NASA Conference Publication 2068

The Saturn System

A workshop held at
The Reston International Conference Center
Reston, Virginia
February 9-11, 1978

NASA

NASA Conference Publication 2068

The Saturn System

Editors:
Donald M. Hunten, *University of Arizona, Tucson, Arizona*
David Morrison, *NASA Office of Space Science*

A workshop sponsored by
NASA Office of Space Science
and held at the Reston
International Conference Center
Reston, Virginia
February 9-11, 1978

National Aeronautics
and Space Administration

**Scientific and Technical
Information Office**

1978

Page intentionally left blank

SATURN SYSTEM WORKSHOP MEMBERSHIP

Dr. Jacques Blamont
Centre Nationale D'Etudes
Universite de Paris
129 Rue de L'Universite
Paris 7, France

Dr. John J. Caldwell
Dept. of Earth & Space Science
State University of New York
Stony Brook, NY 11794

Dr. Sherwood Chang
Mail Stop 239-9
Ames Research Center
Moffett Field, CA 94035

Dr. Lawrence Colin
Mail Stop 245-1
Ames Research Center
Moffett Field, CA 94035

Dr. Giuseppe Colombo
Smithsonian Institution
Astrophysical Observatory
60 Garden Street
Cambridge, MA 02138

Dr. Dale P. Cruikshank
Institute for Astronomy
2680 Woodlawn Drive
Honolulu, HI 96822

Dr. Jeffrey Cuzzi
Space Science Laboratory
University of California
Berkeley, CA 94720

Dr. Rudolph A. Hanel
Code 620
Goddard Space Flight Center
Greenbelt, MD 20771

Dr. Donald M. Hunten
Dept. of Planetary Science
University of Arizona
Tucson, AZ 85721

Dr. Michael J. Klein
Mail Stop 183B-365
Jet Propulsion Laboratory
Pasadena, CA 91103

Dr. David Morrison
Office of Space Science
NASA Headquarters
Washington, DC 20546

Dr. Glenn S. Orton
Mail Stop 183B-365
Jet Propulsion Laboratory
Pasadena, CA 91103

Dr. James B. Pollack
Mail Stop 245-3
Ames Research Center
Moffett Field, CA 94035

Mr. Richard P. Rudd
Mail Stop 161-268
Jet Propulsion Laboratory
Pasadena, CA 91103

Dr. George L. Siscoe
Department of Meteorology
University of California, Los Angeles
Los Angeles, CA 90024

Dr. Bradford A. Smith
Dept. of Planetary Science
University of Arizona
Tucson, AZ 85721

Dr. Edward C. Stone
Mail Code 220-47
California Institute of Technology
Pasadena, CA 91125

Dr. Darrell F. Strobel
Code 7750
Naval Research Laboratory
Washington, DC 20375

Dr. Alan T. Tokunaga
Steward Observatory
University of Arizona
Tucson, AZ 85721

Dr. Laurence M. Trafton
Department of Astronomy
University of Texas at Austin
Austin, TX 78712

Dr. Leonard Tyler
Center for Radar Astronomy
Stanford University
Stanford, CA 94305

Mr. Richard A. Wallace
Code SL
NASA Headquarters
Washington, DC 20546

Dr. James W. Warwick
Dept. of Astro-Geophysics
University of Colorado
Boulder, CO 80302

OTHER PARTICIPANTS

NASA Headquarters

Dr. William E. Brunk
Mr. Daniel H. Herman
Dr. Milton A. Mitz
Dr. Robert E. Murphy

JPL

Mr. Ronald J. Boain
Dr. Albert R. Hibbs

AMES

Dr. Thomas N. Canning

SAI

Dr. William Wells

CONTENTS

CONTENTS (Contd)

INTRODUCTION

In 1982, the Galileo mission (orbiter and entry probe) will be launched toward Jupiter. A logical next step would be a similar mission to Saturn, with probes to Saturn itself and to Titan. One purpose of the Workshop and this document is to provide scientific input to those who are working on plans for SOP[2].

The core of the Workshop was the review papers reproduced here, commissioned from the best available experts on various parts of the Saturn system. Other papers and discussion sessions illustrate the current state of mission planning and the expected state of knowledge after the Voyager encounters in 1980 and 1981. We believe that this report will also be useful as a compendium of the present knowledge of Saturn, its satellites, its rings, and its magnetosphere.

Contributors were able to revise their papers in July 1978. The discussions are reproduced with considerable editing to eliminate repetition and blind alleys.

Thanks are due to the Jet Propulsion Laboratory for their assistance with the workshop and the preparation of this volume. Roy G. Brereton and Albert R. Hibbs handled the physical and financial arrangements for the workshop.

Donald M. Hunten
David Morrison

Page intentionally left blank

BACKGROUND OF THE SOP²* MISSION

Richard A. Wallace

Planetary Division, NASA Headquarters
Washington, DC 20546

ABSTRACT

This paper covers two areas of interest, providing an overview of:

1. Saturn mission design history.
2. Saturn's place in NASA's program plans.

The first area provides a view of how changing concepts and techniques can affect mission design and science return. The second puts Saturn in perspective with regard to its role in NASA's overall planetary program.

SATURN MISSION DESIGN HISTORY

Saturn mission design can be broken into two pieces. The first piece relates to how you reach Saturn from Earth, the second with what you do when you arrive there. The first Table shows a development history for Saturn missions covering the period from 1964 to the present. Throughout this time period, technology and the timely development of interplanetary trajectory techniques have made missions to Saturn more science effective by allowing delivery of larger and larger payloads. The first item in Table 1 shows the requirements of sending a package to Saturn if we do it the same way we did for the Ranger lunar, Mariner 1962 Venus, and Mariner 1964 Mars missions. These were first attempts to scope the outer planet exploration problem. Mission analysts found that direct ballistic trajectories to Saturn were very expensive, quite a bit more so than trajectories to Jupiter.

*SOP² is an abbreviation for Saturn Orbiter Dual Probe—a Saturn bound spacecraft combining three major systems: an orbiter, a Saturn probe, and a Titan probe.

Table 1. Saturn Missions – Development History

Study	Dates	Conclusion
• Specification of ballistic trajectory requirements	1964-65	Energy requirements very high
• Jupiter gravity-assist trajectory discovered	1966-67	Energy requirements comparable to Jupiter mission requirements
• Pioneer/Voyager mission designs	1968-74	Excellent reconnaissance missions to Jupiter and Saturn feasible
• Jupiter Orbiter studies	1969-77	Jupiter Orbiter missions very attractive and feasible; satellite tour techniques defined; outer planet probes studied in detail
• VEGA and ΔVEGA techniques discovered	1974-75	Energy requirements reduced; flight times increased
• Saturn Orbiter/Satellite Tour Study	1975	JOP techniques applied to Saturn; considered VEGA/ΔVEGA
• Titan mission studies	1975-76	Titan lander/probe missions conceptualized; scientifically rewarding missions described
• Ion Drive techniques applied to Saturn mission	1976-78	Energy requirements and flight times reduced
• 1977 SOP^2 study	1977	SOP^2 mission feasible in variety of ways; science priorities required for further mission design

In 1966 Gary Flandro discovered a family of Jupiter gravity-assist trajectories which now brought Saturn into the same launch vehicle range as Jupiter missions. The Pioneer and Voyager missions were designed on the basis of these earlier trajectory analyses, and our first outer planet reconnaissance missions were born. The Voyager mission design aided the solution to the problem of satellite encounter design, developing techniques in timing the launch and providing maneuvers which would maximize satellite science return consistent with planetary science desires.

With the Pioneer and Voyager mission designs underway, interest developed in an exploratory mission to Jupiter which would allow longer times to investigate the

extensive Jupiter system. The Jupiter Orbiter Probe (now Galileo) mission design developed satellite gravity-assist techniques which allowed satellite tours while in orbit around the parent body.

While the Jupiter orbiter design was being developed, a new interplanetary trajectory technique was found which allowed delivery of greater payloads to the outer planets. The technique calls for a trajectory which is first directed in towards the Sun with a possible Venus close flyby and/or deep space propulsion manuever, and then return to Earth for an Earth gravity-assist as the trajectory carries the spacecraft out to the outer planets (VEGA and Δ VEGA trajectories). Not only are the payloads larger, but the opportunities for such missions are available over a greater period of years than the direct Jupiter gravity-assist missions to Saturn. The drawback, and it is a major one, is that launch to arrival times are increased over the already long flight times required by the previously defined techniques.

In 1975, with interest increasing in the Jupiter orbiter mission, analysis of a Saturn orbiter applied the techniques of the Jupiter orbiter mission as well as the new VEGA and ΔVEGA techniques, and found such a mission concept to be feasible enough to warrant further study.

In the last few years technology has been advancing to the point where a new low thrust propulsive technique will be available to NASA which will allow realization of difficult, but scientifically exciting missions. The major problem with Saturn mission designs up through the 1970's was the restriction to relatively low payloads associated with long flight times. Ion drive techniques use a low thrust, continuously operating device acting over a period of years. Combining the ion drive techniques with the Earth gravity-assist techniques discovered earlier provides the possibility of delivering a highly interesting science package to the Saturn system.

Studies conducted last year at JPL and scheduled studies this year are focused on a Saturn Orbiter Dual Probe (SOP^2) mission design. One of the major reasons for holding the Saturn Workshop is to provide science recommendations for an intelligent design of such a mission. What kind of science return should the mission designers focus their study on?

SOP^2 AND NASA's PLANETARY PROGRAM

The timing for this workshop is appropriate. The Pioneer and Voyager missions will be returning important data between 1979 and 1981, in time to focus the SOP^2 design for a launch after 1985. Ion drive and trajectory software development

will be available for launches in the mid-1980's and beyond. Mission concept and feasibility design is now required so that later systems definition and design can take place and dovetail with the technology development and science base. Science recommendations are key to this continuing design process.

Table 2 shows the current 1979-83 planetary exploration five-year plan. This plan is the end result of consultations with the scientific community, mission planners in NASA, Congress, and the Office of Management and Budget.

Several plans were considered. It should be noted that SOP^2 was part of all of them. The SOP^2 mission is considered a high priority mission by NASA.

Table 2. Planetary New Starts – FY 1979-83

Mission	New Start/Launch	Mission Type
Venus Orbital Imaging Radar (VOIR)	1980/1984	Exploratory
Halley/Tempel-2 Rendezvous	1981/1985	Reconnaissance
Saturn Orbiter Dual Probe (SOP^2)	1983/1987	Exploratory
Mars Program Technology Development	1982/-	Intensive Science

DISCUSSION

D. HERMAN: Let me comment on the degree of commitment by NASA to an SOP^2 Mission. First of all, in the Fiscal 1979 Budget, recently submitted to the Congress, there is a separate five million dollar line item for the development of ion drive. The first intended use of that system is to effect a comet rendezvous, probably with comet Tempel 2. The second intended use of that system would be for SOP^2.

At the FY 1979 Budget Press Conference, Dr. Frosch stated that it's time to take ion drive out of being a laboratory curiosity and to develop it towards a flight propulsion system; that's NASA's intent.

With respect to the five-year plan, we were given budget guidelines by the Office of Management and Budget to plan the missions that we want to do in the next five years. We are obliged every fiscal year to submit a revised five-year plan that is consistent with the budget. Our own input to that five-year plan was to show the SOP^2 mission as a Fiscal 1982 new start with a 1986 launch. The Administrator, in reviewing the five-year plan, adjusted the timetable to shift the SOP^2 new start to FY 1983, and that is where it now stands. But we must still plan as if the SOP^2 Mission could indeed be a Fiscal 1982 New Start and a 1986 launch because something could happen to the Mars program to cause us to revert to the original timetable. Our assessment is that the SOP^2 Mission will go either as Fiscal 1982 or a Fiscal 1983 New Start with a launch either in 1986 or 1987.

Page intentionally left blank

ORIGIN AND EVOLUTION OF THE SATURN SYSTEM: OBSERVATIONAL CONSEQUENCES

James B. Pollack

Space Science Division, NASA-Ames Research Center
Moffett Field, California 94035

ABSTRACT

A number of important cosmogonic questions concerning the Saturn system can be addressed with a Saturn-orbiter-dual-probe spacecraft mission. These questions include: the origin of the Saturn system; the source of Saturn's excess luminosity; the mechanism by which the irregular satellites were captured; the influence of Saturn's early luminosity on the composition of its regular satellites; and the origin of the rings. The first two topics can be studied by measurements made from an entry probe into Saturn's atmosphere, while the remaining issues can be investigated by measurements conducted from an orbiter. In this paper, we present background information on these five questions describing the critical experiments needed to help resolve them.

INTRODUCTION

The planets of our solar system can be divided into three compositional classes: the terrestrial planets, which are made entirely of heavy elements; Jupiter and Saturn, which are composed chiefly of hydrogen and helium, although they have heavy element cores; and finally Uranus and Neptune, which are constructed in large measure of heavy element cores, but also contain significant gaseous envelopes. We are in a particularly fortunate situation in our attempts to understand the origin and subsequent evolution of Jupiter and Saturn. In the first place, their current characteristics as well as those of their attendant satellite systems are rife with clues about their history.

For example, the observed excess amount of thermal energy they radiate to space above the amount of absorbed solar energy may represent the embers of internal energy built up during an early rapid contraction phase (Graboske *et al.* , 1975; Pollack *et al.* 1977). In the second place, techniques used to study stellar evolution can be employed to model much of the evolution of these giant planets.

In this paper, we review current cosmogonic theories of the history of the Saturn system and describe how such models can be tested by comparisons with the present properties of Saturn, its rings, and its satellites. Emphasis will be placed on enumerating those cosmogonic clues that might be studied most profitably by a Saturn-Orbiter-Dual Probe (SOP^2) spacecraft mission.

RIVAL COSMOGONIC HYPOTHESES

Present-day Saturn has a mass equal to about 95 Earth masses, of which about 15 Earth masses is sequestered in a heavy element core composed presumably of a mixture of rocky and icy material (Slattery, 1977). The remaining material in the surrounding gaseous-liquid envelope is thought to consist of an approximately solar mixture of elements; i.e. hydrogen and helium are the dominant components. The composition of this envelope closely resembles that of the primordial solar nebula, which served as the source material for planetary construction. There are two logical possibilities for the way in which Saturn could have been assembled within the solar nebula. Either its core was formed first and served to focus a massive gaseous envelope about itself or a gaseous condensation developed initially within the solar nebula and subsequently collected a central core. Both these possibilities have been explored in recent years. Below we describe these alternative models for the formation of Saturn and indicate the stage at which its regular satellites may have formed.

Perri and Cameron (1974) investigated models in which massive planetary cores formed first and subsequently collected a portion of the nearby solar nebula about itself. As might be expected, the gas of the nebula becomes concentrated about the core, with the boundary of this gaseous envelope being the point at which the gravitational attraction of the core and envelope equals the gradient of the gravitational potential of the solar nebula, i.e., it equals the "tidal" radius. Below a certain critical mass, the envelope about the core is hydrodynamically stable, so that only a minor gaseous envelope could be expected at present. But, for cores more massive

than a "critical mass", the envelope becomes hydrodynamically unstable and in a very short period of time assumes a much smaller radius than the tidal value. In this case, the product will be a planet with both a massive core and a massive gaseous envelope.

The value of the critical core mass needed to trigger a hydrodynamic instability in the surrounding gas depends on the temperature structure assumed for the envelope and its boundary conditions. Perri and Cameron (1974) assume that the envelope is convectively unstable, motivated in part by the large opacity expected from dust grains, and that the envelope is on the same adiabat as the solar nebula. Using nominal values for the solar nebula's adiabat, they obtained a critical mass of 115 Earth masses. Since this value was significantly higher than values of several tens of Earth masses found by Podolak and Cameron (1974) from models of the interior structure of the outer planets, they suggested that the instability occurred at a later epoch in the history of the solar nebula, when it was much cooler. Much smaller critical masses can also be realized by postulating an isothermal temperature structure for the envelope. According to Harris (1978), critical masses on the order of 1 Earth mass hold in this case. As mentioned in the introduction, the best current estimate of the mass of Saturn's core places it at 15 Earth masses. Thus, the actual core mass of Saturn may be large enough for it to have been able to initiate a hydrodynamical collapse in the surrounding gas.

An alternative scenario for the origin of Jupiter, and by implication Saturn, was first investigated in detail by Bodenheimer (1974). He suggested that the initial formation stage involved the condensation of the gaseous envelope. As in the case of star formation, a local density enhancement is assumed to be present in the solar nebula. When this density exceeds a critical value, the localized region begins to contract. If the sun has not yet formed and there is little mass in the solar nebula interior to the localized region of interest, the critical density is determined by the condition that the region's gravitational binding energy be comparable to its internal energy, as determined by its temperature. If the sun has formed or at least there is much mass in the solar nebula interior to the local region, the critical density is determined from a tidal criterion. In the case of Jupiter, Bodenheimer estimates the critical density to equal approximately 1.5×10^{-11} gm cm^3 in the former case and about 1×10^{-8} gm/cm^3 in the latter case (Bodenheimer, 1978). For an object of Saturn's mass and distance, a simple scaling of Bodenheimer's prescriptions for the critical density leads to values of about 1×10^{-10} and 2×10^{-9} gm cm^3. The corresponding initial radius for Saturn in both cases is approximately 2000 R_s, where R_s is its current radius.

Once contraction is initiated as a result of the local density enhancement, the gaseous protoplanet will evolve through four stages (Bodenheimer, 1974). The first stage consists of a small contraction (~15%) on a hydrodynamic time scale (~10^2 years), during which the configuration settles into hydrostatic equilibrium. This stage is followed by one characterized by a slow contraction on a Kelvin-Helmholtz time scale (~10^5-10^7 years). As time progresses, the interior temperatures are gradually built up until they reach about 2500 K near the center. At this point significant dissociation of molecular hydrogen occurs, which alters the adiabatic lapse rate in such a way that a hydrostatic configuration is no longer possible and a hydrodynamical collapse phase is initiated. Within a very short time on the order of a few years, the radius of the protoplanet decreases from several hundred times the present value to several times the present value. However, near the end of the collapse, conservation of angular momentum probably leads to a spreading out of the outer regions of the protoplanet into an extended disk. Thus, while the central protoplanet is settling back into a hydrostatic configuration once more, the formation of its regular satellites begins within the extended disk. The fourth stage, which spans almost the entire lifetime of the planet, involves a slow hydrostatic contraction to its present size. From now on, we will refer to these four stages as the first hydrodynamic stage, the first hydrostatic stage, the second hydrodynamic stage, and the second hydrostatic stage, respectively.

Figures 1a and 1b illustrate the nature of the first hydrostatic phase for Saturn (DeCampli *et al.*, 1978). In these figures, radius and luminosity are plotted as a function of time. The time scale of this stage is determined principally by the opacity within the protoplanet, which is almost entirely due to grain opacity. In this calculation, the composition of the major grain species was determined from thermodynamic equilibrium considerations for a solar abundance mixture of elements, with the best available optical constants for each specie being used to determine the Rosseland mean opacity of the ensemble. A protoplanet with Saturn's mass takes about 10^7 years to progress through stage 2, whereas one with Jupiter's mass takes about 10^6 years. Thus, this time scale varies approximately as the square of the mass. Clearly a protoplanet's mass cannot be much less than an order of magnitude smaller than Saturn's mass or it would not complete stage 2 within the age of the solar system. Also, according to these calculations, the second hydrodynamic collapse begins when proto-Saturn has a radius of about 40 R_s.

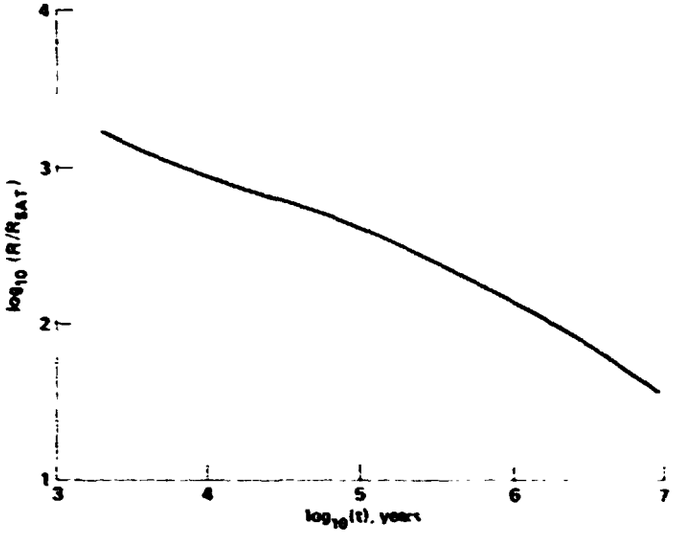

Figure 1a. Radius of Saturn, in units of its present value, as a function of time during the first hydrostatic stage

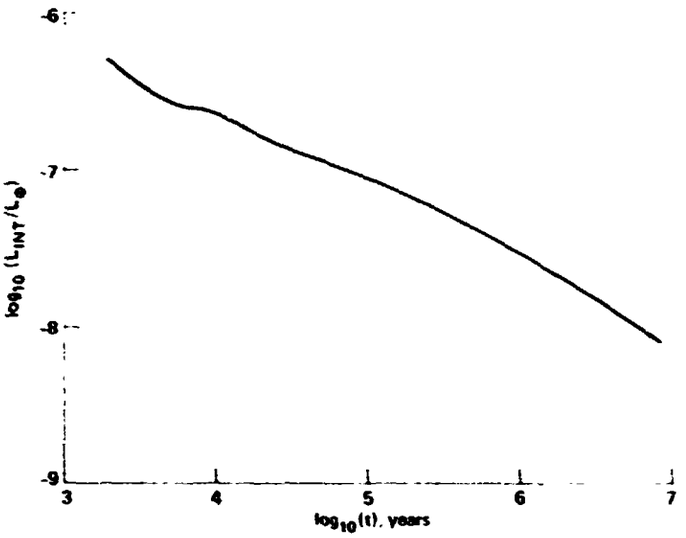

Figure 1b. Luminosity of Saturn, in units of the solar luminosity, as a function of time during the first hydrostatic stage.

Figures 2a and 2b present the temporal variations of Saturn's and Jupiter's radius and luminosity during the second hydrostatic stage (Pollack *et al.* , 1977). The initial radii for these calculations were arbitrarily chosen to be about ten times their current values. However, these curves are equally applicable to other initial conditions, by merely starting at the desired radius and measuring time relative to this initial epoch. Bodenheimer's (1974) calculations of the second hydrodynamic stage suggest that this stage concludes and the second hydrostatic stage begins at a radius of 4 to 5 times the current value. The present day values of radius and excess luminosity are shown by squares and circles in these figures for Jupiter and Saturn, respectively. These calculations refer to a solar mixture model, i.e., one lacking a heavy element core. Inclusion of a core, by design, leads to perfect agreement with the observed radius, but it does not substantially change the time scales nor the luminosity diagram (Grossman, 1978). Possible reasons for the underestimate of Saturn's current excess luminosity will be given below. In any case, we see that these calculations lead to reasonable first order estimates of the observed values. Finally, we note that gases are the only source of opacity for these models. This is reasonable since the interior temperatures are sufficiently high for grains to be evaporated.

An important aspect of Figure 2b is the occurrence of a very high luminosity during the early phases of stage four. Thus, during the time period over which the regular satellites were forming, its planet's luminosity was several orders of magnitude higher than its current value and furthermore was rapidly declining. Consequently, the formation of low temperature condensates, such as ices, may have been inhibited close to the planet at such times and a zonation of composition with distance from the primary may be created (Pollack and Reynolds, 1974; Pollack *et al.* , 1976). We also note from Figure 2b that, during early times of this stage, Jupiter's luminosity was about a factor of ten higher than Saturn's and consequently it was harder to form low temperature condensates close to Jupiter.

So far, we have discussed only the evolution of the gaseous portions of Saturn. There are several ways in which its heavy element core may have been created. First, if proto-Saturn was much more massive than Saturn's current mass, the core could have been formed entirely from grains initially present in the envelope, which were segregated into the central regions. For example, the interior temperatures around the time of the second hydrodynamic stage may have reached the *melting* point of the grains, leading to liquid particles, which rapidly coagulated into much bigger particles; the latter rapidly sank to the center (Cameron, 1977). Subsequently, much

of the gaseous envelope was lost so that the end result was a planet enriched in heavy elements. To be consistent with Saturn's inferred core mass, we would have to postulate that *at least* 80% of the initial protoplanet's mass was later lost!

Alternatively, small rocky and icy bodies may have been produced outside of Saturn's sphere of influence, but at a similar distance in the solar nebula. These objects could have been collected efficiently when proto-Saturn was much larger than its current size, i.e., during the first hydrostatic stage. Planetoids smaller than 10 to 100 km in radius would have become captured by gas drag effects. Continued gas drag would have caused them to spiral very rapidly into the center of the proto-planet (Pollack *et al.*, 1978).

Finally, let us compare the two scenarios of planetary formation. The first hydrostatic stage of the gas instability model bears some resemblance to the stage during which the core is growing to the critical mass in the core instability model. During the core growth period, there will be a gaseous concentration about the core, which will be in hydrostatic equilibrium. The chief differences at this point between the two models is that the core and envelope mass are both growing with time in the core instability model, but not in the gas instability model (except perhaps for the core alone) and that the radius of the envelope in the former model is always determined by the tidal radius, and so will increase with time, not decrease as occurs for the latter model. Both models are characterized by a subsequent rapid hydrodynamical phase. At the end of this stage both models relax into a hydrostatic configuration and follow essentially the same evolutionary path.

PLANETARY OBSERVATIONS

In this section and in the following one, we enumerate critical observations that can be made from a SOP[2] mission that will test and illuminate key cosmogonic issues. In preparing this list of measurements, we have attempted to exclude ones that can be made from the Pioneer 11 and Voyager Flyby missions, which will reconnoiter the Saturn system first.

Assessment of the amount by which Saturn's interior is enriched in heavy elements in excess of their solar abundance values may aid in discriminating between the two theories for the formation of the Saturn system and in obtaining clues about core construction. In principle, the core mass can be determined from a knowledge

of the planet's mass, radius, and rotational period, quantities that are presently well-known. However, such calculations rest on the implicit assumption that the composition of the envelope is known; e.g., that the envelope has a solar elemental abundance composition. But, the envelope may be enriched in such volatiles as water, ammonia, and methane: within the context of the core instability model, a shock wave is set up at the core-envelope interface during hydrodynamical collapse, which may cause the evaporation of some of the icy condensates (Perri and Cameron, 1974). Within the context of the gas instability model, the same result may accrue from the gas drag capture mechanism, as captured bodies are partially volatilized. Indeed some recent models of Saturn's interior have invoked heavy element enrichment of the envelope to fit the measured values of its gravitational moments (Podolak and Cameron, 1974).

While crude estimates of the abundance of methane and ammonia in Saturn's atmosphere can be made from Earth-based observations, truly good determinations can only come from in-situ compositional analyses below the levels at which these gases begin to condense and therefore require an atmospheric entry probe. Such measurements will also yield the water vapor abundance, provided the probe can survive until depths of several tens of bar pressure. Finally, a determination of the helium to hydrogen ratio in the observable atmosphere is also important, since, as discussed below, helium may partially be segregated towards the bottom of the envelope.

Conceivable, not only is the envelope of Saturn enriched in icy species, but also in rocky species (Podolak *et al.*,1977). Since the latter condense way below any altitude to which a probe can reasonably be expected to function, a more indirect assessment of the latter excess is needed. The needed constraint can be provided by the J_2 gravitational moment of Saturn. While this moment is currently known quite well from studies of satellite orbits (~0.1%), there is one important potential source of systematic error in its value. The current estimate of J_2 is based upon the assumption that the rings of Saturn have a negligible mass. Studies of the motion of a Saturn orbiter may provide a check on this assumption. If it turns out that the rings do have a non-trivial mass ($>10^{-6}$ Saturn's mass), corrections can readily be made to the current value of J_2 to convert it into the actual J_2 for Saturn. Similar corrections and refinements to J_4 (currently known to about 7%) will yield a value that will provide a valuable check on the validity of the interior models. Moments higher than J_4 will not be very useful since they are determined principally by the outermost layers of the envelope (Hubbard and Slattery, 1976).

Let us now suppose that the SOP^2 mission provides the needed compositional and gravitational information. Two theoretical steps are needed in order to realize the scientific objectives. First, interior models need to be constructed to define the amount of excess heavy elements and their spatial distribution, i.e., partition between core and envelope. Currently, the chief theoretical factor limiting the accuracy of interior models of the giant planets is the uncertainty in the thermodynamic properties of materials at high temperatures and pressures. In the case of the envelope, the equation of state of a solar elemental mixture is least well known for densities in the range of 0.1 to 1 gm/cm^3. Typically, the needed thermodynamic properties are interpolated from their more well defined values at lower and higher densities. It is reasonable to expect that the uncertainties in this critical density region will be substantially reduced by the time a SOP^2 Mission occurs. This is important since much of Saturn's interior lies within this density domain (~70% by mass!). Also, adequate equations of state for core materials should be available at the time of the SOP^2 mission.

In addition to good interior models, careful determinations are needed of the critical core mass needed to cause hydrodynamic instability in the surrounding gas. Current estimates of this parameter are based on linear stability theory. More reliable values can be obtained from numerical hydrodynamical calculations and these should become available in the next few years. By comparing the inferred excess mass of heavy elements with the critical value, an assessment of the validity of the core instability model can be made.

We next consider the origin of the excess energy Saturn radiates to space. Gravitational energy represents the only plausible source for this excess that would allow Saturn to radiate at its present excess over the lifetime of the solar system (Graboske *et al.*, 1975; Cameron and Pollack, 1976; Pollack *et al.*, 1977). But there are three distinct ways in which Saturn's gravitational energy can be converted into luminosity (ibid). First, rapid contraction in Saturn's early history, when its interior was much more compressible than at present, could have led to a build-up of internal energy, i.e., high interior temperatures, which have subsequently been decreasing. Second, Saturn may be contracting sufficiently rapidly at present to generate the observed excess. Both the above modes of gravitational energy release refer to the behavior of a planet whose interior compositional structure does not change with time. But, according to calculations by Stevenson (1975), when temperatures decline to a certain threshold value in the envelopes of the giant planets, helium will start to become immiscible in metallic hydrogen and begin to sink towards the center of the

planet. As this process proceeds, some helium in the molecular envelope will be mixed into the depleted region of the metallic zone, so that a helium depleted outer region encompassing both regions will be set up. Such a chemical differentiation could generate enough energy to account for much of the observed excess luminosity.

The evolutionary results shown in Figure 2b refer to the contraction history of homogeneous, solar elemental mixtures containing no cores. Thus, the predicted luminosity reflects only the first two gravitational processes. Figure 3 illustrates the relative effectiveness of these two processes for Saturn by displaying the time history of its gravitational and internal energies (Pollack *et al.* , 1977). During the first 10^7 years, contraction proceeds at a rapid enough rate for the internal energy to steadily increase. But, at subsequent times, it declines. Currently, the loss of internal energy is more important than present contraction in accounting for the excess luminosity, although the latter makes a non-negligible contribution. Qualitatively similar statements also hold for Jupiter.

As illustrated in Figure 2b, the calculated excess for Jupiter at a time equal to the age of the solar system is consistent with the observed excess. However, the corresponding theoretical value for Saturn falls noticeably below its observed excess. There are several points that need to be considered before we judge this discrepancy to be real. First determination of the observed value is complicated by the need to subtract out a contribution from the rings at the longer infrared wavelengths, where the two objects cannot be spatially resolved, as well as by uncertainties in calibration standards. Nevertheless, the most recent determinations of Saturn's excess luminosity are crudely consistent with the value displayed in Figure 2b (e.g., Ward, 1977). This situation should be substantially improved by having observations performed when the rings assume an edge-on orientation as viewed from Earth and by utilizing observations from the fly-by missions to obtain an accurate value for the phase integral in the visible. This latter is needed to compute the amount of solar energy absorbed by the planet. In addition to these observational issues, we also need to consider the influence of a core on Saturn's theoretical excess luminosity. Very recent calculations that incorporate a core-envelope structure lead to essentially the same curve as shown in Figure 2b (Grossman, 1978). Hence, the factor of 2 to 3 difference between the computed and observed excess energy may be real.

Is helium segregation an important source of the present excess luminosity? According to Figure 2b, this source is not needed to explain Jupiter's excess. Furthermore, temperatures within Jupiter's metallic zone are at least a factor of two above

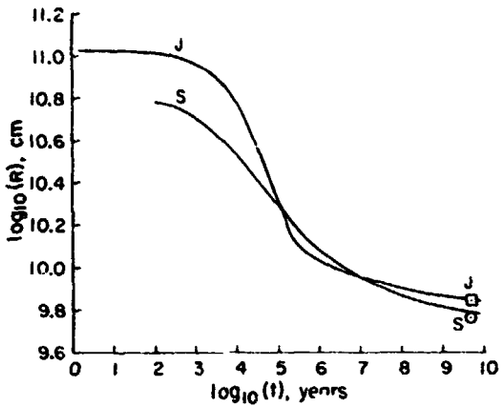

Figure 2a. Radius of Jupiter (J) and Saturn (S) as a function of time, t, during the second hydrostatic phase. The observed values at the 4.5 x 10^9 years time point are indicated by the square and circle for Jupiter and Saturn, respectively.

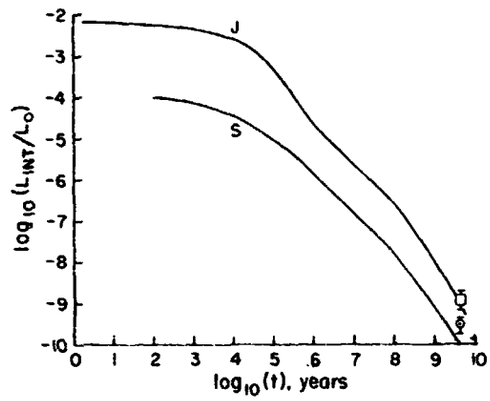

Figure 2b. Excess luminosity of Jupiter (J) and Saturn (S), in units of the solar luminosity, as a function of time, t, during the second hydrostatic stage. Observed values at the 4.5 x 10^9 years time point are indicated by the square and circle for Jupiter and Saturn, respectively.

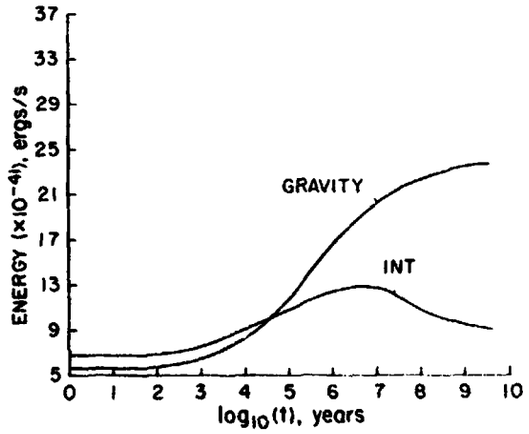

Figure 3. Variation with time during the second hydrostatic stage of ($-E_{GRAV}$), labelled GRAVITY, and E_{INT}, labelled INT, where E_{GRAV} and E_{INT} are the potential energy and internal thermal energy, respectively. These results pertain to a model of Saturn with solar elemental abundances.

the temperature at which phase separation starts to occur (Pollack *et al.* , 1977). But the reverse may be true for Saturn. The computed excess appears to be too low. Also, as illustrated in Figure 4, the interior of a chemically *homogeneous* model crosses the phase separation curve after about 1 billion years of evolution. Allowance for a core-envelope structure leads to higher interior temperatures in the metallic hydrogen zone, wi' . current Saturn lying close to the separation curve. Thus, helium segregation, while apparently not yet an important source for Jupiter, may represent a major source of Saturn's current excess (Pollack *et al.* , 1977).

If the phase separation of helium from hydrogen is in fact a significant source of Saturn's excess energy, planet-wide segregation is required (Pollack *et al.* , 1977). Therefore, an in-situ determination of the helium to hydrogen ratio by experiments carried aboard an entry probe can provide a critical test of this possibility. Not only will it be useful to compare this measurement with solar abundance figures, but, equally important, to compare it with the value found for the atmosphere of Jupiter by experiments aboard the JOP entry probe. This latter comparison is needed since the solar ratio is not as well established as one might like.

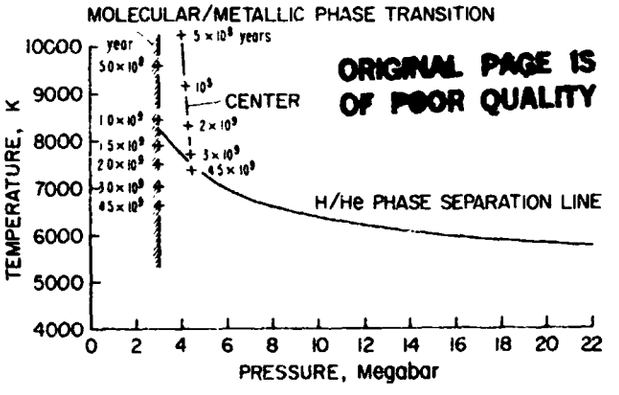

Figure 4. Phase boundaries for the molecular and metallic phases of hydrogen and for the separation of helium from hydrogen. For points lying below the separation line, helium becomes partially immiscible in metallic hydrogen. Also shown on this diagram is the evolutionary track of the center of a solar mix Saturn model. Numbers next to crosses on this track and on the molecular-metallic phase boundary indicate time from the start of the calculation for the second hydrostatic stage.

SATELLITE AND RING OBSERVATIONS

In this section, we discuss sequentially cosmogonically relevant observations of Saturn's irregular satellite(s), regular ones, and the rings. The outer satellites of Jupiter, Saturn, and Neptune differ markedly from the inner satellites of these planets in having highly inclined and eccentric orbits, with about half of them traveling in a retrograde direction. These orbital characteristics suggest that the outer satellites may be captured objects. Pollack *et al.*, (1978) have proposed that capture occurred as a result of the gas drag experienced by bodies passing through the extended gaseous envelopes of the primordial giant planets, just prior to the second hydrodynamical stage. We have earlier pointed out that gas drag capture offers one mechanism of generating core material. In such cases, continued gas drag causes the captured body to quickly spiral into the center of the protoplanet. However, if capture occurs in the outer portion of the protoplanet shortly before initiation of the second hydrodynamical collapse (within $\sim 10^1$ years) and if the captured body is sufficiently large ($\sim 10^2$ - 10^3 km), it will experience only limited orbital evolution prior to the removal of gaseous material from its neighborhood. In this case, the captured body would remain a captured satellite. Pollack *et al.*, (1978) showed that this mechanism could lead to the capture of objects comparable in size to that of the irregular satellites, when nebular densities similar to those exhibited by models of the latest phases of the first hydrostatic stage are utilized (Bodenheimer, 1978). In addition, this model is capable of accounting for many other observed properties of the irregular satellites.

Besides modifying a body's velocity, gas drag also subjects it to mechanical stresses and to significant surface heating. When the dynamical pressure due to gas drag exceeds the body's strength, it will fracture into several large pieces. However, the mutual gravitational attraction between the fragments is larger than the gas drag for so the fragments remain together until separated by collision with a sufficiently large ray body. In this way, Pollack *et al.*, (1978) attempt to account for the existence of Jupiter's two families of irregular satellites with the members of each family being characterized by similar orbital semi-major axes and inclinations.

Figure 5 illustrates the heating rate experienced on the forward hemisphere of a captured body as a function of angular distance θ from the stagnation point. (M. Tauber, private communication). These calculations pertain to typical parameter choices of 5 km/s for the relative velocity between the body and the nebula and

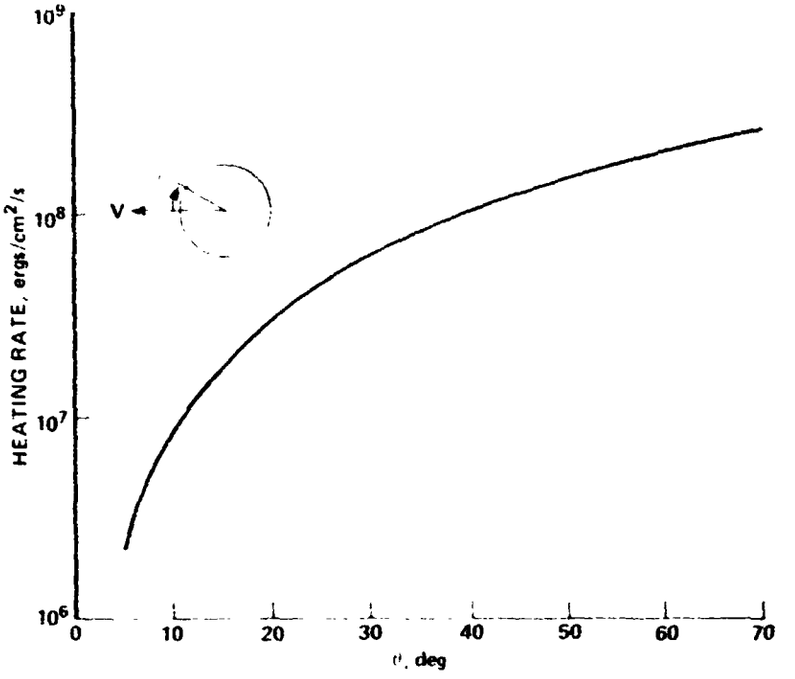

Figure 5 Heating rates on the forward hemisphere of a body experiencing gas drag as a function of angular distance θ from the stagnation point. These calculations were done for a relative velocity of 5 km/s between the body and the gaseous medium and a gas density of 2×10^{-6} gm/cm³.

2×10^{-6} gm/cm^3 for the gas density. Orders of magnitude smaller heating rates occur on the trailing hemisphere. If we use a representative value of 10^8 ergs/cm^2/s for the heating rate and assume it is used simply to enhance the surface temperature, we obtain a surface temperature of 1150 K! Alternatively, if some of the heat is used to melt or vaporize surface deposits of water ice, we find that meters of ice can experience a phase change during the time of the capture process.

Saturn's outermost satellite, Phoebe, is definitely an irregular satellite: it travels in a highly eccentric, highly inclined orbit in the retrograde direction. Conceivably, the second outermost satellite, Iapetus, might also be considered an irregular satellite since its orbital inclination is substantially larger than those of satellites located closer to Saturn. But, Iapetus travels in a prograde direction and has a very low orbital eccentricity.

Photography of Phoebe, its neighborhood, and Iapetus may provide valuable data for assessing the validity of the gas drag capture mechanism. Close-up pictures of Saturn's irregular satellite(s) may reveal morphological features created during the

hypothetical capture event(s). The mechanical stresses experienced during capture may be manifested in extensive fractures, while the strong surface heating may have produced flow features as well as pit-like structures created by outgassing.

As mentioned above, capture led to clusters of irregular satellites in the case of the Jovian system, with cluster members representing fragments of the captured parent body. In the case of the Saturn system, no such families of irregular satellites are known to exist. The presence of single, irregular satellite(s) rather than clusters can be attributed to the following: there were differences in the mechanical properties of the captured bodies so that total fracture never occurred for the Saturn captured objects(s); or fracture did occur, but there was never a subsequent collision with a large enough stray body to separate the pieces; or separation did occur, but the smaller fragments are too faint to be readily observed from the Earth. The last possibility gives rise to the suggestion that a systematic photographic search be conducted from a Saturn orbiter for faint objects with orbital inclinations and semi-major axes similar to those of Phoebe.

We next consider studies of the regular satellites. The Galilean satellites of Jupiter exhibit a systematic increase in their mean density with decreasing distance from Jupiter. This trend has been attributed to the high luminosity of Jupiter during the early phases of its second hydrostatic stage (see Figure 2b) (Pollack and Reynolds, 1974). As discussed earlier, the high luminosity inhibited the condensation of ices in the region close to the planet during the satellite formation period. Saturn's lower luminosity during this epoch means that ices were stable closer to it than to Jupiter during the formation of its satellite system. Nevertheless, a compositional gradient may also be present for the Saturn system.

In Figure 6a, we illustrate the possible effects of Saturn's early high luminosity on the composition of the material forming its satellite system (Pollack *et al.*, 1976). Each curve in this figure shows the temperature of a condensing ice grain at the distance of a given satellite as a function of time from the start of the second hydrostatic stage. The curves are labelled by the first letter of a satellite's name, with A, B referring to the two brightest rings. Analogous curves for the Jovian system are shown in Figure 6b. In both cases, the region of satellite formation has been assumed to have a low opacity to the planet's thermal radiation. Qualitatively similar curves hold in the high opacity case (Pollack *et al.*, 1976).

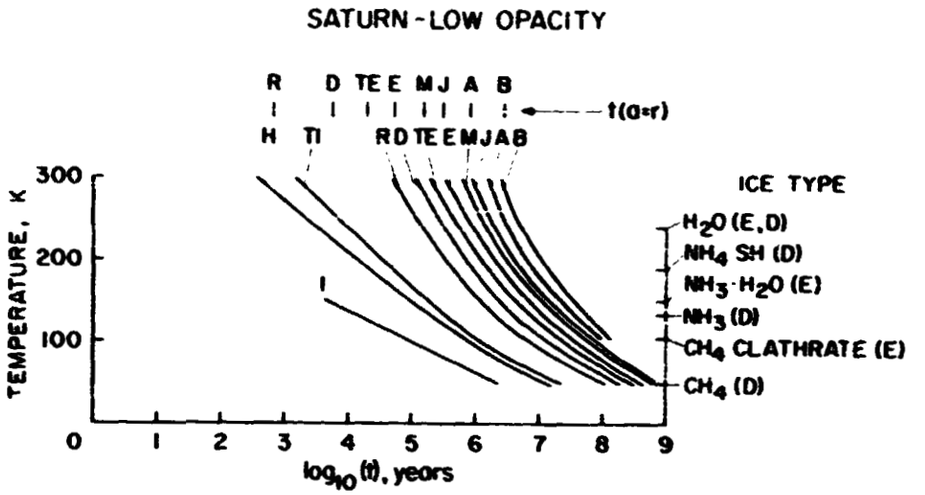

Figure 6a. Temperature of a condensing ice grain as a function of time from the start of the second hydrostatic stage. The calculations of this figure are for the Saturn system and the low-opacity case. Each curve refers to a fixed distance from the center of the planet and is labelled by the first letter of the name of the satellite or ring segment, which is currently at that distance. Further details about this figure are given in the text.

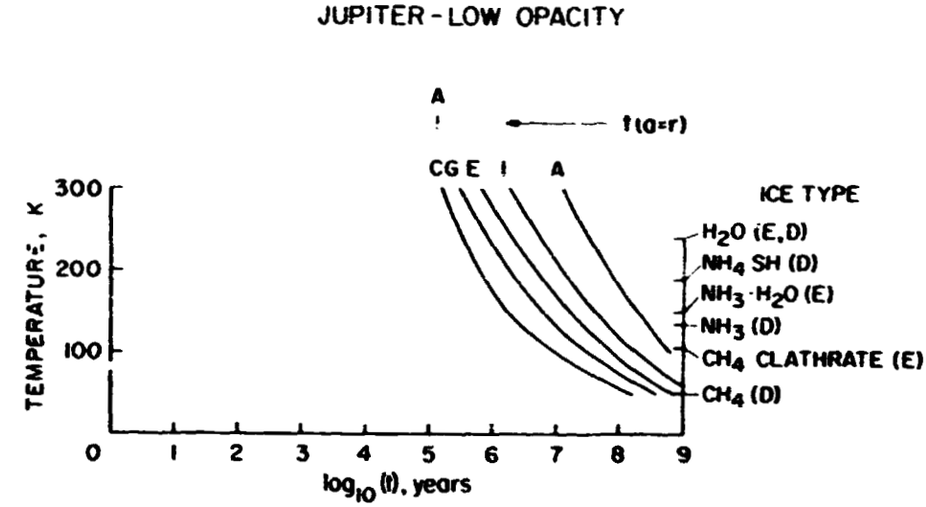

Figure 6b. Same as figure 6a, but for the Jupiter system.

The vertical axis on the right hand side of Figure 6 displays the temperature at which various ice species condense. Thus, at times along a given satellite's curve when the temperature is higher than the condensation temperature of a particular ice specie, it will be entirely in the gas phase and so will not be incorporated into the forming satellite. After a certain time, satellite formation ceases because the disk of material from which they form has been eliminated. If the temperatures have remained too hot for certain ice species to condense up until the end of the satellite formation period, they will be absent from a satellite formed at the distance under consideration. Hence, satellites close to Saturn will lack the more volatile ice species incorporated into satellites formed further away.

The short vertical line segments near the top of Figure 6 indicate the time, t (a = r), at which the radius of the planet equalled the orbital distance of the satellite. Presumably, satellite formation at that distance did not occur at earlier times. Titan may be larger than satellites closer to Saturn because its formation could have started with the commencement of the second hydrostatic stage (Pollack *et al.* , 1977).

Accurate measurements of the mean density of Saturn's regular satellites represent the most important data for assessing the possible influence of Saturn's early excess luminosity on the composition of its satellite system. When graphs, such as Figure 6, are constrained by the currently known compositional properties of Saturn's satellites or the time of satellite formation for Saturn is assumed to be the same as for Jupiter, the following general picture emerges of the bulk compositional gradient within the Saturn system: water ice may represent the only ice species incorporated into the innermost satellites of Saturn; ammonia ices, principally NH_4SH, as well as water ice are present in all the remaining satellites; and methane clathrate is to be found in satellites starting at Titan's distance from Saturn. Also, there may be variations in the fractional amount of rocky material incorporated into the satellites because of the delay in the formation of the inner ones caused by Saturn's size exceeding their orbital distances at the beginning of this period. While the resultant variations in bulk density among the regular satellites of Saturn may not be nearly as spectacular as for the Galilean satellites (Lewis, 1972), they still may be discerned through precise measurements.

Currently, the mean density of five of Saturn's satellites is poorly known and it is not known at all for the remaining ones (Morrison *et al.* , 1977). Undoubtedly, the mean density of a few satellites, especially Titan, will be determined with high precision when Pioneer 11 and the Voyager spacecraft pass through the Saturn system. But accurate values for the remaining satellites will await a Saturn orbiter.

Finally, let us consider the origin of the rings of Saturn. There are two principal competing theories. Either the rings were formed as part of the same process that resulted in the regular satellites, but tidal forces prevented the aggregation of a single large object at the rings' distance from Saturn; or alternatively, they represent fragments from a stray body that passed close to Saturn and was tidally disrupted (Pollack, 1975). The composition of the ring particles offers a way of testing the first possibility. As illustrated in Figure 6a, temperatures may have become cool enough close to the end of the satellite formation period for the Saturn system so that water ice was able to condense in the region of the rings. Any silicate grains, which condensed at earlier times in this region or were present from the start, would have been incorporated into the planet since Saturn's size exceeded the orbital distance of the rings for most of the satellite formation period (see the top of Figure 6a). Thus, if the particles constituting the rings were derived from material generated during Saturn's satellite formation epoch, they should be composed almost entirely of water ice.

There is, in fact, some evidence that the ring particles contain water ice. Near infrared spectra demonstrate that water ice is an important component of the particles' surface material (Pilcher *et al.* , 1970). Constraints on their bulk composition are provided by radar and radio observations. Analysis of these observations show that water ice could be the dominant component of the ring particles, whereas rocky material cannot (Pollack *et al.* , 1973; Pollack, 1975; Cuzzi and Pollack, 1978). However, with the present data, it is more difficult to exclude models in which metals, such as iron, represent the major bulk material (Cuzzi and Pollack, 1978).

We know that the rings have a high brightness temperature in the middle infrared (~10 to 20 μm) and a very low one in the microwave (>3 mm) (Pollack, 1975). Unfortunately, there is conflicting evidence as to where the transition from one brightness temperature regime to the next occurs. In part, this situation arises from the difficulty in spatially resolving the rings from the Earth at the wavelengths of interest. Therefore, it may be worthwhile to have a multi-channel infrared radiometer aboard a Saturn orbiter, which will observe the rings in the 20 μm to 1 mm wavelength region. Determination of the location and shape of the transition point would provide a good means of determining whether water ice is the major component of the ring particles.

SUMMARY

Table 1 provides a summary of the major recommendations given in this paper for an SOP[2] mission. The first column lists the cosmogonic problem, with the second and third columns defining the critical measurements that can be done to help resolve it. Clearly, much insight into the origin and evolution of the Saturn system can be realized from a combined orbiter-probe mission to this system.

Table 1. Cosmogonically Relevant Measurements for an SOP[2] Mission

Cosmogonic Issue	Key Measurements	Observational Technique
Origin of the Saturn system: core instability vs. gas instability.	Assess composition, amount, and distribution of excess heavy elements.	In situ compositional measurements of NH_3, CH_4, H_2O, He, and H_2 from an entry probe; track orbiter to determine the mass of the rings to establish values of J_2 and J_4 for Saturn.
Source of Saturn's current excess luminosity: Is He segregation an important source?	He/H_2 ratio in observable atmosphere.	In situ measurement made from an entry probe.
Capture mechanism for irregular satellites: Did capture occur due to gas drag within the primordial Saturnian nebula?	Morphological properties of the surfaces of the irregular satellites; existence of clusters.	Close-up photography of irregular satellites from an orbiter; photographic search for faint cluster members.
Influence of Saturn's early luminosity on the composition of its regular satellites.	Accurate values of the mean density of the regular satellites.	Good mass and size determinations from tracking an orbiter and from photography during close passages by the satellites.
Origin of the rings.	Composition of the ring particles; especially determining whether they are made primarily of H_2O ice.	Multi-channel infrared radiometer, operating in the 20 μm to 1 mm wavelength region.

REFERENCES

Bodenheimer, P. (1974). Calculations of the early evolution of Jupiter. *Icarus 23*, 319–325.

Bodenheimer, P. (1978). Calculations of the effects of angular momentum on the early evolution of Jupiter, *Icarus*. In press.

Cameron, A. G. W. (1977). Properties of giant gaseous protoplanets. Presented at the "Eighth Planetary Geology Principal Investigators' Symposium," St. Louis.

Cameron, A. G. W., and Pollack, J. B. (1976). On the origin of the solar system and of Jupiter and its satellites. In *Jupiter* (T. Gehrels, ed.), pp. 61–84, University of Arizona Press, Tucson.

Cuzzi, J. N. and Pollack, J. B. (1978). Saturn's rings: particle composition and size distribution as constrained by microwave observations. I: Radar observations: *Icarus 33*, 233–262.

De Campli, W., Bodenheimer, P., Pollack, J. B., and Grossman, A. (1978). Studies of the evolution of gaseous protoplanets. In preparation.

Graboske, H. C. Jr., Pollack, J. B., Grossman, A. S., and Olness, R. J. (1975). The structure and evolution of Jupiter: the fluid contraction phase. *Astrophys. J. 199*, 265–281.

Grossman, A. (1978). The effects of dense rock cores on the structure and evolution of Jupiter and Saturn. Presented at the meeting on "Protostars and Planets," Tucson.

Harris, A. W. (1978). Accumulation of the outer planets. Presented at the meeting on "Protostars and Planets," Tucson.

Hubbard, W. B., and Slattery, W. L. (1976). Interior structure of Jupiter: Theory of gravity sounding. In *Jupiter* (T. Gehrels, ed.), pp. 176–196, University of Arizona Press, Tucson.

Lewis, J. S. (1972). Low temperature condensation from the solar nebula. *Icarus 16*, 241–252.

Morrison, D., Cruikshank, D. P., and Burns, J. A. (1977). Introducing the satellites. In *Planetary Satellites* (J. A. Burns, ed.), pp. 3–17, University of Arizona Press, Tucson.

Perri, F., and Cameron, A. G. W. (1974). Hydrodynamic instability of the solar nebula in the presence of a planetary core: *Icarus 22*, 416–425.

Pilcher, C. B., Chapman, C. R., Lebofsky, L. A., and Kieffer, H. H. (1970). Saturn's rings: identification of water frost. *Science 167*, 1372–1373.

Podolak, M. (1977). The abundance of water and rock in Jupiter as derived from interior models. *Icarus 30*, 155–162.

Podolak, M., and Cameron, A. G. W. (1974). Models of the giant planets. *Icarus 22*, 123–148.

Pollack, J. B. (1975). The rings of Saturn. *Space Sci. Rev. 18*, 3–94.

Pollack, J. B., Summers, A., and Baldwin, B. (1973). Estimates of the size of the particles in the rings of Saturn and their cosmogonic implications. *Icarus 20*, 263–278.

Pollack, J. B., and Reynolds, R. T. (1974). Implications of Jupiter's early contraction history for the composition of the Galilean satellites. *Icarus 21*, 248–253.

Pollack, J. B., Grossman, A. S., Moore, R., and Graboske, H. C. Jr. (1976). The formation of Saturn's satellites and rings, as influenced by Saturn's contraction history. *Icarus 29*, 35–48.

Pollack, J. B., Grossman, A. S., Moore, R., and Graboske, H. C. Jr. (1977). A calculation of Saturn's gravitational contraction history, *Icarus 30*, 111–128.

Pollack, J. B., Burns, J. A., and Tauber, M. E. (1978). Gas drag in primordial circum-planetary envelopes: a mechanism for satellite capture. *Icarus*. In press.

Slattery, W. L. (1977). The structure of the planets Jupiter and Saturn. *Icarus 32*, 58–72.

Stevenson, D. G. (1975). Thermodynamics and phase separation of dense fully-ionized hydrogen-helium fluid mixtures. *Phys. Rev. B 12*, 3999–4007.

Ward, D. B. (1977). Far-infrared spectral observations of Saturn and its rings. *Icarus 32*, 437–442.

DISCUSSION

J. CALDWELL: If you invoke a gas drag mechanism for capturing Phoebe, does that not give you trouble with the very existence of the inner satellites? If the gas drag is enough to capture, how do the others survive?

J. POLLACK: Well, it's a question of the phase at which different things happen. The capture that we're speaking about is occurring at a very early time when Saturn may have been maybe a hundred times bigger than its present size, while in the case of the regular satellites themselves, one is speaking about much later when Saturn was perhaps five times its present size. You're quite right in the sense that one has to be very careful at the stage that the regular satellites are forming. There is a delicate balance between having enough material in the disk for condensation and the aggregation of the satellites, and yet not having so much gas around that the protosatellites spiral into Saturn.

J. CALDWELL: Jupiter doesn't have a major ring system while Uranus has a small one. Is there anything potentially to learn about the Saturn rings from this?

J. POLLACK: Remember that in the Saturn system just before the end of the satellite formation period, temperatures in the ring region could have gotten cold enough for water ice to condense. In the case of Jupiter, its luminosity at the same time was a factor of 10 higher, so that it never got cold enough within its Roche limit for water ice to condense.

In the case of an alternative material like silicates, there may well have been silicates around initially to condense, but at the time that silicates would have been available, Saturn would have been so large that it exceeded the outer boundary of the rings, so that any silicates there would have been incorporated into Saturn itself.

In the case of Uranus, I do not care to speculate very much at this time on why its rings are so different from Saturn's. The only thing I can say is that temperatures could have gotten cold enough to allow material to condense inside the Roche limit.

B. SMITH: But not ice, because the Uranus rings are too dark.

G. ORTON: If helium is capable of segregating from hydrogen at the present time in the interior of Saturn, what does that imply in terms of the heavy elements, methane, water, and silicates.

J. POLLACK: The physics is different, so I'm not sure whether one would expect a phase separation or not. The ultimate answer to the question may require measurements of gravitational moments.

G. ORTON: What precision is required in the measurements of excess thermal flux from Saturn?

J. POLLACK: Well, I'd really like to know whether it's significantly higher than my prediction or not. Thus a precision of ±30% would be quite signiticant, and I think ultimately one might like to go to ±10%.

G. ORTON: For the observations for the presence of water ice in the rings you recommended very long wavelength infrared observations.

J. POLLACK: Longer wavelength observation may distinguish between composition of the surface and the bulk composition. I don't think that there is any question that water ice is the major surface constituent of the particles. In the case of water ice, it's very absorbent up to about 150 μm and then its absorption coefficient starts decreasing very rapidly. And we know from current observation at a few millimeters that the opacity is quite low. The transition wavelength region will surely contain the information we need on the bulk composition.

R. MURPHY: Couldn't radar techniques from orbit or even radio occultation measurements be diagnostic of bulk composition?

J. POLLACK: An occultation basically measures the total cross section, so it is sensitive to the sum of scattering plus absorption. It doesn't separate the two components. Radar is a very nice complementary measurement to the passive brightness temperatures. But we still need to know the brightness temperatures in the long-wave IR region.

SATURN'S ATMOSPHERE: RESULTS OF RECENT INVESTIGATIONS

Laurence Trafton

University of Texas
Austin, Texas 78712

ABSTRACT

We review recent developments in the study of Saturn's atmosphere. Saturn apparently has a high clear layer of H_2 under which lies a comparable layer rich in dusty material. Beneath this is a thicker layer consisting mostly of H_2 mixed with haze particles. An NH_3 cloud deck probably lies below this layer. Evidence for seasonal variations is presented in the form of changes in the NH_3, CH_4 and H_2 absorptions. Finally, the latest mixing ratios for the gaseous constituents are summarized.

EXOSPHERE AND H TORUS

The extent of Saturn's atmosphere is uncertain. L_α emission has been observed from the OAO-C (Copernicus) satellite and a rocket to extend possibly out to Titan's radius. Barker (1977) reports L_α emission of 150 R with FWHM of 75 mÅ for a spectroscopic slit 0.3" × 39" projected on the torus region 5" to 10" inside Titan's orbital position. For Saturn's disk, he reports 250 R emission with FWHM of 100 mÅ. These observations were made during 12-15 April 1976 with OAO-C and are at the limit of photometric accuracy. The strengths are subject to revision depending on the concurrent geocoronal calibration.

Apparently, the first statistically significant detection of L_α emission from Saturn was obtained in March 1975 by Weiser, Vitz and Moos (1977) using a sounding rocket with circular spectroscopic apertures 26" and 53" in diameter. Saturn's disk had an angular extent of 17" by 19" and the outer edge of Ring A had an extent of 43" by 19". Assuming uniform emission intensity over the respective apertures, they

derived a L_α brightness of 700 R ± 50 percent for Saturn's disk and 200 R ± 50 percent for the region outside and immediately adjacent to the disk, out to the radius of the large aperture. Any intensity distribution having zero emission from the region outside the disk is not compatible with the observations. The L_α brightness of Saturn's disk scales well with the 2 kR brightness for Jupiter, suggesting similar excitation mechanisms in the upper atmospheres of both planets (resonant scattering). Weiser *et al.* estimate only 10 R emission for H in the vicinity of the Rings from meteoroid bombardment of the Rings, solar and interstellar wind bombardment, and ice sublimation. Saturn's inclination is high enough so that any contribution of a H torus centered along Titan's orbit to the 200 R observed in the vicinity of the Rings would require ejection velocities of H from Titan nearly comparable to Titan's orbital velocity (5.6 km/s). In this case, many atoms would be escaping the Saturn system so the torus geometry might not be a valid description of the H distribution.

In April of 1977, Barker (1978) repeated his observations and found essentially the same disk intensity but detected no emission (less than 100 R) over the Rings. Therefore, the question of emission next to Saturn's disk, in the immediate vicinity of the Rings, remains open.

IONOSPHERE

The structure of Saturn's ionosphere was recently considered by Capone *et al.* (1977) who included, for the first time, the heating of cosmic-ray ionization as well as that of the extreme ultraviolet radiation of the Sun. These effects are comparable in the outer atmospheres of the major planets beyond Jupiter if the surface magnetic field is 2 Gauss or less and where the insolation is relatively diluted. They neglected the photochemistry of NH_3 and the possible roles of neutral hydrocarbons higher than CH_4. They also neglected negative-ion chemistry and plasma diffusion. They performed their analysis for an isothermal stratosphere and also for Wallace's (1975) model atmosphere to bracket the temperature regime. The electron densities (the quantity most likely to be observed) are plotted in Figure 1 for both cases; the calculated positive ion densities are shown only for the isothermal case. Characteristic of these calculations are two peaks in the electron density, whose altitude separation is diagnostic of the temperature structure in the inversion regime. An occultation experiment with a space probe promises to be a useful tool for investigating the thermal inversion of Saturn's atmosphere.

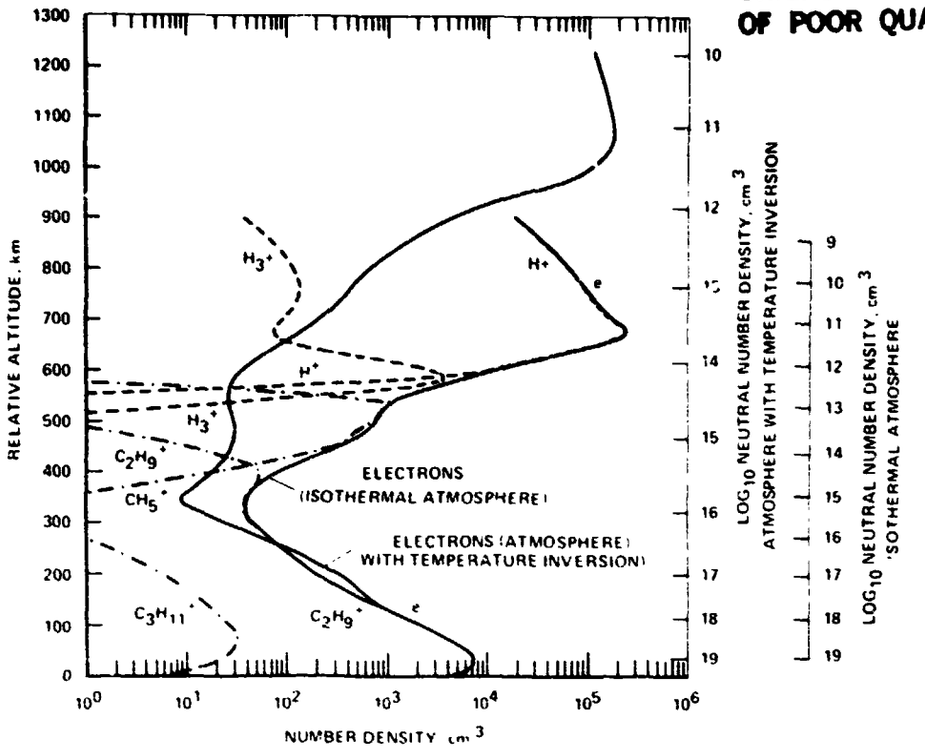

Figure 1. Electron and ion number densities for Saturn. For purposes of clarity, the ion number densities are shown for the isothermal atmosphere only (Capone et al., 1977).

TEMPERATURE INVERSION

The question of Saturn's atmospheric thermal structure in the lower inversion region and troposphere will be addressed at this workshop by Tokunaga, in addition to the question of the magnitude of Saturn's thermal flux. I will consider the aerosol structure and composition of Saturn's atmosphere and also the spatial and temporal variations. I will, therefore, confine this section to a few remarks.

The presence of Saturn's inversion layer was first indicated by the 7.5 - 13.4 μm observations of Gillett and Forrest (1974) at resolution $\lambda/\Delta\lambda$ = 67 (Figure 2). Their spectrum revealed an emission peak at 7.8 μm in the ν_4 CH_4 band similar to that observed for Jupiter. The lack of a brightness temperature minimum around 8.2 μm indicates some unspecified extinction in Saturn's atmosphere which is not strong in

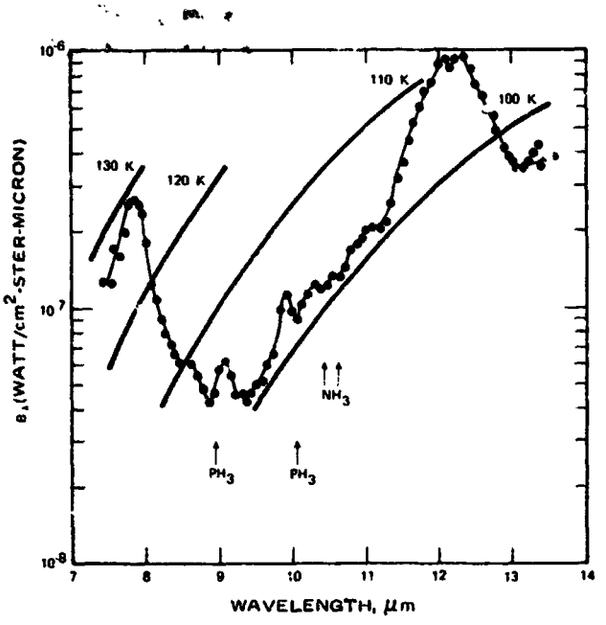

Figure 2. Surface brightness of Saturn versus wavelength. Also shown are the locations of the Q branches of the ν_2 and ν_4 bands of PH_3. (Gillet and Forrest, 1974)

Jupiter's atmosphere. They also detected the bright emission from the ν_9 band of C_2H_6 centered around 12.2 μm. Soon thereafter, Gillett and Orton (1975) obtained several scans across the disk of Saturn at 11.7 μm ($\Delta\lambda$ = 0.18 μm) with a spatial resolution of 2".8 arc sec. These showed limb brightening, confirming the presence of a thermal inversion in Saturn's upper atmosphere. Observations using a broad band filter at 11.7 μm ($\Delta\lambda$ = 1.8 μm) showed less emission at the limb. These observations strongly support Danielson and Caldwell's suggestion that the emission arises from C_2H_6. They also found enhanced emission over the south pole (Figure 3), which they attribute to the increased insolation resulting from the tilt of this pole towards the Sun.

The thermal inversion affects the monochromatic flux primarily in the 7-20 μm spectral region. The continuum is cooler than the region of the inversion emitting hot radiation partly because the deep, hot region of the troposphere is hidden by the NH_3 haze in the spectral region where it is not effectively hidden by the pressure-induced H_2 opacity. The thermal inversion also tends to fill in the absorption features of the S(0) and S(1) pressure induced transitions of H_2, making the spectrum more like a black body. This filling in cannot be too strong, as in the case of Caldwell's (1977) model, because this would cause H_2 to radiate efficiently in the inversion zone. This would tend to destroy the inversion because a temperature inversion can only exist when there is no efficient radiator at thermal wavelengths in the inversion region to release the energy absorbed there from the solar heating of gas molecules and dust particles.

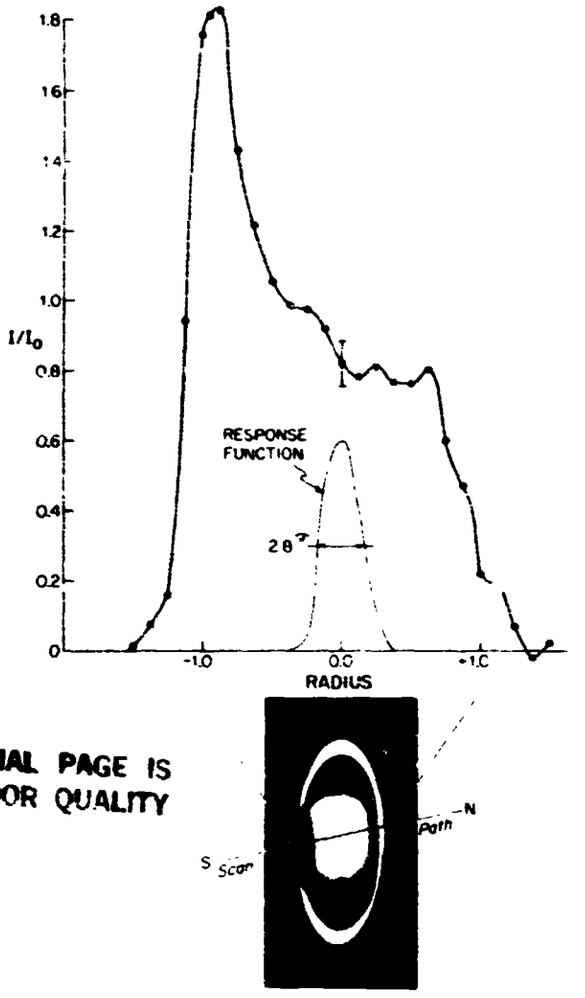

Figure 3. Single polar scan at 11.7 μm through the pole. (Gillet and Orton, 1972).

THE TROPOSPHERE AND NH_3 MIXING RATIO

Below the inversion region is the troposphere and associated haze layers and cloud decks. Below its sublimation level, NH_3 should be uniformly mixed with the other atmospheric bulk constituents. The microwave spectral observations permit the NH_3 distribution to be studied to depths much greater than for any other spectral region containing NH_3 bands. Several authors have *assumed* an isothermal stratosphere and convective troposphere in order to calculate synthetic spectra of the 1.25 cm NH_3 "inversion" band which they then compared with observations (Gulkis *et al.* 1969;

Wrixon and Welsh, 1970; Gulkis and Poynter, 1972). Models with solar NH_3 abundance below the saturation level and saturation values of the NH_3 partial pressure above the saturation level fitted the observations well. Ohring and Lacser (1976) dispense with the need for making these assumptions by using temperature profiles derived directly from inverting the emission spectrum of the 7.7 μm CH_4 band (Ohring, 1973), and using them to derive the NH_3 distribution directly from inverting the observed microwave emission spectrum. This spectrum they approximated by a smooth curve between 1 - 20 cm, using the points with higher signal to noise ratios. Their results, shown in Figure 4, depend on the CH_4/H_2 mixing ratio but are rather insensitive to the He/H_2 ratio for values ≤ 0.2. For a nominal $CH_4/H_2 = 5 \times 10^{-4}$, they obtain a relatively constant value of $NH_3/H_2 = 1 \times 10^{-4}$ below the saturation level and, as for Jupiter (Ohring, 1973), they find NH_3 to be saturated (not supersaturated) above the saturation level. This level lies at 154 K and 4 atm for the nominal model. Its variation with CH_4 mixing ratio may be ascertained by reference to Figure 4.

Saturn's NH_3 abundance determined from the 6450 Å band has been relatively constant in the three year period ending 1975 (Woodman, Trafton and Owen, 1977). The abundance is 2 ± 0.5 m-am NH_3 "above the clouds" (equivalent reflecting layer model). Ohring and Lacser (1976) indicate that the level of line formation of NH_3 for an abundance of 2 m-am is above the highest level for which they have inferred NH_3 concentrations. The microwave results have the advantage that they pertain to much deeper layers than do the visual spectra.

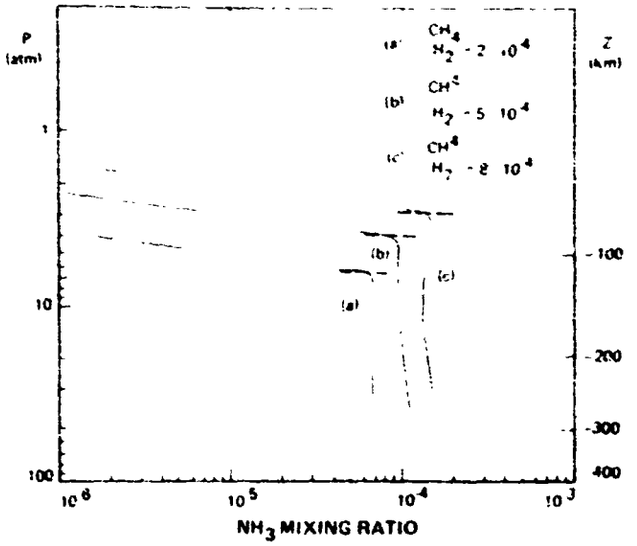

Figure 4. Ammonia mixing ratio profiles for nominal temperature profile and for extreme temperature profiles. The level at which saturation begins is indicated by a dashed line (Ohring and Lacser, 1976).

HAZE

There appears to be an extended haze in Saturn's atmosphere near the 100–105 K levels. Gillett and Forrest's (1974) spectra show a brightness temperature in the 9–11 μm region of only 100–105 K, compared to ~130 K for Jupiter. They point out that this is too cold for the dominant gaseous opacity to be NH_3; the partial pressure of NH_3 in the layers responsible for Saturn's 9–11 μm emission is 10^{-2} to 10^{-3} times that in the layers responsible for Jupiter's 9–11 μm emission (which arises in the ν_2 band of NH_3). My radiative convective models suggest that the top of Saturn's convective zone is at the 108–112 K level, well above the NH_3 saturation level, in contrast to Jupiter. If Saturn's haze consists of NH_3 particles suspended by convective currents, its extent in depth is much larger than for Jupiter. Caldwell (1977a) finds that indeed solid NH_3 crystals provide a good fit to Saturn's spectrum in the region of the 9.5 μm absorption feature visible in Gillett and Forrest's (1974) data. He also finds that the haze must be inhomogeneously distributed in depth, being concentrated at lower levels rather than mixed throughout the inversion. This haze layer is quite transparent at microwave wavelengths and is sufficiently thin at visual wavelengths that weak NH_3 lines are detectable in the 6450 Å band. Visible light penetrates below the 105 K level, where it undergoes multiple scattering.

The haze causes the subdued behavior of the equivalent widths of H_2, CH_4 and NH_3 from the center of the disk to the limb. The H_2 quadrupole lines are roughly constant over the disk; they are slightly stronger at the south pole and slightly weaker near the equatorial limbs (Trafton, 1972). The 6450 Å NH_3 band is strongest at the center of the disk, slightly weaker at the south pole, and quite weak near the equatorial limb (Woodman, Trafton and Owen, 1977) as indicated in Figure 5. Methane absorption is weaker in the equatorial belt and either about the same over the south pole and the center of the disk or slightly weaker over the pole (Teifel, Usoltseva and Kharitonova, 1971; 1973).

Saturn's limb darkening and polarization are not characteristic of pure Rayleigh scattering but of a haze with particles having an average radius of ~1 μm (Teifel, 1975).

The shapes of the R-branch manifolds of the 3 ν_3 CH_4 band indicate the presence of some aerosol scattering (Trafton, 1973; Trafton and Macy, 1975; Macy, 1976) but they are much more compatible with a reflecting layer model (RLM) than a homogeneous scattering model. These observations were obtained along Saturn's central

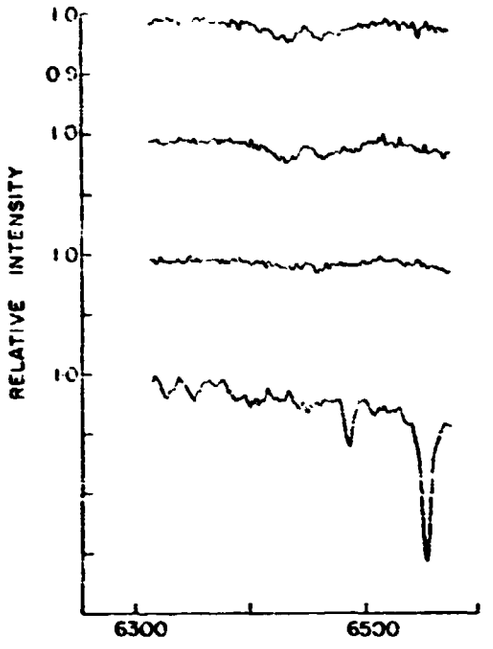

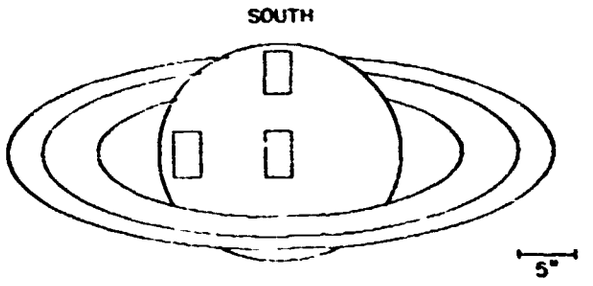

Figure 5. Spatial variation of 6450 Å NH_3 band over the disk of Saturn, with ring spectrum for comparison. Size and placement of spectrograph slit are also illustrated. The top ratio spectrum corresponds to the south pole and the bottom one to the equatorial limb. (Woodman et al., 1977)

meridian, excluding the equatorial belt and Rings. For this area, the RLM approximation may not be bad, at least in this wavelength regime. Figure 6a shows spatial scans I obtained along Saturn's central meridian at three wavelengths located in various CH_4 bands. They illustrate the CH_4 absorption increasing strongly towards the pole. Figure 6b shows the CH_4 absorption at these three wavelengths increasing toward the south pole.

Another manifestation of Saturn's haze is the lower abundance determinations in the infrared than in the visual spectrum (see the section below on Composition). Also, abundances determined from lines of very different strength at the same wavelength lead to conflicting values when analyzed in the RLM approximation. See de Bergh and Maillard (1977) for a discussion of this. Finally, we have already noted that the brightness temperatures at 8.2 μm and 9.5 μm indicate a haze.

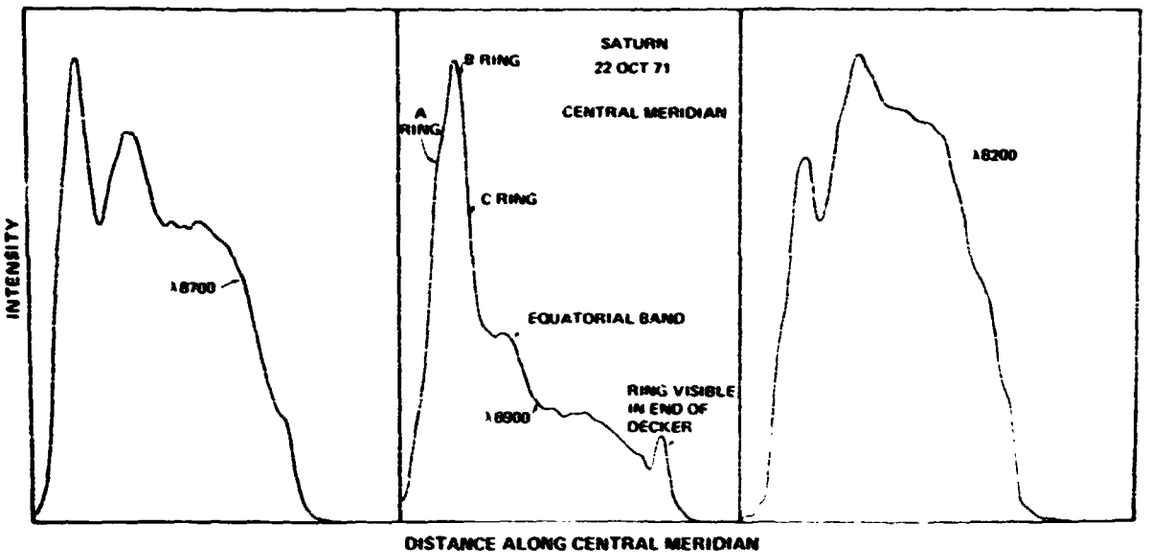

Figure 6a. Spatial scans along Saturn's central meridian at three wavelengths in various CH_4 absorptions.

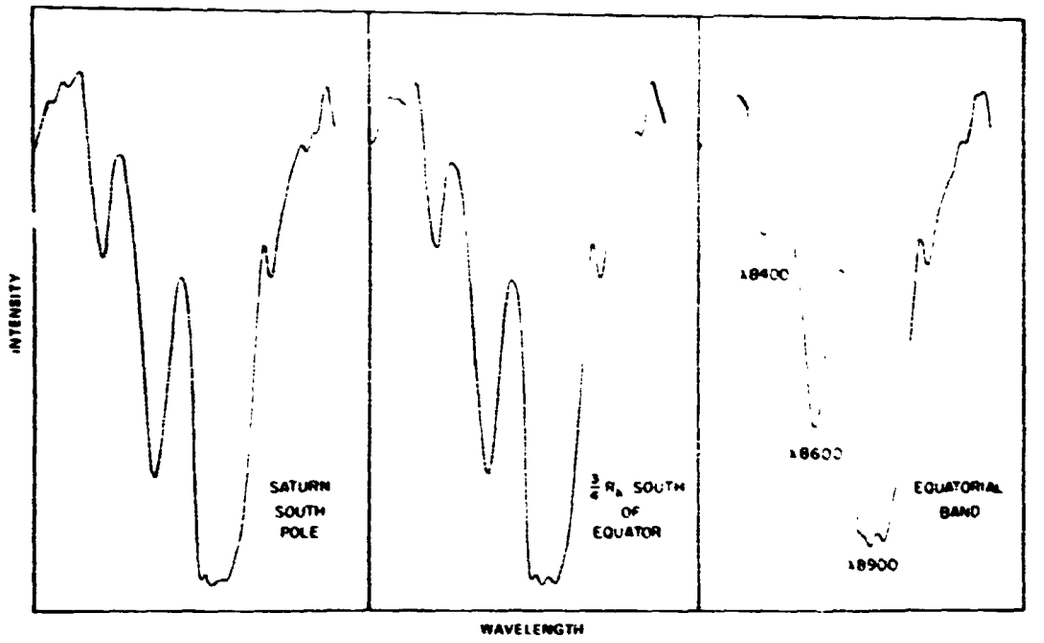

Figure 6b. Spectral scans at three points along Saturn's central meridian covering the wavelengths of Fig. 6a.

DUST

The presence of dust in Saturn's atmosphere is deduced from the sharp drop in albedo between 5000 Å and 3000 Å. It probably arises from photochemistry of CH_4 photodissociation products (Caldwell, 1977a). Podolak and Danielson (1977) have modeled this albedo in terms of a homogeneous dust layer mixed with 28 km-A (kilometer-Amagat) H_2 above a cloud deck and under a clear layer H_2 7 km-A thick. The parameters of the dust follow: The real part of the index of refraction = 2.0; the imaginary part $\sim\lambda^{-2.5}$; and a flat distribution in particle radii from 0 to 0.1 μm. The dust parameters are the same as those successfully used to model the blue-UV albedos of Jupiter and Titan. At 5000 Å, the optical depth for extinction of the dust is 0.7. The fit is shown in Figure 7. It should be noted that these models of the dust distribution are not unique. The effect of an inhomogeneous depth distribution of the dust would be to change the value of the exponent α in the imaginary part of the refractive index (Barker and Trafton, 1973).

The presence of a high, clear region of the atmosphere, free of dust and aerosol particles, is required by the increase in albedo shortwards of 3000 Å (cf. Figure 7). This occurs as a result of a sharply increasing cross section of Raleigh scattering. A layer of 7-28 km-A is needed, depending on the model. Podolak and Danielson (1977) place 7 km-A H_2 in the clear region; Teifel (1975) places "less than 13" km-A H_2 there; and Macy (1977) places 27 km-A H_2 there.

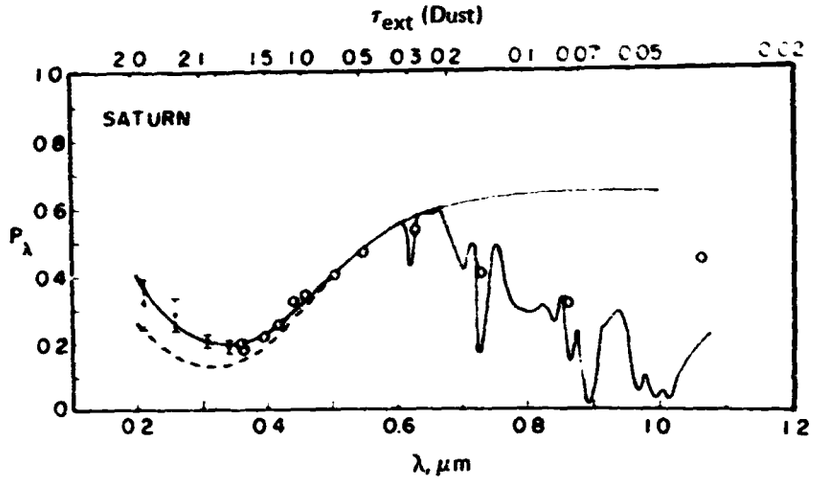

Figure 7. Variation of geometric albedo with wavelength for Saturn. The solid curve is the theoretical fit to the data with a 7 km-am-region of H_2 above the dust. The dashed curve is the fit without such a clear layer. The methane absorptions are also shown. (Podolak and Danielson, 1977).

More accurate modeling of this region is needed. The presence of limb brightening in the UV (Marin, 1968) also requires a relatively clear upper atmosphere. New measurements, such as those of Franz and Price (1977) may help the modeling. They find pronounced limb brightening in U, moderate limb brightening in B and limb darkening in V.

AEROSOL STRUCTURE

The best model to date of Saturn's aerosol structure is Macy's (1977) but this model does not agree with all observations so there is room for improvement. For the thermal structure, Macy uses the temperature profile of Caldwell's thermal model (1977a) but adjusts the effective temperature to 97 K instead of 93.5 K and uses a surface gravity of 1050 cm s^{-2}. Caldwell's inversion region is too low for it causes H_2 to appear in emission in his model but this does not significantly affect the aerosol structure. The various models for the inversion converge in the troposphere although they disagree in the inversion regime. The convergence is a result of the H_2-He opacities being relatively well known because these opacities control the radiative transfer in the troposphere.

Macy's model is constructed to agree with photometric and spectroscopic data in the UV, visible and near IR while Caldwell's (1977a) thermal model is concerned with the spectral characteristics for wavelengths longer than 8 μm, except for solar heating. Scattering is not included in the radiative transfer of Caldwell's model but is included in Macy's model. Other differences are that Macy's model includes a clear region above the absorbing dust and has the cloud deck at the NH_3 sublimation level rather than at the radiative-convective boundary. The former is motivated by the UV limb brightening and rise in albedo. The latter is motivated by the visibility of weak gaseous NH_3 absorptions, relatively large H_2 equivalent widths and high rotational temperatures for CH_4. Macy's model also distinguishes the equatorial from the temperate zones, as indicated in Table 1.

Figure 8 shows Macy's schematic for Saturn's atmosphere. Above the opaque cloud deck is 52 km-A H_2 mixed with haze particles. Multiple scattering in this region enhances the equivalent widths of the H_2 lines but obscures the gaseous NH_3 absorption. Above the haze is a layer of absorbing particles (or dust) 15-23 km-A H_2 thick and above this there is the clear region 19-27 km-A H_2 deep. The dust layer accounts for the drop in albedo in the blue-UV spectral region and helps to heat the upper atmosphere. The

Table 1. Particle Distribution

Layer	H_2 Abundance (km-A)		Pressure at Layer Bottom, Equator (atm)	Pressure at Layer Bottom, Temperate (atm)
	Equator	Temperate		
Clear gas	19	27	0.2	0.3
Absorbing Particle	23	15	0.4	0.4
Haze Particle	52	52	1.1	1.1

haze layer also helps to explain the shapes of the $3\nu_3$ CH_4 manifolds and the low brightness temperature at 9.5 μm (but the cross section for the particles may be quite different at visual wavelengths than at 9.5 μm). Macy's model incorporates the Raleigh phase function for scattering by the gases and an isotropic phase function for scattering by the particles. The particle albedo is scaled according to the van de Hulst similarity relations to account for their anisotrapy. Because greater polarization is observed in the temperate region than in the equatorial belt, Macy argues that absorbing particles should lie deeper in the temperate region. His model is also constrained by molecular line observations: in particular, the (3-0) and (4-0) H_2 quadrupole lines, lines from the weak 6450 Å NH_3 band, and manifolds from the $3\nu_3$ CH_4 band R branch.

Macy's model fits the spectral reflectivity well (Figure 9). On the other hand, the fit of the reflectivity from the center of the disk to the equatorial limb is rather poor (see Figure 10). This is due in part to approximating anisotropic scattering by isotropic. There is also a problem with the high rotational temperature of the $3\nu_3$ CH_4 band. The high-J manifolds are too strong relative to those in his model. He discussed this problem in a previous paper (Macy, 1976) which analyzed the $3\nu_3$ CH_4 band and H_2 absorptions simultaneously using an inhomogeneous model atmosphere. He found that if the

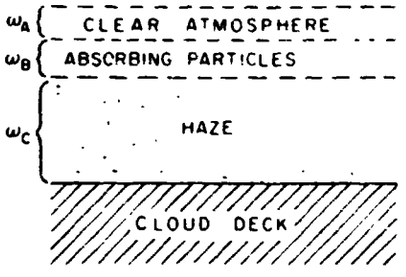

Figure 8. Diagram of the model. Values for the H_2 abundance in the clear layer, ω_a, the absorbing particle layer, ω_b, and the haze layer, ω_c, are given in Table 1. The absorbing particle-haze layer boundary corresponds to the radiative-convective boundary. The bottom of the cloud deck is at the ammonia sublimation level.

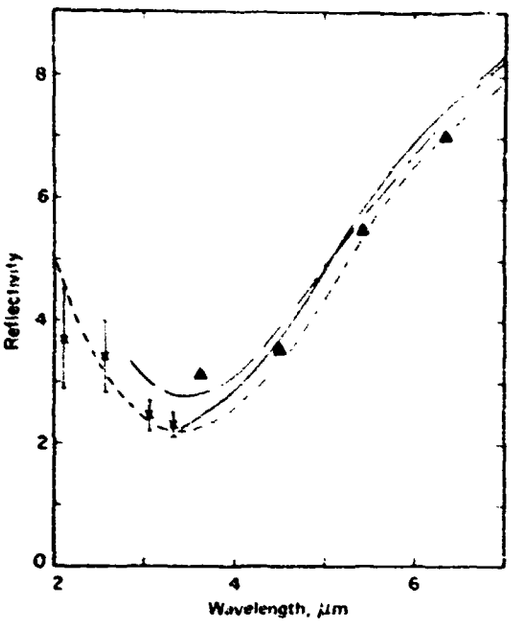

Figure 9. Observed reflectivity as a function of wavelength in the equatorial region (solid line), the temperate region (at latitude 40°S in the south temperate zone (Reese, 1971)) (triangles), and OAO II geometric albedo (Caldwell, 1975), which have been increased by 20% to give an estimated equatorial reflectivity (error bars). Calculated reflectivities are for the equatorial region (R_{planet}) = 0.03 (long-dashed line) and the temperate region (R_{planet}) = 0.4 (short-dashed line).

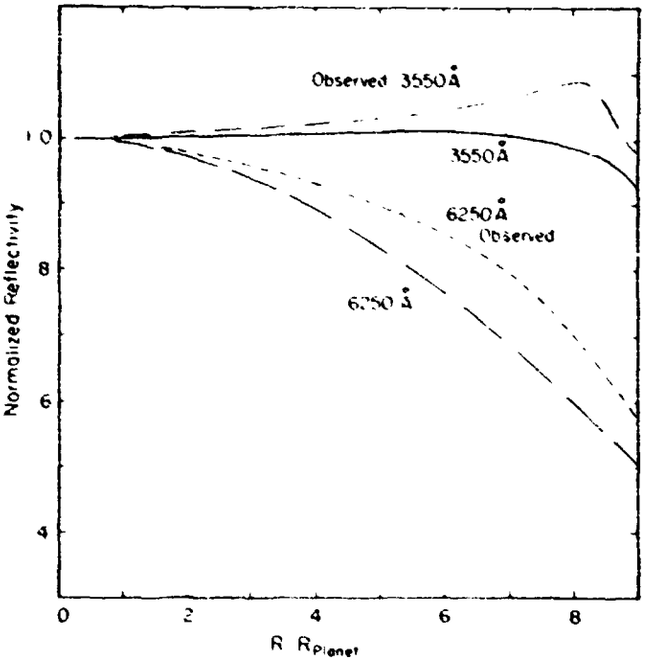

Figure 10. Observed reflectivity along the equator normalized to unity at the center of the disk (Marvin, 1968), at 6250 Å (short-dashed line) and 3550 Å (dash-dot line). Calculated reflectivity at 6250 Å (long-dashed line) and 3550 Å (solid-line). The theoretical curves have not been convolved with a point spread function. A full treatment of the limb darkening must take into account the anisotropy of the scattering phase function and smearing due to seeing.

optical thickness of the haze layer was adjusted to fit the observed H_2 absorption, the effective depth of absorption for the $3\nu_3$ CH_4 band was so shallow that the rotational temperature of the band came out too low.

It seems to me that this problem could be resolved if the mean cross section of the haze particles in his model were allowed to decrease with increasing wavelength rather than be held constant. This variation is required to explain the (3-0) and (4-0) H_2 absorptions in Uranus' atmosphere (Trafton, 1976). Then deeper, hotter layers would contribute to the $3\nu_3$ CH_4 absorption at 1.1 μm while shallower layers limit the

H_2 absorption at 0.64 μm and 0.82 μm. This modification should also result in a revision of the derived CH_4/H_2 ratio.

Finally, there appears to be some uncertainty about the depth of the NH_3 sublimation level. Macy's model gives 1.1 atm but that derived from inversion of the NH_3 microwave spectrum (Ohring and Lacser, 1976) is 4 atm for a $CH_4/H_2 = 5 \times 10^{-4}$. Macy's model has four times the methane mixing ratio. The microwave results are brought into closer agreement with Macy's sublimation level if Macy's methane mixing ratio is assumed. This would require a larger NH_3 mixing ratio, however, so the depth, at present, must be considered uncertain.

SEASONAL VARIATIONS

Spectra of H_2, NH_3 and CH_4 obtained over a long time base indicate that significant seasonal variations occur. The visibility of the 6450 Å NH_3 band has ranged from zero to almost the strength of Jupiter's band. Dunham (1933) was able to see as many lines of this band in Saturn's spectrum as he saw in Jupiter's spectrum. This is not surprising in view of the exponential dependence of the equilibrium NH_3 vapor pressure on the temperature and the deep NH_3 haze layer. Small changes in temperature could cause much bigger changes in the NH_3 visibility.

Observations of the H_2 quadrupole lines over the past decade are shown in Figure 11 (Trafton, 1976) and indicate a seasonal variation correlated with the shading of the planet's disk by the Rings. Figure 12 shows more recent data for strong CH_4 bands. If the trend given by the earlier H_2 points is correct, Saturn's atmosphere mimics the deep, clear atmosphere of Uranus at a time when the Rings are edge on (minimum shading) which also happens to be when the planet is farthest from the Sun. The Ring shading and orbital eccentricity each produce 15% variations in the insolation of the disk. The H_2 equivalent widths appear to be minimum at the time of maximum shading, suggesting a lot of haze opacity in the deeper atmosphere. The CH_4 bands, which probe shallower regions of Saturn's atmosphere, show a recent increase in strength, suggesting that haze may be settling out of Saturn's upper atmosphere after the time of maximum Ring shading. Further monitoring of Saturn's H_2, NH_3 and CH_4 absorption is needed to confirm the seasonal behavior and to understand its causes. The scatter of the points in Figure 11 indicates that the diurnal and short term variations are typically less than 10%.

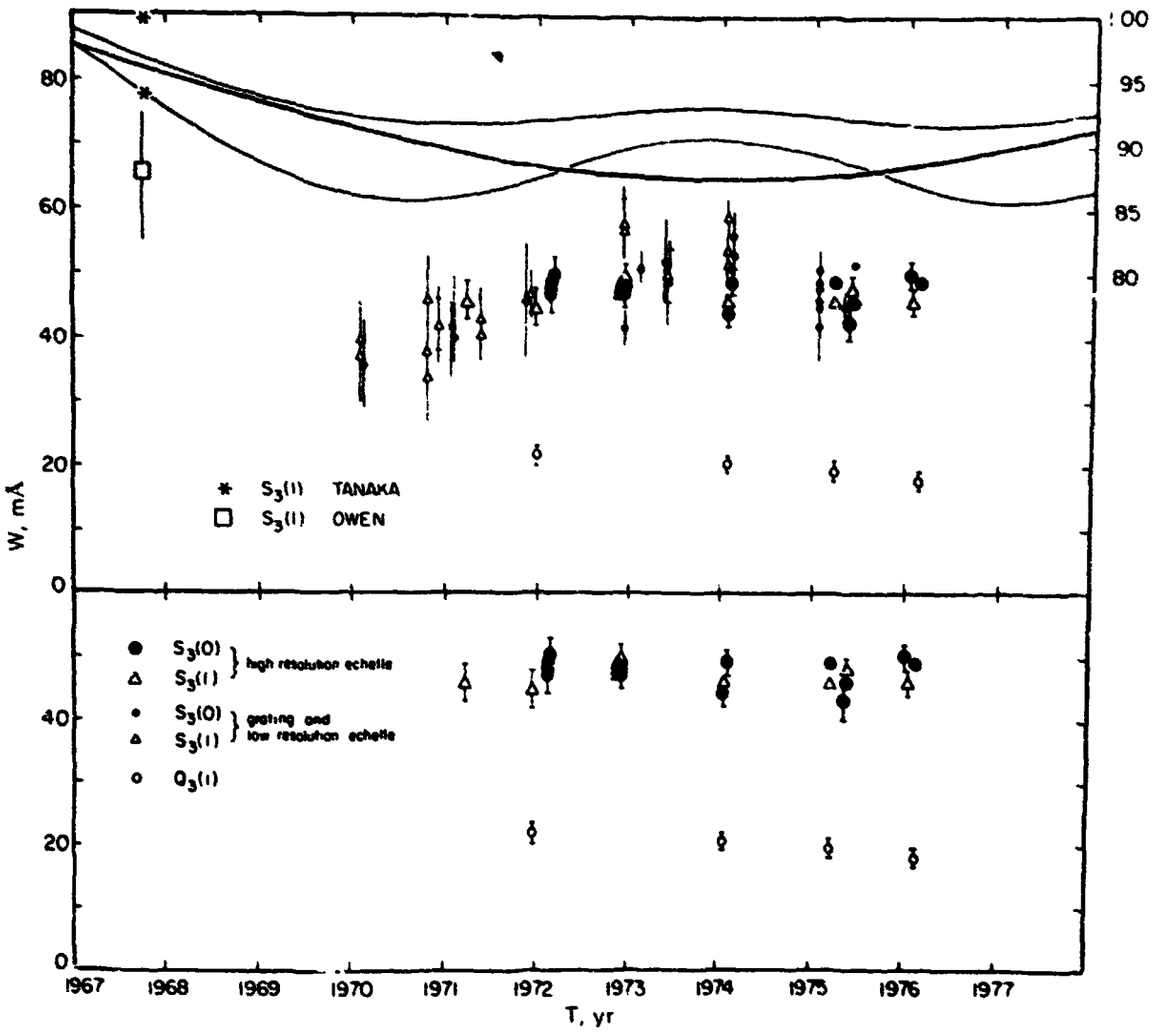

Figure 11 Time variation of H_2 equivalent widths. The long term behavior is presumably seasonal. An upper limit to the diurnal behavior is given by the scatter. (a) Values from all spectra. The wavelength scale on the right is for the curves at the top of the figure. The heavy curve describes the square of Saturn's distance from the Sun normalized to unity in January 1966. It was maximum in May of 1959. It is inversely proportional to the insolation. The light curves bracket the fractional shading of Saturn's disk by the rings. The absorption was minimum at the time the shading of the rings was maximum. When shading was minimal, the H_2 absorption may have been greatest when Saturn was farthest from the Sun. Near this time, the depth of the NH_3 cloud should have been greatest. (b) Values from the high-resolution spectra alone. These have a lower scatter and are less susceptible to errors resulting from blended telluric H_2O lines. Encrenaz and Owen (1973) measured values in February of 1973 for the (3−0) lines. Their value for $S_3(0)$ agrees with our data well but their value (41 + 7 mÅ) for $S_3(1)$ is 15% lower.

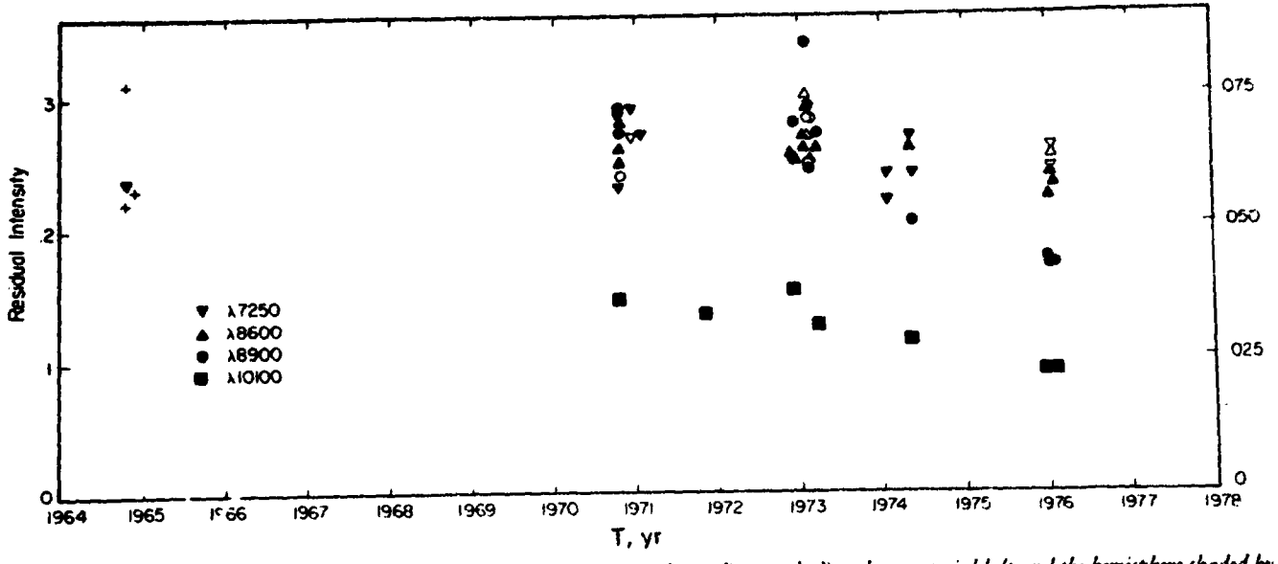

Figure 12. Long-term variation of Saturn's CH_4 absorption on the central meridian, excluding the equatorial belt and the hemisphere shaded by the rings. The precise wavelengths are shown in Figure 5. The scale on the right is for the λ 8900 band's residual intensity. The scale on the left is for the other three bands. The uncertainty of the values from the λ 10 100 band is equal to the height of the symbol. These points have the highest accuracy owing to no blending with telluric H_2O and a fairly wide band minimum. The uncertainty of the other values is best estimated from their scatter. The open symbols indicate greater measurement uncertainty. The + symbol plots points taken with the slit set parallel to Saturn's equator in the northern hemisphere during 1964. All bands indicate an increase in absorption.

COMPOSITION

The questions of composition are what gases compose Saturn's atmosphere and what are their relative abundances? In addition to H_2, NH_3 and CH_4; detected gases include H (Weiser *et al.*, 1977), $^{13}CH_4$ (Combes *et al.*, 1975), HD (Smith and Macy, 1977; Trauger, Roesler and Mickelson, 1977), C_2H_6 (Tokunaga, Knacke and Owen, 1975), PH_3 and CH_3D (Fink and Larson, 1977). Helium has not yet been detected; its presence is inferred from cosmogony and possibly from the shape of the thermal spectrum. Solid NH_3 appears to be responsible for the absorption at 9.5 μm and possibly at 8.98 μm (Caldwell, 1977a). There appears to be a weak feature at 10.1 μm in the spectra of Gillett and Forrest (1974) which might arise from solid NH_2D (Caldwell, 1977) but higher resolution spectra are needed to confirm this possibility.

The controversy on whether the features at 10-11 μm are due to PH_3 (Bregman *et al.*, 1975) or to C_2H_4 (Encrenaz *et al.*, 1975) appears to be resolved in favor of PH_3 since Fink and Larson (1977) have detected PH_3 in Saturn's 5 μm spectrum. They find the absorption to be considerably stronger than on Jupiter. About 50 cm-A of laboratory PH_3 is needed to match the broad PH_3 feature at 4.73 μm. These authors also find the Q and P branches of CH_3D to be quite prominent in Saturn's spectrum and the line strengths are comparable to those of CH_3D on Jupiter. About 5 cm-A of laboratory CH_3D is needed to match their absorption. Smith and Macy (1977) derive a value for $D/H = (6.6 \pm 3.1) \times 10^{-5}$ from the $R_5(0)$ line of HD and Trauger *et al.*, (1977) report a similar value $(5.1 \pm 0.7) \times 10^{-5}$ from the $P_4(1)$ line of HD. Modeling the emission from the ν_9 band of C_2H_6 at 12.2 μm, Caldwell (1977a) estimates a mixing ratio $C_2H_6/H_2 = 1.8 \times 10^{-6}$.

A number of abundances for H_2, NH_3 and CH_4 have been given in the literature in the reflecting layer approximation. For the (3-0) and (4-0) H_2 quadrupole lines, Encrenaz and Owen (1973) quote 77 ± 20 km-A H_2 using the curve of growth of Fink and Belton (1969) which is now outmoded because the pressure broadening coefficients have since been improved (Macy, 1973). For the $Q_2(1)$ line, de Bergh *et al.* (1977) obtain a H_2 abundance of 25^{+9}_{-6} km-A also by using Fink and Belton's curve of growth. For the pressure-induced fundamental, Martin derived 25^{+10}_{-9} km-am H_2 with a base temperature of 150 K and a base density of $0.52^{+0.26}_{-0.17}$ amagats. For the first overtone of the pressure-induced H_2 band, Lecacheux *et al.* (1976) derived 63^{+13}_{-8} km-A H_2. From the 6450Å NH_3 band, Woodman *et al.* (1977) derived 2.0 ± 0.5 m-A NH_3.

But from the 1.56 μm NH_3 band, Owen *et al.* (1976) derived an upper limit of 0.15 m-A. Using the 3 ν_3 CH_4 band, Trafton (1973) derived a CH_4 abundance of 54 ± 13 m-A (Trafton and Macy, 1975) and Lecacheux *et al.* (1976) derived 59^{+15}_{-7} m-A. On the other hand, Lutz *et al.* (1976) analyzed the weak blue and green bands and derived ~150 m-A CH_4.

It is easily seen from this that the abundances derived in the RLM approximation vary both with the wavelength of the band analyzed and with the strength of that band. Except perhaps for the central meridian, the RLM approximation is probably poor. Even comparing bands at the same wavelength but of different strengths requires that the radiative transfer include scattering. Meaningful abundance ratios may be obtained without analysis of the radiative transfer if absorption features of the two gases in question can be found and measured which have comparable strengths (de Bergh and Maillard, 1977). This ratio is independent of the radiative transfer, at least for weak lines. Therefore, duplicating these absorptions with cold laboratory spectra yields the abundance ratio. This method has been applied successfully for C/H and $^{12}C/^{13}C$ in the atmospheres for Jupiter and Saturn. For Saturn, Lecacheux *et al.* (1976) derive C/H = $4.7^{+2.0}_{-1.3} \times 10^{-4}$ and Combes *et al.* (1977) derive 89^{+25}_{-18}, respectively. Figure 13 shows several manifolds of Saturn's $^{13}CH_4$ spectrum and the

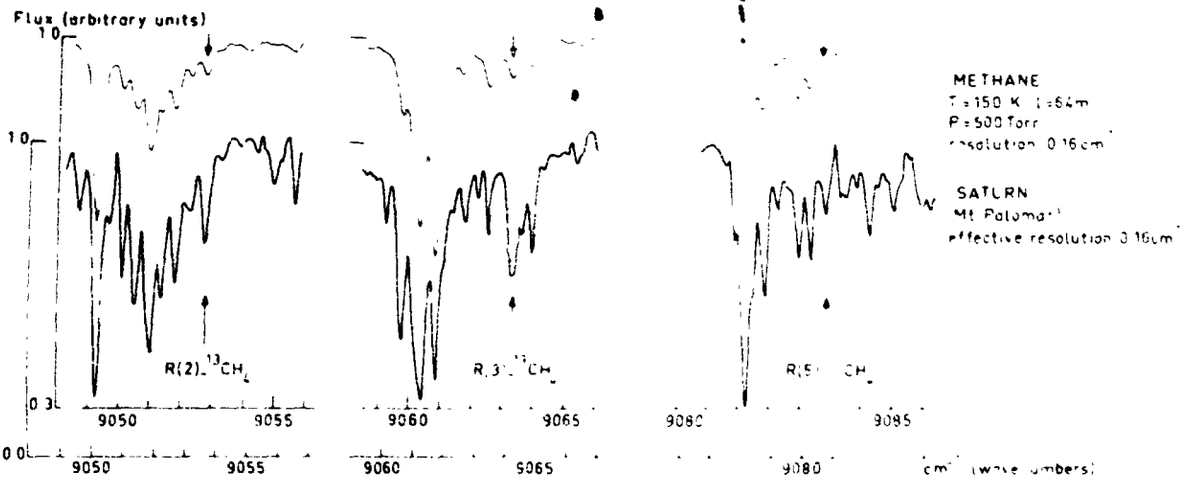

Figure 13. Lower curve. Portions of a spectrum of Saturn recorded at Mt. Palomar in 1974 with a Connes interferometer. Resolution for planetary lines: 0.16 cm^{-1} S/B (B=2σ)=2×4 per curve. Portions of a laboratory spectrum of CH_4 (as in Figure 11). The spectral resolution has been degraded to 0.15 cm^{-1} for a better comparison with the Saturn spectrum (Combes et al., 1977).

laboratory CH_4 features used to compare them. These values are essentially the same as the solar values, and the same as the telluric value in the case of $^{12}C/^{13}C$.

Podolak and Danielson (1977) have shown the importance of including dust and haze in determining abundances from atmospheric models. They were successful in constructing such models which give both the observed absorptions for the weak blue bands of CH_4 and the stronger bands the red and near infrared.

Some results for the CH_4/H_2 mixing ratio from such models follow: Podolak and Danielson (1977); 5x solar C/H ($CH_4/H_2 = 3.5$ to 3.9×10^{-3}); Caldwell (1977a): 4.7x solar ($CH_4/H_2 = 2.1 \times 10^{-3}$); Mach (1977): 4.5x solar. These are all higher than the value of Lecacheux *et al.* (1976), who derive approximately the solar ratio. This discrepancy requires further study.

Saturn's UV spectrum obtained by the TD1a and OAO-2 satellites shows no definite absorption features (Caldwell, 1977b). Saturn's albedo from 2100Å to 2500Å is similar to Jupiter's, implying that there is a common UV absorber. This absorber cannot be NH_3 on either planet because it is frozen out to much deeper levels in Saturn's atmosphere so that it should affect Saturn's spectrum differently. Caldwell (1977b) models the H_2S absorption and finds that a mixing ratio of $H_2S/H_2 = 1.4 \times 10^{-8}$ fits Saturn's UV spectrum (see Figure 14). This compares with the upper limit of 4×10^{-7} on this mixing ratio reported by Owen *et al.* (1976) for Saturn from the 6289 cm^{-1} band. Caldwell's value is much less than the corresponding solar S/H ratio, implying that S is bound in other molecules.

Scattergood and Owen (1977) consider the composition of the blue-UV "dust" in terms of the production of organics by proton bombardment of H_2, CH_4 and NH_3 mixtures. Their results show that CH_4+H_2 mixtures remain clear but the addition of N (e.g. NH_3) or S (e.g., H_2S) leads to the production of colorful liquids and solids. None has the spectral behavior identical to those shown by the planets so mixtures would be required to explain the haze. As yet, there is no satisfactory explanation for what material is causing the absorption between 5000-3000 Å in Jupiter, Saturn or Titan. This remains a major unsolved problem.

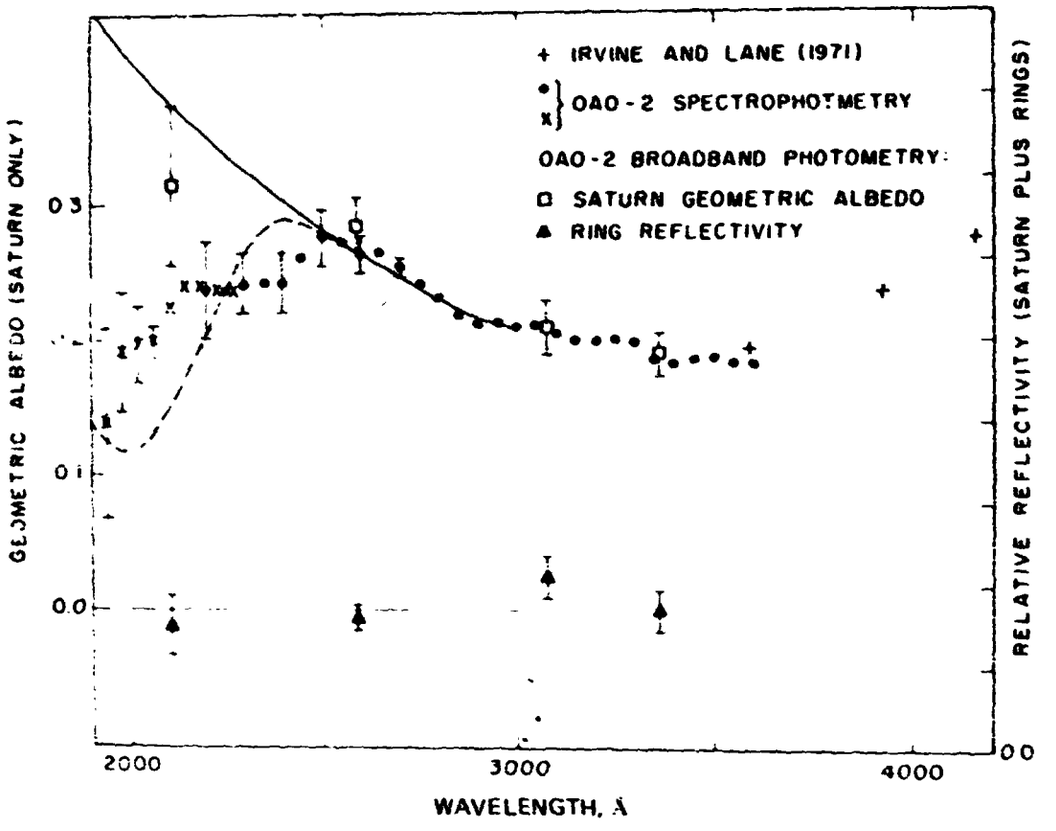

Figure 14. Ultraviolet spectrophotometry of the Saturn system. The observational points (X, ●, +) are described by the right hand ordinate, which is the ratio of the brightness of the planet plus rings divided by the Sun. Regular OAO-2 spectrophotometry (⧫), replotted from WCS, and long integration time spectrophotometry (⧓), are shown with error bars only due to background uncertainty. The ring reflectivity (▲) error bars are due only to the uncertainty in extrapolating the total brightness to zero ring inclination. The Saturn geometric albedo points (Φ) were used to normalize the geometric albedo scale on the left. This scale is valid only shortward of 3500 Å. The solid curve is a model calculation including absorption by a trace amount of H_2S (Caldwell, 1977b).

REFERENCES

Barker, E. (1977). Progress Report Copernicus observations of solar system objects. *Bull. Amer. Astron. Soc.* 9, 456.

Barker, E. (1978) Private communication

Barker, E., and Trafton, L. (1973). Ultraviolet reflectivity and geometric albedo of Titan. *Icarus* 20, 444–454.

Bregman, J., Lester, D., and Rank, D. (1975) Observation of the ν2 band of PH_3 in the atmosphere of Saturn. *Astrophys. J.* 202, L55–L56.

Caldwell, J. (1977a) The atmosphere of Saturn: an infrared perspective. *Icarus* 30, 493–510.

Caldwell, J. (1977b). Ultraviolet observations of Mars and Saturn by the TDIA and OAO-2 satellites. *Icarus* 32, 190–209.

Capone, L., Whitten, R., Prasad, S., and Dubach, J. (1977) The ionospheres of Saturn, Uranus, and Neptune. *Astrophys. J.* 215, 977–983.

Combes, M., Maillard, J., and deBergh, C. (1977) Evidence for a telluric value of the $^{12}C/^{13}C$ ratio in the atmospheres of Jupiter and Saturn. *Astron. Astrophys.* 61, 531–537.

deBergh, C., Lecacheux, J., and Maillard, J. (1977) The 2-0 quadrupole spectrum of H_2 in the atmospheres of Jupiter and Saturn. *Astron. Astrophys.* 56, 227–233.

REFERENCES (Contd)

deBergh, C., and Maillard, J. (1977). Abundances from near infrared spectroscopy (in the giant planets). In *Proceedings of Symposium on Planetary Atmospheres* (A. V. Jones, ed.), pp. 9–18. Ottawa.

Dunham, T., Jr. (1933). Note on the spectra of Jupiter and Saturn. *Publ. Astron. Soc. Pac. 45*, 42–44.

Encrenaz, Th., and Owen, T. (1973). New observations of the hydrogen quadrupole lines on Saturn and Uranus. *Astron. Astrophys. 28*, 119–124.

Encrenaz, Th., Combes, M., Zeau, Y., and Vapillon, L. (1975). A tentative identification of C_2H_4 in the spectrum of Saturn. *Astron. Astrophys. 42*, 355–356.

Fink, U., and Belton, M. (1969). Collision-narrowed curves of growth for H_2 applied to new photoelectric observation of Jupiter. *J. Atmos. Sci. 26*, 952–962.

Fink, U., and Larson, H. (1977). The 5 μm spectrum of Saturn. *Bull. Amer. Astron. Soc. 9*, 535.

Franz, O., and Price, M. (1977). UBV pinhole scans of Saturn's disc. *Bull. Amer. Astron. Soc. 9*, 535.

Gillett, F., and Forrest, W. (1974). The 7.5 to 13.5 micron spectrum of Saturn. *Astrophys. J. 187*, L37–L38.

Gillett, F., and Orton, G. (1975). Center-to-limb observations of Saturn in the thermal infrared. *Astrophys. J. 195*, L47–L49.

Gulkis, S., McDonough, T., and Craft, H. (1969). The microwave spectrum of Saturn. *Icarus 10*, 421–427.

Gulkis, S., and Poynter, R. (1972). Thermal radio emission from Jupiter and Saturn. *Phys. Earth Planet. Interiors 6*, 36–43.

Lecacheux, J., deBergh, C., Combes, M., and Maillard, J. (1976). The C/H and $^{12}CH_4/^{13}CH_4$ ratios in the atmospheres of Jupiter and Saturn from 0.1 cm^{-1} resolution near-infrared spectra. *Astron. Astrophys. 53*, 29–33.

Lutz, B., Owen, T., and Cess, R. (1976). Laboratory band strengths of Methane and their application to the atmospheres of Jupiter, Saturn, Uranus, Neptune, and Titan. *Astrophys. J. 203*, 541–551.

Macy, W. (1973). Inhomogeneous models of the atmosphere of Saturn. Ph.D. Thesis, Princeton University, 70 pp.

Macy, W. (1976). Analyses of Saturn's methane 3 ν_3 band profiles in terms of an inhomogeneous atmosphere. *Icarus 29*, 49–56.

Macy, W. (1977). Inhomogeneous models of the atmosphere of Saturn. *Icarus 32*, 328–347.

Marin, M. (1968). Photometric photographique de Saturne. *J. Obs. 51*, 179–192.

Ohring, G. (1975). The temperature profile in the upper atmosphere of Saturn from inversion of the thermal emission observations. *Astrophys. J. 195*, 223–225.

Ohring, G., and Lacser, A. (1976). The ammonia profile in the atmosphere of Saturn from inversion of its microwave emission spectrum. *Astrophys. J. 206*, 622–626.

Owen, T., McKellar, A., Encrenaz, Th., Lecacheux, J., deBergh, C., and Maillard, J. (1977). A study of the 1.56 μm NH_3 band on Jupiter and Saturn. *Astron. Astrophys. 54*, 291–295.

Podolak, M., and Danielson, R. (1977). Axel dust on Saturn and Titan. *Icarus 30*, 479–492.

Scattergood, T., and Owen, T. (1977). On the sources of ultraviolet absorption in spectra of Titan and the outer planets. *Icarus 30*, 780–788.

Smith, W., and Macy, W. (1977). Observation of HD on Saturn and Uranus. *Bull. Amer. Astron. Soc. 9*, 516.

Teifel, V. (1975). Limb darkening on Saturn's disc. *Astron. Zh. 52*, 823–831.

Teifel, V., Usoltseva, L., and Kharitonova, G. (1971). Optical properties and structure of Saturn's atmosphere. I. Preliminary results of studies of CH_4 absorption bands on the planetary disc. *Sov. Astron. 15*, 296–302.

Teifel, V., Usoltseva, L., and Kharitonova, G. (1973). Optical properties and structure of Saturn's atmosphere. II. Latitudinal variations of absorption in the 0.62-μm CH_4 band and characteristics of the planet in the near ultraviolet. *Sov. Astron. 17*, 108–111.

Tokunaga, A., Knacke, R., and Owen, T. (1975). The detection of ethane on Saturn. *Astrophys. J. 197*, L77–L78.

Trafton, L. (1972). Quadrupole H_2 absorption in the spectra of Jupiter and Saturn. *Bull. Amer. Astron. Soc. 4*, 359.

Trafton, L. (1973). Saturn: A study of the 3 ν_3 methane band. *Astrophys. J. 182*, 615–636.

Trafton, L. (1976). The aerosol distribution in Uranus' atmosphere. Interpretation of the hydrogen spectrum. *Astrophys. J. 207*, 1007–1024.

Trafton, L. (1977). Saturn: Long-term variation of H_2 and CH_4 absorptions. *Icarus 31*, 369–384.

Trafton, L., and Macy, W. (1975). Saturn's 3 ν_3 methane band. An analysis in terms of a scattering atmosphere. *Astrophys. J. 196*, 867–876.

Trauger, J., Roesler, F., and Mickelson, M. (1977). The D/H ratios on Jupiter, Saturn, and Uranus based on new HD and H_2 data. *Bull. Amer. Astron. Soc. 9*, 516.

Wallace, L. (1975). On the thermal structure of Uranus. *Icarus 25*, 538–544.

Weiser, H., Vitz, R., and Moos, H. (1977). Detection of Lyman α emission from the Saturnian disk and from the ring system. *Science 197*, 755–757.

Woodman, J., Trafton, L., and Owen, T. (1977). The abundances of ammonia in the atmospheres of Jupiter, Saturn, and Titan. *Icarus 32*, 314–320.

Wrixon, G., and Welch, W. (1970). The millimeter wave spectrum of Saturn. *Icarus 13*, 163–172.

DISCUSSION

J. CALDWELL: Concerning the controversy over ethylene and phosphine at 10.5 μm, I don't think that the observations of Fink and Larson rule out ethylene. If ethylene is being seen at that wavelength, it's in emission at a very high altitude. And if that were true, you would see emission from ethylene on top of any possible absorption by phosphine so that, in fact, both observations could be right; they're not mutually exclusive.

L. TRAFTON: The observations of Fink and Larson show that the phosphine is fairly strong, stronger than in Jupiter, so it would also be absorbing in the 9 to 10 μm region fairly strongly.

J. CALDWELL: But if ethylene is emitting above that, you see the ethylene.

G. SISCOE: Do the Copernicus Lyman-alpha measurements give a density value or a density limit for the Titan torus?

L. TRAFTON: They give an intensity of about 150 Rayleighs for the Titan torus. E. Barker (1977) pointed out from OAO data, that within ten arc-sec of Titan a 39-arc-sec measurement gave about 150 Rayleighs, which would be a limit for their detection. And when he looked again, I believe he saw about the same number.

J. POLLACK: When you speak about the observations of the Titan torus, is that a discrete torus?

L. TRAFTON: The observations are made through a 39-sec slit superimposed over the torus about five or ten-sec away from Titan. I understand there is a problem with the geocoronal calibration of atomic hydrogen data. That has to be subtracted out, and you're subtracting two large numbers which are roughly equal to each other and in that circumstance, there can be large uncertainties. It's a difficult problem and I think even more observations are needed to convince a majority of the community one way or another whether the hydrogen emission really is present at all, to say nothing of the detailed geometry.

D. HUNTEN: You were praising the use of spectral features of comparable strengths in getting relative abundances, but there's another important point that I've recently become sensitive to: you want comparable physics as well. You don't want to compare a pressure-induced feature with a pressure-narrowed feature, for example, if you can possibly help it, because every time the physics is different like that, you have a different depth weighting in the formation of the spectral feature. You must go a lot further than just to look for comparable features, and unfortunately, in comparing hydrogen and methane, nothing is really comparable. Every time you look for a useful pair, you find that the depth weighting is totally different.

L. TRAFTON: Unfortunately, I have to agree.

THE THERMAL STRUCTURE OF SATURN: INFERENCES FROM GROUND-BASED AND AIRBORNE INFRARED OBSERVATIONS

Alan Tokunaga

Steward Observatory, University of Arizona
Tucson, Arizona 85721

ABSTRACT

Spectroscopic and photometric infrared observations of Saturn are reviewed and compared to the expected flux from thermal structure models. Large uncertainties exist in the far-infrared measurements, but the available data indicate that the effective temperature of the disk of Saturn is 90 ±5 K. The thermal structure models proposed by Tokunaga and Cess and by Gautier *et al.* (model "N") agree best with the observations. North-South limb scans of Saturn at 10 and 20 μm show that the temperature inversion is much stronger at the South polar region than at the equator.

INTRODUCTION

The importance of infrared observations of Saturn in constraining model atmospheres and identifying trace atmospheric constituents has been recently emphasized by Caldwell (1977). Since Saturn radiates nearly all of its energy at wavelengths longer than 10 μm, the infrared spectral region is particularly important in establishing the thermal structure of Saturn. It is not surprising, therefore, that the increasing quality and wavelength coverage of infrared observations has been accompanied by a corresponding increase in the number of thermal structure models. In this paper, we review observations of Saturn in the 8-1000 μm wavelength region and relate these observations to model atmospheres. In Section II, we summarize ground-based and

airborne observations of Saturn, and we critically examine uncertainties in the effective temperature of Saturn. In Section III, thermal structure models are briefly reviewed and compared to the observations.

THE EFFECTIVE TEMPERATURE OF SATURN

One of the fundamental input parameters in an interior and atmospheric model for Saturn is the effective temperature. This is a particularly difficult quantity to measure in the case of Saturn because most of its radiant energy is in the far-infrared, a spectral region which is almost totally inaccessible to ground-based observatories. Observations of the brightness temperature of Saturn at wavelengths longer than 10 μm are shown in Tables 1 and 2. Work prior to 1972, not included here, is summarized by Newburn and Gulkis (1973). The far-infrared observations shown in Table 1 are particularly important since Saturn radiates approximately 80% of its energy at wavelengths longer than 30 μm. Unfortunately, the relatively small telescope aperture

Table 1. Airborne and Balloon Far-Infrared Photometry[a]

λ_{eff} (μm)	$\Delta\lambda$(μm)	T_B (K)	Reference
--	30 - 45	84 ± 4	Armstrong *et al.* (1972)[b]
--	45 - 80	85 ± 2	Armstrong *et al.* (1972)[b]
--	65 - 110	89 ± 5	Armstrong *et al.* (1972)[b]
--	125 - 300	79 ± 4	Armstrong *et al.* (1972)[b]
--	30 - 300	85 ± 2	Armstrong *et al.* (1972)[b]
--	45 - 300	86 ± 2	Armstrong *et al.* (1972)[b]
--	40 - 250	90 ± 5	Fazio *et al.* (1976)
39	30 - 50	91.3 ± 2.9	Loewenstein *et al.* (1977)[c]
58	45 - 80	88.1 ± 3.3	Loewenstein *et al.* (1977)[c]
80	45 - 300	87.9 ± 3.4	Loewenstein *et al.* (1977)[c]
150	100 - 400	78.7 ± 3.0	Loewenstein *et al.* (1977)[c]
410	200 - 700	95 ± 2	Loewenstein *et al.* (1977)[c]

[a]Brightness temperatures include emission from the rings. Fractional area of the rings was 0.65 during the Armstrong *et al.* observations and 0.55 during the Loewenstein *et al.* observations.

[b]The "reconciled" values given by Wright (1976) are shown here.

[c]From Tables 2 and 3 in their paper.

Table 2. Ground-Based Infrared Photometry[a]

λ_{eff} (μm)	Δλ(μm)	T_B (K)	Reference
11	6	101 ± 3	Morrison (1974)
20	11.5	92 ± 2	Morrison (1974)
20	11.5	94 ± 3[b]	Murphy (1973)
450	≥300	205 ± 15[c]	Hudson *et al.* (1974)
21	8	92 ± 1.5	Rieke (1975)
22.5	5	93 ± 1.5	Rieke (1975)
33.5	12	91 ± 2	Rieke (1975)
17.8	1	92 ± 2	Knacke *et al.* (1975)
18.4	1	90 ± 2	Knacke *et al.* (1975)
21	6	90 ± 2	Knacke *et al.* (1975)
35	14	96 ± 6	Nolt *et al.* (1977)
39	8	98 ± 2.5	Nolt *et al.* (1977)
17.8	0.6	90.3 ± 1.5	Tokunaga *et al.* (1978)
19.8	1.7	90.7 ± 1.7	Tokunaga *et al.* (1978)
22.7	2.3	88.9 ± 1.9	Tokunaga *et al.* (1978)

[a]With the exception of the measurement by Hudson *et al.*, the photometry included here have beam sizes which are smaller than the disk of Saturn.

[b]Revised value from Nolt *et al.* (1977).

[c]Includes emission from the rings.

available with aircraft and balloon telescopes has intrinsically large diffraction which prevents a measurement of the disk of Saturn independent of its rings.

The measured far-infrared brightness temperature in Table 1 includes emission from both the disk and rings of Saturn. Loewenstein *et al.* (1977) find that the effective temperature of the disk is approximately 89 K if they assume that the disk and the A and B rings have the same brightness temperature. This is approximately consistent with the broad-band brightness temperatures of Armstrong *et al.* (1972)and Fazio *et al.* (1976), and with the ground-based observations shown in Table 2.

Spectroscopic observations of the Saturn-ring system in the 20-110 μm spectral range have been made by Erickson *et al.* (1978) and by Ward (1977). These observations are shown in Figures 1 and 2. In order to remove the contribution from the rings, both assume constant A and B ring brightness temperatures with wavelength and use the

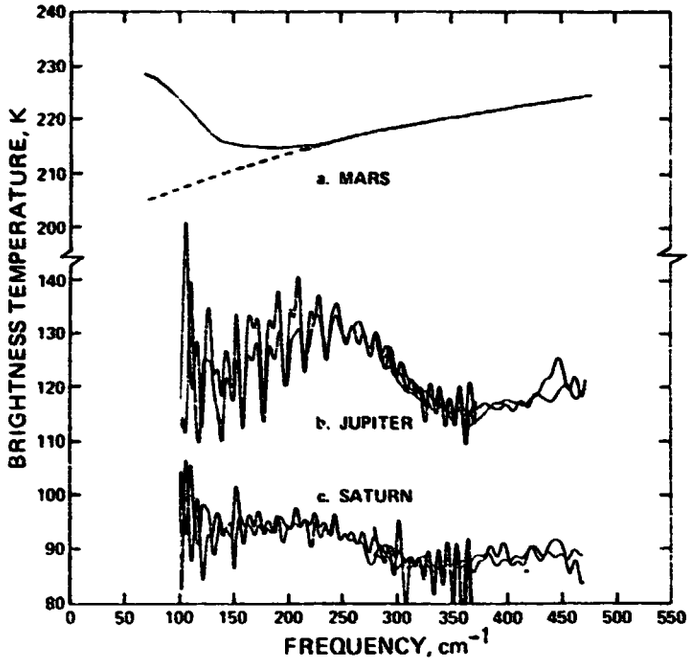

Figure 1. (a) The brightness temperature of Mars for Jan. 26, 1976 is given as a function of frequency in the solid curve. The values calculated by Wright (1976) are given by the dashed curve. (b) The average brightness temperatures for Jupiter are plotted for each of the four flights. (c) The average brightness temperatures for Saturn are plotted for each of the four flights. (From Erickson et al. 1978)

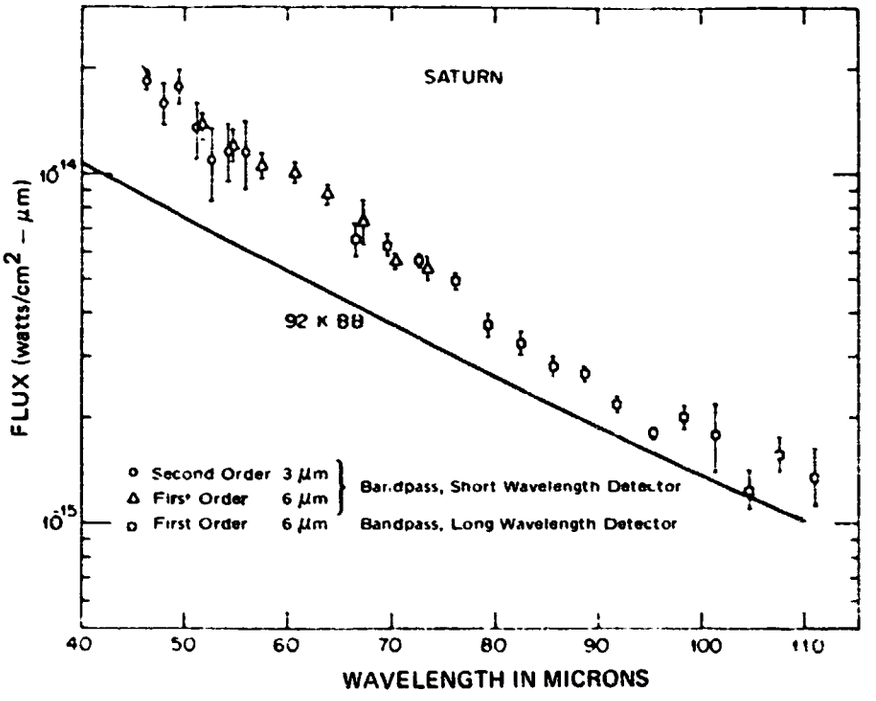

Figure 2. Flux received from Saturn and its rings. The solid line is the flux that would be received from a 92 K black body subtending the same solid angle as Saturn partially occulted by the A and B rings. (From Ward 1977)

ring optical depths given by Rieke (1975). However, Erickson *et al.* (1978) used a ring temperature of 89.3 K, while Ward used 96 K. This gives rise to a discrepancy in the effective temperature of Saturn with Erickson *et al.* (1978) finding $T_{eff} = 97 \pm 3$ K but Ward obtaining $T_{eff} = 89 \pm 3$ K. Since both groups observed Saturn in the first half of 1976, most of the disagreement in the effective temperature is probably caused by the different ring temperature used.

Ward finds the brightness temperature of Saturn, after the ring emission is removed, is 65 ± 10 K in the 80-110 μm wavelength range. Such a low brightness temperature is inconsistent with the models discussed in the next section, but Ward points out that the ring emission could be lower than he assumed if the ring particle size were small. In this case, the calculated brightness temperature of Saturn's disk could be raised. It is also possible that Mars, Ward's calibration source, may deviate from the assumed brightness temperature as predicted by Wright (1976). This possibility is raised by Erickson *et al.* who find that the brightness temperature of Mars disagrees with Wright's model at wavelengths longer than 50 μm. The increasing brightness temperature of Mars observed by Erickson *et al.*, at the longer wavelengths could partly explain the low brightness temperature of Saturn found by Ward. The validity of using Mars as a far-infrared calibration standard is clearly subject to question at the present time.

Since the ring contribution to the observed far-infrared flux is considerable, it is necessary to consider the risks involved in assuming a ring brightness equal to the disk. At the time near maximum ring tilt, Rieke (1975) found equal disk and ring brightness temperatures in the 20-34 μm spectral range, but recent observations of the rings show changes in the A, B, and C ring brightness temperature (Nolt *et al.*, 1978). We expect, therefore, that the assumption of equal ring and disk brightness temperatures to be valid only near the time of maximum ring tilt. In addition, the C ring appears to be bright in the infrared. Observations of the rings by Murphy (1973), Rieke (1975), and Nolt *et al.* (1978) find that the emission from the C ring is substantial, although Morrison (1974) did not detect it. We must therefore view with caution any correction for the ring emission at far-infrared wavelengths.

The effective temperature of Saturn is more difficult to extract from the shorter wavelength infrared data shown in Table 2. In the 8-14 μm spectral region, the continuum is greatly affected by CH_4 and C_2H_6 emission, NH_3 ice absorption, and other not yet positively identified minor constituents (Caldwell 1977, Gillett and Forrest 1974). In the 17-25 μm spectral range, the temperature inversion contributes

significantly to the observed flux (as shown in the next section). We are therefore compelled to use far-infrared data in order to obtain the effective temperature of Saturn. Any atmospheric model for Saturn, however, should be consistent with the data in Table 2.

We conclude from the available far-infrared data that the effective temperature of Saturn is 90 ± 5 K. For an equilibrium temperature of 76 K (Rieke 1975, Erickson *et al.* 1978), the ratio of emitted to absorbed power is in the range 1.6 - 2.4. Obviously more observations are necessary, and we expect that far-infrared observations in 1980, when the rings are edge-on, will provide a good value for the effective temperature. The largest experimental uncertainty will likely be in the absolute calibration.

MODEL ATMOSPHERES

We know relatively little about the thermal structure of Saturn's atmosphere compared to the Jovian atmosphere. Since Trafton (1967) first constructed a model atmosphere for Saturn, six other atmospheric models have been proposed - all within the last five years. In this section, we review the properties of these models and compare them to observations in the infrared.

The 8-14 μm spectrum of Saturn is shown in Figure 3 (Gillett and Forrest,1974). The emission peaks at 7.9 and 12.2 μm are produced by emission from methane and ethane in a temperature inversion region. Scans across the disk of Saturn in the ethane emission band (Gillett and Orton 1975) show equatorial limb brightening and an intensity enhancement at the South pole which is consistent with a temperature inversion. Saturn is not unusual in having a temperature inversion since a temperature inversion in the Jovian atmosphere has been firmly established (Gillett, Low, and Stein 1969, Gillett and Westphal 1973, Ridgway 1974) and strong evidence for a temperature inversion has been found on Titan and Neptune (Gillett 1975, Macy and Sinton 1977, and Gillett and Rieke 1977). In this paper, we assume that the absorption of solar radiation by aerosols and methane in the upper atmosphere is sufficient to power the temperature inversion (Gillett, Low, and Stein 1969, Wallace *et al.*, 1974, Caldwell 1977).

Atmospheric models by Wallace (1975), Caldwell (1977), Tokunaga and Cess (1977), and Gautier *et al.* (1977) have incorporated a temperature inversion, and these models are shown in Figure 4. The models by Cess and Khetan (1973) and by Encrenaz and Combes (1977) are similar to the Wallace (1975) model below the

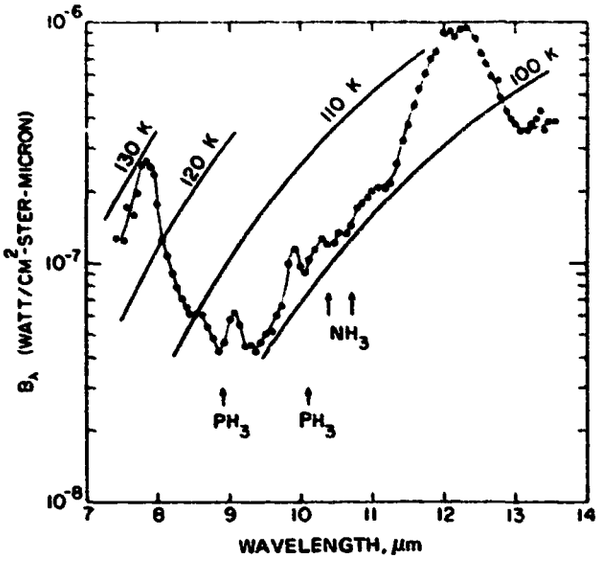

Figure 3. Surface brightness of Saturn versus wavelength. Also shown are the locations of the Q-branches of the ν_2 band of NH_3 and the ν_2 and ν_4 bands of PH_3. (From Gillett and Forrest, 1974)

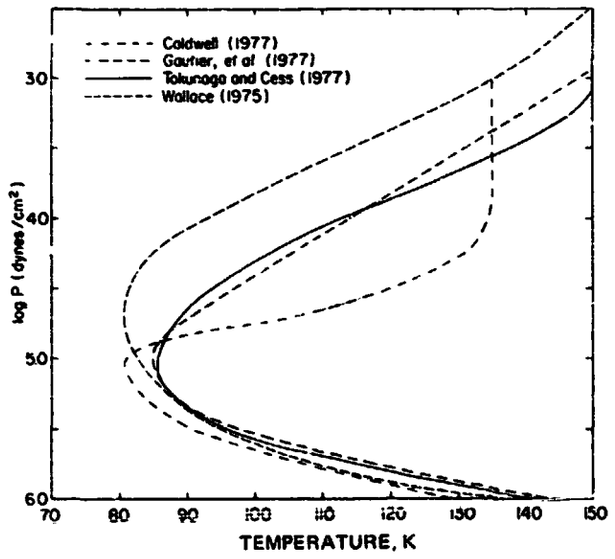

Figure 4. Thermal structure models for Saturn. The model for Tokunaga and Cess corresponds to the model in their Figure 4 (j = 0.2 and $f_E = 2 \times 10^{-6}$). The Gautier et al. *model shown is their model N.*

temperature minimum, but both models have a weaker temperature inversion (see Figure 1 of Encrenaz and Combes, 1977). The discussion of the Wallace model in this section will apply equally well to the Cess and Khetan and to the Encrenaz and Combes model. All the models, with the exception of the Wallace and the Gautier *et al.* models, have an effective temperature which is consistent with the far-infrared data discussed in the previous section. In Figure 4, it is evident that the models agree to ±10 K at any pressure level below the temperature minimum, but they are very discrepant in the temperature inversion region.

Some of the models have been compared to the far-infrared data by Erickson *et al.* (1978), as shown in Figure 5. The Tokunaga and Cess model provides a good fit throughout with a ring temperature of 89.3 K, and the Wallace model can also provide as good a fit with a higher ring temperature. The 20 μm center of disk measurements in Table 2, however, are not consistent with the Wallace model. These results depend on a uniform ring brightness temperature at all wavelengths - an assumption which may not be valid at the longer wavelengths (Ward 1977). It is important to note that the observations by Erickson *et al.* and by Ward probe to the 0.6 - 0.8 atm level in the 50-100 μm spectral range. Encrenaz and Combes (1977) show that observations of the continuum at wavelengths longer than 100 μm can test thermal structure models at higher pressures in the convective region, since the ammonia opacity is much reduced compared to Jupiter. The effect of clouds may be a serious obstacle, however.

In Figure 6, the Wallace, Caldwell, and Tokunaga and Cess models are compared to spectroscopic observations in the 17-25 μm spectral region. Observations at these wavelengths can distinguish between the various models of the temperature inversion since optical depth 1 is reached slightly below the temperature minimum. The Wallace model has a temperature inversion which is too cold, while the Caldwell model is too warm. In the latter model, the S(0) and S(1) pressure-induced rotational lines of molecular hydrogen appear slightly in emission. The Tokunaga and Cess model provides a reasonable fit to the data, and the Gautier *et al.* model "N" also fits well (see Figure 3 of their paper). The Trafton (1967) model lacks a temperature inversion, and its predicted spectrum is similar to the Wallace model. A comparison of the Tokunaga and Cess model to part of the data given in Table 2 is shown in Figure 7. This model agrees to within several standard deviations with all the disk-resolved data in the 13-40 μm spectral region.

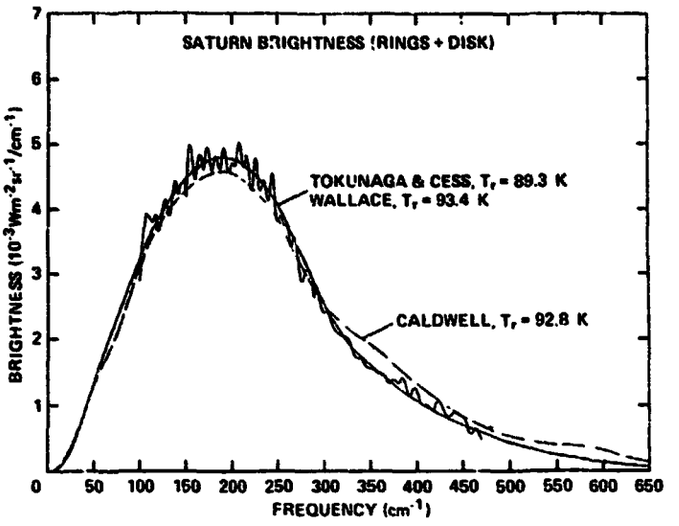

Figure 5. Comparison of observed far-infrared brightness of Saturn and its rings with model predictions. (From Erickson et al., *1978)*

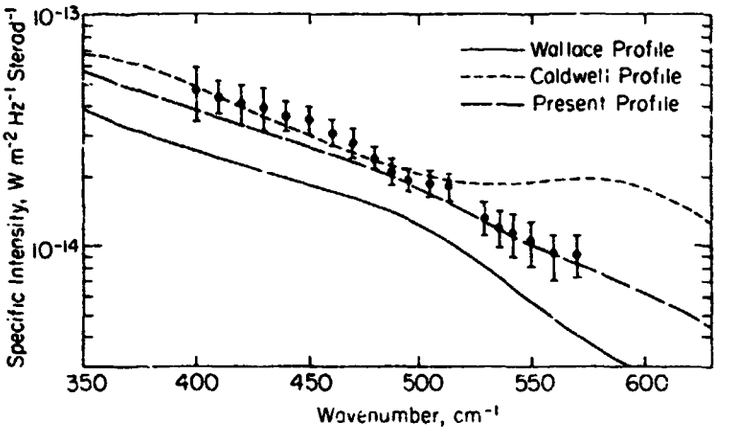

Figure 6. Comparison of the model full-disk intensities with the spectroscopic data of Tokunaga et al. *(1977). ("Present profile" refers to the Tokunaga and Cess model.) (From Tokunaga and Cess, 1977)*

The atmospheric models can also be tested by limb scans in the infrared. Caldwell *et al.* (1978) compare equatorial limb scans at three wavelengths in the 17-25 μm spectral region to the model predictions, and the results are shown in Figures 8, 9, and 10. The beam profile determined by Nolt *et al.* (1978) was used to produce the predicted limb emission profile. As a figure of merit, the deviation of the model predictions from the observed profile was computed and is shown in Table 3. Within the uncertainties in the beam profile, both the Tokunaga and Cess model and Gautier *et al* model "N" provide a good fit to the limb scans. The other models differ significantly from the observed limb profile.

We now review the evidence for differences in the thermal structure between the equatorial and the South polar region. North-South scans of the disk of Saturn at 12 and 20 μm have shown an intensity enhancement at the South polar region (Gillett and Orton, 1975; Rieke, 1975; Tokunaga *et al.*, 1978) and this effect is illustrated in Figure 11. The scans in the methane and ethane emission bands (at 7.9 and 12.2 μm) show an intensity enhancement at the South pole, but the scans in the continuum (at 11.14 and 13.31 μm) show much less limb brightening. There appears to be a slight amount of polar limb brightening at 13.31 μm, but it is not clear whether this results from molecular hydrogen or acetylene emission. The 12.2 μm scan is similar to the 12 μm scans obtained by Gillett and Orton (1975) and Rieke (1975).

The 7.9 μm scan suggests that the enhanced polar emission is mostly the result of a hotter inversion since we expect methane to be uniformly mixed over the disk of Saturn. Scans obtained in the molecular hydrogen continuum indicate that the temperature inversion is indeed hotter at the South polar region. As shown in Figure 12, the strongest limb brightening occurs at 17.8 μm, the wavelength which is closest to the maximum in the molecular hydrogen opacity. The degree of polar limb brightening can be judged by comparing Figure 12 with equatorial scans shown in Figures 8, 9, and 10.

Tokunaga *et al.* (1978) proposed a model for the South pole which was constructed in a similar fashion to the model by Tokunaga and Cess (1977), but it includes the higher acceleration of gravity at the pole and the increased value for the diurnally-averaged insolation. In Figure 13, we show the South pole model along with an equatorial model and the Tokunaga and Cess model for comparison. Note that the Tokunaga and Cess model is a global model since a diurnally-averaged insolation over all latitudes was used (for a Saturn-Sun distance of 9.5 AU). The equatorial model uses a diurnally-averaged insolation for the Saturnian equator at the time of the

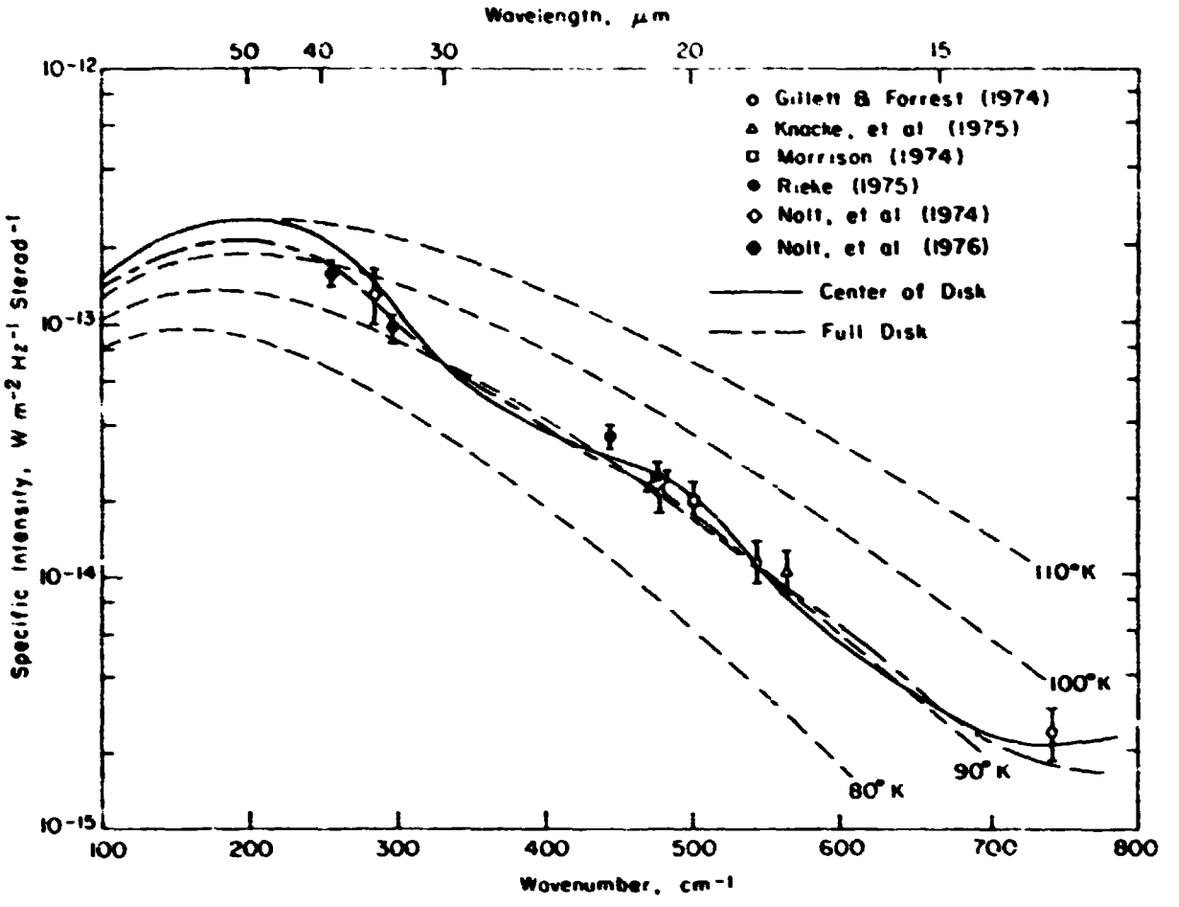

Figure 7 Comparison of the Tokunaga and Cess model with photometric data (From Tokunaga and Cess, 1977)

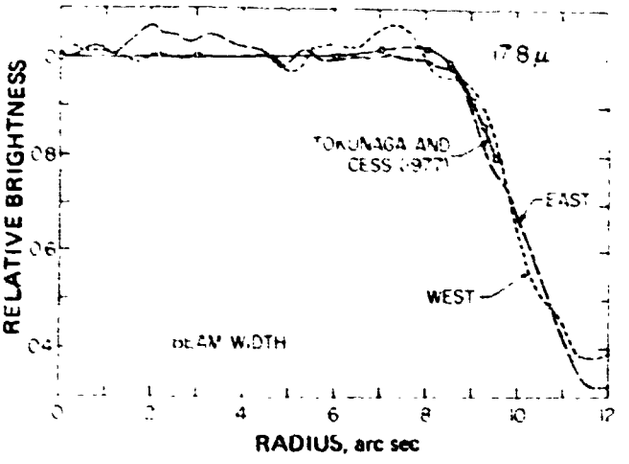

Figure 8 Center-to-limb scans near the equator of Saturn at 17.8 μm compared with the spatially smeared brightness variations from a model by Tokunaga and Cess (1977). East and West limb scans have been folded onto each other as a means of demonstrating experimental reproducibility. The signal does not go to zero at the planetary limb (10.05 arc sec) because of the ring contribution. (From Caldwell et al., 1978)

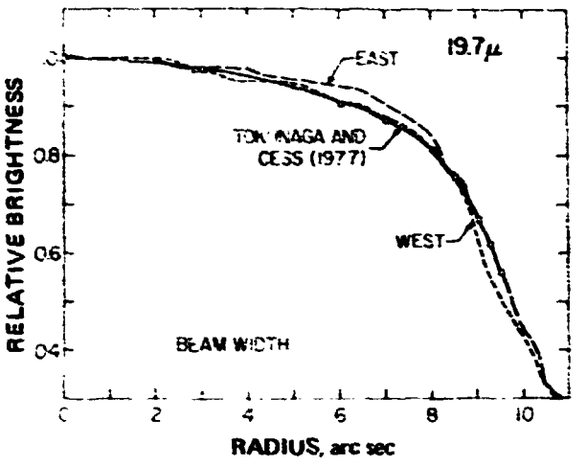

Figure 9. Center-to-limb scans near the equator of Saturn at 19.7 μm compared with the spatially smeared brightness variations from a model by Tokunaga and Cess (1977). East and West limb scans have been folded onto each other as a means of demonstrating experimental reproducibility. The signal does not go to zero at the planetary limb (10.05 arc sec) because of the ring contribution. (From Caldwell et al, 1978)

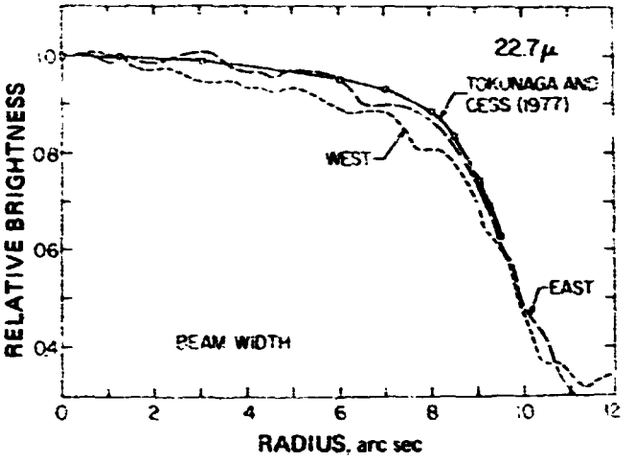

Figure 10. Center-to-limb scans near the equator of Saturn at 22.7 μm compared with the spatially smeared brightness variations from a model by Tokunaga and Cess (1977). East and West limb scans have been folded onto each other as a means of demonstrating experimental reproducibility. The signal does not go to zero at the planetary limb (10.05 arc sec) because of the ring contribution. (From Caldwell et al, 1978)

Table 3. Center to Limb Brightness Variations[1]
(from Caldwell *et al.*, 1978)

Wavelength	17.8 μm			19.7 μm			22.7 μm			RMS
Fraction of Radius from Center	0.6	0.8	0.95	0.6	0.8	0.95	0.6	0.8	0.95	
Tokunaga and Cess (1977)	-0.8	+2.2	+0.4	-2.3	-2.0	+6.1	+3.3	+3.7	+4.7	5.32
N[2]	+0.4	+5.5	+5.7	-2.4	-1.4	+8.4	+3.6	+7.4	+7.6	5.44
C	0.0	+2.8	-0.1	+3.7	+8.4	+19.8	+6.4	+10.9	+9.6	9.04
W	+4.5	+16.7	+23.0	-7.9	-7.4	+5.8	+2.9	+10.8	+16.8	12.4
N'	-1.3	-6.3	-21.3	+7.5	+8.9	+17.9	+8.7	+8.0	+3.5	11.7
C'	+6.5	+23.4	+36.9	+3.2	+12.0	+34.2	+6.6	+15.8	+23.1	23.1
W'	-1.2	-9.4	-19.2	+7.3	+12.1	+20.3	+8.7	+11.5	+5.8	12.1
Wallace (1975)	-9.8	-19.7	-33.0	-5.9	-13.1	-16.0	-1.4	-6.6	-16.6	16.1
Caldwell (1977)	+14.4	+42.6	+65.9	+9.6	+32.2	+75.8	+12.7	+33.2	+53.8	43.9

(1) [(Computed-Observed)/Observed] x 100.

(2) Models by Gautier *et al.* (1977).

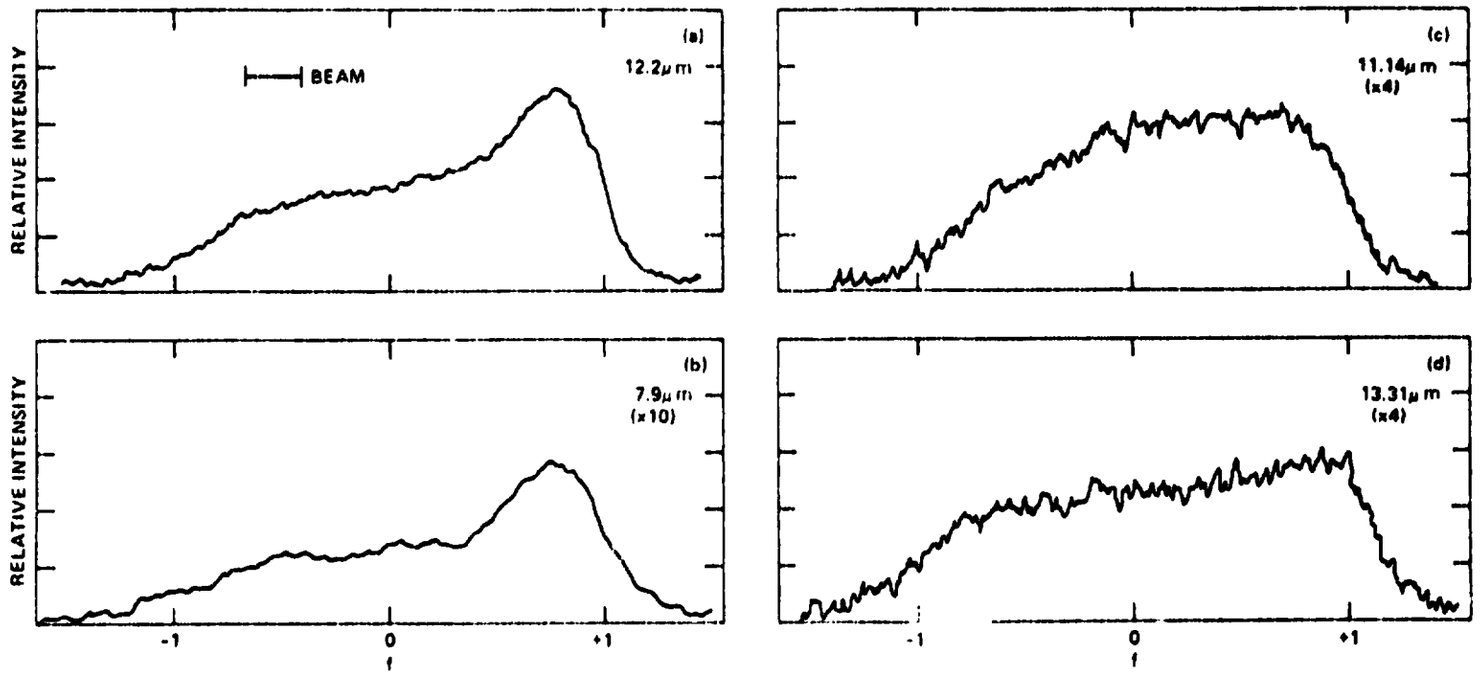

Figure 11. North-South disk scans of Saturn obtained in Feb. 1975. The abscissa is the normalized radius where 0 represents the subearth point and +1 is the southern limb of the disk. The half-power beam width for all the scans is 2.8 arc sec. The number in parenthesis is the factor by which the ordinate has been multiplied relative to Figure 11(a). The tilt to the pole toward the sun was 24.°4. (From Tokunaga et al., *1978)*

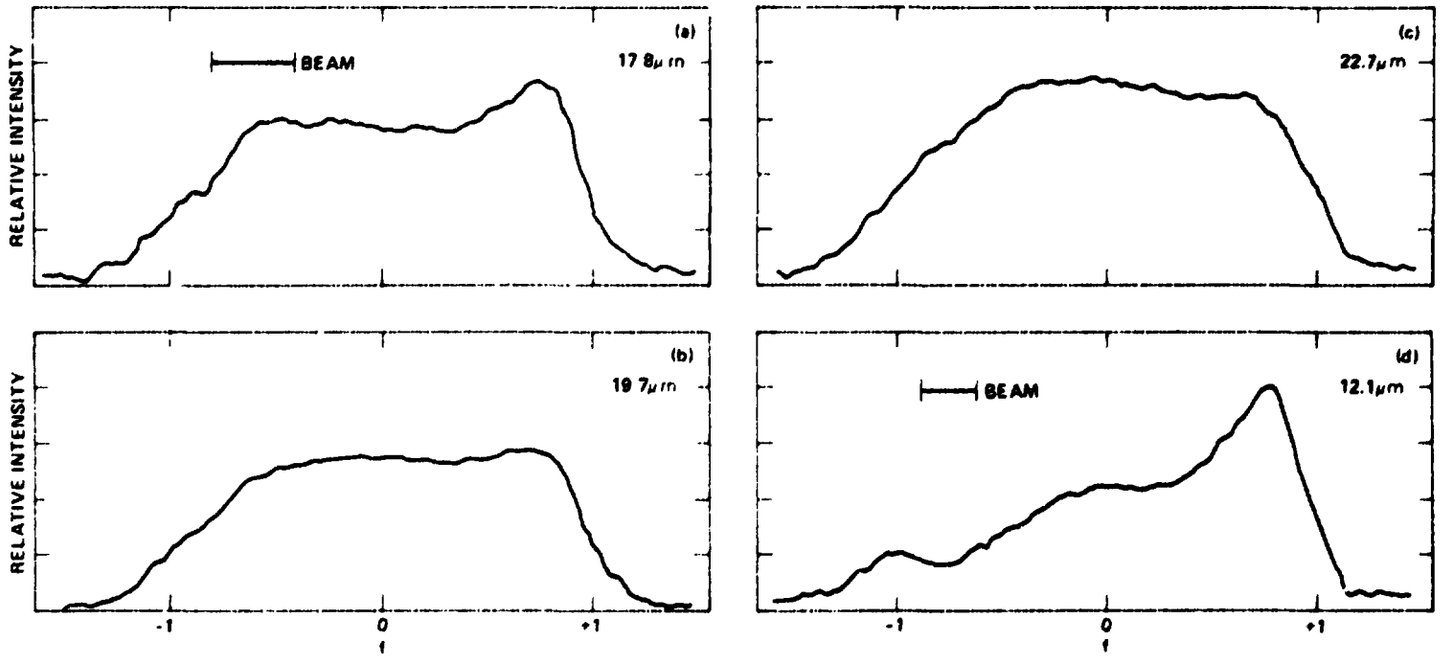

Figure 12 North-South disk scans of Saturn obtained in March 1977. The half-power beam width was 5.5 arcsec for the 20μm scans and 2.8 arc sec for the 12 μm scan. The tilt of the pole toward the sun was 16.5°. (From Tokunaga et al., 1978).

observations (9.14 AU). The South pole and equatorial models therefore have hotter temperature inversions than the global model of Tokunaga and Cess. The differences between the equatorial and global models are not large enough to affect the results obtained by Caldwell *et al.* (1978) as discussed earlier in this section.

A comparison between the predicted and observed brightness temperature for the South pole is shown in Figure 14. While the South pole model predicts a greater brightness temperature than is observed, this is partly a result of the relatively large telescope beam used (3.5 arc sec) which includes emission over a range of latitude. Tokunaga *et al.* (1978) find that at a latitude of -70° (corresponding to a distance from the pole equal to the radius of the beam), the computed temperature inversion is uniformly 3 K colder than the South pole model. From this result, roughly one-half of the brightness temperature discrepancy between the South pole model and the observations can be ascribed to beam-size effects. The South pole model appears to overestimate the heating by methane and aerosols. This result suggests that the stronger temperature inversion at the South pole could be powered with somewhat less than "normal" concentration of UV-absorbing aerosols.

We conclude that: (1) recent observational tests in the infrared favor the Tokunaga and Cess model and the Gautier *et al.* model "N", and (2) the South polar region has a stronger temperature inversion than the equatorial region. We expect that the intensity enhancement at the South pole to greatly diminish in the next few years as it tilts away from the Sun.

SUMMARY

In spite of the increasing quality of far-infrared data, the effective temperature of Saturn is not well known. Large uncertainties exist in the correction for the ring emission and in the absolute calibration. The far-infrared spectrum of Mars, the primary standard for most far-infrared observations, has only recently been measured, and more work on far-infrared calibration sources is necessary. The available far-infrared data indicates that the effective temperature of the disk of Saturn is 90 ± 5 K.

Current thermal structure models of Saturn are roughly similar in the lower atmosphere below the temperature inversion, but they differ greatly in the temperature inversion region. Ground-based observations in the 17-25 μm spectral region favor the Tokunaga and Cess (1977) model and the Gautier *et al.* (1977) model "N". There is greater uncertainty in the thermal structure below the temperature minimum, but observations at wavelengths longer than 40 μm can help to constrain models down to the

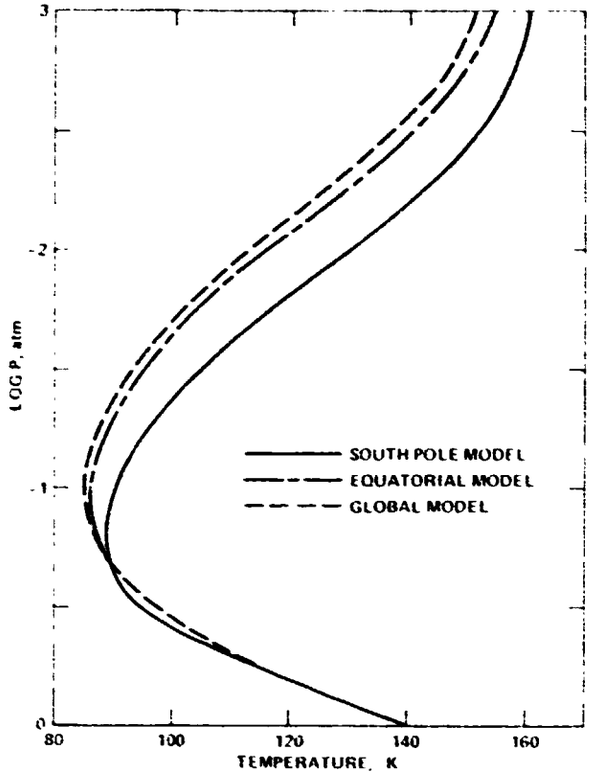

Figure 13. Models of the temperature inversion of Saturn. The global model is the same as in Tokunaga and Cess (1977) with the fraction of sunlight absorbed by aerosols = 0.2 and ethane mixing ratio = 2×10^{-6}. (From Tokunaga et al 1978)

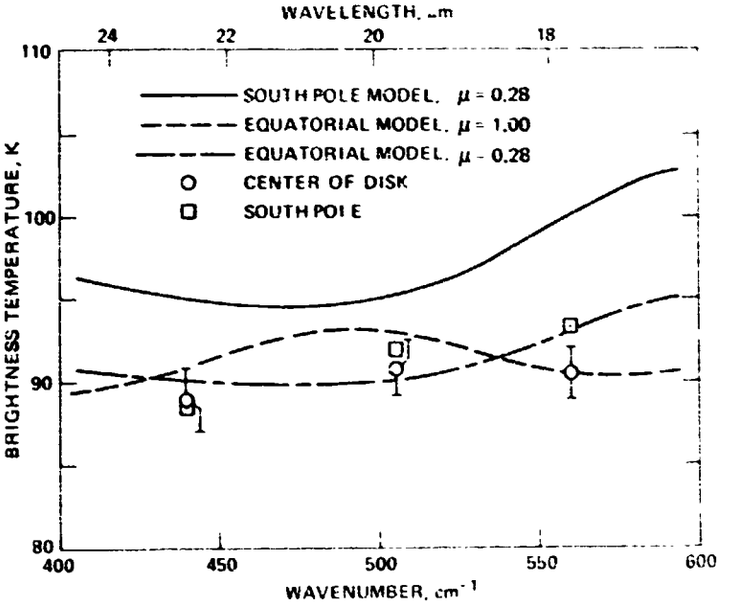

Figure 14. Comparison of the observed (see Figure 12) and model brightness temperature. The brightness temperature of the South pole model has been computed for $\mu = \cos\theta = 0.28$ where θ is the angle from the normal to the surface at which we observe Saturn. The brightness temperature of the equatorial model has been computed at the center of the disk ($\mu = 1.0$) and at the South pole ($\mu = 0.28$). (From Tokunaga et al., 1978).

cloud deck. Strong differences exist between the temperature inversion in the equatorial and the South polar regions. There are several possible ways to explain this effect, and more data concerning the deposition of solar radiation in the upper atmosphere is required.

REFERENCES

Armstrong, K. R., Harper, D. A., and Low, F. J. (1972). Far-Infrared Brightness Temperatures of the Planets. *Astrophys. J. 178*, L89–L92.

Caldwell, J. (1977). The Atmosphere of Saturn: An Infrared Perspective. *Icarus 30*, 493–510.

Caldwell, J., Gillett, F. C., Nolt, I. G., and Tokunaga, A. (1978). Spatially Resolved Infrared Observations of Saturn. I. Equatorial Limb Scans at 20 Microns. *Icarus 35*

Cess, R. D., and Khetan, S. (1973). Radiative Transfer Within the Atmospheres of the Major Planets. *J. Quant. Spectrosc. Radiat. Transfer 13*, 995–1009.

Encrenaz, T., and Combes, M. (1977). The Far-Infrared Spectrum of Saturn: Observability of PH_3 and NH_3. *Astron. Astrophys. 61*, 387–390.

Erickson, E. F., Goorvitch, D., Simpson, J. P., and Strecker, D. W. (1978). Far-Infrared Spectrophotometry of Jupiter and Saturn. *Icarus 35*, 61–73.

Fazio, F. G., Traub, W. A., Wright, E. L., Low, F. J., and Trafton, L. M. (1976). The Effective Temperature of Uranus. *Astrophys. J. 209*, 633–637.

Gautier, D., Lacombe, A., and Revah, I. (1977). Saturn: Its Thermal Profile from Infrared Measurements. *Astron. Astrophys. 61*, 149–153.

Gillett, F. C. (1975). Further Observations of the 8 - 13 Micron Spectrum of Titan. *Astrophys. J. 201*, L41–L43.

Gillett, F. C., and Forrest, W. J. (1974). The 7.5 to 13.5 Micron Spectrum of Saturn. *Astrophys. J. 187*, L37–L39.

Gillett, F. C., Low, F. J., and Stein, W. A. (1969). The 2.8 - 14 Micron Spectrum of Jupiter. *Astrophys. J. 157*, 925–934.

Gillett, F. C., and Orton, G. S. (1975). Center-to-Limb Observations of Saturn in the Thermal Infrared. *Astrophys. J. 195*, L47–L49.

Gillett, F. C., and Rieke, G. H. (1977). 5 - 20 Micron Observations of Uranus and Neptune. *Astrophys. J. 218*, L141–L144.

Gillett, F. C., and Westphal, J. A. (1973). Observations of 7.9 Micron Limb Brightening of Jupiter. *Astrophys. J. 179*, L153–L154.

Hudson, H. S., Lindsey, C. A., and Soifer, B. T. (1974). Submillimeter Observations of Planets. *Icarus 23*, 374–379.

Knacke, R. F., Owen, T., and Joyce, R. R. (1975). Infrared Observations of the Surface and Atmosphere of Titan. *Icarus 24*, 460–464.

Loewenstein, R. F., Harper, D. A., Moseley, S. H., Telesco, C. M., Thronson, H. A., Hildebrand, R. H., Whitcomb, S. E., Winston, R., and Steining, R. F. (1977). Far-Infrared and Submillimeter Observations of the Planets. *Icarus 31*, 315–324.

Macy, W., and Sinton, W. (1977). Detection of Methane and Ethane Emission on Neptune but not on Uranus. *Astrophys. J. 218*, L79–L83.

Morrison, D. (1974). Infrared Radiometry of the Rings of Saturn. *Icarus 22*, 57–65.

Murphy, R. E. (1973). Temperatures of Saturn's Rings. *Astrophys. J. 181*, L87–L90.

Newburn, R. L., and Gulkis, S. (1973). A Survey of the Outer Planets Jupiter, Saturn, Uranus, Neptune, Pluto, and their Satellites. *Space Sci. Rev. 14*, 179–271.

Nolt, I. G., Sinton, W. M., Caroff, L. J., Erickson, E. F., Strecker, D. W., and Radostitz, J. V. (1977). The Brightness Temperatures of Saturn and Its Rings at 39 Microns. *Icarus 30*, 747–759.

Nolt, I. G., Tokunaga, A., Gillett, F. C., and Caldwell, J. (1978). The 22.7 Micron Brightness of Saturn's Rings Versus Declination of the Sun. *Astrophys. J. 219*, L63–L66.

Ridgway, S. T. (1974). Jupiter: Identification of Ethane and Acetylene. *Astrophys. J. 187*, L41–L43.

Rieke, G. H. (1975). The Thermal Radiation of Saturn and Its Rings. *Icarus 26*, 37–44.

Sinton, W., and Good, J. (1977). Saturn: Predicted Seasonal Variation of Thermal Flux. *Bull. Am. Astron. Soc. 9*, 511.

Tokunaga, A., Caldwell, J., Gillett, F. C., and Nolt, I. G. (1978). Spatially Resolved Infrared Observations of Saturn. II. The Temperature Enhancement at the South Pole of Saturn. *Icarus 36*. In press.

Tokunaga, A., and Cess, R. D. (1977). A Model for the Temperature Inversion within the Atmosphere of Saturn. *Icarus 32*, 321–327.

Tokunaga, A., Knacke, R. F., and Owen, T. (1977). 17 - 25 Micron Spectra of Jupiter and Saturn. *Astrophys. J. 213*, 569–574.

Trafton, L. M. (1967). Model Atmospheres of the Major Planets. *Astrophys. J. 147*, 765–781.

Wallace, L. (1975). On the Thermal Structure of Uranus. *Icarus 25*, 538–544.

Wallace, L., Prather, M., and Belton, M. J. S. (1974). The Thermal Structure of the Atmosphere of Jupiter. *Astrophys. J. 193*, 481–493.

Ward, D. B. (1977). Far-Infrared Spectral Observations of Saturn and Its Rings. *Icarus 32*, 437–442.

Wright, E. L. (1976). Recalibration of the Far-Infrared Brightness Temperatures of the Planets. *Astrophys. J. 210*, 250–253.

DISCUSSION

G. ORTON: Do you have any estimate for the effects of this rather high and proportionately very pervasive haze (assumed to be ammonia) in the wavelengths you've been looking at?

It is a very effective absorber and scatterer in certain areas of the 8 to 14 μm region, over and above ammonia vapor absorption. One of my greatest concerns for Voyager is, what is the effect of the phenomena going to be in the far infrared which is really where we would like to get most thermal structure information, hydrogen/helium ratio, etc.

A. TOKUNAGA: We haven't addressed that question. In the 20-μm region, we don't think we see deep enough in the atmosphere of Saturn for ammonia ice opacity to affect our results.

J. CALDWELL: Optical depths in the 20-μm region at the ammonia haze level are at least 3 and typically 10 or more, at least in our model. At 17.8 μm, they're of the order of 10, so you're not seeing the effects of the haze. At very much longer wavelengths, of the order of 40 μm, it's entirely possible that on Saturn ammonia haze is a very strong contributor to the opacity. That may well foul up remote observations.

G. ORTON: I'd like to comment on the fact that we would expect to see large variations in the thermal structure, both at the equator and the pole, because of Saturn's large obliquity and the variation in insolation with time. We would like to see what sort of changes take place, what sort of equilibrium is taking place, as the insolation varies. I can say that in the 12-μm area, comparing observations made last year and this year, there is less limb brightening at the South Pole in the 12.2-μm region.

A. TOKUNAGA: We have somewhat contradictory information on that point in that we made another 12-μm scan a few weeks ago but with a smaller aperture. The brightening is about the same as you see it here. This was done a year ago. March of 1977.

J. CALDWELL: Orton is right that there are large, strong seasonal effects present. There's no indication yet of limb brightening at any wavelength in the northern hemisphere, while there's very strong limb brightening in the southern hemisphere that varies with position.

J. POLLACK: A lot of the far infrared observations that you show have been calibrated on Mars, which has become a popular standard in recent years, and particularly a lot of it has been based on very nice work by Wright (1976, *Astrophys. J. 210*, p. 250). Unfortunately, there may be a problem since Wright and others assumed that except at times of great dust storms, the atmosphere of Mars was essentially clear of dust. We now know from Viking that there is no time of the year in which that assumption can effectively be made, and that has two implications for Mars as a calibration standard in the infrared: (1) The effect of dust in the atmosphere is to reduce the ground temperature during the daytime, and that's the side that you see when you use Mars as a calibration standard. (2) The dust has significant optical depth at, say 20 μm, and will tail off at longer wavelengths, so there is a potential wavelength dependence of brightness temperature as well. I wouldn't rule Mars out as a calibration source, but I think it's going to be a lot harder to standardize.

J. CALDWELL: I think Alan Tokunaga is being a bit modest in assessing the various Saturn models. In Figure 4, the power of the limb scans is sufficient to differentiate between the two in the middle, and, in fact, Tokunaga and Cess are about twice as good as Gautier *et al.*, and in my judgment that is significant. These earlier models, including my own, were done without the limb scans. I don't think the variety you see really represents the uncertainty we now have in the models.

A. TOKUNAGA: In the 17 to 25 μm spectral region we're probing 0.2 atmosphere to about 0.05 atmosphere. We don't have very strong constraints either above or below that region. Observations in the methane band which would be sensitive to higher altitudes would be important, and with longer wavelength observations, longer than 40 μm, we can probe to lower altitudes.

G. ORTON: What is needed to determine a thermal methane/hydrogen ratio? Can we ever get observations far enough out in the wings of the 8 μm methane band, for example, to probe the same depth that can be reached in the H_2 continuum? Limb scans might be a particularly good way to relate these two opacity sources.

J. CALDWELL: If you get too far out on the wings of the methane band you also run into CH_3D opacity.

THE RINGS OF SATURN: STATE OF CURRENT KNOWLEDGE AND SOME SUGGESTIONS FOR FUTURE STUDIES

Jeffrey Cuzzi

Space Science Division, University of California
Berkeley, California

ABSTRACT

In this brief overview, the state of our current knowledge of the properties of the ring system as a whole, and of the particles individually, is assessed. More detailed review papers are cited for further discussion and attention is primarily devoted to recent results and possibilities for exploration of the ring system by a Saturn orbiter. In particular, the infrared and microwave properties of the ring system are discussed. The behavior of the ring brightness is not well understood in the critical transition spectral region from $\sim 100\ \mu$m to ~ 1 cm. Also, the dynamical behavior of the ring system is discussed. Recent theoretical studies show that ongoing dynamical effets continually affect the ring structure in azimuth (possibly producing the A ring brightness asymmetry) and in the vertical direction (possibly preventing the rings from flattening to a monolayer).

Orbital spacecraft-based studies of the rings will offer several unique advantages and impact important cosmogonical questions. Bistatic radar studies and millimeter-wavelength spectrometry/radiometry will give us the particle size and composition limits needed to resolve the question of the density of the rings, and provide important boundary conditions on the state of Saturn's protoplanetary nebula near the time of planetary formation.

Detailed study of the radial structure of the rings near resonance "gaps" will shed light on the whole question of ring formation and in a larger sense on planetary formation as influenced by dynamical effects. The recent discovery of the rings of Uranus further motivates such dynamical studies. Topics which would benefit from further study, either from spacecraft or from Earth, are noted.

I. INTRODUCTION

Due to their great beauty and uniqueness, the rings of Saturn have been studied as much or perhaps more in the past than Saturn itself. Their scientific importance is in fact also quite great. Trapped within the Roche limit of Saturn by the gravitational perturbations of the satellite Mimas, the ring particles have been unable either to escape or to accrete into a large body. Thus, if the rings formed in their current place, they represent a practically untouched remnant of the protoplanetary nebula, a direct condensate unaffected by thermal, chemical, or impact metamorphosis. However, it is also possible that the rings formed through tidal breakup of a pre-existing comet or satellite. Knowledge of the size distribution and bulk composition of these particles could permit final discrimination between these two origin hypotheses. For instance, the existence or absence of kilometer-sized "particles" would permit or disprove the breakup hypothesis. Even the bulk composition of the particles has not been definitely established. Current work indicates that cosmogonically plentiful ices could compose the bulk of the ring material. However, fairly pure metal may not as yet be ruled out. Thus, study of the rings could provide valuable constraints on theories of Solar System origin and evolution. In Section II the global structure of the rings (radial, vertical, azimuthal) is reviewed. In Section III current knowledge of particle size and composition is discussed. In Section IV likely advances due to Pioneer, Voyager, and interim Earth-based studies are mentioned. In Section V, important scientific questions will be presented which are appropriate for study by SOP[2]. This brief paper will only touch the surface of existing research on Saturn's rings. For further background, the reader is referred to review papers by Bobrov (1970) Cook, Franklin, and Palluconi (1973), and Pollack (1975).

II. OVERALL PHYSICAL STRUCTURE OF THE RING SYSTEM

Radial Structure

The ring system exhibits obvious radial structure which has evolved a particular nomenclature. Currently accepted values for, and uncertainties in, ring element boundaries are given along with standard nomenclature in Table 1. Below we discuss

Table 1. Ring Element Boundaries (After Cook *et al.*, 1973)

Ring Region	Boundaries Radius (km)	Planetary (Equatorial) Radii*	Arc sec at 9.5388 AU
A Outer	137,400 ± 700 (est)	2.29	19.52" ±0.1" (est)
A Inner	121,800 ± 700	2.03	17.57" ±0.1" (est)
Cassini Division: Width	4,800 ± 700	0.08	0.7"
B Outer	117,000 ± 700	1.95	16.87 ±0.1" (est)
B Inner	91,800 ± 700	1.53	13.21 ±0.1" (est)
C Inner	72,600 ± 1,400	1.21	10.5 ±0.2"

*R_e = 8.65" ±0.02 at 9.5388 " (Cook *et al.* 1973)

= 6×10^4 km (Dollfus 1970)

the radial structure in some detail and then review currently accepted values for optical depth of the rings at visible wavelengths as a function of radial distance.

1. Mechanisms governing radial structure.

   The most likely explanation for the radial structure of the rings is that it arises from the effects of gravitationally induced perturbations in ring particle orbits which lie near commensurability with Mimas, one of Saturn's smaller satellites (see, e.g., Franklin and Colombo, 1970). The perturbation characterizing commensurability increases the eccentricity of the "resonant" particle until a collision removes the particle from the resonant orbit. Thus such commensurate orbits are unstable. This simple explanation serves very well to explain the inner and outer boundaries of the ring system. Given that only empty space exists beyond the resonance in either case, the collision which removes the particle from its unstable orbit is most likely to be with another particle *within* the rings and in such a case the final orbit will be more likely *within* the ring boundary than *beyond* the ring boundary. In this way the resonances are seen to present at least partially effective barriers to mass flow. The inner edge of the B ring, inner edge of Cassini's division, and the outer

edge of the A ring represent such unstable orbits with periods equal to 1/3, 1/2, and 2/3 of the period of Mimas, respectively. The real radial brightness distribution is, of course, more complex (see Figure 1). However, the picture is more complex regarding the widths of the resonances.

2. Gaps within the rings

It has been recently realized (Greenberg and Franklin 1977) that the above mechanism will "clear out" only a region of radial extent ≤ 30 km, much less than the observed width of the Cassini division (see Table 1). Particles moving under the resonance, but more than ~30 km distant from it, do so "in phase" in their orbits and do not collide. Several mechanisms have been proposed to explain the observed width. Goldreich and Tremaine (1978) suggest that a density wave, induced at the resonances, travels outward and decreases the angular momentum of particles in a range which agrees well with the width of Cassini's division. Cook (1978) suggests that the system is evolving radially outwards, due possibly to magnetic or gaseous drag. High-quality observations near the edges of all the resonances and within Cassini's division will be necessary to supply further constraints on these hypotheses.

3. Optical depths in the rings

The optical depth, τ_o, provides an important boundary condition relating particle volume densities to particle sizes. By definition,

$$\tau_o = \iint n(r, z)\, \pi\, r^2 dr dz$$

where r is particle radius and n(r, z) is volume density. The normal optical depth of the rings, τ_o, varies significantly with radial distance from the planet. Values of τ_o have been obtained by two general methods: transmission of light through the rings ($I_{trans} = I_{inc}\, e^{-\tau_o/\cos\theta}$), where θ

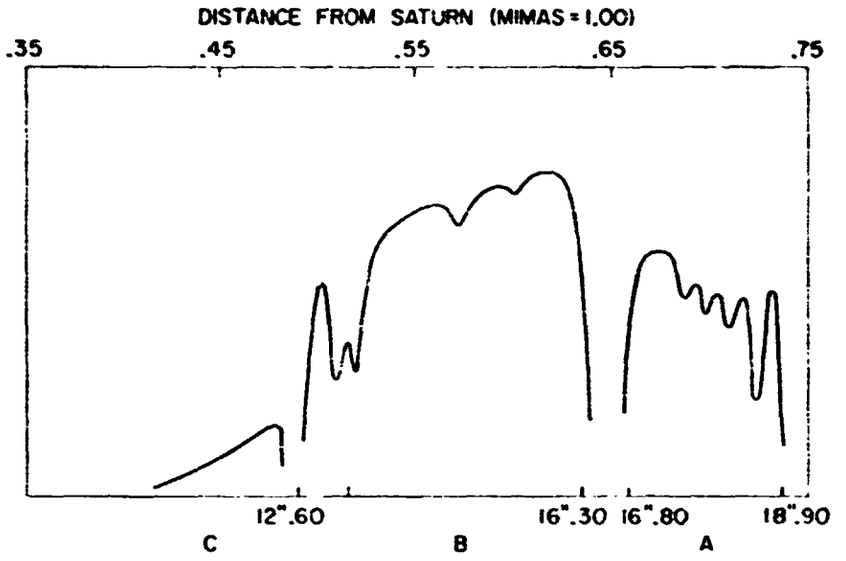

Figure 1. Brightness of the ring system as a function of radial distance from the center of Saturn at 10 AU (Dollfus 1970).

is the angle from the ring normal, and reflection of light from the rings. The former method is more direct as fewer assumptions about the ring structure, particle albedos, and phase functions are required. However, most quoted values have been obtained from the latter method, in which a simple scattering-layer model is used to calculate reflected brightness. Using the variation of brightness with tilt angle, one solves for both a particle albedo and local optical depth. Uncertainties in the optical depths so obtained may be quite large and the values themselves may be systematically low (Pollack, 1975; Cuzzi and Pollack 1978). Best current values for optical depth as a function of radial position are given in Figure 2 along with their sources and likely uncertainties. The optical depth of the Cassini Division is highly uncertain due to the many difficult and important corrections which must be applied to observations (smearing, scattered light, etc.) These values are azimuthal averages. Azimuthal variations are discussed below.

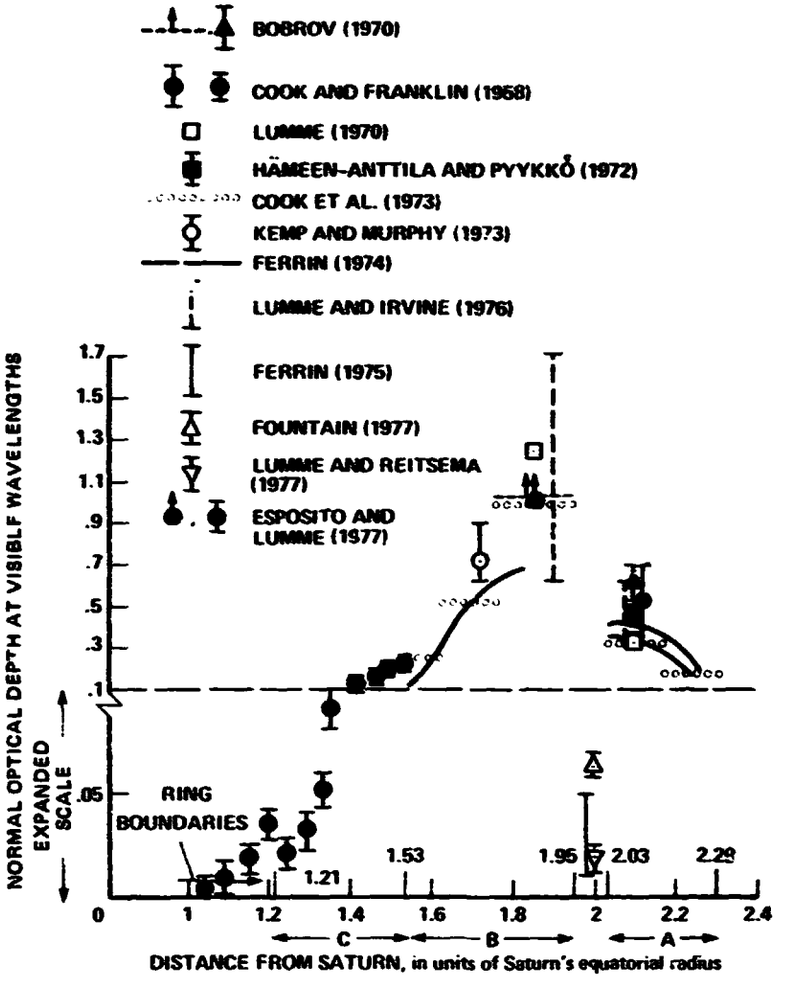

Figure 2. A comparison of several estimates of the optical thickness of the rings as a function of radial distance.

Vertical and Azimuthal Structure

The vertical and azimuthal structure are related in that they both deal with the local "internal" structure of the rings; that is, whether the rings are one particle thick (a "monolayer") or are many particles thick.

Perhaps the most significant observation constraining this question is the phase effect of the rings (see Figure 3). The net increase in brightness (about a factor of two) over 6° of observable phase is similar in magnitude to the lunar opposition brightening. Both arise from the fact that shadowing of particles in the lit surface by

each other ceases rapidly as the directions to Sun and Earth become coincident at zero degrees phase angle. Detailed analyses of the effect for the rings (Irvine 1966, Bobrov 1970, Kawata and Irvine 1974) yield a volume density of particles $\sim 10^{-2}$ to 10^{-3} in a many-particle thick ring (see Figure 4), far lower than the lunar soil volume density (Hämeen-Anttila and Vaaraniemi 1975) and characterizing a layer containing particles which are separated by many times their own radius.

Until recently, dynamical arguments (Jeffreys 1947) indicated that inter-particle collisions would cause the rings to flatten and spread to a monolayer. This would require the opposition effect to arise from surface microstructure. However,

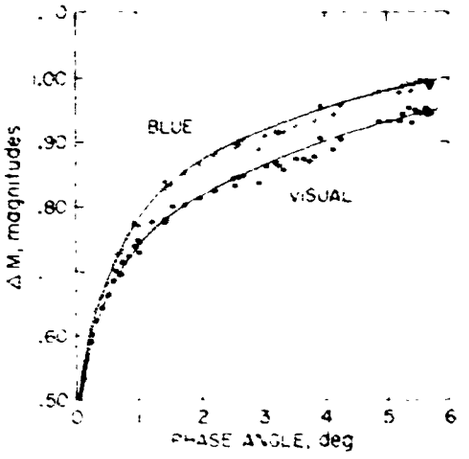

Figure 3. Phase curve for Saturn's B ring showing relative brightness, in magnitude units, as a function of phase angle, in degrees. From Franklin and Cook (1965).

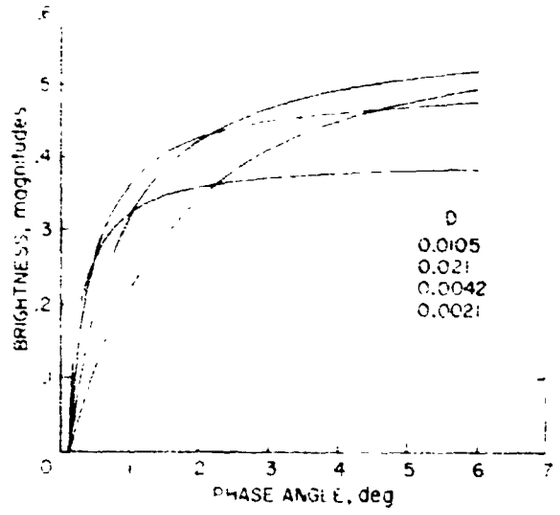

Figure 4. Theoretical curves for first-order scattering by a many-particle-thick ring with optical depth unity, and a ring tilt angle of 25°. The curves are labeled by the value of ring volume density. From Kawata and Irvine (1974).

recent studies of energy sources within the ring system (differential rotation, Mimas) indicate that a finite thickness may be maintained (Brahic, 1977; Goldreich and Tremaine, 1978a; Cuzzi *et al.*, 1978). The characteristic thickness is on the order of a few times the size of the largest particles. Should the rings also include a substantial number of much smaller particles, they would be "many particles thick." We return to this in Section III. In addition, other natural high-albedo surfaces (e.g., the Galilean satellites) show much less dramatic opposition effects (see Figure 5) than do the rings. The opposition effect for these objects, due to surface microstructure, is probably smaller due to particle transparency and multiple scattering. These, as well as other such observations, such as the color dependence of the opposition effect and of polarization, favor the many-particle-thick hypothesis slightly over the monolayer hypothesis (Pollack 1975).

The absolute thickness of the rings has not been observationally established. Observations at the time when the rings appeared edge on (Focas and Dollfus, 1969; Kiladze, 1969; Bobrov, 1970) have been recently re-analyzed (Lumme and Irvine, 1977) with the result that they appear to give only an upper limit of 3 km full thickness. The true thickness characterizing macroscopic particles is almost certainly two orders of magnitude smaller, if the rings are of the age of the solar system (Brahic, 1977; Goldreich & Tremaine, 1978a; Cuzzi *et al.*, 1978). However, radiation pressure could cause micron-sized particles to have vertical excursions as large as a kilometer (Vaaraniemi, 1973).

The rings present an interesting environment for horizontal structural variations as well. Gravitational perturbations by Saturn's satellites will theoretically produce a ripple, or wave, with largest components due to Titan, the Sun, Tethys and Mimas. Orbiting particles will attain vertical excursions as large as ~10 m or so, adjacent particles moving coherently in "roller-coaster" fashion (Burns *et al.*, 1978).

In addition it has been recently confirmed by several groups (Lumme and Irvine 1976; Reitsema, Beebe, and Smith, 1976) that Saturn's A ring exhibits azimuthal variations in brightness (see Figure 6). The amplitude of the effect is ~10% at maximum ring opening (26°) and increases slightly (to 15%) as the rings close to 16° (Lumme *et al.*, 1977). The "sign" of the effect (bright quadrants precede conjunctions) is not related to the position of the Sun or Earth, but the amplitude of the effect decreases at opposition (Lumme *et al.*, 1977). The effect is not shown by the B ring. Two classes of hypotheses have been advanced to account for the effect. One class invokes some use of large, synchronously rotating bodies which are either elongated or

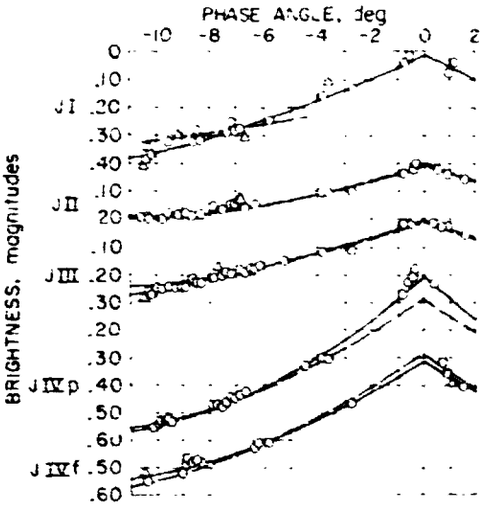

Figure 5. Phase curve for the Galilean satellites, JI, JII, JIII, and JIV. From Stebbins and Jacobsen (1928).

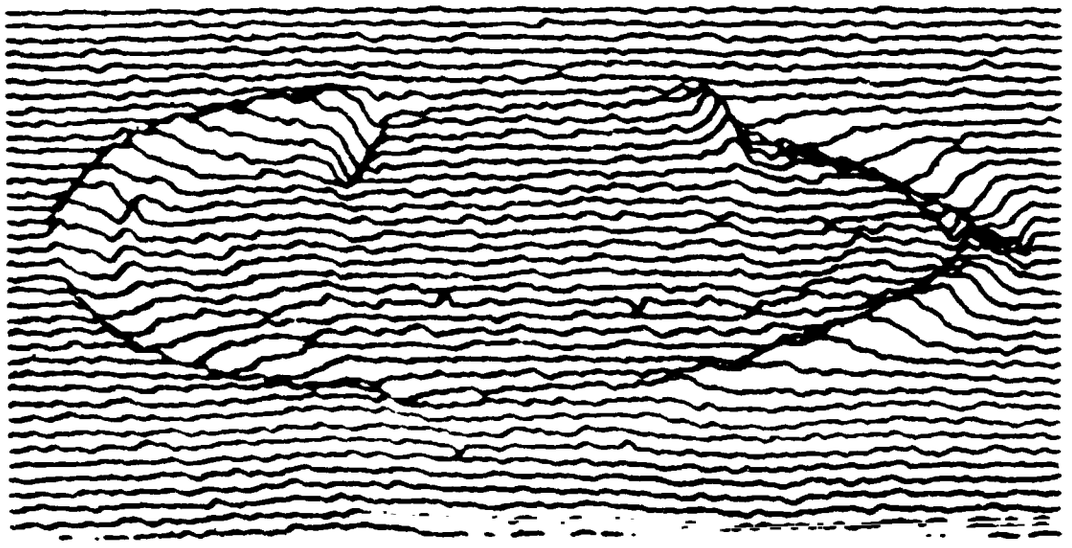

Figure 6. Quadrant asymmetry in the brightness of Saturn's A ring derived from a digitized Saturn image of 1977 January 26. Pseudo 3D plot shows the brightness when a mirrored image (left for right) is subtracted from the original. Upper left and lower right quadrants of the A ring are maxima, while the upper right and lower left are minima (thus). East is to the right, and orbital phase angle increases clockwise). Shadow of planet on ring visible in upper portion. From Lumme et al. 1977.

asymmetrically reflective (Lumme and Irvine 1976, Reitsema *et al.*, 1976). The other class invokes transient, gravitationally induced, "clumping" of swarms of small particles in trailing "wakes" (e.g., Colombo, *et al.*, 1977). The predominance of very large (many-meter) particles in the rings is not in good agreement with microwave results discussed in Section III. Therefore some variant of the "clumping" hypothesis is favored.

Summary

The radial structure of the rings is determined primarily by orbital resonances with Mimas. The width of the Cassini Division is not completely understood, but may reflect the presence of a density wave driven by Mimas. The large opposition effect of the rings and other optical effects continue to favor the hypothesis that the rings are many particles thick, although some contribution from surface microstructure undoubtedly does exist. Dynamical arguments, including likely sources of particle random motions, are now apparently consistent with the many-particle-thick idea as well. However, the true "thickness" may in fact be no more than some tens of meters. A monolayer hypothesis would imply that the individual "particles" are many meters in size and, at least in the A ring, in synchronous rotation.

III. RING PARTICLE PROPERTIES

A full treatment of the great quantity of material dealing with particle properties such as narrowband and broadband geometric albedo, phase function, surface vs. bulk composition, and particle size is beyond the scope of this summary. In this article only a brief review of known or inferred particle properties is given. The reader is referred to review articles by Cook, Franklin, and Palluconi (1973), and Pollack (1975) for fuller details of the observations and their significance.

Particle Albedos and Temperatures

1. Albedos.

   The particle albedos ($\tilde{\omega}_0$) must be obtained simultaneously with ring optical depths by solving the multiple scattering problem and matching data such

as the phase variation, tilt variation, and absolute value of the ring reflectivity. Many authors have approached this problem, usually by assuming isotropic scattering. The most sophisticated recent analyses, which include the use of both isotropic and anisotropic scattering phase functions, indicate that isotropic scattering is not consistent with the data (Kawata and Irvine, 1974, 1975; Esposito and Lumme, 1977). Particle albedos obtained in these analyses are shown for the brightest parts of the A and B rings in Table 2. The best-fit phase function is somewhat, but not strongly, backscattering, with derived values of the phase integral g ranging from ~0.9 to 1.6 (Lumme and Irvine, 1976; Esposito and Lumme, 1977). This value represents a surface intermediate between a Lambert surface and the lunar surface in degree of backscattering, similar to the characteristics of typical snowbanks (Veverka, 1970). The large range of allowed values of g and $\tilde{\omega}_o$ is due in part to the very small range of observable phase angles.

2. Particle temperatures.

Thermal balance calculations giving the physical temperature of the ring particles are quite complex in the case of the rings because of: (a) The gradient in insolation with optical depth in the rings and the associated diffuse radiation; (b) Heating of particles by the infrared emission of other particles; and (c) Heating of particles by emission from Saturn. In addition, the variation of (a) with ring tilt angle must be considered. These calculations have been carried out by Kawata and Irvine (1975), for likely upper and lower limits of bolometric Bond albedo $A_B = 0.54$ and 0.38 respectively. In addition to the uncertainties in Bond albedos at blue and visual wavelengths mentioned above, the large uncertainty in albedo from 0.7-1.1 μm wavelengths leaves the bolometric Bond albedo quite uncertain. The results (see Figure 7) are grossly consistent with thermal infrared observations (see Table 3 and Morrison, 1976) but, for the more realistic case $A_B \sim 0.5$, calculated temperatures are somewhat lower than recent observations. More study and better observations of the rings over a wider range of wavelengths and phase angles (i.e. from an orbiter) could help greatly to resolve this apparent discrepancy.

Table 2. Albedos at the Brightest Part of Each Ring Element

Ring Element	Mean Radius/R_E	λ	p	q	$\tilde{\omega}_o$	Source
A	2.10	V	1.1	0.57*	0.63	Cook *et al.*, 1973
		V	0.48-0.61	1.57	0.75-0.95	Esposito & Lumme, 1977
		V	0.72 ± 0.05	1.0-1.5	0.5-1.0	Lumme & Irvine, 1976
		V	---	---	0.75	Kawata & Irvine, 1976
		V	0.64 ± 0.04	1.0-1.5	0.8-1.0	Lumme & Irvine, 1976
B	1.85	V	1.1	0.57*	0.63	Cook *et al.*, 1973
		V	0.51-0.61	1.57	80-0.95	Esposito & Lumme, 1977
		B	0.86	0.57*	0.49	Cook *et al.*, 1973
		B	---	---	0.48	Kawata & Irvine, 1975

*Assumed value

Spectral Observations and Compositional Implications

Water ice was first identified in the rings by Pilcher *et al.* (1970), and Kuiper *et al.* (1970) using 1-3 μm spectroscopy (see Figure 8). The shapes of the spectral features in this region vary both with temperature (Kieffer 1974, Fink and Larson 1975) and particle size (Pollack *et al.* , 1973). Pollack *et al.*. 1973, used this effect to infer the grain size of the ice particles doing the absorbing to be ~ 30-40 μm (see Figure 9). As discussed in section C below, this is probably the size of individual grains on the surfaces of much larger particles. The variation of ring reflectivity over the entire visible-near IR range, however, (Lebofsky *et al.*, 1970), is not consistent with a pure water ice composition, which would have constant reflectivity in the 0.3-1.0 μm region. In fact, the spectral reflectivity of the rings (see Figure 10) closely resembles that of Jupite 's innermost (and highly reddened) satellite Io (Johnson and McCord, 1970) in overall behavior. The spectra of the A and B rings are quite similar. This

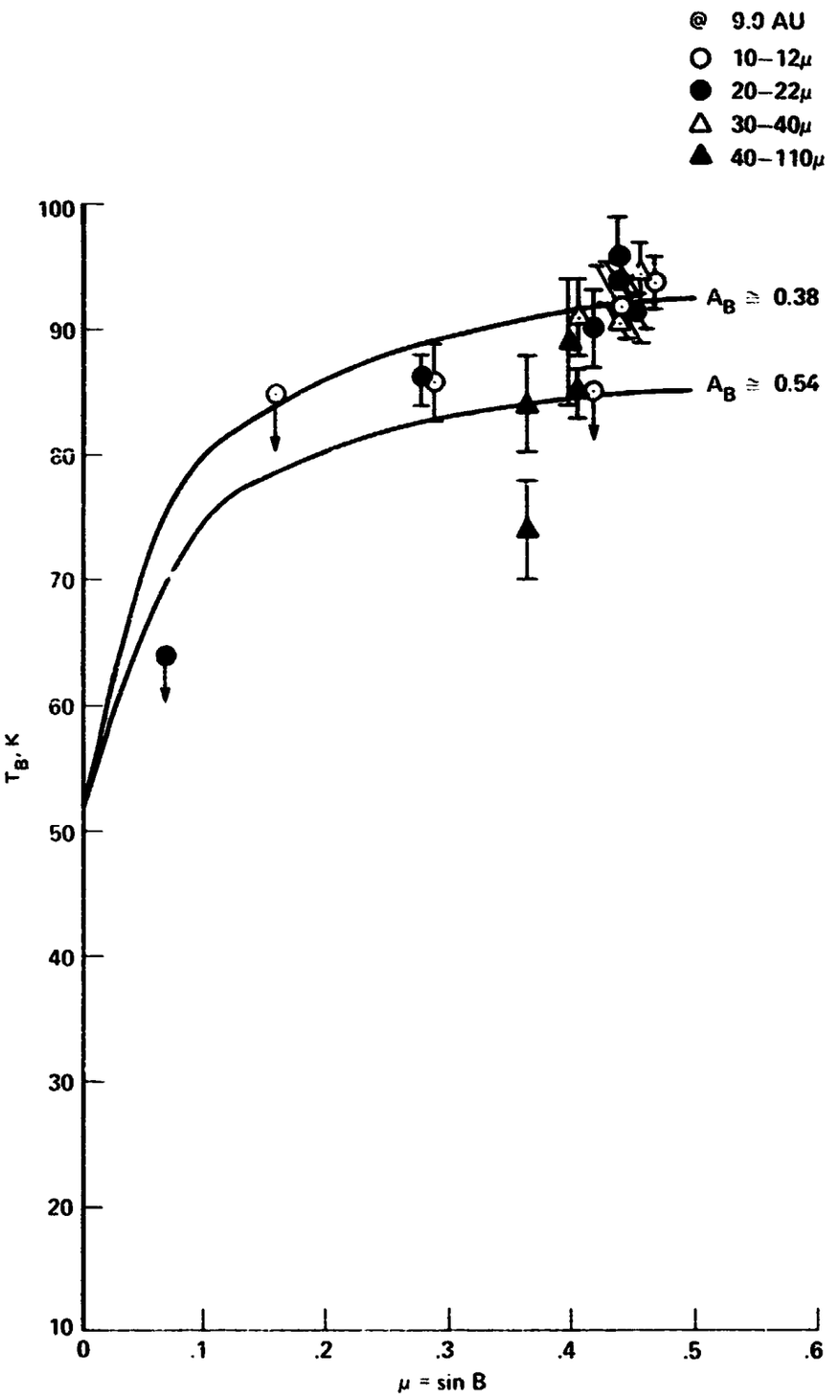

Figure 7. Calculated infrared brightness of Saturn's B ring as a function of ring tilt angle for two choices of particle Bolometric albedo, from Kawata and Irvine (1975). Observations from Table 3 are plotted, normalized to a heliocentric distance of 9.0 AU.

Table 3. Observations of the Brightness Temperature of the B Ring in the Thermal Infrared*

Year	λ, μm	T_B (B ring), K	Tilt Angle, B	Observers
1964	10	<85	~9°	Low (1965)
1965	21	<64	~4° ± 1°	Low (unpublished)
1969	12	86 ± 3	17°	Allen & Murdock (1971)
1971	20	90 ± 3	25°	Murphy *et al.* (1972)
1971	11	<85	11	Armstrong *et al.* (1972)
1971-72	45-80	85 ± 7	255°	Armstrong *et al.* (1972)
	65-110	89 ± 5	255°	Wright (1976) recalib.
1972	20	94 ± 2	26°	Murphy (1973)
1973	20	96 ± 3	26°	Morrison (1974)
1973	11	92 ± 3	26°	Morrison (1974)
1973	35	92-97	26°	Nolt et al (1974)
1973	~33	91 ± 2	26°	Rieke (1975)
1974	~11	94 ± 2	26°	Rieke (1975)
1974	~22	91.5 ± 1	26°	Rieke (1975)
1975	39	91 ± 3	24.5°	Nolt *et al.* (1977)
1976	45-80	84 ± 4	21.8°	Ward (1978)
	65-110	74 ± 4		
1977	22.7	86 ± 2	16°	Nolt *et al.* (1978)

*Corrected to heliocentric distance of 9.0 AU

reddening effect is not understood, but could be due to trace impurities (sulfur? phosphorus? Axel dust?) and/or the effect of charged particle bombardment on the ice lattice (Pollack, 1975). An even stronger reddening is seen in the spectrum of Titan (see Figure 11). The existence of water ice comes as no surprise due to its abundance and stability compared to methane and ammonia ice in the outer solar system. Hydrate clathrates of methane or ammonia with water ice are also possible (Miller, 1961). Their existence has not yet been established observationally, as near-IR spectra (Smythe, 1975) do not distinguish water ice from clathrates. Spectra at longer wavelengths, however, (Bertie *et al.*, 1973) could be quite useful.

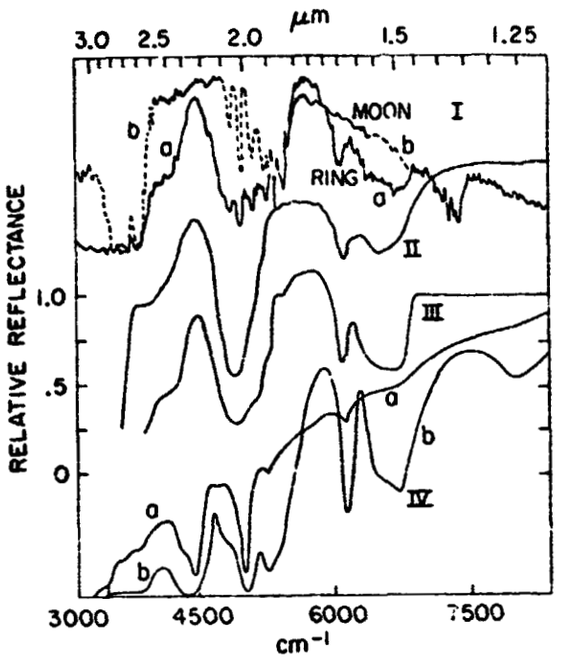

Figure 8. Comparison of the reflectance spectra for H_2O and NH_3 frosts and Saturn's rings. (Ia): The Saturn ring spectrum of Kuiper et al. *(1970) (Ib): Lunar comparison spectra; (II): Fine-grained H_2O frost spectrum; (III): Spectrum of the rings divided by that of the moon; (IV): NH_3 frost, fine grained, a; coarse grained, b. From Pilcher* et al. *(1970).*

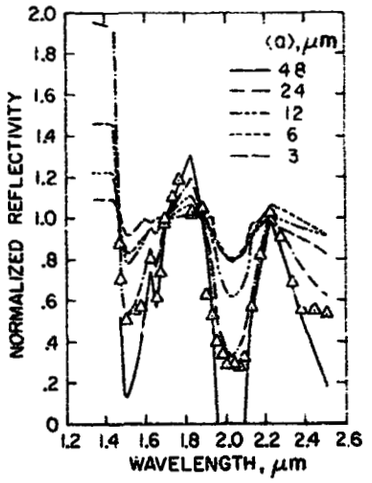

Figure 9. Comparison of the reflectivity spectrum of the rings (triangles) with theoretical curves for the reflectivity behavior of a water frost surface characterized by a mean given radius (a). The observed values were obtained from Kuiper et al. *(1970). From Pollack* et al. *(1973).*

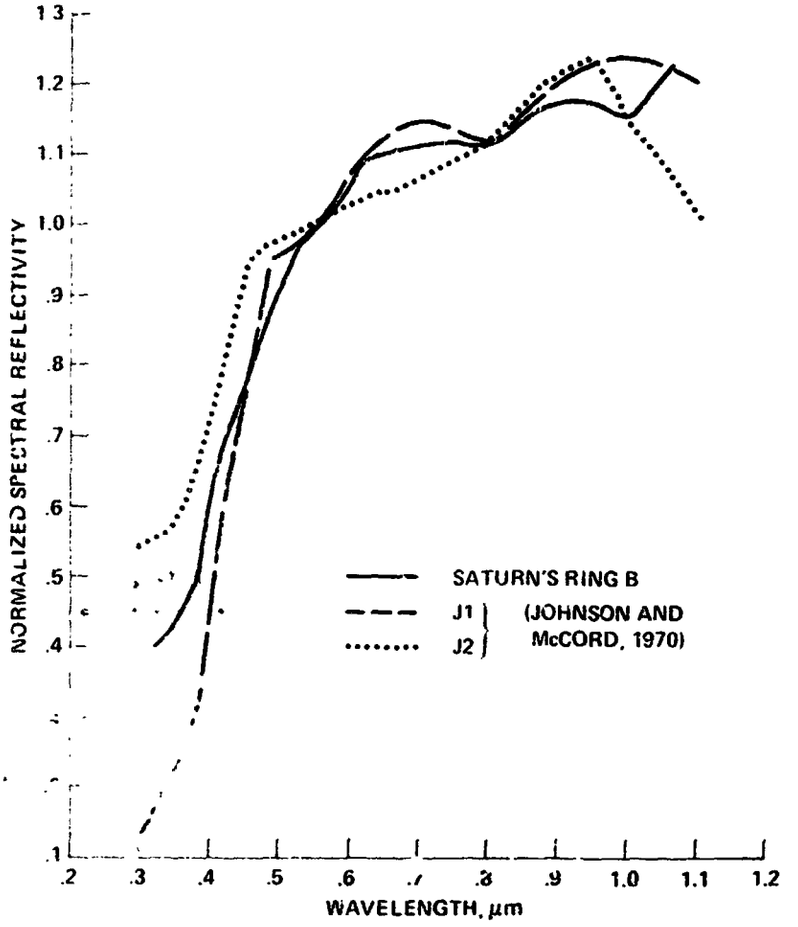

Figure 16. The normalized spectral reflectivity of Saturn's B ring is shown, compared with spectra of J1 and J2. From Lebofsky et al. *(1970).*

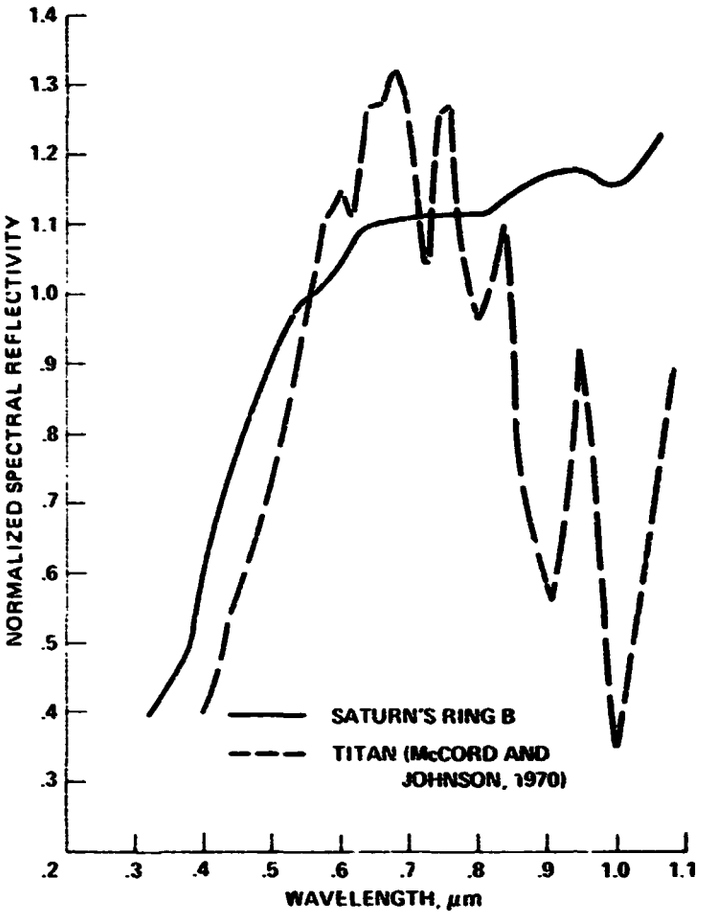

Figure 11. The spectral reflectivity of Saturn's B ring is shown along with the spectral reflectivity of Titan. From Lebofsky et al. (1970).

The above observations sample only the surface layers of the ring particles, and do not constrain the bulk particle composition. Observations at microwave wavelengths sample depths of centimeters to meters, giving a better idea of the bulk composition. However, particle size effects may be significant at these longer wavelengths. Therefore, we discuss these two aspects simultaneously below.

Particle Size Distribution and Composition as Constrained by Microwave Observations

The brightness temperature of the rings at wavelengths ≥ 0.86 cm is $\leq 10 \pm 3$ K, significantly lower than their physical temperature of 95 K or so. This result comes from current model analysis (Cuzzi and Pollack, 1978) of published interferometric (high resolution) observations (Briggs, 1974; Cuzzi and Dent, 1975; Janssen and Olsen, 1974). Recent interferometer maps of the rings (Muhleman *et al.*, 1976, Schloerb, 1977) are in agreement with this low, but non-zero, ring brightness. The low temperature is due to an emissivity effect, as the optical depth of the rings at centimeter-decimeter wavelengths is comparable to its value at visible wavelengths based both on the above observations and on the high radar reflectivity of the rings (Goldstein and Morris, 1973; Goldstein et al., 1977). In fact, for the high reflectivity implied by the radar observations, it is not difficult to show that most, if not all, of the microwave brightness of the rings is scattered radiation from the planet, and not "emission" at all. At longer wavelengths, the rings seem colder (Berge and Muhleman, 1973; Briggs, 1974; Jaffee. 1977) and perhaps less optically thick.

Two possibilities exist for the low emissivities. First, the bulk material of the particles could have an intrinsically low emissivity. To match the observations by this "compositional" means alone for particles much larger than the wavelength in size, nearly pure metallic particles or particles possessing dielectric loss orders of magnitude lower than the least lossy of naturally occurring materials (ices) would be required. Second, as pointed out by Pollack *et al.* (1973) particles of size comparable to a wavelength may have extremely low emissivity, and yet high scattering efficiency, in the presence of a realistic value of dielectric loss such as possessed by ices. Using radio brightness limits and the observed radar reflectivity at two wavelengths, 3.5 and 12.6 cm, Pollack (1975) and Cuzzi and Pollack (1978a, 1978b) have set constraints on the possible particle size distribution and composition using realistic scattering models. First, silicates are excluded except possibly as a minor (<10% by mass) constituent of the particles. Second, water ice (or clathrate) particles with radii distributed following a power law distribution $n(r) = n_0 r^{-3}$ for $1\ \text{cm} \lesssim r \lesssim$ several meters could satisfy the observations if distributed in a many-particle-thick layer (see Section II). The upper limit on r here depends on the value of dielectric loss for the ice at 100 K and is not known to better than a factor of three or so (Whalley and Labbé, 1969). Third, an optical depth ≥ 1.5 at visible wavelengths in the thickest part of the B ring is indicated. Fourth, metallic particles larger than a

centimeter in radius are still a possibility. Fifth, very large (many-meter) particles of very low density ($\lesssim 10^{-1}$ g cm^{-3}) with subsurface scatterers of the composition and sizes discussed above could also satisfy the existing observations based on analogy with the high radar reflectivity and depolarization characterizing the Galilean satellites (Campbell *et al.*, 1977; Ostro and Pettengill, 1977). Some of the results leading to these constraints are shown in Figures 12-14, and these results are summarized in Table 4. The important aspects of the radar observations are their high absolute value and depolarization, and apparent wavelength independence.

Another point of interest is that the radial variation of radar reflectivity is in fairly good agreement with the radial variation of visible depth (Pettengill *et al.*, 1977). A corollary of the microwave results is that the fraction of the rings (by surface area) composed of particles smaller than a centimeter or so must be quite small. This result is in good agreement with the results of analysis of eclipse cooling of the particles by Aumann and Kieffer (1973) and observations by Morrison (1974) that the particle size is greater than about 1.5 cm. These results are also in agreement with the likely structure of the ring as discussed in Section II and with the expected lifetime of small particles against Poynting-Robertson drag. However, one should not be surprised to find some small particles ($\ll 1$ cm in size) in the rings, possibly being continually produced in collisions.

The rings are largely unobserved in the interesting transition wavelength range between 100 μm and 1 cm within which the temperature drops from ~90 K to ~10 K. Far-infrared observations (about 10-400 μm) over the last ten years appeared to show a clear contribution from the rings at their physical temperature (see Table 5). In addition, observations of Saturn relative to Jupiter at ~1 mm wavelength (Low, 1966; Rather *et al.*, 1975) appeared to show some ring contribution at a brightness temperature of 30-40 K. However, recent observations are not in agreement with these results. From a scan of Saturn at 400 micrometers, it appears that the brightness of the rings is less than 0.35 of the disk brightness (Werner, private communication). Also Werner *et al.* (1978) see no evidence for excess flux due to the rings (in an unresolved observation comparing total flux with Jupiter) at 1 mm wavelength. These important short wavelength observations will become more difficult as the solid angle of the rings decreases further in coming years, but will be essential to understanding the composition and size distribution of the ring particles.

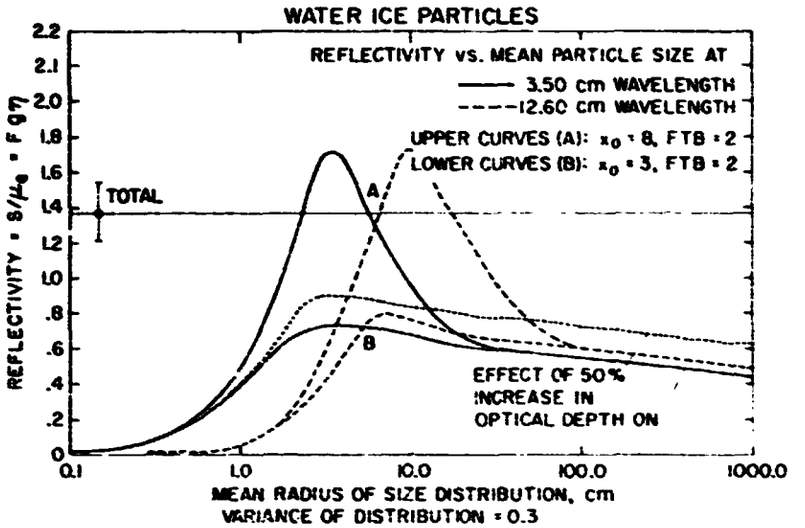

Figure 12. Comparison of observed radar reflectivity with the calculated reflectivity of a many-particle-thick layer with a relatively narrow size distribution. The parameters x_0 and FTB characterize scattering by nonspherical particles and are fairly typical values for rough (x_0 = 3) and smooth (x_0 = 8) particles respectively. From Cuzzi and Pollack (1978).

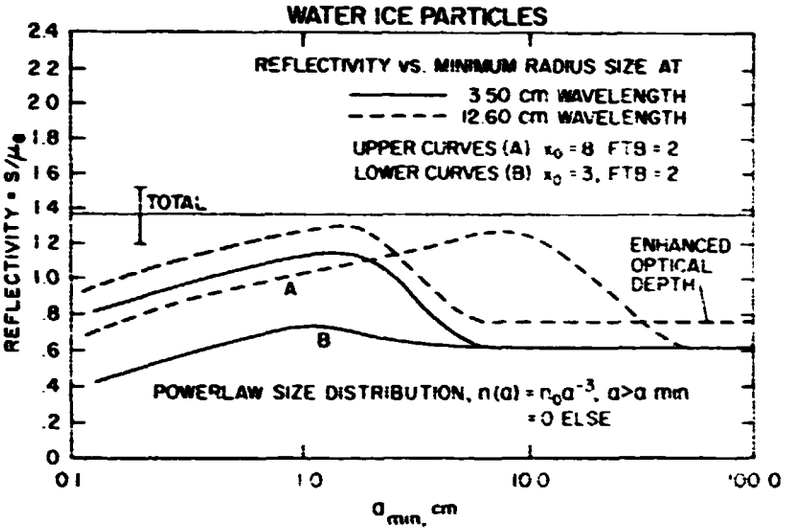

Figure 13. Comparison of observed radar reflectivity with the calculated reflectivity of a many-particle-thick ring layer composed of ice particles with a broad (power law) size distribution. From Cuzzi and Pollack (1978).

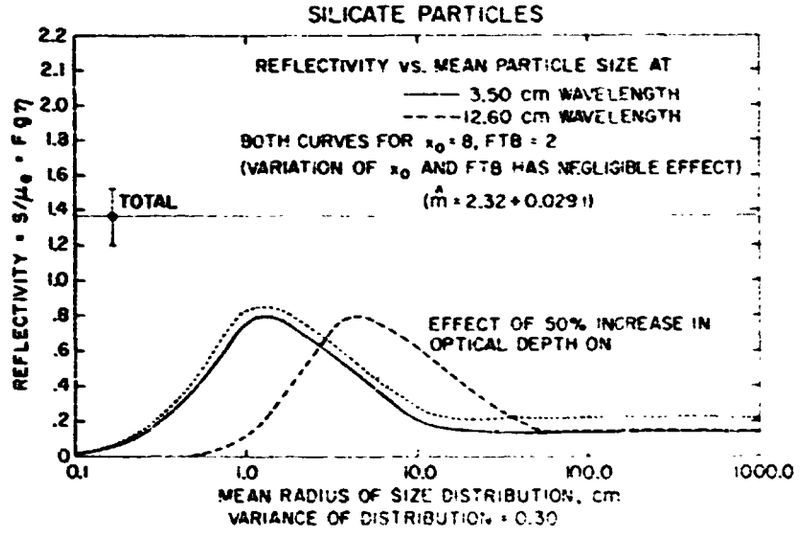

Figure 14. Comparison of observed radar reflectivity with the calculated reflectivity of a many-particle-thick ring layer composed of silicate particles. From Cuzzi and Pollack (1978).

Table 4. Acceptability of Ring Models of Different Structure, Composition, and Particle Size

Model Structure	Particle Composition: Ice	Rock	Metal
Extended layer:			
A: $a << \lambda$ ($a < 1$ cm)	No, due to low net reflectivity and strong λ-dependence	No, due to low net reflectivity and strong λ-dependence	No, due to strong λ-dependence
B: $a \gtrsim \lambda$ (narrow size distribution)	Possible ($\bar{a} = 6 \pm 1$ cm only)	No, due to low net reflectivity	Possible
C: $a >> \lambda$ ($a > 1$ m) (narrow size distribution)	No, due to low net reflectivity	No, due to low net reflectivity	Possible
D: Power law ($a > 1$ cm) $n(a) = n_o a^{-3}$	Possible	No, due to low net reflectivity	Possible
Monolayer:			
A: $a << \lambda$ ($a < 1$ cm)	No, due to low net reflectivity and strong λ-dependence	No, due to low net reflectivity and strong λ-dependence	No, due to strong λ-dependence
B: $a \gtrsim \lambda$ ($a > 1$ cm)	Unlikely, due to low depolarization	Unlikely, due to low depolarization	Unlikely, due to low depolarization
C: $a >> \lambda$ ($a > 1$ m) (narrow size distribution)	Possible (multiple internal scattering)	No, due to low net reflectivity	Unlikely, due to low expected depolarization
D: Power law ($a > 1$ cm) $n(a) = n_o a^{-3}$	Unlikely, due to low depolarization	No, due to low net reflectivity	No, due to low net reflectivity

Table 5. Far Infrared Observations of Saturn and Its Rings: Variation of Net Flux Coming from Disk Using Values of Disk T_B Derived on Two Different Assumptions
F1: T_B obtained assuming no flux from rings.
F2: T_B obtained assuming rings & disk of equal temperature

Date	Tilt Angle	Area (Disk + Rings)/Area (Disk)	$\left(\frac{F_1 \text{ (date)}}{F_1 \text{ (1968)}}\right)$	$\left(\frac{F_2 \text{ (date)}}{F_2 \text{ (1968)}}\right)$	Source
Dec. 1968 (1-350 μm)	-11°	1.0	1.0	1.0	Aumann *et al.* (1969)
Winter 1975-76 (40-300 μm)	-21°	1.6	1.5 ± 0.3	1.0 ± 0.1	Loewenstein *et al.* (1977)
(100-400 μm)[b]			1.8 ± 0.1[b]	0.93 ± 0.03	
Oct. 1971 (30-300 μm)	-24°	1.8	1.7 ± 0.1	1.0 ± 0.1	Armstrong *et al.* (1972) and
(125-300 μm)[b]			2.0 ± 0.1[b]	0.97 ± 0.03	Wright (1976)
Winter 1973-74 (300-500 μm)[b]	-26°	1.9	1.9 ± 1[b]	0.9 ± 0.1	Hudson *et al.* (1974)

a) approximate correction for ring blockage by planet included.
b) Rayleigh-Jeans limit assumed in scaling temperature to flux.

Summary

The albedos of the ring particles are somewhat uncertain, but quite high ($\tilde{\omega}_o \gtrsim 0.8$) at blue and visible wavelengths. The scattering phase function is fairly backscattering, but not as highly backscattering as that of the lunar surface. These properties are similar to those of typical snowbanks. Particle temperatures calculated for a range of values for the bolometric albedo consistent with the above results decrease with ring tilt angle as observed, but seem slightly low (5-10 K) with respect to observations in the thermal IR. Water ice (and possibly clathrate hydrates) apparently constitutes the major part of the ring material, although ice-coated metal may not be ruled out on the basis of existing infrared, radio, or radar observations.

Metal may, however, be regarded as unlikely both on grounds of cosmic abundance and on grounds of its high density. If the ring particles were of metal, the Roche limit would lie well within the rings and accretion could proceed. Also, the

net ring mass based on the observed volume density would very likely be so large as to cause a noticeable discrepancy in the location of Cassini's division (see Section II).

It appears that the particles must be larger than a centimeter or so in size. A very broad size distribution, possibly $n(r) = n_o r^{-3}$, is consistent with all existing data if the largest particles are several meters in radius. Such a situation would explain the probable ring "many-particle" thickness and azimuthal variations (Section II) as well, in terms of dispersion of the numerous small particles by the few large ones. Another possibility is that the "particles" are much larger, with internal scatterers of centimeter-to-meter size fixed in a low-density matrix.

IV. NEAR-TERM INFORMATION EXPECTED (1978 – 1984)

Earth-based Studies

1. Further investigations of the opposition effect and the azimuthal brightness variations with decreasing ring tilt angle and at longer (red, IR) wavelengths. These will hopefully constrain the particle albedo more closely, impacting the question of the "infrared discrepancy."

2. An interferometric observation of the ring brightness at 3 mm wavelength may be possible in the near future, but in general critical short microwave-wavelength observations (100 μm - 1 cm) will become more difficult as the rings close up. Hopefully, laboratory measurements of the microwave (and infrared) dielectric properties of ices and clathrates at low temperatures will be obtained, as these will eventually be critical for final analyses of ring particle size and composition.

3. Continuation of radar backscatter observations of the rings as they close up may allow us to discriminate between monolayer and many-particle-thick models.

Pioneer and Voyager

1. Pioneer 11 will "probe" the region exterior to ring A for particles, but due to the low value of ring tilt angle, may not provide much other information.
2. Voyager will encounter Saturn at a ring tilt angle of 5 degrees. The Voyager Radio Science experiments (Eshleman *et al.*, 1978; Tyler, 1978) will obtain high-quality information on ring optical depths for regions with low ($\tau_o < 1$) optical depths. Parts of the B ring may still be opaque. Good radial resolution will be obtained (~100 km) giving new information on dynamics and radial structure. Proper use of the two Voyager spacecraft in different modes (one in direct occultation, one in large-angle bistatic reflection) will provide information on particle sizes spanning the whole range of interest. Oblique scattering angles are desirable both in studying particles between 1 cm and several meters in size, and in obtaining interesting polarization results, which bear directly on particle shape.
3. Voyager IRIS experiments will obtain independent "mean" size information from observations of eclipse cooling of the particles. Spectral observations from 0.3-50 μm will provide useful information on composition and temperature of the particles observed. Photography may reveal the existence of extremely large "parent" bodies with sizes on the order of a kilometer or more.
4. Determination of the ring mass with an accuracy of ~10^{-6} M_S will be possible. This measurement will probably discriminate between ices and metal as major material constituents. However, if the rings are of ice, their mass may very well be less than the above detection limit.

V. POTENTIAL USES OF SOP[2] FOR STUDY OF THE RINGS

Composition Determinations and Relevance to Studies of Solar System Formation

As mentioned in Section 1, the origin of the rings is still not well-established. However, indications are that very large (> 1 km) particles are, at best, a rarity in the rings. As internal strength would limit the size of fragments produced by Roche

breakup of a larger satellite to a value at least this large (Harris, 1975; Greenberg *et al.*, 1977), this may be taken as at least an indication that the ring material is a direct condensate from the proto-planetary nebula. Because the ring particles have not been chemically or thermally altered by atmospheric or tectonic processes, they provide a valuable boundary condition on conditions in the protoplanetary nebula.

For instance, Lewis (1973) and Miller (1973) have suggested that methane and ammonia hydrates are stable at temperatures around or below 90 K. Thus, one would expect them to exist currently, if they ever formed. Pollack *et al.* (1977) have shown that the early high-luminosity phase of proto-Saturn may have kept the region of the rings too warm for anything but pure water ice to form there, and then only very close to the end of the accretion period. Thus, determination of the clathrate *vs* ice composition will provide an important constraint on the formation history of Saturn and the outer solar system in general. This may well be accomplished by an IRIS-type experiment operating out to long wavelengths (~1-100 μm) where spectral discrimination of clathrates appears to be possible (Bertie *et al.*, 1973). Some evidence for spectral structure in the 10 and 20 μm region has been inferred in observations by Morrison (1974). Laboratory work is needed to determine critical wavelength intervals and sensitivity required. In addition, trace silicate impurities which may be admixed in the ice may be representative of the composition of the original interstellar grains, and may be present in sufficient amounts to be detectable by an IRIS experiment. Hydrated silicates appear to be likely constituents of the Galilean satellites (Pollack *et al.*, 1978) and observable even from the ground. High-resolution spectra at visible wavelengths would help resolve the source of the "reddening" which seems to characterize all outer solar system objects. Organic photo-products have been suggested for this "Axel dust" on Titan, but the rings have no atmosphere in which to form such products.

Both in ice vs clathrates and ice vs silicate, compositional gradients may exist with distance from Saturn at a level which might be detectable only with substantial integration time, requiring repeated observations from an orbiter.

Particle Size Distribution and the Evolution of the Rings

A detailed knowledge of the particle size distribution, possibly a function of distance from the planet, may tell us a good deal about the evolution of rings. Smaller particles will be affected more by drag effects and will drift inwards. Also

particles undergoing the most collisions (the smaller, more numerous particles) will diffuse inwards and outwards the most rapidly. Thus, information may be gained as to whether the rings originated in one place and diffused radially, or remain in much the same location in which they were formed. The exact form of the size distribution may be compared with distributions characterizing meteorites and with theoretical studies of accretion/comminution processes (Greenberg *et al.*, 1978) to give us a greater understanding of the accretion process itself.

These studies would be best accomplished using bistatic radar reflectivity and polarization studies over as large a range of view angles as possible. This implies observations from a fairly inclined orbit (~10-20°) with respect to the ring plane. Such an inclined orbit would also improve our chances of obtaining a ring mass as separable from the higher gravitational harmonics of Saturn itself. A full knowledge of the diffuse scattering properties of the rings (see Figure 15) would provide an excellent constraint on the distribution of particle sizes from less than one centimeter to several meters radius. Studies of the polarization would allow inferences as to particle shape and irregularity to be made, giving qualitative information on the collisional processes shaping the particles. Repeated ring occultations at a time when the rings are fairly open (~20 degrees in 1984) will give us full knowledge of the optical depth in the thickest regions of the rings which will be necessary for understanding of the intensity and polarization results. Coherent radio occultations also provide a good means of detecting small (<<1 cm radius) particles, by the phase shift of the coherent signal.

Radiometry at short microwave wavelengths (100 μm-1 mm) would be of great value in establishing limits on the size of the largest particles. These maximum sizes might also vary with radial distance. Current values of ring brightness temperature at millimeter wavelengths are not in agreement; however, model calculations (Cuzzi and Pollack 1978) indicate that brightness temperatures of 30-50 K could be expected, if the particles are composed of ice. Better knowledge of the critical transition zone between 100 μm and several millimeters wavelength will be essential to better knowledge of the particle sizes and compositions. Improved knowledge of the phase effect at visible wavelengths would lead to good determination of the volume density of the rings critical for proper analysis of the microwave scattering behavior. The volume density may vary with radial distance, especially near the resonances, providing indirect information on the dynamics of resonances and ring thickness.

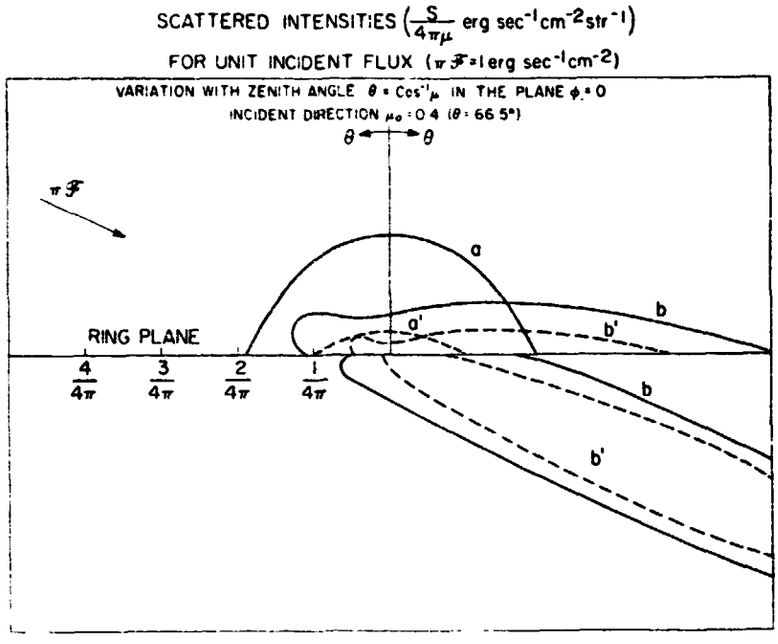

Figure 15. The angular distribution of diffusely scattered and transmitted radiation in the plane of incidence. The incident plane wave has unit flux normal to itself. Curves a and a': total and singly scattered intensities reflected by a semi-infinite layer of isotropic scatterers with $\bar{\omega}_0 = 1$. Curves b and b': total and singly scattered intensities diffusely reflected and transmitted by a typical ring model composed of centimeter-to-meter-sized particles in a many-particle-thick ring layer. From Cuzzi and Pollack (1978).

The ring system as a dynamics laboratory: The recent discovery of the rings of Uranus shows that ring systems are more common than had been thought, and vary greatly in nature. These two systems afford us a great opportunity to study large-scale gravitational perturbations which could lead to a better knowledge of the accretion processes forming resonant pairs of satellites, and even planets themselves (Goldreich and Nicholson, 1978), as well as large-scale dynamical effects influencing galactic structure. For instance, the exact shape and optical depth of the gaps in the rings will allow tests to be made of density wave theory in differentially rotating disks (Goldreich and Tremaine, 1978). Knowledge of the "strengths" of the Mimas resonances as barriers to mass motion (from theory), studies of the optical depth variations across the resonances, and the "spreading rate" of the rings as determined by velocity dispersion (thickness) may be compared with observations of radial diffusion of particles as evidenced by radial variations in composition on particle size distribution. More detailed study of local ring irregularities such as the non-axisymmetric disturbances in ring A and the physical thickness of the rings, even from $3R_s$ orbital distance, appears to be difficult as these are probably tens of meters in size, requiring angular resolution less than 0.1 arc sec.

Summary

Several points of interest are noted vis-a-vis use of SOP[2] to study the rings and the relevance of these studies to solar system formation. Studies of particle composition and size distribution, and their variations with distance from the planet, could provide several useful constraints on conditions prevailing in the proto-planetary nebula. These are best accomplished from inclined orbit (10-20°) with visible photometry at several wavelengths (or spectroscopy), an IRIS experiment operating from 1-50 μm (100 μm?) wavelength, a multiband radiometer operating from ~100 μm to several millimeters wavelength, and extensive bistatic radar mapping. Studies of the dynamics of particles in the rings will greatly improve our theoretical understanding of the gravitational processes that influenced, and might have initiated, planetary accretion and evolution. These will arise from extensive photography of the rings and repeated radio occultations of an orbiter by the rings.

REFERENCES

Allen, D. A., and Murdock, T. L. (1971). Infrared photometry of Saturn, Titan, and the Rings. *Icarus 14*, 1–2.

Armstrong, K. R., Harper, D. A., Jr., and Low, F. J. (1972). Far-infrared brightness temperatures of the Planets. *Astrophys. J. 178*, L89–L92.

Aumann, H. H., Gillespie, C. M., Jr., and Low, F. J. (1969). The internal powers and effective temperatures of Jupiter and Saturn. *Astrophys. J. 157*, L69–L72.

Aumann, H. H., and Keffer, H. H. (1973). Determination of Particle Sizes in Saturn's rings from their eclipse cooling and heating curves. *Astrophys. J. 186*, 305–311.

Berge, G. L., and Muhleman, D. O. (1973). High-angular-resolution observations of Saturn at 21.1 cm wavelength *Astrophys. J. 185, 373–381.*

Bertie, J. E., Othen, D. A., and Solinas, M. (1973). The infrared spectra of ethylene oxide hydrate and hexamethylenetetramine at 100 K. In *Physics and Chemistry of Ice* (E. Whalley, S. J. Jones, and L. W. Gold, eds.) pp. 61–65. Ottawa. Royal Soc. of Canada.

Bobrov, M. S. (1970), Physical Properties of Saturn's Rings. In *Surfaces and Interiors of Planets and Satellites* (A. Dullfus, ed.), pp. 377–458, Academic Press, N.Y., New York.

Brahic, A. (1977). Systems of colliding bodies in a gravitational field. I-numerical simulation of the standard model *Astron. Astrophys. 54*, 895–907.

Briggs, F. H. (1974). The microwave properties of Saturn's rings. *Astrophys J. 189*, 367–377

Burns, J. A., Hamill, P., Cuzzi, J. N , and Durisen, R. (1977). On the "thickness" of Saturn's rings caused by satellite perturbations. In Preparation.

Campbell, D. B., Chandler, J. F., Pettengill, G. H., and Shapiro, I. I. (1976). The Galilean Satellites: 12.6 cm radar observations. *Bull. Amer Astron. Soc 8*, 46.

Cook, A. F., 1976; Gravitational resonances in Saturn's rings. II. Perturbations due to Janus, Mimas, and Enceladus: the initial profile in Saturn's equatorial plane and warping of the rings. Center for Astrophysics, preprint No. 588.

Cook, A. F., and Franklin, F A. (1958). Optical properties of Saturn's rings. I. Transmission. *Smithsonian Contrib. Astrophys 2*, 377–383.

Cook, A. F., Franklin, F. A., and Palluconi, F. D. (1973). Saturn's Rings - A Survey. *Icarus 18*, 317–337.

Colombo, G., Goldreich, P., and Harris, A. (1976). Spiral structure as an explanation for the asymmetric brightness of Saturn's A ring. *Nature 264*, 344–345.

Cuzzi, J. N., and Dent, W. A., (1975) Saturn's Rings: The determination of their brightness temperature and opacity at centimeter wavelengths. *Astrophys. J. 198*, 223–227.

REFERENCES (Contd)

Cuzzi, J N , and Pollack, J. B. (1977). Saturn's rings. Particle composition and size distribution as constrained by microwave observations. I Radar Observations, *Icarus* In press.

Cuzzi, J. N., and Pollack, J. B. (1978). Saturn's rings. Particle composition and size distribution as constrained by microwave observations. II. Radio brightness observations In preparation.

Cuzzi, J. N., Durisen, R , Burns, J. A., and Hamill, P. (1978). On the vertical structure of Saturn's rings In preparation.

Dollfus, A (1970). New optical measurements of the diameters of Jupiter, Saturn, Uranus, and Neptune. *Icarus 12*, 101−117

Eshelman, V. R., Tyler, G. L., Anderson, J. D., Fjeldbo, G., Levy, G. S., Wood, G. E., and Croft, T A (1978). Radio science investigations with Voyager. *Space Sci. Rev.* In press.

Esposito, L. W., and Lumme, K. (1977). The tilt effect for Saturn's rings *Icarus 31*, 157−168

Ferrin, I R (1974). Saturn's rings. I. Optical thickness of rings A, B, D and structure of ring B. *Icarus 22*, 159−174.

Ferrin, I. R. (1975). Saturn's Rings II Condensations of light and optical thickness of Cassini's division. *Icarus 26*, 45−52.

Fink, U , and Larson, H. P. (1975). Temperature dependence of the water-ice spectrum between 1 and 4 microns. Application to Europa, Ganymede, and Saturn's Rings. *Icarus 24*, 411−420.

Focas, J. H., and Dollfus, A. (1969). Propriete's optiques et l'epaisseur des anneaux de Saturne observes par la tranche en 1966. *Astron. Astrophys. 2*, 251−265

Fountain, J. W. (1977). Saturn's ring: Physical thickness and the optical depth of Cassini's division. *Bull. Amer Astron Soc. 9*, 463.

Franklin, F. A., and Colombo, G. (1970). A dynamical model for the radial structure of Saturn's rings. *Icarus 12*, 338−347

Franklin, F. A., and Colombo, G. (1977). On the azimuthal brightness variations of Saturn's rings. Submitted to *Icarus* Jan. 1977, Center for Astrophysics Preprint No. 685.

Franklin, F. A., Colombo, G. and Cook, A F. (1971). A dynamical model for the radial structure of Saturn's rings *Icarus 15*, 80−92.

Franklin, F. A., and Cook, A. F. (1965). Optical properties of Saturn's rings, II: Two-color phase curves of the two bright rings. *Astron. J. 70*, 704−720.

Goldreich, P., and Nicholson, P. (1978). Revenge of Tiny Miranda. *Nature 269*, 783−785.

Goldreich, P., and Tremaine, S. (1978a). The velocity dispersion in Saturn's rings. Submitted to *Icarus*

Goldreich, P., and Tremaine, S. (1978b). The formation of the Cassini division in Saturn's rings. Submitted to *Icarus*

Goldstein, R. M., and Morris, G. A., (1973) Radar observations of the rings of Saturn. *Icarus 20*, 260−265.

Goldstein, R M., Green, R R , Pettengill, G. H , and Campbell, D. B., (1977). The rings of Saturn: Two frequency radar observations. *Icarus 30*, 104−110.

Greenberg, R., Davis, D. R., Hartmann, W. K., and Chapman, C R , (1977). Size distribution of particles in planetary rings. *Icarus 39*, 769−779.

Greenberg, R , Wacker, J., Hartmann, W K., Chapman, C. R , and Davis, D. R. (1978). Accretion of planets from planetesimals Paper presented at meeting on "Protostars and Planets", Tucson, Arizona, January 1978.

Hameen-Anttila, K. A., and Pyykkö, A (1972). Photometric behavior of Saturn's rings as a function of the Saturnocentric latitudes of the Earth and Sun. *Astron. Astrophys. 19*, 235−247.

Hameen-Anttila, K A , and Vaaraniemi, P. (1975). A theoretical photometric function of Saturn's rings *Icarus 25*, 470−478.

Harris, A. W (1975) Collisional breakup of particles in a planetary ring. *Icarus 24*, 190−192

Hudson, H. S , Lindsey, G A., and Soifer. B T. (1974). Submillimeter observations of planets *Icarus 23*, 374−379.

Irvine, W. M (1966). The shadowing effect in diffuse reflection. *J. Geophys. Res 71*, 2931−2937.

Jaffee, W. (1977). 6 cm radio observation of Saturn. Preprint.

Janssen, M A. and Olsen E T. (1976). Saturn's rings. Brightness temperature measurements at λ8mm *Bull Amer. Astron Soc. 8*, 461.

Jeffreys, Sir H. (1947) The effects of collisions of Saturn's rings. *Monthly Not. Royal Astron. Soc. 107*, 263−267.

Johnson, T. V. and McCord, T. B. (1970). Galilean satellites: The spectral reflectivity 0.30-1.10 microns. *Icarus 13*, 37−42

Kawata, Y. and Irvine, W. M. (1974). Models of Saturn's Rings Which Satisfy the Optical Observations. In *The Exploration of the Planetary System* (Woszczyk and Iwaniszewska, eds.) pp. 441−464. Reidel Pub. Boston.

Kawata, Y., and Irvine, W M. (1975) Thermal emission from a multiple scattering model of Saturn's rings *Icarus 24*, 472−482.

Kemp, J. C. and Murphy, R. E. (1973). The linear polarization and transparency of Saturn's rings. *Astrophys. J. 186*, 679−686.

Kieffer, H. (1974). Ring particle sizes and composition derived from eclipse cooling curves and reflection spectra, in The Rings of Saturn (G. H. Pettengill and F. D. Palluconi, eds.), NASA SP-343, 51−65.

Kiladze, R. I. (1969). Observations of Saturn's rings at the moment of the Earth's transit through their plane (in Russian) *Byull Abastuman Astrofiz. Obs 37*. 151−164.

Kuiper, G. P., Cruikshank, D. P., and Fink, U. (1970). The composition of Saturn's rings. *Sky and Tel 39*, 14.

Lebofsky, L. A , Johnson, T V , and McCord, T. B (1970). Saturn's rings· Spectral reflectivity and compositional implications. *Icarus 13*, 226−230.

Lewis, J S. (1973). Chemistry of the outer solar system. *Space Sci Rev., 14*, 401−411.

Loewenstein, R. F., Harper, D. A., Moseley, S. H., Telesco, C. M., Thronson, H. A., Jr., Hildebrand, R. H., Whitcomb, S. E., Winston, R., and Stiening, R. F. (1977). Far-infrared and submillimeter observations of the planets *Icarus 31*, 315−324.

Low, F. J. (1965). Planetary Radiation at infrared and millimeter wavelengths. *Bull. Lowell Obs.* 5, 184−187.

REFERENCES (Contd)

Lumme, K. (1970). On photometric properties of Saturn's rings. *Astrophys. Space Sci. 8*, 90–96.

Lumme, K. and Irvine, W. M. (1976a). Azimuthal brightness variations of Saturn's rings. *Astrophys. J. 204*, L55–L57.

Lumme, K. and Irvine, W. M. (1976b). Photometry of Saturn's rings. *Astron. J. 81*, 865–893.

Lumme, K., and Irvine W. M., (1977). Low tilt angle photometry and the thickness of Saturn's ring. *Bull Amer. Astron. Soc. 9*, 521.

Lumme, K., and Reitsema, H. J. (1977). Five color photometry of Saturn and its rings. *Bull. Amer. Astron. Soc. 9*, 463.

Lumme, K., Esposito, L. W., Irvine, W M., and Baum, W. A. (1977). Azimuthal brightness variations of Saturn's rings. II. Observations at an intermediate tilt angle. *Astrophys. J. 216*, L123–L126.

Miller, S. L. (1961). The occurrence of gas hydrates in the solar system. *Proc Nat. Acad. Sci. U.S. 47*, 1798–1808.

Miller, S. L. (1973). The clathrate hydrates-their nature and occurrence. In *Physics and Chemistry of Ice* (E. Whalley, S. J. Jones, and L. W. Gold, eds.). pp. 42–50. Roy. Soc of Canada, Ottawa, Canada.

Morrison, D. (1974). Infrared Radiometry of the Rings of Saturn. *Icarus 22*, 57–65.

Morrison, D. (1976). Radiometry of satellites and the rings of Saturn. In *Planetary Satellites* (J. Burns, ed.) pp. 269–301. University of Arizona Press.

Muhleman, D., Schloerb, F. P., and Berge, G. L., (1976). A Radio synthesis map of the Saturn system at a wavelength of 3.71 cm. *Bull. Amer. Astron. Soc. 8*, 475.

Murphy, R. E. (1973). Temperatures of Saturn's rings. *Astrophys. J. 181*, L87–L90.

Murphy, R. E., Cruickshank, D. P., and Morrison, D. (1972). Limb Darkening of Saturn and Thermal Properties of the Rings from 10 and 20 micron Radiometry. *Bull. Amer. Astron. Soc. 4*, 358.

Nolt, I. G., Radostitz, J. V., Donnelly, R. J., Murphy, R. E., and Ford, H. C. (1974). Thermal emission of Saturn's rings and disk at 34 μm. *Nature 248*, 659–660.

Nolt, I. G., Sinton, W. M., Caroff, L. F., Erickson, E. F., Strecker, D. W., and Radostitz, J. V. (1977). The brightness temperatures of Saturn and its rings at 39 microns. *Icarus 30*, 747–759.

Nolt, I. G., Tokunaga, A., Gillett, F. C., and Caldwell, J. (1978). The 22 μm brightness of Saturn's rings versus declination of the Sun. *Astrophys. J. 219*, L63–L66.

Ostro, S. F., and Pettengill, G. H. (1977). Icy craters on Europa, Ganymede, and Callisto. *Bull. Amer. Astron Soc. 9*, 523.

Pettengill, G. H., Ostro, S. J., Campbell, D. B., and Goldstein, R. M. (1977). Saturn's rings: Radial distribution of radar scatterers. *Bull. Amer. Astron. Soc. 9*, 462.

Pilcher, C. B., Chapman, C. R., Lebovsky, L. A., and Kieffer, H. H. (1970). Saturn's rings Identification of water frost. *Science 167*, 1372–1373.

Pollack, J. B. (1975). The Rings of Saturn. *Space Sci. Rev. 18*, 3–93.

Pollack, J. B., Summers, A. L., and Baldwin, B. (1973). Estimates of the size of the articles in the rings of Saturn and their cosmogonic implications. *Icarus 20*, 263–278.

Pollack, J. B., Grossman, A. S., Moore, R., and Graboske, H. C. (1977). The formation of Saturn's satellites and rings, as influenced by Saturn's contraction history. Submitted to *Icarus*.

Pollack, J. B., Witteborn, F., Erickson, E., Strecker, D., Baldwin, B., and Bunch, T. (1978). Near-infrared spectra of the Galilean satellites-observations and compositional implicates. Submitted to *Icarus*.

Rather, J. D. G., Ulrich, B., and Ade, P. A. R. (1974). Planetary brightness temperature measurements at 1.4mm wavelength. *Icarus 23*, 448–453.

Reitsema, H. J., Beebe, R. F., and Smith, B. A., (1976). Azimuthal brightness variations in Saturn's rings. *Astron. J. 81*, 209–215.

Rieke, G. H (1975). The thermal radiation of Saturn and its rings. *Icarus 26*, 37–44.

Schloerb, F. P. (1978) Radio Interferometric Investigations of Saturn's Rings at 3.71 - and 1.30-cm Wavelength. Thesis, California Institute of Technology, California.

Smythe, W. D. (1975). Spectra of hydrate frosts: Their application to the outer solar system *Icarus 24*, 421–427.

Stebbins, J., and Jacobsen, T. S. (1928). Further photometric measures of Jupiter's satellites and Uranus, with tests for the solar constant. *Lick Obs. Bull. 13*, 180–195.

Tyler, G. L., and Eshelman, V. P. (1978). Voyager radio occultation investigations at Saturn. This volume.

Vaaraniemi, P. (1973). The Short-Periodic Perturbations in Saturn's Rings. NASA Publication N73-19854 Report 14, Aarne Karjalainen Observatory, University of Oulu, Oulu, Finland.

Veverka, J. F. (1970). Photometric and polarmetric studies of minor planets, planets and satellites. Doctoral dissertation, Harvard University, Cambridge, Massachusetts.

Ward, D. B. (1968). Far infrared spectral observations of Saturn and its rings. Submitted to *Icarus*. 1978.

Werner, M. W., Neugerbauer, G., Houck, J. R., and Hauser, M. G. (1978). One millimeter observations of the Planets Submitted to *Icarus*. 1978.

Whalley, E., and Labbe, H. J., (1969). Optical spectra of orientationally disordered crystals. III. Infrared spectra of the sound waves, *J. Chem. Phys. 51*, 3120–3127.

Wright, E. L. (1976). Recalibration of the far-infrared brightness temperatures of the planets *Astrophys. J. 210*, 250–253.

DISCUSSION

J. CALDWELL: I would like to show a Figure A taken from Caldwell, J. (1975) Ultraviolet observations of small bodies in the Solar System (Icarus 25, 384-396) and compare it with one of Jeff's (see Figure 9)

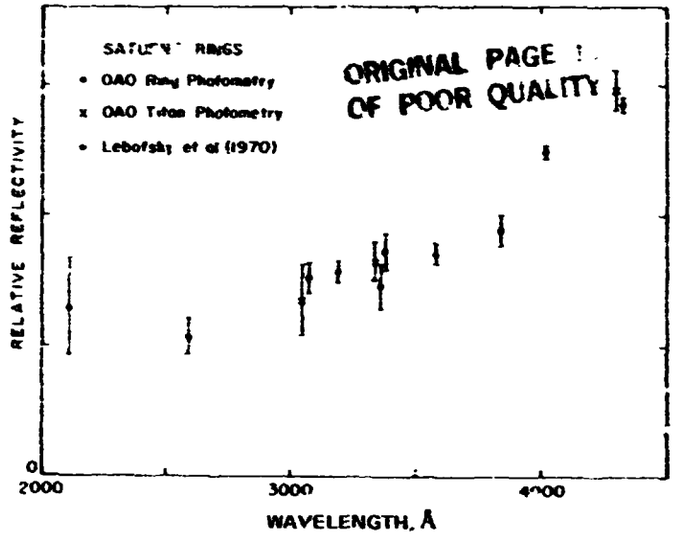

This figure shows OAO data that extend the reflectivity measurements of the rings below 3000 Å to practically 2000 Å. The precipitous drop in reflectivity implied by McCord and his colleagues stops around 3000 Å.

The reflectivity in the 2000-3000 Å region is flat and is consistent with water frost. It also appears to me that the total spectrum would be consistent with two components. I don't know whether they are spatially separated or mixed together.

The ultraviolet reflectivity of the rings does not look like that of the Galilean satellites, which continue to decrease noticeably all the way down to 2000 Å, at least for those for which measurements are possible (Callisto, Ganymede, and Europa).

L. TRAFTON: Although the rings are brighter than Titan, the relative reflectivities from 5000 Å down to at least 3000 Å are very similar. So whatever makes up the dust on Titan, may be the same stuff which helps to color the rings.

B. SMITH: During the recent Iapetus eclipse we did confirm the existence of the Encke division or minimum, so we have a little more than Dollfus's visual observation to go on.

Also, with regard to ring thickness seen at the time the Earth goes through the ring plane, its true that the rings never completely disappear, but the model that Cook has developed has turned up edges near the resonance divisions. Thus the rings can be very thin and still appear thicker when seen edge on.

J. CUZZI: Yes, however it is uncertain whether Cook's inclination resorance, which produces the "turned-up" edges, lies in a region containing particles, or in fact within an empty region near the ring edge.

D. MORRISON: In your upper limit on the amount of silicates that can be included in the particles and still be consistent with the radar measurements, I presume that it refers to the centimeter or perhaps the 10-cm particles. If you had a silicate core in some of the large objects, could you tell the difference?

J. CUZZI: Probably not. The meter-sized and larger objects in the power law distribution contribute relatively little to the radar signal, so their properties do not constrain the model.

D. MORRISON: So, in fact, a component of a relatively small number of meter-sized objects made of anything would be consistent with existing data.

J. CUZZI: Yes, as long as their total surface area, or optical depth, is less than a few percent of that of the entire ring system.

THE D AND E RINGS OF SATURN

Bradford A. Smith

Department of Planetary Sciences and Lunar and Planetary Laboratory
University of Arizona
Tucson, Arizona 85721

ABSTRACT

CCD observations of Saturn Ring D, discovered by Guerin in 1969, confirm the existence of this inner ring and indicate that its surface brightness ranges from 0.03 (inner edge) to 0.05 (outer edge) relative to the maximum surface brightness of Ring B. If Ring D is composed of spherical, diffusely reflecting particles with average surface reflectivity equal to that of the particles in Ring B, the average normal optical thickness of Ring D is 0.02. Reanalysis of a photograph taken by Feibelman during the 1966 ring plane passage suggests a normal optical thickness for Ring E between 10^{-6} and 10^{-7}, depending upon the average reflectivity of the particles. No new observations of this outer ring will be possible until the earth passes through the Saturn ring plane in 1979–80.

I will discuss two rings of Saturn which cannot normally be seen; by that I mean rings which would be invisible to a visual observer using even the largest of telescopes. It must be said that, until quite recently, the very existence of both of these rings -- located interior to and exterior to the three bright rings -- was in serious question. Today we feel quite confident of the reality of the inner ring, while the outer ring probably still remains, in reality space, somewhere between Farrah Fawcett-Majors and Tinker Bell. The International Astronomical Union does recognize at least the hypothetical existence of both rings, however, and has designated the inner and outer as Rings D and E, respectively.

The outer ring has been reported by several visual observers since the turn of the century (Alexander, 1962), most notably by the famous French observer,

G. Fournier, and by the even more famous astrophysicist, Sir Arthur Stanley Eddington. Since we now know that the E ring is *much* too faint to be seen visually, it was perhaps an exercise of good judgement when Eddington decided to pursue a theoretical career. Ring E is in fact so faint that the only opportunity for detecting it at all happens during the time when the earth is passing through the Saturn ring plane. The most recent opportunity occurred in 1966 and we will have another chance in 1979-80.

The inner ring was first reported by Pierre Guérin after examining photographs that he had taken at Pic du Midi in 1969 (Guérin, 1970). Subsequent reexaminations of photographs by S. Larson at the Lunar and Planetary Laboratory of the University of Arizona and by myself at New Mexico State University tended to confirm the existence of Ring D, but the signal was buried uncomfortably far down in the noise of the light scattered by the bright rings and by Saturn itself. In 1975 JPL's Saturn Ring Study Team produced an impressive 150 page document entitled "The D Ring - Fact or Fiction" (JPL Document 760-134). The study concluded that the existence of the D ring could not be verified and that the maximum brightness of Ring D would have to be less than 0.01 of the maximum brightness of Ring B. However, recent studies by Larson (1978), using images obtained with a CCD camera, have provided quantitative confirmation of Ring D.

Looking more closely now at Ring E, the only quantitative data currently available (Smith *et al.*, 1975) are those which have been extracted from a single blue-light photographic image obtained during the 1966 opportunity by W.A. Feibelman at the Allegheny Observatory of the University of Pittsburgh (Feibelman, 1967). Although Feibelman had actually taken several dozen photographs of varying exposure with the Allegheny 76-cm refractor, only a single, 30-minute, overexposed image of Saturn showed a faint extension* of the visible rings. Fortunately, Feibelman's photograph also contains a dozen or so faint stars, thereby allowing a quantitative estimate of the brightness of the extended ring material. The only additional photographs known to show Ring E are several taken at the Catalina Observatory of the University of Arizona during the same opportunity in 1966 (Kuiper, 1974). Although the Arizona photographs tend to confirm the existence of the outer ring, the field of view was so small that no field stars were recorded and no quantitative brightness estimates are possible.

*The extension is most visible to the east of Saturn. The west side is cluttered by the overexposed images of Dione, Enceladus, Rhea and Titan

At the time that the Allegheny observation was made (15 November 1966), the ring plane was inclined 0°.233 to the line of sight. The projected width of Ring E would then be approximately 0.5 arc sec, considerably less than the 3.6 arc sec star images appearing on the same photograph. Thus, for photometric purposes, it is possible to treat the ring extension as a line source. The range over which the outer ring is seen extends from 3.3 to 6.5 Saturn radii (approximately 200,000 to 400,000 km) from the center of the planet. The inner limit is set by the core of the greatly overexposed image of Saturn itself, while the outer limit seems to be coincident with the edge of the annular halation area around the overexposed core. It seems likely that the faint ring extension is made visible by the photographic "inertia" provided by the halation annulus. If so, the ring may extend well beyond 6.5 Saturn radii. The uniformity over the observed range would also suggest that it probably extends inward to the outer edge of the visible rings.

Microdensitometry of the Feibelman image gives a line-source brightness of $m_B = 19.5 \pm 0.5$ magnitudes per linear arc sec. If we make the simplifying assumption that the ring is composed of diffusely reflecting, spherical particles, we can arrive at a normal optical thickness of the ring for any assumed average albedo of the individual ring particles. Assuming that the albedo extremes are bounded by granular, ice-covered surfaces (0.8) at one end and bare, carbonaceous-chrondritic material (0.05) at the other, we find the normal optical thickness to lie between $\tau = 1.0 \pm 0.5 \times 10^{-7}$ and $\tau = 1.6 \pm 0.7 \times 10^{-6}$.

The size distribution of particles in Ring E must be governed by the mechanisms of production and depletion. The Poynting-Robertson effect, for example, would have removed all primordial particles smaller than 7 cm over the age of the solar system. On the other hand, we might expect that new particles are being continuously created by meteoritic bombardment of larger particles near the outer edge of Ring A. Those spalled particles should then spiral outward under the influence of plasma drag. Such a mechanism would be increasingly effective with decreasing particle size and would tend, therefore, to populate the E ring with the smaller end of the spalled particle size-distribution range.

The hazard to spacecraft passing through Ring E depends, of course, on the distribution of particle size. As an example, if nearly all of the particles are very large, the separation between particles will be large compared to the size of the spacecraft and the probability of impact will be merely the normal optical thickness times a

projection effect which is approximately the cosecant of the trajectory inclination. For even low inclination trajectories, this could hardly be considered a serious hazard. If the particles are very small, impacts are assured, but damage will likely be negligible. It is in the millimeter range of particle sizes that the hazard to spacecraft becomes greatest, but this may also be a range where primordial particles are depleted and steady-state production is relatively small.

Turning to the region inside the bright rings, our study of Ring D (Larson, 1978) has made use of CCD images of Saturn obtained in the 886-nm absorption band of methane. The absorption of reflected light within this band by methane in Saturn's atmosphere appreciably reduces one component of the scattered light which has made earlier attempts to detect this inner ring so difficult. Suppression of reflected light from Saturn is variable over the disk, as it depends upon height and scattering properties of the reflecting cloud layer. Averaged over the disk, however, the reduction in light reflected from the planet relative to that from the rings is about a factor of 10.

CCD images of Saturn and its rings were recorded in February and April 1977, using the University of Arizona 154-cm Catalina telescope. The phase angle was $0.^{\circ}14$ and $6.^{\circ}3$, respectively, and the ring plane was inclined 17° and 18° to the line of sight. Intensity profiles along the major axis of the rings were then compared with model intensity profiles convolved two-dimensionally with an appropriate point spread function (PSF). In order to provide a realistic PSF which would properly fit both the core and the wings of a smeared stellar image, we used a summed double gaussian. The model intensity profile for the three bright rings was based on microdensitometry of high-resolution photographic images obtained by Larson with the same telescope in 1974. The results are shown in Figure 1 which displays the observed profile along with both the convolved and unconvolved profiles of the model. It can be seen that the model requires a reflecting region interior to Ring C and that the surface brightness of the interior ring must decrease toward the planet. The surface brightness of Ring D at 886 nm varies between 0.03 and 0.05 that of Ring B.

If we again assume that Ring D is made up of spherical, diffusely reflecting particles, and that the average surface reflectivity is approximately equal to that of the particles in Ring B, the average normal optical thickness of the Ring D is 0.02. On the other hand, if the particles in Ring D are not ice covered, the normal optical thickness would be correspondingly higher. Larson (1978) further notes that the Ring D seems to follow the same opposition effect as that exhibited by the bright rings. The so called

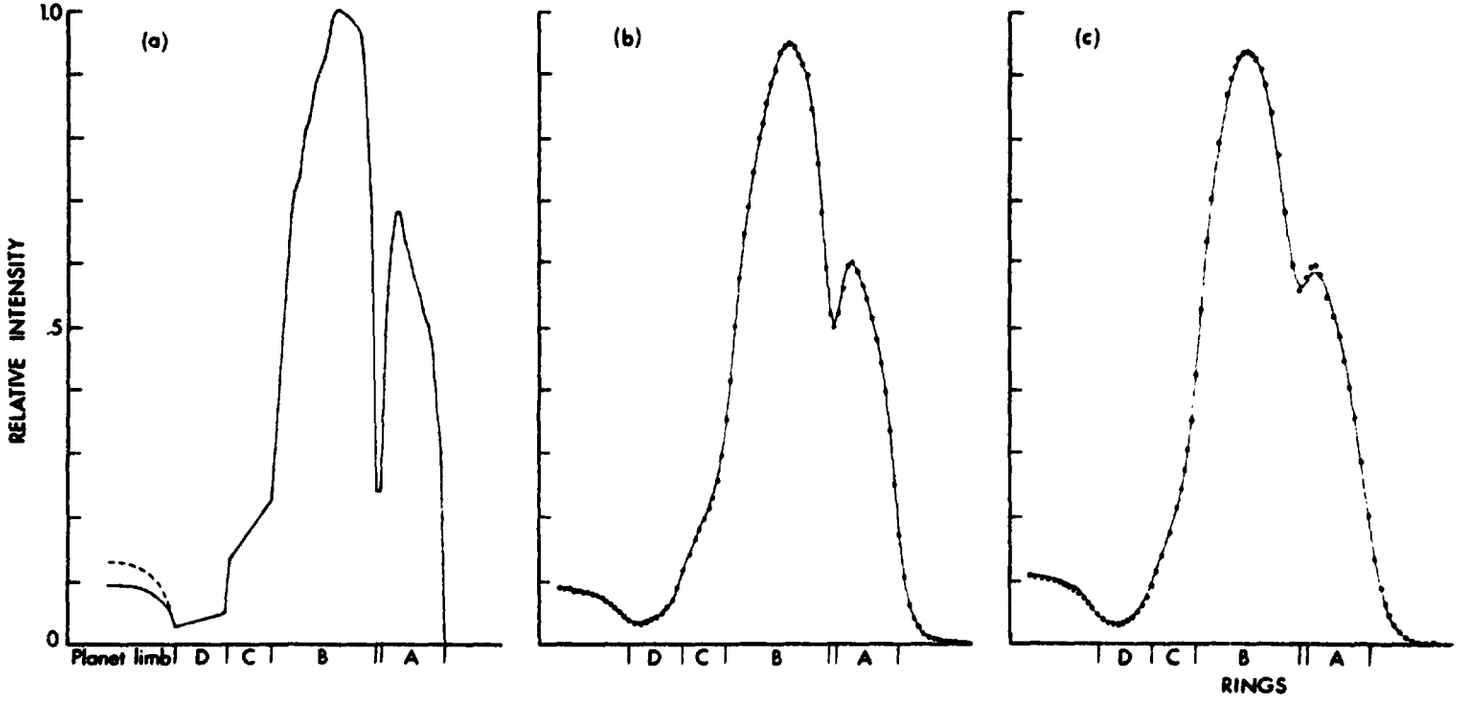

Figure 1. (a) Model intensity profiles of the rings. The solid and dashed lines represent the relative disk brightness at phase angles of 0.°14 and 6.°3 respectively. (b) Model convolved in two dimensions with a smearing function consisting of summed gaussians of 0.66 and 2.20 arc sec full width at half maximum. The dots are observational data from both ansae on 3 February 1977 at a phase angle of 0.°14. (c) Gaussians of 1.10 and 2.64 arcsec full width at half maximum. Dots are observational data from the east ansa on 22 April 1977 at a phase angle of 6.°3.

"Guérin Division" between Rings C and D was not observed, but this may be due to image quality which is somewhat inferior to that obtained by Guérin.

With regard to potential hazards to any future spacecraft attempting to fly through Ring D at any trajectory inclination, it is difficult to see any hope for survival unless all of the particles are large compared to the dimensions of the spacecraft itself.

As for future observations of these faint rings, I have already mentioned that 1979-80 will provide a good opportunity for groundbased telescopic studies of Ring E. Because of its very small optical thickness, it is unlikely that either Pioneer or Voyager will contribute anything new to our knowledge of the optical properties of this region. There is, however, the possibility that charged particle investigations will provide some new information, if indeed there is interaction between the trapped radiation and particulate material in the E Ring, as has been suggested by Van Allen (1976). The next good opportunity for ground-based studies of Ring D will not come until the mid to late 1980's. Long before that, Voyager should provide quantitative measurements of surface brightness, optical thickness and structure.

REFERENCES

Alexander, A. F. O'D (1962). *The Planet Saturn*, 1st ed. Faber and Faber, London. 474 pp.

Feibelman, W. A. (1967). Concerning the "D" ring of Saturn. *Nature 214*. 793–794.

Guérin, P. (1970). Sur la mise en evidence d'un quatriéme anneau et d'une novelle division obscure dans le systéme des anneaux de Saturn. *Comptes Rend., Serie B, Sci. Phys., 270*, 125–128.

Kuiper, G. P. (1974). On the origin of the solar system, I. *Celest. Mech.* 9. 321–348.

Larson, S. M. (1978). Observations of the Saturn D Ring. Submitted to *Icarus*.

Smith, B. A., Cook, A. F., Feibelman, W. A. and Beebe, R. F. (1975). On a suspected ring external to the visible rings of Saturn. *Icarus 25*, 466–46°.

Van Allen, J. A. (1976). Personal Communication.

DISCUSSION

J. CALDWELL: You said that Pioneer and Voyager wouldn't tell us much about the Ring E. But what about when Pioneer and Voyager actually go through the Ring E?

B. SMITH: The Voyager trajectory is such that it crosses the Saturn ring plane sometime shortly after leaving Jupiter and does not cross it again until it is very close to Saturn. So, as far as imaging is concerned, there's no hope of timing an exposure to look right in the plane. Yet, the optical thickness is so low you'd have to be exactly in the plane to be able to see it.

D. MORRISON: Perhaps one should note here that the first Voyager will not go that close to the rings, but both Pioneer 11 and the second Voyager, if it's on a Uranus trajectory, will go at about 2.37 Saturnian radii from the center of the planet.

D. WALLACE: Would you suggest that an Orbiter should be in the ring plane? You would discriminate then.

B. SMITH: Well, that might be discriminating the hard way. I don't recommend an orbiter in the ring plane.

J. POLLACK: Actually, from the point of view of other aspects of the ring, it probably would be useful to have the orbiter slightly inclined for two reasons: (1) You get a better ability to separate the ring mass from Saturn. (2) You have the ability to do some of the interesting bistatic radar experiments that I spoke about earlier.

D. HUNTEN: Not to mention imaging, which also requires being out of the ring plane.

D. MORRISON: This is an issue that we'll certainly want to come back to later, because if you are very far out of the plane of the rings, you may find that Titan is the only satellite that you can come close to, and there may be some trades that have to be made between multiple satellite encounters and getting a good look at the rings.

LOW SURFACE PRESSURE MODELS FOR TITAN'S ATMOSPHERE

John Caldwell

Depts. of Mechanical Engineering and of Earth and Space Science
SUNY at Stony Brook, New York 11794

ABSTRACT

The inversion model for the atmosphere of Titan, first proposed by Danielson, Caldwell and Larach, is reviewed. The basic features of the model are: a cold surface (80 K), a warm stratosphere (160 K) and a low surface pressure (20 mbar). The model is consistent with all existing thermal infrared spectrophotometry, but it cannot preclude the existence of an opaque, cloudy, thick atmosphere. The model is strongly supported by the recent scattering analysis of Podolak and Giver, which, together with the early analysis by Trafton, excludes other gases than methane as bulk constituents. Radio wavelengths observations, including recent data from the Very Large Array, are discussed. These long wavelength observations may be the only direct means of sampling the surface environment before an entry probe or flyby. The differences between the inversion model and Hunten's model must be resolved before detailed probe design studies can be performed meaningfully.

INTRODUCTION

It has been known for more than three decades (Kuiper, 1944) that Titan is unique among the well-observed satellites in the Solar System in having a substantial atmosphere, including at least some CH_4. However, for much of the intervening time, this datum was ignored by most of the astronomical community.

In 1972, there began a revolution in our understanding of this enigmatic satallite. Trafton (1972a) reported the possible detection of H_2 on Titan and also re-evaluated the quantitative analysis of the observed CH_4 absorption at 1.1 μm, revising upward the

estimate of the minimum column abundance of the Titanian atmosphere (Trafton, 1972b). Allen and Murdock (1971) had observed an anomalously high brightness temperature at 12 μm and concluded that the satellite had an atmospheric greenhouse. Morrison *et al.* (1972), influenced by their own radiometric observations at 20 μm and by the papers cited above, proposed a greenhouse model in which the opacity due to the broad, pressure-induced rotational transitions in H_2 at 17 μm and 28 μm, together with the relative transparency of H_2 in the 8-14 μm terrestrial atmospheric window, produced the observed infrared properties of Titan. Pollack (1973) presented a detailed greenhouse model, which also included the pressure-induced opacity of CH_4. He derived a surface temperature $\simeq$150 K, with a minimum surface pressure $\simeq$400 mbar and a minimum column abundance $\simeq$50 km-atm total of H_2 and CH_4.

There was an alternate interpretation of the new Titan data, however. Danielson *et al.* (1973) and Caldwell (1977) developed and refined a model atmosphere with a surface temperature $\simeq$80 K, a surface pressure $\simeq$20 mbar and a column abundance of $\simeq$2 km-atm of CH_4. This class of model, with its relatively low surface pressure, has become known as the inversion model, because it features a high altitude temperature inversion that is capable of reproducing all of the infrared observations of Titan.

There are other candidate models as well. Hunten (e.g., 1977) has been a forceful advocate for the inclusion of N_2 and has pointed out the theoretical difficulties in maintaining a substantial H_2 component on Titan against its high escape rate. Cess and Owen (1973) have included the effects of noble gases on greenhouse models.

The differences between these models must be resolved if there is to be an accurate understanding of the current state of Titan, and if its clues to the larger question of the origin and evolution of the outer Solar System are to be exploited. On a more practical level, an improved knowledge of the atmosphere is a prerequisite for many of the more useful potential spacecraft explorations of Titan.

It is the purpose of this paper to review the original inversion model, to discuss the impact of recent results on the model, and to speculate on imminent developments. In the following chapter, Hunten describes the current status of models with higher surface pressures and column densities.

THE INVERSION MODEL

The details of this model have previously been given by Danielson *et al.* (1973) and by Caldwell (1977). This section summarizes those papers.

The starting point for the model was the adoption of the smallest column abundance for the Titanian atmosphere that was consistent with observations. From the work of Trafton (1972b), that was 2 km-atm CH_4, with no other major molecular constituent. The motivation for choosing this extreme value was originally to counterbalance the then-prevailing trend among planetary scientists to favor the largest tenable column abundance. However, as will be discussed below, this choice is further justified by considerations of CH_4 vapor pressure and of the global radiation budget.

The 2 km-atm abundance was determined by Trafton from his analysis of the $3\nu_3$ band of CH_4 at 1.1 μm. Podolak and his colleagues have shown that it can be reconciled with the visible and near infrared absorption bands of CH_4 in the spectrum of Titan. This work will be summarized in the next section. However, toward shorter wavelengths, the reflectivity of Titan is not determined by CH_4 alone.

From 6000 Å down to 2600 Å, the reflectivity decreases monotonically. The shortest wavelength point, determined from broadband photometry by OAO-2 (Caldwell, 1975), corresponds to a geometric albedo of 0.033 for a radius of 2900 km. Caldwell (1974) has emphasized that such a low value is inconsistent with Rayleigh scattering even from the minimal 2 km-atm of CH_4. Models with higher abundances have greater disagreement with the observations.

The low ultraviolet albedo requires the presence of an absorbing species high in the atmosphere of Titan. The Rayleigh scattering constraint means that there can be at most a clear layer of $\approx$0.1 km-atm column abundance above the absorber if it is completely black at 2600 Å.

No molecule has been identified with the spectral characteristics necessary to reproduce the variation in reflectivity exhibited by Titan. However, laboratory simulations of Titan-like atmospheres exposed to natural energy sources such as far ultraviolet light generally produce a dark reddish-brown polymer (e.g., Khare and Sagan, 1973) that has the qualitative properties to explain the trend of Titan's ultraviolet to visual albedo curve. In this process, CH_4 is decomposed, and the fragments recombine to form the large colored particles. Such particles will henceforth be called "dust" to differentiate them from possible condensatic products.

The original inversion model was based on an assumption that such a process actually occurs on Titan. Although the details on Titan are not fully understood, as will be discussed below, the short wavelength absorption is definite. It is therefore certain that a significant fraction of the non-reflected Solar radiation incident upon Titan is absorbed high in the atmosphere, and not at the surface.

An object at Titan's distance from the Sun which has a high thermal emissivity will acquire an equilibrium temperature of the order of 100 K. The actual value will depend on the object's albedo. If the object does not have a high thermal emissivity at the wavelength of peak emission (≈30 μm for 100 K) the temperature will rise until the integral over all wavelengths of the emissivity multiplied by the Planck function equals the absorbed energy.

Titan's upper atmosphere has in fact reached an equilibrium temperature well above 100 K. The evidence for this is found in the middle infrared spectrophotometry of Gillett *et al.* (1973) and Gillett (1975). These data show a brightness temperature of ≈160 K in the ν_4 fundamental band of CH_4 at 3 μm. Since this band is very strong, it is optically thick at very high altitudes, and this brightness temperature must be very close to the actual physical temperature there.

At lower altitudes, there must be an opaque, colder level because, without an internal energy source, there is not enough incoming radiant energy to maintain the outer skin of the satellite at this elevated temperature against radiation to space. Hence, Titan has a temperature inversion, with warmer layers overlying cooler ones.

It is possible that an atmospheric greenhouse effect could maintain warmer layers below the cold, opaque level. This conjecture cannot be disproven now. The simplest model, advocated here, is that the opaque layer is in fact the physical surface.

It is postulated in the inversion model that the surface is CH_4 ice and that the atmosphere is in vapor pressure equilibrium with the surface. This fixes the surface temperature at ≈80 K, because this value, combined with the CH_4 saturated vapor pressure (20 mbar) gives the correct column abundance (2 km-atm). As discussed by Danielson *et al.* (1973), this temperature also leads to a reasonably accurately balanced global radiation budget for the model atmosphere and surface.

The inversion model has been successful in explaining the infrared emission of Titan. Figure 1 shows the 8–14 μm region, with the model compared to Gillett's (1975) data.

The emission peaks centered at 7.7 μm, 12.2 μm and 13.7 μm in the model are due respectively to CH_4, C_2H_6 (ethane) and C_2H_2 (acetylene). CH_3D and C_2H_4 have not

been included in the model. Between the peaks, the emission is due to the (ultraviolet-absorbing) dust. This effect is more evident in the next figure. The surface in the model is too cold to influence the emission shown in Figure 1.

Figure 2 shows the computed emission out to 40 μm. The dust has been taken to have a temperature of 160 K, with an emissivity proportional to $1/\lambda$. This is a simplifying approximation, consistent with an index of refraction that is constant with wavelength.

The surface is modelled as a black body with unit emissivity at 78 K. (This value will be discussed presently.) In the model, most of the radiation at 20 μm is due to the dust; and beyond 40 μm, most is due to the surface.

The parameters of any model fitted to reflected and emitted light from a planet are sensitive to the radius. A flux is the measured datum, but the radius is required for computing the physically meaningful quantities, brightness and albedo. In refining the original inversion model, Caldwell (1977) used the occultation radius of 2906 km measured by Elliot *et al.* (1975) for the effective radiating layer and the effective reflecting layer of the atmosphere. The surface radius is unknown, but for a specific value of the surface radius, a definite surface temperature can be calculated that balances the absorbed and emitted radiation. With the vapor-pressure equilibrium envisaged in the model, this also determines the surface pressure and column abundance. Caldwell (1977) chose a baseline model with a surface radius of 2700 km, leading to a surface temperature of 78 K, surface pressure of 16 mbar and column abundance of 1.3 km-atm. The amount by which these values change as a function of surface radius is summarized in Figure 3.

In the inversion model as described above, there are no clouds of condensate particles. This is not unreasonable, even though the entire surface is postulated to be in vapor pressure equilibrium with the atmosphere, because the high altitude heating may be sufficient to cause a positive temperature lapse rate everywhere. Such an atmosphere would be extremely stable against vertical convection.

If the radiative interchange between surface and atmosphere is such that a condensation cloud forms at low altitudes, the basic features of the model would not change greatly. The situation where a major constituent of an atmosphere is condensable has been discussed by Lewis and Prinn (1973) and Hunten (1977).

Because of the postulated vapor pressure equilibrium, the atmosphere will act as an effective thermostat, to keep the surface everywhere isothermal at the temperature determined by the global average visible transmission of the atmosphere and by

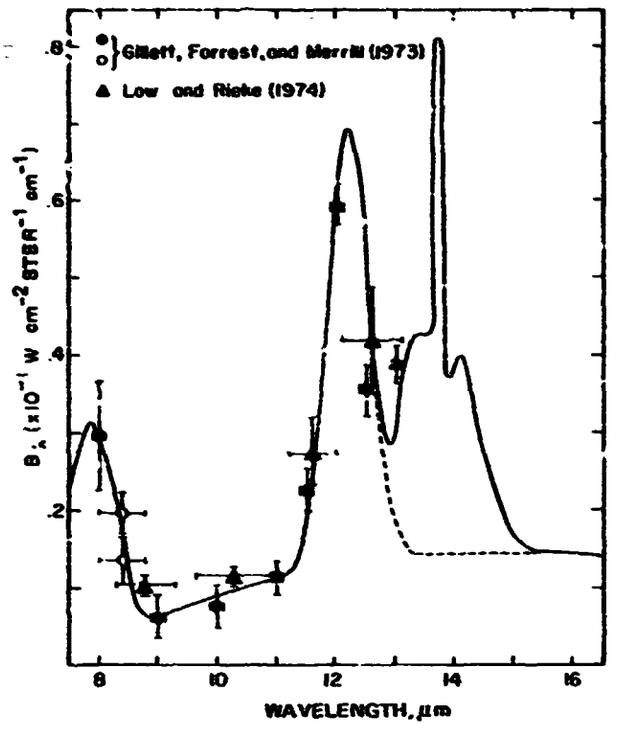

Figure 1. Details of the molecular band emission from Titan. The solid line includes emission from optically thin dust, approximate CH_4 emission and calculated emission from 0.5 cm-atm C_2H_6 and from 1.0 cm-atm C_2H_2; the broken line shows the emission with no C_2H_2. Emissions from C_2H_6 (10.5μm), CH_3D (8.7μm) and CH_3 (16.5μm) are not included in the model. The surface is not significantly bright at these wavelengths. See Gillett (1975) for further data, including additional points confirming the C_2H_2 feature. All figures in this article are reproduced from Planetary Satellites, *J. A. Burns, Editor, University of Arizona Press (1977).*

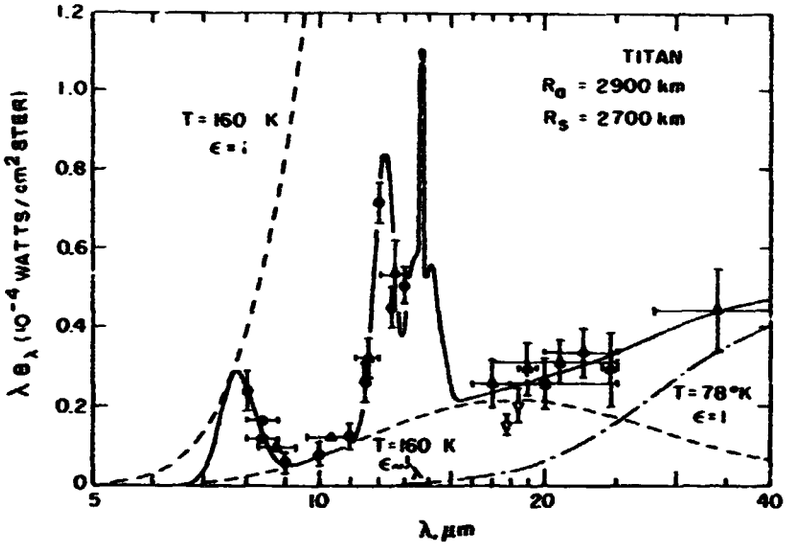

Figure 2. Comparison of the infrared photometric observations with the temperature inversion model. Axes are drawn so that the area under the curves is proportional to the energy traversing the atmospheric radius. Bandpasses for the closed circle data points are similar to the width of the circles. The solid line represents the total calculated emission from molecular bands and optically thin dust in a temperature inversion region at 160 K and a surface with unit emissivity at 78 K. The molecular abundances are 0.5 cm-atm C_2H_6 (12.2μm), and 1.0 cm-atm C_2H_2 (13.7μm). The CH_4 peak at 7.7μm is only approximate. The predicted ratio of atmospheric emission to surface emission was used to calculate the effective radius for each observational point. Closed circles are data from Gillett et al. *(1973), closed triangles are from Low and Rieke (1974), open triangles are from Knacke* et al. *(1975), and the closed square is from Morrison* et al. *(1972).*

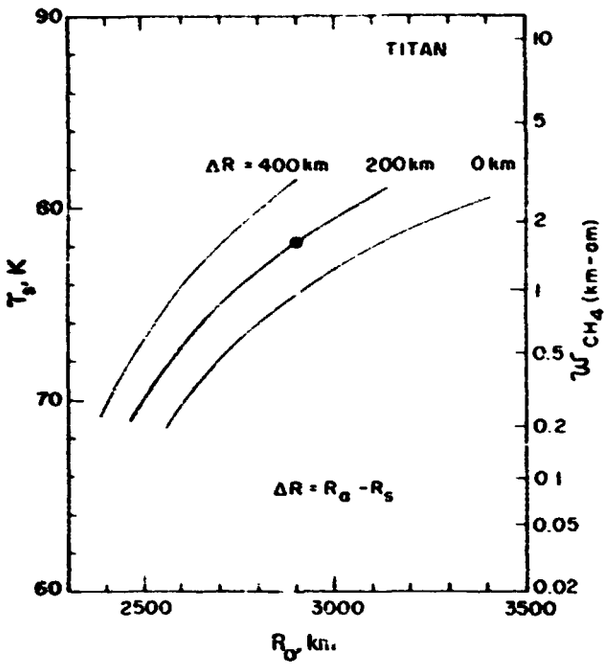

Figure 3. The energy balance of Titan. The ordinate is the surface temperature necessary in the inversion model to balance emitted and absorbed radiation from Titan, for various atmospheric and surface radii. On the right, the column abundance of CH_4 (W) corresponding to the surface temperature at the left is shown. A value of $g = 125$ cm s^{-1}, consistent with the baseline radius, was used to calculate W.

the downward infrared atmospheric emission. Any local region that found itself departing from the mean temperature in either sense would attempt to adjust its local vapor pressure by increased condensation or sublimation. Because of the sharp variation of CH_4 vapor pressure with temperature, winds would arise to restore an isobaric surface condition. The substantial latent heat of phase change of CH_4 would oppose the hypothetical temperature differential, and the local transient winds would continue until the differential disappeared.

In particular, Danielson *et al.* (1973) have shown that the atmosphere won't condense at the winter pole of Titan, because that pole never cools down. Assuming that the obliquity of Titan is the same as Saturn's, they calculated that about 5 percent of the atmosphere would condense on the winter polar during that season, without changing the surface temperature. This must be replenished by sublimation in the other hemisphere. The operative criterion in this calculation is that the surface cannot dissipate the latent heat of condensation faster than a blackbody at 80 K can radiate to space.

The assumption concerning the obliquity of Titan is not critical. For any general orientation of Titan's polar axis, precession will alter Titan's seasonal year, but most probably not enough to matter.

If the obliquity assumption is even approximately correct, then each Titan pole at its summer solstice will experience the largest diurnally-averaged solar flux of any point on the surface. Thus there are probably no absolute sinks of CH_4 on Titan. At some point during a Titan year, all locations will sublime some CH_4. However, on an annual average, the poles receive less flux than the equator, so there will be a steady, cumulative movement of CH_4 from the equator to the poles.

This situation is clearly statically unstable. Titan will respond by an equatorward flux of CH_4 glaciers to maintain its spherical shape. One effect of this motion will be to overturn the surface layer continually. Dust particles settling on the surface will not pave it over. The surface will not be hermetically sealed from the interior, and there will be fresh CH_4 exposed to the atmosphere to replenish those molecules irreversibly lost to photochemical action.

An alternate surface scenario, suggested by R. E. Danielson is that a modest greenhouse effect could raise the surface temperature to $\simeq$90 K, the CH_4 triple point. This would permit the formation of CH_4 oceans. In this case, ocean currents, and not glaciers, would recycle the CH_4 to the equatorial zone.

RECENT DEVELOPMENTS RELATED TO THE INVERSION MODEL

1. The Hydrogen Abundance.

   Recently, Münch *et al.* (1977) observed the (3-0) S1 quadrupole line region on Titan, and found *no* evidence for absorption there. They established a 3σ upper limit corresponding to a column abundance of 1 km-atm. This result differs from Trafton's (1972a) finding of 5 km-atm. It could represent an exotic variability on Titan, but the preferred interpretation of the author is that it means there is little and possibly no H_2 there. Münch *et al.* (1977) had superior spectral resolution to Trafton (1972a), and Trafton required a sophisticated statistical analysis to extract information not evident in the raw data.

   If true, the new result of Münch *et al.* (1977) does not directly alter the inversion model. As Danielson *et al.* (1973) stated: "Although no H_2 is required, the presence of some H_2 as reported by Trafton is readily accommodated." However, the absence of H_2 will provide an obstacle to all greenhouse models which require it to provide opacity between 15 μm and 35 μm. As will be discussed below, an atmosphere free of H_2 could have important photochemical implications. Further, it has been

a continuing problem (Hunten, 1977) to understand how an appreciable steady-state concentration can accumulate on Titan because of its rapid loss to space.

2. The Methane Abundance.

Trafton (1972b) estimated the CH_4 column abundance to be 2 km-Amagat if CH_4 is the only major constituent of the atmosphere. Lesser abundances would have been allowed if there was another major gas to broaden the lines of the $3\nu_3$ band of CH_4 observed by Trafton.

Lutz *et al.* (1976) derived a CH_4 abundance of 80 m-A, thereby implying the presence of $\simeq$20 km-A of some other gas, such as N_2 or Ne. Their result came from laboratory and planetary observations of the visible and near infrared overtone and combination bands of CH_4. Their two kinds of observations were scaled by a simple reflecting layer model for Titan's atmosphere.

However, Podolak and Danielson (1977) and Podolak and Giver (1978) have argued that the reflecting layer model is inadequate to represent all the CH_4 bands observed on Titan. These bands vary in intrinsic strength by several orders of magnitude. Even the strongest of them in Titan spectra have finite residual central intensity. These papers explain the central band reflectivity as being due to backscattered light from the same dust particles that cause the previously discussed ultraviolet absorption. The change in optical properties from ultraviolet to red is due to the assumed variation of the imaginary index of refraction of the dust with wavelength and also due to the modelled particle size distribution. By judiciously limiting the permitted particle sizes, Podolak and Danielson (1977) find that ultraviolet photons see the particles as large compared to wavelength, and hence experience strong forward scattering, whereas red photons see small particles and are isotropically scattered. Podolak and Danielson (1977) simultaneously explain most of the CH_4 spectral features and the continuum variation in albedo with their dust model. They require a CH_4 column abundance $\simeq$1 km-atm.

Podolak and Giver (1978) have modified the model by confining the dust to the upper layers of Titan's atmosphere. This is reasonable if the dust is formed at high altitudes, grows continuously in size, and settles rapidly to the surface after reaching a critical size. This

adjustment increases the observed strengths of weak bands relative to strong ones. They ultimately derive a CH_4 abundance of at least 2 km-A.

When the results of Podolak and Giver (1978) are combined with those of Trafton (1972b), the inversion model, with its column abundance of 2 km-A, is entirely consistent with the methane absorption spectrum.

3. Dust.

One of the interesting claims of Podolak and Danielson (1977) is that the continuum reflectivities of both Titan and Saturn from 2500Å to 10,000 Å can be explained by dust particles with the same optical properties for both planets. The only changes required are in the total amount of the dust and its vertical distribution. While this conclusion is not universally accepted (Scattergood and Owen, 1977; see also the discussion below), it will be stipulated for the present for the purpose of illustrating, if not proving, a point.

Although Saturn's atmosphere shows pronounced variations in color according to season, its equator is usually very dark in the ultraviolet. The standard interpretation is that this corresponds to a latitudinally restricted concentration of dust particles. However, photographs taken through a narrowband filter in the strong 8900 Å CH_4 band show the equatorial region to be relatively brighter than the rest of the planet (Owen, 1969).

Although Owen interpreted his observation as a high-altitude CH_4 condensation cloud at Saturn's equator, more recent models (e.g., Caldwell, 1977b) do not favor this interpretation. The one-way optical depth for absorption in this band is probably in the range from 1 to 3 above the cloud tops. It is more probable that Owen (1969) has actually recorded scattered light from high altitude dust particles. Unfortunately, it is not now possible to exhibit such an effect visually for Titan, because of the limits of spatial resolution. This alternate interpretation of Owen's results supports the concepts of Podolak and Danielson (1977) and of Podolak and Giver (1978).

Laboratory experiments on dust particle formation have recently been performed by Scattergood and Owen (1977). They used high energy

proton bombardment of simulated planetary atmospheres to dissociate such species as H_2, N_2, CH_4, NH_3, and H_2S, and then observed the resulting particulate formation. Their work was an advance over that of Khare and Sagan (1973) because Scattergood and Owen could initiate reactions in mixtures excluding the long wavelength photon acceptors NH_3 and H_2S. Because of experimental difficulties, Khare and Sagan required these molecules to absorb light longward of 2000 Å before they could initiate any reactions. Chang (this volume) has further discussed the relevance of high energy.

Scattergood's and Owen's result indicate that particles suitably colored to reproduce observed planetary reflectivities from visual to ultraviolet wavelengths do not form unless such species as N_2, NH_3, or H_2S are present. Specifically, they claim that simple mixtures of H_2 and CH_4 do not produce particles with the required coloration.

The inversion model can readily accommodate minor amounts of most of these gases without changing the basic features of the model. However, they could not be major species, or the simultaneous satisfaction of the limits imposed by Trafton (1972b) and by Podolak and Giver (1978) would be impossible. N_2 has a high vapor pressure, and could be the remnant from primordial NH_3 previously photodissociated. H_2S also has a higher vapor pressure than NH_3, and is not excluded by any spectroscopic observations. It could conceivably have a source in the interior of Titan.

IMMINENT DEVELOPMENTS IN TITAN STUDIES

1. Ultraviolet Spectroscopy.

   On January 26, 1978, the International Ultraviolet Explorer was launched successfully. This satellite will extend the wavelength range and the resolution significantly beyond the capabilities of OAO-2 (Caldwell, 1974, 1975). The possible detection of Rayleigh scattering below 2600 Å and of spectral signatures of specific molecules could lead to model constraints too various to outline here. Titan is a high priority target for the IUE, so significant results may be expected soon.

2. Radio Wavelength Observations.

At millimeter and centimeter wavelengths, it is a fair prospect that Titan's atmosphere will be transparent. Measurements there offer the possibility of sampling the surface unambiguously and of differentiating between candidate molecules. A major problem has been that diffraction makes the detection of a relatively weak signal from Titan difficult in the presence of the very strong confusion from Saturn itself.

Existing and future radio observations are summarized in Table 1. Briggs (1974) used the NRAO interferometer at Greenbank with three baselines of 0.5, 1.9, and 2.4 km, observing at 3.7 cm for 19 hours. Scaling his result to the baseline surface radius of 2700 km (Caldwell, 1977a) gives a brightness temperature of 99 ±34K. This result supports the inversion model. The limiting factor in Briggs' work is signal to noise.

Table 1. Radio Observations of Titan

Reference	Instrument	Wavelength	T_B*	Limitations
Briggs (1974)	NRAO Interometer (Greenbank)	3.7 cm	99 ± 34	Signal to Noise, confusion with Saturn
Conklin *et al.* (1977)		3.3 mm	213 ± 38	Confusion with Saturn
Jaffe *et al.* (1978)	VLA	1.3, 2, 6 cm	90 ± 30	Signal to Noise
---	Bonn 100 m dish	1.3 cm	---	No Data Yet

* Assumed surface radius = 2700 km

Conklin *et al.* (1977) used the 36-foot millimeter dish at NRAO Tucson in the photometer mode. They made two observations three months apart. Saturn was out of the primary beam, but currently unmeasured side lobes can generate 200% systematic errors from such a close, bright object. Conklin *et al.* were careful to measure the background after Titan had moved away, but they cannot rule out temporal changes in the side lobes. The measurements were in two broad bandpasses near 3.3 mm, with the

resulting brightness temperature of 213 ± 38 K for a surface radius of 2700 km.

If their measurement represents the surface temperatures, as Conklin *et al.* (1977) conclude, then the inversion model would need a major revision, along the lines suggested by Figure 20.2 of Hunten (1977), or Hunten's article in this volume.

The disagreement between the two published observations could be real because they are at different wavelengths, but the requisite atmospheric opacity to produce such numbers seems unphysical. Further observations were clearly needed. Recently, Jaffe *et al.* (1978) used the Very Large Array interferometer at Socorro, New Mexico to remeasure Titan at 1.3, 2 and 6 cm. The total observing time was 35 hours on three nights, including simultaneous observations at different wavelengths on one night. From night to night, between 4 and 8 dishes were available, with baselines up to 10 km. Ultimately, 27 dishes with baselines up to 35 km will be operable. Currently, signal to noise limits the data, but since this improves as the square of the number of working dishes, this problem will eventually diminish greatly. Confusion with Saturn is of relatively low importance. In fact, the instrument will eventually be capable of measuring the radius of the surface of Titan.

Preliminary analysis of VLA observations at 6 cm indicates a nominal brightness temperature of 90 K ± 30 K(1σ) for a surface radius of 2700 km, with an upper limit of 180 K (3σ). This is in good agreement with Briggs (1974) but disagrees with Conklin *et al.* (1977). Further analysis, to reduce the remaining uncertainty, is underway.

Finally, it is noted in Table 1 that the 100 meter dish in Bonn will also be capable of making useful measurements for Titan, but such measurements have not yet been done.

SUMMARY AND PROSPECT

Pending a clarification of the radio brightness measurements outlined immediately above, the inversion model for Titan, as proposed by Danielson *et al.* (1973) and modified by Caldwell (1977a), remains completely viable. Baseline parameters of the model are: surface temperature = 78 K; column abundance of CH_4 = 1.6 km-atm; surface

pressure = 16 mbar. Engineering studies for Titan probe missions must consider these numbers.

It is probable that Titan is a highly evolved planet. It is different from the Jovian planets in that significant quantities of its atmosphere can escape over the life of the solar system. It also lacks a means of thermally recycling atmospheric dust particles to fully reduced compounds in its interior. It is reasonable to expect that the current wide range of Titan atmospheric models will soon be narrowed greatly. When this preliminary phase is complete, future studies should address the task of unravelling Titan's evolutionary history. Direct exploration by space vehicles seems to be the only means available for doing this.

ACKNOWLEDGEMENTS

This work represents one phase of research being done at Stony Brook with the support of NASA grant NSG-7320 and NSF grant ENG 75-02986-A01.

REFERENCES

Allen, D. A. and Murdock, T. L. (1971). Infrared photometry of Saturn, Titan and the rings. *Icarus 14*, 1–2.
Barker, E. S. (1977). Progress report: Copernicus observations of solar system objects (abstract). *Bull. Amer. Astron. Soc. 9*, 465.
Briggs, F. H. (1974). The radio brightness of Titan. *Icarus 22*, 48–50.
Caldwell, J. (1974). Ultraviolet observations of Titan from OAO-2. In *The Atmosphere of Titan* (D. M. Hunten, ed.) pp. 88–91. NASA-SP 340.
Caldwell, J. (1975). Ultraviolet observations of small bodies in the solar system by OAO-2. *Icarus 25*, 384–396.
Caldwell, J. (1977). Thermal radiation from Titan's atmosphere. In *Planetary Satellites* (J. A. Burns, ed.) pp. 438–450. University of Arizona Press, Tucson.
Caldwell, J. (1977b). The atmosphere of Saturn: an infrared perspective. *Icarus 30*, 493–510.
Cess, R. D. and Owen, T. (1973). Titan: The effect of noble gases on an atmospheric greenhouse. *Nature 244*, 272–273.
Conklin, E. K., Ulich, B. L., and Dickel, J. R. (1977). 3-mm observations of Titan. *Bull. Amer. Astron. Soc. 9*, 471.
Danielson, R. E., Caldwell, J., and Larach, D. R. (1973). An inversion in the atmosphere of Titan. *Icarus 20*, 437–443.
Gillett, F. C., Forrest, W. J., and Merrill, K. M. (1973). 8-13 micron observations of Titan. *Astrophys. J. 184*, L93–L95.
Gillett, F. C. (1975). Further observations of the 8-13 micron spectrum of Titan. *Astrophys. J. 201*, L41–L43.
Hunten, D. M. (1977). Titan's atmosphere and surface. In *Planetary Satellites* (J. A. Burns, ed.) pp. 420–437 University of Arizona Press, Tucson.
Jaffe, W., Caldwell, J., and Owen, T. (1978). Centimeter observations of Titan with the VLA. In preparation.
Knacke, R. F., Owen, T., and Joyce, R. R. (1975). Infrared observations of the surface and atmosphere of Titan *Icarus 24*, 460–464.
Kuiper, G. P. (1944). Titan: A satellite with an atmosphere. *Astrophys. J. 100*, 378–383.
Lewis J. S., and Prinn, R. A. (1973). Titan revisited. *Comments Ap. Space Phys. 5*, 1–7.
Low, F. J., and Rieke, G. H. (1974). Infrared photometry of Titan. *Astrophys. J. 190*, L143–L145.
Lutz, B. L., Owen, T., and Cess, R. D. (1976). Laboratory band strengths of methane and their application to the atmospheres of Jupiter, Saturn, Uranus, Neptune, and Titan. *Astrophys. J. 203*, 541–551.
Morrison, D., Cruikshank, D. P., and Murphy, R. E. (1972). Temperatures of Titan and the Galilean satellites at 20 microns. *Astrophys. J. 173*, L143–L146.
Munch, G., Trauger, J. T., and Roesler, F. L. (1977). A search for the H_2 (3,0) S1 line in the spectrum of Titan. *Astrophys. J. 216*, 963–966.
Owen, T. (1969). The spectra of Jupiter and Saturn in the photographic infrared. *Icarus 10*, 355–364.
Podolak, M., and Danielson, R. E. (1977). Axel dust on Saturn and Titan. *Icarus 30*, 479–492.
Podolak, M., and Giver, L. P. (1978). On inhomogeneous scattering models of Titan's atmosphere. Submitted to *Icarus*.
Pollack, J. B. (1973). Greenhouse models of the atmosphere of Titan. *Icarus 19*, 43–58.
Scattergood, T., and Owen, T. (1977). On the sources of ultraviolet absorption in spectra of Titan and the outer planets. *Icarus 30*, 780–788.
Trafton, L. M. (1972a). On the possible detection of H_2 in Titan's atmosphere. *Astrophys. J. 175*, 285–293.
Trafton, L. M. (1972b). The bulk composition of Titan's atmosphere. *Astrophys. J. 175*, 295–306.
Trafton, L. M. (1975). Near-infrared spectrophotometry of Titan. *Icarus 24*, 443–453.

A TITAN ATMOSPHERE WITH A SURFACE TEMPERATURE OF 200 K

Donald M. Hunten

Department of Planetary Sciences and Lunar and Planetary Laboratory
University of Arizona
Tucson, Arizona 85721

ABSTRACT

The brightness temperature of Titan at 3 mm wavelength is around 200 K, according to Ulich, Conklin, and Dickel (1978). Although an earlier measurement by Briggs is much colder, we adopt 200 K as the surface temperature and build an atmospheric model with a surface pressure of 21 bars. CH_4 clouds form between 100 and 120 km altitude. The visual limb is near 200 km. The methane mixing ratio is 0.25% above the clouds and 7% below; the dominant gas is assumed to be N_2. The thermal opacity is due to pressure-induced absorption in N_2 and a trace (0.5%) of CH_4, with some help from cloud particles; unit opacity is reached at 600 mbar, 110 km from the surface. The radius of the solid body in this model is 2700 km, in reasonable agreement with 2600 km obtained if the density is the same as that of Ganymede and Callisto. Deeper atmospheres can be obtained if the temperature gradient is subadiabatic or greater CH_4 abundance is assumed.

INTRODUCTION

It has been clear for some years that a deep, cloudy atmosphere, with a surface pressure of many bars, was not ruled out for Titan by any existing data (Lewis and Prinn, 1973; Pollack, 1973). On the other hand, no data required it. Recently, however, Ulich *et al.* (1978) have obtained a 3-mm brightness temperature of 200 K. It is, therefore, worthwhile to explore the properties of a deep atmosphere in some detail. The model has quite a bit in common with the established picture of Venus, with a surface temperature 3-4 times the effective temperature, and a dense cloud

layer tens of km deep. Because of the lower gravity, however, this depth is achieved with a lower surface pressure, only 21 bars.

Since the next three sections are devoted to a variety of detailed discussions, we refer ahead to the final model illustrated in Figure 3. There is a clear layer 100 km deep composed of N_2 with a few % of CH_4. Dense methane clouds form at 100 km and extend up another 10–20 km. Their top is diffuse enough to have an important effect on the formation of the observed absorption bands. We do not treat the question of how much solar radiation penetrates to the surface to drive the greenhouse, but we can appeal to the analogy with Venus to suggest that the mechanism is at least plausible.

The model presented here is far from unique, but we feel it to be conservative, in the sense that any plausible variant with a 200 K surface would have a still deeper atmosphere and greater surface pressure. An absorbing layer at the 200 K level is one possibility; another has more methane vapor, which increases the scale height and gives a deeper region of small (wet adiabatic) lapse rate. Or the lapse rate could be less than the adiabatic.

A summary of numerical data for Titan is given in the Appendix. Earlier reviews appear in the books edited by Hunten (1974) and Burns (1977). We make no attempt to summarize this material, but some of it is surveyed and updated in the preceding article by Caldwell.

THE RADIO DATA

The brightness temperature T_B deduced from a radio flux measurement is inversely proportional to the square of the assumed radius. Table 1 shows the data of Ulich *et al* (see also Conklin *et al.*, 1977) and Briggs (1974) as given and as converted to a radius of 2700 km, justified below.

Table 1. Radio Data

Source	Wavelength (mm)	T_B (K)	Radius (km)	T_B (2700) (K)
Ulich *et al.*	3	200	2900	231
Briggs	37	103	2550	115

Although each result has fairly large error bars, they do not overlap. Since we do not know how to resolve the discrepancy, we take a round value of 200 K for the present work, assuming it to be the surface temperature. The bias above the mean of the data is partly to account for an emissivity less than unity. The radiating layer could also be within the atmosphere if there is enough microwave opacity, due perhaps to NH_3. For convenience, however, we shall use the term "surface". A lower temperature, if required by later data, is readily accommodated by inserting a new "surface" at the appropriate height.

COMPOSITION OF THE VISIBLE ATMOSPHERE

Quantitative interpretation of the "red" bands of CH_4 (which extend from 4410 to 9000 Å) has only recently become possible through the laboratory work of Lutz, Owen, and Cess (1976) (hereafter, LOC), Fink, Benner, and Dick (1977), and Giver (1978). For practical purposes, the absorption at each wavelength is purely exponential and independent of pressure; an observation of Titan, therefore, gives a methane abundance, and LOC obtained 80 m-A (meter-Amagat). Lines of the $3\nu_3$ band are pressure-dependent in a known way; LOC used a result by Trafton (1975b), with their methane abundance, to obtain a total abundance of 21 km-A (if the major gas is N_2); the corresponding pressure is 300 mbar for a gravity of 117 cm s^{-2}, and the CH_4 mixing ratio 0.4%. There is no direct evidence that the gas is N_2, but we feel the indirect arguments for it are strong (Hunten, 1973, 1977).

This analysis assumes that the visible atmosphere is a clear gas above a discrete cloud top: the reflecting layer model or RLM. If, on the other hand, the cloud top is very fuzzy, the homogeneous scattering model or HSM is more appropriate. Indeed, Trafton (1975a) has already clearly demonstrated that the RLM does not fit the data; the analysis below merely substitutes laboratory data for the Saturn data he was forced to use. A crude HSM analysis has kindly been carried out by L. Wallace, as illustrated in Figure 1. The residual intensities, as a fraction of the nearby continuum, were estimated for several wavelengths from the spectra published by Trafton (1975a), and were plotted against the laboratory absorption coefficients of Giver (1978). It can hardly be claimed that the HSM, represented by the solid curves, is a good fit to the points, but at least it is much better than the RLM, which is simply an exponential. Some of the discrepancies may derive from the assumed location of the continuum at

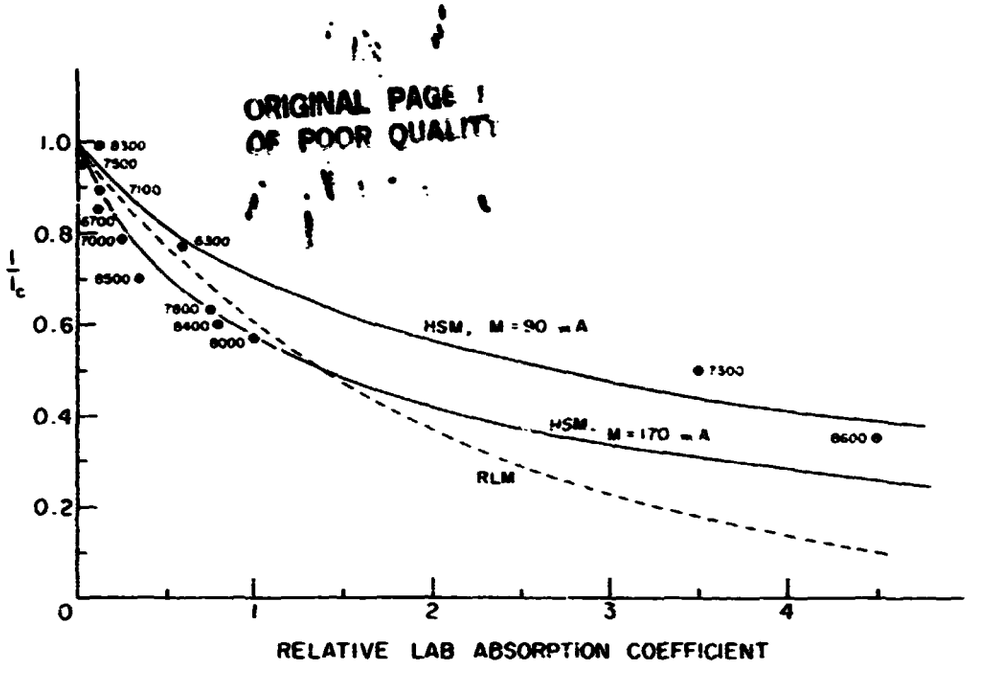

Figure 1. Rough analysis of Titan's "red" CH_4 bands. Points are estimates of intensity I divided by continuum intensity I_c. The solid curves are HSM models for two different specific amounts M, and the dashed line shows an RLM. (Wavelengths are ± 30 Å, except "6300" which should be 6165. The "8300" point should be at .012, not 0.12.)

longer wavelengths: it may be that the continuum is never reached. The best fit lies between the two curves of Figure 1; we adopt a specific methane abundance M of 150 m-A per mean free path.

To interpret the $3\nu_3$ line, we use the curve of growth (their Figure 12) derived by Wallace and Hunten (1978), which takes account of the varying pressure through the scattering atmosphere. With the specific abundance and equivalent width as input, we get a value for p_1, the pressure at unit scattering optical depth. For this first rough analysis, we divided Trafton's (1975b) equivalent width of 1.0 Å, and the laboratory strength, by 2, since the line can be approximated as a doublet with only slight overlap. The broadening coefficient at 1 bar is $\alpha^\circ = 0.169\ cm^{-1}$ for N_2 at 100 K (Darnton and Margolis, 1973). The result is p_1 = 900 mbar; the N_2 abundance corresponding is 63 km-A which, like the CH_4 specific abundance, is referred to unit mean free path. The ratio, 0.24%, is therefore, the CH_4 mixing ratio according to the HSM. It makes little difference whether we use the RLM or the HSM, but we shall adopt the latter value, which is clearly uncertain by at least a factor of 2.

Methane photolysis and escape of the resulting H_2 gives a predictable H_2 mixing ratio of 0.47% (Hunten, 1973, 1977). Our picture of the visible atmosphere is therefore:

- A gas, predominantly N_2 containing 0.25% CH_4 and 0.5% H_2;
- A cloud (argued below to be mainly liquid CH_4) with a very diffuse top, and unit optical depth at 900 mbar;
- A haze of "Axel dust" (Danielson *et al.*, 1973; Caldwell, 1977) extending well into the stratosphere. Since it is probably a mixture of methane photolysis products, it is likely to dissolve readily in the methane cloud droplets and give them also a dark color.

Elliot, Veverka, and Goguen (1975) have obtained a radius of 2900 km by analysis of a lunar occultation. It is known that a scattering atmosphere closely resembles a Lambert sphere, the model that was used (Harris, 1961). But what pressure level does the radius refer to? A ray grazing the limb encounters unit optical depth due to molecular scattering alone at a pressure of 50 mbar. In Titan's impure atmosphere, the level might be higher by 1 or 2 scale heights, or the pressure as low as 10 mbar. About 4 scale heights, or 100 km, separate this level from the 900 mbar level; the latter is, therefore, close to 2800 km radius, a value we henceforth adopt.

FAR-INFRARED OPACITIES

It is now necessary to tie the optical structure to the thermal structure. As on Venus, a high surface temperature can be sustained only by a large opacity, probably greater than 100, through the whole thermal infrared. Pollack (1973) has laid much of the groundwork for study of a Titan greenhouse. We have simply adopted his illustrative result for pressure-induced absorption in H_2, scaling by the factor 2.67 (Kiss, Gush, and Welsh, 1959) appropriate for collisions with N_2 instead of H_2. Nitrogen opacity (Bosomworth and Gush, 1965) dominates at the lower frequencies below 350 cm^{-1}, and totally swamps the CH_4 absorption which has a similar shape. Bosomworth and Gush give N_2 data only at 298 K; we have omitted the temperature correction to both width and strength of the absorption, discussed by them and also by Pollack (1973). The adopted curve is shown in Figure 2.

As found below, the gases alone have plenty of opacity to blanket the warm surface. But it is known that the structure due to the H_2 S(0) and S(1) lines does not appear

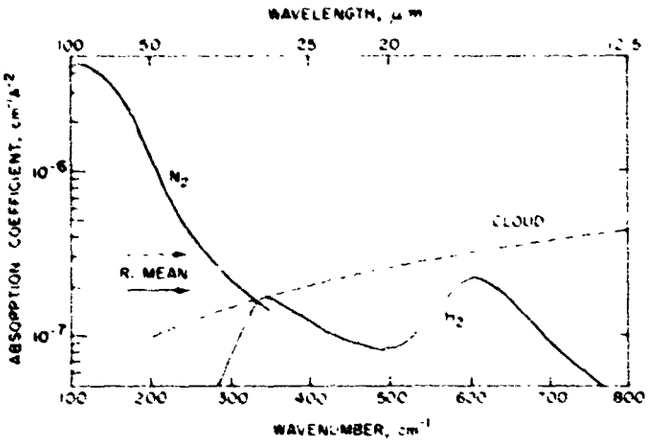

Figure 2. Pressure-induced opacities for N_2 with 0.5% H_2, and an assumed cloud opacity. The latter is referred to the N_2 pseudo-Rosseland mean; the mean with and without cloud

in Titan's thermal emission spectrum (Pollack, 1973; Low and Rieke, 1974; Hunten, 1977). It is reasonable to suppose that the cloud particles provide enough opacity above 350 cm^{-1} to smooth out the structure. Liquid methane alone would not be adequate, but the dissolved hydrocarbons already referred to might give enough absorption at all frequencies. Following Danielson *et al.* (1973), we have adopted the curve shown in Figure 2, with opacity proportional to frequency. Use of the HSM implies uniform mixing of particles and gas; if, however, the particle mixing ratio increases downwards, the corresponding absorption can be crudely represented in the same terms as the N_2 absorption.

We now form the Rosseland mean of the data in Figure 2 (e.g., Schwarzschild, 1958):

$$\frac{1}{\bar{A}} = \frac{15}{4\pi^4}\int_0^\infty \frac{x^4 e^{-x}\,dx}{A_x (1-e^{-x})^2} \qquad (1)$$

where $x = h\nu/kT$ and A is the absorption coefficient. Without cloud opacity, the result is

$$\bar{A} = 1.87 \times 10^{-7}\ cm^{-1}\ A^{-2};$$

with clouds included, we have

$$\bar{A}_c = 3.10 \times 10^{-7}\ \mathrm{cm}^{-1}\ \mathrm{A}^{-2}.$$

The level having temperature T_e, the effective temperature, is taken at the depth where the optical depth τ is unity. For pressure-induced absorption,

$$\tau = \frac{\bar{A}}{2H} w^2(N_2), \tag{2}$$

where H is the scale height and $w(N_2)$ is the abundance. Solving for the latter, and converting to pressure, we find

$$p = 790 \text{ mbar (no cloud)}$$
$$= 610 \text{ mbar (with cloud)}$$

We adopt the latter estimate and give it the equilibrium temperature 77 K. It is slightly above the 900 mb level that has unit cloud optical depth in the red. For the stratosphere we simply accept the thermal-inversion model of Caldwell (1977 and preceding chapter of this volume).

THE DEEPER ATMOSPHERE

We shall, somewhat loosely, use the name "tropopause" for the point (610 mbar, 77 K) just derived. For the deeper structure we assume an adiabat, making allowance for the latent heat of condensation of the methane that forms the cloud.

Sagan (1969) has given a conveniently parameterized discussion of radiative and convective temperature gradients, and finds them so nearly the same that the tropopause location is often very sensitive to small changes. Conversely, the profile is insensitive to just where the tropopause occurs.

As a first approximation we neglect latent heat and find the pressure that corresponds to 200 K. The adiabatic lapse rate for N_2 is $\Gamma = \mu g/C_p = 1.16$ K/km and the scale-height gradient is $\beta = -1/3.5$. With the standard expression (e.g., Hunten, 1971) for the barometric law,

$$\frac{p}{p_o} = \left(1 + \frac{\beta z}{H_o}\right)^{-1/\beta} = \left(\frac{H}{H_o}\right)^{-1/\beta}, \tag{3}$$

we can substitute the ratio of temperatures (200/77) for H/H_o and obtain a pressure ratio of 28.2. This estimate of the surface pressure is therefore, $0.61 \times 28.2 = 17.2$ bars. After allowance for condensation as described below, a better estimate is 19.7 bars of N_2. A possible surface material is methane clathrate hydrate, whose vapor pressure is 1.38 bars at 200 K (see Appendix). The atmospheric composition at the surface would thus be about 6.6% CH_4, 93% N_2, which gives a total pressure

p_s = 21.1 bars, as well as plenty of material to condense into the clouds. Since the vapor pressure of CH_4 is about 2 orders of magnitude greater than that of clathrate, there will be an extended clear region above the surface. Once the cloud is reached, the dry adiabat used for the preliminary estimate is not satisfactory. Various expressions for the wet lapse rate appear in the literature (Brunt, 1933, 1939; Danielson *et al.*, 1977), but the best seems to be that of Lasker (1963). In practice the differences are minor, especially since the fate of the condensate is uncertain. If it falls out or remains at the height where it condenses, its specific heat should be omitted, and the curve is called a "pseudoadiabat". If the condensate moves with the gas, the situation is truly adiabatic. Lasker's expression for the pseudo-adiabat is

$$-\beta = \frac{d \ln T}{d \ln p} = \frac{1 + \gamma(1 + \alpha)}{(C_p/R) + \gamma\alpha(1 + \alpha)} . \qquad (4)$$

Here β is the same quantity used in (3), which, however, is valid only over a region where β is constant. The specific heat C_p pertains to the mixture of gas and vapor; γ is the mixing ratio $[CH_4]/[N_2]$; and $-\alpha$ is the exponent in the vapor-pressure relation. For CH_4, $\alpha = 1024/T$ (see Appendix). As suggested by Lasker, a suitable method is to find the (T, p) relation from (4) and then obtain the height scale from the hydrostatic equation. Where β is independent of height, (3) may be used, and it gives useful accuracy even where β is slowly varying. In the present case, γ varies from 0.070 to essentially zero and $\alpha \simeq 12.5$; $-\beta$ is 0.282 below the cloud, and drops to 0.127 at the cloud base, back to 0.286 above the cloud.

Figure 3 shows the model. The vertical scale is linear in the logarithm of pressure, with an auxiliary (nonlinear) height scale. The Danielson-Caldwell stratospheric model does not specify a pressure scale; the one adopted is by analogy with the Jupiter model of Orton (1977).

The cloud base is at 103 km and has a methane partial pressure of 70 mbar at a total pressure of 1080 mbar. The potential cloud mass is the amount contained in a scale height, or 600 g cm^{-2}. In the form of 10 μm diameter droplets, this amount would have a scattering optical thickness of over 10^6. Thus, most of it could precipitate out and still leave a very respectable cloud. The temperature is 87 K, somewhat below the freezing point (89 K); the form may therefore be either crystals or supercooled droplets. The level found in Section 3 for unit optical depth in the "red" is a few km above the base, a reasonable location.

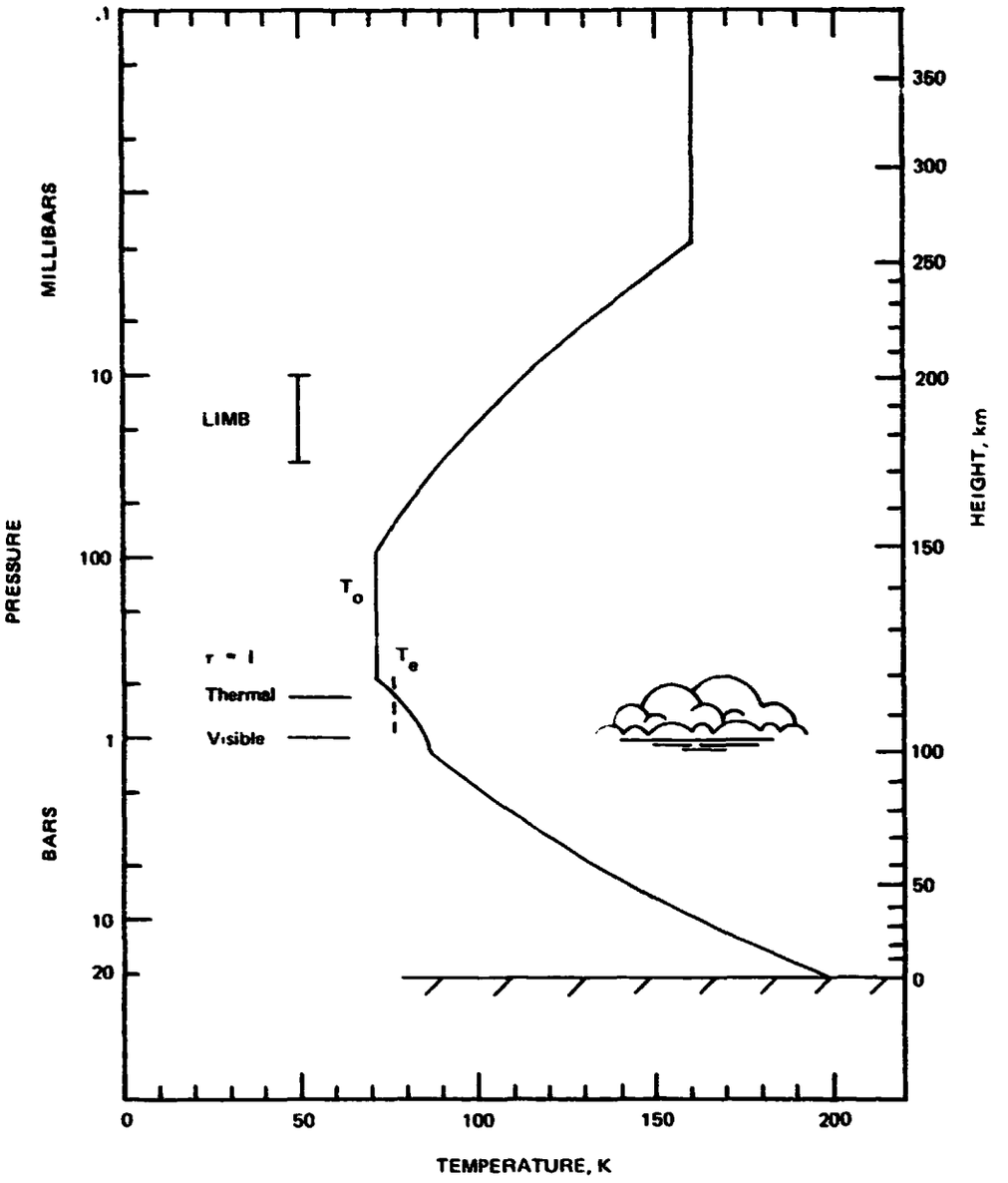

Figure 3. Temperature as a function of log pressure, along with a height scale. The position of the cloud layer is sketched, and the levels of unit thermal and visible opacity are indicated. If the surface is at a radius of 2700 km, the limb position shown is in agreement with the observed radius of 2700 km.

DISCUSSION

As pointed out in the Introduction, the present model is conservative in the sense that any other that gives a "surface" temperature of 200 K requires an even deeper atmosphere. A totally different argument is to estimate the radius of solid Titan from its known mass and a reasonable mean density. For the latter, we take Callisto and Ganymede as analogs, weighting the densities of Morrison *et al.* (1977) inversely by the stated errors. The result (1.89 g cm^{-3}) combines with a mass of 1.40×10^{26} g to give a radius of 2605 km. A 10% change of density reflects into a radius change of 80 km. Titan is likely to be less dense, if anything, than any Galilean satellite; if so, a reasonable range for the radius is 2600–2700 km, which just includes the value from the atmospheric model.

The vapor pressure of NH_3 dissolved in ice is roughly 1 mbar at 200 K. The mixing ratio could thus be around 5×10^{-5}. The optical depth of this amount is about 8 at 3 mm wavelength, according to the approximate treatment of Field (1959). Perhaps the ammonia is kept out of the atmosphere by a layer of hydrocarbons on the surface.

Much of this paper is built on the assumption that the surface temperature is 200 K, as suggested by the microwave observations. The issue of ammonia opacity only serves to point up the crucial nature of such data, and the importance of data at other wavelengths. The disagreement shown in Table 1 is particularly disturbing, and a resolution is badly needed. The measurements are, however, so difficult that progress is sure to be slow. Ammonia opacity cannot be called on, because it is nearly the same at the two wavelengths. The preliminary VLA results reported by Caldwell at the end of the preceding chapter support a lower temperature, although they would still permit it to be above 150 K. However, a temperature of, say, 100 K can be accommodated by placing the surface at 2 bars or 85 km in Figure 1. The model is unchanged at greater heights.

Added after the Workshop:

Shortly after the Workshop, a preprint by Podolak and Giver (1978) became available. This work, an extension of Podolak and Danielson (1977), adopts as its model an atmosphere of pure CH_4, 2 km-A deep, with a layer of Axel dust occupying the top

50 m-A. This dust is nearly opaque in the blue, grading rather suddenly in the red to essentially transparent in the infrared. The surface (or cloud top) has an albedo of 50-60%. An excellent fit is obtained to the observed CH_4 bands from 5000 to 10,000 Å. Although the $3\nu_3$ band is not discussed, the model is consistent with Trafton's analysis for a reflecting-layer model, which requires 1.5 km-A if the atmosphere is pure CH_4. At this and longer wavelengths, the Podolak-Giver model reduces to a reflecting layer.

How might a choice be made between this model and the one described here? They were both fitted to the same data; thus we require some additional information. Two recent lines of evidence can in fact be brought forward: (1) the work of Rages and Pollack reported in Chapter 11 of this volume; (2) spectra of the 1-3 μm region.

Rages and Pollack find the mean particle radius to be 0.2-0.4 μm, and strongly exclude the value (slightly under 0.1 μm) required by Giver and Podolak to obtain the necessary optical properties.

The infrared spectra, shown in Figure 4, were obtained by U. Fink and H. Larson in 1975, and are reproduced here by their kind permission.

A detailed analysis has not yet been done, but two facts stand out clearly:

(1) The Titan spectrum is utterly unlike the laboratory spectrum of 1.5 km-A of methane.

(2) The closest analog to Titan in this spectral region is Neptune.

The laboratory spectrum is the analog of a clear atmosphere of pure methane (the Podolak-Giver model at these wavelengths). Neptune is an analog of a deep scattering atmosphere with a small fraction of methane. Although the major gas is assumed to be H_2-He on Neptune and N_2 on Titan, the important thing is the scale height, not the composition, and the scale heights are rather similar. These arguments strongly suggest that the deep, N_2-CH_4, atmosphere is preferred over the pure-CH_4 one. A detailed analysis is highly desirable, but in this spectral region it is very difficult because of the fine structure of the bands.

A direct comparison of a laboratory spectrum with Titan may be misleading because of the gross differences in the temperatures and pressures at which the CH_4 is observed. It has been shown by Ramaprasad *et al.* (1978) in a study of liquid CH_4 that band shapes are somewhat different at 90 K than they are at a room temperature. For example, a band may be seen at 9170 Å in the spectra of the cold liquid and of Titan which is completely masked by the wing of the strong band at 8890 Å. The sensitivity of the populations of high J levels to temperature must be accounted for before a truly meaningful comparison can be made.

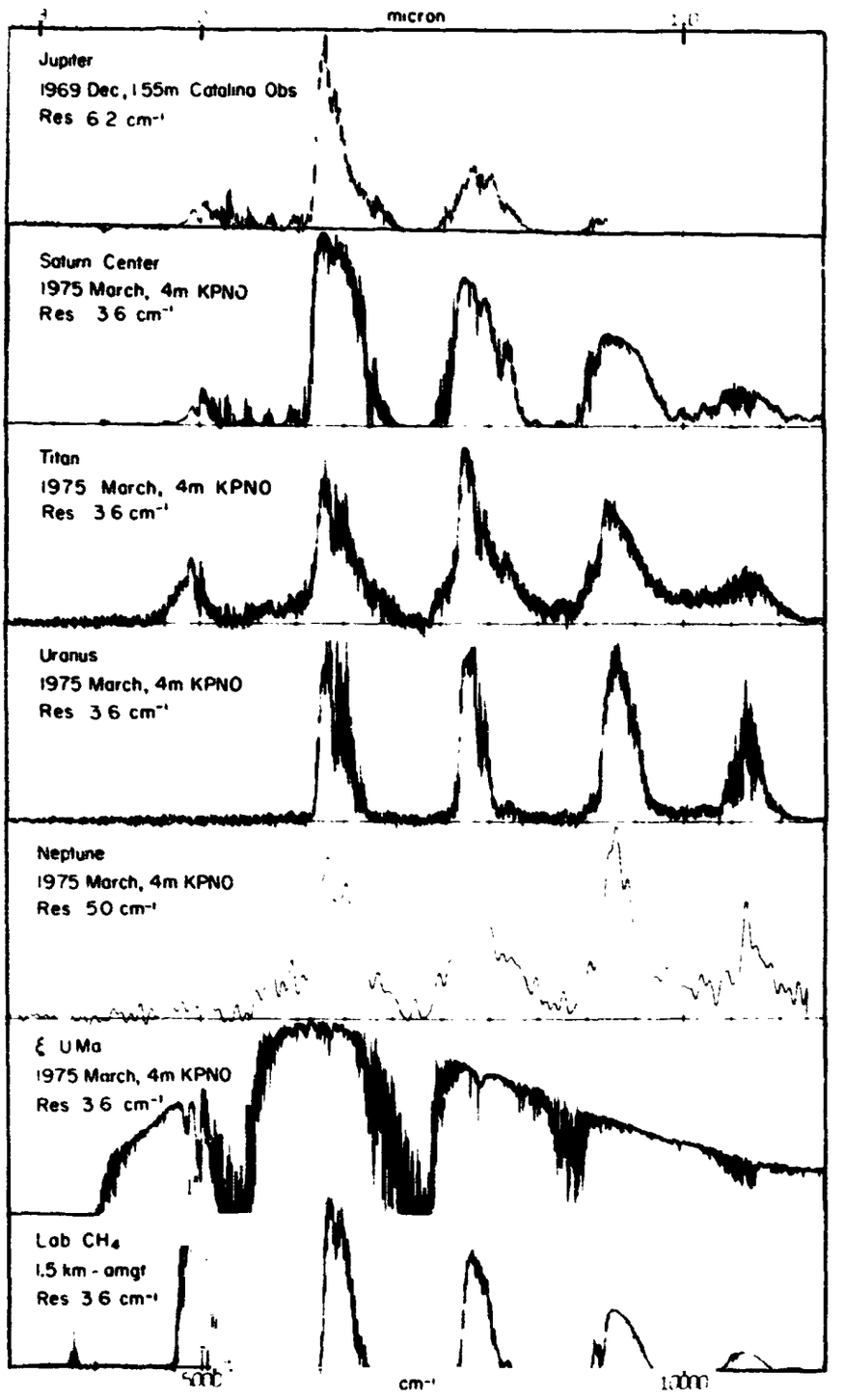

Figure 4. 1-2 5 μm spectra obtained in 1975 by U. Fink and H. Larson, reproduced by their kind permission. A solar-type star shows the atmospheric transmission.

Clearly, all this evidence refers only to the region that can be probed optically, and bears only on the composition of this region. The issue of the surface temperature and pressure is totally independent.

Atreya *et al.* (1978) have discussed in detail the production of N_2 by photolysis of NH_3, and have found that a surface partial pressure of 14-19 bars could reasonably be generated over the age of the solar system.

ACKNOWLEDGMENTS

I am indebted to B. L. Ulich for discussion of his microwave results, to L. Wallace for numerous discussions and contributions, to L. P. Giver and S. K. Atreya for preprints, and to U. Fink and H. Larson for permission to use Figure 4.

APPENDIX

Table 2 gives various quantities for three radial distances r corresponding to heights of 0, 100, and 200 km in the model. They are the acceleration of gravity g, the scale height for pure N_2 at a reference temperature of 100 K, the base pressure for an N_2 abundance of 1 km-Amagat, and the dry adiabatic lapse rate for N_2.

Table 2. Quantities for Three Radial Distances

r (km)	2700	2800	2900
g (cm s^{-2})	125	117	109
H (km)	23.8	25.5	27.2
p/N (mb/km-A)	15.6	14.6	13.6
r (dry) (K/km)	1.20	1.13	1.05

Table 3 gives constants in the vapor-pressure equation, $p = A \exp(-B/T)$, from Delsemme and Wenger (1970) and the Handbook of Chemistry and Physics. The melting point of methane is 89 K.

Table 3. Constants in the Vapor-Pressure Equation

Form	A(bar)	$B = \alpha T$
Clathrate	75,300	2182
Liquid	9,714	1024
Solid	59,662	1190

REFERENCES

Atreya, S. K., Donahue, T. M., and Kuhn, W. R. (1978). Evolution of an N_2 atmosphere on Titan. *Science* 201, 611–613.

Bosomworth, D. R., and Gush, H. P. (1965). Collision-induced absorption of compressed gases in the far infrared, Part II. *Can. J. Phys.* 43, 751–769.

Briggs, F. H. (1974). The radio brightness of Titan. *Icarus* 22, 48–50.

Brunt, D. (1933). The adiabatic lapse-rate for dry and saturated air. *Q. J. Roy. Met. Soc.* 59, 351–360.

Brunt, D. (1939). *Physical and Dynamical Meteorology* Cambridge at the University Press.

Burns, J. A. (ed.) (1977). *Planetary Satellites*. University of Arizona Press, Tucson. 598 pp.

Caldwell, J. (1977). Thermal radiation from Titan's atmosphere. In *Planetary Satellites* (J. A. Burns, ed.), pp. 438–450. University of Arizona Press, Tucson.

Conklin, E. K., Ulich, B. L., and Dickel, J. R. (1977). 3-mm observations of Titan. *Bull. Am. Astron. Soc.* 9, 471.

Danielson, R. E., Caldwell, J. J., and Larach, D. R. (1973). An inversion in the atmosphere of Titan. *Icarus* 20, 437–443.

Danielson, R. E., Cochran, W. D., Wannier, P. G., and Light, E. S. (1977). A saturation model of the atmosphere of Uranus. *Icarus* 31, 97–109.

Darnton, L. and Margolis, J. S. (1973). The temperature dependence of the halfwidths of some self- and foreign-broadened lines of methane. *J. Quant. Spectrosc. Radiat. Transfer* 13, 969–976.

Delsemme, A. H., and Wenger, A. (1970). Physico-chemical phenomena in comets. I. *Planet. Space Sci.* 18, 709–715.

Elliot, J. L., Veverka, J., and Goguen, J. (1975). Lunar occultation of Saturn. I. *Icarus* 26, 387–407.

Field, G. B. (1959). The source of radiation from Jupiter at decimeter wavelengths. *J. Geophys. Res.* 64, 1169–1177.

Fink, U., Benner, D. C., and Dick, K. A. (1977). Band model analysis of laboratory methane absorption spectra from 4500 to 10500 Å. *J. Quant. Spectrosc. Radiat. Transfer* 18, 447–457.

Giver, L. P. (1978). Intensity measurements of the CH_4 bands in the region 4350 Å to 10,600 Å. *J. Quant. Spectry. Radiat. Transfer* 19, 311–322.

Harris, D. L. (1961). Photometry and colorimetry of planets and satellites. In *Planets and Satellites* (G. P. Kuiper and B. M. Middlehurst, eds.) pp. 272–342. University of Chicago Press.

Hunten, D. M. (1971). Composition and structure of planetary atmospheres. *Space Sci. Rev.* 12, 539–599.

Hunten, D. M. (1973). The escape of H_2 from Titan. *J. Atmos. Sci.* 30, 726–732.

Hunten, D. M. (ed.) (1973). *The atmosphere of Titan*. NASA SP-340. 177 pp.

Hunten, D. M. (1977). Titan's atmosphere and surface. In *Planetary Satellites* (J. A. Burns, ed.), pp. 420 – 437. University of Arizona Press, Tucson.

Kiss, Z. J., Gush, H. P., and Welsh, H. L. (1959) The pressure-induced rotational absorption of hydrogen. I. *Can. J. Phys.* 37, 362–376.

Lasker, B. M. (1963). Wet adiabatic model atmosphere for Jupiter. *Astrophys. J.* 138, 709–719.

Lewis, J. S. and Prinn, R. G. (1973). Titan revisited. *Comments Ap. Space Phys.* 5, 1–7.

Low, F. J. and Rieke, G. H. (1974). Infrared photometry of Titan *Astrophys J.* 190, L143–145.

Lutz, B. L., Owen, T. C., and Cess, R. D. (1976). Laboratory band strengths of methane and their application to the atmospheres of Jupiter, Saturn, Uranus, Neptune, and Titan *Astrophys. J.* 203, 541–551.

Morrison, D., Cruikshank, D. P. and Burns, J. A. (1977) Introducing the satellites. In *Planetary Satellites* (J. A. Burns, ed.), pp. 3–17. University of Arizona Press, Tucson.

Orton, G. S. (1977). Recovery of the mean Jovian temperature structure from inversion of spectrally resolved thermal radiance data. *Icarus* 32, 41–57.

Podolak, M. and Danielson, R. E. (1977). Axel dust on Saturn and Titan *Icarus* 30, 479–492

Podolak, M. and Giver, L. P. (1978). On inhomogeneous scattering models of Titan's atmosphere *Icarus* (in press).

Pollack, J. B. (1973). Greenhouse models of the atmosphere of Titan *Icarus* 19, 43–58

Ramaprasad, K. R., Caldwell, J., and McClure, D. (1978). The vibrational overtone spectrum of liquid methane in the visible and near infrared. application to planetary studies. *Icarus*. In press.

Sagan, C. (1969). Gray and nongray planetary atmospheres. structure, convective instability, and greenhouse effect. *Icarus* 10, 290–300.

Schwarzschild, M. (1958). *Structure and evolution of the stars*. Princeton University Press. 296 pp.

Trafton, L. M. (1975a). The morphology of Titan's methane bands. I. *Astrophys. J.* 195, 805–814.

Trafton, L. M. (1975b). Near-infrared spectrophotometry of Titan. *Icarus* 24, 443–453.

Ulich, B. L., Conklin, E. K., and Dickel, J. R. (1978). Private communication.

Wallace, L. and Hunten, D. M. (1978). The Jovian spectrum in the region 0.4-1 1 μm: The C/H ratio. *Rev. Geophys. Space Phys.* In press.

TITAN'S ATMOSPHERE: COMMENTS ON HAZE CONTENT, METHANE ABUNDANCE, BAND SHAPES, AND HYDROGEN UPPER LIMIT

Laurence Trafton

Department of Astronomy
University of Texas at Austin
Austin, Texas 78712

ABSTRACT

This is a reply to the presentations of Caldwell and Hunten and was presented as part of the "discussion" following their papers.

I would like to reply to Caldwell's and to Hunten's presentations. First, I remind you that I have already demonstrated the existence of scatterers in Titan's atmosphere in a paper I published in the *Astrophysical Journal* three years ago (Trafton, 1975b). My conclusion is not affected by recent laboratory investigations showing that certain CH_4 bands are independent of pressure because I showed that the reflecting layer model fails to explain Titan's CH_4 absorptions *regardless* on which portion of the curve of growth Titan's CH_4 lines lie. In that paper, I used Saturn's atmosphere along the central meridian as my "laboratory" for studies of CH_4 absorption, arguing that my conclusion is insensitive to the moderate scattering there.

The quite pronounced role of scattering in Titan's atmosphere strongly suggests that Titan's surface is obscured. This is compatible with the lack of variation of Titan's brightness with orbital phase (Noland *et al.*, 1974), unless Titan has a featureless surface, because Titan almost certainly rotates synchronously about Saturn. Even if a smooth, featureless, or "tarry" surface exists (Hunten, 1973), the scattering probably veils it enough so that the ambiguity in interpreting Veverka's (1973) polarization measurements should be resolved in favor of atmospheric scattering rather than

reflection from a smooth surface. So as the case for a significant haze is strengthened, the case for a smooth surface is weakened.

My second point is that the fact that certain CH_4 bands studied in the laboratory do not depend on pressure does not alter the CH_4 abundances I have derived in previous papers. While I concede that laboratory measurements have since shown that certain CH_4 bands behave like a linear opacity (following Beer's law), at least for the pressures and temperatures investigated, it is well known that the R branch of the $3\nu_3$ CH_4 band deviates from this behavior in the atmospheres of Jupiter and Saturn (Belton, 1969; Trafton, 1973b) and, consequently, at lower pressures. That is, the absorption of the $3\nu_3$ CH_4 band depends on the pressure as well as the CH_4 abundance throughout the physical regime spanning the conditions between the atmospheres of Titan and Saturn. In my original paper on Titan's bulk composition (Trafton, 1972), I argued qualitatively that the bulk of Titan's atmosphere is large because the strong CH_4 bands should depend on pressure but I derived the quantitative relation between CH_4 abundance and bulk composition on the basis of the Q branch of Titan's $3\nu_3$ CH_4 band, arguing that since the R branch is saturated, the Q branch is too. So the recent laboratory results refute my qualitative argument based on the strong CH_4 bands but not my quantitative result based on the Q branch of the $3\nu_3$ CH_4 band.

This analysis yielded 1600 m-A (meter-Amagat) CH_4 in the case of a pure CH_4 atmosphere and less CH_4 if another bulk constituent is present. In a following paper (Trafton, 1974), I revised this figure to 2 km-A based on a correction to the airmass factor for saturated bands pointed out to me by Hunten. I also reported three independent observations of the R(5) manifold of Titan's $3\nu_3$ CH_4 band and noted that the strength relative to Saturn's R(5) manifold was approximately the same as for the Q branches, supporting my analysis based on the Q branches. Figure 1 reviews my observations of the Q branches and R(5) manifolds. Since only part of the Q branch was observed on Titan, owing to the very low signal level, this confirmation was important.

The three independent observations of Titan's R(5) manifold shown are similar, giving confidence that their sum is accurate. The Ring spectrum shows the limited contribution of telluric H_2O. The equivalent width of the summed Titan spectrum divided by the Ring spectrum is proportional to the product of the effective pressure times the CH_4 abundance, in the reflecting layer approximation. For homogeneous scattering, it is proportional to the effective pressure times the CH_4 abundance along a scattering

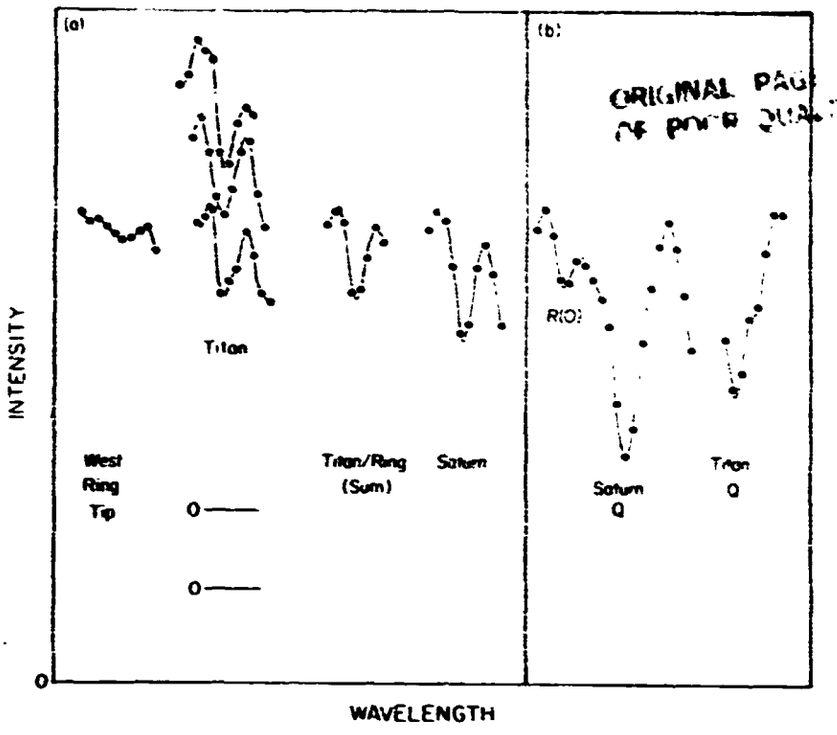

Figure 1. (a) The R(5) manifold (10973Å) of Titan's $3\nu_3$ CH_4 band at a resolution of 4.0 Å. Three independent observations of this manifold are shown. The telluric H_2O absorption is indicated by the scan of the west ring tip. The first channel corresponds to the first channel of the lowest Titan spectrum. The scale is 1.3Å/ch. (b) Comparison of a segment of Titan's Q branch of the $3\nu_3$ CH_4 band (11054Å) with Saturn's Q branch at a resolution of 6.6Å. As for the R(5) manifold the strength is about two thirds of that of Saturn's features, assuming a symmetrical profile. The scale is 2.0Å/Ch.

mean free path (since in scattering models lines move over to the square root regime of the curve of growth for smaller values of the equivalent width [Chamberlain, 1970]). In a third paper, I analyzed the equivalent width of the R(5) manifold to obtain at least 1600 m-A for the pure CH_4 case in the reflecting layer approximation (Trafton, 1975a).

The figure 1600 m-A is a lower limit for the bulk atmosphere in this approximation. If there is less CH_4 than this, there is an even greater proportion of some other gas present. This figure can be greater if the local continuum in the center of the manifold is higher than in the wings (because of possible blending with neighboring features). The figure is not likely to be much less owing to superposition of some unidentified absorption at the same wavelength as the R(5) manifold because the absorption at this wavelength in Titan's spectrum relative to that in Saturn's spectrum is in essentially the same proportion as the Q branches. I have since discovered that telluric OH emission from the $P_1(3)$ doublet occurs in the blue wing of the R(5) manifold and may raise

the local continuum and, hence, the derived equivalent width. The agreement, however, of the shapes of the R(5) manifold between Titan and Saturn indicates that the correction for this is small. Consequently, 1600 m-A remains essentially unchanged as the *lower limit* to Titan's *visible* (1.1 μm) *bulk atmosphere* or as a rough *upper limit* to Titan's spectroscopically *visible* CH_4 *abundance*, according to the reflecting layer approximation.

A more serious objection would be the invalidity of the reflecting layer model when the presence of significant scattering has been demonstrated. A scattering analysis has not yet been attempted which includes the $3\nu_3$ CH_4 band. I estimate on the basis of Titan's low albedo and whole-disk contribution to the spectrum that an analysis of the equivalent width of the R(5) manifold using a homogeneously scattering model atmosphere will yield a pressure-abundance product comparable with that using a reflecting layer model. But now abundance refers to the specific abundance and pressure to the effective level of line formation. [A crude analysis along these lines is given in Hunten's paper above].

My third point is that at sufficiently low pressures, or for sufficient haze, Titan's infrared CH_4 bands may show a pressure dependence after all. Chamberlain (1970) has shown that absorption lines depart from the linear portion of the curve of growth for smaller values of the equivalent width in a scattering atmosphere than in a clear one. This is a consequence of the "random walk" character of photon scattering, and the effect increases with the mean number of scatterings.

Figure 2 compares the 0.9 μm and 1 μm CH_4 bands of Titan and Saturn. It shows that the regions of high absorption are anomalously weak in Titan's spectrum. This point is reinforced in Figure 3 which plots the mean transmission over a small wavelength interval for Titan vs that for Saturn. The mean transmission is defined to be the residual intensity (relative to the apparent local continuum) averaged over a small wavelength interval. Since a given mean transmission may occur at several wavelengths within the band complex, it is surprising that a curve rather than an area results from such plots. I have interpreted this behavior both in terms of an elevated haze layer (Trafton, 1973a) and as differences in the region of the curve of growth on which Titan's and Saturn's bands lie (Trafton, 1975b). An argument that pressure does play some role is that in spite of the significant differences between Jupiter's and Saturn's haze distributions, their CH_4 spectra are remarkably similar compared to the difference between Titan and Jupiter, or Titan and Saturn. It is difficult to imagine an aerosol

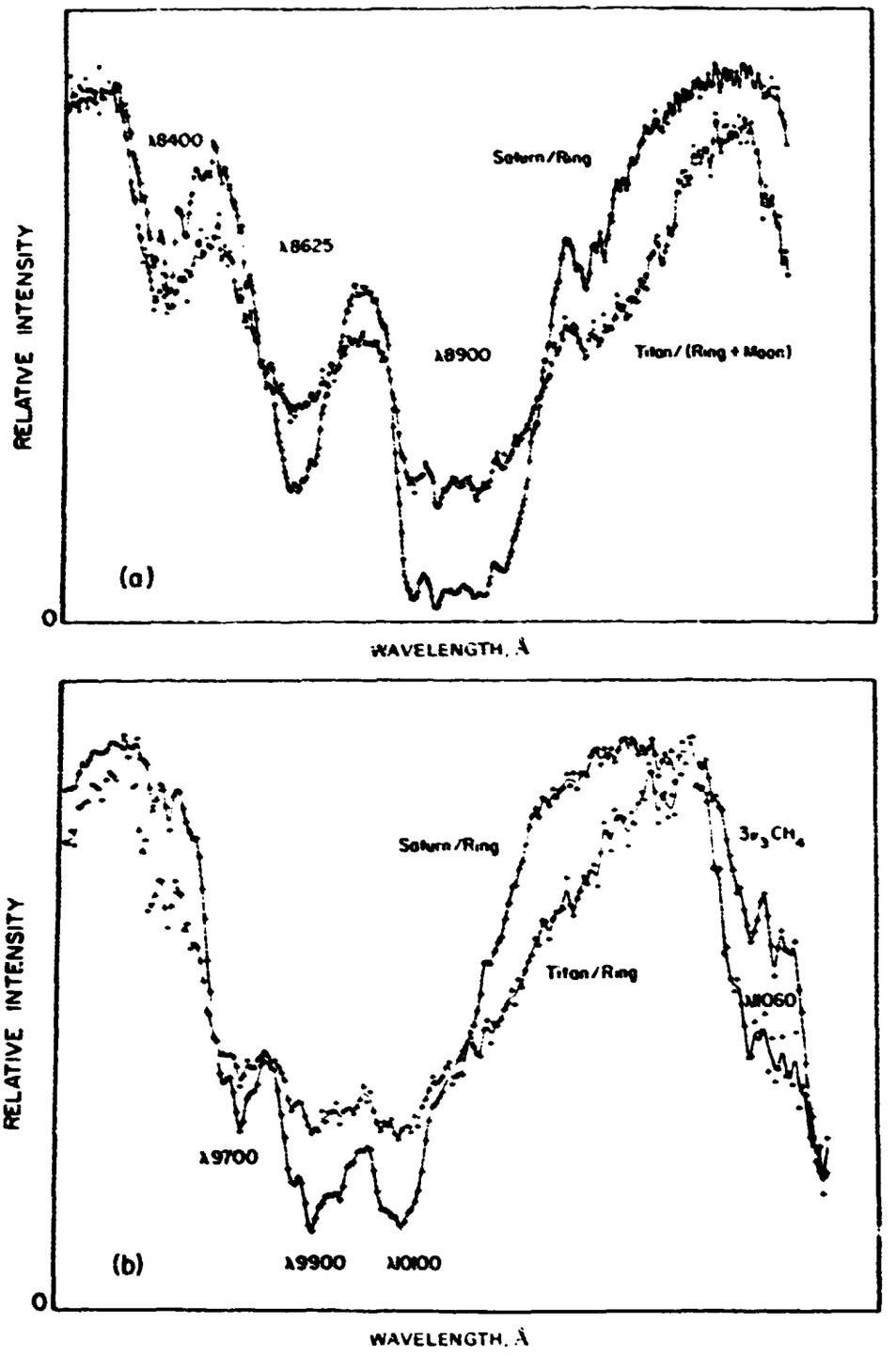

Figure 2 Comparative spectra of Titan and Saturn. (a) The 0.9 μm band complex. The resolution element is 9 Å. (b) The 1 μm band complex. The resolution element is 35 Å.

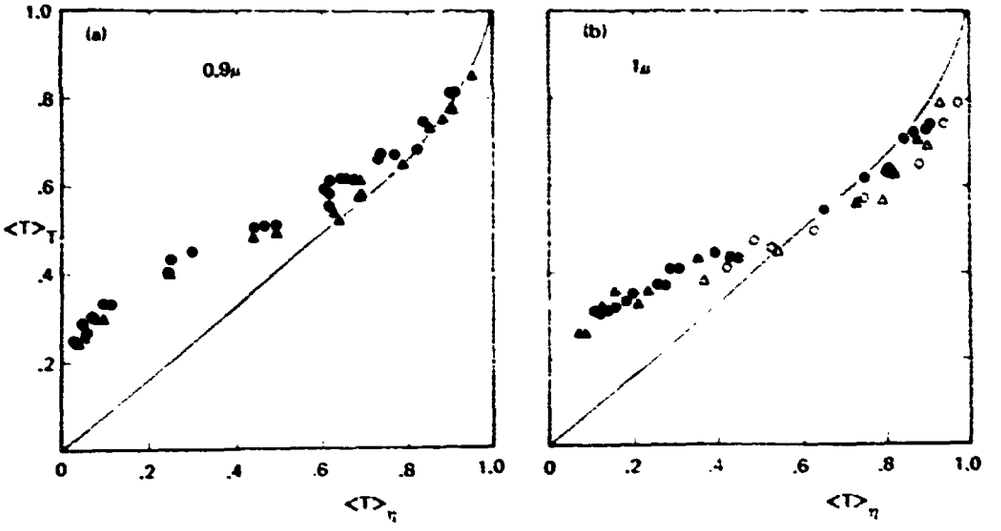

Figure 5. Plots of Titan's band transmission vs. Saturn's band transmission. Transmission is defined to be the residual intensity averaged over the residual. Each element. The circles and triangles correspond to different observations independently reduced (see Trafton, 1975b). Each planetary spectrum was taken relative to a lunar or Ring spectrum to remove telluric features and vignetting effects. The solid line corresponds to the behavior of a reflecting layer model for band absorption, illustrating the departure of Titan from this model. (a) The 0.9 μm CH_4 bands. (b) The 1 μm CH_4 bands. The open symbols denote points in the longer wavelength wing of the 1 μm band. The deviant behavior of the open symbols indicates that another gas is absorbing in the red wing of the 1 μm band complex.

distribution on Saturn which might duplicate Titan's band morphology. Of course, now that CH_4 absorption coefficients are available, the sensitivity of CH_4 band shapes to aerosol distribution should be tested using model atmospheres to determine whether the haze distribution suffices to explain the band shapes.

My fourth point concerns the existence of the 8151 Å feature in Titan's spectrum. Although Münch *et al.* (1977) have used higher resolution than I have, their spectra are too noisy to reveal the weak telluric H_2O line at 8151.3 Å which should be visible at their resolution and is visible in my lower-resolution spectra having higher signal to noise ratio (Trafton, 1975a). They may have therefore underestimated the upper limit on the H_2 abundance. I feel that an upper limit of about 2 km-A is more appropriate.

It is important to remember that the existence of a feature at this wavelength does not necessarily mean it arises from H_2. There are a number of unidentified lines in Titan's spectrum near 1.06 μm (Trafton, 1974) and the responsible gas might conceivably absorb at 8151 Å. Giver and Podolak (1977) have shown that long-path CH_4 spectra reveal many lines in this region so CH_4 cannot be ruled out as the source of

the feature visible in my spectra of Titan. The same instrument has detected the slightly stronger (5mÅ vs Münch's *et al.* upper limit of 3 mÅ for $S_3(1)$ on Titan) S(1) line of the (5–0) band of H_2 in Uranus' spectrum (Trafton, 1978). I still believe there is an absorption feature at or close to this wavelength; the question is from what gas does it arise?

REFERENCES

Belton, M. J. S. (1969) An estimate of the abundance and the rotational temperature of CH_4 on Jupiter. *Astrophys. J.* 157, 469–472.

Chamberlain, J. (1970) Behavior of absorption lines in a hazy planetary atmosphere. *Astrophys. J.* 159, 137–138.

Giver, L. P., and Podolak, M. (1977) Interpretation of the red methane absorption bands in the spectrum of Titan. *Bull. Amer. Astron. Soc.* 9, 471.

Hunten, D. M. (1973) Scientific summary. In *The Atmospheres of Titan* (D. M. Hunten, ed.), pp. 4–8. NASA SP-340.

Munch, G., Trauger, J. T., and Roesler, F. L. (1977) A search for the H_2 (3,0) S1 line in the spectrum of Titan. *Astrophys. J.* 216, 963–966.

Noland, M., Veverka, J., Morrison, D., Cruikshank, D. P., Lazarewicz, A., Morrison, N. D., Elliot, J., Goguen, J., and Burns, J. (1974) Six color photometry of Iapetus, Titan, Rhea, Dione, and Tethys. *Icarus* 23, 334–354.

Trafton, L. M. (1972) The bulk composition of Titan's atmosphere. *Astrophys. J.* 175, 285–306.

Trafton, L. M. (1973a). Interpretation of Titan's infrared spectrum in terms of a high-altitude haze layer. *Bull. Amer. Astron. Soc.* 5, 305.

Trafton, L. M. (1973b) Saturn: A study of the 3.3 CH_4 band. *Astrophys. J.* 182, 615–636.

Trafton, L. M. (1974) Titan: Unidentified strong absorptions in the photometric infrared. *Icarus* 21, 178–187.

Trafton, L. M. (1975a) Near-infrared spectrophotometry of Titan. *Icarus* 24, 443–455.

Trafton, L. M. (1975b) The morphology of Titan's methane bands. I. Comparison with a reflecting layer model. *Astrophys. J.* 202, 805–814.

Trafton, L. M. (1978) Detection of H_2 quadrupole lines belonging to the (5,0) overtone band in the spectrum of Uranus. *Astrophys. J.* In press.

Veverka, J. (1973) Titan: Polarimetric evidence for an optically thick atmosphere. *Icarus* 18, 651–660.

Page intentionally left blank

PHYSICAL PROPERTIES OF AEROSOLS IN TITAN'S ATMOSPHERE AS DEDUCED FROM VISIBLE OBSERVATIONS

Kathy Rages and James B. Pollack

Space Science Division, NASA-Ames Research Center
Moffett Field, California 94035

ABSTRACT

Analysis of the absolute value of Titan's albedo and its variation with increasing phase angle has yielded constraints on the optical properties and average particle size of the aerosols responsible for the scattering of visible light. The real index of refraction of the scattering material lies within the range $1.5 \leq n_r \leq 2.0$ and the average particle size is somewhere between 0.2 μm and 0.4 μm. The amount of limb darkening produced by these models leads to an occultation radius of ~2700 km.

The reflection of visible light by Titan is believed to be due chiefly to scattering by an optically thick layer of particles analogous to the blue absorbing "Axel dust" present in the upper atmospheres of the outer planets. By comparing observed properties of Titan with model calculations, we have obtained preliminary estimates of some of the properties of the aerosols, including particle size and spectral absorption characteristics. In addition, these characteristics allow us to predict Titan's limb darkening, thereby removing an ambiguity in the determination of Titan's radius found from lunar occultation observations.

We evaluated the scattering characteristics of our aerosol models with a computer program based on the doubling method that provides an accurate solution to the multiple scattering problem. The single scattering properties of the aerosols were

computed using a scheme developed for nonspherical particles (Pollack *et al.*, 1977). The free parameters of the model include the real part of the index of refraction n_r; the imaginary index n_i; optical depth of the aerosol layer at a reference wavelength of 0.55 μm, τ; particle size distribution function f(r), where r is the radius of an equal volume sphere; and three parameters, α_o, FTB, and SAR, which are related to the nonspherical nature of the particles. We used the two parameter size distribution proposed by Hansen and Hovenier (1974), since the scattering properties of the aerosol layer depend almost entirely on one of these parameters, $\bar{r}$, the cross section (geometric) weighted average particle radius. The second parameter b is a measure of the width of the distribution function. The nonspherical parameters α_o, FTB, and SAR are, respectively, the ratio of particle circumference to wavelength below which the particles act like spherical scatterers and above which they depart from Mie scattering; the ratio of light singly scattered into the forward hemisphere to that scattered into the backward hemisphere for the non-Mie domain; and the ratio of actual surface area to that of an equal volume sphere.

In the calculations discussed below, we selected the following values for the above parameters: n_r = 1.3, 1.4, 1.5, 1.7, 1.8, 2.0, 2.5, 3.0; $n_i(\lambda)$ to be found from the observations; τ = 10 (essentially infinite optical depth); $\bar{r}$ to be determined from the observations; b = 0.05 (a narrow distribution); α_o = 8 (typical of particles lacking sharp edges); FTB = 2; and SAR = 1.3.

Even though the phase angle dependence of Titan can only be observed over a 6.5° range from Earth, it is still possible to obtain some information on the mean particle size $\bar{r}$ from this data. The magnitude of the phase angle variation depends on the shape of the single scattering phase function near a scattering angle θ of 180°. This in turn depends on $\bar{r}$. When $\bar{\alpha} = 2\pi\bar{r}/\lambda \ll 1$, where λ is the wavelength, the aerosol exhibits a Rayleigh scattering phase function, which decreases only slightly with decreasing θ when θ is near 180°. When $\bar{\alpha} \gg \alpha_o$, the phase function increases with decreasing θ, but when $1 < \bar{\alpha} < \alpha_o$, it decreases significantly as θ decreases slightly from 180°. Thus, the second $\bar{\alpha}$ domain exhibits the smallest decrease in brightness with increasing phase angle (decreasing θ), the third $\bar{\alpha}$ domain exhibits the largest decrease, and the first $\bar{\alpha}$ domain exhibits an intermediate behavior. Hence, some bounds on $\bar{r}$ can be obtained from the observed phase effect.

We have computed the phase effect of our model aerosol layers for a wide range of values of $\bar{r}$. For each choice of $\bar{r}$, we have evaluated $n_i(\lambda)$ by demanding that the computed geometric albedo match the observed value at wavelength λ (Nelson and Hapke, 1978). We compared the predicted phase effects with those observed by Noland, *et al.* (1974) at six wavelengths ranging from 0.35 μm to 0.75 μm. The large decrease in brightness with increasing phase angle found at the shorter wavelengths implies that $1 < \bar{\alpha} < \alpha_o$, or 0.05 μm $< \bar{r} <$ 0.45 μm. Within this size domain it is possible to obtain an actual value for $\bar{r}$ from the data. Figure 2 shows a plot of the ratio of Titan's disk integrated intensity at 6.4° and 0° phase angle as a function of wavelength. Filled squares and vertical lines indicate the observed values and their associated error bars, as found from a least squares fit to the observations, while the curves indicate the predicted behavior of several models that come closest to fitting the data. The middle curve corresponds to a model with $n_r = 1.5$, $\bar{r} = 0.35\mu$m, while the top and bottom curves refer to $\bar{r} = 0.32$ μm and $\bar{r} = 0.40$ μm, respectively. We see that the middle curve is not only capable of matching the observed phase effect at two wavelengths, as might be expected since there are two free parameters n_r and $\bar{r}$, but is also able to reproduce the observed spectral dependence over all six wavelengths. We also see that $\bar{r}$ can be altered by at most a few hundredths of a micron from its optimum value before the fit to the observations becomes unacceptable. However, the value of $\bar{r}$ can be changed by a somewhat larger amount if n_r is also varied.

In Figure 2, the model curves coming closest to fitting the observations are shown for several different values of n_r. In addition to the cases shown, fits to the observations were attempted using $n_r = 1.3$, 1.4, 2.5, and 3.0. A refractive index of 1.4 or less is unable to produce a phase variation much less than 0.98, which makes it clearly unacceptable at the shorter wavelengths. Refractive indices greater than 2 yield insufficient variation of the phase function with wavelength, a trend which can already be detected in the model curve shown for $n_r = 2.0$. So judging from the results shown in Figure 2, $1.5 \lesssim n_r \lesssim 2.0$ and 0.2 μm $\lesssim \bar{r} \lesssim$ 0.4 μm.

The inferred value of $\bar{r}$ is consistent with the requirements of the inversion model of Titan (Danielson *et al.*, 1973). This model requires that the mean size of the aerosols absorbing some of the incident sunlight be small enough so that they are poor radiators in the thermal region of the spectrum, i.e. $\bar{\alpha} << 1$ for $\lambda \sim 10$ μm or longer. This condition allows the upper atmosphere to assume higher temperatures than the effective temperature.

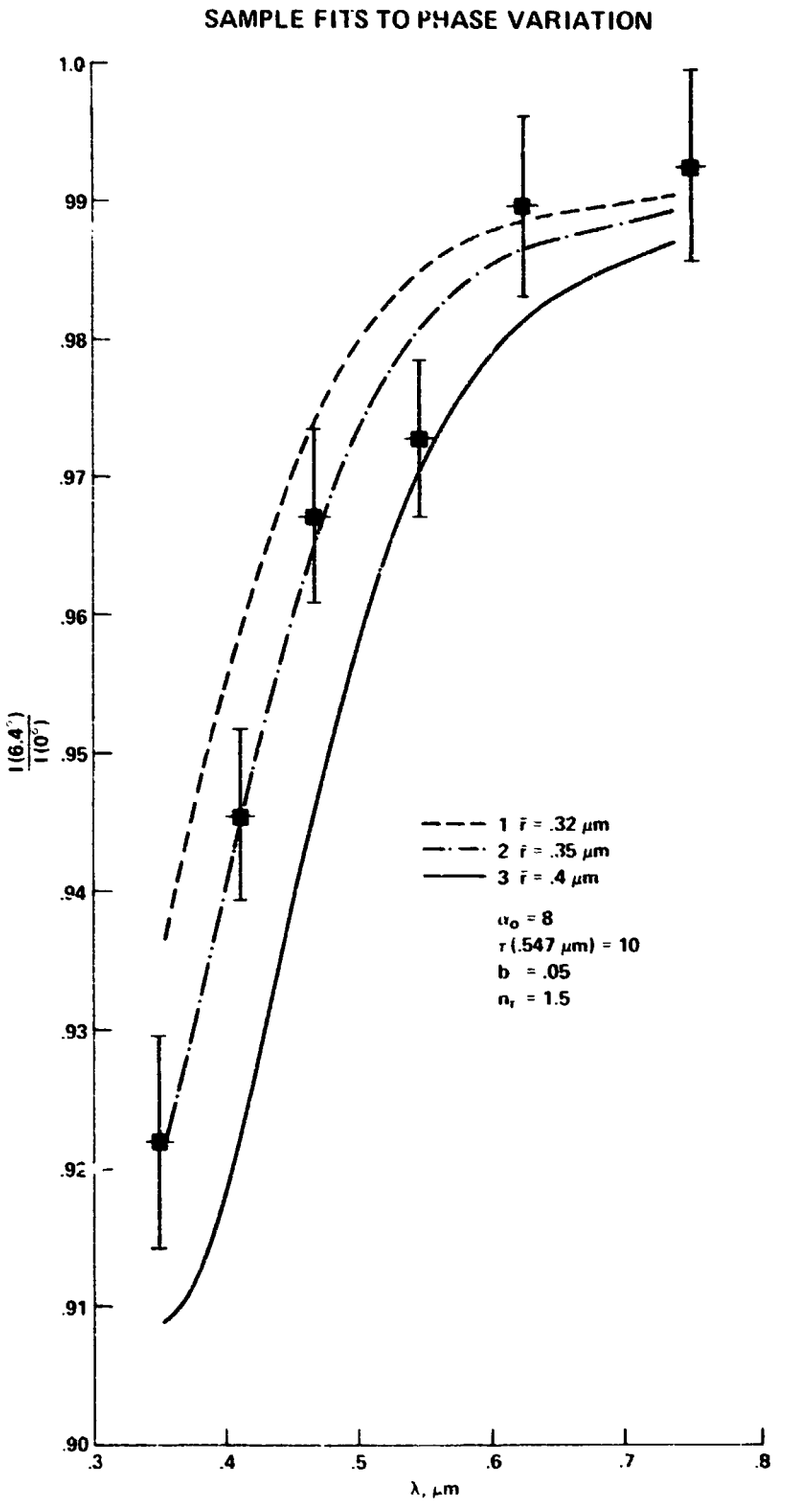

Figure 1. Illustration of the phase effect calculated for Titan as a function of wavelength, for n_r = 1.5 and three different mean particle sizes. The values derived from the observations of Noland et al. *(1974) are indicated by filled squares with error bars.*

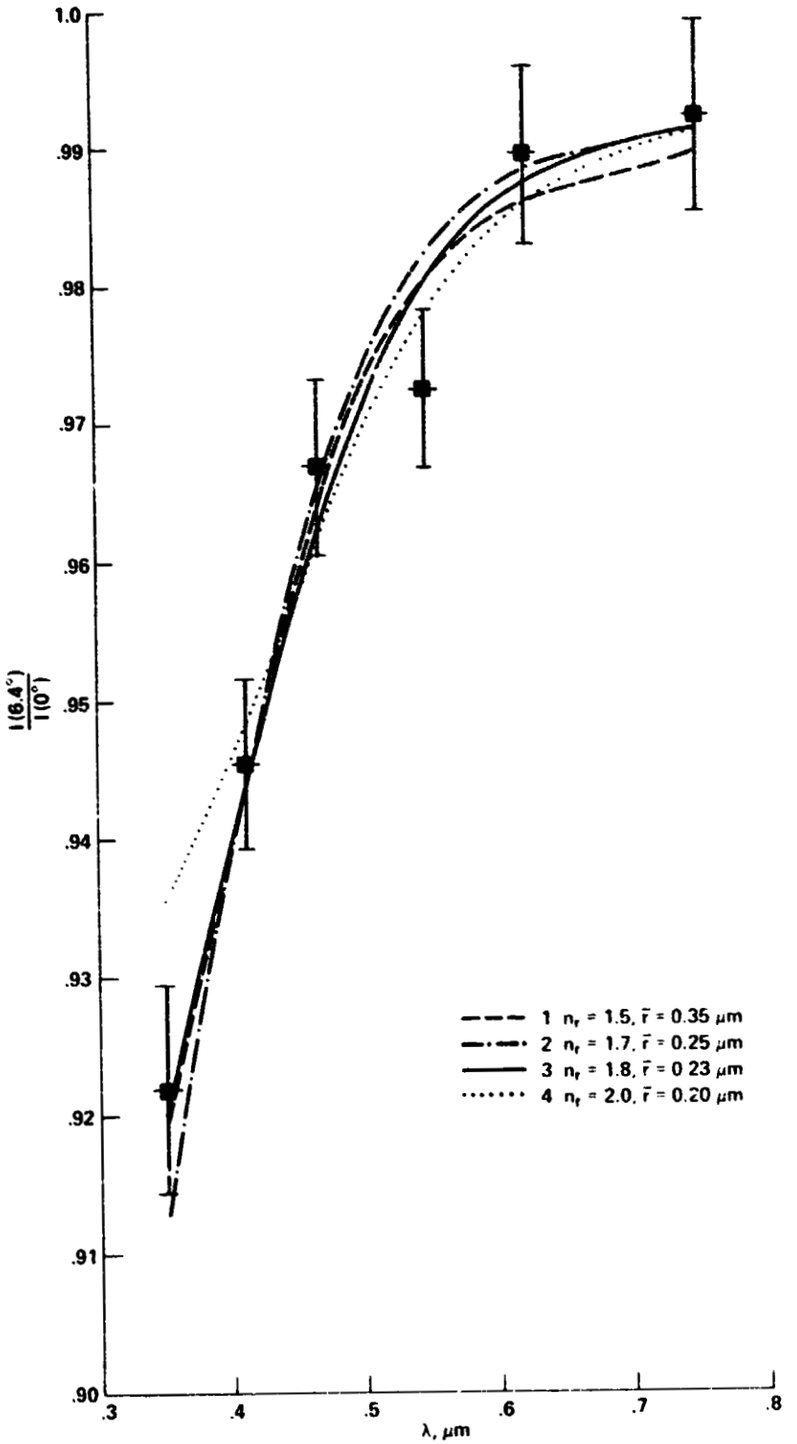

Figure 2. The best fit to the observed spectral dependence of the phase variation obtainable by varying $\bar{r}$, for four different values of n_r.

Figure 3 displays the imaginary index of refraction as a function of wavelength, as found by matching Titan's geometric albedo for an assumed visible "surface" radius of 2700 km. The four curves of this figure correspond to the four models shown in Figure 2. We see that the absorption coefficient of the aerosols decreases by about one order of magnitude between 0.35 μm and about 0.6 μm, but that it flattens toward longer wavelengths. Both the deduced spectral shape and approximate absolute value of n_i should provide useful constraints on the composition of the aerosols.

Finally, we consider the limb darkening behavior of our most successful models. In Figure 4, $I(\mu)/I(\mu = 1)$ is plotted as a function of μ at wavelengths of 0.49 μm and 0.62 μm, where μ is the cosine of the angle between the local vertical and the line of sight. These predictions refer to zero degrees phase angle. Also given in the figure for comparison is the behavior of a Lambert surface.

These results have relevance for the inference of Titan's radius from lunar occultation observations (Elliot *et al.*, 1975). These data do not permit the simultaneous solution of both the limb darkening law and the satellite's radius at the occultation level. For a uniformly bright satellite ($I(\mu) = I(\mu = 1)$), the occultation radius is about 2500 km, while for a Lambert law, it has a value of 2900 km. The expected limb darkening illustrated in Figure 4 implies that the occultation radius should be about 2600 to 2700 km. We plan to make a more precise determination of this important quantity.

REFERENCES

Danielson, R. E., Caldwell, J. J., and Larach, D. R. (1973). An inversion in the atmosphere of Titan. *Icarus 20*, 437–443.

Elliot, J. L., Veverka, J., and Goguen, J. (1975). Lunar occultation of Saturn I. *Icarus 26*, 387–407.

Hansen, J. E. and Hovenier, J. W. (1974). Interpretation of the polarization of Venus. *J. Atmos. Sci. 31*, 1137–1159.

Nelson, R. M. and Hapke, B. W. (1978). Spectral reflectivities of the Galilean Satellites and Titan, 0.32-0.86 micrometers. Submitted to Icarus.

Noland, M., Veverka, J., Morrison, D., Cruikshank, D. P., Lazarewicz, A. R., Morrison, N. D., Elliot, J. L., Goguen, J., and Burns, J. A. (1974). Six-color photometry of Iapetus, Titan, Rhea, Dione, and Tethys. *Icarus 23*, 334–354.

Pollack, J. B., Colburn, D., Kahn, R., Hunter, J., Van Camp, W., Carlston, C. W., and Wolf, M. R. (1977). Properties of aerosols in the Martian atmosphere, as inferred from Viking lander imaging data, *J. Geophys. Res. 82*, 4479–4496.

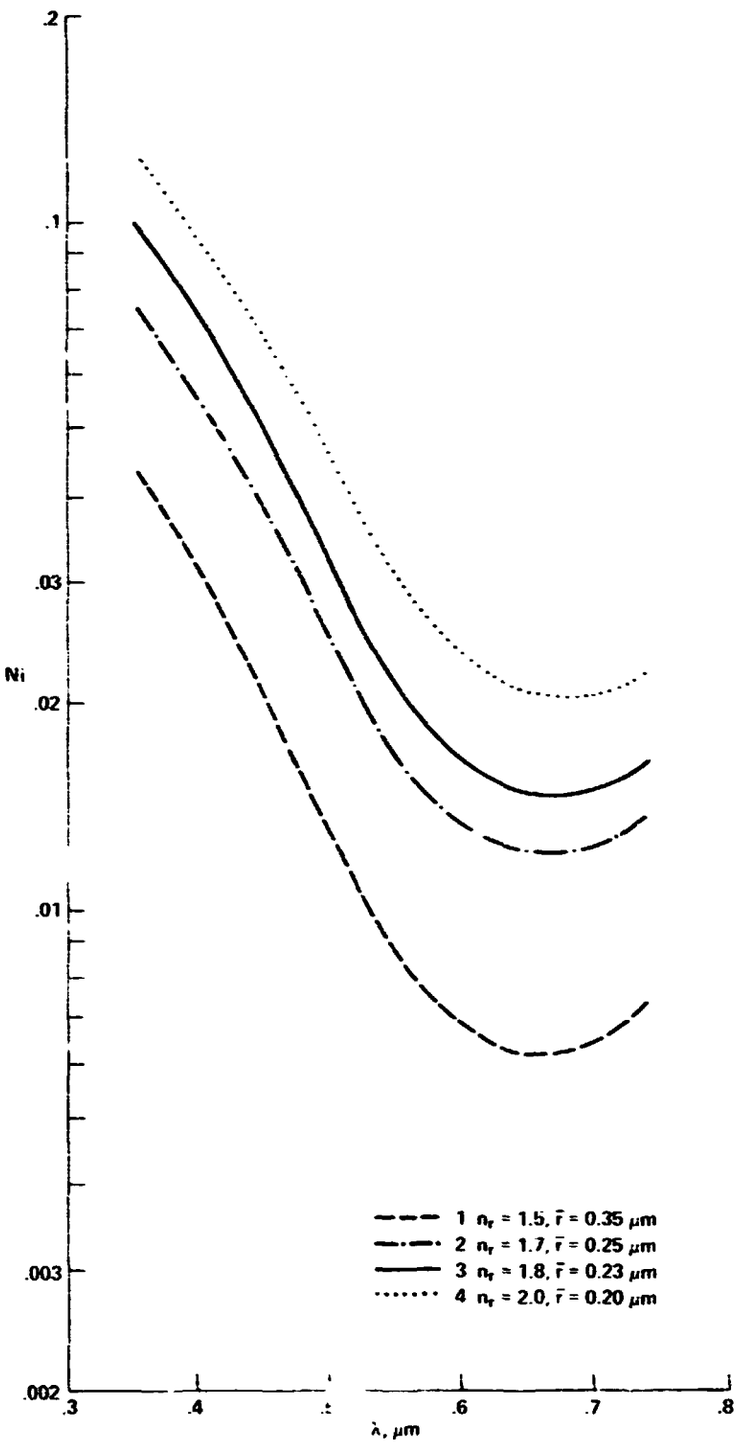

Figure 3. Imaginary index of refraction as a function of wavelength for the cases shown in Figure 2. Numbering of the curves is the same as in Figure 2.

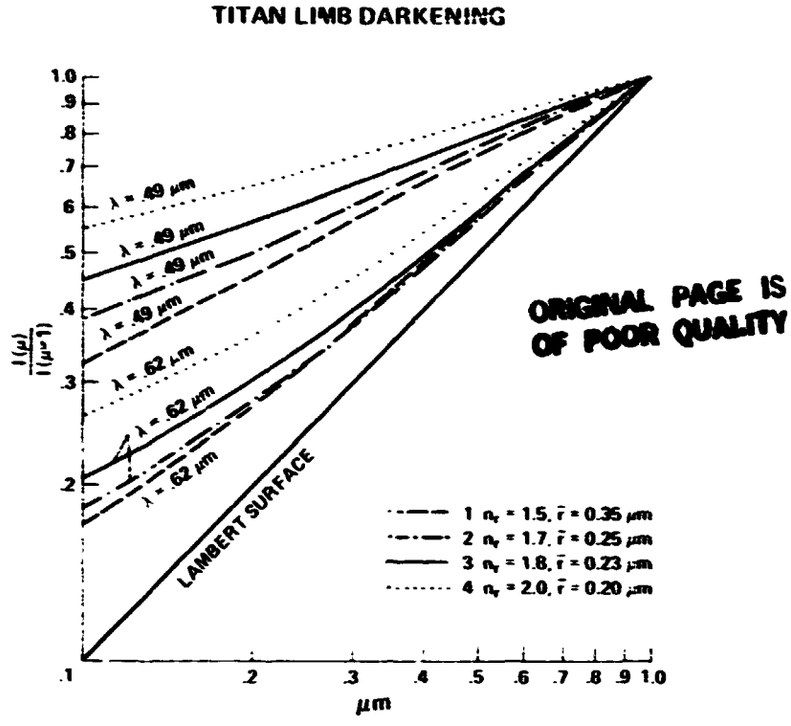

Figure 4. Limb darkening at wavelengths corresponding to two of the channels used in the lunar occultation observations of Elliot et al. *(1975). The numbering of the curves is the same as in Figure 2. The limb darkening of a Lambert surface is shown for comparison.*

DISCUSSION

D. MORRISON: It seems clear that the surface properties as they could be derived from photometric or polarimetric measurements are important for distinguishing between the models. You could have a surface, John, where Don has the top of a cloud level. I would like to read to you from Veverka's paper given at the Titan Workshop (p. 54)--"the single most important conclusion to be drawn from the photometry and polarimetry of Titan is that a Saturn-like cloud model may be required to explain the sum of the observations." Can you comment on this?

D. HUNTEN: That is a perfectly reasonable interpretation, but it's not unique. On p. 57 of that book I point out that Titan could also be paved with a glassy layer of asphalt, which would have polarization properties indistinguishable from those of a cloud. And that's not an entirely improbable kind of appearance for a Titan surface.

J. CALDWELL: I don't think it's quite right to conclude that the cloud has to be like Saturn. The optical depth of the atmosphere and dust layer, even in these low surface pressure models, is very large in the visible and ultraviolet. It seems to me perfectly reasonable that the polarization might be due to the properties of the dust.

B. SMITH: What optical depth do you use?

J. CALDWELL: Podolak and Danielson calculate an optical depth due to dust of ≈ 5 at 5000 Å.

B. SMITH: Either way, there is no hope of seeing the surface.

D. HUNTEN: And no hope of seeing the cloud top of my model either.

J. POLLACK: The successful model by Rages and myself shows, starting about 0.6 μm, a tremendously sharp increase in the imaginary index to shorter wavelengths; at somewhat longer wavelengths, it tends to flatten out. So, in effect, whatever is making up this layer is something that has very strong and very sharp ultraviolet absorption band. I think that both the shape and the absolute absorption coefficient here may allow us to choose between different compositional possibilities.

With a model we can, of course, define what the limb darkening of Titan would be like, and the relevance of that is that the lunar occultation measurement of the size of Titan is very dependent upon what limb darkening law you assume. If you assume a uniformly bright surface, which would be a flat line in Figure 4, then you get a radius of 2500 km. If you assume a Lambert law, you get about 2900 km.

What our models would say is that you're somewhere in between, but closer to the Lambert surface, so therefore, the occultation radius would be something on the order of 2600 to 2700 km.

Finally, I would like to note that I've become increasingly impressed that the apparent secular brightening of Titan is, in fact, a real phenomenon, and there's now something like six years of observations that indicate that Titan's brightness has increased by maybe five or so percent. If we assume that that's right, and we also assume that what we see is a photochemical layer, then it's quite conceivable that plausible solar variability could indeed have a very interesting climatic feedback. For example, if you have ultraviolet solar variations, which we know from satellite observation do occur, variations in intensity will cause a variation in the production rate of the smog, which in turn could affect the size of the particles somewhat, and

therefore, affect the overall brightness of Titan. If this sort of linkage is true, it's very interesting in the sense that a very small energy change in the Sun is able to enormously amplify the amount of solar energy that is deposited in Titan.

D. HUNTEN: But we should also remember that ordinary seasonal variations may be the answer.

J. CALDWELL: Podolak and Danielson have done a lot of work to derive the photometric properties of the dust, and they have a size of about 0.1 μm.

J. POLLACK: This size (0.1 μm) is incompatible with the phase angle variations (see Figure 1 of this article). Also, they make some arbitrary assumptions about the analytic dependence of the imaginary index; they assumed a power law. I think you can see from Figure 3 of this article that this is not true over the whole spectral range of the observations.

B. SMITH: What do you mean by the particle size?

J. POLLACK: Any time you derive particle size information from brightness measurements, what you're really doing is just deriving one gross property of the size distribution, namely, the cross-sectional averaged particle size. For Podolak and Danielson, the number given is the maximum radius of a flat distribution, and the effective size is a bit smaller.

J. POLLACK: On the difference between the equivalent widths on Titan and Saturn for the methane bands, it could equally well be the result of the differences in the properties of the scattering medium that's present in the two atmospheres.

L. TRAFTON: Possibly. But look at the differences between the spectrum of Jupiter and Saturn where you have appreciably different haze layers. The haze layer of ammonia is really thin on Jupiter, it's really thick on Saturn, and yet these big differences in the aerosol structure between the two planets lead to only small differences in the shapes of the spectra when you compare them against the shapes of methane in Titan's atmosphere.

J. POLLACK: Let me be a little bit more specific. In the case of Jupiter and Saturn, there is an optically thin haze layer and then a fairly thick, dense cloud layer beneath that. In the case of Titan, there is an optically thick haze layer which means that a lot more multiple scattering happens in Titan's atmosphere, while on Jupiter and Saturn it's closer to simple reflecting.

L. TRAFTON: Yes, but there are really three different regimes. I really don't see Jupiter and Saturn being in one regime and Titan being entirely different. But in terms of differences in the spectrum, I do see very little differences between the shapes of the spectrum of Jupiter and Saturn.

J. POLLACK: That is what I would expect for the photochemical haze; it is much thinner in the case of Jupiter and Saturn than it is on Titan. I believe most of the line formation takes place within the actual dust in the case of Titan.

D. MORRISON: Why should Titan have so much more of this dust or smog than Jupiter or Saturn?

J. POLLACK: I think it goes back to abundances; for one thing, the fractional abundance of methane is a lot more on Titan.

D. HUNTEN: I don't agree that it's a lot more; what is different is the absence of hydrogen in the photochemical processes, so that the reducing power of the atmosphere is negligible.

J. POLLACK: Yes, and nitrogen in Titan's atmosphere could also be a critical element there.

L. TRAFTON: What is needed is laboratory data for methane at a very low pressure like a hundredth atmosphere to maybe a tenth to know whether or not there is indeed any pressure dependence at the methane level.

J. CALDWELL: Such a measurement requires a very long path length. Lutz applied tremendous lengths already to do this. You may be asking the impossible.

SUMMARY OF DISCUSSION AMONG TRAFTON, HUNTEN, AND POLLACK: Fink, Benner, and Dick (1977) find below 8000 Å that the bands obey Beer's law and are pressure-independent. Their explanation is that there are many lines per half-width even at zero pressure. Pressure effects begin to be evident at longer wavelengths and might be expected in the wings of all bands. Podolak and Giver have explored possible saturation effects for the lowest pressures. Temperature effects must also be kept in mind.

M. KLEIN: (addressed to Hunten) If you really have this cloud at the 77 K level of 600 g cm^{-2}, the opacity to microwaves at 3 mm is no longer unappreciable. This effect may not be insignificant.

D. HUNTEN: The particles would have to be very large to have a significant scattering opacity. Pure methane, either liquid or solid, should have very low millimeter-wave absorption, because the molecule is nonpolar. I think it would need polar impurities to be much of an absorber.

In addition, I don't really believe the cloud is that dense. I believe that most of that mass must precipitate out and leave a much thinner cloud. All I did in the paper was follow the Lewis-type prescription in which you condense out all the mass that is available at each height and call it a cloud.

D. STROBEL: Do your methane cloud properties satisfy the observations that Low and Rieke (*Astrophys. J.* 190, 1.143, 1974) made at 5 μm? It could be thermal emission at 165 K or solar reflection with an albedo of 0.10.

D. HUNTEN: My methane cloud top is about 79 or 80 K, but I don't see why it couldn't explain the observations as reflected sunlight.

J. CALDWELL: Is your cloud opaque at all in the 10 μm region? There are many transparent gaps between the fundamental bands of CH_4, C_2H_6 and C_2H_4 in this region.

D. HUNTEN: I would think so. In one of my models I did simply postulate an opaque cloud. I rationalize this by suggesting that Axel dust dissolves in methane and gives it some additional absorption that pure methane wouldn't have.

J. CALDWELL: In my models, the optical depth of the Axel dust is the order of 0.05. If the optical depth gets much larger than that, the emission of the dust will go up at 10 μm in contradiction to the observations.

D. HUNTEN: But I'm not talking of dust itself, rather the same material after it's dissolved in the cold methane clouds.

J. CALDWELL: My reason for emphasizing this point is that any model must be consistent with Gillett's observations at 10 μm, which exclude a high brightness temperature. If there's a 200 K surface below the haze, something has to hide that from an outside observer.

D. HUNTEN: I think pressure induced hydrogen will do that. Even at 10 μm, with twenty atmospheres of nitrogen and several km-A of hydrogen at the surface, that's a very opaque medium. It's very much like Venus.

G. SISCOE: What is the hydrogen escape rate from Titan?

D. HUNTEN: My estimate in *Planetary Satellites* is 9×10^9 molecules cm^{-2} s^{-1}. That is based simply on photolysis of the methane we see to be present, and is firm unless someone can find a stronger source.

ORGANIC CHEMISTRY ON TITAN

Sherwood Chang, Thomas Scattergood,* Sheldon Aronowitz, and Jose Flores

Extraterrestrial Biology Division, NASA-Ames Research Center
Moffett Field, California 94035

ABSTRACT

Observations of nonequilibrium phenomena on the Saturn satellite Titan indicate the occurrence of organic chemical evolution. Greenhouse and thermal inversion models of Titan's atmosphere provide environmental constraints within which various pathways for organic chemical synthesis are assessed. Experimental results and theoretical modeling studies suggest that the organic chemistry of the satellite may be dominated by two atmospheric processes: energetic-particle bombardment and photochemistry. Reactions initiated in various levels of the atmosphere by cosmic ray, "Saturn wind," and solar wind particle bombardment of a CH_4 - N_2 atmospheric mixture can account for the C_2-hydrocarbons, the uv-visible-absorbing stratospheric haze, and the reddish color of the satellite. Photochemical reactions of CH_4 can also account for the presence of C_2-hydrocarbons. In the lower Titan atmosphere, photochemical processes will be important if surface temperatures are sufficiently high for gaseous NH_3 to exist. Hot H-atom reactions initiated by photo-dissociation of NH_3 can couple the chemical reactions of NH_3 and CH_4, and are estimated to produce organic matter at a rate of about 10^{-13} to 10^{-14} g cm^{-2} s^{-1}. Electric discharges are highly improbable on Titan; if they occurred at all, they would be restricted to the lower atmosphere. Their yield of organic matter might approach that of hot H-atom reactions if the conversion of solar to electrical discharge energy on Titan was as efficient as on Earth.

*NAS-NRC Resident Research Associate.

I. INTRODUCTION

Two fundamental observations make the satellite Titan an object of great interest to exobiologists and organic cosmochemists: the unique occurrence of abundant methane (CH_4) in the atmosphere (Trafton, 1972) unaccompanied by higher amounts of H_2 (Münch *et al.*, 1977) and the presence of a reddish "surface" (Morrison and Cruikshank, 1974). Although there is some doubt in interpreting this surface as the top of a cloud layer or as the actual surface of the satellite, it does exist and its implications are significant for chemical evolution in the atmosphere. Interpretation of spectroscopic (Caldwell, 1974; Trafton, 1975), and polarimetric (Veverka, 1973; Zellner, 1973) observations of Titan indicate the existence of a thick particle layer in the atmosphere that absorbs ultraviolet and visible light, a layer characterized as a "photochemical haze" (Danielson *et al.*, 1973; Podolak and Danielson, 1977). Ethane (C_2H_6), ethylene (C_2H_4), and acetylene (C_2H_2) (Gillett, 1975) are attributable to, but should not be uniquely identified with, stratospheric CH_4 photochemical reactions (Strobel, 1974). In the context of Lewis' (1971) physical and chemical model of Titan, the presence of C_2H_6, C_2H_2, and C_2H_4, the red surface, and a particle layer that absorbs ultraviolet and visible light clearly indicate a chemical nonequilibrium in the atmosphere. To the organic cosmochemist, this indicates reactions that yield organic molecules in a prebiotic environment perhaps related to those of primitive Earth (Sagan, 1974) and the parent bodies of carbonaceous meteorites. In turn, this draws the interest of exobiologists to the possibility that life may have originated or that terrestrial organisms may survive on Titan.

Recently, Margulis *et al.* (1977) discussed the models that have been proposed for Titan's atmosphere and their implications for life. No basis now exists to alter their conclusion that "the likelihood of growth of a terrestrial microbe is vanishingly small." By implication, the probability of the origin of life forms resembling terrestrial organisms on Titan is also "vanishingly small." If organisms with biochemistry fundamentally different from those of terrestrial organisms evolved and populate Titan today, there are no obvious methods for detecting and identifying them except, perhaps, by imaging techniques.

Rather than addressing a highly speculative issue such as Titan exobiology, in this paper, we discuss several more fundamental issues concerning the satellite's organic chemistry. Current models of Titan's atmosphere described in Section II will be used to help identify the nature and distribution of possible sources of organic matter. Data from the literature and this laboratory will be used to assess the rele-

vance and productivity of those sources as well as to characterize the nature of the products derived from them. The upper and lower atmospheres will be treated separately in Sections III and IV, respectively. A summary of our conclusions is presented in Section V.

II. WORKING MODELS OF THE ATMOSPHERE

Observations of Titan have provided support for two types of thermal atmosphere models. In the temperature-inversion model (Danielson *et al.*, 1973; Podolak and Danielson, 1977; Caldwell, 1977, 1978) the surface temperature (<100 K) and pressure (≤ 20 mbar) are low, but absorption of ultraviolet and visible sunlight by a high particle layer heats the upper atmosphere to as high as 160 K. In the greenhouse model (Sagan, 1973; Pollack, 1973; Cess and Owen, 1973; Hunten, 1978) the stratospheric temperature is also high as a result of dust particles, but it decreases with depth to a CH_4 cloud. Below this cloud, the temperature increases with depth to the surface where there are high temperatures (>150 K) and pressures (≥300 mbar). Podolak and Giver (1978) point out that with available data, it is not possible to distinguish the "surface" of the inversion model from the top of a thick dust-covered cloud layer below which a massive greenhouse atmosphere might prevail. Radio measurements by Briggs (1974) at 8085 MHz suggest a surface temperature of 135 ± 45 K, which is consistent with the inversion model as well as some greenhouse models. Microwave data of Conklin *et al.* (1977) favor a massive atmosphere with a pressure of several bars at the surface and a corresponding temperature near 260 K, although more recent data indicate that the temperature is closer to 100 K, consistent with the earlier measurements (Owen, 1978). These observations conflict in supporting a greenhouse model. Nonetheless, for any such model, the low H_2 concentrations observed by Münch *et al.* (1977) indicate that a different gas must drive the greenhouse. Nitrogen may fulfill this purpose (Hunten, 1972, 1978; Owen and Cess, 1975).

For purposes of discussion, we shall view the Titan atmosphere as a composite model with the following features taken from various sources: (1) a stratospheric dust layer that absorbs ultraviolet and visible sunlight; (2) a stratospheric temperature of 160 K decreasing to < 100 K at the top of a thick, dust-covered, reddish cloud layer consisting primarily of hydrocarbon ices; (3) CH_4 or CH_4 and N_2 comprise the bulk of the atmospheric gases above and below the cloud layer; (4) a clear atmosphere from the bottom of the clouds at >100 K to the surface where the temperature is about 135 K

and the pressure about one bar; (5) NH_3 abundances below the clouds are determined by its vapor pressure at the surface either in the form of $NH_3 - H_2O$ ice or aqueous NH_3 solution.

III. UPPER ATMOSPHERE

Several factors must be reconciled about the chemistry of the upper atmosphere: evidence for C_2H_6, C_2H_4, and C_2H_2 as minor constituents, with a C_2H_6/C_2H_4 ratio of about 250 (Gillett, 1975); evidence for dust particles that strongly absorb ultraviolet and visible light; and the red color of the observable surface.

Dust and Acetylene Polymerization

The dust particles are thought to be "photochemical smog" arising from CH_4 photolysis (Strobel, 1974). Scattergood and Owen (1977) suggested that a component of the dust particles might be a yellowish acetylene polymer, similar to cuprene $(C_2H_2)_n$, formed by particle or photo-induced polymerization of C_2H_2, or both. Although polymers are routinely formed during the photolysis and thermal decomposition of C_2H_2, the conditions on Titan may not support such processes.

Plasma polymerization of acetylene (Kobayashi *et al.*, 1974), alone and in the presence of saturated (C_2H_6) and unsaturated (C_2H_4) hydrocarbons readily occurs at pressures as low as 0.7 mbar to yield gaseous oligomers and solid polymers. The presence of H_2 in the gas mixture, however, partially inhibits polymerization. The solid polymers are insoluble and appear to consist of a highly cross-linked, three-dimensional network containing carbon-carbon double bonds and aromatic structures. It is not clear whether or not these polymers are closely related to the polymers identified as $(C_2H_2)_n$ produced during radiation-induced gas-phase polymerizations of C_2H_2 (Jones, 1959), because the infra-red spectra are dissimilar in many respects. Ultraviolet irradiation of pure C_2H_2 at 1470 Å (McNesby and Okabe, 1964) and 1849 Å (Zelikoff and Aschenbrand, 1956) also yields an ill-characterized solid polymer with smaller amounts of diacetylene ($HC \equiv C - C \equiv CH$), vinylacetylene ($CH_2 = CH - C \equiv CH$), ethylene and benzene. At 1849 Å, quantum yields for C_2H_2 disappearance and the apparent chain length of polymers decrease with decreasing pressure. While these

polymers form readily under many conditions through many different energy sources (Jones, 1959; Lind, 1961, Kobayashi, 1974) their chemical constitutions are not uniquely defined; they are described, however, as near-white to yellowish and as lacking color-depth.

Recent laboratory studies provide the bases for assessing the possible existence of acetylene polymers on Titan. As a model for interstellar organic synthesis, Floyd *et al.* (1973) bombarded a solid film of C_2H_2 at 55 K with 150-eV electrons. They reported evidence for a variety of unsaturated and aromatic compounds, all of which are ultraviolet absorbers from 2000 - 3000 Å (Table 1). No mention was made of a solid cuprene-like product, although such a product would have been interesting in the context of interstellar organic chemistry. If polymers were absent, Floyd's work reveals an important temperature dependence for polymer formation, because previous polymer syntheses were achieved at room temperature or higher. Polymer synthesis on Titan may be inhibited by the low temperature of the stratosphere.

Recent experiments by Scattergood (1975), Flores *et al.* (1978) and Bar-Nun (1975, 1978) provide stronger additional arguments against the formation of solid acetylene polymers on Titan. Bombardment of gaseous CH_4, C_2H_2, and CH_4 - C_2H_2 mixtures with Mev protons (Scattergood, 1975) produced a yellowish powdery polymer in pure C_2H_2 and in mixtures of CH_4 and C_2H_2 where the CH_4/C_2H_2 ratio was < 2. Clear, colorless liquids consisting primarily of simple saturated hydrocarbons resulted when the ratio was raised to 10. Apparently, under highly favorable total pressure conditions, a low mixing ratio of C_2H_2 in CH_4 prohibits formation of solid-colored polymer. We conclude that the CH_4/C_2H_2 ratio on Titan, which is estimated to exceed 10 by at least several orders of magnitude (Gillett, 1975; Strobel, 1974), also would be prohibitively high for C_2H_2 polymer synthesis by proton bombardment.

When 2.6 mbar of pure CH_4 is photolyzed with 1236 Å light (Flores *et al.*, 1978), the major products are the saturated hydrocarbons C_2H_6 and C_3H_8 (see Figure 1). After 30% CH_4 decomposition, when the system approached a photochemical steady-state, no hydrocarbons higher than C_4 were observed by gas chromatography, even when the total product was concentrated into a small volume by liquid nitrogen prior to sampling (Table 2). Not only did hydrocarbon production terminate at the C_4 stage, synthesis of unsaturated compounds was inhibited. These results essentially agree with experiments performed by Bar-Nun (1978). At the H_2/C_2H_2 ratio of 40 produced by CH_4 decomposition, the secondary process of C_2H_2 photopolymerization to a solid polymer is expected to be inhibited (Bar-Nun, 1975, 1978). Bar-Nun (1978) also found

Table 1. Ultraviolet Absorption Properties of Compounds Synthesized by 150 eV Electron Bombardment of C_2H_2 Films at 55 K

Compound	λ_{max} Å[a]	log ϵ [a]
Diacetylene (HC_4H)	2340	-
Benzene (C_6H_6)	2030	2.5
	2540	3.9
Phenylacetylene ($C_6H_5C_2H$)	2350	4.2
	2720	2.5
Naphthalene ($C_{10}H_8$)	2200	5.0
	2750	3.8
Indene (C_9H_8)	2490	4.1

[a]Data taken from Hirayama (1965).

during irradiation of C_2H_2 that production of photopolymers decreased with lowerings of temperature and initial acetylene pressure below 300 K and 260 mbar, respectively. If the experimental data are extrapolated to Titan, and if CH_4 were the only hydrocarbon in the initial atmosphere, then the combined effects of low C_2H_2 mixing ratio, high H_2/C_2H_2 ratio, substantially lower temperatures, and pressures orders of magnitude lower would make photochemical formation of an acetylene polymer like $(C_2H_2)_n$ highly unlikely in the Titan stratosphere. This conclusion is consistent with the region

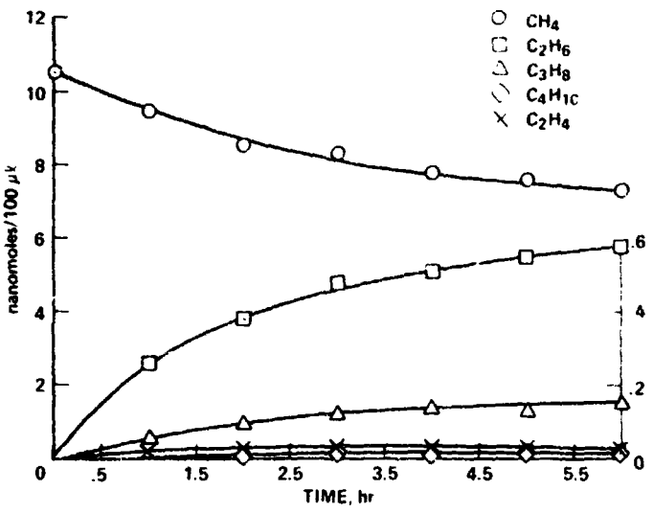

Figure 1. Product distributions at various times by irradiation of 2.6 mbar of CH_4 with 1236 Å light. Hydrocarbon abundances were determined by gas-chromatography and are given in nanomoles per 100 μl sample. Left scale, CH_4, right scale, other gases.

Table 2. Mole Fractions and Quantum Yields of Products Obtained by 1236 Å Irradiation of 2.6 mbar CH_4 at 300 K[a]

Product	Mole Fraction[b]	Molecules Photon^{-1}[c]
CH_4	0.699	0.56[d]
C_2H_2	0.0016	0.0002
C_2H_4	0.0048	0.014
C_2H_6	0.107	0.15
C_3H_6	0.0003	
C_3H_8	0.0228	0.03
i - C_4H_{10}	0.0019	0.001[e]
n - C_4H_{10}	0.0021	
H_2	0.162	

[a] Performed in a stirred 2196-cm^3 flask with an Opthos lamp emitting (6 ± 2) × 10^{15} photons s^{-1}.

[b] Includes H_2 abundance calculated by mass balance. Mole fractions apply to near steady-state condition after 30% CH_4 decomposition.

[c] Calculated at 10% CH_4 decomposition, unless otherwise specified. Errors estimated at ± 30%.

[d] Molecules of CH_4 destroyed per absorbed photon.

[e] Calculated when first observed, after 18% CH_4 decomposition.

[f] Calculated for 30% CH_4 decomposition.

of CH_4 -photolysis occurring at levels in the atmosphere corresponding to number densities of 10^9 to 10^{12} cm^{-3}. Furthermore, the planetary data of Gillett (1975) and Münch *et al.* (1977) indicate a C_2H_2/CH_4 ratio < 10^{-5} and an $H_2/{}_2H_2$ ratio ≤10^4.

Although synthesis of acetylene polymers in Titan's atmosphere is improbable, their contribution to the stratospheric dust cannot be ruled out. However, they certainly cannot account for Titan's reddish surface. On the other hand, ultraviolet absorbance by these polymers is assured by their double-bond and aromatic-ring content. Interestingly, electron micrographs of polymer produced by alpha-particle irradiation of C_2H_2 show them to consist of 0.1 to 0.13 μm-diameter spheres. As candidates for the photochemical smog, if they form in a low pressure medium, these particles conveniently remain solid at the relatively high stratospheric temperatures (150 K) postulated for both the inversion and greenhouse models, and are of the proper size to satisfy recent albedo (haze) models (Podolak and Giver, 1978).

If cuprene-like polymers at most comprise a minor component of the dust, what is the bulk of it? Apparently, the photochemistry of CH_4 alone cannot produce colored material. The products observed experimentally (Table 2) cannot account for even the observed absorption of ultraviolet light in Titan's stratosphere. Scattergood and Owen (1977) pointed out that production of colored material would require the presence of a nitrogen gas such as N_2 along with CH_4. According to the working models, gases like NH_3 and H_2S cannot be involved because they become frozen below the stratosphere.

For purposes of comparison, the ultraviolet-visible and infrared spectra of condensable materials produced during Mev-proton irradiation of gas mixtures are shown in Figures 2 and 3. Table 3 contains a list of the major types of products. For N-containing mixtures, the spectra are similar and resemble those of the colored product obtained by 2537 Å irradiation of NH_3 - H_2S - CH_4 - C_2H_6 - H_2O mixtures (Khare and Sagan, 1973). Because not one of these materials has spectral properties identical to those on Titan, Scattergood and Owen (1977) proposed that mixtures of materials similar to the CH_4 - H_2 and CH_4 - N_2 products were present. This is an attractive alternative because the components in appropriate proportions, more readily than the Khare-Sagan polymer alone, would permit the rapid increase in absorption toward the ultraviolet that is exhibited by dust in Titan's stratosphere (see Danielson *et al.*, 1973). Therefore, production of dust having the observed spectroscopic properties requires the coupling of C and N in a CH_4 - N_2 atmosphere.

From the incident proton energies of 2 Mev (with 0.75 Mev absorbed by the gas) and fluxes of 1.7×10^{13} cm^{-2} s^{-1} used in his experiments and estimates of the total CH_4 decomposition (based on decreases in infrared absorption), Scattergood (1975) calculated that 1.7×10^4 CH_4 molecules per proton are converted to product (equivalent to 44 eV per CH_4). Coupling this figure with Titan's cosmic ray energy flux of 2.3×10^9 eV cm^{-2} s^{-1} $ster^{-1}$ (Capone, 1978) leads to an estimated CH_4 loss rate of 5×10^7 cm^{-2} s^{-1} or production of 1.3×10^{-15} g cm^{-2} s^{-1} of colored, condensable, carbonaceous matter. With this estimate, we assume that conversion of kinetic energy to chemical energy in the laboratory experiments is similar to that in Titan's lower ionosphere, despite orders of magnitude differences in flux density and total pressure. Assuming condensable matter with density of one is produced at a constant rate, 7.6×10^{10} s or 3×10^3 y would be required to deposit a 1-μm-thick layer of dust. After 4.5×10^9 y, the total column density would be about 180 g $\times$ cm^{-2}. Maximum energy deposition occurs around the 10^{18} cm^{-3} level of the atmosphere (Capone, 1978).

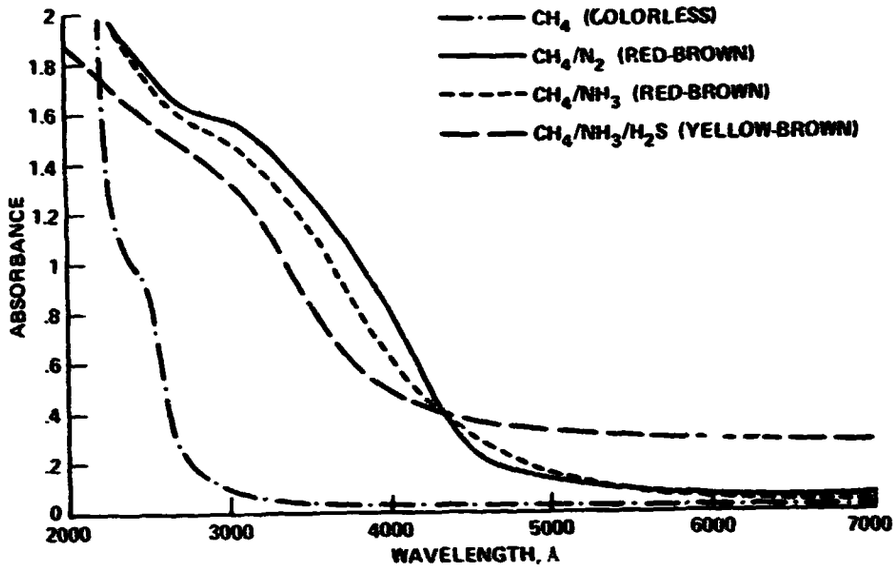

Figure 2. Ultraviolet-visible absorption spectra of liquid-phase products synthesized by MeV-proton irradiation of gas mixtures (Scattergood et al., 1975; Scattergood, 1975; Scattergood and Owen, 1977).

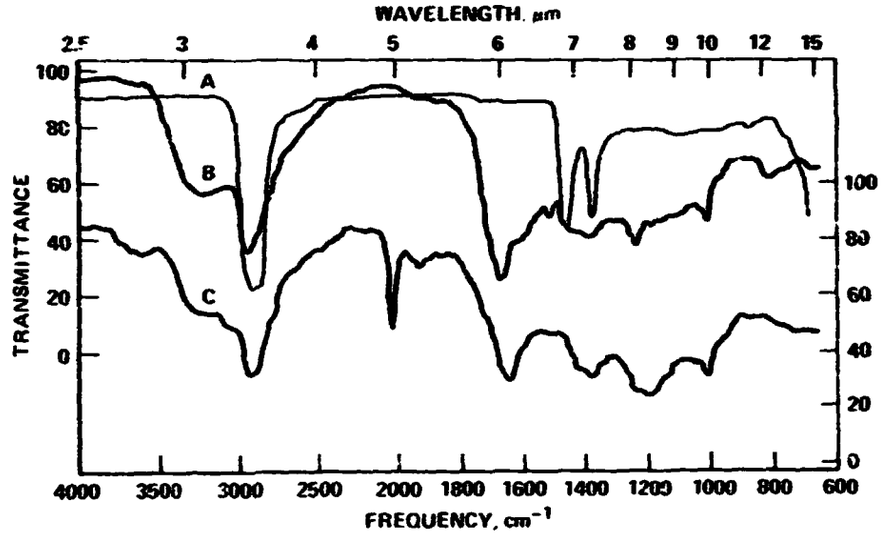

Figure 3. Infrared transmission spectra of liquid phase products obtained from MeV proton irradiation of gas mixtures: A. CH_4 - H_2; B. CH_4 - N_2 and CH_4 - NH_3; C. CH_4 - NH_3 - H_2S (from Scattergood et al., 1975, Scattergood, 1975; Scattergood and Owen, 1977). Plot for mixture C is offset for clarity.

Recent calculations of Siscoe (1978) provide models for the magnetosphere associated with various possible values of Saturn's magnetic field. For a value as low as 0.5 gauss, the magnetosphere would extend to twenty Saturn radii and include Titan within its boundary 90% of the time. As a consequence of a 1.7 cm^{-3} particle density and a 200 km s^{-1} particle velocity, the flux of 150-eV "Saturn wind" protons striking the upper atmosphere of Titan would amount to 3.4×10^{7} cm^{-2} s^{-1}. Calculated as above, these figures lead to an organic matter production rate at least twice that afforded by cosmic rays. Because of the shallow depth to which 150-eV protons can penetrate, consequent reactions should occur above the stratosphere in the region of maximum photochemistry, unlike the cosmic rays that penetrate deeper.

If Titan has no magnetic field, if the solar wind energy (avg, 1 keV $nucleon^{-1}$) and particle flux (2×10^{6} cm^{-2} s^{-1}) are unaffected by Saturn's proximity, and if the assumptions given above for the production rate resulting from cosmic ray particles are applied, then an upper estimate can be made for the rate of synthesis of condensable carbonaceous matter by solar wind bombardment of the atmosphere. This estimate amounts to 1.1×10^{-15} g cm^{-2} s^{-1} and is comparable to the cosmic ray production rate.

Table 3. Products Resulting from MeV Proton Irradiation of Various Gas Mixtures[a]

Gas mixture	
CH_4	Aliphatic hydrocarbons[b]
$CH_4 - H_2$	Aliphatic hydrocarbons[b]
$CH_4 - N_2$	Aliphatic hydrocarbons[b]; Aliphatic and alicyclic amines[c]; Acetonitrile (CH_3CN); Red-brown polymer
$CH_4 - NH_3$	Aliphatic hydrocarbons[b]; Aliphatic and alicyclic amines[c]; Acetonitrile (CH_3CN); Red-brown polymer

[a] From Scattergood (1975); Scattergood *et al.* (1975); Scattergood and Owen (1977).

[b] Includes saturated and unsaturated compounds up to C_{22} in length. Less than 10 ppm aromatics (e.g., benzene).

[c] Cyclic amines include hexamethylenetetramine ($C_6H_{12}N_4$) and its methyl and dimethyl nomologues.

Clearly, the assumptions used to obtain these estimates require that they be used with caution. Nonetheless, the role of particle radiation in producing condensable and gaseous trace constituents in Titan's atmosphere cannot be dismissed. Models of CH_4-rich atmospheres, which included cosmic ray ionization processes (Capone *et al.*, 1976), predicted CH_3 radical concentrations that were three orders of magnitude higher than those predicted by strictly photochemical models (Strobel, 1974). Because attainment of higher CH_3 concentrations without significantly lowering the CH_3/H radical ratios is expected to favor a high hydrocarbon production, the predictions support the view that particle irradiation would enhance organic synthesis.

Electrical Discharges

In addition to synthesis of C_2H_2 polymers by way of CH_4 photolysis and synthesis of condensable organic matter by particle irradiation of CH_4 - N_2 mixtures, vacuum ultraviolet photolysis of CH_4 - N_2 or electric discharges may generate Titan's stratospheric dust and coloration. Electric discharges through CH_4 - N_2 mixtures at 30 mbar produce many different saturated and unsaturated hydrocarbons and nitriles (Toupance *et al.*, 1974) that could subsequently undergo photochemistry and condensation-polymerization reactions to readily form reddish substances if formed in Titan's atmosphere. To account for the occurrence of stratospheric dust in the absence of strong atmospheric mixing, however, electrical discharges must occur above the dust layer at pressures < 1 mbar in a dry atmosphere containing no clouds. Although they could conceivably occur, discharges under such conditions are sufficiently implausible as to permit discounting them.

Photochemistry

In the only report describing the coupling of C and N in the photochemistry of a CH_4 - N_2 mixture, Dodonova (1966) found that irradiations at 7 - 10 mbar with a hydrogen lamp (10^{15} - 10^{16} photons s^{-1}) produced HCN after 8 - 10 hr; hydrocarbons comprised the other products. HCN was detected with a picrate color test sensitive to 10^{-7} g. The explanation given for this result was "the photoactivation of nitrogen and its interaction with CH radicals resulting from the decomposition of methane." The author described that the photoactivation of nitrogen occurred at 1273 Å. A crude estimate based on the reported data places the quantum yield for HCN at about 10^{-5}.

Although several attempts were made at NASA Ames Research Center (Bragin and Nicoll, 1976) to duplicate the Russian work with a 1236 Å lamp, they failed to produce any HCN detectable by high sensitivity gas-chromatographic analyses. If formed on Titan by Lyman-α photons at the estimated yield, however, HCN would be produced at the insignificant rate of about 10^3 cm^{-2} s^{-1} or 4.5×10^{-8} g cm^{-2} s^{-1}. Further attempts to study the photochemistry of CH_4 - N_2 at Lyman-α and other wavelengths would be desirable because gaseous HCN is photochemically converted to more complex organic compounds and reddish-brown solids (Mizutani *et al.*, 1975).

Thus, the most attractive mechanism for production of stratospheric dust on Titan that we have discussed involves high-energy proton irradiation, which requires a CH_4 - N_2 atmosphere. This source could provide the colored condensates that are responsible for the reddish surface of the satellite and its low ultraviolet-visible albedo. Unless vacuum ultraviolet photolysis of CH_4 - N_2 yields HCN more efficiently than 10^{-5} molecules per photon, it can be discounted along with electric discharges as a tenable mechanism.

If we now return to the data for 1236 Å photolysis of CH_4 (see Figure 1, Table 2), we can make additional observations pertinent to Titan's atmospheric photochemistry. Although a photochemical steady-state had not been reached at the time of measurement of the mixing ratios in Table 2, it was sufficiently close (see Figure 1) that the assumption of steady-state is justified. The relative abundances of experimental products suggest that propane (C_3H_8) may also be detectable in Titan's atmosphere along with the previously observed ethane (C_2H_6) and acetylene (C_2H_2). This idea has also been proposed by Bar-Nun and Podolak (1978). Propane should actually be more abundant than C_2H_2. On the other hand, C_2H_2 should be the least abundant of these hydrocarbons. The experimental C_2H_2/C_2H_6 ratio of 0.050 is lower by a factor of 10 than the ratio predicted by the CH_4-photochemical model of Strobel (1974). Furthermore, the ratio of quantum yields for C_2H_4 and C_2H_6 point to an experimental C_2H_4/C_2H_6 ratio of 0.045, which is 10 - 100 times the ratio obtained in the model calculations. Although spectroscopic observations do not provide a useful measure of the C_2H_2/C_2H_6 ratio, they do indicate a C_2H_4/C_2H_6 ratio of 4×10^{-3} (Gillett, 1975), consistent with the CH_4-photolysis calculations. Clearly, there are difficulties in duplicating planetary environments in computer and laboratory simulations of CH_4 photolysis. Whether these difficulties may account for the discrepancies between the results of the simulations remains to be evaluated.

IV. LOWER ATMOSPHERE

Recently, Woodman *et al.* (1977) established an upper limit of 30 cm-am for the abundance of ammonia on Titan. In the context of the inversion model described in Section II, low surface temperatures of < 100 K remove essentially all NH_3 from the gas phase by condensation. If the temperature reaches 115 K, however, gas-phase NH_3 photochemistry can occur, as we discuss below. Because of the ambiguity about the nature of the Titan surface and the possible range of surface temperatures measured by radio (135 ± 45 K, Briggs, 1974) and microwave (260 K, Conklin *et al.*, 1977) observations, we considered ammonia photolysis at temperatures ranging from 115 to 200 K. If the "surface" of the inversion model corresponds to the actual surface, a temperature of 115 K implies that pure solid CH_4 is unlikely to be a major surface constituent. If the surface is the top of a cloud layer, the 115 K implies cloud particles that consist of hydrocarbons other than CH_4 or possibly NH_3. Photolysis at >115 K is considered to occur in the atmosphere below the clouds of the greenhouse models.

Ammonia Photochemistry

Although Hunten (1973) discussed NH_3 photolysis as a means for generating large amounts of N_2 on Titan, the process has not been modeled for Titan. In theoretical studies of Jovian atmospheric chemistry, NH_3 and CH_4 photolysis reactions are decoupled from each other (Prinn, 1970; Strobel, 1973a, 1973b; Prasad and Capone, 1976). Except in the work of Kuhn *et al.* (1977), production of organic compounds by means other than CH_4 photolysis high in the stratosphere is discounted. However, laboratory experiments (Sagan and Khare, 1973; Becker *et al.*, 1974; Ferris and Chen, 1975; Ferris *et al.*, 1977) suggest that hot H atoms generated by photodissociation of NH_3 or H_2S (or both) can initiate reactions with CH_4 and C_2H_6 to produce organic compounds by way of hydrocarbon radicals such as CH_3 and their recombination with each other and with NH_2 radicals. Data in Table 4 summarize results reported by Ferris *et al.* (1977) and include estimated production rates at Titan obtained by extrapolation of their results. The product yields in the 115 K experiment were based on an experimental quantum yield for NH_3 decomposition of 0.12 at 208 K (Nicodem and Ferris, 1973). In the low-temperature experiments, some NH_3 is considered and the gas-phase abundances of NH_3 correspond to the equilibrium vapor pressures. Entries in the bottom two lines of Table 4 show that from 115 - 347 K photolysis of ammonia is accompanied by induced hot-atom decomposition of CH_4 at levels higher than 0.6 CH_4

Table 4. Photolysis of a Mixture of H_2 (0.623 bar), He (0.080 bar), CH_4 (0.125 bar), and NH_3 (0.040 bar) with 1849 Å Light at Various Temperatures: Product Yields and Estimated Production Rates at Titan[a]

Product	Product Yield (molecules/photon)			Estimated Production Rate at Titan[b] (g cm^{-2} s^{-1})
	347 K	200 K	115 K	
H_2	0.67			
N_2	0.14	0.040	0.007	0.93×10^{-12}
N-organics[c]	0.02	0.04	0.103	1.0×10^{-12}
HCN	1.2×10^{-4}	0.94×10^{-4}	0.79×10^{-4}	2.1×10^{-15}
C_2H_6	2.3×10^{-4}			
C_3H_8	0.59×10^{-4}			
$C_4H_{10} + C_4H_x$	0.59×10^{-5}			
C_5H_y	0.5×10^{-7}			
N_2H_4	1.7×10^{-6}	0.56×10^{-3}	1.09×10^{-5}	1.5×10^{-14}
(NH_3 loss)	(0.30)	(0.12)	(0.12)	(0.6×10^{11} cm^{-2} s^{-1})[d]
(CH_4 loss)	(0.25)	(0.073)	(0.083)	(0.4×10^{11} cm^{-2} s^{-1})[d]

[a]Product yields calculated from data of Ferris *et al.* (1977), using quantum yields for NH_3 photolysis obtained at 347 K (Ferris *et al.*, 1977) and 208 K (Nicodem and Ferris, 1973).

[b]Calculated from yields at 200 K using a photon flux of 2×10^{12} cm^{-2} s^{-1} between 1600 - 2270 Å at Titan divided by 4.

[c]Assumed to be CH_3NH_2; other possibilities may include NH_2CN, CH_3CN, NH_2NHCH_3.

[d]Column photodecomposition rate.

molecule per NH_3 molecule dissociated. Furthermore, photolytic losses of CH_4 and NH_3 cannot be accounted for by summing the observed products. This lack of mass balance undoubtedly results in part from the difficulty of the analyses. Also, other compounds not specifically sought were likely to have evaded detection.

Mass balance for nitrogen requires the formation of the "N-organics" designated in Table 4. Methylamine (CH_3NH_2) with a N/C ratio of 1 and molecular weight 31 is taken to represent these compounds. Early on, Becker and Hong (1977) detected CH_3NH_2 in similar experiments, but not after long irradiations. Apparently, facile conversion of CH_3NH_2 to other compounds under the irradiation conditions accounts for its absence in most experiments. Formation of complex and colored organic matter from HCN or CH_3NH_2 or both by secondary photolytic processes can be readily envisioned. Mass balance for carbon also indicates the formation of more hydrocarbons than are reported in Table 4. Using the data for 200 K, and assuming that the missing carbon is in the form of $(CH_2)_n$, a hydrocarbon production rate of 0.4×10^{-12} g cm^{-2} s^{-1} is required for mass balance. The total production rate of organic matter from NH_3 photochemistry and hot hydrogen-atom chemistry amounts to 1.4×10^{-12} g cm^{-2} s^{-1}. At this rate, a 1-μm-thick layer of organic matter (with unit density) would take about eight days to produce on Titan, and 4.5×10^9 yr of production would yield a 2-km-thick layer of organic matter and liberate 10^3 km-am of N_2 (or a column density of 28×10^{26} molecules cm^{-2}). Even if only 0.1% of the photons from 1600 - 2270 Å penetrated the cloud layer of Titan, the production of organic matter and N_2 would be significant.

The 115 and 200 K experiments of Table 4 represent relevant laboratory simulations of organic photochemistry on Titan. In greenhouse models, 115 K may occur at the top of the cloud layer, within it, or at some level below it. The high CH_4 partial pressure of this experiment, however, disqualifies its relevance to the inversion model. The 200 K temperature corresponds to a level somewhere below the clouds of the greenhouse models, either at or above the surface. The presence of H_2 and He are also relevant, not because they exist on Titan at the experimental abundances, but because they represent agents for collisional thermalization of the hot H atom. On Titan, N_2 may be the thermalizing agent. However, H_2 and He are expected to be more efficient thermalizers than N_2 (Wolfgang, 1963).

Hot Hydrogen Atom Chemistry

To explore hot atom chemistry under other possible planetary conditions, Aronowitz *et al.* (1978) developed a novel use of a computational method. Their approach couples hot-atom chemistry with the general kinetic problem by incorporating the kinetic theory of Wolfgang (1963) for hot atoms. Temperature, pressure, and incident photon energy are explicitly taken into account. A complete discussion of the approach is beyond the scope and intent of this report, however, and will appear in full detail elsewhere (Aronowitz *et al.*, 1978).

In these computations, the photochemistry is approximated in the following manner. An assemblage of molecules corresponding to an atmospheric composition is exposed to an arbitrarily chosen total number of photons in a series of incremental steps. A small fraction of the available NH_3 is dissociated by each increment of photons; the resulting primary products, H (hot) and NH_2 are allowed to interact with each other and with other gas components in the system according to the reactions in Table 5. The resulting mole fractions of reactants (e.g., NH_3) and products (e.g., N_2H_4) are determined iteratively. The calculations are allowed to run to the point at which additional iterations have negligible effect on the mole fractions of stable end products. The photodissociation of NH_3 was kept low ($\leq 5\%$) by limiting the number of photons introduced in the calculations. For purposes of simplification, the quantum yield for NH_3 was assigned a value of 1.0 for all wavelengths. Use of an appropriate scaling factor, however, permits correction of the calculated quantum yields for any photodissociation quantum yield < 1.0. Secondary photolysis of products is neglected. Quantum yields obtained for various products were calculated from the number of photons and the mole fractions of products. The simulated environmental parameters and derived quantum yields are listed in Table 6. In each experiment, the NH_3 partial pressure is governed by its equilibrium vapor pressure (estimated from a fitted equation of the Antoine form) at the indicated temperature. These estimates are smaller than those determined by Gulkis *et al.* (1978) and hence constitute a lower bound on the NH_3 abundance.

Data in Table 6 reveal several interesting aspects of hot-atom chemistry over the range of conditions simulated. Under all conditions, C_2H_6 and CH_3NH_2 are formed, and CH_3NH_2 is the dominant product. With temperature and wavelength constant, total pressure increases (Experiments I, II, III) lead to increased CH_4

Table 5. Reactions Pertinent to Ammonia Photolysis and Hot Atom Chemistry on Titan

Reaction	Rate Constant[a]	Reference
(1) $H(hot) + H_2 \rightarrow H(thermal) + H_2$	Calculations used hot atom theory	
(2) $H(hot) + CH_4 \rightarrow H_2 + CH_3$	Calculations used hot atom theory	
(3) $H(hot) + NH_3 \rightarrow H_2 + NH_2$	Calculations used hot atom theory	
(4) $2H(thermal) + M \rightarrow H_2 + M$	$2.9 \times 10^{15} (300/T)^{0.6}$	Ham *et al.*, 1970[b]
(5) $H(thermal) + CH_3 \rightarrow CH_4$	2.3×10^{14}	Cheng *et al.*, 1977
(6) $CH_3 + CH_3 + M \rightarrow C_2H_6 + M$	2.2×10^{19} (M)	Dodd and Steacie, 1954[b]
(7) $H(thermal) + NH_2 \rightarrow NH_3$	1.8×10^{13}	Boyd *et al.*, 1971[b]
(8) $NH_2 + CH_3 \rightarrow CH_3NH_2$	6.6×10^{13}	Kuhn *et al.*, 1977
(9) $NH_2 + NH_2 \rightarrow N_2H_4$	1.5×10^{13}	Pham Van Khe *et al.*, 1977

[a] The rate constants are in units of cm^3 $mole^{-1}$ s^{-1} for two body and cm^6 $mole^{-2}$ s^{-1} for three body reactions.

[b] From Strobel (1973a), Table 4.

decomposition, which is also reflected in higher yields of C_2H_6. Formation of CH_3NH_2 appears to be favored by lower pressure. Lowering the temperature from 155 to 125 K (Experiments II, IV) causes little change in the product yields. Quantum yields for CH_4 decomposition decrease as the irradiating wavelength increases (Experiments V, II, VI). This decrease occurs because the hot H atoms produced at longer wavelengths are less energetic ("hot"). The influence of H_2 as a thermalizing agent is striking (Experiments IX, XI). When the H_2/CH_4 ratio is high, CH_4 and NH_3 decomposition are inhibited, and recombination of CH_3 and NH_2 radicals with thermalized H atoms takes place. As a result of inefficient production of CH_3 radicals by hot H atoms, substantially diminished yields of C_2H_2 and CH_3NH_2 occur. Excess N_2 exerts no influence on the thermalization of hot H atoms (Experiments II, IX). However, when the model calculations permit inelastic rather than elastic collisions of the

Table 6. Calculated Quantum Yields for Consumption of Reactants and Formation of Products by Hot-Atom Reactions Under Various Titan Conditions

Experiment	$CH_4/H_2/N_2/NH_3$ (mole ratios)	T, P (K, bar)	λ(Å)	Quantum Yields (molecules/photon)				
				$-NH_3$	$-CH_4$	N_2H_4	C_2H_6	CH_2NH_2
I.	1/1/1/[6.7(-6)]	125, 0.022	1850	0.996	0.913	0.128	0.087	0.740
II.	1/1/1/[2.9(-7)]	125, 0.526	1850	0.984	0.926	0.266	0.237	0.452
III.	1/1/1/[1.1(-7)]	125, 1.316	1850	0.977	0.932	0.340	0.217	0.298
IV.	1/1/1/[1.6(-3)]	155, 0.526	1850	0.986	0.925	0.249	0.218	0.489
V.	1/1/1/[2.9(-7)]	125, 0.526	1686	0.986	0.956	0.279	0.264	0.428
VI.	1/1/1/[2.9(-7)]	125, 0.526	2014	0.980	0.875	0.265	0.213	0.449
VII.	100/1/1/[2.2(-4)]	125, 0.022	1850	0.999	0.998	0.064	0.063	0.872
VIII.	100/1/1/[9.5(-6)]	125, 0.526	1850	0.999	0.999	0.305	0.305	0.389
IX.	1/1/400/[3.8(-5)]	125, 0.526	1850	0.984	0.926	0.266	0.237	0.452
X.[a]	1/1/400/[3.8(-5)]	125, 0.526	1850	0.482	0.141	0.194	0.024	0.094
XI.	1/100/400/[4.8(-5)]	125, 0.526	1850	0.371	0.018	0.180	0.003	0.011

[a]Same as IX except calculations provided for inelastic collisions between N_2 and the hot atoms.

hot H atom with N_2 (Experiment X), quantum yields for CH_4 decomposition and C_2H_6 and CH_3NH_2 synthesis drop by factors of 7, 10, and 5, respectively.

Over the range of conditions tested by the model calculations, changes in temperature, total pressure and irradiating wavelength cause relatively small variations in the yields of products. The presence of high abundances of the moderating gases N_2 and H_2 (e.g., $CH_4/N_2 \leq 0.003$) reduces the yields by up to one order of magnitude. Although H_2 is a more effective thermalizer than N_2, its abundance on Titan is not expected to exceed that of CH_4 (Münch *et al.*, 1977). Conditions of 125 K and 22 mbar (total pressure) represent the closest experimental simulation of the surface environment of the inversion model. Other simulations correspond to locations below the clouds of the greenhouse models.

To estimate production rates on Titan from the data in Table 6, a value of 0.12 for the quantum yield of NH_3 photodissociation is assumed. This value was measured at 208 K in excess H_2 ($H_2/NH_3 = 749$) by Nicodem and Ferris (1973), who found its magnitude had increased from a value of 0.04 at 313 K. This inverse correlation with temperature suggests that the value of 0.12 may be a lower limit below 208 K. For conditions that apply to atmospheric levels above the clouds, transmission of 10% of the incident sunlight is assumed; below the clouds, 1% transmission is assumed. Product quantum yields at 1850 Å are taken to represent average yields from 1600 - 2270 Å. The resulting total production rates of hot atom products corresponding to various conditions are listed in Table 7. Production rates based on the experimental data of Table 4 are also included as the bottom two lines, and are in reasonable agreement with theoretical results.

If the surface temperature of the inversion model were 125 K, a 1 μm layer of organic matter would accumulate every 46 days, leading to a 360-m-thick layer after 4.5×10^9 yr. Organic synthesis occurs at 115 K and may extend to even lower temperatures provided that some NH_3 exists in the gas phase. The possibility of hot-atom-mediated synthesis in the solid phase at low temperatures remains to be evaluated. If the lowest production rate in Table 7 is taken to represent synthesis below the clouds of greenhouse models, then settling of products to the surface would yield a 1 μm-thick layer after 900 yr and a 5-m layer after 4.5×10^9 yr.

Table 7. Production Rates for Organic Matter Synthesized by Ammonia Photolysis and Hot H-Atom Chemistry Under Various Simulated Titan Conditions

$CH_4/H_2/N_2/NH_3$ (mole ratios)	Experiment (Table VI)	T, P (K, bar)	Production Rates[a] (mole. cm^{-2} s^{-1})	Production Rates[a] (g cm^{-2} s^{-1})
1/1/1/ 6.7(-6)	(I)	125, 0.022	5.0×10^{10}	2.5×10^{-13}
1/1/1/ 1.1(-7)	(III)	125, 1.316	3.1×10^{10}	1.6×10^{-14}
1/1/1/ 1.6(-3)	(IV)	155, 0.526	4.3×10^{10}	2.1×10^{-14}
100/1/1/ 2.2(-4)	(VII)	125, 0.022	5.6×10^{10}	2.8×10^{-13}
1/1/400/ 3.8(-5)	(X)	125, 0.526	0.7×10^{10}	0.35×10^{-14}
0.2/1/0/0.06[b]		200, 0.87	2.9×10^{10}	1.0×10^{-14}
0.2/1/0/0.06[b]		115, 0.87	5.2×10^{10}	2.6×10^{-14}

[a] Calculated for 1% transmission through cloud layer, except on lines 1 and 4.

[b] Corresponds to initial NH_3 abundance at room temperature, data from Table 4.

Electrical Discharges

Electric discharge is the last mechanism considered for organic synthesis in Titan's lower atmosphere. Toupance *et al.* (1974), have shown that electric discharges through CH_4 - N_2 mixtures in a flow system (26 mbar) produce mainly HCN, hydrocarbons, and a variety of saturated and unsaturated nitriles. Starting with a 90% N_2/10% CH_4 mixture, about 60% of the CH_4 was converted to HCN. This conversion factor is used to estimate production of organic matter by electric discharges on Titan.

From the solar constant at Titan and an effective albedo of 0.2, the energy flux available is calculated to be 1.1×10^{-3} J cm^{-2} s^{-1}. For lack of other relevant data, the conversion of this energy to electric discharges is assumed to proceed on Titan as it does on Earth with an efficiency of 10^{-3}%. Therefore, the energy flux carried as electric discharges would be 1.1×10^{-8} J cm^{-2} s^{-1}. Assuming a 5-km lightning stroke with a shock column of 80 cm^2 cross-section and a total energy of 10^{10} J (after Bar-Nun, 1975), a CH_4 number density of 5×10^{18} cm^{-3} in a 90% N_2 atmosphere, and a discharge energy flux of 1.1×10^{-8} J cm^{-2} s^{-1}, a production rate of 1.3×10^{8} molecules cm^{-2} s^{-1} or 6×10^{-15} g cm^{-2} s^{-1} is obtained. This figure is appropriate for the lower atmosphere of the greenhouse models, and compares favorably with the production rates derived from hot H-atom reactions. However, the laboratory simulations of electric discharges on which the calculations are based may have little relevance to lightning discharges in a planetary atmosphere. Moreover, there is no clear information regarding the conversion efficiency of solar energy to electric discharge energy on any planet other than Earth. These considerations make statements about electric discharge synthesis of organic matter on Titan speculative. Interestingly, Bar-Nin (1975, 1978) suggests that the high C_2H_2/C_2H_6 ratios observed on Jupiter may be manifestations of electric discharge phenomena.

V. SUMMARY

In recent years, several models have been proposed to account for available observations of Titan and to explain the processes that may be responsible. Although these models may differ in concept and function (e.g., greenhouse vs. inversion), several features must be common to all. Titan is undeniably red, which is most likely a result of the production of a colored organic layer on the surface or in the clouds.

Spectroscopic and polarimetric data indicate the existence of a layer of particles (photochemical haze) in the atmosphere, which may be thick enough to constitute clouds. Finally, in light of thermochemical equilibrium models, the presence of observable amounts of C_2H_6, C_2H_2 and C_2H_4 indicate the occurrence of active organic chemical processes.

Nitrogen appears to be required in the atmosphere for the production of the uv-visible light absorbing dust in the stratosphere and of the reddish surface or clouds, or both. Although N_2 has not been observed in Titan's atmosphere, the probability of its existence is indicated by the inability of CH_4 and $CH_4 + H_2$ mixtures to yield colored products from particle bombardment or photochemistry. The presence of N_2 would require the existence of NH_3 in the atmosphere at some time in Titan's history and its subsequent photodissociation to produce the N_2. Incorporation of nitrogen from NH_3 or N_2 or both into organic molecules by various processes would produce materials with the necessary spectroscopic properties.

In the upper Titan atmosphere where the gas densities are low, reactions initiated by particles (protons, electrons) may predominate, especially those coupling N_2 with CH_4. It is not clear whether CH_4 can be coupled with N_2 photochemically ($\lambda > 1000$ Å), but this will be insignificant at best. Production rates of organic compounds of about 10^{-15} g cm^{-2} s^{-1} are estimated for processes initiated by solar winds, Saturn "wind," and cosmic rays. Cosmic-ray-induced reactions, however, will maximize much lower in the atmosphere than will the other particle-induced reactions. Hydrocarbons will be formed from particle reactions as well as from photochemical breakdown of CH_4. Over 4.5×10^9 y spectroscopically observable materials (e.g., clouds or surface materials) should easily be produced.

Photochemical processes may predominate in the lower atmosphere below the clouds. Although the ultraviolet flux may be reduced by 2 - 4 orders of magnitude from the incident value, atmospheric photochemistry may nevertheless be significant from the occurrence of hot H atom reactions. The hot H atom may be produced from small amounts of NH_3 in the lower atmosphere. Production rates for organic matter are estimated to be about 10^{-14} g cm^{-2} s^{-1} (Table 7), or ten times the upper-atmosphere rates. Electric discharges, if they occur, should produce about the same level of organic chemicals.

Thus, the surface of Titan should be covered by ancient or recent organic matter produced in the atmosphere. This material should include both hydrocarbons

and N-organics. Therefore, study of the satellite's surface in any lander mission should include organic analysis as a prime science objective, with particular attention to the chemistry of the organogenic elements H, C, N, O, and S.

ACKNOWLEDGMENTS

The authors are indebted to L. Giver, L. A. Capone, and D. Goorvitch for their helpful discussions on Titan observations and models. S. Aronowitz acknowledges support under NASA-Ames Contract No. A39942B.

REFERENCES

Aronowitz, S., Chang, S., and Scattergood, T. (1978). In preparation.
Bar-nun, A. (1978). Thunderstorms and Acetylene Formation on Jupiter. Private communication.
Bar-nun, A. (1975). Thunderstorms on Jupiter. *Icarus 24*, 86–94.
Bar-nun, A., and Podolak, M. (1978). The Chemistry of Hydrocarbons on Titan. Private communication.
Becker, R. S., Hong, K., and Hong, J. H. (1974). Hot hydrogen-atom reactions of interest in molecular evolution and interstellar chemistry. *J. Mol. Evol.* 4, 157–172.
Becker, R. S., and Hong, J. H. (1977). Private communication of research performed at the University of Houston.
Boyd, A. W., Willis, C., and Miller, O. A. (1971). Reexamination of the yields in the high dose rate radiolysis of gaseous ammonia. *Can. J. Chem.* 49, 2283–2289.
Bragin, J. and Nicoll, G. (1976). Vacuum ultraviolet photolysis of methane-nitrogen mixtures. Unpublished report of work conducted at Ames Research Center.
Briggs, F. H. (1974). The radio brightness of Titan. *Icarus 22*, 48–50.
Caldwell, J. J. (1974). Ultraviolet observations of Titan from OAO-2. In *The Atmosphere of Titan* (D. M. Hunten, ed.), pp. 88–91. NASA SP-340.
Caldwell, J. J. (1977). Thermal radiation from Titan's atmosphere. In *Planetary Satellites* (J. Burns, ed.), pp. 438–450. University of Arizona Press, Tucson.
Caldwell, J. J. (1978). Low pressure model of Titan's atmosphere. In this volume.
Capone, L. A. (1978). Private communication.
Capone, L. A., Whitten, R. C., Dubach, J., Prasad, S. S., and Huntress, W. T. (1976). The lower ionosphere of Titan. *Icarus 28*, 367–378.
Cess, R., and Owen, T. (1973). Titan: The effect of noble gases on an atmospheric greenhouse. *Nature 244*, 272–273.
Cheng, J-T., Lee, Y-S., and Yeh, C-T. (1977). The triplet mercury photosensitized decomposition of ethane at high intensity. *J. Phys. Chem. 81*, 687–690.
Conklin, E. K., Ulich, B. L., and Dickel, J. R. (1977). 3-mm observations of Titan. *Bull. Amer. Astron. Soc. 9*, 471.
Danielson, R. E., Caldwell, J. J., and Larach, D. R. (1973). An inversion in the atmosphere of Titan. *Icarus 20*, 437–443.
Dodd, D. E., and Steacie, E. W. R. (1954). The combination of methyl radicals: photolysis of acetone at low pressures. *Proc. Roy. Soc. A223*, 283–295. (London)
Dodonova, N. Ya. (1966). Activation of nitrogen by vacuum ultraviolet radiation. *Russian Journal of Physical Chemistry 40*, 969–970.
Ferris, J. P., Nakagawa, C., and Chen, C. T. (1977). Photochemical synthesis of organic compounds on Jupiter initiated by the photolysis of ammonia. *Life Sciences and Space Research XV*, 95–99.
Ferris, J. P., and Chen, C. T. (1975). Photosynthesis of organic compounds in the atmosphere of Jupiter. *Nature 153*, 587–588.
Flores, J., Scattergood, T., and Chang, S. (1978). To be presented at the Am. Astron. Soc. Div. of Planetary Sci. Meeting, Oct. 31–Nov. 3, Pasadena, CA.
Floyd, G. R., Prince, R. H., and Duley, W. W. (1973). A method of forming complex molecules in interstellar space. *J. Roy. Astron. Soc. Can. 67*, 299–305.
Gillett, F. C. (1975). Further observations of the 8–13 micron spectrum of Titan. *Astrophys. J. 201*, 141–143.
Gulkis, S., Janssen, M. A., and Olsen, T. (1978). Evidence for the depletion of ammonia in the Uranus atmosphere. *Icarus 34*, 10–19.
Ham, D. O., Trainor, D. W., and Kaufman, F. (1970). Gas phase kinetics of H + H + H_2 → 2H_2. *J. Chem. Phys. 53*, 4395–4396.
Hirayama, K. (1965). Ultraviolet absorption. Infrared absorption. In *Handbook of Organic Structural Analysis* (Y. Yukama, ed.), pp. 1–450. W. A. Benjamin, New York.

REFERENCES (Contd)

Hunten, D. M. (1972). The atmosphere of Titan. *Comm. Astrophys. Space Phys.* 4, 149–151.

Hunten, D. M. (1973). The escape of H_2 from Titan. *J. Atmos. Sci.* 30, 726–732.

Hunten, D. (1978). A Titan atmosphere with a surface temperature of 200 K. In this volume.

Jones, A. R. (1959). On the radiation induced gas phase polymerizations of acetylene and benzene. *J. Chem. Phys.* [illegible], 953–954.

Khare, B. N., and Sagan, C. (1973). Red clouds in reducing atmospheres. *Icarus* 20, 311–321.

Kobayashi, H., Bell, A. T., and Shen, M. (1974). Plasma polymerization of saturated and unsaturated hydrocarbons. *Macromolecules* 7, 277–283.

Kruger, F. P., Dawson, G. A., and Uman, M. A. (1968). The energy dissipated in a single stroke lightning flash. *J. Geophys. Res.* 73, 3335.

Kuhn, W. R., Atreya, S. K., and Chang, S. (1977). The distribution of methylamine in the Jovian atmosphere. *Geophys. Res. Lett.* 4, 203–206.

Lewis, J. S. (1971). Satellites of the outer planets: their physical and chemical nature. *Icarus* 15, 174–185.

Lind, S. C. (1961). *Radiation Chemistry of Gases*. Reinhold, New York. 333 pp.

Margules, L., Halvorson, H. O., Lewis, J., and Cameron, A. G. W. (1977). Limitations to growth of microorganisms on Uranus, Neptune and Titan. *Icarus* 30, 795–808.

Mizutani, H., Mikami, H., Takahashi, M., and Noda, H. (1975). Study on the photochemical reaction of hydrocyanic acid and its polymer products relating to primary chemical evolution. *Origins of Life* 6, 513–525.

McNesby, J. R. and Okabe, H. (1964). Vacuum ultraviolet photochemistry. *Adv. Photochem.* 3, 157–240.

Morrison, D. and Cruikshank, D. P. (1974). Physical properties of the natural satellites. *Space Sci. Rev.* 15, 641–739.

Münch, G., Trauger, J. T., and Roesler, F. L. (1977). A search for the $H_2S(0,0)$ S_1 line in the spectrum of Titan. *Astrophys. J.* 216, 963–966.

Nicodem, D. E. and Ferris, J. P. (1973). Ammonia photolysis on Jupiter. *Icarus* 19, 495–498.

Owen, T. (1978). Private communication.

Owen, T., and Cess, R. D. (1975). Methane absorption in the visible spectra of the outer planets and Titan. *Astrophys. J.* 197, L37–L40.

Pham Van Khe, Soulignac, J. C., and Lesclaux, R. (1977). Pressure and temperature dependence of amino radical recombination rate constant. *J. Chem. Phys.* 81, 210–214.

Podolak, M. and Danielson, R. E. (1977). Axel dust on Saturn and Titan. *Icarus* 30, 479–492.

Podolak, M. and Green, L. (1978). On anhomogeneous scattering models of Titan's atmosphere. Private communication.

Pollack, J. B. (1973). Greenhouse models of the atmosphere of Titan. *Icarus* 19, 43–58.

Prasad, S. S., and Capone, L. A. (1976). The photochemistry of ammonia in the Jovian atmosphere. *J. Geophys. Res.* 81, 5596–5600.

Pritan, R. G. (1970). UV radiative transfer and photolysis in Jupiter's atmosphere. *Icarus* 13, 424–435.

Sagan, C. (1974). Organic chemistry in the atmosphere. In *The Atmosphere of Titan* (D. M. Hunten, ed.), pp. 134–142. NASA SP-340.

Sagan, C. (1973). The greenhouse of Titan. *Icarus* 18, 649–656.

Scattergood, T., Lester, P., and Owen, T. (1975). Production of organic molecules in the outer solar system by proton irradiation: laboratory simulations. *Icarus* 24, 465–471.

Scattergood, T., and Owen, T. (1977). On the sources of ultraviolet absorption in spectra of Titan and the outer planets. *Icarus* 30, 780–788.

Scattergood, T. (1975). Proton simulated chemistry in the outer solar system. Ph.D. Thesis, State University of New York at Stony Brook. 216 pp.

Sicsic, G. (1978). Magnetosphere of Saturn. In this volume.

Strobel, D. F. (1973a). The photochemistry of NH_3 in the Jovian atmosphere. *J. Atmos. Sci.* 30, 1209–1209.

Strobel, D. F. (1973b). The photochemistry of hydrocarbons in the Jovian atmosphere. *J. Atmos. Sci.* 30, 489–498.

Strobel, D. F. (1974). The photochemistry of hydrocarbons in the atmosphere of Titan. *Icarus* 21, 466–470.

Toupance, G., Raulin, F., and Bruet, R. (1974). Formation of prebiochemical compounds in models of the primitive Earth's atmosphere (CH_4 – NH_3 and CH_4 – N_2 atmospheres). In *Chemical Evolution and the Origin of Life II* (J. Oro and S. L. Miller, eds.), 83–90. Reidel, Boston.

Trafton, L. M. (1972). The bulk composition of Titan's atmosphere. *Astrophys. J.* 175, 295–306.

Trafton, L. (1975). The morphology of Titan's methane bands. I. Comparison with a reflecting layer model. *Astrophys. J.* 197, 805–814.

Veverka, J. (1973). Titan: polarimetric evidence for an optically thick atmosphere. *Icarus* 18, 657–660.

Wolfgang, R. (1963). Kinetic theory of hot-atom reactions. II. Evaluation of collisional energy loss. Application to reactive mixtures. *J. Chem. Phys.* 39, 2983–2993.

Woodman, J. H., Trafton, L., and Owen, T. (1977). The abundances of ammonia in the atmospheres of Jupiter, Saturn and Titan. *Icarus* 32, 314–320.

Zelikoff, M. and Aschenbrand, L. M. (1956). Vacuum ultraviolet photochemistry. Part III. Acetylene at 1849 Å. *J. Chem. Phys.* 24, 1054.

Zellner, B. (1973). The polarization of Titan. *Icarus* 18, 661–664.

AERONOMY OF SATURN AND TITAN

Darrell F. Strobel

Naval Research Laboratory
Washington, DC 20375

ABSTRACT

The Saturn system presents exciting and unique objects for planetary aeronomy. The photochemistry of H_2 and H_e leads to the formation of an ionosphere. Methane photolysis results in the formation of spectroscopically detectable amounts of C_2H_6 and C_2H, and in the case of Titan, C_2H_4. Density profiles of C_2H_6, C_2H_2, and PH_3 should be indicative of the strength of atmospheric mixing processes.

INTRODUCTION

The Saturn system presents exciting and unique objects for planetary aeronomy. The presence of hydrocarbons on Titan raises interesting possibilities for organic chemistry. Light gases may escape Titan's gravitational field but not the stronger planetary field of Saturn and thus lead to the formation of a gaseous toroidal cloud around Saturn (McDonough and Brice, 1973a, b). From our limited information Saturn's upper atmosphere appears similar in thermal structure, composition, and photochemistry to the Jovian upper atmosphere.

THERMAL STRUCTURE

A distinctive feature of the Saturn system is the thermal IR emission. On Saturn the pronounced emission peak of CH_4 at 7.7 μm suggests a warm stratosphere, $T \geq 130$ K, while the same feature on Titan is indicative of temperatures ≥ 160 K. The

most plausible interpretation of these emission spectra is the presence of a temperature inversion in their stratospheres similar to the Earth's O_3 layer with solar IR heating in the 3.3 μm CH_4 band balanced by IR cooling in the 7.7 μm CH_4 band, the 12.2 μm C_2H_6 band, and the 13.7 μm C_2H_2 (Gillett *et al.*, 1969; Danielson *et al.*, 1973). Additional heating may be required to achieve these observed "temperatures" and fine absorbing particles which absorb UV and visible sunlight have been suggested (Axel, 1972; Danielson *et al.*, 1973). Since these particles are very small, they are poor emitters and will heat up and collisionally transfer their energy to atmospheric gases.

Strobel and Smith (1973) concluded that the globally averaged vertical temperature contrast in the thermospheres of Saturn and Titan was ~10 K and ~90 K, respectively, for solar EUV heating only. It should be remembered that Pioneer 10 measured a Jovian ionospheric scale height that implied a much warmer thermosphere than solar EUV heating could maintain (Fjeldbo *et al.*, 1975). The above temperature contrast for Saturn's thermosphere should be regarded as a minimum value.

PHOTOCHEMISTRY OF H_2

Molecular hydrogen, the major constituent of the outer planets, has a dissociation continuum below 845 Å and an ionization continuum below 804 Å (Cook and Metzger, 1964). Discrete absorption in the Lyman and Werner bands can lead to fluorescent dissociation of H_2 (cf. Field *et al.*, 1966; Stecher and Williams, 1967). The deposition of solar EUV radiation in a H_2 atmosphere results initially in the production of primarily H_2^+ ions, which react with H_2 to produce $H_3^+ + H$ and break a H_2 bond. If He is present the production of He^+ ions will result in the dissociation of H_2 by ion-molecule reactions. For each H_2 molecule and He atom ionized at least two H atoms will be produced. Three body recombination of H atoms is exceedingly slow in the ionosphere and consequently there is a large downward flux of H atoms on Saturn from this region. For Saturn the globally averaged downward H atom flux is $\sim 2 \times 10^8$ cm^{-2} s^{-1} (Strobel, 1973c).

The planetary albedo at Ly-α is in simple terms a measure of the H atom column density above the absorbing CH_4 layer. This column density is a sensitive function of the eddy diffusion coefficient, K, in the vicinity of the turbopause

(Hunten, 1969; Wallace and Hunten, 1973). The recent rocket measurement of Ly-α from the Saturn system by Weiser *et al.* (1977) gave ~700 R for the disk. This is comparable to a 2kR signal from Jupiter and, based on Wallace and Hunten (1973), would suggest an eddy diffusion coefficient near the turbopause of $10^{(6-7)}$ cm^2 s^{-1}. In addition Weiser *et al.* (1977) detected ~200 R of Ly-α in the vicinity of Saturn which may be indicative of a hydrogen atmosphere associated with the ring system. Measurements of the Ly-α brightness around the satellites will provide important information on processes that produce the gaseous toroidal clouds discussed in the Introduction.

The formation of an ionosphere H_2-dominated atmosphere has been most recently discussed by Atreya and Donahue (1975). Of particular importance are the major sources of H^+ ions as a H^+ plasma can only recombine radiatively at a slow rate ($\sim 7 \times 10^{-12}$ cm^3 s^{-1}). The H_3^+ ions produced by the reaction $H_2^+ + H_2$ dissociatively recombine rapidly ($\sim 4 \times 10^{-7}$ cm^2 s^{-1}). Thus H^+ will be the major ion down to a level where the three body reaction $H^+ + H_2 + H_2 \rightarrow H_3^+ + H_2$ proceeds rapidly. This behavior is illustrated in Figure 1 for Saturn. In the lower ionosphere ($\leq$ 125 km, Figure 1) hydrocarbon ions, produced by hydrogen ions (H^+, H_2^+, H_3^+) reacting with CH_4 and photoionization of CH_3 radicals (Prasad and Tan, 1974), dominate. They dissociatively recombine an order of magnitude faster than H_3^+ and would lead to lower electron densities (up to a factor of 3) in this region than illustrated in Figure 1. Ionospheric models have also been developed for Titan by Whitten *et al.* (1977).

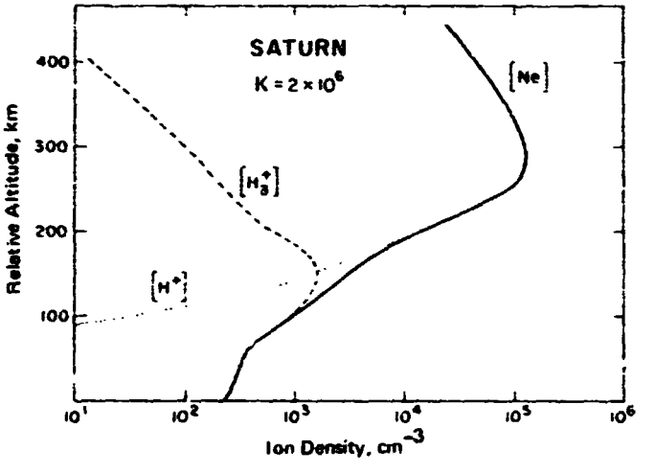

Figure 1. A Model for Saturn's ionosphere with $K = 2 \times 10^6 cm^2 s^{-1}$, and He mixing ratio of 0.24. The vertical scale gives the height above a reference level where the H_2 density is $1 \times 10^{16} cm^{-3}$. (after Atreya and Donahue, 1975).

PHOTOCHEMISTRY OF HYDROCARBONS

The principal hydrocarbon in the outer solar system is CH_4. C_2H_6 has been detected in the atmospheres of Saturn, and Titan (Ridgway, 1974; Gillett and Forrest, 1974; Gillett *et al.*, 1973). Hydrocarbons in the presence of UV radiation can form polymers. Based on photochemical models for the outer planets Strobel (1975) concluded that only a small percentage of dissociated CH_4 molecules are converted to complex hydrocarbons. To first order a closed photochemical model can be constructed; the principal reactions are schematically presented in Figure 2. Approximately 70% of the solar photons which dissociate CH_4 are at Ly-α where the primary processes are (Rebbert and Ausloos, 1972; Ausloos, 1972)

$$\begin{aligned} CH_4 + h\nu\,(\text{Ly-}\alpha) &\rightarrow {}^1CH_2 + H_2 \quad 92\% \\ &\rightarrow CH + H + H_2 \quad 8\% \end{aligned} \qquad (1)$$

where $^1CH_2$ denotes the singlet state of CH_2.

The only chemical means (other than energetic photons) for breaking the bond of two C atoms is the reaction sequence: $H + C_2H_4 \rightarrow C_2H_5$, $H + C_2H_5 \rightarrow 2CH_3$. For this destruction to be important a large H atom concentration is required at pressures ~10 mbar. As a consequence there is some production of higher hydrocarbons. To conserve C atoms a downward flow of C_2H_6 and C_2H_2 is balanced by an upward flow of CH_4. It is postulated that a deep circulation is present in Saturn that transports higher hydrocarbons to the hot, dense interior where they undergo thermal decomposition to produce fresh CH_4 which is transported upwards to replenish the CH_4 destroyed in photolysis.

The photochemical model is most sensitive to the $[CH_4]/[H_2]$ mixing ratio, the escape rate of H atoms from the atmosphere, and the atmospheric mixing rate (eddy diffusion coefficient). From Figure 2 it is evident that as the $[CH_4]/[H_2]$ ratio increases, the production rates of C_2H_4 and C_2H_2 will increase. The fate of the CH_3 radical depends on the $[H]/[CH_3]$ ratio and determines the rate at which CH_4 is recycled. Although the escape rate of H atoms from Saturn is negligible, it can be substantial from the satellites and actually control the H atom density distribution. A large escape rate depresses the H concentration and results in large conversion rates of CH_4 to C_2H_6 and C_2H_2 (>90% for Titan (Strobel, 1974a)). Also large con-

centrations of C_2H_2 will efficiently remove H atoms by catalytic recombination as illustrated in Figure 2, $H + C_2H_2 \rightarrow C_2H_3$, $H + C_2H_3 \rightarrow H_2 + C_2H_2$ (Strobel, 1973a).

The most abundant hydrocarbons produced in CH_4 photolysis are C_2H_6 and C_2H_2. They have vertical density distributions of the form (Strobel, 1974b):

$$n = c \exp\left[\frac{-z}{H_{av}}\right] + \frac{\phi_0}{K}\left[\frac{1}{H_{av}} - \frac{1}{H_k}\right]^{-1} \qquad (2)$$

where $K = K_0 \exp(z/H_k)$, H_{av} is the atmospheric scale height, C is an integration constant, and ϕ_0 is the downward flux approximately equal to the column production rate. Typical hydrocarbon densities are illustrated in Figure 3 for Saturn. C_2H_6 is a stable molecule in a cold, reducing atmosphere. If the interior conditions do not require rapid downward flow, then the C_2H_6 density profile is given approximately by the first term of (2), i.e., C_2H_6 is mixed. For rapid downward flow the C_2H_6 density profile will exhibit the scale height of K and be represented by the second term of Equation (2). For C_2H_2 some chemical removal occurs when the ratio $[H]/[H_2]$ is very small. A large downward flux is required to balance this loss. Consequently its density profile is represented by the second term of Equation (2). The

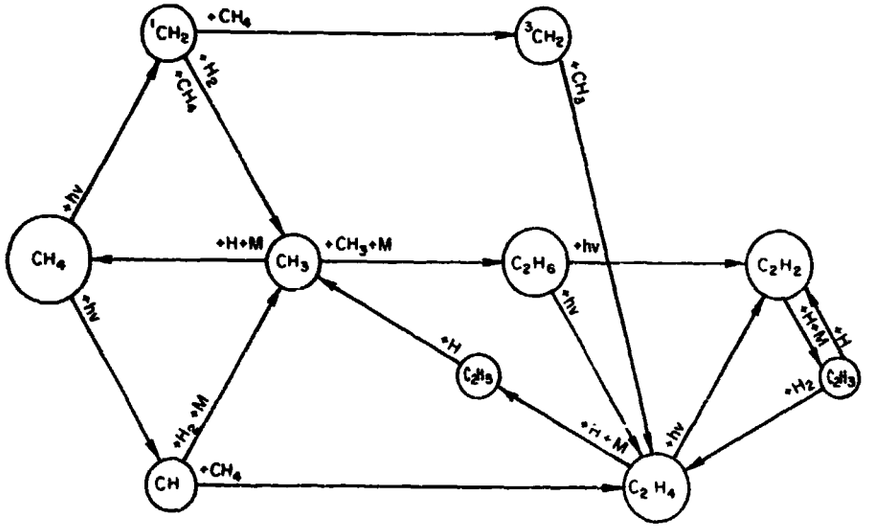

Figure 2. Principal reactions of hydrocarbon photochemistry in the outer solar system atmosphere (after Strobel, 1975).

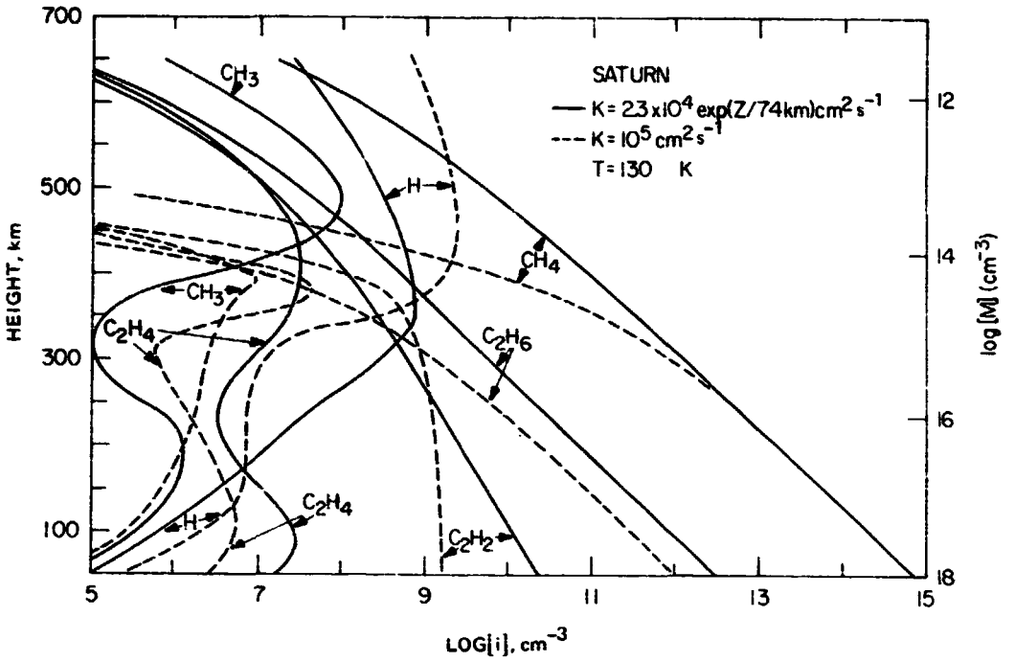

Figure 3. Hydrocarbon density profiles for the Saturnian atmosphere with indicated eddy diffusion profile. Solid line. $K \propto \{M\}^{-0.5}$, dashed lined: $K = 10^5 cm^2 s^{-1}$, where $\{M\}$ = number density of atmospheric gas. Lower boundary condition for C_2H_6 is a small downward flux (see Strobel, 1973a).

rapid decrease in the H concentration below 200 km is due to catalytic removal by C_2H_2 (Strobel, 1973a). It should be noted that for C_2H_2 (and C_2H_6 if rapid downward flow is required) that the very rapid mixing characteristic of the troposphere will result in a substantial decrease in the number density below the tropopause (on the order of the eddy diffusion coefficient ratio).

Products of CH_4 photolysis on Titan are removed by condensation at a cold tropopause and possibly dissolve on the cold surface. As a consequence a large downward flux of photolysis products is anticipated ($\sim 10^{10}$ cm^{-2} s^{-1}, primarily C_2H_6 and C_2H_2). Over the age of the solar system this would represent an accumulation of 30 kg cm^{-2}. Photochemical models for Titan predict observable amounts of C_2H_6 and C_2H_2 for slow mixing rates in the lower stratosphere (eddy diffusion coefficients $\leq 10^5$ cm^2 s^{-1}) as illustrated in Figure 4. Their density profiles are represented by the second term of Equation (2), from which it follows that large densities are associated with slow mixing. The other essential features of the model are that the C_2H_6 abundance is sensitive to the eddy diffusion coefficient, the composition of Titan's atmosphere, and the net escape rate of H atoms from the exobase, whereas the C_2H_2 abundance is principally sensitive to the eddy diffusion coefficient.

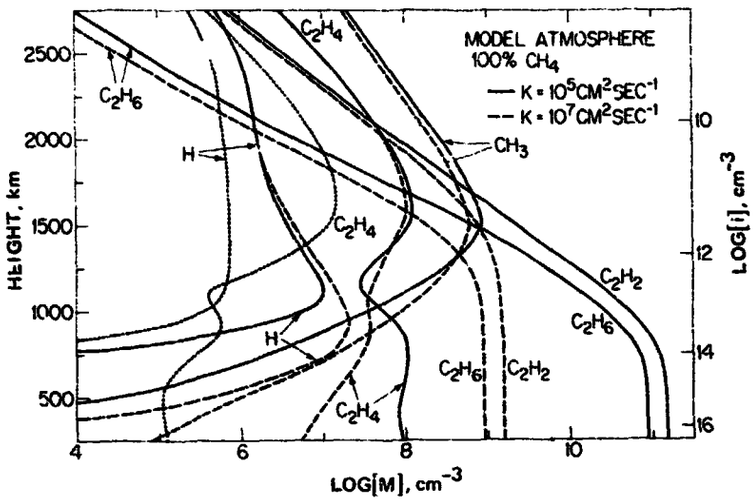

Figure 4. Hydrocarbon densities as a function of the eddy diffusion coefficient for a pure CH_4 atmosphere on Titan. The dotted lines represent a model with $K = 10^5 cm^2 s^{-1}$ and a negligible reaction rate for $CH_2 + CH_3 \rightarrow C_2H_4 + H$.

PHOTOCHEMISTRY OF PH_3 AND NH_3

On Saturn and Titan the cold trap temperatures at the tropopause are sufficiently low and restrict the NH_3 mixing ratio above this level to less than 10^{-12}. As a consequence only the more abundant PH_3 on Saturn is aeronomically important. The Prinn and Lewis (1975) model is applicable with the addition of the reaction $H + PH_3 \rightarrow PH_2 + H_2$, which effectively doubles the dissociation rate (Lee *et al.*, 1976; Strobel, 1977). One questionable feature of this model is the absence of any direct mechanism for partial recycling of PH_3 in the photolysis region. Each absorbed UV photon by PH_3 leads to irreversible conversion to P_4 (red phosphorus).

The vertical PH_3 density profile is given by

$$[PH_3] \propto \exp\left[-\frac{z}{2H_{av}} \left(1 + \sqrt{1 + r}\right) \right] \qquad (3)$$

where $r = \frac{4 H_{av}^2 \epsilon J}{K}$, J is the PH_3 dissociation rate and $\epsilon \sim 2$ as discussed above. For sufficiently slow mixing, this expression reduces to

$$[PH_3] \propto \exp\left[- z \sqrt{\frac{\epsilon J}{K}} \right]$$

For Saturn $\epsilon J \sim 2 \times 10^{-7}$ s^{-1} and if $K \sim 10^4$ cm^3 s^{-1}, then the effective PH_3 scale height is ~2 km, i.e. PH_3 is confined to the lower stratosphere. The vertical distribution of $[PH_3]$ is thus indicative of K(z) in the lower stratosphere.

SUMMARY

The photochemistry of H_2 and He leads to the formation of the main ionosphere and, through ion chemistry and recombination, H atoms. Observations of electron density and ion composition will yield information on the chemistry and structure of the ionosphere. H atoms can be observed by Ly-α emission and interpretation of the data should yield the mixing rate near the turbopause. CH_4 photolysis leads principally to the formation of C_2H_6 and C_2H_2. C_2H_6 is a photochemically stable molecule and, depending on the lower boundary condition, is either quasi-mixed or $K[C_2H_6]$ is quasi-conserved above the tropopause. Also $K[C_2H_2]$ is quasi-conserved in this region. Thus observations of the C_2H_2 and C_2H_6 density profiles can yield information on K(z) and the magnitude of the downward C_2H_6 flow to the interior in the case of Saturn. The extent of catalytic removal of H atoms by C_2H_2 requires a measurement of H density profile. The models predict $[C_2H_4]/[C_2H_2] \ll 1$ and that C_2H_4 can only be detected on Titan where its scale height is an order of magnitude larger than on Saturn. Attempts to observe C_2H_4 would serve as a useful internal check on the models.

NH_3 should be frozen out below the tropopause on Saturn and Titan and thus be aeronomically unimportant. On Saturn the vertical PH_3 density profile should be indicative of K(z) in the lower stratosphere in a similar manner as the NH_3 profile on Jupiter (Strobel, 1973b).

REFERENCES

Atreya, S. K. and T. M. Donahue (1975). Ionospheric models of Saturn, Uranus, and Neptune *Icarus 24*, 358–362.

Ausloos, P., (1972). Private communication.

Axel, L. (1972). Inhomogeneous Models of the Atmosphere of Jupiter, *Astrophys. J. 173*, 451–468.

Cook, G. R , and P. H. Metzger (1964). Photoionization and absorption cross sections of H_2 and D_2 in the vacuum ultraviolet region. *J. Opt Soc. Amer. 54*, 968–972.

Danielson, R. E., J. J. Caldwell, and D. R. Larach (1973). An inversion in the atmosphere of Titan. *Icarus 20*, 437–443.

Field, G. B., W. B. Somerville, and K. Dressler (1966). Hydrogen molecules in astonomy. *Ann. Rev. Astr. and Astrophys. 4*, 207–244.

Fjeldbo, G., A. J. Kliore, B. Seidel, D. Sweetman, and D. Cain (1975). The Pioneer 10 radio occultation measurement of the ionosphere of Jupiter. *Astron. Astrophys. 39*, 91–96.

Gillett, F. C., F. J. Low, and W. A. Stein (1969). The 2.8-14 micron spectrum of Jupiter. *Astrophys J. 157*, 925–934.

Gillett, F. C., W. J. Forrest, and K. M. Merrill (1973). 8-13μm observations of Titan. *Astrophys. J. 184*, L93–L95.

Gillett, F. C. and W. J. Forrest (1974). The 7 5 to 13.5 micron spectrum of Saturn. *Astroyphys. J. 187*, L37–L39.

Hunten, D. M. (1969). The upper atmosphere of Jupiter. *J. Atmos. Sci. 26*, 826–834.

Lee, J. H., J. V. Michael, W. A. Payne, D. A. Whytock, and L. J. Stief (1976). Absolute rate constant for the reaction of atomic hydrogen with phosphine over the temperature range 209 to 495K. *J. Chem. Phys. 65*, 3280–3283.

McDonough, T. R. and N. M. Brice (1973a). A new kind of ring around Saturn? *Nature 242*, 513.

McDonough, T. R. and N. M. Brice (1973b). A Saturnian gas ring and the recycling of Titan's atmosphere. *Icarus 20*, 136–145.

Prasad, S. S. and A. Tan (1974). The Jovian ionosphere. *Geophys. Res. Lett. 1*, 337–340.

Prinn, R. G. and J. S. Lewis (1975). Phosphine on Jupiter and implications for the great red spot. *Science 190*, 274–276.

Rebbert, R. E., S. G. Lias, and P. Ausloos (1973). Pulse radiolysis of methane. *J. Res. Nat. Bur. Stand. (U.S.) 77A*, 249–257.

Ridgway, S. T. (1974). Jupiter: Identification of ethane and acetylene. *Astrophys. J. 187*, L41–L43.

Stecher, T. P., and D. A. Williams (1967). Photodestruction of hydrogen molecules in HI Regions. *Astrophys. J. 149*, L29–L30.

Strobel, D. F. (1973a). The Photochemistry of hydrocarbons in the Jovian atmosphere. *J. Atmos. Sci. 30*, 489–498.

Strobel, D. F. (1973b). The Photochemistry of NH_3 in the Jovian atmosphere. *J. Atmos. Sci. 30*, 1205–1209.

Strobel, D. F. (1973c). The Jovian upper atmosphere. In *Physics and Chemistry of Upper Atmospheres*. (B. M. McCormac, ed.), pp. 345–353. D. Reidel Publishing Co., Holland.

Strobel, D. F. (1974a). The Photochemistry of hydrocarbons in the atmosphere of Titan. *Icarus 21*, 466–470.

Strobel, D. F. (1974b). Hydrocarbon abundances in the Jovian atmosphere. *Astrophys. J. 192*, L47–L49.

Strobel, D. F. (1975). Aeronomy of the major planets: Photochemistry of ammonia and hydrocarbons. *Rev. Geophys. Space Phys. 13*, 372–382.

Strobel, D. F. (1977). NH_3 and PH_3 photochemistry in the Jovian atmosphere. *Astrophys. J. 214*, L97–L99.

Strobel, D. F. and G. R. Smith (1973). On the temperature of the Jovian thermosphere. *J. Atmos. Sci. 30*, 718–725. (see also Corrigenda, p. 964)

Wallace, L. and D. M. Hunten (1973). The Lyman-Alpha albedo of Jupiter. *Astrophys. J. 182*, 1013–1031.

Weiser, H., R. C. Vitz, and H. W. Moos (1977). Detection of Lyman α emission from the Saturnian disk and from the ring system. *Science 197*, 755–757.

Whitten, R. C., L. A. Capone, L. McCulley, and P. F. Michaelson (1977). The Upper Ionosphere of Titan. *Icarus 31*, 89–96.

DISCUSSION

S. CHANG: If a probe went into Jupiter's atmosphere or Saturn's atmosphere and actually found significant amounts of ethane in the troposphere, would you conclude that some process other than methane photochemistry is responsible?

STROBEL: That would be one possible interpretation. The other is that thermodynamically there were large amounts in the deep interior and that the mixing was violent enough to carry it up to the observable region.

A. TOKUNAGA: Is there any evidence that the eddy diffusion coefficient is different at the poles relative to the equator? If that were the case, the ethane mixing ratio might vary with latitude.

D. STROBEL: The eddy diffusion coefficient works best when it is regarded as a global average. As one tries to ascribe to it horizontal variations, I think one is stretching the use of the concept. It's a convenient factor to use as a first estimate of what's going on in the atmosphere, but when the subject becomes sufficiently mature, one should use actual dynamical equations to calculate the transport.

J. POLLACK: Didn't Don Hunten once nickname it the eddy confusion coefficient?

D. HUNTEN: The straight answer to Alan's question is that there could be large variations in vertical transport rates with latitude on a planet like Saturn, very large.

D. STROBEL. Especially if the vertically propagating waves are the cause of the phenomena and depending on where they are excited.

D. HUNTEN: George Siscoe was quite interested in hydrogen production rates and, of course, they can be derived implicitly from these computations. The vertical curves at the bottom right of Figure 4 give a downward flux of the things left over, once you've made hydrogen. The corresponding hydrogen is escaping, and the rate is 9×10^{9} cm^{-2} s^{-1}.

D. STROBEL: Right. I should emphasize that the atmosphere is considerably larger than the solid body, and therefore captures more solar photons than you might think.

SATURN'S MICROWAVE SPECTRUM: IMPLICATIONS FOR THE ATMOSPHERE AND THE RINGS

M. J. Klein, M. A. Janssen, S. Gulkis and E. T. Olsen

Earth and Space Sciences Division, Jet Propulsion Laboratory
California Institute of Technology
Pasadena, California 91103

ABSTRACT

Measurements of Saturn's disk temperature are compiled to determine the planet's microwave spectrum from 1 mm to 100 cm wavelength. The data were adjusted to conform with a common flux density scale. A model of Saturn's rings is used to remove the effects of the rings from the atmospheric component at centimeter and decimeter wavelengths. Theoretical spectra for a number of convective atmospheric models were computed and compared with the observed spectrum. Radiative-convective models with approximately solar composition and with an effective temperature of ~89 K are in good agreement with the observations. The agreement between the observed and theoretical spectra is a strong indication that gaseous ammonia is present in Saturn's atmosphere. A good fit to the data is obtained with an ammonia mixing ratio of $\sim 5 \times 10^{-4}$. Lower values of the NH_3 mixing ratio can also provide a good fit provided an additional source of microwave opacity is present in Saturn's atmosphere. Liquid water droplets in the troposphere could provide a substantial microwave opacity. A comparison of the millimeter wavelength data with the "best-fitting" atmospheric spectrum indicates that the thermal component of the ring brightness temperature near 1 mm wavelength is ~25 K.

INTRODUCTION

Theoretical studies have shown that Saturn's microwave spectrum can be explained by thermal emission from the tropospheric region of an atmosphere with generally solar composition and with ammonia as the primary source of microwave

opacity (Gulkis *et al.*, 1969; Wrixon and Welch, 1970; Gulkis and Poynter, 1972; Ohring and Lacser, 1975). In all of these studies, the influence of the rings on the observed brightness temperatures was assumed to be negligible. Because the available data consisted almost entirely of observations made with very low spatial resolution, the microwave properties of the rings were virtually unknown. In recent years, measurements of the planet and rings have been made with radio interferometers operating at wavelengths from 0.8 to 21 cm. These new data provide strong constraints on the microwave properties of the rings and hence their influence on the microwave spectrum can now be estimated. In addition, the microwave flux-density scale, which is used to calibrate the planetary measurements, has been defined with better accuracy and over a larger wavelength interval than it was only a few years ago. In this paper we make use of the new data to re-analyze Saturn's microwave spectrum.

We have compiled a new list of the published measurements of Saturn's microwave disk temperature for wavelengths between 1 mm and 100 cm. The data are normalized to a uniform calibration scale and the effects (e.g., obscuration, scattering and emission) of the rings are computed for a simple model of the rings. Computed spectra for several atmospheric models are compared with the spectrum from 0.8 cm to 100 cm. The influence of the rings in this spectral region is found to be small and it can be removed with confidence. Two "best fit" models are determined, one with an NH_3 mixing ratio which is somewhat greater than a solar value, and the other with a solar-like NH_3 mixing ratio but with an additional opacity source near the 270 K level in the troposphere. When either of these atmospheric models are extended to millimeter wavelengths, the computed temperatures fall systematically below the observed disk temperatures. This result is explained if the thermal component of the ring brightness temperature, assuming both the A and B rings are uniformly bright, is ~25 K for wavelengths near 1 mm. Finally, we computed the vertical transmission loss that a probe communication link is likely to encounter as it penetrates Saturn's atmosphere.

SATURN'S MICROWAVE SPECTRUM

Data Normalization Factors

Our list of measurements of Saturn from 1 mm to 100 cm is given in Table 1. Because most of the observations were obtained with single antennas having low spatial resolution, the majority of the reported temperatures include the integrated flux density

Table 1. Saturn's Microwave Spectrum

(1)	(2)	(3)	(4)	(5)[a]	(6)[b]	(7)[c]	(8)[c]	Reference
λ	T_D	Error (rel, abs)	|B|	f_{CAL}	$f_\Omega(B)$	T_s/T_D^*	T_s	
(cm)	(K)	(K)	(deg)				(K)	
0.1	145	(7 , 14)	22.0	1.0	0.983	0.937	133.4	Werner *et al.* (1978)
0.12	140	(15 , 22)	10.2	0.940	0.996	1.007	132.0	Low and Davidson (1965)
0.14	194	(8 , 21)	26.6	0.983	0.975	0.888	165.2	Rather *et al.* (1974)
0.14	120	(- , 30)	20.0	1.070	0.985	0.911	115.3	Kostenko *et al.* (1971)
0.14	184	(6 , 13)	26.6	1.0	0.975	0.898	161.1	Courtin *et al.* (1977)
0.14	188	(5 , 14)	25.4	1.0	0.977	0.914	168.0	Courtin *et al.* (1977)
0.213	164	(5 , 12)	26.4	0.980	0.976	0.876	137.4	Ulich (1974)
0.309	148	(5 , 11)	21.0	1.0	0.984	0.973	141.7	Ulich *et al.* (1973)
0.33	150	(6 , -)	8.0	1.0	0.998	1.024	153.2	Epstein *et al.* (1970)
0.33	155	(3 , -)	16.2	1.0	0.990	1.016	156.0	Epstein (1978)
0.341	144	(2 , -)	10.5	1.0	0.996	1.043	149.5	Ulich (1978)
0.35	132	(6 , 13)	16.3	1.220	0.990	1.035	165.1	Pauliny-Toth and Kellermann (1970)
0.353	151	(3 , -)	25.2	1.0	0.978	0.939	138.6	Ulich (1978)
0.387	115	(3 , 15)	26.4	1.286	0.976	0.923	133.2	Voronov *et al.* (1974)
0.428	148	(7 , -)	25.9	1.0	0.977	0.932	134.7	Ulich (1978)
0.6	156	(7 , -)	25.9	1.0	0.977	0.955	145.4	Ulich (1978)
0.696	158	(4 , -)	10.1	1.0	0.996	1.053	165.7	Ulich (1978)
0.82	132	(4 , 9)	17.6	1.0	0.989	1.059	138.2	Kuzmin and Losovsky (1971)
0.833	147	(4 , 9)	24.9	1.0	0.978	*	144.0	Janssen and Olsen (1978)

Table 1. Saturn's Microwave Spectrum (contd.)

(1)	(2)	(3)	(4)	(5)[a]	(6)[b]	(7)[c]	(8)[c]	
λ	T_D	Error (rel, abs)	|B|	f_{CAL}	$f_\Omega(B)$	T_s/T_D^*	T_s	Reference
(cm)	(K)	(K)	(deg)				(K)	
0.845	151	(3 , 7)	17.7	0.980	0.988	1.056	154.5	Wrixon and Welch (1970)
0.95	127	(3 , 13)	4.0	1.087	0.999	1.028	141.8	Pauliny-Toth and Kellermann (1970)
0.955	135	(7 , -)	25.9	1.0	0.977	0.981	129.3	Ulich (1978)
0.955	136	(4 , 6)	22.0	1.0	0.983	1.037	138.6	Dent (1972)
0.955	126	(- , 6)	6.0	1.059	0.999	1.043	139.0	Hobbs and Knapp (1971)
1.176	131	(3 , 6)	17.7	0.980	0.988	1.073	136.1	Wrixon and Welch (1970)
1.265	127	(4 , 6)	18.4	0.980	0.988	1.074	132.0	Wrixon and Welch (1970)
1.304	139	(2 , 8)	23.6	0.918	0.981	*	125.0	Schloerb (1977)
1.463	131	(3 , 5)	17.0	1.0	0.989	1.084	140.4	Wrixon and Welch (1970)
1.53	141	(10 , 15)	10.2	0.967	0.996	1.070	145.4	Welch *et al.* (1966)
1.95	145	(4 , -)	4.0	0.938	0.999	1.038	141.1	Pauliny-Toth and Kellermann (1970)
2.07	162	(4 , 7)	26.5	1.0	0.976	1.020	161.2	Gary (1974)
3.12	137	(7 , 12)	6.2	1.053	0.999	1.043	150.3	Berge (1968)
3.56	170	(2 , 6)	26.5	1.0	0.976	1.011	167.7	Gary (1974)
3.56	158	(2 , 6)	17.9	1.0	0.988	1.091	170.3	Turegano and Klein (1978)
3.71	161	(5 , 7)	26.1	1.035	0.976	*	163.0	Cuzzi and Dent (1975)
3.71	171	(5 , -)	15.3	1.0	0.991	*	169.0	Schloerb (1977)
3.75	168	(7 , 11)	5.8	1.048	0.999	1.045	183.7	Seling (1970)
6.0	175	(17 , 19)	10.0	1.040	0.996	1.072	198.8	Kellermann (1966)

Table 1. Saturn's Microwave Spectrum (contd.)

(1)	(2)	(3)	(4)	(5)[a]	(6)[b]	(7)[c]	(8)[c]	
λ (cm)	T_D (K)	Error (rel, abs) (K)	$\|B\|$ (deg)	f_{CAL}	$f_\Omega(B)$	T_s/T_D^*	T_s (K)	Reference
6.0	190	(- , 45)	0.2	1.0	1.000	1.000	190.0	Hughes (1966)
6.2	162	(12 , 18)	24.8	1.037	0.978	1.044	171.6	Gerard and Kazes (1973)
9.0	165	(- , 25)	1.1	1.060	1.000	*	175.0	Berge and Read (1968)
10.0	196	(- , 44)	17.9	0.988	0.988	1.086	207.7	Drake (1962)
10.7	172	(- , 20)	5.4	1.061	0.999	*	182.0	Berge and Read (1968)
11.1	186	(20 , 25)	25.[illegible]	1.050	0.978	1.033	197.2	Gerard and Kazes (1973)
11.3	182	(4 , 18)	14.7	1.024	0.992	1.085	200.5	Davies *et al.* (1964)
11.3	196	(17 , 20)	8.0	1.025	0.998	1.056	211.6	Kellermann (1966)
21.1	208	(13 , -)	16.8	1.010	0.989	*	208.0	Berge and Muhleman (1973)
21.1	231	(9 , -)	21.8	0.978	0.983	*	222.0	Berge and Muhleman (1973)
21.1	230	(10 , 15)	25.2	0.988	0.978	*	222.0	Briggs (1973)
21.2	286	(10 , 37)	18.0	0.950	0.988	1.089	292.0	Davies and Williams (1966)
21.2	193	(20 , 25)	21.5	0.988	0.983	1.071	200.8	Gerard and Kazes (1973)
21.2	207	(20 , 25)	25.0	0.988	0.978	1.031	206.2	Gerard and Kazes (1973)
21.4	214	(14 , 15)	26.2	1.029	0.976	1.015	218.1	Condon *et al.* (1974)

Table 1. Saturn's Microwave Spectrum (contd.)

(1)	(2)	(3)	(4)	(5)[a]	(6)[b]	(7)[c]	(8)[c]	
λ	T_D	Error (rel, abs)	|B|	f_{CAL}	$f_\Omega(B)$	T_s/T_D^*	T_s	Reference
(cm)	(K)	(K)	(deg)				(K)	
49.5	390	(- , 65)	21.8	1.050	0.983	1.074	432.2	Yerbury *et al.* (1971)
69.7	385	(45 , 49)	26.3	1.0	0.976	1.019	382.8	Condon *et al.* (1974)
94.3	540	(- ,110)	24.7	1.0	0.979	1.040	549.6	Yerbury *et al.* (1973)

[a]The factor f_{CAL} is the multiplier used to normalize the observed disk temperatures to the microwave flux density scale of Baars, Genzel, Pauliny-Toth and Witzel (1977) for $100 > \lambda > 1$ cm; and the spectrum of DR-21 for $1 > \lambda > 0.3$ cm (Dent, 1972 ; B. L. Ulich private communication). For $\lambda < 0.3$ cm, we rely on the calibration of the most recent observations, and we normalize the older data to this calibration via the observed ratios of Saturn to Jupiter and Venus.

[b]The disk temperatures listed in column 2 are based on the solid angle given by the polar and equatorial semi-diameters of Saturn published in the AENA. The factor $f_\Omega(B)$ corrects this reference solid angle to the value for an oblate spheriod inclined to the observer at the angle B.

[c]The ratio T_s/T_D^* , where $T_D^* = T_D f_{CAL} f(B)$, is computed based on the ring model described in the text.

T_D^* is thus the equivalent disk temperature of the Saturn-ring system, adjusted to a common flux density scale and corrected for viewing geometry, while T_s is the average brightness temperature of the disk alone.

from both the planet and the rings. The temperatures given in the second column of the table are based on the assumption that all of the observed flux density is emitted from the solid angle of the apparent disk of Saturn, i.e., emission, scattering and obscuration by the rings was ignored for all but the nine interferometric observations. We treat the interferometric data separately because the influence of the rings was already removed by the authors. In the following discussion we describe the various correction factors we have applied to the original data to derive the final disk temperatures (Column 8), which represents the microwave spectrum of Saturn's atmosphere.

All of the observed temperatures were adjusted to a common flux-density scale given by Baars *et al.* (1977), and to the solid angle computed from the polar and equatorial semi-diameters given in the American Ephemeris and Nautical Almanac. The flux scale normalization factors, f_{CAL}, are listed in Column 5 of Table 1. An additional correction was applied to the data to account for the fact that the solid angle of an oblate spheriod varies with B, which is the angle the planet is tipped toward (or away from) the Earth at the time of the observation. The corresponding correction factors for the solid angle, $f_{\Omega}(B)$, are given in Column 6.

Influence of the Rings

To remove the influence of the rings from Saturn's microwave spectrum, we adopt a model for the microwave properties of the rings and use this model to derive correction factors to be applied to the single antenna measurements. These correction factors, given in Column 7, convert the measured disk temperatures, which include the influence of the rings, to the temperatures that would have been observed if there were no rings. We account for the finite beamwidth of the antenna used for each measurement. The latter correction is primarily important at the short wavelengths where the spatial resolution of antennas can be comparable to the angular size of Saturn's Ring system. The correction factors account for the weak thermal emission from the rings, for the fraction of thermal emission from Saturn's disk reflected off the rings, and for the attenuation of atmospheric emission transmitted through the sector of the rings which obscures the planet. The three components are schematically identified in Figure 1.

The nominal ring model incorporates the following assumptions and approximations. First, we assume that only the A and B rings are important to this discussion and that the microwave properties of these two rings are identical. We adopt $\tau = 0.7$

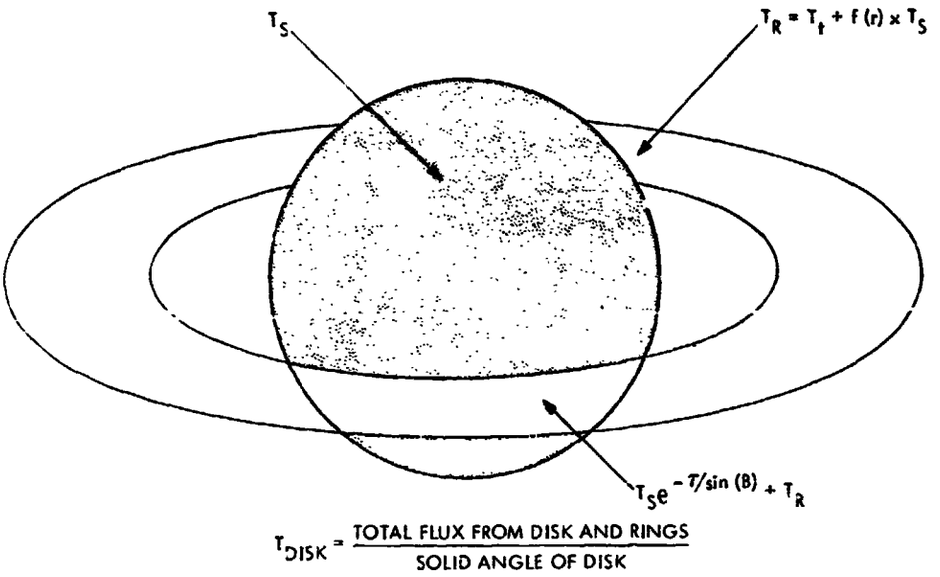

Figure 1. Schematic model of the brightness distribution of Saturn and the rings. Given the ring parameters T_r and τ, the brightness temperature, T_s, of Saturn's disk can be determined for any ring-inclination B. T_s is the temperature that would be measured in the absence of the rings.

for the optical depth of the rings at normal incidence and compute the absorption of the atmospheric emission by the obscuring sector of the rings (see Figure 1). We further assume that the opacity is independent of frequency over the microwave spectrum. These assumptions are based on the results of recent interferometric observations (Briggs, 1973; Berge and Muhleman, 1973; Cuzzi and Dent, 1975; Schloerb, 1977; Janssen and Olsen, 1978).

The ring brightness temperature, T_R is given by the sum of T_t and $f(r)T_S$, where T_t is the thermal brightness temperature of the rings, f(r) is an expression for the radial dependence of the reflected atmospheric temperature, T_S. The function f(r) is computed with the assumption that the rings form a perfectly-reflecting Lambertian-scattering surface. This assumption is an acceptable approximation to the more physically realistic models with multiple scattering computations (see e.g., Schloerb, 1977). The observational results for $\lambda > 1$ cm show that T_R is consistent with the reflected component as the primary source of brightness with the possibility of a small thermal component. For our nominal model, we set $T_t = 2 \pm 2$ K and calculate an average total ring contribution of $T_R \sim 7$ K. This choice encompasses the results of all interferometric measurements at centimeter wavelengths.

There is evidence that T_t increases with decreasing wavelength shortward of ~1 cm, but the wavelength dependence is strictly unknown. The computations of the

correction factors listed in the table are based on the assumption that T_t increases monotonically from $T_t \sim 7$ K near 8 mm (Janssen and Olsen, 1978) to $T_t \sim 25$ K near 1 mm wavelength. We show in a following section that this increase in T_t is consistent with the millimeter observations.

A computer program was written to calculate the disk temperature of the model illustrated in Figure 1 and described above. The brightness temperature T_S was adjusted to give the corrected disk temperature $T_D^* = T_D f_{CAL} f_\Omega(B)$. The corresponding correction factor T_S/T_D^* was then calculated for each single antenna observation in Table 1 and is listed in Column 7. The brightness temperature T_S (Column 8) is the disk temperature of Saturn which would be measured in the absence of rings.

ATMOSPHERIC MODELS

We computed theoretical microwave spectra for several models of Saturn's atmosphere to compare with the observational data. Each model is in hydrostatic equilibrium throughout, with the lower troposphere in convective equilibrium. The temperature-pressure profile in the upper stratosphere is given by the solution of the Eddington equation for a constant-flux, gray radiative atmosphere. The range of models is constrained by the effective temperature, T_e, that we allow in the solution. Current estimates of Saturn's effective temperature, derived from infrared observations, are near 90 K (e.g., Ward, 1977). We will restrict our discussion to three models which we designate Nominal (T_e = 89 K), Cool (T_e = 84 K) and Warm (T_e = 94 K).

The composition for each model is assumed to be primarily H_2 and He with CH_4, NH_3 and H_2O as minor constituents. The H_2, He and CH_4 are assumed uniformly mixed throughout the atmosphere with a He/H_2 number mixing ratio of 0.2 and $CH_4/H_2 = 2.1 \times 10^{-3}$ (Caldwell, 1977). Ammonia is assumed to be uniformly mixed in the troposphere and saturated in the upper troposphere. The partial pressure of saturated ammonia is controlled by the temperature according to the condensation relation

$$\text{Log } P_{NH_3} = 9.9974 - 1630\ T^{-1} \qquad (1)$$

where the pressure is in millimeters of Hg and T is degrees Kelvin.

The procedure for calculating the models begins with an initial estimate of a pressure-temperature point on an adiabat deep in the atmosphere (p > 10 atm). Solutions to the equation of hydrostatic equilibrium give the pressure at successively higher altitudes as the temperature decreases with the adiabatic gradient. For our choices of composition and gravitational acceleration (g = 905 cm^2 s^{-1}) the adiabatic gradient is ~0.97 K km^{-1}. Both the adiabatic lapse rate and a radiative lapse rate are calculated at each pressure point, until the adiabatic gradient overtakes the radiative gradient. Above this point, the temperature follows the radiative profile with increasing altitude. With this procedure, each pressure-temperature profile is uniquely specified either by a single pressure-temperature point or by the effective temperature. A more complete discussion of this procedure is given by Klein and Gulkis (1978).

The pressure-temperature profiles for our Warm, Nominal and Cool models are shown in Figure 2. The condensation temperatures for water and ammonia are marked to indicate the respective pressures where cloud bases are expected. The solid curves represent the convective portion of the atmosphere and the broken curves show the radiative regime. The thermal profile in and above the stratosphere does not

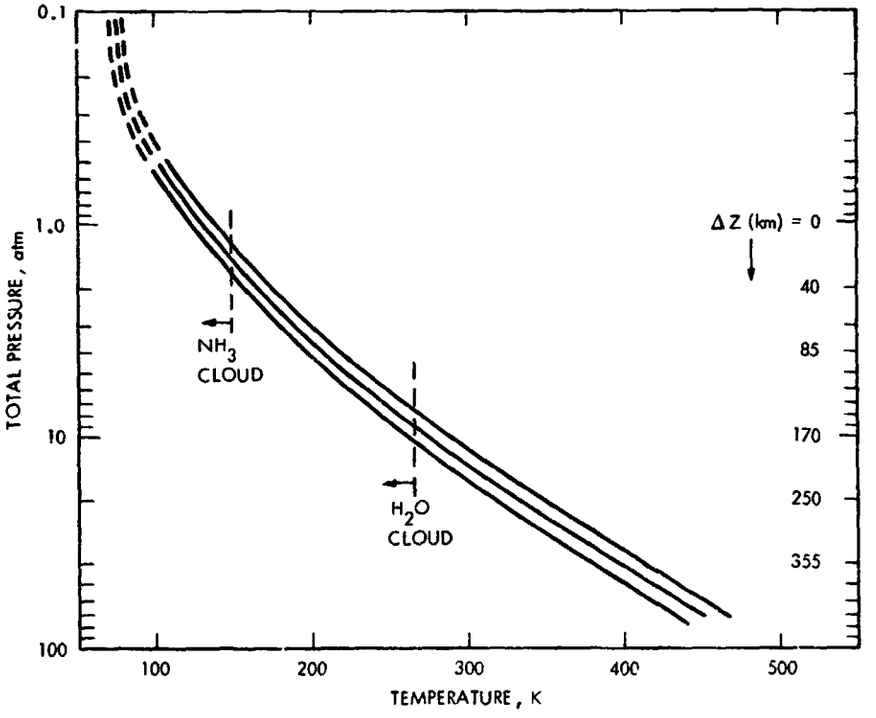

Figure 2. Pressure-Temperature profiles are shown for three atmospheric models of Saturn described in the text. The Cool, Nominal and Warm models correspond to the effective temperatures, respectively shown from left to right, T_e = 84K, 89K, 94K.

affect our interpretation of Saturn's microwave spectrum because the microwave opacity is very small in this region. For this reason we are not concerned with a temperature inversion which might form at high altitudes.

The atmospheric parameters, i.e., pressure, temperature and composition are related to the observed microwave brightness temperature through the equation of radiative transfer. The final step of our modeling program (see Klein and Gulkis, 1978) is to compute the distribution of the microwave brightness over the planet and from this we compute the mean brightness temperature of Saturn's oblate disk as a function of frequency. The resultant microwave spectrum for each model can then be compared with the spectrum, of the "ring free" temperature, T_S.

INTERPRETING THE SPECTRUM

The NH_3 Abundance

Among the various molecular species that have been detected or that are likely to be found in Saturn's atmosphere, ammonia is by far the most effective source of microwave opacity. For this reason, the observed microwave spectrum contains information on the average concentration and vertical distribution of ammonia on a global scale. In particular, the shape of the computed spectra corresponding to different atmospheric models depends upon our choice of $[NH_3]$, which is the number mixing ratio of ammonia at depth, and upon the pressure-temperature profile of each model. In this section the observed spectrum of Saturn's atmosphere is compared with the computed spectra for our Nominal model (T_e = 89 K). Several values of $[NH_3]$ are obtained and the sensitivity of the result to variations in other model assumptions is discussed.

For our study of the ammonia mixing ratio we concentrate on the spectral region from 0.8 to ~50 cm. Our confidence in both the ring-model corrections and the accuracy of the flux density scale is considerably greater for $\lambda > 8$ mm. The long-wavelength limit is imposed by the uncertainty of extrapolating microwave absorption coefficients to the deep atmosphere where pressures exceed 1000 atmospheres; emission from these regions begins to contribute significantly to the brightness temperature for wavelengths beyond ~50 cm. Exclusion of data at wavelengths longer than 50 cm minimizes the possible effects of non-thermal (synchrotron) emission from trapped radiation

belts. Condon *et al.* (1974) show that postulated components of synchrotron emission are insignificant for $\lambda \leq 21$ cm.

The measurements of Saturn's microwave spectrum for wavelengths >8 mm are plotted in Figure 3. Theoretical spectra for our Nominal model with selected values of $[NH_3]$ are represented by the four curves. It is evident that mixing ratios between 3×10^{-4} and 10×10^{-4} yield acceptable fits to the data. A formal analysis with weighted Chi-square tests gave an optimum abundance of $[NH_3] \sim 5 \times 10^{-4}$. For this analysis we included all data in the range $0.8 \leq \lambda \leq 21$ cm, each weighted by the square of the reciprocal of the relative error.

A constant multiplier, which was an additional free parameter in the analysis, allows for a uniform uncertainty in the absolute flux density scale. The minimum Chi-square solution was found with this constant equal to 0.96, which is consistent with this uncertainty. However, factors less than unity can also be explained (1) if we have underestimated the thermal emission from the rings; (2) if the ring opacity is less than 0.7; or (3) by atmospheric model assumptions that are invalid. One plausible example of the latter is the increase in disk temperature that occurs if the NH_3 is not completely saturated in the cloud regions. For example, the relative NH_3 humidity might differ from one area to the next on the disk (e.g., belts and zones).

The relative insensitivity of the computed spectra to nominal changes in T_e and the He abundance is demonstrated in Figures 4 and 5. The small changes in slope of the computed spectra that occur at the longer wavelengths can be compensated in the model by incrementing the value of $[NH_3]$ an insignificant amount.

Model with H_2O Cloud

Noting that atmospheric models predict the formation of a water cloud near the 270 K temperature region, one might ask if there is any evidence of such a cloud in Saturn's microwave spectrum. To investigate this possibility, we added a variable opacity term to our model near the 270 K level and recalculated the microwave spectrum for the Nominal pressure-temperature model. The ammonia mixing ratio was reduced to 1.5×10^{-4} to bring it into agreement with the solar N abundance. The microwave opacity in the "cloud" region was assumed to be $\tau_{cl} = \tau_o \nu^{-2}$, where $\tau_o = 1$ at 1 GHz and ν is the frequency in GHz. Our choice of opacity is based on the microwave absorption of small (<1 mm) water droplets and a cloud density of ~ 35 g m^{-3}

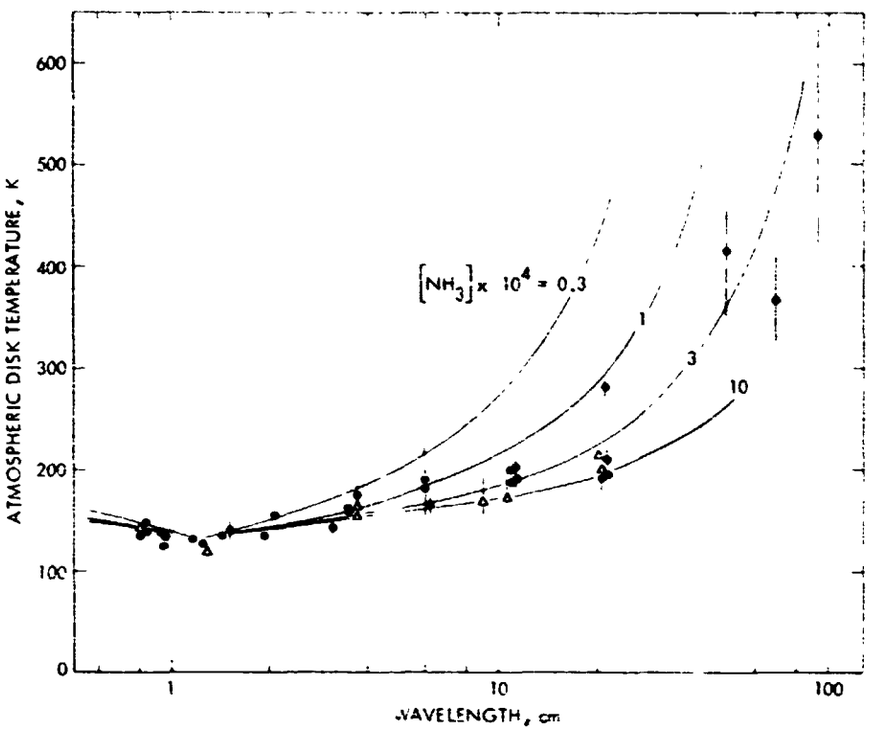

Figure 3. The microwave spectrum of Saturn's atmospheric temperature in the wavelength interval 0.8 to 100 cm. The filled circles represent single antenna data which have been adjusted slightly to remove the influence of the rings. The eight triangles represent the interferometric measurements which do not require ring corrections. The four curves represent the computed spectra for our Nominal Model with four values of the NH_3 mixing ratio.

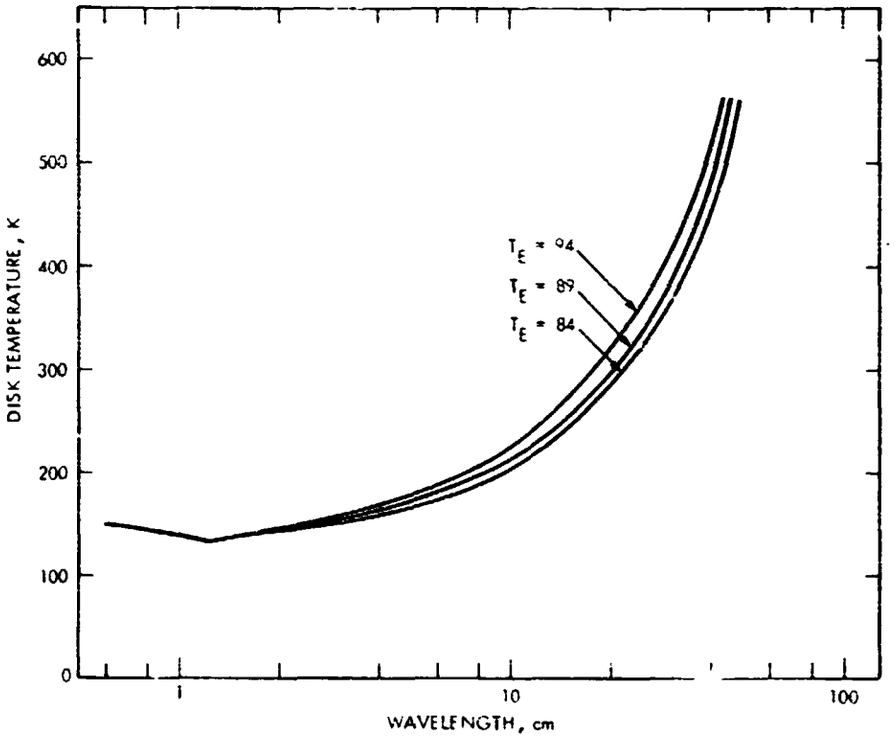

Figure 4. The effect of varying T_e, the effective temperature, on the computed microwave spectrum.

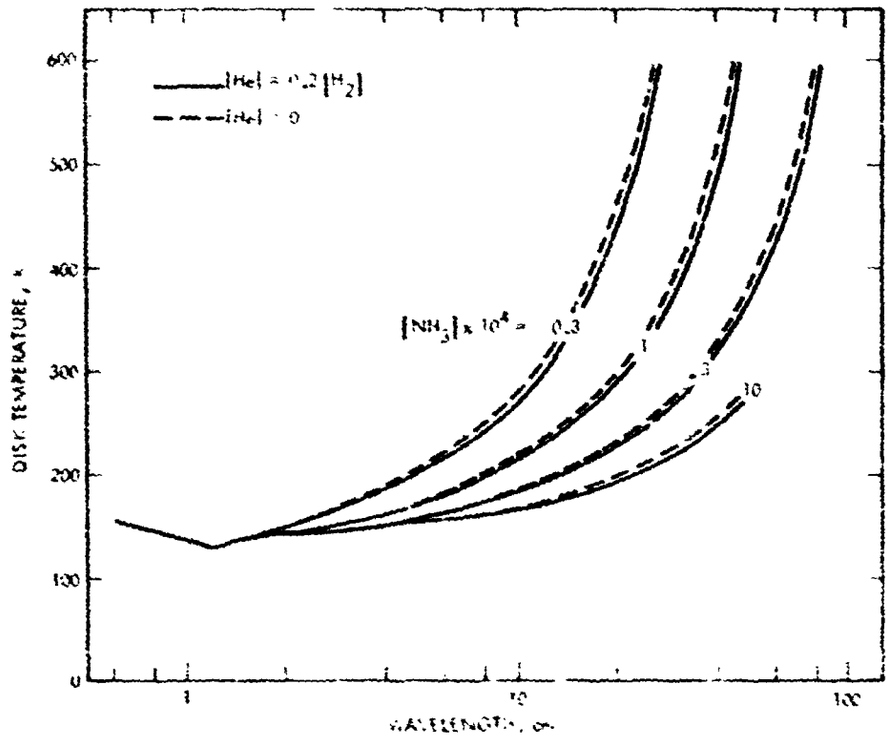

Figure 5. The effect of varying the helium abundance on the computed microwave spectra for four values of NH_3 mixing ratio (cf. Figure 3).

(from Weidenschilling and Lewis, 1973). In Figure 6 we show the calculated optical depth of this type of cloud as a function of frequency.

The result of the cloud model computation is shown in Figure 7. The solid curve is the spectrum of the model with no cloud ($\tau_o = 0$) and the dashed curve shows the effect of adding a cloud with $\tau_o \sim 1$. The trend is correct, i.e., the slope of the spectrum between ~6 and 21 cm is flattened just as the data tend to be; but the model curve misses the dense cluster of points near $\lambda = 21$ cm. Increasing the cloud opacity does not solve the discrepancy. The 21 cm temperature is only reduced an additional 2K when τ_o is doubled.

This very simple cloud approximation shows promise even though our first attempt failed to provide a good fit to the data. There is a need for further investigation of the vertical extent of the cloud model. Weidenschilling and Lewis (1973) suggest that cloud condensation might occur at altitudes above the saturation level, and that cloud particles might be swept up to higher altitudes by convection. These conditions would shift the peak of the cloud opacity to higher altitudes and lower temperatures. In a preliminary test, we computed the spectrum for $\tau_o = 1$ at the 250 K level and found that the 21 cm disk temperature was suppressed 10 K, bringing it into qualitative agreement with the observations.

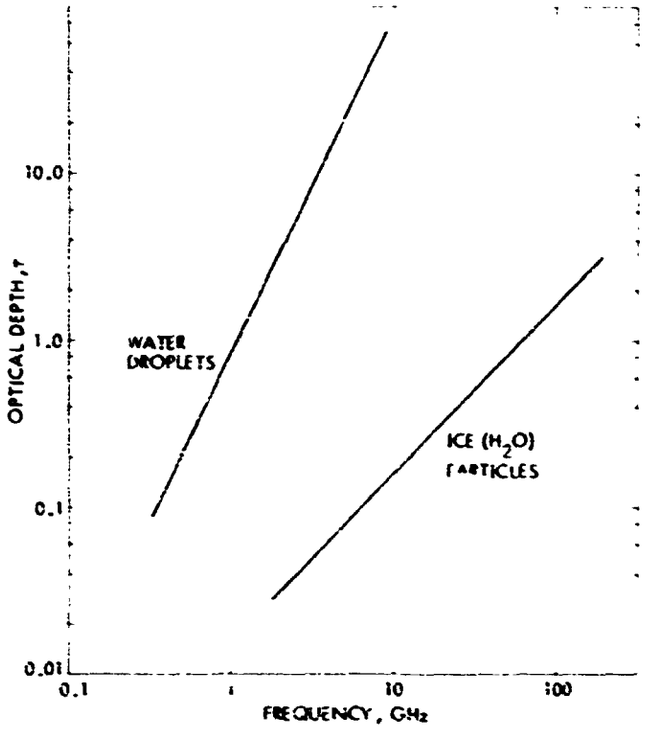

Figure 6. Opacity as a function of frequency computed for a cloud of water droplets with density 35 g/m³. Such a cloud has been postulated for Saturn by Weidenschilling and Lewis (1973).

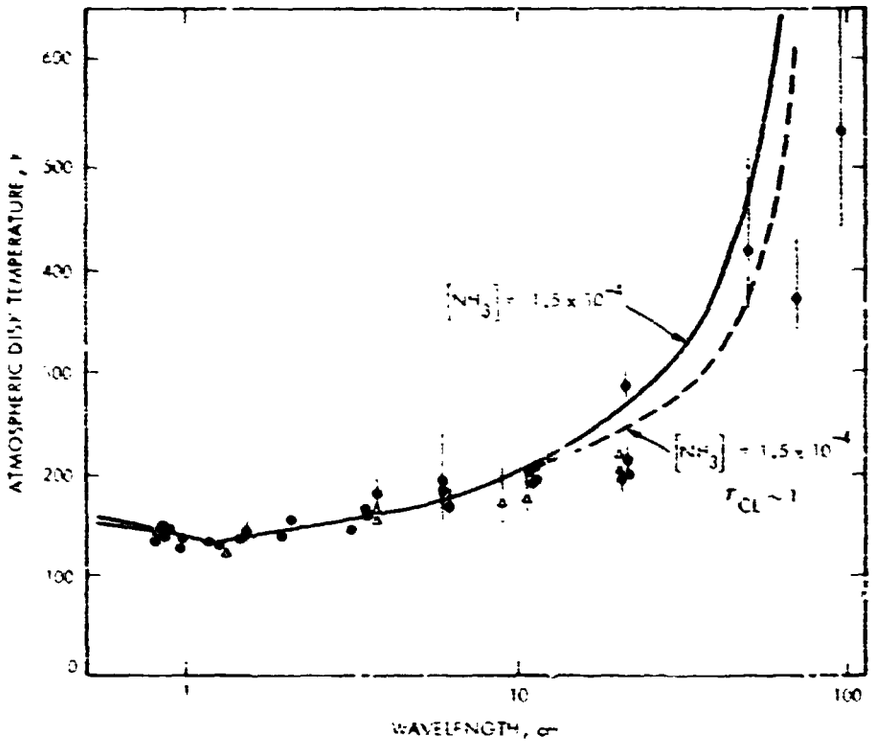

Figure 7. The microwave spectrum of Saturn's atmosphere compared with the nominal model. Curves for a solar value of NH_3 mixing ratio are shown with and without cloud opacity near the 270 K level of the atmosphere.

THE MILLIMETER SPECTRUM OF THE RINGS

The atmospheric models that fit the spectrum at centimeter wavelengths can be used to investigate the thermal spectrum of the rings at millimeter wavelengths. The atmospheric brightness temperatures, which are controlled by the ammonia opacity, are only weakly dependent on the exact choice of the NH_3 mixing ratio because the peak opacity at short radio wavelengths occurs near the cloud forming region where the ammonia is saturated. If we assume that the millimeter spectrum of the atmosphere is adequately determined by the models that fit the longer wavelength data, any excess emission at millimeter wavelengths can be attributed to thermal emission from the rings.

The short-wavelength data between 0.1 and 0.8 cm are shown with theoretical spectra in Figure 8. The solid curves represent the spectra for the two values of ammonia mixing ratio considered above, i.e., $[NH_3] = 1.5$ and 5×10^{-4}. The data have been corrected for ring obscuration and scattering effects, but the thermal component, T_t, is set to zero. The intent here is to demonstrate that these partially corrected temperatures are systematically higher than the model curves, which implies that the rings do emit thermally at millimeter wavelengths.

The dashed curves in Figure 8 demonstrate the magnitude of the increase in the computed microwave spectrum that occurs if the rings emit thermally. Because the thermal flux density received from the rings at a given frequency will vary with the solid angle of the ring surface, we show the computed spectra for two values of ring inclination. The ring brightness temperature spectrum shown in Figure 9 is assumed for these computations.

We obtain a ring brightness temperature spectrum by attributing the excess flux (measured minus predicted with $T_t = 0$) to thermal emission from the rings. The resulting spectrum is shown in Figure 9. Intrinsic thermal emission from the rings is indicated. The average of the excess temperatures between 1 mm and 2 mm, weighted by their absolute errors, gives $T_t \sim 25$ K. This result is consistent with the ring brightening from $T_t \sim 7$ K at 8.6 mm (Janssen and Olsen, 1978). An increase of thermal ring emission at millimeter wavelengths is not surprising since the brightness must approach ~95 K, the observed temperature at 10 μm. Furthermore, ice is a likely candidate for the ring particle composition, and its absorption coefficient increases markedly in the millimeter wavelength region.

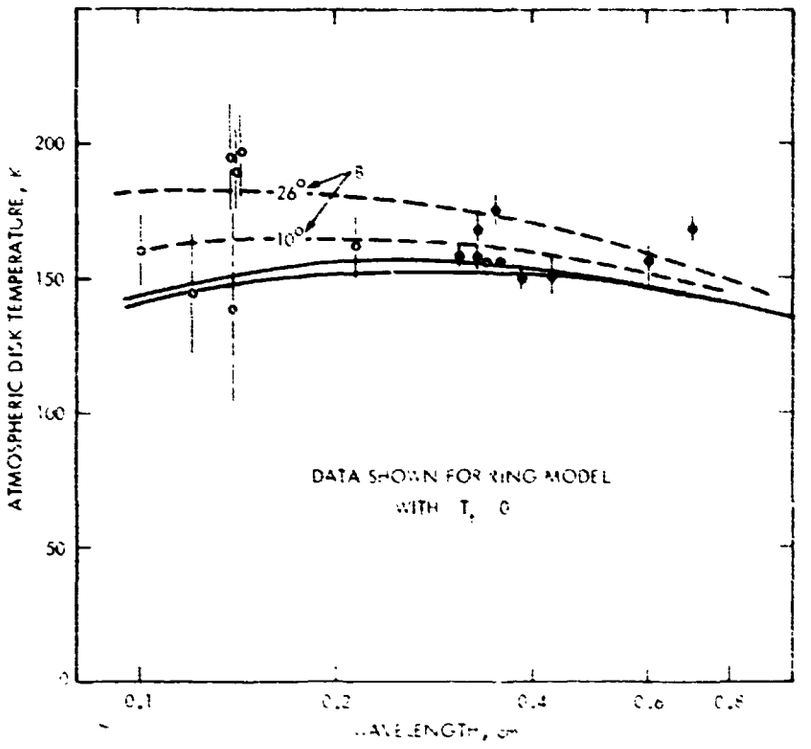

Figure 8. Saturn's 0.1-0.8 cm Spectrum with ring-model correction. The measured disk temperatures have been adjusted to account for the presence of the rings with the assumption that there is no thermal emission from the rings. The two solid curves represent the short wavelength spectra for the range of atmospheric models that fit the 0.8-100 cm microwave spectrum. The tendency for the data to fall systematically above the model spectra suggests that thermal emission from the rings is present. The two dashed curves show the increase in the computed spectra for two values of B and the ring spectrum shown in Figure 9.

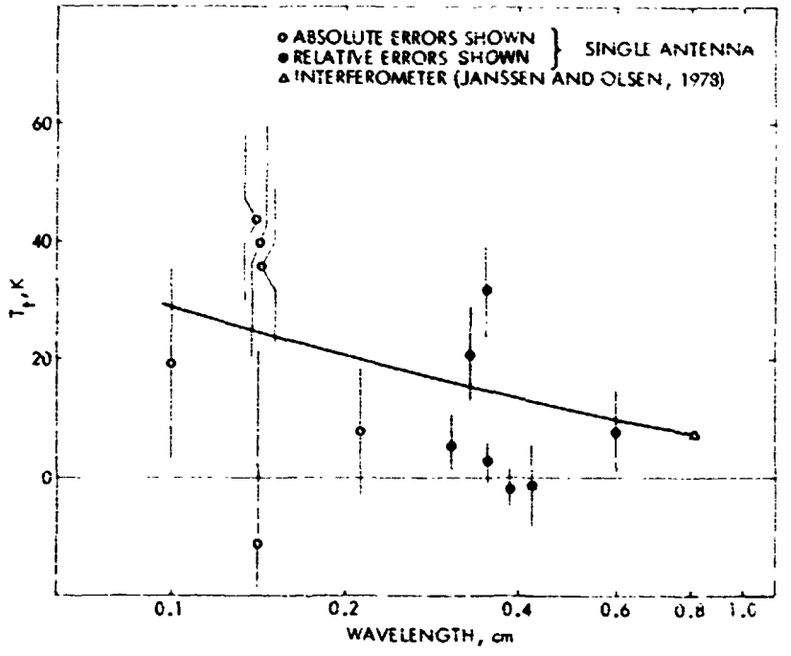

Figure 9. A millimeter spectrum for the thermal emission of Saturn's rings. The points are derived from the disk temperature measurements by assuming that the atmospheric spectrum is given by the $NH_3 = 5 \times 10^{-4}$ mixing ratio model, and that the excess observed emission may be ascribed to uniformly distributed thermal emission from the A and B rings. The curve is drawn to interpolate between the mean value $T_r = 25$ K at 0.14 cm and the interferometric determination at $T_r = 7$ K at 0.8 mm. Error bars from points shown as open circles are the given absolute errors, while the error bars from the points marked by filled circles show the given relative errors of measurement.

THE MICROWAVE SPECTRUM OF SATURN'S ATMOSPHERE

The microwave spectrum of the thermal emission from Saturn's atmosphere is shown in Figure 10. The effects of the rings have been removed from the data as discussed above. The nominal ring model was used with the ring brightness-temperature spectrum shown in Figure 9. Two model spectra are shown; the solid curve represents the computed spectrum with $[NH_3] = 5 \times 10^{-4}$, whereas the broken curve represents the spectrum for the model with a lower NH_3 abundance and the additional source of opacity near the 270 K level (i.e., an H_2O cloud).

There is good agreement between the model spectra and the ring-corrected data over the entire band, which spans three decades in wavelength. This agreement provides a strong argument that ammonia is present in Saturn's atmosphere, since NH_3 is the primary source of microwave opacity in the models. The shape of the spectrum in the wavelength interval centered on the 1.25 cm inversion band of NH_3 and the 130–135 K disk temperatures that are observed near the band center are in excellent agreement

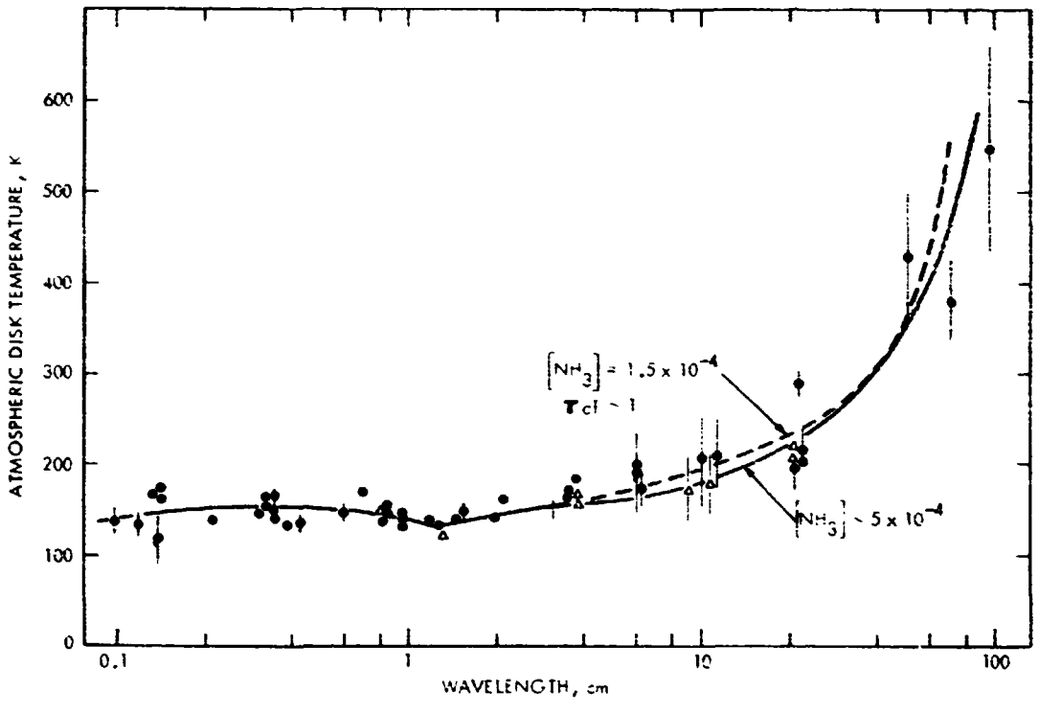

Figure 10. Saturn's microwave spectrum with data corrected for ring effects. Computed spectra are shown for the Nominal Model (Te = 89 K) for two values of ammonia mixing ratio, one with a cloud opacity near T = 270 K (dashed curve), and one without an additional source of opacity (solid curve).

with the models. Without the NH_3 opacity, these models yield disk temperatures in excess of 200 K at these wavelengths.

In the 10-21 cm region there is some evidence that the observed spectrum is slightly flatter than the model spectra. The agreement is good for both models shown, when one considers the statistical scatter in the data over the entire spectrum. Nevertheless, some improvement may be possible if more sophisticated cloud models are investigated and applied.

The model spectra at the longest wavelengths (>50 cm) are probably the most uncertain. Our assumptions regarding the absorption coefficient of the atmosphere at great depths, where temperatures and pressures exceed 1000 K and 1000 atmospheres, surely become invalid. Additional sources of opacity, e.g., from pressure induced ionization, may become important. A component of nonthermal emission from a Saturnian radiation belt is also plausible at these long wavelengths. Nevertheless, it is encouraging that the three measured temperatures are completely consistent with the relatively simple models that we have presented here.

ATMOSPHERIC TRANSMISSION LOSSES FROM A PROBE

With the models of Saturn's atmosphere in hand, one can readily compute the atmospheric attenuation that must be considered in the design of a probe communication system. We have performed the calculations for our nominal model atmosphere with a nominal ammonia mixing ratio of $[NH_3] = 3 \times 10^{-4}$. Cloud opacities were not included. The single-path absorption for three plausible probe frequencies are plotted as functions of pressure in Figure 11. The attenuation refers to the accumulated signal loss from a probe transmitting from a given pressure level in the atmosphere, e.g., a 2 GHz signal from the 10 atmosphere pressure level would be attenuated 4 db when transmitted vertically through the atmosphere.

A different representation of the results is shown in Figure 12, where we plot the vertical path absorption *vs* frequency for probe penetrations to pressure levels of 10, 30 and 100 atmospheres. We also show a computed attenuation curve (dashed line) for a probe in Jupiter's atmosphere. Note that the vertical attenuation to a given pressure level in the Jovian atmosphere is considerably less than the

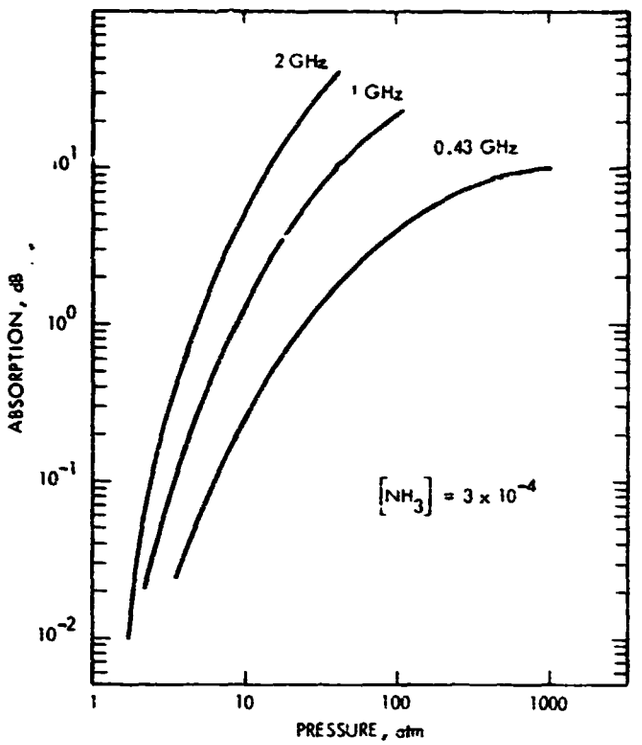

Figure 11. Vertical (single path) transmission loss in Saturn's atmosphere for plausible probe communication frequencies. The nominal atmospheric model with $(NH_3) = 3 \times 10^{-4}$ is assumed.

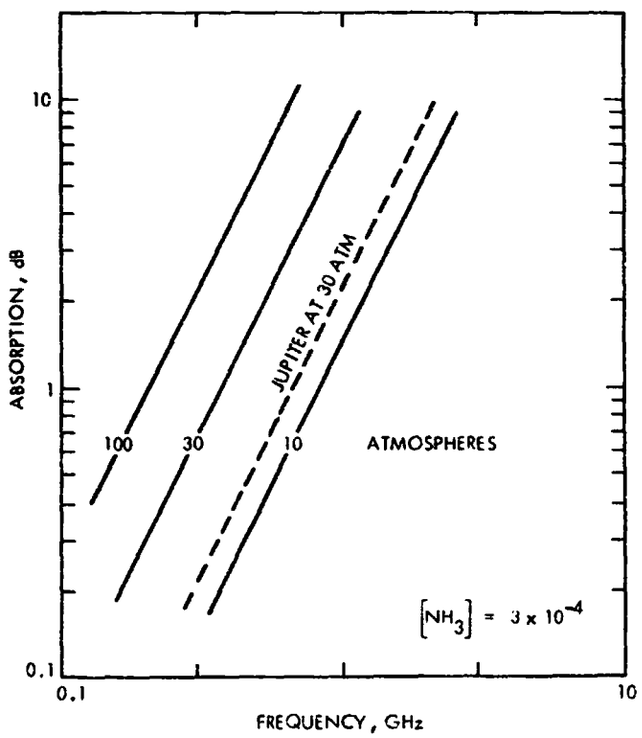

Figure 12. Vertical transmission loss from a probe at three pressure levels in Saturn's atmosphere. Computed loss vs. frequency is based on the nominal model atmosphere with ammonia mixing ratio = 3×10^{-4}. Dashed curve shows a similar attenuation vs. frequency curve for the 30 atmosphere level in Jupiter's atmosphere, where the predicted signal loss is not as great as in Saturn's atmosphere.

corresponding loss in Saturn's atmosphere. From the figure, we note that the "dB-loss" in Saturn's atmosphere is approximately three times greater. At 600 MHz, the vertical loss to 30 atmosphere pressure is 3 dB greater in Saturn's atmosphere. In general, the relation can be expressed as

$$\text{Loss dB}_{\text{Saturn}} \simeq 3 \times \text{Loss dB}_{\text{Jupiter}}. \qquad (2)$$

ACKNOWLEDGEMENTS

This paper is JPL atmospheres Publication Number 978-33 and represents one phase of research carried out at the Jet Propulsion Laboratory, California Institute of Technology, under Contract No. NAS 7-100, sponsored by the National Aeronautics and Space Administration.

REFERENCES

Baars, J. W. M., Genzel, R., Pauliny-Toth, I. I. K., and Witzel, A. (1977). *Astron. Astrophys. 61*, 99–106.
Berge, G. L. (1968). Recent observations of Saturn, Uranus, and Neptune at 3.12 cm. *Astrophys. Lett. 2*, 127–131.
Berge, G. L., and Read, R. B. (1968). The microwave emission of Saturn. *Astrophys. J. 152*, 755–764.
Berge, G. L., and Muhleman, D. O. (1973). High angular-resolution observations of Saturn at 12.1-centimeter wavelength. *Astrophys. J. 185*, 373–381.
Briggs, F. H. (1973). Observations of Uranus and Saturn by a new method of radio interferometry of fain moving sources. *Astrophys. J. 182*, 999–1011.
Caldwell, J. (1977). The atmosphere of Saturn: An infrared perspective. *Icarus 30*, 493–510.
Condon, J. J., Yerbury, M. J., and Jauncey, D. L. (1974). Interpretation of Saturn's decimetric radio emission. *Astrophys. J. 193*, 257–261.
Courtin, R., Coron, N., Encrenaz, Th., and Gispert, R. (1977). Observations of giant planets at 1.4 mm and consequences on the effective temperatures. *Astron. Astrophys. 60*, 115–123.
Cuzzi, J. N., and Dent, W. A. (1975). Saturn's rings: The determination of their brightness temperature and opacity at centimeter wavelengths. *Astrophys. J. 198*, 223–227.
Davies, R. D., Beard, M., and Cooper, B. F. C. (1964). Observations of Saturn at 11.3 centimeters. *Phys. Rev. Letters 13*, 325–327.
Dent, W. A. (1972). A flux-density scale for microwave frequencies. *Astrophys. J. 177*, 93–99.
Drake, F. D. (1962). Microwave spectrum of Saturn. *Nature 195*, 893–894.
Epstein, E. E., Dworetsky, M. M., Montgomery, J. W., Fogarty, W. G., and Schorn, R. A. (1970). Mars, Jupiter, Saturn and Uranus: 3.3 mm brightness temperatures and a search for variations with time and phase angle. *Icarus 13*, 276–281.
Epstein, E. E. (1978). Private Communication.
Gary, B. L. (1974). Jupiter, Saturn, and Uranus disk temperature measurements at 2.07 and 3.56 cm. *Astron. J. 79*, 318–320.
Gerard, E., and Kazes, I. (1973). Observations of Saturn at wavelengths of 6.2, 11.1 and 21.2 cm. *Astrophys. Lett. 13*, 181–184.
Gulkis, S., McDonough, T. R., and Craft, H. (1969). The microwave spectrum of Saturn. *Icarus 10*, 421–427.
Gulkis, S., and Poynter, R. L. (1972). Thermal radio emission from Jupiter and Saturn *Phys. of Earth and Planetary Interiors* 6, 36–43.
Hobbs, R. W., and Knapp, S. L. (1971). Planetary temperatures at 9.55 mm wavelength. *Icarus 14*, 204–209.
Hughes, M. P. (1966). Planetary observations at a wavelength of 6 cm. *Planet. Space Sci. 14*, 1017–1022.
Janssen, M. A., and Olsen, E. T. (1978). A measurement of the brightness temperature of Saturn's rings at 8 mm wavelength. *Icarus 33*, 263–278.
Kellermann, K. I. (1966). The thermal radio emission from Mercury, Venus, Mars, Saturn and Uranus. *Icarus 5*, 478–490.
Klein, M. J., and Gulkis, S. (1978). Jupiter's atmosphere· Observations and Interpretation of the microwave spectrum near 1.25 cm wavelength. *Icarus*. In press.
Kostenko, V. I., Pavlov, A. V., Sholomitsky, G. B., Slysh, V. I., Soglasnova, V. A., and Zabolotny, V. F. (1971). The brightness temperature of planets at 1.4 mm. *Astrophys. Lett. 8*, 41–42.
Kuzmin, A. D., and Losovskii, B. Ya. (1971). Measurements of 8.2 mm radio emission from Saturn and estimate of the rings optical thickness. *Astron. Vestnik 5*, 78–81.

REFERENCES (Contd)

Low, F. J., and Davidson, A. W. (1965). Lunar observations at a wavelength of 1 millimeter. *Astrophys J. 142*, 1278–1282

Ohring, G., and Lacser, A. (1976). The ammonia profile in the atmosphere of Saturn from inversion of its microwave emission spectrum. *Astrophys. J. 206*, 622–626.

Pauliny-Toth, I. I., and Kellermann, K. I. (1970) Millimeter-wavelength measurements of Uranus and Neptune. *Astrophys. Lett. 6*, 185–187.

Rather, J. D. G., Ulich, B. L., and Ade, P. A. R. (1974) Planetary brightness temperature measurements at 1.4 mm wavelength. *Icarus 22*, 448–453.

Schloerb, F. P. (1977). Radio Interferometric investigations of Saturn's rings at 3.71 and 1.30 cm wavelengths. Ph.D. Thesis, California Institute of Technology.

Seling, T. V. (1970). Observations of Saturn at 3.75 cm *Astron. J. 75*, 67–68

Turegano, J. A. and Klein, M. J. (1978). Paper in preparation.

Ulich, B. L., Cogdell, J. R., and Davis, J. H. (1973). Planetary brightness temperature measurements at 8.6 mm and 3.1 mm wavelengths. *Icarus 19*, 59–82.

Ulich, B. L. (1974). Absolute brightness temperature measurements at 2 1 mm wavelength. *Icarus 21*, 254–261.

Ulich, B. L. (1978). Private Communication.

Voronov, V. N., Kislyakov, A. G., and Troitskii, A. V. (1974). Brightness Temperatures of Venus, Saturn, and Mercury at 3.87 mm. *Astron. Vestnik 8*, 17–19.

Ward, D. B. (1977). Far infrared spectral observations of Saturn and its rings. *Icarus 32*, 437–442.

Weidenschilling, S. J., and Lewis, J. S. (1973) Atmospheric and cloud structures of the Jovian planets. *Icarus 20*, 465–476.

Welch, W. J , Thornton, D. D., and Lohman, R. (1966). Observations of Jupiter, Saturn, and Mercury at 1.53 centimeters. *Astrophys. J. 146*, 799–809.

Werner, M. W., Neugebauer, G., Houck, J. R., and Hauser, M. G. (1978). One millimeter brightness temperatures of the planets NASA-TM-[illegible]. 21 pp.

Wrixon, G. T., and Welch, W. J. (1970). The millimeter wave spectrum of Saturn. *Icarus 13*, 163–172.

Yerbury, M. J., Condon, J. J , and Jauncey, D. L. (1971). Observations of Saturn at a wavelength of 49.5 cm. *Icarus 15*, 459–465.

Yerbury, M. J., Condon, J. J., and Jauncey, D. L. (1973). The brightness temperature of Saturn at decimeter wavelengths. *Icarus 18*, 177–180.

DISCUSSION

J. WARWICK: Mike, do you see any evidence for possible synchrotron emission in this spectrum?

M. KLEIN: There's no compelling evidence. What we see is that even at wavelengths near 90 cm there doesn't seem to be any excess in the brightness temperature. But there could be some contribution due to synchrotron emission because as we get down to 90 cm the thermal models are rather uncertain. The ammonia absorption coefficient is not well known at several thousand degrees temperature and thousands of atmospheres of pressure. However, all I can say is that we see no compelling reason to assume that we need synchrotron radiation to explain the spectrum.

D. CRUIKSHANK: In the models and the observations of the Jupiter microwave spectrum, the ammonia line at 1.25 cm is fairly pronounced. Is there some simple-minded reason why that doesn't show up very strongly either in the observations or the models of Saturn?

M. KLEIN: For Saturn we have a higher-pressure model than we had for Jupiter because the lapse rate is different. Then since we are looking at a higher pressure, the line is spread out by collisional broadening.

PHYSICAL PROPERTIES OF THE SATELLITES OF SATURN

Dale P. Cruikshank

University of Hawaii, Institute for Astronomy
Honolulu, Hawaii 96822

ABSTRACT

The photometric and bulk parameters of the known and suspected satellites of Saturn are presented in updated tables and are compared. The surface compositions of all the satellites are discussed in terms of modern photometry and spectroscopy; most if not all of the inner bodies have water frost surfaces, but the outer three satellites have surfaces of unknown composition. The few reliable mass values of some inner satellites, together with the best current values for the satellite radii, suggest mean densities representative of bulk compositions dominated by frozen volatiles, though Titan may have a substantial volume fraction of silicates. The special case of Iapetus is considered in the light of new studies of its two distinct faces and polar cap.

INTRODUCTION

In spite of a superficial resemblance, the satellite system of Saturn is quite distinct from that of Jupiter, and is, in fact, unique in the Solar System. This review includes a cursory discussion of the dynamics of the satellite system, but concentrates on the current stage of understanding of the compositions, masses, bulk densities, and interior structures of the known and suspected objects orbiting Saturn outside the confines of the rings. The atmospheric composition and structure of Titan is left for other papers in this collection, though the photometric and bulk properties of this largest of the satellites are included in the scope of this review.

SATURN'S FAMILY OF SATELLITES

The search for and discovery of satellites of Saturn has occupied astronomers for over three centuries, and the result of these endeavors is a retinue of at least ten, and probably more, objects orbiting the planet outside the confines of the ring system. The search continues to this date and is currently concentrated on the region between Mimas and the outer extremity of the rings.

The population of satellites of Saturn includes (1) the small bodies of unknown number that appear to exist just outside the rings, (2) six satellites, of which Titan is by far the largest, lying in circular orbits in the plane of the rings, (3) two irregular satellites, including Hyperion in an eccentric orbit at very nearly the 4:3 commensurability with Titan, and Iapetus with an inclined but nearly circular orbit, and (4) Pho be in a highly inclined retrograde orbit. In this paper we consider the physical properties of all these bodies.

Before examining the details of the Saturn satellites, we must first consider the evidence for the existence of the most recently discovered members of the family, those orbiting just exterior to the rings. From photographic observations made at the time of the 1966 passage of the earth through the ring plane, Dollfus (1967 a, b) announced the discovery of a probable satellite (Janus, S 10) near the extremity of the ring system, and the presence of a new object was confirmed by Texereau (1967) and Walker (1967). Fountain and Larson (1978) have studied some of the original photographs by Dollfus, Texereau, and Walker, plus data acquired at the Lunar and Planetary Laboratory at the time of ring-plane passage (Figure 1), and have shown evidence for a small object in addition to Janus, though no name has so far been proposed for it. Aksnes and Franklin (1978) analyzed the available photographs independently and concluded that the orbital characteristics of Janus should still be regarded as questionable, as should those of the Fountain/Larson object because unique orbits cannot be computed from the sparse observations available. While Fountain and Larson (1978) suggest even another object in addition to Janus and S 11, Aksnes and Franklin find the evidence uncompelling. The latter authors conclude that whatever the exact identities and orbits of the objects might be, ". . . the efforts of Dollfus, Fountain and Larson have seemingly established the important fact that the region just outside ring A may well contain several bodies in nearby orbits - a sort of highly attenuated, large-particle 'ring' near the Roche limit."

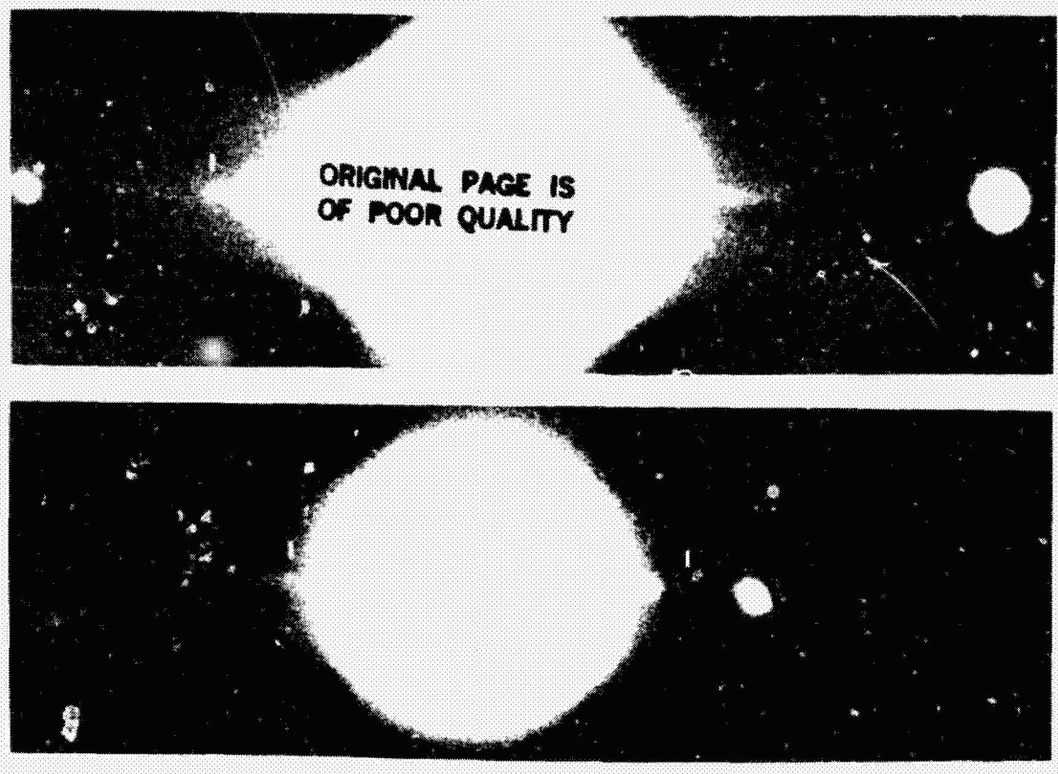

Figure 1. Photographs of Saturn and several satellites at the time of the passage of the earth through the ring plane in 1967. The upper photograph shows (tick mark) the possible S 11. The other satellites in order, left to right, are Enceladus, Rhea, Tethys (in planet's glare), and Titan (17 December 1967, 0230 UT). The lower photograph (18 December 1967, 0249 UT) shows S 10 Janus on the left, Enceladus, S 11 (tick mark) and Tethys. From Fountain and Larson (1978).

In spite of the uncertainties attached to the existence and nature of S 11 and Janus, they are listed in Tables 1 and 2 with their provisional orbital parameters and brightnesses, though these quantities are subject to large revision at the time of the next observing opportunity, that is, when the earth again intersects the ring plane in 1980.

Aksnes and Franklin (1978) have also reanalyzed the evidence for the satellite that was reported early in this century by Pickering (1905, 1908) and named Themis. The evidence does not withstand careful scrutiny and detailed comparison with deep photographs of the background star fields, and Aksnes and Franklin (1978) conclude that while the space where Themis was reported is likely on dynamical grounds to contain a satellite (4:3 resonance with Titan), Pickering's object does not exist.

Table 1. Orbital Data for the Satellites of Saturn

Satellite	Orbital Radius (10^3 km)	Orbital Radius (Planetary Radii)	Period (Days)	Eccentricity	Inclination (°)
11 No name	151.3	2.93	0.69378*	0	0
10 Janus	159 5	2.65	0.74896	0	0
1 Mimas	186.	3.09	0.942	0.0201	1.5
2 Enceladus	238.	3.97	1.370	0.0044	0.0
3 Tethys	295.	4.91	1.888	0.0000	1.1
4 Dione	377.	6.29	2.737	0.0022	0.0
5 Rhea	527.	8.78	4.518	0.0010	0.4
6 Titan	1222.	20.4	15.95	0.0289	0.3
7 Hyperion	1481.	24.7	21.28	0.1042	0.4
8 Iapetus	3560.	59.3	79.33	0.0283	14.7†
9 Phoebe	12930.	216.	550.4	0.1633	150.

†Variable
*Eastern elongation 1966 Oct 29.596 ET

Data from Morrison and Cruikshank (1974) except those for S 11, which come from Fountain and Larson (1978).

THE DYNAMICS OF THE SATELLITE SYSTEM

Recent studies of the dynamics of the system of Saturn's satellites have explored old and new ideas in great detail and need not be repeated here. The review by Greenberg (1977) clarified the question of orbital resonances in the Saturn system as they pertain to orbital evolution, while the review by Kovalevsky and Sagnier (1977) considered details of the orbital motion of these and the other natural satellites. Burns (1977) considered the effects of tides and of accretion drag in the evolution of satellite orbits, while Peale (1977, 1978) has recently addressed the nature and evolution of the Titan-Hyperion commensurability.

The 1:2 resonance in the Mimas:Tethys orbital periods and the 1:2 resonance in the Enceladus:Dione pair have permitted mass determinations of these four bodies,

Table 2. Light Curve Data for Saturn's Satellites

Satellite	Sources	$\frac{dV}{d\alpha}$	Light Curve Amplitude ΔV	θ_{min}	θ_{max}	Remarks
11 (No name)	1	-	-	-	-	No information
10 Janus	1,2,3	-	-	-	-	No information
1 Mimas	4,5	-	-	-	-	No information
2 Enceladus	6	~0.08 (?)	0.4	~90° (?)	~270° (?)	More data needed
3 Tethys	6,7,8,9,10	~0.02	~0.15	~270°	~90°	Confirmation needed
4 Dione	6,7,8,9,10	~0.01	~0.4	~290 ±30°	~120 ±30	Not well determined
5 Rhea	7,8,9,10 11,16	0.05	0.2	270 ±5°	90° ±50°	Well established
6 Titan	9	~0.005	<0.02	-	-	
7 Iapetus	9,10, 12,13	~0.05** ~0.03	1.9*	90°	270°	Well established
8 Hyperion	14,15	-	$0.05 \stackrel{?}{-} 0.10$	30°,210°	120°,300°	Needs confirmation
9 Phoebe	14,15	-	~0.3	270°,0°	90°,180°	More data required

Source Code

1. Fountain and Larson (1978)
2. Dollfus (1967)
3. Aksnes and Franklin (1978)
4. Franz (1975)
5. Koutchmy and Lamy (1974)
6. Franz and Millis (1975)
7. McCord *et al.* (1971)
8. Blair and Owen (1974)
9. Noland *et al.* (1974)
10. Harris (1961)
11. Blanco and Catalano (1971)
12. Millis (1973)
13. Morrison *et al.* (1975)
14. Andersson (1978)
15. Andersson, Degewij and Zellner (1978)
16. Franklin and Cook (1974)

*Depending on polar axis tilt at epoch of observation.
**Larger value corresponds to dark face ($\theta = 90°$) and smaller value corresponds to bright face ($\theta = 270°$).

though the precision is low. Titan dominates the pair Titan:Hyperion so that only the effect of the largest satellite on the smallest can be observed, resulting in a mass value for Titan alone.

The motion of Iapetus is affected about equally by the sun and Saturn, and is also influenced by massive Titan. The retrograde orbit of Phoebe is slightly perturbed by the sun and departs slightly from an ellipse.

PHOTOMETRY OF THE SATURN SATELLITES

The goals of photometric studies of a planetary satellite are (1) to search for clues to the surface composition and the microstructure of the body, (2) to determine the rotation period from the periodicities in the light curve induced by zonal brightness (albedo) inhomogeneities, (3) to draw inferences on the distribution of albedo features that may be related to the satellite's rotational history or that can lead to a rudimentary map of the surface, and (4) to determine either the body's radius or surface geometric albedo when the other parameter is known.

The first goal is most satisfactorily met by spectrophotometry or spectroscopy, and the results of this work for the Saturn satellites will be discussed below. In this section we consider the results of photometric studies of the rotation of satellites and the changes in global brightness related to changing solar phase angle.

Photometric studies of those satellites that lie at sufficient angular separation from Saturn to permit precise measurements from ground-based telescopes have shown orbital phase angle variations in the brightness (V-mag) ranging from less than 2 percent (Titan) to a factor of more than five (Iapetus) with a sinusoidal or near sinusoidal pattern having the same period as the orbital period (with the possible exception of Hyperion noted below). These observations have been reviewed by Morrison and Cruikshank (1974) and Veverka (1977) in the context of similar measurements of satellites of other planets, and the patterns are similar for the four Galilean satellites of Jupiter, though the amplitude of the variation in V of Iapetus is uniquely high.

The measurement of orbital phase angle (θ) variations in the brightness of satellites must necessarily be made over a period of many days, during which time the solar phase angle (α) varies. For dark objects, or dark portions of spotted satellites, the solar phase coefficient is different from that of bright surfaces or parts of surfaces. The solar phase curve at the V wavelength (0.56 μm) has a linear portion at $\alpha > 5^{\circ}$, of about $dV/d\alpha = 0.02$ mag deg^{-1} for both dark and bright surfaces,

but for $\alpha < 5^\circ$, $dV/d\alpha$ is somewhat larger for dark surfaces and nearly unchanged for bright surfaces. This is, of course, a qualitative description of the opposition effect, or brightness surge seen on airless bodies having irregular surface micro and macrostructures when viewed at small phase angles. The opposition effect is dependent on albedo, and to some degree, on color of the satellite, asteroid, and planetary surfaces. Veverka's (1977) discussion of this property of satellite surfaces observed from the Earth is especially lucid and relevant in the present context.

With a sufficient quantity of observations the effects of changing α and θ can be separated, though for the outer planets where the observable range of α is small, the distinction of the two effects is more difficult. Saturn's satellites are observable over a range of about 6°, so that the establishment of the exact magnitude of the opposition surge on top of the normal linear phase coefficient requires a large number of high-quality data. As noted below, the only Saturn satellites for which the solar phase functions are adequately known are Titan, Rhea and Iapetus.

The question of the information content of the solar phase function has recently been reviewed by Veverka (1977). Borrowing freely from Veverka's study, we note that the phase function depends on (1) the effective scattering phase function and albedo for the single particles comprising the surface, (2) the shadowing function of a surface element determined by small-scale texture, and (3) the large-scale shadowing function resulting from surface topography, such as craters and mountains. While unique surface properties cannot be derived directly from the observed phase function, satellites with the roughest surface structures on both micro and macro scale would be expected to have the largest phase coefficients, and for those surfaces in which multiple scattering is significant (such as frosts) the phase coefficient is less than for a surface in which single scattering dominates. The nonlinear opposition effect is most pronounced in low-albedo pulverized surfaces where shadowing and single scattering are dominant. Bright powders also show an opposition effect, but it is less than in dark powders, and is most pronounced at extremely small phase angles. Various analytical models of the opposition effect and phase functions of pulverized materials are reviewed in some detail by Veverka (1977).

Adequate determinations of the orbital phase angle variations or rotation curves, in various colors, have been obtained for Tethys, Dione, Rhea, and Iapetus (e.g., Noland *et al.*, 1974); observations of the innermost satellites are especially difficult because of the proximity to the bright rings and planet, while the faint outer satellites can be measured only with very large telescopes. Figure 2 (from Noland

et al. 1974) shows the y (5470 A) curves for two satellites after removal of the solar phase function; the ordinates are plotted in stellar magnitudes, where

$$0.4\ (m_1 - m_2) = \log \frac{\text{Brightness}_2}{\text{Brightness}_1} .$$

All those satellites for which the orbital phase curve has been satisfactorily observed show a rotation period synchronous with the period of revolution around the planet, as is expected from rotational dynamics. Hyperion may be an exception inasmuch as the scanty data available suggest a double maximum and minimum in one revolution around Saturn, but this can also be explained as a shape factor (asteroids commonly show double maxima and minima in one rotation). This cannot be regarded as a firm conclusion because of the very few data available (Andersson 1974, Degewij *et al.*, 1978). The rotation of Phoebe may not be synchronous with the revolution period, but there are no data relevant to this problem. The 550.4-day period of

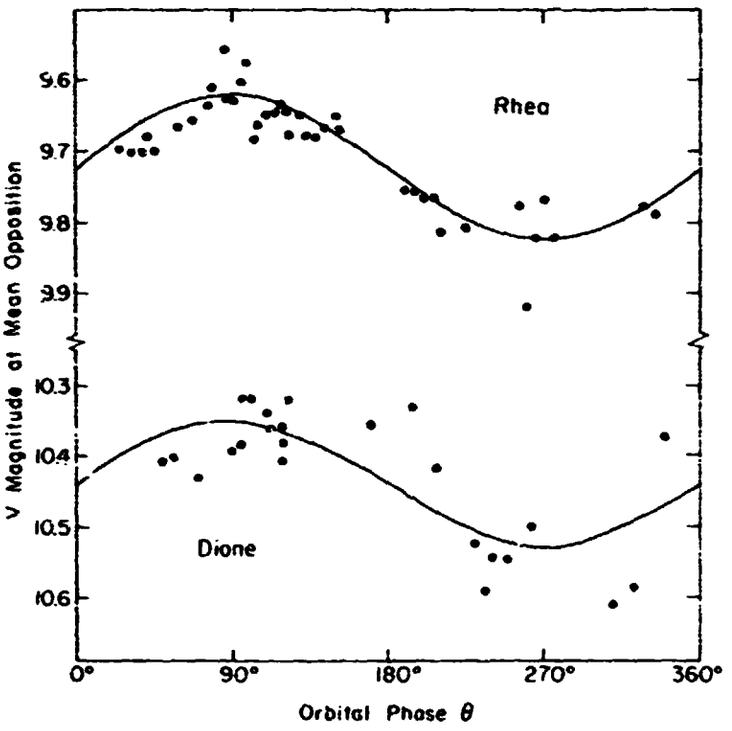

Figure 2 Orbital photometric variations of Rhea and Dione in the y band. The solid curve for Rhea is given by y = 9.72 − 0.10 sin θ, and for Dione by 4 = 10.44 − 0.09 sin θ. The dependence of the magnitude on solar phase angle was removed by using phase coefficients of 0.025 and 0.009 mag deg $^{-1}$, respectively. From Morrison and Cruikshank (1974), adapted from observations by Noland et al. (1974).

Phoebe makes an observational study of the rotation quite difficult unless the rotation period of the satellite is on the order of several hours, as is expected if it is not synchronously locked to the motion around Saturn. The innermost satellites (S11, Janus) can be observed only under very rare conditions, as noted earlier, and Mimas and Enceladus can normally be observed only at elongations, so the observational conformation of the virtually certain synchronous rotation will be difficult to achieve.

The nonuniformities in the brightness and color of a satellite that yield the lightcurve often show a symmetry with respect to the leading and trailing hemispheres of a synchronously rotating body. "Leading" is used in the sense of the hemisphere in the direction of the satellite's orbital motion around the planet; the leading hemisphere is that viewed from Earth at eastern elongation ($\theta = 90^{\circ}$) of the satellite with respect to its primary. The leading-trailing asymmetry is clearly seen in photometry of the Galilean satellites of Jupiter and of Iapetus, as well as several other satellites of Saturn. In Table 2 are given lightcurve data for the Saturn satellites as well as the best available values for $dV/d\alpha$. In the Table, θ_{min} corresponds to the orbital phase angle where the satellite is faintest, and θ_{max} to maximum brightness. For many of the satellites these parameters are not well known because of a paucity of data.

A significant point is that some satellites have darker trailing hemispheres and others have darker leading hemispheres. Iapetus is the prime example of the latter, as noted below, and Enceladus may share this property, though to a much lesser degree. Tethys, Dione, and Rhea appear to have darker trailing hemispheres, though corroborating data are needed. The leading-trailing asymmetries have led to interesting speculation on their causes, but there are still no adequate explanations, especially for the great contrast in the two hemispheres of Iapetus. The Galilean satellites of Jupiter also exhibit significant rotational curves, but the alignment with the leading and trailing hemispheres is most distinct for Europa.

The rotation curve of Titan, as noted above, shows an extremely small amplitude at the wavelengths at which it has been observed, presumably owing to the satellite's cloudy, or at least deep, atmosphere. It is possible that the methane atmosphere of Titan exhibits zonal inhomogeneities, as does the atmosphere of Neptune (Cruikshank 1978), and that the rotational curve can be determined from observations with filters centered in strong methane absorption bands in the near infrared. The required studies should be performed in order to ascertain if the inhomogeneities exist, if they change on an observable time scale, and to determine if the atmosphere rotates with the same period as the (presumably) synchronously rotating solid satellite.

SURFACE COMPOSITIONS OF THE SATELLITES OF SATURN

Multi-color photometry (see Table 3) of the satellites of Saturn, has yielded information on their surface compositions. Leaving aside variations in the colors as a function of α and θ, broad- and narrow-band photometry in the spectral regions where compositional information occurs as a result of absorption in the constituents of the surfaces, has, in the past few years, led us to a fairly satisfactory understanding of the surface compositions of four of the inner satellites plus the bright hemisphere of Iapetus. UBV and other visible region photometry (Harris 1961, McCord *et al.*, 1971, Noland *et al.*, 1974), though carefully done, gave only clues to the composition of the inner satellites (Tethys, Dione, Rhea, and Iapetus) because the relevant compositional information lies further into the infrared. Broadband UBV photometry of the more difficult satellites, Hyperion and Phoebe, has also been accomplished (Andersson 1974, Degewij *et al.*, 1977) with significant results, but the infrared work on these bodies is in its infancy, chiefly as a result of their faintness.

Narrow-band photometry of four satellites obtained by McCord *et al.* (1971) is shown in Figure 3, where the data are presented normalized to intensity equal 1.0 at wavelength 0.56 μm; this normalization was necessary at the time the data were acquired because the diameters and geometric albedos of the satellites were not known. While some variations are seen from satellite to satellite, and there may even be broad absorption features, notably at about 0.57 μm or longer wavelengths for some objects, the spectra are largely uninterpretable. They do show, however, that the sharp brightness decrease in the violet seen on many other solar system bodies (e.g., Mars, Mercury, the Moon, the Jovian satellites, and the rings of Saturn) is largely absent on the satellites for which data were obtained. This is significant because the rings of Saturn, now known to be similar in composition to Tethys, Dione, and Rhea, do show the steep violet absorption, and questions arise as to the differences among these surfaces.

In Figure 4 are shown photometric results in the near infrared where solid surfaces of ices and mineral assemblages show stronger and more diagnostic absorptions than in the visible region of the spectrum. The simplest interpretation of Figure 4 comes from the comparison of the Saturn satellites with the Jovian satellites, two of which (Europa and Ganymede) are known to have partial covers of water ice (cf. Morrison and Cruikshank 1974 and Morrison and Burns 1977). The photometry of the Saturn satellites closely mimics that of Ganymede, from which it was concluded

Table 3. Colors of the Satellites of Jupiter and Saturn

	Satellite	V_o	U-B	B-V	J	J-H	J-K	J-L
J1	Io	5.0	1.3	1.15	3.7 ±0.1	0.35 ±0.01	0.43 ±0.02	0.43 ±0.03
J2	Europa (L)	5.3	0.5	0.89	4.1 ±0.1	-0.31 ±0.02	-0.66 ±0.03	-2.90 ±0.04
J2	Europa (T)				±	-0.37 ±0.02	-0.91 ±0.04	-3.25 ±0.05
J3	Ganymede (L)	4.6	0.53	0.81	3.6 ±0.1	-0.10 ±0.03	-0.18 ±0.04	-2.08 ±0.14
J3	Ganymede (T)					-0.07 ±0.02	-0.14 ±0.03	-1.58 ±0.04
J4	Callisto	5.6	0.55	0.88	4.4 ±0.1	0.27 ±0.01	0.34 ±0.02	-0.67
S1	Mimas	12.9	-	0.65 ±0.1	-	-	-	-
S2	Enceladus	11.8	-	0.62	10.6 ±0.1	-0.16 ±0.05	-0.33 ±0.07	>-0.66
S3	Tethys	10.3	0.34 - 0.32	0.74	9.3 ±0.1	-0.20 ±0.05	-0.36 ±0.07	>-0.46
S4	Dione	10.4	0.27 - 0.30	0.71 - 0.82	9.6 ±0.2	-0.20 ±0.05	-0.32 ±0.07	>-0.42
S5	Rhea	9.7	0.35	0.76	8.6 ±0.1	-0.05 ±0.05	-0.29 ±0.07	-1.89 ±0.18
S6	Titan	8 4	0.75	1.30	-	-	-	-
S7	Hyperion	14.2	0.33	0.78	13.0 ±0.1	0.15 ±0.05	-0.03 ±0.07	> 0.55
S8	Iapetus (L)	10.2	0.38 ±0.03	0.78 ±0.02	10.3 ±0.1	0.20 ±0.03	0.28 ±0.04	-0.82 ±0.25
S8	Iapetus (T)	11.9	0.29 ±0.03	0.69 ±0.01	9.4 ±0.1	-0.11 ±0.02	-0.24 ±0.03	>-1.35
S9	Phoebe	16.5	0.30	0.63	-	-	-	-
S10	Janus	14	-	-	-	-	-	-

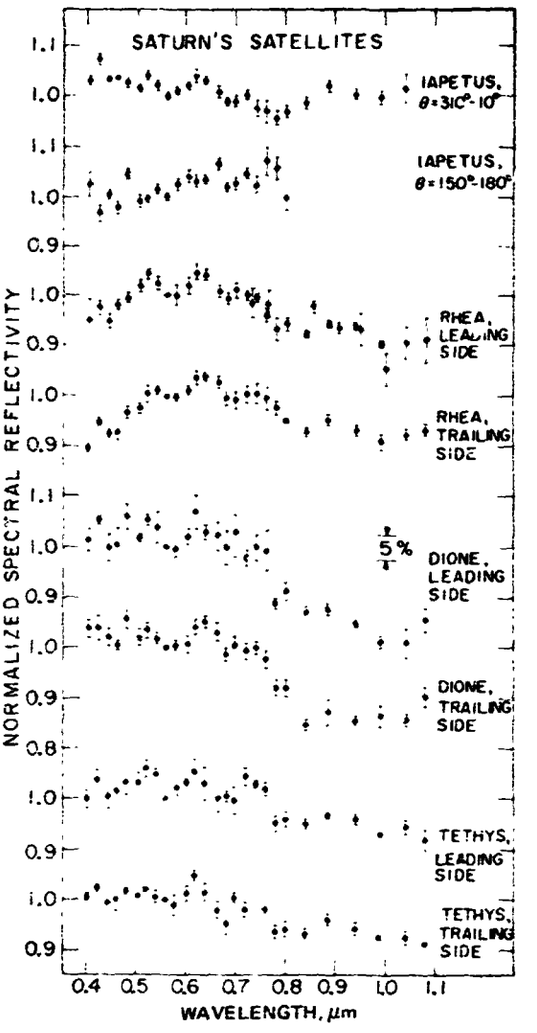

Figure 3. Spectrophotometric data for several Saturn satellites, normalized at 0.56 microns. From McCord et al. *(1971).*

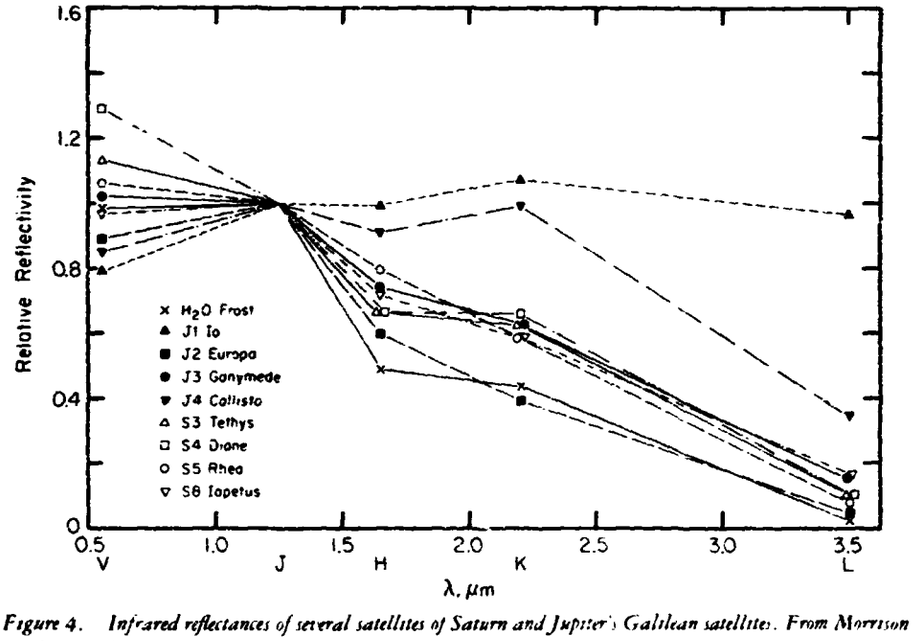

Figure 4. Infrared reflectances of several satellites of Saturn and Jupiter's Galilean satellites. From Morrison et al. *(1976).*

(Morrison *et al.*, 1976), that Tethys, Dione, Rhea, and the bright hemisphere of Iapetus have at least partial coverings of water frost at a low temperature presumably in equilibrium with the solar insolation.

This conclusion was reached nearly simultaneously (but published first) by Fink *et al.* (1976), who obtained the remarkable first infrared spectra of the same satellites. Their spectra, together with a stellar comparison, are shown in Figure 5, and in Figure 6 are shown the ratios of the satellite spectra to the comparison. Those deep absorptions at 1.6 and 2.0 μm in the spectra of Iapetus, Rhea, Dione, and Tethys are clearly a result of water ice absorption, as shown by the laboratory comparison and the accompanying spectrum of Saturn's rings.

Thus, the presence of water ice is clearly established on the surfaces of Rhea, Dione, Tethys, and the bright hemisphere of Iapetus. The fact that Rhea, Dione, and Tethys show relatively small variations of brightness with θ (Figure 2) suggests that the areal distribution of water frost or ice is more or less uniform.

Although fully satisfactory infrared spectra have not yet been obtained for the other satellites or the dark hemisphere of Iapetus, JHK photometry of Enceladus, Hyperion, and darker Iapetus has given some interesting results. The spectrum of Iapetus (Morrison *et al.*, 1976) is similar to that of Callisto. The reflectivity of Enceladus is shown in Figure 7 in comparison with data for ice-covered Rhea, plus four other satellites (Cruikshank *et al.*, 1977). The similarity of Enceladus to Rhea has led Cruikshank *et al.*, to conclude that this small satellite is similarly water-frost covered, a result corroborated by a new spectrum (1.9-2.6 μm) of Enceladus obtained by Cruikshank (1979) in 1978.

The reflectance of Hyperion appears to be quite another problem. As shown in Figure 7 it resembles not Enceladus and Rhea, but two satellites of Uranus and Neptune's Triton. As pointed out by Cruikshank *et al.* (1977), the reflectance characterized by Hyperion and the others does not appear to represent volatiles, and these objects constitute a class different from the groups into which most of the other satellites of the solar system fall. The reflectance class, of which Hyperion is a member, is shown in relation to the other recognized classes in Figure 8 (from Cruikshank *et al.* 1977), and the membership and probable natures of these classes are described in Table 4.

Cruikshank and C. B. Pilcher succeeded in obtaining a low-resolution infrared spectrum of Hyperion with the Kitt Peak 4-m telescope in 1976, in the region 1.4 - 2.6 μm (see Figure 9), but the reflectance of the satellite, while bearing

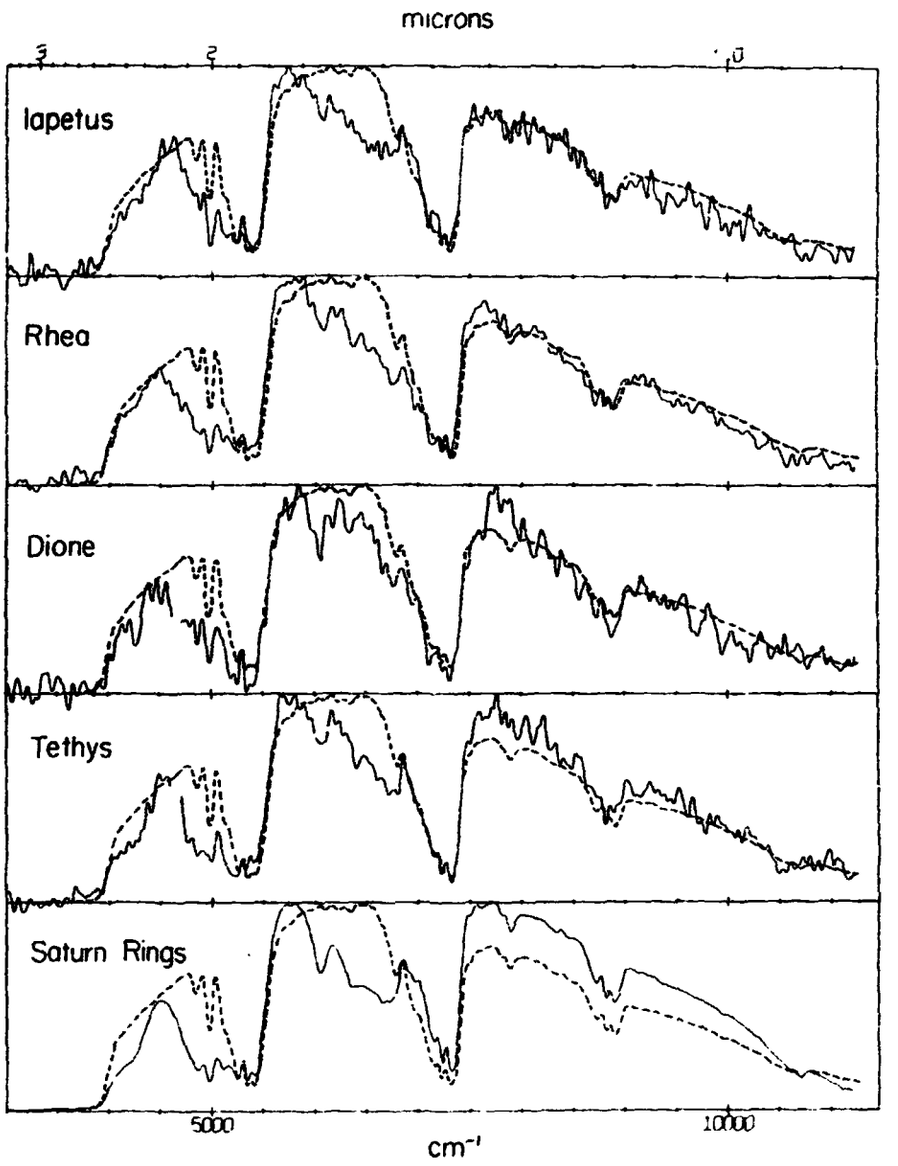

Figure 5. Near infrared spectra of Saturn's satellites and the rings, showing residual absorptions attributed to water frost or ice. From Fink et al. *(1976)*

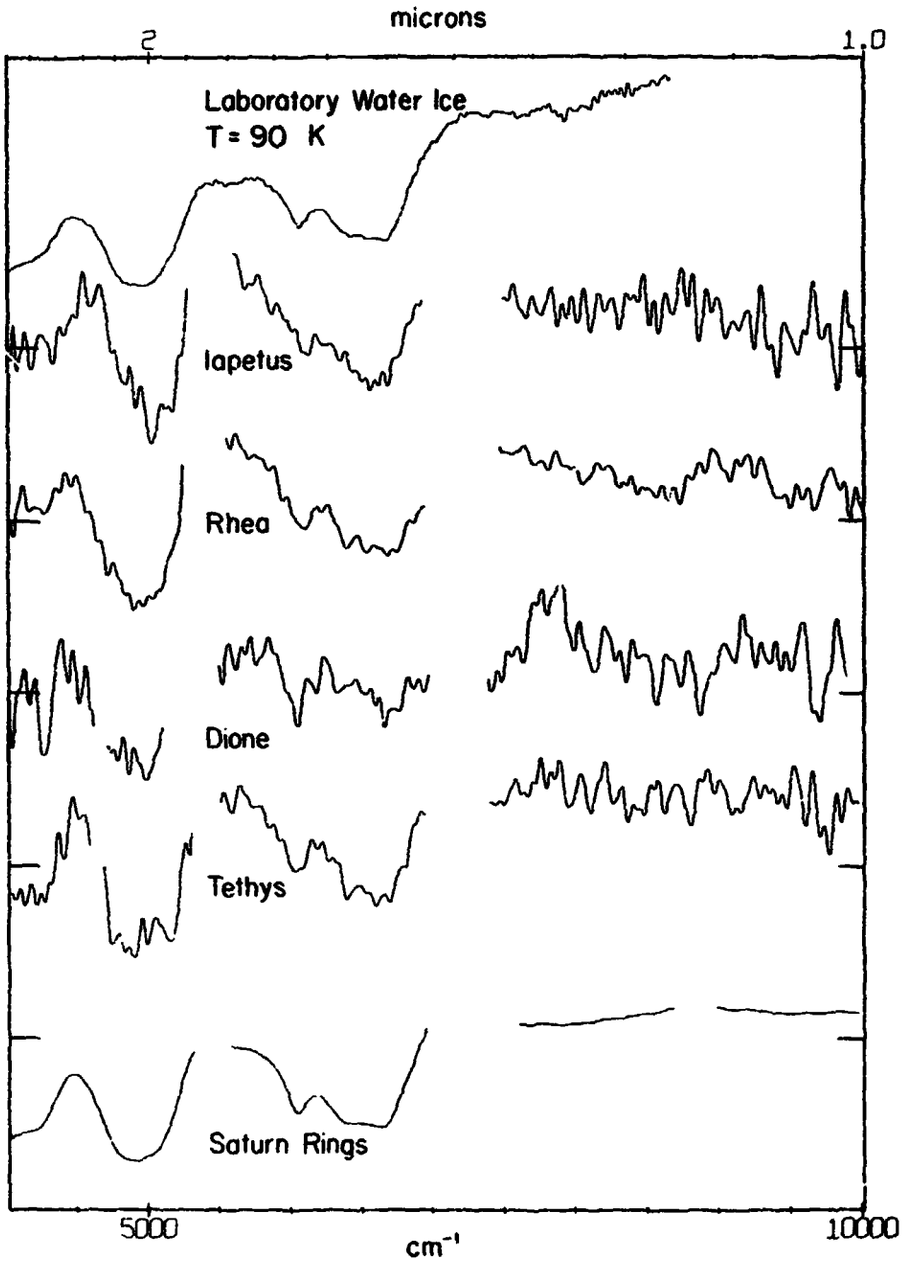

Figure 6. Ratio spectra of the satellites and rings of Saturn showing absorptions attributed to water frost or ice. From Fink et al. *(1976).*

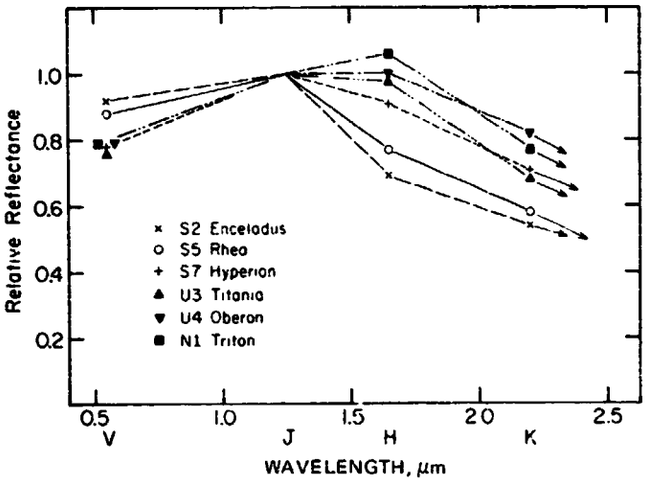

Figure 7. Infrared reflectance spectra of three satellites of Saturn, Triton, Titania, and Oberon. From Cruikshank et al. *(1977).*

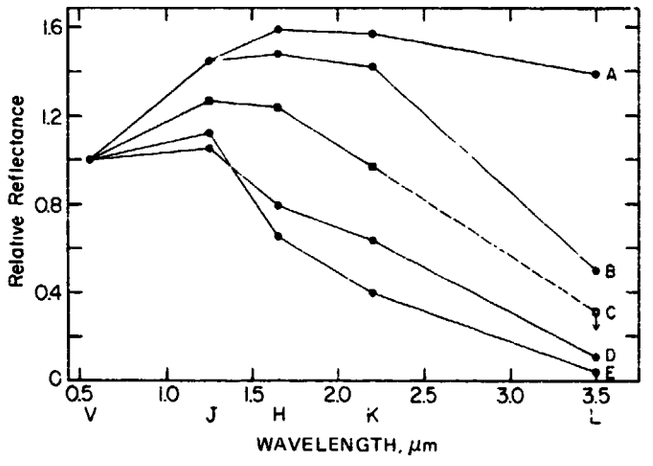

Figure 8. Reflectances, normalized at V, of five categories of solar system bodies. The categories and their members are identified in Table 4.

Table 4. Reflectance Classes of Solar System Bodies

Group	Members of Group	Surface Composition	Average Reflectance Relative to J (λ = 1.25 μm)			
			a_V	a_H	a_K	a_L
A	Io	Evaporite salts ?	0.69	1.10	1.08	0.96
B	Callisto	Rock	0.69	1.02	0.99	0.35
C	Hyperion, Titania, Oberon, Triton	?	0.79	0.98	0.77	<0.25
D	Ganymede, Enceladus, Tethys, Dione, Rhea, Iapetus (trailing)	H_2O ice (frost) + neutral material	0.94	0.75	0.60	0.11
E	Europa, Rings of Saturn	H_2O ice (frost)	0.88	0.58	0.35	0.04
F	Pluto	CH_4 ice (frost)	0.92	0.94	0.57	<0.36
-	Asteroids 88, 511	[C-type asteroids]	-	1.16	1.23	-
-	Asteroids, 5, 6, 7, 116, 433	[S-type asteroids]	-	1.13	1.09	-
-	Asteroid 64	[E-type asteroid]	-	1.08	1.09	-

a superficial resemblance to water frost, is not immediately identifiable. In particular, the upturn in reflectance at the extreme long wavelength end of the spectrum, if real, is atypical of water frost, and in fact precludes the presence of a substantial H_2O frost component on the surface. Additional data are needed, not only for Hyperion, but for Triton and the other two members of the class of which they are members in common. The Hyperion spectrum resembles that of volatiles rather than asteroids or any known meteorites (Gaffey 1976), but the identification from a spectrum of such low resolution and insufficient precision is not easy. UBV photometry of Hyperion (Degewij *et al.* 1977) shows this satellite to be distinct from the dark asteroids, including Trojans.

The only relevant data on Phoebe's surface composition are contained in UBV photometry obtained by Degewij *et al.* (1977) (Figure 10). In a UBV color plot Phoebe clusters together with Himalia and Elara (J6 and J7), which are very dark objects (Cruikshank 1977). As is seen in the figures, Phoebe and the Jovian satellites form a small group quite separate from the Trojans (also very dark; Cruikshank 1977) and other asteroids of low albedo, and fall generally within the field in the UBV color plot occupied by C-type asteroids.

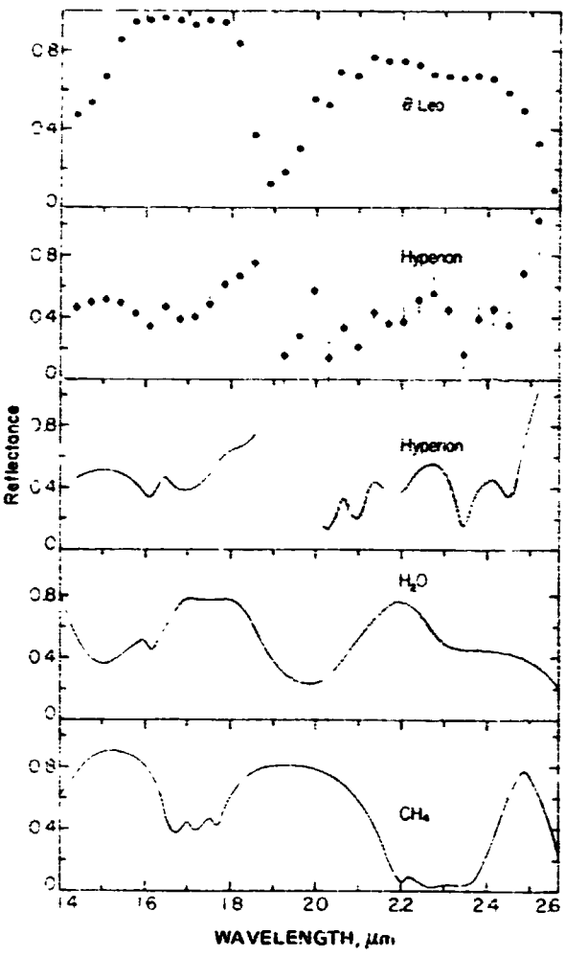

Figure 9. Preliminary infrared spectrum of Hyperion rattoed to Theta Leo. The second panel from the top shows the individual data points with error bars, and the third panel is a "maximum interpretation" version of the same data. Reflectance spectra of water and methane ices are also shown. From Cruikshank and Pilcher (in preparation).

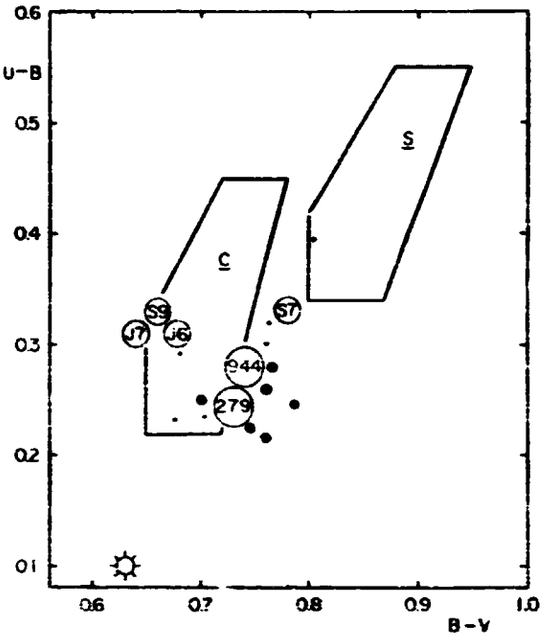

Figure 10. This U-B, B-V color plot shows several solar system objects known or suspected to be very dark. Hyperion (S 7) and Phoebe (S 9), are shown with Himalia (J 6) and Elara (J 7), Trojan asteroids (large dots), and Hilda asteroids (small dots) plus 279 Thule and 944 Hidalgo. From Degewij et al. 1977.

The compositions of Mimas, Janus, and the possible S11 are completely unknown from direct observations, though inferences might be made on the basis of the known frost composition of the rings and the satellites nearby these three bodies. Mimas and Janus lie in a region of special interest because of the great difference in reflectance between the rings and satellites Tethys, Dione, and Rhea, specifically the violet turn-down in the ring spectrum, as noted above. Lebofsky and Fegley (1976) suggest that the violet absorption in the ring spectrum results from solar ultraviolet irradiation or trapped particle bombardment of polysulfide or other impurities in the ring frost, with the implication that such impurities do not occur in the frosts of the satellite surfaces, or that the bombarding particles in the vicinity of Saturn (either past or present) do not extend spatially outward to the neighborhood of the satellites. Spectrophotometric observations of Mimas and Janus are thus of special interest in order to ascertain (1) if they are composed of water frost, and (2) if the frost shows radiation damage similar to the rings.

DIAMETERS AND ALBEDOS

In terms of observations made from Earth, the diameter and surface geometric albedo of a satellite or asteroid are inextricably related by

$$5 \log r = V_o - V_o - 2.5 \log p_V + 5 \log (R \cdot \Delta),$$

where r is the radius of the object, V_o is the V-mag of the Sun (usually taken as -26.77), p_V is the visible geometric albedo, R is the distance of the satellite from the Sun, and Δ is its distance from the Earth (or observer). V_o is reasonably well known for most of the satellites, but the computation of r or p_V requires knowledge of one or the other.

With the largest telescopes in the finest seeing conditions, the disks of the satellites of Saturn are occasionally discernable, and in 1954 Kuiper published his measurements of the diameters of Enceladus, Dione, Tethys, Rhea, Titan, and Iapetus, made with a visual diskmeter on the Hale 5-m telescope. Other measurements of the diameters of the Saturn satellites have been made by more or less direct means. In 1974, Elliot *et al.* (1975) observed the occultations of several satellites by the dark limb of the moon and measured the time required for extinction of the light from the satellites with a high-speed photometer. The lunar occultation technique gives the highest intrinsic accuracy of the methods so far used, but the interpretation

of the results depends on a model of the brightness distribution across the surface of the occulted object, a model dependent on both the spatial distribution of dark and bright materials (frost and rock, for example) and the limb darkening/brightening of the disk. The identification of water frost on the surfaces of several of the satellites has aided in establishing the limb brightening coefficients used in modeling the brightness distribution (e.g. Veverka *et al.*, 1978). Double-image micrometric measurements have also been made with large telescopes (Dollfus 1970) using rare moments of excellent seeing and image definition when the disks of the satellites are discernible. In addition, photometric measurements of the thermal fluxes of six satellites have been used to derive "radiometric" diameters. All of these results are collected in Table 5 together with similar determinations of the radii of the Galilean satellites and Triton for comparison.

Beyond the measurements of the type described above, none others have been successfully applied, though the techniques of speckle interferometry and fringe interferometry can in principle be used for further independent determinations.

Diameters of planetary satellites can be calculated from *assumed* values of p_V. For example if we allow that the surface of Enceladus is covered with water frost, as deduced from the infrared photometry, we can assume that the albedo lies in the range of that of other ice-covered satellites, such as Europa, Ganymede, Rhea, etc., or about 0.40 - 0.65. The radius is then in the range 295 - 375 km. The frost-cover assumption may be quite valid for Janus, S11, and Mimas by analogy with the rings and the next several satellites, but it is not valid for Titan, Hyperion, the dark side of Iapetus, or Phoebe.

The photometric/radiometric method of radius determination in fact yields the geometric albedo if certain assumptions are made about the infrared emissivity of the surface and the phase integral of the satellite. The radius is then computed from p_V and V_o. The sensitivity of the photometric/radiometric method to uncertainties in the values of various parameters has been discussed by Morrison (1977). Assembled in Table 6 are the "accepted" radii and corresponding values of p_V for several of the Saturn satellites. For the remaining satellites, the radii are calculated from assumed albedos, and these values are enclosed in parentheses. In this table, V(1,0) corresponds to the V-mag at unit distance from the sun and earth and seen at $\alpha = 0^\circ$, with no allowance for an opposition surge in brightness at small phase angles, but with the $dV/d\alpha$ indicated in Table 2.

Table 5. Various Determinations of Satellite Diameters

Object	Kuiper Diskmeter Radius (km)	Occultation Radius (km)	Radiometric Radius (km)	Double Image Radius (km)	Accepted Radius (km)
Enceladus (S2)	275	-	-	-	-
Tethys (S3)	410	520 ±60[1]		-	520 ±60
Dione (S4)	410	415 ±75[1]	575 ±100[6]	-	500 ±120
Rhea (S5)	820	790 ±45[1]	800 ±125[6,7]	-	800 ±100
Titan (S6)	2290	2915 ±25[1]	2800 ±150[8]	2425 ±150[12]	2900 ±200
Hyperion (S7)	-	-	112 ±15[9]	-	112 ±15
Iapetus (S8)	670	725 ±100[2]	835 $^{+50}_{-75}$[10]		725 ±100
Io (J1)	1650	1820 ±5[3]	-	1750 ±75[13]	1820 ±10
Europa (J2)	1420	1500 ±100[4]	-	1550 ±75[13]	1500 ±100
Ganymede (J3)	2460	2635 $^{+15}_{-100}$[5]	-	2775 ±65[13]	2635 ±25
Callisto (J4)	2290	-	-	2550 ±75[13]	2500 ±150[14]
Triton (N1)	1900	-	≤2630[11]	-	2200 ±500

Notes:

(1) Elliot *et al.* (1975). The values given are those computed for a Lambert limb-darkened model. The uniform-disk model yields radii 10-15 percent smaller than those given here. The values tabulated here are rounded off from those actually given by Elliot *et al.*

(2) Veverka *et al.* (1978)

(3) O'Leary and van Flandern (1972). See also Taylor (1972) and discussion in Morrison and Cruikshank (1974).

(4) Based on mutual occultations of the Galilean satellites (Aksnes and Franklin, 1974; Vermillion *et al.* 1974).

(5) Carlson *et al.* (1973).

(6) Morrison (1974).

(7) Murphy *et al.* (1972).

(8) W. M. Sinton, private communication (1975). See also Low and Rieke (1974).

(9) Cruikshank (1978b).

(10) Morrison *et al.* (1975).

(11) Cruikshank *et al.* (1978).

(12) Dollfus (1970).

(13) Dollfus (1970), Morrison and Cruikshank (1974).

(14) Cruikshank and Stockton (1978).

Table 6. Bulk Parameters of the Satellites of Saturn

Satellite	V(1,0)	p_V	R(km)	M(10^{23} g)	$\bar{\rho}$
1 Mimas	+3.3	(0.6)	(180)	0.37 ±0.01	~1.5
2 Enceladus	+2.2	(0.6)	(300)	0.84 ±0.03	~1
3 Tethys	+0.7	0.8	520 ±60	6.2 ±0.11	~1.1
4 Dione	+0.88	0.6	500 ±120	11.6 ±0.3	~1.5
5 Rhea	+0.16	0.6	800 ±100	-	~1
6 Titan	-1.20	0.21	2900 ±200	1399 ±2	1.4
7 Hyperion	+4.6	0.47	112 ±15	-	-
8 Iapetus	0.6/2.3	0.35/0.05	725 ±100	-	-
9 Phoebe	+6.9	(0.05)	(120)	-	-
10 Janus	+4	(0.6)	(100)	-	-
11 -	+4	(0.6)	(100)	-	-

Values in parentheses are estimated on the basis of an assumed ice or frost-covered surface.

MASSES AND MEAN DENSITIES

The masses of five of the satellites in the resonance pairs Mimas: Tethys, Enceladus:Dione, and Titan:Hyperion, have been determined from observations of the mutual gravitational interactions. The values in Table 6 are from the review by Duncombe *et al.* (1974). While Duncombe *et al.* give mass values for Rhea, Hyperion, Iapetus, and Phoebe taken from the literature, they cannot be considered reliable enough for inclusion in the table; this conclusion was adopted by Morrison and Cruikshank (1974) in their review, and more recently by Morrison *et al.* (1977) in an updated consideration of the same material.

Mean densities of the satellites are calculated from the adopted radii and masses, but only for Tethys, Dione, and Titan can these densities be given much credence. The formal calculations of density of Enceladus gives a value less than 1.0, which is considered unlikely. A composition of mostly frozen volatiles is consistent with mean densities on the order of 1 - 1.5 g cm^{-3}, as noted below, but for most of the Saturn system of satellites these basic parameters are still largely unknown. If masses are required for dynamical computations, the best values might be calculated from an assumed mean density of 1 - 1.5 g cm^{-3} using the estimated radii

given in the table, at least for the inner satellites. Hyperion, Iapetus, and Phoebe may be exceptions, but there is no relevant information presently available.

THE SPECIAL CASE OF IAPETUS

The problem of the large range of brightness of Iapetus between eastern and western elongations was solved by Murphy *et al.* (1972), who showed that thermal emission was maximum when the visible brightness was at a minimum, that is, the visible and thermal "lightcurves" are anticorrelated. The brightness variations are therefore a result of nonuniform albedo rather than a shape factor, and subsequent work by Morrison *et al.* (1975) provided a detailed (but unique only to first order) solution to the distribution of dark and bright areas on the satellite surface. From a new analysis of early and recent photometry of Iapetus, plus observations of the thermal flux throughout an orbit, Morrison *et al.* (1975) derived an albedo distribution map, shown in Figure 11, that satisfactorily accounts for the visual lightcurve seen at various aspects. The distribution of albedo shown in Figure 11 is not unique in that (small) variations may occur across the bright face and across the dark face. In order to reproduce the observed lightcurves, a polar cap of bright material intruding

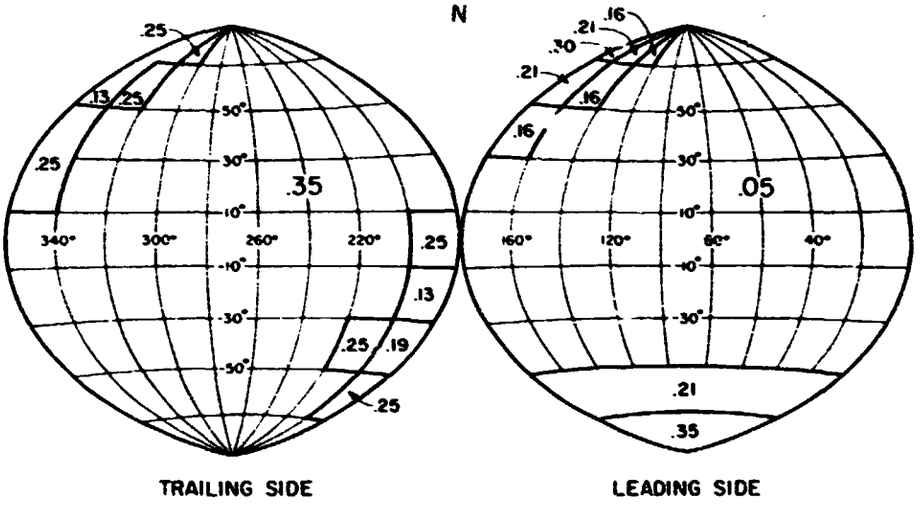

Figure 11. Model albedo distribution for Iapetus, shown on an Aitoff equal-areas projection. Each area is labeled by its visual geometric albedo. The coordinate system is defined such that the longitude on the satellite is equal to the orbital longitude, measured prograde from superior geocentric conjunction, and the axis of rotation is assumed normal to the satellite's orbital plane. Longitude increases to the east as seen from the earth, and north is at the top. From Morrison et al. 1975

on the dark face was necessary, as were darker limbs on the bright face. The average geometric albedo of the bright face must be about 0.35 and that of the dark face about 0.05 in order to yield the observed thermal fluxes, and the phase integral for the bright side must lie in the range 1.0 - 1.5. An artistic rendition of the albedo map is shown in Figure 12. The thermal (20 μm) observations at different orbital phase angles (Morrison *et al.*, 1975) are shown in Figure 13, together with model curves for two values of the phase integral, and the visual light curve from three different observers is shown in Figure 14.

A new analysis of the occultation lightcurve of Iapetus by Veverka *et al.* (1978) corroborates the Morrison *et al.* (1975) model requiring approximately, but not exactly, a two-hemisphere albedo distribution. Veverka *et al.*, suggest that the dark hemisphere shows no limb darkening (similar to the moon), but that the bright hemisphere exhibits limb darkening according to the Minnaert relationship (Veverka *et al.*, equation 2). With the limb darkening coefficient and the time duration of the occultation, Veverka *et al.*, compute the diameter of the satellite, and then the albedo of the bright hemisphere (Elliot *et al.*, 1978). The diameter is that given in Tables 5 and 6, while the geometric albedo is $p_V = 0.54^{+0.20}_{-0.16}$. The dark hemisphere is then $p_V = 0.11^{+0.04}_{-0.03}$. Both values are appreciably higher than those derived by Morrison *et al.* (1975). The higher albedo derived by Veverka *et al.*, and Elliot *et al.* for the dark hemisphere does not appear to be sufficiently low to produce the infrared thermal flux measured by Morrison *et al.* (1975), though the bright hemisphere albedos derived in both studies are adequately included in the range expected for water frost.

The question of the polar cap has been further studied by Millis (1977) who has continued the photoelectric photometry of Iapetus in recent years as the aspect angle changes. The inclination of the satellite's orbit to the ring plane, though it amounts to less than 15°, results in a small change in aspect from year to year such that in the interval 1970 to the present the south pole is tilting out of view. As a result, the integrated brightness of the dark (leading) side has decreased in the past few years, as shown in Millis' photometry in Figure 15. Concurrently, the thermal flux of the dark side is increasing (Cruikshank 1979, in preparation) as less bright material is exposed.

We noted earlier that the composition of the material on the bright face of Iapetus is at least partially water frost. The composition of the dark material on the leading face is unknown, but its reflectance from broadband filter photometry in the near infrared appears to resemble that of Callisto. Callisto's surface mineralogy is not yet understood, but the presence of bound water has been revealed by infrared

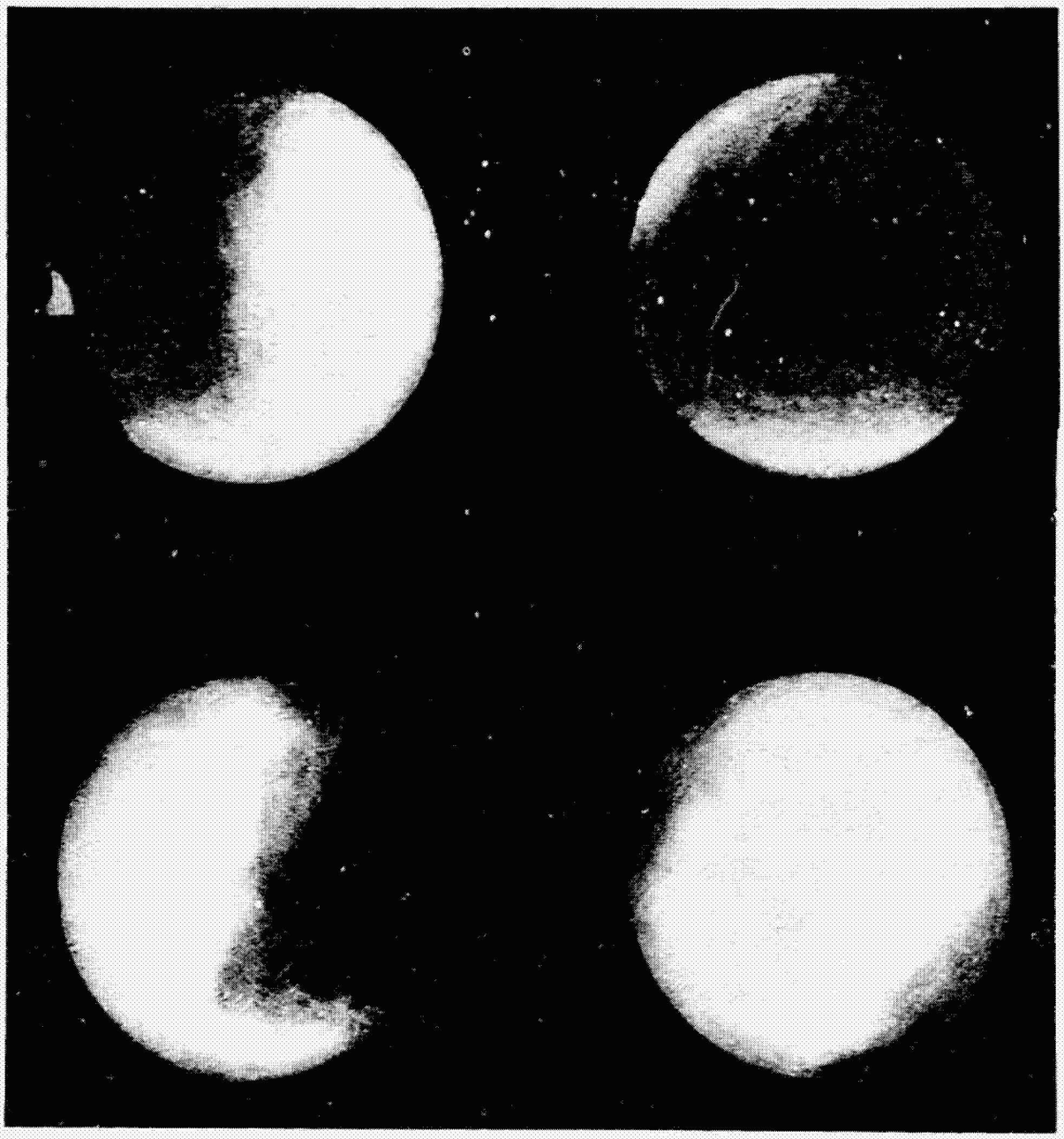

Figure 12. Artistic representation of the surface of Iapetus as seen with linear resolution about 0.02 arcsec, based on the computed albedo distribution model shown in Figure 11. The longitudes of the central meridian (equal to the orbital longitude) for these four views are (u.l.) 0° (superior geocentric conjunction), (u.r.) 90° (eastern elongation), (l.l.) 180° (inferior conjunction), (l.r.) 270° (western elongation). Note that these drawings illustrate only one of a range of similar albedo distributions that are consistent with the available data. From Morrison et al. *(1975).*

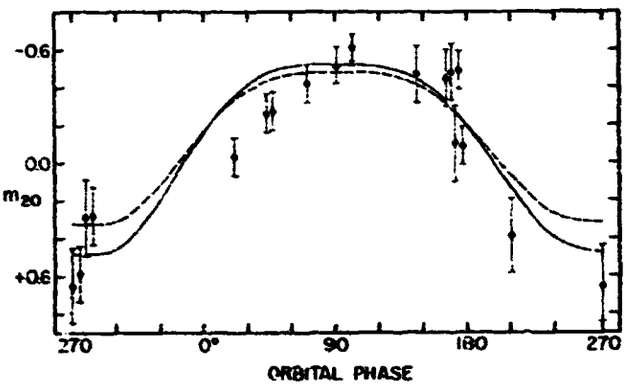

Figure 13. Brightness variations of Iapetus at 20 microns as a function of orbital (rotational) phase, compared with two theoretical curves calculated from the albedo distributions in Figure 11. The solid curve provides the best fit and corresponds to a phase integral for the bright material $q = 1.3$. The dashed line is for $q = 1.1$. From Morrison et al. *(1975).*

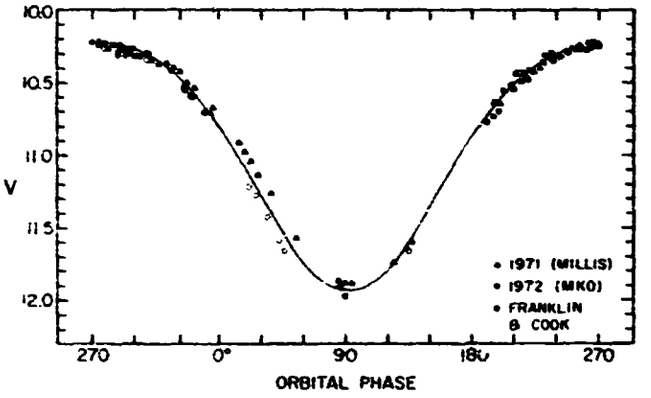

Figure 14. The visible light curve of Iapetus from 1971–1973 compared with the theoretical curve generated from the albedo distribution shown in Figure 11.

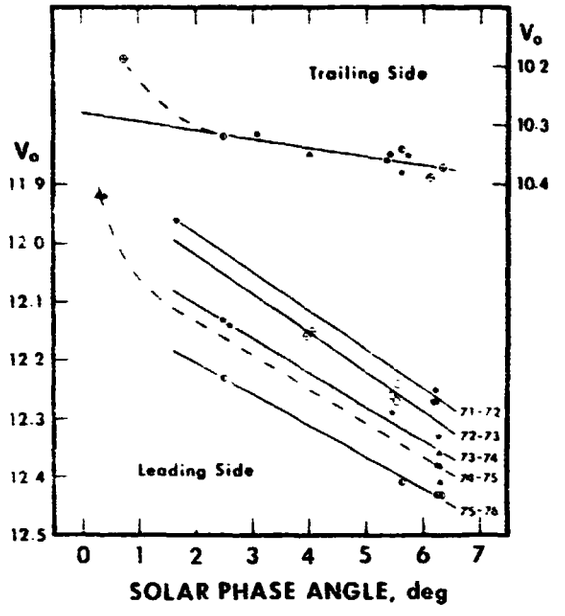

Figure 15. V-photometry of the leading and trailing sides of Iapetus versus solar phase angle for a number of different apparitions. The increase in brightness of the leading (dark) side of the satellite each successive year since 1971–1972 is attributed to the gradual tilting of the polar cap out of the angle of view from the earth. From Millis (1977).

spectrophotometry near 3 μm (Lebofsky 1977, Pollack *et al.*, 1977, and Cruikshank *et al.*, 1977). This absorption also occurs in certain dark asteroids (Pallas and Ceres) but not in Vesta (Cruikshank and Gaffey 1978, in preparation). The bound water band should be sought on Iapetus, and this problem is within present observational capabilities with narrow-band filters. Discrete mineral absorptions should also be sought, but it should be noted that such observations must be made at the exact time of eastern elongation so that the feeble light from the dark surface materials is not contaminated with the bright reflected light from the ice and snow. This requirement places a rigid constraint on an already difficult observational problem, but with persistence it can be solved.

A rare eclipse of Iapetus by Saturn and its rings in January 1978 afforded an opportunity to observe for the first time since the invention of the bolometer the change in brightness temperature of the satellite with changes in solar insolation. Portions of the event were successfully observed at 20 μm in Hawaii, California, and Arizona, though the results are in a very preliminary state at this time. The Hawaii observations (Cruikshank and Becklin 1978) are shown in Figure 16; the changing 20-μm flux occurred as Iapetus passed through the shadow of Ring A and into full sunlight;

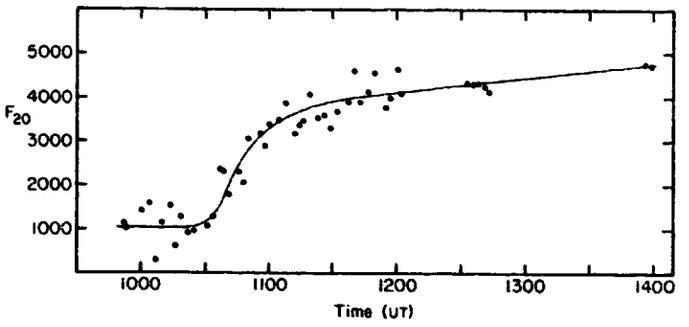

Figure 16. Thermal observations at 20 microns of the reappearance of Iapetus from the shadow of Saturn's Ring A, 8 January 1978. This preliminary curve shows the increase in thermal flux following reheating of the satellite surface by sunlight after reappearance from the shadow. From Cruikshank and Becklin (in preparation).

emersion from the ring shadow was predicted (by Alan Harris) at 1100 UT, but the satellite surface had clearly begun to warm up starting at about 1030 UT. This suggests that the outer extremities of Ring A are partly transparent, a result known earlier from observations of stellar occultations. There is evidence that the thermal response of the uppermost surface layer(s) of the regolith of Iapetus is almost instantaneous, indicating, as in the case of the Galilean satellites (Morrison and Cruikshank 1973, Hansen 1973) that the thermal conductivity and the thermal inertia are extremely low. Detailed models of the Iapetus data may put realistic constraints on the presence of atmospheric gases on this satellite because of the strong effect of an atmosphere on the thermal conductivity of the dendritic surface microstructure presumed to exist on Iapetus.

The reason for the stunning asymmetry in the distribution of frost, hence the brightness, on the leading and trailing faces of Iapetus is not understood. Hypotheses proposed have included both preferential deposition of frost on the trailing hemisphere and preferential removal of frost from the leading hemisphere, but neither can be satisfactorily modeled, especially in view of the more nearly uniform distribution of bright (or dark) materials on the other satellites. A more recent hypothesis suggests that dark material generated from impacts on Phoebe might preferentially accumulate on the leading face of Iapetus as the particles spiral toward Saturn, but this, too, requires detailed modeling. In this context, the determination of the nature (at least albedo) of the surface of Phoebe is of interest.

ATMOSPHERES

Except for Titan, nothing is known about the presence of atmospheres on the satellites of Saturn, but the Fink *et al.* (1976) spectra would have shown methane or ammonia had either gas been present in even very small amounts. Water frost has a finite vapor pressure, and water vapor will dissociate in the presence of solar ultraviolet light with spectroscopically identifiable oxygen as one byproduct. Searches for oxygen surrounding the icy Galilean satellites have so far been negative, however, and the reduced vapor pressure at the lower temperature of the Saturn satellites, plus the lesser solar ultraviolet flux, makes the detection from earth of oxygen around Rhea, for example, unlikely.

INTERIOR STRUCTURES OF THE SATELLITES

The principal studies of the interior structures and thermal histories of small bodies in the outer solar system have been those of Lewis (1971a, b, 1972) and Consolmagno and Lewis (1976), who have described equilibrium and disequilibrium models of condensation from the solar nebula. In the most recent exposition of this work, Consolmagno and Lewis (1977) have shown that for condensation at T = 160 K or less, a body will have a bulk composition consisting of C1 chondritic material and water ice in roughly equal proportions if the process is slow enough to permit maintenance of chemical equilibrium with the surrounding solar nebula. If condensation occurs too fast, disequilibrium occurs and the body is built up of layers that do not interact chemically with one another. Such a body will have a high-density core surrounded by a mantle of ice and ammonium hydrosulfide, with an ultimate crust of ammonia ice.

The total mean densities of both types of satellite will be about the same, and within the range of the probable densities of the Saturn satellites, except Titan. The higher mean density of Titan suggests a larger volume fraction of silicate material.

The thermal histories of the small satellites depend on their compositions because of the different melting temperatures of various ices. If only C1 material and water ice are present, satellites less than 650 km in radius will probably not melt, and bodies as large as 1000 km will melt and differentiate only slightly. In models where ammonia compounds are present, smaller bodies will melt because of the lowered melting temperature, and satellites of 700 to 1000 km radius will be significantly

differentiated with a core of silicates, a mantle consisting of water ice and an ammonia-water solution, plus a crust of water ice a few hundred kilometers thick.

The thermal history of Titan is much more complex because of its greater size (with higher internal pressure) and possible larger volume fraction of silicate minerals. Melting occurs early in the history of a satellite this large, and accelerates as energy is released by the gravitational settling of denser fractions. The thermal histories of large bodies are perhaps more properly termed cooling histories, and the formation of different pressure phases of the ices in the interiors of these objects, plus the chemical interactions of the different constituents has only begun to be studied.

SUMMARY

It is useful at this point to summarize our understanding of each satellite individually; we consider them radially outward from Saturn.

1. S 11 If it exists, S 11 is probably an icy satellite with high albedo and radius several tens of kilometers. It may be, as Aksnes and Franklin suggest, just one member of a family of extended ring particles near the Roche limit. Verification of its existence will probably await the next passage of the earth through the ring plane, or perhaps spacecraft imagery.

2. Janus If Janus really exists, it is probably indistinguishable from S 11 and any other members of the ring-tip family of satellites, but additional data are clearly required.

3. Mimas By inference and analogy, the surface, and perhaps the bulk composition, of Mimas is dominated by water frost. Mimas is less than half the size of the largest asteroids.

4. Enceladus The only relevant data indicate that Enceladus is a frost-covered satellite, though there is a suggestion of a leading-trailing asymmetry in the same sense as that observed on Iapetus. If correct, there may exist a further clue to the puzzling case of Iapetus. Enceladus is about the same size as Mimas, but there is marginal evidence that its mean density is a bit greater, though still in the range of total volatile composition.

5. Tethys Another icy satellite, Tethys is about the same size as the largest asteroids, though its albedo is much higher. The frost appears uniformly distributed around the body.

6. Dione Dione is indistinguishable from Tethys at the present level of precision of the relevant data.

7. Rhea Frost dominates the surface of Rhea, and the albedo is uniformly high around the satellite. It is larger than the largest asteroids, but is still only half the size of Titan and the Galilean satellites. The mass, hence the density, is unknown, but frozen volatiles probably are the bulk compositional constituents.

8. Titan Titan dominates the satellite family in terms of diameter and mass, and exerts a measurable gravitational force on other bodies in the system. Its opaque atmosphere controls its photometric properties, and we know nothing of its surface. The mean density of Titan is uncertain, but is probably less than 2 g cm^{-3}, suggesting that the interior contains only a very small fraction of silicates in addition to the presumed condensed volatiles. Titan presents an interesting contrast to the icy satellites interior to it.

9. Hyperion Apparently another non-icy satellite, Hyperion exists in a gravitational relationship with Titan, and its orbital (and rotational) history may have been controlled by the larger body. Sketchy evidence appears to show a compositional similarity between the surface of Hyperion and satellites of Uranus and Neptune, but the nature of the material has not yet been deciphered. Hyperion is very small.

10. Iapetus One of the great puzzles of the solar system is the asymmetry in the distribution of frost on the surface of this satellite; the leading face may be dark, and the trailing hemisphere is largely covered with water frost. Iapetus is comparable in size with the largest asteroids, and it is the first satellite outward from Saturn whose orbit is inclined significantly to the ring/satellite plane. Thermal eclipse data appear to indicate a very low density upper surface layer.

11. Phoebe Marginal evidence suggests that Phoebe's surface is dark, in which case material removed by impacting space debris may be the source of the dark material on Iapetus. Phoebe moves retrograde in its large orbit, at a high inclination to the ring plane. There is no evidence on the question of surface composition.

Ground-based observational techniques have not been exhausted in the study of the satellites of Saturn. Infrared spectra can be obtained for all members of the system with the exception of Janus and S 11, with instruments in existence or under development, thus giving us the possibility of studying the composition of Mimas, Hyperion, the dark side of Iapetus, and Phoebe. The largest telescopes and most sensitive detectors are required, however, so progress on these problems will be slow.

ACKNOWLEDGMENTS

I thank my colleagues for permission to quote their results in advance of publication, particularly K. Aksnes, F. Franklin, S. Larson, J. Fountain, J. Gradie, J. Degewij, B. Zellner, L. Andersson, E. Becklin, and C. Pilcher. Supported in part by NASA Grant NGL 12-001-057.

REFERENCES

Aksnes, K., and Franklin, F. A. (1978). The evidence for new faint satellites of Saturn reexamined. *Icarus*. In press.

Andersson, L. E. (1974). A photometric study of Pluto and satellites of the outer planets. Ph.D. thesis, Indiana University. 226 pp.

Burns, J. A. (1977). Orbital evolution. In *Planetary Satellites* (J. A. Burns, ed.), pp. 113–156. University of Arizona Press, Tucson.

Consolmagno, G. J., and Lewis, J. S. (1976). Structure and thermal models of icy Galilean Satellites. In *Jupiter*, pp. 1035–1051. University of Arizona Press, Tucson.

Consolmagno, G. J., and Lewis, J. S. (1976). Structure and thermal models of Icy Galilean Satellites. In *Jupiter* (T. Gehrels, ed.), pp. 1035–1051. University of Arizona Press, Tucson.

Cruikshank, D. P. (1977). Radii and albedos of four Trojan asteroids and Jovian satellites 6 and 7. *Icarus 29*, 224–230.

Cruikshank, D. P. (1978). On the rotation period of Neptune. *Astrophys. J. 220*. L57–L58.

Cruikshank, D. P. (1978). The radius and albedo of Hyperion. *Icarus*. In press.

Cruikshank, D. P. (1979). Enceladus: Conformation of water frost on the surface. *Icarus*. In preparation.

Cruikshank, D. P. Dyck, H. M., and Becklin, E. E. (1978). On the diameter and geometric albedo of Triton. Submitted to *Icarus*.

Cruikshank, D. P., Pilcher, C. B., and Morrison, D. (1977). Evidence for a new class of satellites in the outer solar system. *Astrophys. J. 217*, 1006–1010.

Cruikshank, D. P. and Stockton, A. (1978). The nature of Triton. Submitted to *Icarus*.

Degewij, J., Gradie, J., and Zellner, B. (1977). UBV photometry of distant asteroids and faint satellites. *Bull. Amer. Astron. Soc.* 9, 503.

Degewij, J. Andersson, L., Gradie, J., and Zellner, B. (1978). Photometric and polarimetric properties of the satellites J6 (Himalia), J7 (Elara), S7 (Hyperion), S9 (Phoebe), and N1 (Triton). *Icarus*. In preparation.

Dollfus, A. (1967a). IAU Circular 1987.

Dollfus, A. (1967b). IAU Circular 1995.

Dollfus, A. (1970). Diameters des planètes et satellites. In *Surfaces and Interiors of Planets and Satellites* (A. Dollfus, ed.), pp. 45–139. Academic Press, New York.

Duncombe, R. L., Klepczynski, W. J., and Seidelman, P. K. (1974). The masses of the planets, satellites, and asteroids. *Fundam. of Cosmic Phys. 1*, 119–165.

Elliot, J. L., Veverka, J., and Goguen, J. (1975). Lunar Occultation of Saturn. I. The diameters of Tethys, Dione, Rhea, Titan, and Iapetus. *Icarus 26*, 387–407.

Fink, U., Larson, H. P., Gautier, T. N. III, and Treffers, R. R. (1976). Infra red spectra of the satellites of Saturn: Identification of water ice on Iapetus, Rhea, Dione, and Tethys. *Astrophys. J. 207*, L63–L67.

Fountain, J. W., and Larson, S. M. (1978). Saturn's ring and nearby faint satellites. *Icarus*. In press.

Franz, O. G. (1975). A photoelectric color and magnitude of Mimas. *Bull Amer. Astron. Soc. 7*, 388.

Franz, O. G., and Millis, R. L. (1975). Photometry of Dione, Tethys, and Enceladus on UBV system. *Icarus 24*, 433–442.

Gaffey, M. J. (1976). Spectral reflectance characteristics of the meteorite classes. *J. Geophys. Res. 81*, 905–920.

Greenberg, R. (1977). Orbit-orbit resonances among natural satellites. In *Planetary Satellites* (J. A. Burns, ed.), pp. 157–168. University of Arizona Press, Tucson.

Hansen, O. L. (1973). Ten micron eclipse observations of Io, Europa, and Ganymede. *Icarus 18*, 237–246.

Harris, D. L. (1961). Photometry and colorimetry of planets and satellites. In *Planets and Satellites* (G. P. Kuiper and B. M. Middlehurst, eds.), pp. 272–342. University of Chicago Press, Chicago, IL.

Kourtchmy, S., and Lamy, Ph. L. (1975). Study of the inner satellites of Saturn by photographic photometry. *Icarus 25*, 459–465.

Kovalevsky, J., and Sagnier, J-L. (1977). Motions of natural satellites. In *Planetary Satellites* (J. A. Burns, ed.), pp. 43–62. University of Arizona Press, Tucson.

Lebofsky, L. A. (1977). Identification of water frost on Callisto. *Nature 269*, 785–787.

Lebofsky, L. A., and Fegley, Jr. M. B. (1976). Chemical compositon of icy satellites and Saturn's rings. *Icarus 28*, 379–388.

Lewis, J. S. (1971a). Satellites of the outer planets: Their physical and chemical nature. *Icarus 15*, 174–185.

Lewis, J. S. (1971b). Satellites of the outer planets: Thermal models. *Science 172*, 1127–1128.

Lewis, J. S. (1972). Low temperature condensation from the solar nebula. *Icarus 16*, 241–252.

McCord, T. B., Johnson, T. V., and Elias, J. H. (1977). Saturn and its satellites. Narrow-band spectrophotometry (0.3 - 1.1 u). *Astrophys. J. 165*, 413–424.

Millis, R. L. (1977). UBV photometry of Iapetus: Results from five apparitions. *Icarus 31*, 81–88.

Morrison, D. (1974). Albedos and densities of the inner satellites of Saturn. *Icarus 22*, 51–56.

Morrison, D., and Burns, J. A. (1976). The Jovian satellites. In *Jupiter* (T. Gehrels, ed.), pp. 991 – 1034. University of Arizona Press, Tucson.

REFERENCES (Contd)

Morrison, D. 1977. Asteroid sizes and albedos. *Icarus 31*, 185–220.

Morrison, D., and Cruikshank, D. P. (1973). Thermal properties of the Galilean satellites. *Icarus 18*, 224–236.

Morrison, D., and Cruikshank, D. P. (1974). Physical properties of the natural satellites. *Space Sci. Rev. 15*, 641–739.

Morrison, D., Jones, T. J., Cruikshank, D. P., and Murphy, R. E. (1975). The two faces of Iapetus. *Icarus 24*, 157–171.

Morrison, D., Cruikshank, D. P., Pilcher, C. B., and Rieke, G. H. (1976). Surface compositions of the satellites of Saturn from infrared photometry. *Astrophys. J. 207*, L213–L216.

Morrison, D., Cruikshank, D. P., and Burns, J. A. (1977). Introducing the satellites. In *Planetary Satellites* (J. A. Burns, ed.), pp. 3–17. University of Arizona Press, Tucson.

Murphy, R. E., Cruikshank, D., and Morrison, D. (1972). Radii, albedos, and 20-micron brightness temperatures of Iapetus and Rhea. *Astrophys. J. 177*, L93–L96.

Noland, M., Veverka, J., Morrison, D., Cruikshank, D. P., Lazarewicz, A. R., Morrison, N. D., Elliot, J. L., Goguen, J., and Burns, J. A. (1974). Six-color photometry of Iapetus, Titan, Rhea, Dione and Tethys. *Icarus 23*, 334–354.

O'Leary, B. T., and van Flandern, T. C. (1972). Io's triaxial figure. *Icarus 17*, 209–215.

Peale, S. J. (1977). Rotation histories of the natural satellites. In *Planetary Satellites* (J. A. Burns, ed.), pp. 87–112. University of Arizona Press, Tucson.

Peale, S. J. (1978). An observational test for the origin of the Titan-Hyperion orbital resonance. Submitted to *Icarus*.

Pickering, W. H. (1905). The ninth and tenth satellites of Saturn. *Harvard Ann. 53*, 173–185.

Pickering, W. H. (1908). An investigation of the orbit of the tenth satellite of Saturn. *Harv. Ann. 61*, 86–94.

Pollack, J. B., Witteborn, F. C., Strecker, D. W., Erickson, E. F., Baldwin, B. J., and Bunch, T. E. (1977). Observations of the near infrared spectra of the Galilean satellites. *Bull. Amer. Astron. Soc. 9*, 524.

Taylor, G. E. (1972). The determination of the diameter of Io from its occultation of β Scorpii C on May 14, 1971. *Icarus 17*, 202–208.

Texereau, J. (1967). Observing Saturn's edgewise rings. *Sky and Telescope 33*, 226–227.

Veverka, J. (1977). Photometry of satellite surfaces. In *Planetary Satellites* (J. A. Burns, ed.), pp. 171–209. University of Arizona Press, Tucson.

Veverka, J., Burt, J., Elliot, J. L., and Goguen, J. (1978). Lunar occultation of Saturn. III. *Icarus 34*, 301–310.

Walker, R. (1967). A faint satellite of Saturn? *Sky and Tel. 33*, 93.

DISCUSSION

D. MORRISON: Since you mentioned the recent Iapetus eclipse, I think it would be appropriate to read into the record the abstract of a preprint that I received from K. Aksnes and F.A. Franklin of a paper called Mutual Phenomena of Saturn's Satellites in 1979–1980. (This paper has since appeared in *Icarus* (1978), *34*, 194–207.)

> *"Using two sets of orbital elements and the radii of the Saturnian satellites 1 (Mimas) through 7 (Hyperion), we find that from Oct. 1979 until Aug. 1980 nearly 300 mutual eclipses and occultations involving these bodies will occur. To allow for the expected errors in the satellite ephemerides, we repeat these calculations in order to obtain the additional events that occur when all satellite radii (save Titan's) are increased by 1000 km. A third listing predicts eclipses of satellites by (the shadow of) the ring. Photometric observations of a large number of these events will add much precise information to our knowledge of the Saturnian system at a critical time."*

D. CRUIKSHANK: These eclipses and occultations will be tough to observe.

G. SISCOE: Are the leading faces of all the satellites interior to Titan brighter than the trailing faces?

D. CRUIKSHANK: No, they're not. There is some marginal evidence that Enceladus is oriented the same way that Iapetus is, namely, that the face in the leading direction is darker than the trailing face. That conclusion was based on insufficient photometric data that are intrinsically very difficult to get.

In the case of Mimas, we have no data whatever. But it is interesting to speculate about the difference between the reflectance of the icy satellites and the reflectance of the rings, specifically short of 500 nm. The rings, as you know, drop off toward the UV, while the satellites are flat. Where does the transition occur? Does it occur at the edge of the rings? Does it occur with S-11 or Janus or Mimas? It would be very interesting to find out.

I might point out that a lot of these problems that still remain on the satellites of Saturn are soluble. We can get better spectra and better photometry, but it takes big telescopes with sensitive detectors.

D. MORRISON: There also will be a much improved opportunity in the next couple of years because of the rings being on edge. The scattered light problem will be substantially less for the inner satellites.

J. CUZZI: In the spectra of Callisto and Ganymede, can you resolve the rock component from the ice component? Also, do you see less reddening in the outer Galilean satellites than you do in Io and Europa? In the Saturn system you see the Saturn satellites having flat spectra and the rings being red, and I wondered if a similar effect was seen in the Galilean satellites.

D. MORRISON: There are such major compositional differences from one Galilean satellite to another that such a systematic effect is probably masked. That's why it's interesting to talk about the ensemble of the rings and the satellites for Saturn. As far as we know, they all have surfaces with about the same composition - mainly water ice. It is a more homogeneous sample, at least to first order.

NON-THERMAL RADIO EMISSION FROM SATURN

James W. Warwick

Department of Astrogeophysics, University of Colorado
Boulder, Colorado 80309

ABSTRACT

Direct, strong evidence for non-thermal radio emission from Saturn exists in the hectometric data observed by Imp 6 and studied by L. W. Brown. With the approaches of the Voyager and Pioneer spacecraft, new and specific information on Saturn's magnetic field will become available by the end of 1979. The planet has been tentatively identified as a decametric source by several investigators, but the most sensitive and most recent data fail to confirm this. At metric or decimetric wavelengths Saturn has no non-thermal emission like Jupiter's synchrotron sources. Finally, a comparative study of earth and Jupiter radio emissions suggests what we may expect from giant planets in the way of evidence for lightning discharges.

Let T be source temperature in the usual thermodynamic sense (a measure of E_{av} per molecule); then, non-thermal radio emission occurs where the source is brighter than the radiance, $2E_{av}/\lambda^2$ $Wm^{-2}Hz^{-1}sr^{-1}$. λ is wavelength; $E_{av} = kT$ where $k = 1.38 \times 10^{-23}$ J per deg, and T = absolute temperature.

Hectometric radio emission from Saturn (at wavelengths of 100's of meters) has probably been observed from the Imp-6 Spacecraft by L. W. Brown (1975) (see Figure 1). At the peak, 300 m = λ, the flux density in this emission seen near the earth approximately equals the cosmic background radio flux, as well as the peak flux density of Jupiter's emission at 8 MHz (Brown, 1974). Its occurrence probability is less than 5% of that for Jupiter emission at 1 MHz. This may explain the lack of detection (Kaiser, 1977) of Saturn from the Radio Astronomy Explorer-2 spacecraft.

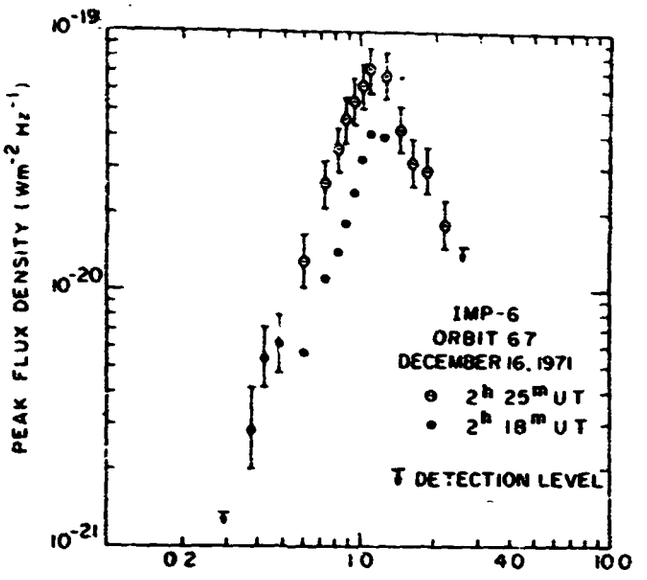

Figure 1. Hectometric Saturn burst (L. W. Brown, 1975). (Reproduced courtesy The Astrophysical Journal.)

Decametric radio emission from Saturn was tentatively detected by Smith and Douglas (1959), Carr *et al.* (1961), and Braude (1972). Further measurements to a very high sensitivity at 11.4 m (Shawhan *et al.*, 1973 and Mutel, 1974) indicate no continuous flux greater than about 1×10^{-26} flux units. Since the latter observations took place close to the maximum tilt of Saturn's southern pole towards the earth, it seems clear that there is little or no south pole emission. If Saturn is asymmetric, and favors its north pole, however, the Yale observations could have been consistent with northern emission, like Jupiter produces.

The possibility of Saturn synchrotron emission has generated many attempts to estimate and to measure polarization and spectral properties of Saturn's metric and decimetric radiations. This emission may well be significant only at metric wavelengths; measurements have not yet detected it (see Shawhan, 1978).

Phenomenologically distinct from these types of emission, there exists on the earth strong broadband impulsive radio emission associated with electrical discharges. It seems as though virtually all prognosticators believe that lightning also will occur in the giant planets' atmospheres near the water ice freezing levels (Lewis, 1969), and even in the atmosphere of Saturn's largest satellite, Titan (Sagan, 1974). My favorite magazine center-fold illustration is from *National Geographic* (February, 1975). It shows, I think, what we might all hope to record sometime aboard probes into the atmospheres of the giant planets and, perhaps, to Titan.

There are no measurements of Saturn's magnetic field as such. Brown's (1975) data represent indirect evidence for the field like (although it lacks polarization) the evidence on which Jupiter's field was inferred 20 years ago (Franklin and Burke, 1958). The inference that Saturn's polar surface field is 2 gauss follows from the comparison of the radio frequency of terrestrial kilometric radiation with that of Jupiter's decametric radiation. The one peaks at about 300 KHz, and the other, at about 8 MHz. The field strengths in the sources are directly proportional to these radio frequencies. This kind of agreement, as put forth by Kaiser and Stone (1975), is based on many different authors' theoretical and experimental results.

Theoretical inferences on Saturn's polar surface field cover an enormous range. Excluding predictions that it has no field at all (Smoluchowski, 1971), they range from 1/20 to 5 gauss (Stevenson, 1974; Warwick *et al.*, 1977), a factor of 100 Smoluchowski doubts the existence of the necessary liquid metallic core, Stevenson allows for only a small core (1/6 the planetary radius) and Warwick *et al.* use a physical scaling for magnetic theory, but do not discuss metallicity or conductivity of Saturn's interior. Many people (Luthey, Van Allen, Siscoe, Scarf, and others) adopt their own solutions to this problem of Saturn's internal fluidity and magnetism.

As I write (1 February, 1978), Brown's (1974) hectometric Jupiter signals would lie about 3 dB above cosmic noise at the Voyager spacecraft about 3 AU from Jupiter. The Voyager PRA experiment (Warwick *et al.*, 1977) at hectometric wavelengths uses a narrow bandwidth, only 1 kHz, and cannot detect the cosmic noise, both as a result of this bandwidth limitation, and also the presence of a small residual interference unsynchronized with the spacecraft clock. However, it has detected Jupiter in this range since 28 December 1977. The approach to Jupiter renders its signals much stronger than noise of Saturn. After Jupiter encounter, Saturn emission rapidly gains the advantage. At the time of the Pioneer 11 encounter in September, 1979, Voyager 1 should show Saturn signals comparable, at 1 MHz, to Jupiter signals and 10 dB stronger than the cosmic noise. At Titan's distance from Saturn, its signals will be 60 dB stronger than at Earth, and far above minimum detectable signals.

For more than one year before Voyager's Saturn encounter, and possibly as soon as Pioneer 11's Saturn encounter, the Voyagers will receive Saturn's hectometric radio emissions for measurements of spectrum, time variations, and polarization. If the emission is detected at all, and Brown's success in this respect is at

the 95 percent confidence level, we can learn about Saturn the same things we learned about Jupiter from ground-based radio observations. These are: (1) rotation period of Saturn's internal magnetic field sources to a precision of a few seconds or better in 10 hours; (2) presence of satellite or ring interactions with Saturn's magnetospheric plasma; (3) asymmetries in the magnetic field on Saturn's surface; (4) strength and sense of the surface magnetic fields. In the latter data, we will, of course, perhaps only verify crudely what Pioneer 11 has already by then measured with considerable precision. However, it is comfortable to consider that whatever is Pioneer 11's fate almost two years from now, we can reasonably expect to learn something about Saturn's field just from Voyager data alone, and as soon as September, 1979. And finally, the radio period of rotation determined over a baseline of more than 10^3 rotations, will probably remain more precise than *in situ* field measures can provide over the 20 or 30 rotations of close encounter.

Electrical discharges from man-made sources, such as frictional electrification of synthetic fabrics, are a commonplace feature of everyday life. In their extreme natural form, they are dangerous, not common, and not understood. If the sole precondition for thunderstorm electrification in a planetary atmosphere is turbulent convection near the water freezing level, then we expect electrification in Saturn's and Titan's atmospheres, as well as Jupiter's.

Bar-Nun (1975) goes further, to compute the explicit intensity of thunderstorms like those on earth that would be required on Jupiter, according to his theory of the origin and chemical kinetics of ammonia and acetylene, to produce the observed acetylene. Many authors seek to explain the presumed existence of complex prebiotic chemistry in the giant planets, through laboratory experiments patterned after those of Miller and Urey (see Ponnamperuma, 1974) who sparked test tubes containing the cosmic mixture and analyzed the prebiotic products. No doubt, if lightning does occur out there, these reactions occur, whether or not their products are sufficiently abundant to produce the coloration visible in the giant planets' atmospheres. There is controversy on this point, which, to repeat, is whether there is evidence, from either chemistry, spectroscopy, or photometry, that lightning discharges take place on the giant planets.

What the space program might provide is *in situ* evidence for the occurrence of electrical discharges in giant planet atmospheres. The remainder of my report will discuss what evidence there may be from Earth-based data, and what evidence

may be collected in the future from the Voyager spacecraft, as well as might have been already observed from the Pioneer spacecraft at the two Jupiter encounters.

Direct radio emission evidence, including the low-frequency phenomena of whistlers, is lacking from the Pioneers for the simple reason that neither of them carried a wave experiment at any frequency. These were energetic-particles-intensive spacecraft, and provided definitive evidence especially for engineering design of future spacecraft for flights around Jupiter.

On the other hand, optical experiments in the infrared and visual spectral regions showed Jupiter's atmosphere to be turbulent, on a scale no larger than a few hundred kilometers, everywhere, including polar regions. Furthermore the infrared experiment showed outward heat fluxes constant (Ingersoll *et al.*, 1976) over the entire planet accessible to observation, which implies that the forces driving convection are omnipresent. It is obviously not possible within the time scales of the Pioneer scanning photopolarimeter to record lightning flashes; this most direct of all methods does not work on those spacecraft.

Earth orbiting satellites can on the other hand detect nighttime lightning storms (Sparrow and Ney, 1971; Sizoo and Whalen, 1976). Signal levels from the Defense Meteorological Satellite Program (DMSP) satellites at just under 1000 km altitude easily detect city lights and squall lines, the latter through a unique streak of response by the scanning detector to intense flashes of lightning. From the Jupiter periapsis of Voyager 1 at more than 300 times the distance of DMSP from Earth's lightning strokes, the same effect must require about 50 dB greater lightning intensity. Success of the Voyager polarimeters must under these circumstances be doubted insofar as their detection of lightning is concerned, even though Bar-Nun (1975) requires essentially a thunderstorm on each element of area on Jupiter's surface measuring 10 x 10 km, each producing strokes once every 10 s, like a violent terrestrial storm.

In some particularly active centers, such as the Great Red Spot, he infers 10 x even that level, which is itself 10^4 x as active, per unit area averaged over Jupiter's surface, as is the level of terrestrial lightning.

It is well worth remembering that the earliest explanations of Jupiter's decametric emission were in terms of enormous lightning flashes requiring energies more than 10^8 x greater than those on Earth (Burke, 1961, and see below). This enormous enhancement is necessary if the fine time structure of the planetary emissions, fluctuations violent on a scale of 0.1 s to 10 s, represents individual flashes. Since, however, there are convincing reasons to believe this variability has more to

do with scintillations produced in the solar wind plasma, than time variability in the sources on Jupiter, the early explanation is no longer accepted. Instead, Jupiter's radio sources today are understood in terms of magnetospheric physics, including the generation and precipitation of energetic electron streams into Jupiter's upper atmosphere.

Therefore we accept Bar-Nun's requirement of 10^4 enhancement in the average rate of occurrence of lightning flashes on Jupiter as compared with the Earth, rather than enormously enhanced individual flashes. Flashes are, by assumption, identical in physical structure on the two planets, and we will not discuss whether Bar-Nun's conclusion is, in its own terms, acceptable from a physical chemical point of view.

Thunderstorm activity on Earth produces radio emissions at all frequencies ranging from ELF to VHF. At high frequencies (HF), from 3 to 30 MHz, the emissions from individual flashes may escape the ionosphere of the earth and be recorded in space. Figure 2 shows a typical flash consisting of several return strokes, with coupled impulsive radio emissions at 15 kHz and 34 MHz, as well as quasi-continuous

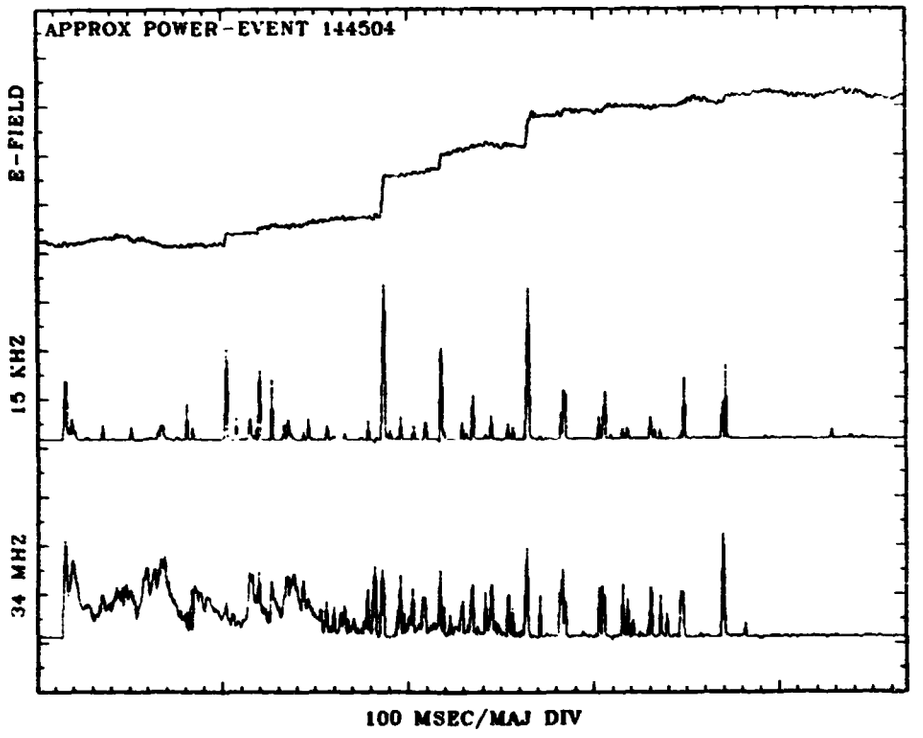

Figure 2. Electromagnetic fields in the lightning flash. The "E-field" curve is essentially the DC variations in the electrostatic field. The other two curves are, respectively, broadband emission centered on 15 KHz, and relatively narrow band emission centered on 34 MHz. The observations were made at the University of Colorado Radio Astronomy Observatory, near Nederland, Colorado, in September, 1977.

emission lasting for several tenths of one second at 34 MHz. Field strengths in an individual stroke at 34 MHz are typically a few millivolts per meter per root hundred kilohertz at ranges of a few kilometers (see Uman, 1969).

High frequency emission from a single, given, stroke seen from satellite altitudes, say, 1000 kilometers, about equals the cosmic background. To produce this much signal if its source were Jupiter, the stroke would have to be 120 dB more energetic, since Jupiter is about 10^6 x farther away (600, 000, 000 km at opposition). This is a much larger ratio than the one given by Gallet (1961), which was only a factor of 10^8 to 10^9 in energy.

Instead of individual flashes, observations of terrestrial discharges from space refer to the largest scale storm centers on Earth covering millions of square kilometers of tropical continents. These have been effectively observed by the Radio Astronomy Explorer-1 spacecraft at an altitude of 6000 km over the Amazon basin (Herman *et al.*, 1973). In southern winter, December, 1968, direct observations showed this particular terrestrial radio emission source to have a brightness about 50 dB above the cosmic noise level at 9 MHz. These are well calibrated results, by the spacecraft's Ryle-Vonberg comparison radiometer in 32 s averages. Furthermore, the lower Vee antenna of this spacecraft possesses a pattern 13° x 27° in dimensions, quite appropriate to a determination of the brightness variations over sources the size of Amazonia, seen from an altitude of 6000 km.

Thirty-four MHz stroke emission seen at 6000 km from a single stroke, should be 15 dB below the cosmic noise level. To enhance a single stroke by additional strokes sufficient to build the total emission 50 dB above the cosmic noise requires more than 3 x 10^6 strokes to occur simultaneously. Since only 10^3 storms are simultaneously present over the entire Earth, it may be that RAE-1's Amazonia observations are due to man-made interferences as well as to thunderstorms.

Our interest is, however, in Saturn, and to the extent it provides a model, also Jupiter. Taken at face value, that is, without allowance for man-made noise in the Amazonia data, the RAE-1 results suggest that thunderstorms on Jupiter, just like those on earth in stroke intensity and in rate of stroke occurrence per square km per s, are not far below the Earth-based detection level at 9 MHz. With the greater areal frequency of thunderstorms proposed by Bar-Nun, the radio emission should have already been recorded in Earth-based radio astronomical observations.

To demonstrate this we note that RAE-1's terrestrial "thunderstorm" levels at 9.1 MHz are 50 dB greater than the cosmic noise when the spacecraft is 6000 km above Amazonia. If the spacecraft were at Jupiter's distance 600,000,000 km instead, it would receive the signals from 10^5 x farther away, and therefore 100 dB weaker. This would result in the terrestrial signals there being 50 dB below the cosmic noise. Jupiter's area is 21 dB greater than the earth's, and as a result, if it is the source of thunderstorms exactly like those observed by RAE-1, but greater in number because of this greater area, Jupiter storms seen from the Earth should be just 29 dB below the cosmic noise at 9.1 MHz.

But Bar-Nun states that the normalized rate of occurrence of thunderstorm strokes on Jupiter needs for chemical reasons to be 10^4 x that of the Earth. Since there are no more than 10^3 storms in progress on the Earth at a given moment, the terrestrial areal occurrence frequency is no more than 1.96×10^{-6} km^{-2}, which requires one storm in each area measured 714 km on the sides over the entire Earth. Bar-Nun suggests that this figure on Jupiter would be, instead, 7.14 km on one side.

The total number of Jupiter storms visible at the Earth on Bar-Nun's hypothesis becomes 21 dB + 40 dB - 3 dB = 58 dB greater than are terrestrial storms visible from Jupiter. Since the latter are 50 dB below the cosmic noise, we conclude that in combination with the BAE-1 terrestrial data, Bar-Nun's theory predicts that terrestrial observations of Jupiter thunderstorms should lie 8 dB above the cosmic noise level at 9.1 MHz.

One caveat would be the possibility that at 9.1 MHz, Jupiter's ionosphere cuts off thunderstorm radio emissions. They are, of course less intense at higher VHF frequencies so that we would expect smaller signal to noise ratios there. And, in addition, decametric emissions will strongly cover thunderstorm emissions at higher frequencies. In any case, the Pioneer 10/11 ionosphere critical frequencies were only about 5 to 6 MHz (see Fjeldbo *et al.*, 1976). Finally, Bar-Nun suggests that the Great Red Spot, because of its obvious convective activity as well as strong color, should be an active thunderstorm region, 10 x more than other regions of Jupiter.

We have several years of high gain interferometer data recorded by the University of Colorado-High Altitude Observatory near Boulder, at 8.9 MHz. This should be an ideal base on which to investigate whether this effect occurs. These data have been scaled for Jupiter emissions, alongside similar data taken at 10.1 MHz (see Dulk and Clark, 1966) at the US Department of Commerce Observatory

in B ılder. These authors analyzed their data for structures in the radio longitude system and in the Io longitude system. If, however, a putative atmospheric source contributes to these data the slower rotation rate of the GRS than the magnetic field of Jupiter might make it hard to observe. This smearing amounts to about 90° in only one observing season; while, at decametric wavelengths, features are much narrower than this value, it might be that in a few longitude ranges, say perhaps where GRS is located, a new peak would appear at the low frequency of 8.9 MHz.

Figure 3 shows the results of reanalyzing the 1964 apparition data at 8.9 MHz, and additional, unpublished material for the apparition of 1965. In essence, the new analyses, in radio longitude system III (1965) and as well, in temperature-altitude longitude system II, show as expected a very broadly distributed emission of almost global occurrence around the planet. The features are more consistent in system III, and shift backwards, towards smaller longitudes, in system II. This is precisely what should happen if the emission is totally dominated in these records by the familiar decametric emissions that relate to magnetospheric interactions. In particular, there is little evidence that a narrow new source appears at the LCM of the GRS, which is about 020° in system II at this time.

The upshot of all this is that it appears as though Bar-Nun's conclusion, alongside the RAE-1 data, together imply thunderstorm activity from Jupiter 8 dB above cosmic noise levels. The Jupiter decametric levels on these ground-based records are, although it has not been mentioned earlier, about 10 dB below the cosmic noise. Therefore, we conclude that our hypotheses are in error by 18 dB at least, and possibly some greater amount. If we conclude that our failure to find a system II connection is at the 10 dB level below the level of the Jupiter emissions themselves, we are probably safe in concluding that thunderstorm activity is at least 30 dB below the RAE-1-Bar-Nun prediction.

How should we understand this discrepancy? In the first place, suppose that the terrestrial thunderstorm data at 6000 km are 15 dB above cosmic noise instead of 50 dB. Herman *et al.* (1975) indicate, for United States thunderstorms, the levels are 6 to 12 dB higher than in the usual circumstances, when man-made noise dominates. This corresponds to the assumptions that there are 10^3 storms simultaneously in the antenna of RAE-1 over Brazil, and we know HF emission levels from strokes. In that case, we have made up the discrepancy vis-a-vis the 8.9 MHz observational data, and with only 5 dB required from Bar-Nun's theory (i.e., 35 dB enhancement over earth's thunderstorm activity, instead of 40 dB) to make it fit the data.

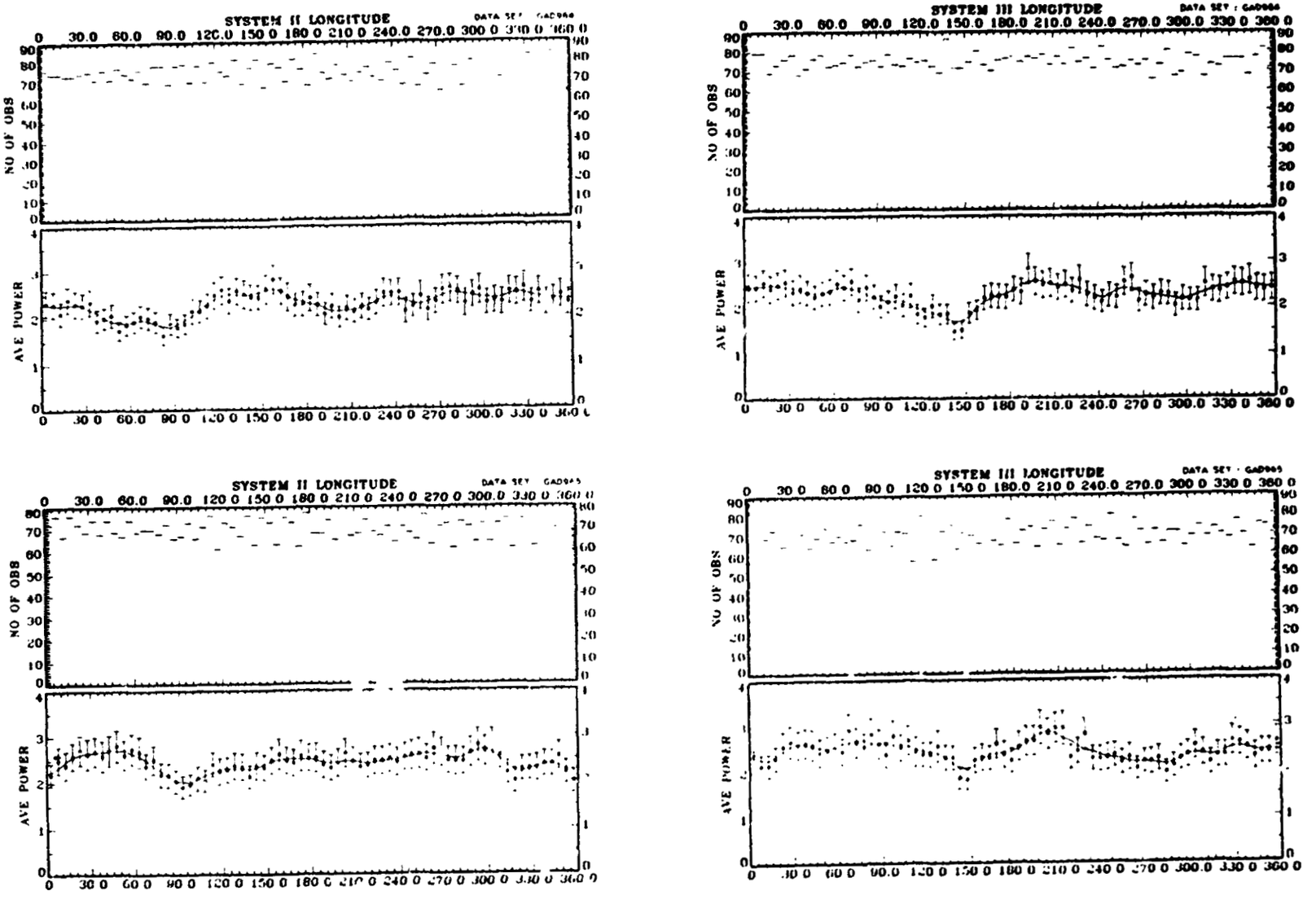

Figure 3 — 8.9 MHz radio emission from Jupiter in 1964 and 1965. The longitude systems are, system II, as defined in the American Ephemeris and Nautical Almanac (P_{II} = 9 hour, 55 minutes 40.632 seconds), and system III (1965), as defined in Seidelmann and Divine (1977) (P_{III} = 9 hours 55 minutes 29.711 seconds).

Conversely, we might suggest that some Jupiter thunderstorm activity is indeed apparent in the Boulder 8.9 MHz data.

Voyager 1 passes by Jupiter at about 350,000 km distance, $(350)^2 = 51$ dB, away from the standard 1000 km distance at which a single stroke produces an equivalent radiation to the cosmic noise at decametric wavelengths. But there are 58 dB more storms there (if we accept Bar-Nun's hypothesis) than are visible from the earth, and the latter number is 30 dB more than one stroke. We expect to see thunderstorm activity, granted validity of Bar-Nun's conclusions, at a level 58 dB + 30 dB - 51 dB = 37 dB above the cosmic noise. This value exceeds the spacecraft interference levels at all frequencies, and suggests detectability of Bar-Nun's thunderstorms from both Voyagers.

The spacecraft are implemented so that observations on a time resolution of about 0.1 milliseconds are possible for a lot of observing time within the Jupiter system. The statistics of these data may reveal lightning storms on Jupiter, even if individual strokes are not distinguishable from the great bulk of emissions. In particular, enhancements associated with optical features such as the GRS are worth a careful search. Perhaps within a year or so, we can answer the vexing question of lightning occurrence on Jupiter, and then, within two and a half years, similar questions for Saturn and Titan.

ACKNOWLEDGEMENT

The research in this note was supported by NASA and by NSF.

REFERENCES

Bar-Nun, A. (1975). Thunderstorms on Jupiter. *Icarus 24*, 86–94.

Braude, S. Ya. (1972). In *Pravda Ukrainy* 16 April, p. 3. Reported by Library of Congress-Federal Research Division, S. and T. News Alert, Item 839.

Brown, L. (1974). Spectral behavior of Jupiter near 1 MHz. *Astrophys J. 194*, L159–L162.

Brown, L. (1975). Saturn radio emission near 1 MHz. *Astrophys. J. 196*, 189–192.

Burke, B. F. (1961). Radio observations of Jupiter. I. In *Planets and Satellites* (G. P. Kuiper, and B. M. Middlehurst, eds.), pp. 473–498. University of Chicago Press, Chicago 37.

Carr, T. D., Smith, A. G., Bollhagen, H., Six, Jr., N. F., and Charterton, N. E. (1961). Recent decameter-wave-length observations of Jupiter, Saturn, and Venus. *Astrophys. J. 134*, 105–125.

Dulk, G. A., and Clark, T. A. (1966). Almost-continuous radio emission from Jupiter at 8.9 and 10 MHz. *Astrophys J. 145*, 945–948.

Fjeldbo, G., Kliore, A., Seidel, B., Sweetnam, D., and Woiceshyn, P. (1976). The Pioneer 11 radio occultation measurements of the Jovian ionosphere. In *Jupiter* (T. Gehrels, ed.), pp. 238–246. University of Arizona, Tucson.

Franklin, K. L., and Burke, B. F. (1958). Radio observations of the planet Jupiter. *J. Geophys. Res. 63*, 807–824.

Gallet, R. M. (1961). Radio observations of Jupiter II. In *Planets and Satellites* (G. P. Kuiper, and B. M. Middlehurst, eds.), pp. 500–533. University of Chicago Press, Chicago.

Herman, J. R., Caruso, J. A., and Stone, R. G. (1973). Radio Astronomy Explorer RAE-1. Observations of terrestrial radio noise. *Planet. Space Sci. 21*, 443–461.

Herman, J. R., Stone, R. G., and Caruso, J. A. (1975). Radio detection of thunderstorm activity with an earth-orbiting satellite. *J. Geophys. Res. 80*, 665–672.

Ingersoll, A. P., Munch, G., Neugebauer, G., and Orton, G. S. (1976). In *Jupiter* (T. Gehrels, ed.), pp. 197–205. University of Arizona, Tucson.

Kaiser, M. L. (1977). A low-frequency radio survey of the planets with RAE-2. *J. Geophys. Res. 82*, 1256–1260.

Kaiser, M. L., and Stone, R. G. (1975). Earth as an intense planetary radio source: similarities to Jupiter and Saturn. *Science 189*, 285–287.

Lewis, J. S. (1969). Observability of spectroscopically active compounds in the atmosphere of Jupiter. *Icarus 10*, 393–409.

Mutel, R. (1974). Personal communication, and letter to John Rather, University of California, Irvine, California 92664, dated 8 May.

Ponnamperuma, C. (1974). The chemical basis of extraterrestrial life. In *Interstellar Communication: Scientific Perspectives* (C. Ponnamperuma, and A. G. W. Cameron, eds.), pp. 45–58. Houghton Mifflin, Boston.

Sagan, C. (1974). Organic chemistry in the atmosphere. In *The Atmosphere of Titan* (D. M. Hunten, ed.), pp. 134–141. NASA SP-340.

Seidelmann, P. K. and Divine, N. (1977). Evaluation of Jupiter longitudes in system III (1965). *Geophys. Res. Letters 4*, 65–68.

Shawhan, S. D. (1978). Magnetospheric plasma waves. In *Solar System Plasma Physics—A Twentieth Anniversary Review* (C. F. Kennel, L. J. Lanzerotti, E. N. Parker, eds.), North Holland.

Shawhan, S. D., Clark, T. A., Cronyn, W. M., and Basart, J. P. (1973). Upper limit to the 11.4 m flux of Saturn using VLBI. *Nat. Phys. Sci. 243*, 65–66.

Sizoo, A. H., and Whalen, J. A. (1976). Lightning and squall line identification from DMSP satellite photographs. AFGL-TR-76-0256, *Air Force Surveys in Geophysics*, No. 355 (Air Force Geophysical Laboratory, Hanscom Air Force Base, MA 01731).

Smith, H. J., and Douglas, J. N. (1959). Observations of planetary nonthermal radiation. In *Paris Symposium on Radio Astronomy*, (R. N. Bracewell, ed.), pp. 53–55. Stanford University Press, Stanford California 94305.

Smoluchowski, R. (1977). Metallic interiors and magnetic fields of Jupiter and Saturn. *Astrophys. J. 166*, 435–439.

Sparrow, J. G., and Ney, E. P. (1971). Lightning observations by satellite. *Nature 232*, 540–541.

Stevenson, D. (1974). Planetary magnetism. *Icarus 22*, 403–415.

Uman, M. A. (1969). *Lightning* McGraw-Hill, New York. 264 pp.

Warwick, J. W., Pearce, J. B., Peltzer, R. G., and Riddle, A. C. (1977). Planetary Radio Astronomy experiment for Voyager missions. *Space Sci. Rev. 21*, 309–327.

DISCUSSION

B. SMITH: Jim, what is the hope that new observations will determine the radio rotation period (the equivalent of Jovian System III) for Saturn?

J. WARWICK: I believe that the possibility of observing non-thermal emission by Saturn from space remains for Voyager. Voyager I will be the first to detect Saturn, and that will be from a distance of about 4 AU in September of 1979. Until then, there won't be any more data than Brown's. To determine a Saturn rotation period will be a "first order of business" for us.

L. TYLER: What about the possibility of detecting lightning in other regions of the spectrum?

J. WARWICK: With a flyby of Jupiter, that's one of the things the plasma wave experiment would be looking for. The question is: Will there be any precursor events to identify the wave sources as lightning, such as the snap followed by the whistle? We may not be able to see the individual snap followed by the individual whistle. If there's as much activity as Bar-Nun thinks, we may not be able to see anything separately: just see a mishmash of noise comprising all the lightning strokes over the surface of Jupiter.

MAGNETOSPHERE OF SATURN

George L. Siscoe

Department of Atmospheric Sciences, University of California at Los Angeles
Los Angeles, California 90024

ABSTRACT

Models of the Saturnian magnetosphere based on the application of magnetospheric scaling relations to a spin-aligned planetary magnetic dipole that produces a surface equatorial field strength in the range 0.5 to 2 gauss exhibit the following properties: (1) the orbit of Titan lies inside of the magnetosphere essentially all of the time, even when variations in the size of the magnetosphere resulting from solar wind pressure changes are taken into account; (2) the Brice-type planetary plasmasphere reaches a peak density of about 10 protons cm^{-3} at $L \approx 7$ (L = planetocentric distance in units of planetary radii); (3) Saturn's rings have a profound effect on the energetic particle population and the plasmaspheres derived from interstellar neutrals and Titan's torus; (4) the model calculation suggests that the Titan-derived plasmasphere may be self-amplifying with a feedback factor greater than unity, which implies the possibility of a nonlinearly saturated, highly inflated Saturnian magnetosphere; (5) this same source can have important eroding effects on the outer edge of the rings as determined by Brown-Lanzerotti sputtering rates.

INTRODUCTION

The observation of radio bursts from Saturn strongly imply that that planet, like Mercury, Earth and Jupiter has a rich and interesting magnetosphere. We here apply the arguments and relationships that comprise the subject of comparative magnetospheres to explore in terms of specific models some of the likely properties of the Saturnian magnetosphere. Each magnetosphere presently known has one or more distinguishing characteristics which set it apart from the others: at Mercury a small, quick, ionospherically-unrestrained magnetosphere; at Earth a compromise

magnetosphere, intermediate in almost all respects, and at Jupiter a rotation and, as now appears likely, satellite dominated magnetosphere. In the case of Saturn, unique characteristics can be expected to result from the presence of the rings which act as a particle absorption feature extending far into the magnetosphere, and from the presence of Titan with its relatively massive atmosphere and neutral particle torus acting as a strong ion source in the outer magnetosphere.

The principal results from the subject of comparative magnetospheres to be used here are taken from Kennel (1973) and Siscoe (1978a). Concerning the magnetospheres of Jupiter and Saturn specifically, the articles by Scarf (1973, 1975), Coroniti (1975), and Kennel and Coroniti (1975, 1978) should also be consulted. To go through our subject systematically, we consider separately the magnetospheric features and processes arising from the solar wind interaction, from the ionization of the planetary atmosphere and interstellar medium, and from the ionization of Titan's neutral particle torus (see Figure 1).

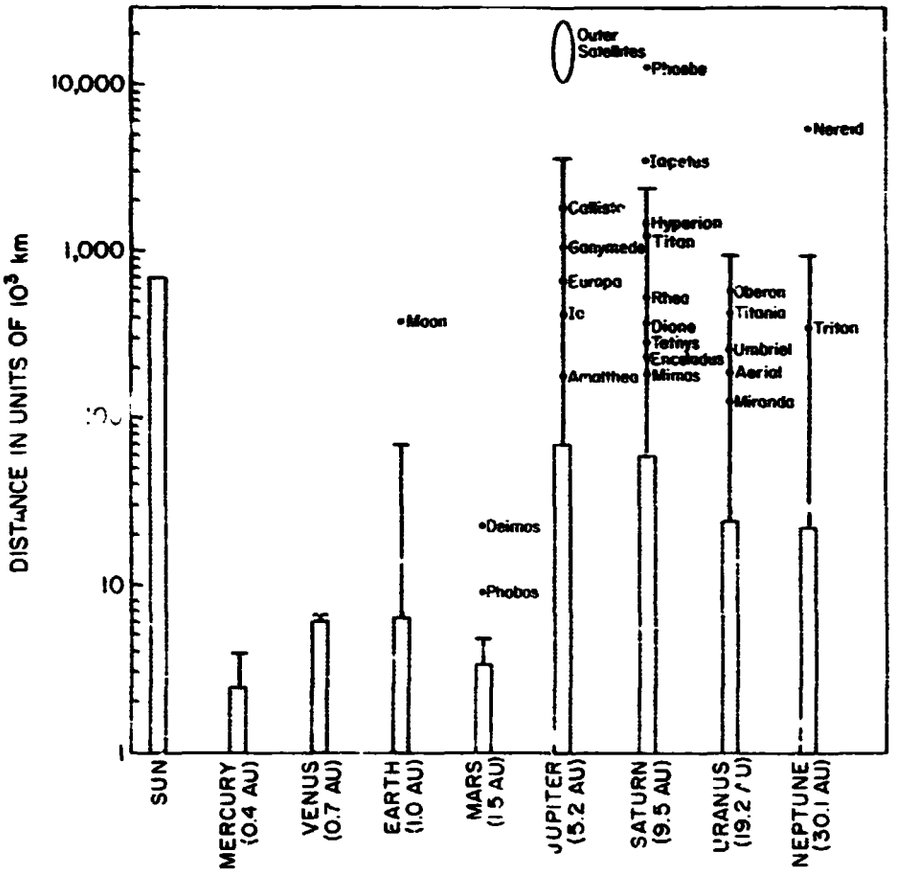

Figure 1. Scale sizes of the planets, their satellite systems and their magnetospheres as characterized by the distance from the planet's center to the subsolar stagnation point. Planetary and solar radii are indicated by the hatched bars and the magnetospheric dimensions by the T's. (From Siscoe, 1978a).

SOLAR WIND FEATURES AND PROCESSES

The solar wind boundary, or magnetopause, is the first item we will consider under this heading. The distance from the planet into the wind at which the shielding effect of the planetary magnetic field brings the solar wind to rest and causes the flow to be deflected in the manner of a flow past a blunt body is given in the case of Saturn, under the assumption of a pure dipole field and a vacuum magnetosphere, by

$$R_m = 34 \left(\frac{\langle nV^2 \rangle}{nV^2} \right)^{1/6} B_{ES}^{1/3} \text{ (gauss)} \qquad (1)$$

where R_m is in units of Saturnian radii, nV^2 is the product of solar-wind proton density and speed-squared at Saturn, expressed as in Figure 3 in terms of the ratio to the mean value 8×10^{13} $cm^{-1}s^{-2}$ extrapolated from measurements at 1 AU (Formisano *et al.*, 1974), and B_{ES} is the surface equatorial field strength in gauss. We assume here that the planetary field is a spin-aligned dipole (see Figure 2).

Arguments based on the absence of detectable Saturnian radio emissions at earth analogous to Jovian decimetric emissions (Scarf, 1973), on the detection of Saturnian magnetospheric radio bursts analogous to Jovian decametric bursts and geomagnetospheric kilometric bursts (Kaiser and Stone, 1975; Kennel and Maggs, 1976), and on an empirical planetary scaling relation (Kennel, 1973) suggest that B_{ES} lies in the range 0.5 to 2 gauss.

The solar wind quantity proportional to momentum flux, nV^2, varies in response to solar wind streams, which undergo appreciable nonlinear evolution between the orbit of Earth, where the characteristics of the flux are well known, and the orbit of Saturn, where the characteristics must be determined by nonlinear extrapolation from 1 AU. Such calculations have been performed by Hundhausen and Pizzo (private communication, 1976) and are shown in Figure 3. The effect of stream evolution is evident in the comparison of the histograms at 1 AU and 10 AU. At 1 AU the modal and average values are approximately equal whereas at 10 AU the modal value is considerably less than the average, and there is a compensating increase in the population of the high value tail. This change in the character of the histogram reflects the fact that at 10 AU the streams have evolved into narrow regions of high compression separated by wide regions of rarefaction. The magnetospheric consequence of this stream evolution is that compared to Earth the value of R_m for Saturn will be relatively more variable and values larger than average will occur relatively more frequently (see Smith *et al.*, 1978).

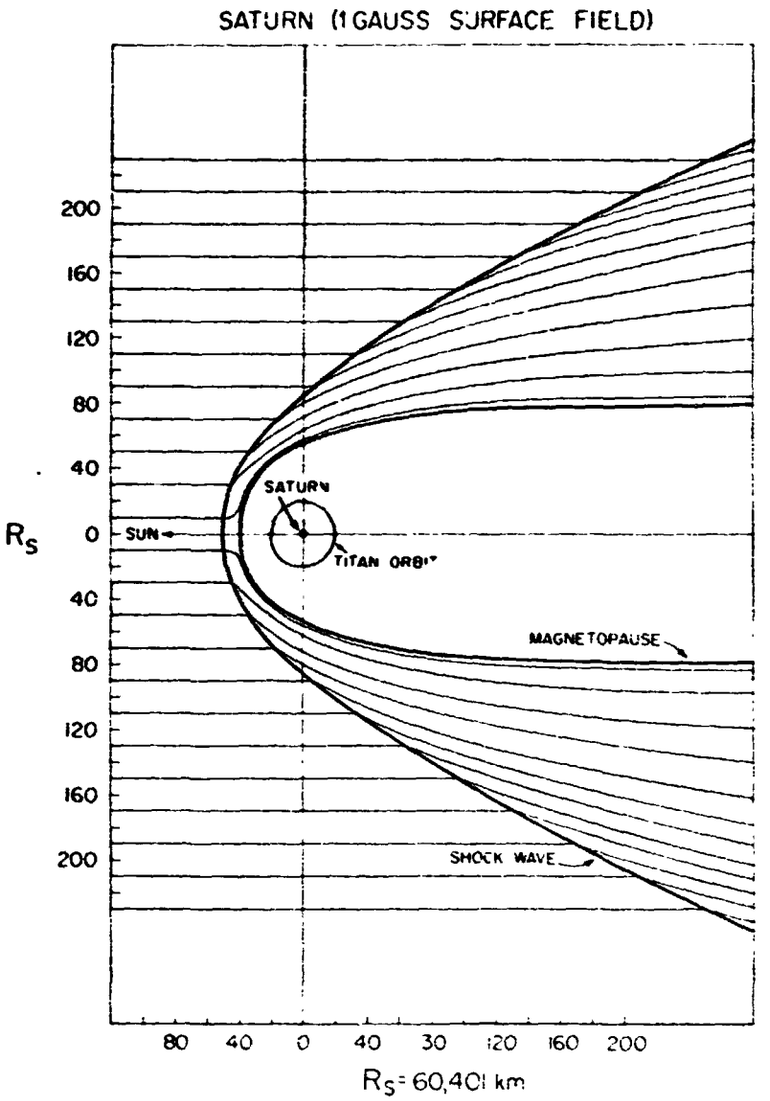

Figure 2. Schematic of the solar wind flow pattern past a hypothetical saturnian magnetosphere with an upstream dimension of 40 R_s (Saturnian radii)

The histogram in Figure 3 can be used in combination with equation (1) to determine probability distributions for the size of the Saturnian magnetosphere as measured by R_m and these are shown in Figure 4. We see from the figure that the probability that the subsolar magnetopause lie beyond the orbit of Titan is greater than 90% even for the case $B_{ES} = 0.5$ gauss. For the case $B_{ES} = 2$ gauss, there is a 50% probability that it will lie beyond twice the orbital distance of Titan.

The values of R_m determined from equation (1) are actually lower limits that would be revised upwards when the effects of interior plasma populations are considered. In the case of earth such revisions are relatively small, except possibly during geomagnetic storms, when the solar wind-derived interior plasma feature referred to as the ring current becomes important. In the case of Jupiter, interior plasma populations evidently dominate in providing the stagnation pressure at the subsolar magnetopause, creating in effect a magnetic dipole 2 to 3 times greater than that of Jupiter alone (Davis and Smith, 1976). As equation (1) shows, such an effective increase in B_{ES} would increase R_m by a factor of 1.3 to 1.4. The increased internal pressure might result simply from the addition of the static thermal and magnetic pressures of the resident, quasi-trapped charged particle populations, or from the dynamic pressure of a centrifugally driven, radially flowing magnetospheric wind (Coroniti and Kennel, 1977, and references therein). As we will see, in the case of Saturn, Titan might be the source of a major internal plasma feature with a magnetic moment exceeding that of Saturn. Thus, the actual size of Saturn's magnetosphere might be considerably larger than predicted on the bases of a vacuum interior.

We have dwelt at length on the magnetopause and what determines its size because of the importance of the answer to this question to later discussions. With regard to the remaining solar wind features and processes, it is both reasonable and expedient to adopt the philosophy first expressed by Scarf (1973 and also 1975). In all essentials that are likely to be important in determining magnetospheric features and processes, both in regard to solar wind parameters and planetary parameters, Jupiter and Saturn are very similar. To arrive at Saturn's magnetosphere then, we should start with Jupiter's magnetosphere and make appropriate adjustments. The Jovian magnetospheric tail is expected to be very long, perhaps 2 to 4 AU (Kennel and Coroniti, 1975, 1977), and the same expectation should apply to Saturn. The polar caps that map along field lines from the plane into the tail have angular radii

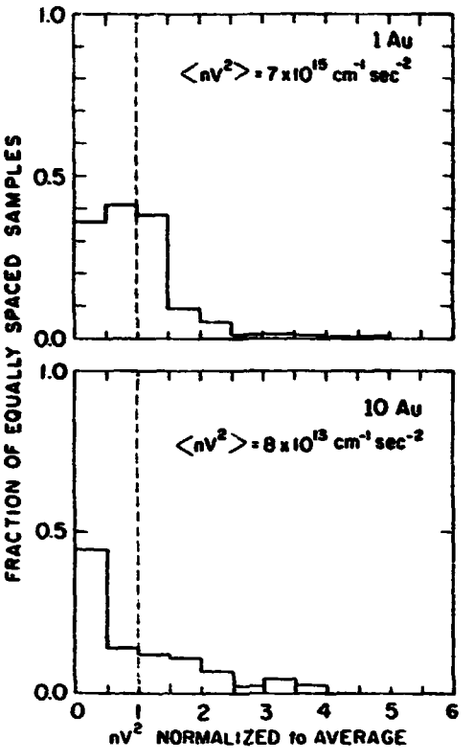

Figure 3. Histograms of the solar wind nv^2 as measured at 1 AU (top) and as computationally extended to 10 AU (bottom) (Hundhausen and Pizzo, 1976 personal communication). The averages at 1 AU have been set equal to those obtained by Formisano et al. (1974).

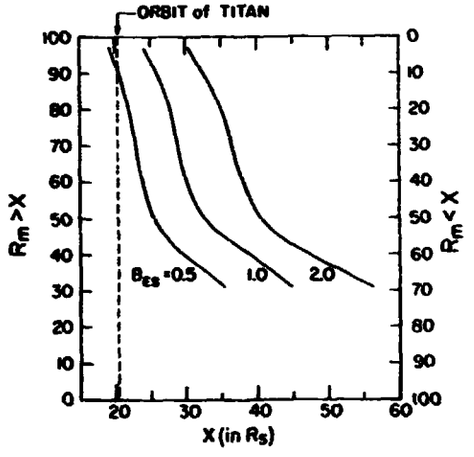

Figure 4. Probabilities relating to the location of the subsolar stagnation point of Saturn's magnetosphere based on the histogram of Figure 3 and the vacuum dipole scaling relations.

expressed in degrees measured from the magnetic poles of 10° for Jupiter and 11° for Saturn, compared to 20° for the case of Earth. The naive scale length that characterizes the extent of planetary control through the domination of corotation over solar wind-induced convection is 530 R_J for Jupiter and 320 R_S for Saturn, compared to 12 R_E for the case of Earth. This characteristic length is called naive because its computation ignores several complicating factors, all of which tend to reduce its size (Kennel and Coroniti, 1975; Chen and Siscoe, 1977). In the case of Earth, the actual size is closer to 5 R_E. We will assume in the following that the unknown reduction factor in the case of Saturn does not exceed an order of magnitude. This has the consequence that Titan lies in the corotation dominated portion of the magnetosphere.

With regard to the final solar wind-derived feature that we will consider, the trapped energetic particle radiation belts, the argument first advanced by Scarf (1973) would still seem to apply. Solar wind-derived particle intensities at Saturn should be less than at Jupiter at corresponding magnetospheric locations for two reasons. Compared to Jupiter, the magnetosphere of Saturn is expected to be smaller, and large particle intensities result essentially from compression through large volume ratios. The second, and probably more important reason is that compared to Jupiter, the rings of Saturn extend outward by more than a factor of two the inner absorption boundary to the inward diffusing particles. The effect of moving the absorbing boundary closer to the source is to reduce the intensities everywhere in between. However before this appealingly simple argument can be accepted, the effects of particle losses resulting from pitch angle scattering into the loss cone and from satellite sweep-up need still to be looked at. If electron intensities are set by the stably trapped limit determined by whistler mode turbulence, as appears to be the case at Jupiter between L = 6 and L = 20 (Coroniti, 1975), then at a fixed value of L, the intensity at Saturn should be about half that at Jupiter. In spite of prior expectations of larger effects, Pioneer 10 measurements revealed relatively small, factors of 2 to 5, reductions in particle intensities across the orbit of Io, and lesser reductions at the other satellites. Thus without going into the detailed calculations required for a definitive answer, the anticipation is that it would be surprising if the intensities at Saturn exceeded those at Jupiter at corresponding locations in the magnetospheres.

PLANETARY AND INTERSTELLAR PLASMASPHERES

Figure 5 shows schematically the local sources for internal magnetospheric plasma features that result from ionization of the planet's atmosphere, the interstellar medium passing through the magnetosphere, and the neutral particle torus and atmosphere of any satellite. We consider here the first two sources and treat the Titan-derived plasmasphere in a separate section.

In all three cases we are faced with a basic transport problem in which specification of the source characteristics, loss mechanisms, and mode of transport determine the density and kinetic properties of the plasma everywhere in the solution domain. As stated above, we assume initially at least that the magnetosphere is corotation dominated, which implies that the mode of transport is cross-L diffusion as opposed to convection or a centrifugally driven wind. The appropriate transport equation is for this case

$$\frac{d}{dL}\left[\frac{D_{LL}}{L^2}\frac{d}{dL}(L^2N)\right] + S - R = 0 \qquad (2)$$

where we assume steady state, NdL is the total number of ions in a flux shell of thickness dL, SdL and RdL are the source and loss rates in the same shell, and D_{LL} is the diffusion coefficient.

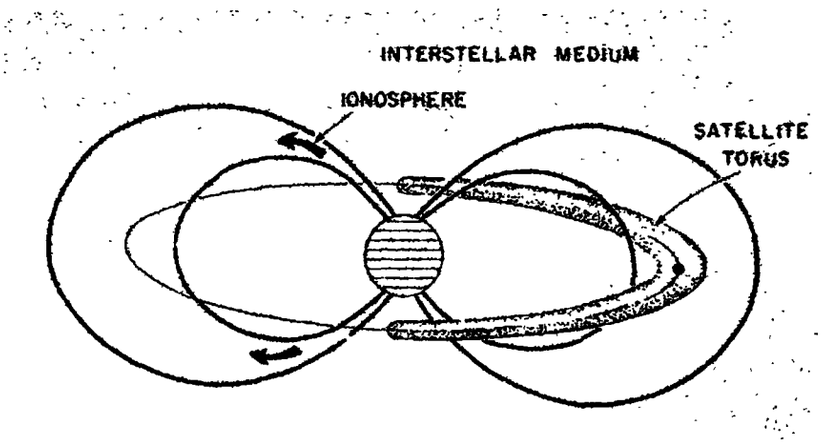

Figure 5. The three sources of plasmaspheres for the giant planets, ionization of the planets atmosphere, the local interstellar medium, and the neutral particle torii of any satellites.

Solutions of this equation appropriate to the planetary and interstellar plasmaspheres in the Jovian magnetosphere have already been presented (Siscoe, 1978a, b). The first reference also treats the Saturnian magnetosphere, but ignores the absorption of the particles by the rings. We refer the interested reader to these articles for a fuller discussion of the problem. A couple of points, however, should be repeated here. The boundary conditions are full absorption at inner and outer boundaries. The outer boundary is set at 30 R_S or 40 R_S. For the planetary plasmasphere there are two "opposite extreme" models. One, the maximum plasmasphere model, is based on the idea of complete magnetospheric trapping of the ionospheric photoelectron-plus-ion flux (Goertz, 1976). The other extreme allows a return flux to the ionosphere in the strong diffusion limit (that is it assumes an isotropic pitch angle distribution) and represents an application of the familiar idea of ambipolar diffusion (first applied to the Jovian magnetosphere by Ioannidis and Brice, 1971, and extended by Mendis and Axford, 1974). For the maximum planetary and interstellar plasmaspheres, the inner boundary to the cross-L diffusion domain is the outer edge of the rings, which is assumed to absorb and neutralize fully the inward diffusing flux. For the ambipolar plasmasphere, the inner boundary to the cross-L diffusion domain is marked simply by the transition to the ambipolar diffusion dominated domain. The cross-L diffusion coefficient, D_{LL}, is taken to be KL^3, with $K = 2 \times 10^{-10}$ s^{-1}, a theoretically based expression successfully used to interpret Jovian data. We apply it here to Saturn assuming similarity to the Jovian situation (justified more fully in Siscoe, 1978a). The source functions for the two types of plasmaspheres can be specified with little uncertainty. The only loss mechanism considered other than flux into the loss cone, included in the ambipolar model, is recombination, which for the problem in hand turns out to be negligible.

Figure 6 shows the characteristic shape of the ambipolar planetary plasmasphere for the giant planets (Ioannidis and Brice, 1971; Mendis and Axford, 1974; Scarf, 1973; Siscoe, 1978 a, b). The ambipolar diffusion and cross-L diffusion domains interface near L = 7, where a maximum density of roughly 20 cm^{-3} is achieved. The density decreases outward because of the absorption boundary at L = 40, and decreases inwards because of a field aligned flux into the atmosphere. If field aligned fluxes are prohibited, we arrive at the maximum planetary plasmasphere shown in Figure 7. In this case the density continues to increase inward, reaching roughly 500 cm^{-3} at $L \approx 3$ before dropping to zero at the contact with the rings.

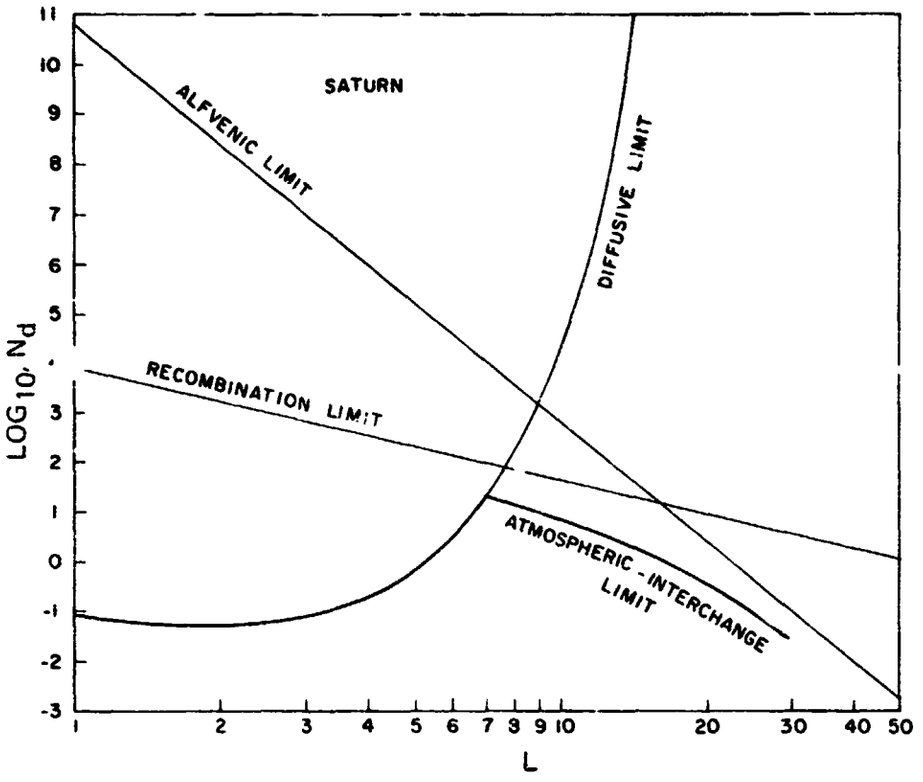

Figure 6. The planetary plasmasphere resulting from the combined effects of ambipolar and cross-L diffusion (See Sisco 1978a, b for details).

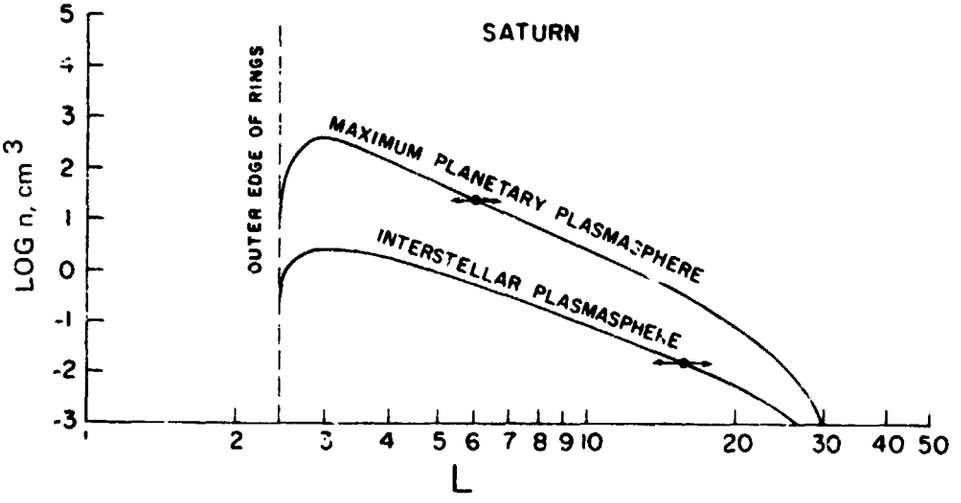

Figure 7. The planetary plasmasphere that results from complete trapping of the ionospheric flux coupled with cross-L diffusion. The interstellar plasmasphere based on a local interstellar hydrogen density of 0.1 cm^{-3} is also shown.

The back-to-back arrows mark the division between outward and inward diffusing fluxes. In this model, all of the photoelectron-plus-ion flux leaving the ionosphere between the latitudes corresponding to L = 2.3 (49°) and L = 3 (55°) diffuses into and is absorbed by the outer edge of the rings. This amounts to a maximum total flux of about 5×10^{26} s^{-1} for the planetary plasmasphere. The maximum energy of the inward diffusing ions at the ring contact is 11 M_i (eV) where M_i is the atomic mass of the ion in AMU. Most ions will arrive with lesser energy.

The calculated density for the interstellar plasmasphere is also shown in Figure 7. The actual plasmasphere resulting from this source will depend on the location of Saturn in its orbit relative to the asymmetric distribution of the interstellar neutral hydrogen around the solar system (Johnson, 1972). The profile shown corresponds to the maximum density encountered by Saturn, and assumes that the interstellar density, unaffected by the sun, is 0.1 cm^{-3}. The plasmasphere density reaches a maximum of roughly 2 cm^{-3} at $L \approx 3$. Since the plasma density is linearly proportional to the interstellar density at Saturn n_{Is}, we can say more generally that the maximum density is about 20 n_{Is}. Between L = 3 and 5 or 6, the density of the interstellar plasmasphere illustrated here exceeds that of the ambipolar plasmasphere. The inward diffusing flux that results from ionization of the interstellar neutral hydrogen between L = 2.3, the edge of the rings, and L = 15, the edge of the inward diffusion domain, is 2×10^{24} n_{Is} s^{-1} based on photoionization alone. The maximum energy of the particles comprising that flux at L = 2.3 is 36 keV. The flux at L = 2.3 for the illustrated case is 2×10^{23} s^{-1}, but we note that during encounters of the solar system with high density interstellar clouds, that flux can be greater by several orders of magnitude.

THE SATELLITE PLASMASPHERE

We come now to the plasmasphere derived from ionization of the neutral particle torus of Titan. Our purpose here is to determine the density, flux, and energy of such a plasmasphere assuming that Titan lies wholly in the corotation, cross-L diffusion dominated portion of the magnetosphere. The grounds for this assumption have been presented, but we must admit that the uncertainties of the matter are large enough that the applicability of the results based on the assumption are somewhat speculative.

We assume that the effective radius of the Titan torus is about 1 R_s (Fang *et al.*, 1976), and that the tilt angle between the dipole and rotational axes of Saturn is 10°. The satellite ion disc that then results from cross-L diffusion can be calculated (Siscoe, 1977) and it is shown in magnetic-meridian profile in Figure 8. The Titan-derived plasmasphere will under the stated conditions be confined to lie essentially within the indicated profile, except for violations of the first and second invariants by coulomb and wave scattering that occur during the diffusion process. Pitch angle scattering, which we ignore in the present treatment, will extend the boarders of the plasma disc to higher latitudes.

Consider first the plasma density at Titan's orbit, n_T. We assume the plasma to be derived from photoionization of the neutral hydrogen torus. The total ion production rate, F_T, is then N/τ_{ph} where N is the total number of hydrogen atoms in the torus and τ_{ph} the photoionization lifetime ($\sim 2 \times 10^8$ s). The total density N is related to the total neutral particle flux, F_{NT} which includes both H_2 and H (H_2 is assumed then to be dissociated in the ring) by

$$F_{NT} = \left(\frac{1}{\tau_{ph}} + \frac{1}{\tau_{ch}} \right) N \tag{2}$$

where τ_{ch} is the charge exchange lifetime ($= 1/V_T\, n_T\, \sigma_{ch}$, with $V_T = \Omega R_s L_T$ and $\sigma_{ch} = 1.6 \times 10^{-15}$ cm^2 the charge exchange cross section). Thus we find

$$F_T = \frac{F_{NT}}{1 + 7 n_T} \tag{3}$$

Now F_T and n_T are also related by the solution to the diffusion equation, namely by

$$n_T = \frac{F_T}{4\pi\theta R_s^3 K} \frac{\ln \dfrac{L_o}{L_T}}{\ln \dfrac{L_o}{L_r}} \frac{\ln \dfrac{L_T}{L_i}}{L_T^4} \tag{4}$$

where θ is the 10° magnetic tilt angle, L_o is the distance to the outer absorption boundary and is taken to be 30 R_s, $L_T = 20\ R_s$, and $L_i = 2.3\ R_s$ are the distances to the orbit of Titan and the outer edge of the rings respectively. Equations (3) and (4) give a quadratic equation for n_T in terms of F_{TN} and other known or assumed quantities. The solution is

$$n_T = \frac{\left(1 + 6.3 \times 10^{-25} F_{NT}\right)^{\frac{1}{2}} - 1}{14} \text{ cm}^{-3} \tag{5}$$

There is however an upper limit on n_T imposed by the constraint that the corotational kinetic energy density should not exceed the magnetic energy density, the so-called Alfvenic limit (Michel and Sturrock, 1974). This gives

$$n_T \leq 1.7\ B_{ES}^2 \text{ (gauss)} \tag{6}$$

Figure 9 shows n_T as a function of F_{NT} assuming a 1 gauss surface field. We see that for $F_{NT} \geq 10^{27}\ s^{-1}$, density is Alfven limited at the value of 1.7 cm^{-3}. Since fluxes larger than this are expected (e.g., Hunten, 1973a, b) the density at Titan for this case is in effect clamped at 1.7 cm^{-3}, and this fixes the interior solution.

Figure 10 shows the same effect for other surface field strengths. A 2 gauss surface field becomes Alfven limited at a flux of $10^{28}\ s^{-1}$ and a 3 gauss field at a flux of about $4 \times 10^{28}\ s^{-1}$.

Parameters for the Titan-derived plasmasphere normalized to the values at Titan's orbit are shown in Figure 11. The density peaks near L = 3 at a value ~200 n_T. The energy of all the particles at the inner boundary is about 150 keV. The particle intensity at the peak is close to 5×10^3 that at Titan. In the case of a 1 gauss surface field, the peak density is 340 cm^{-3} and the peak intensity is $2 \times 10^{11}\ cm^{-2}\ s^{-1}$ at an energy per particle greater than 100 keV.

The beta of the plasma, the ratio of thermal to magnetic energy density, is greater than 1 between L = 3.4 to L = 20. The high β condition which results from the fact that the density is Alfven limited at the source, alerts us to the possibility that the Titan-derived plasmasphere can have major effects on the magnetosphere. To make a quantitative evaluation of one such effect, we calculate the magnetic moment of the ring current associated with the plasmasphere, which turns out to be given approximately by

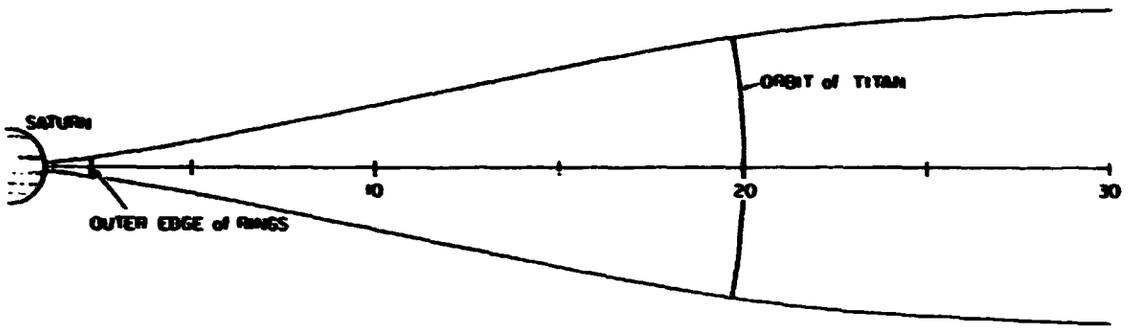

Figure 8. Meridian plane cross section through the confinement disc of a Titan-derived plasmasphere. The disc profile is based on the assumption of the neutral cloud being confined to within 10° of the magnetic equator of Saturn, and on the assumption of cross-L diffusion in the absence of pitch angle scattering (Sittler, 1977).

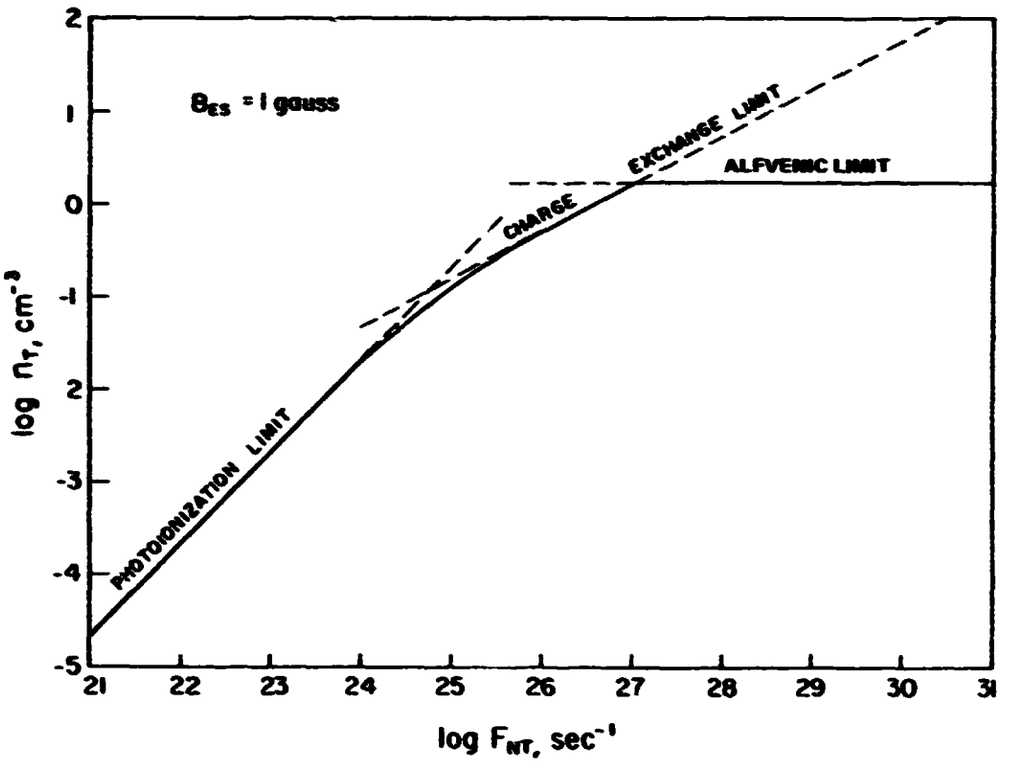

Figure 9. The proton number density at the orbit of Titan (n_T) as a function of the total (net) loss rate of H and H_2 from Titan. The mass-loading or Alfvenic limit is based on a surface equatorial magnetic field of 1 gauss at Saturn.

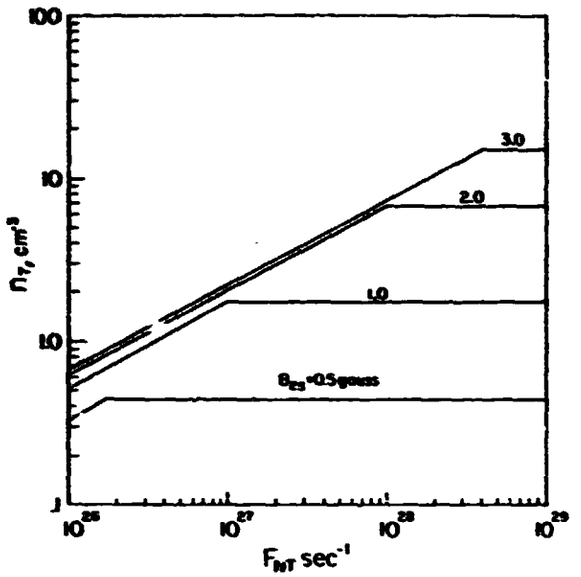

Figure 10. Same as Figure 9 but with different assumed strengths of the surface equatorial magnetic field.

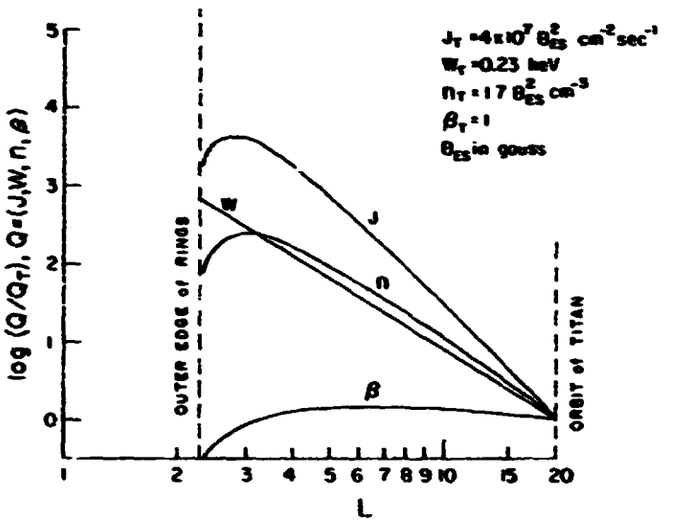

Figure 11. Parameters of the Titan-derived plasmasphere in the region between the outer edge of the rings and Titan's orbit. Values are normalized to Titan's orbit, which are given explicitly. J is the proton intensity, W is the proton kinetic energy, n is the proton number density, and β is the ratio of proton kinetic energy density to magnetic energy density.

$$M_R = \frac{1}{3.5} \frac{H_T}{R_s} M_s \qquad (7)$$

where H_T is the thickness of the disc at L_T and M_s is the Saturnian magnetic moment. If we continue to assume by analogy with the tilt angles for Mercury, Earth and Jupiter that $\theta \approx 10^\circ$, then $M_R \approx 2\ M_s$.

Now since the density at Titan is Alfven limited, or so it seems, the field at Titan now determined by the sum of M_s and M_R, will be larger, which corresponds to a higher density limit, by equation (6), which in turn leads to a higher value for M_R. When this feedback mechanism is considered explicitly, we find that if the proportionality factor in equation (7) is greater than about 1/2, the solution is unstable. That is, each increases in M_R brings in more particles which then produce an even greater increase in M_R. The result is that the magnetosphere either reaches a non-linear saturation, or the increase in M_R reaches a point where the density at Titan is no longer Alfven limited. As shown in Figure 12, which gives the dependence of n_T on B_{ES} (or in the present application on $M_s + M_R$) for given and fixed values of F_{NT}, once the field rises to the point where n_T leaves the Alfven limit curves, further increases in the field produce only small increases in n_T.

In conclusion if Titan lies in the corotation, cross-L diffusion dominated portion of the magnetosphere, it should cause the magnetosphere to become grossly inflated by the production of a massive, self-limiting plasmasphere. In effect in this model Titan blows up the Saturnian magnetosphere in a way that is unique in the solar system.

CONSEQUENCES FOR SATURN'S RINGS

Cheng and Lanzerotti (1978) have drawn attention to possibly interesting magnetospheric consequences for Saturn's rings. They invoke recently measured ice sputtering rates (Brown *et al.*, 1978) and energetic particle intensities scaled from Jupiter to infer a net rate of erosion of the outer edge of the rings of 10^{-6} cm year^{-1}. We note here that the ion flux from Titan can considerably increase this rate.

The inward flux from Titan in the Alfvenic limit is $1.2 \times 10^{25} (B^*_{ES})^2\ s^{-1}$, where B^*_{ES} is the effective equatorial surface field which takes into account the magnetic moment of the plasmasphere. In light of the previous discussion, a flux range

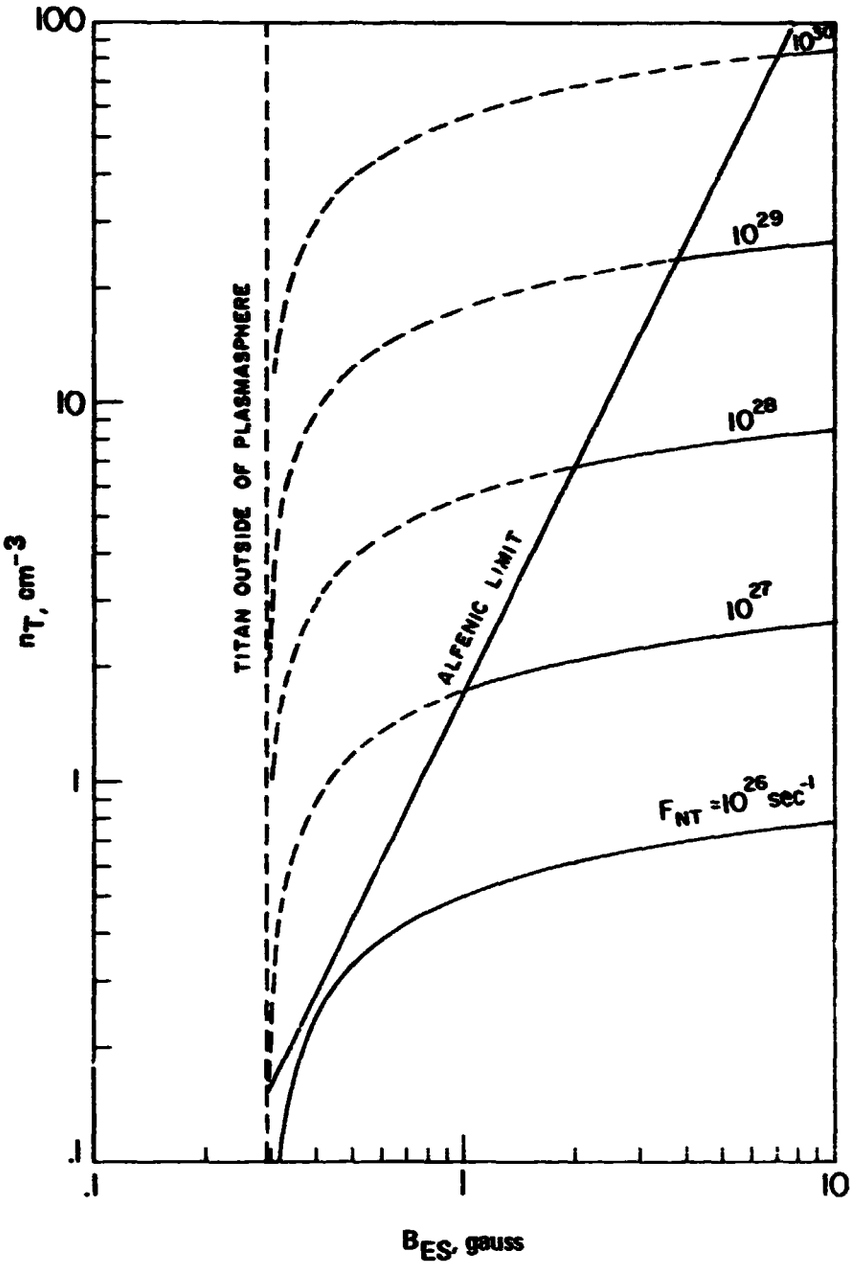

Figure 12. Proton number density at Titan's orbit (n_T) as a function of the (equivalent) strength of the surface equatorial magnetic field at Saturn (B_{ES}) for various assumed loss rates of H_2 and H from Titan (F_{NT}).

of 10^{25} to 10^{26} s^{-1} might reasonably be expected to result from a fully magnetospherically engaged, Titan-derived plasmasphere. At a particle energy of 150 keV, a sputtering efficiency of 0.5 is given, and thus a molecular erosion rate of 5×10^{24} to 5×10^{25} s^{-1} is here inferred to result from the absorption of the inward diffusing Titan-ion flux by the outer edge of the ring. If we assume a molecular density equivalent to a uniform disc of water ice with a thickness of 10 cm, we find an erosion rate between 5×10^{-3} to 5×10^{-2} cm yr^{-1}.

REFERENCES

Brown, W. L., Lanzerotti, L. J., Poate, J. M., and Augustyniak, W. M. (1978). "Sputtering" of ice by MeV light ions. Bell Laboratories. Preprint, Jan. 1978.

Chen, C. -K., and Siscoe, G. L. (1977). A method for finding plasmasphere statistics from solar wind measurements. *J. Geophys. Res. 82*, 1158–1162.

Cheng, A. F., and Lanzerotti, L. J. (1978). Ice sputtering by radiation belt protons and the rings of Saturn and Uranus. Submitted to *J. Geophys. Res.*

Coroniti, F. V. (1975). Dénouement of Jovian radiation belt theory. In *The Magnetospheres of the Earth and Jupiter* (V. Formisano, ed.), pp. 391–410. D. Reidel Publishing Co., Boston, MA.

Coroniti, F. V., and Kennel, C. F. (1977). Possible origins of time variability in Jupiter's outer magnetosphere 1, Variations in solar wind dynamic pressure. *Geophys. Res. Lett. 4*, 211–214.

Davis, L., Jr., and Smith, E. J. (1976). The Jovian magnetosphere and magnetopause. In *Magnetospheric Particles and Fields* (B. M. McCormac, ed.), pp. 301–310. D. Reidel Publishing Co., Boston, MA.

Fang, T. M., Smyth, W. H., and McElroy, M. B. (1976). The spatial distribution of long lived gas clouds emitted by satellites in the outer solar system. *Planet. Space Sci. 24*, 577–588.

Formisano, V., Moreno, G., and Amata, E., (1974). Relationships among the interplanetary plasma parameters: Heos 1, December 1968 to December 1969. *J. Geophys Res. 79*, 5109–5117.

Goertz, C. K. (1976). Plasma in the Jovian magnetosphere. *J. Geophys. Res. 81*, 2007–2014.

Hunten, D. M. (1973a). Blowoff and escape of H_2. In *The Atmosphere of Titan* (D. M. Hunten, ed.), pp. 110–117. NASA SP-340.

Hunten, D. M. (1973b). The escape of H_2 from Titan. *J. Atmos. Sci. 30*, 726–732.

Ioannidis, G., and Brice, N. M. (1971). Plasma densities in the Jovian magnetosphere. Plasma slingshot or Maxwell demon? *Icarus 14*, 360–373.

Johnson, H. E. (1972). Backscatter of solar resonance radiation-I. *Planet Space Sci. 20*. 829–840

Kaiser, M. L., and Stone, R. G. (1975) Earth as an intense planetary radio source: Similarities to Jupiter and Saturn. *Science 189*, 285–287.

Kennel, C. F. (1973). Magnetospheres of the planets. *Space Sci. Rev. 14*, 511–533.

Kennel, C. F., and Coroniti, F. V. (1975). Is Jupiter's magnetosphere like a pulsars on Earth's? In *The Magnetospheres of Earth and Jupiter* (V. Formisano, ed.), pp. 451–477. D. Reidel Publishing Co., Boston, MA.

Kennel, C. F., and Maggs, J. E. (1976). Possibility of detecting magnetospheric radio bursts from Uranus and Neptune. *Nature 261*. 299–301.

Kennel, C. F. and Coroniti, F. V. (1977). Possible origins of time variability in Jupiter's outer magnetosphere, 2, Variations in solar wind magnetic field. *Geophys. Res Lett. 4*, 215–218.

Kennel, C. F., and Coroniti, F. V. (1978). Jupiter's magnetosphere. In *Solar System Plasma Physics—A Twentieth Anniversary Review* (C. F. Kennel, L. J. Lanzerotti, and E. N. Parker, eds.), North Holland Publishing Co.,

Mendis, D. A., and Axford, W. I. (1974) Satellite and magnetospheres of the outer planets. *Ann. Rev. Earth Planet Sci. 2*, 419–474.

Michel, F. C , and Sturrock, P. A. (1974). Centrifugal instability of the Jovian magnetosphere and its interaction with the solar wind. *Planet Space Sci. 22*. 1501–1510

Scarf. F. L. (1973). Some comments on the magnetosphere and plasma environment of Saturn. *Cosmic Electrodynamics 3*, 437–447.

Scarf, F. L. (1975). The magnetospheres of Jupiter and Saturn. In *The Magnetospheres of the Earth and Jupiter* (V. Formisano, ed.), pp. 433–449. D. Reidel Publishing Co , Boston, MA.

Smith, E. J., Fillius, R W., and Wolfe, J. H. (1978). Compression of Jupiter's magnetosphere by the solar wind. Submitted to *J. Geophys. Res.*

Siscoe, G. L. (1977). On the equatorial confinement and velocity space distribution of satellite ions in Jupiter's magnetosphere. *J. Geophys. Res. 82*, 1641–1645

Siscoe, G. L. (1978d). Towards a comparative theory of magnetospheres In *Solar System Plasma Physics—A Twentieth Anniversary Review* (C. F. Kennel, L. J. Lanzerotti, and E. N. Parker, eds.), North Holland Publishing Co.,

Siscoe, G. L. (1978b) Jovian plasmaspheres *J Geophys. Res.* In press.

DISCUSSION

D. CRUIKSHANK: The idea of sputtering from the edge of the rings is interesting. I wonder if you might not be sputtering water off the inner satellites and depositing it on the rings?

G. SISCOE: Yes, that's one of the calculations that should also be done. The satellites are going to be absorbing this inward flux just as the rings are. Current estimates suggest that the satellites will not absorb a significant fraction of the flux, that the rings are still going to get most of it. But from the point of view of the satellites, they're still absorbing their full complement. I would guess an absorption rate of perhaps 10 molecules per square centimeter per second.

S. CHANG: If Titan is inside Saturn's magnetosphere, what would be the flux of the particles into the atmosphere of Titan?

G. SISCOE: That would be just the product of the density (1.7 particles per cm^3) and the velocity (200 km s^{-1}).

B. SMITH: If the E Ring actually exists and extends out perhaps as far as 20 Saturnian radii, essentially out to the orbit of Titan, then it represents an important absorption surface. If the particles are oscillating back and forth across the ring plane with a period of a few seconds, and the E Ring has an optical thickness of the order 10^{-6}, then there's a depletion time constant of the order of months. The question is: Does the inward diffusion swamp that or will there be an appreciable effect on the distribution of particles?

G. SISCOE: It's comparable. If the actual time scale for depletion is of the order of months, there might be a significant effect.

B. SMITH: In that case, measurement of the particle flux as a function of the distance from Saturn would present an excellent way of mapping out this medium which is too thin to be seen optically.

E. STONE: What is the possibility that if Titan is such a pro[illegible] producer of plasma, then the magnetic field just cannot retain the plasma at all, and one has essentially a wind blowing?

G. SISCOE: That is a necessary consequence of the model I just presented. There would be a Titan wind of more than 10^{26} particles per second going out. You need a band with a thickness of about a thousand kilometers to carry that wind. It's not a big feature.

J. WARWICK: Do you have any comments on possible effects at Saturn analogous to those due to Io's interaction with Jupiter's magnetosphere, either from the rings or interior satellites or Titan?

G. SISCOE: The potential difference across Titan is about 10 kilovolts, which is probably not enough. The potential difference across the Earth's ionosphere is about 50 kilovolts and that does all kinds of interesting things. So my guess is that there probably is an electrodynamic coupling having some small effects, but nothing comparable to Io.

D. HUNTEN: All this work assumed that everything that gets emitted from Titan is quickly ionized, isn't that right?

G. SISCOE: It assumes that the mechanism of particle loss is through ionization. A neutral density will build up to the point where the ionization rate balances the loss rate. The amount of neutral hydrogen in the torus should build up to something like 10^{35} particles.

VOYAGER INVESTIGATIONS OF THE SATURNIAN SYSTEM

E. C. Stone*

California Institute of Technology
Pasadena, California 91125

ABSTRACT

This paper provides a brief review of the objectives and capabilities of the Voyager Mission at Saturn. In addition to a brief description of the eleven Voyager Investigations and the Saturn encounter geometry, the scientific capabilities are discussed in the areas of Atmospheric, Satellite, Magnetospheric, and Ring studies.

INTRODUCTION

In 1977 two Voyager spacecraft were launched toward encounters with Jupiter, Saturn, and possibly Uranus. In this paper the eleven scientific investigations and the encounter geometry at Saturn will first be briefly reviewed, followed by a discussion of the planned studies of the Saturnian system. This discussion, which will be organized into the four broad categories of Atmospheres, Satellites, Magnetosphere, and Rings, will necessarily be preliminary, since design of the sequence of observations will not begin until 1979. More detailed information on the mission and each of the eleven investigations is available in two special issues of *Space Science Reviews* (Stone, 1977).

*Voyager Project Scientist

INVESTIGATIONS

The eleven investigations and the corresponding Principal Investigators and Team Leaders are listed in Table 1. Although not shown, a total of ~100 scientific investigators from 38 institutions are involved in the Voyager mission. A brief summary of the nominal characteristics of the instruments is contained in Table 2, while Figure 1 illustrates their location on the Voyager spacecraft. The four boresighted remote sensing instruments (ISS, IRIS, PPS, and UVS) share the scan platform which has two axes of articulation for nearly complete angular coverage.

ENCOUNTER CHARACTERISTICS

The heliocentric trajectories of the Voyager spacecraft are illustrated in Figure 2, and details of the Saturn encounters are summarized in Table 3.

Table 1. Voyager Science Investigations

Investigation Area	Principal Investigator/Institution
Imaging Science (ISS)	Smith/Univ. Arizona (Team Leader)
Infrared Spectroscopy and Radiometry (IRIS)	Hanel/GSFC
Photopolarimetry (PPS)	Lillie/Univ. Colorado
Ultraviolet Spectroscopy (UVS)	Broadfoot/KPNO
Radio Science (RSS)	Eshleman/Stanford Univ. (Team Leader)
Magnetic Fields (MAG)	Ness/GSFC
Plasma (PLS)	Bridge/MIT
Plasma Wave (PWS)	Scarf/TRW
Planetary Radio Astronomy (PRA)	Warwick/Univ. Colorado
Low Energy Charged Particles (LECP)	Krimigis/JHU/APL
Cosmic Rays (CRS)	Vogt/Caltech

Table 2. Instrument Characteristics

Investigation	Nominal Characteristics
ISS	Two Se-S vidicon cameras (f = 1500 mm and f = 200 mm); Narrow angle camera: 19 μrad/line pair, 2900 - 6400 Å
IRIS	Michelson interferometer (3.3 - 50 μm) and radiometer (0.33 - 2 μm); 51 cm telescope; 0.25° FOV
PPS	Photomultiplier with 15 cm telescope; 2350 - 7500 Å; 3.5°, 1°, 1/4°, 1/16°, FOV; 3 linear polarizers
UVS	Grating spectrometer; 500 - 1700 Å with 10 Å resolution; airglow (1° × 0.1° FOV) and occultation (1° × 0.3° FOV)
RSS	S-Band (2.3 GHz) and X-band (8.4 GHz); Ultra Stable Oscillator ($<4 \times 10^{-12}$ short term drift)
MAG	Two low field ($<10^{-6}$ - 0.5 G) and two high field (5×10^{-4} - 20 G) magnetometers; 13 m boom; 0 - 16.7 Hz
PLS	Earth-pointing sensor (10 eV - 6 keV ions) and lateral sensor (10 eV - 6 keV ions, 4 eV - 6 keV electrons)
PWS	Sixteen channels (10 Hz - 56.2 kHz); waveform analyzer (150 Hz - 10 kHz); share PRA antennas
PRA	Stepping receiver (1.2 kHz and 20.4 kHz - 40.5 MHz); right and left circular polarization; orthogonal 10 m monopole antennas
LECP	Two solid state detector systems on rotating platform; 10 keV - 10 MeV electrons; 10 keV/nuc - 150 Mev/nuc ions
CRS	Multiple solid state detector telescopes; 3 - 110 MeV electrons; ~1 - 500 MeV/nuc nuclei; 3-dimensional anisotropies

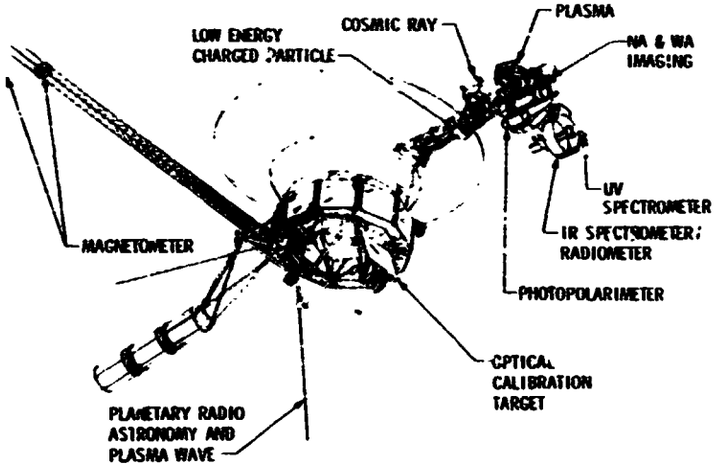

Figure 1. A drawing of the Voyager spacecraft showing the location of the science instruments. The Radio Science Investigation uses the dual-frequency spacecraft transmitters, an Ultra Stable Oscillator, and the 12' parabolic antenna.

The trajectory of the first-arriving spacecraft at Saturn is labeled JST (Jupiter-Saturn-Titan) because the trajectory includes a close encounter with Titan. Since the second arriving spacecraft can be targeted to either the Uranus aim point at Saturn or to a close Titan flyby, the trajectory is referred to as JSX. Figure 2 illustrates both the Uranus option (X=U) and the Titan option (X=TB).

The targeting of JSX will affect the nature of the investigations possible at Saturn. As shown in Table 3, for example, the JSX(X=U) trajectory does not have an

Table 3. Saturn Encounters

		JST	JSX(X=U)	JSX(X=T)
Date, Closest Approach		11/12/80	8/26/81	8/27/81
Radius, Closest Approach		3.0 R_S	2.7 R_S	3.4 R_S
Radius, Ring Plane Crossing		19.6 R_S 6.2 R_S	2.9 R_S	19.6 R_S 5.7 R_S
Distance (10^3 km), Earth Occultation	Saturn	230	156	218
	Rings	~250	-	~200
	Titan	29	-	23
Distance (10^3 km), Sun Occultation	Saturn	235	158	219
	Rings (A, B)	~300	-	~190
	Titan	24	-	25

occultation of the sun and Earth by either the Rings or Titan. Thus, the Uranus option will be selected only if JST accomplishes the major scientific objectives at Saturn, Titan, and the Rings, and only if the Voyager 2 spacecraft appears healthy enough to be sent on an additional 4-year mission to Uranus. The geometries of the JST and JSX(X=U) flybys is illustrated in Figures 3 and 4.

ATMOSPHERIC STUDIES

There are several interrelated aspects of the Saturnian and Titanian atmospheres which will be studied by Voyager, including dynamics, structure, and composition. Some of the general characteristics of these studies will be discussed below, with subsequent papers by B. A. Smith, R. A. Hanel, and G. L. Tyler providing more specific details for the Imaging, Infrared, and Radio Science investigations.

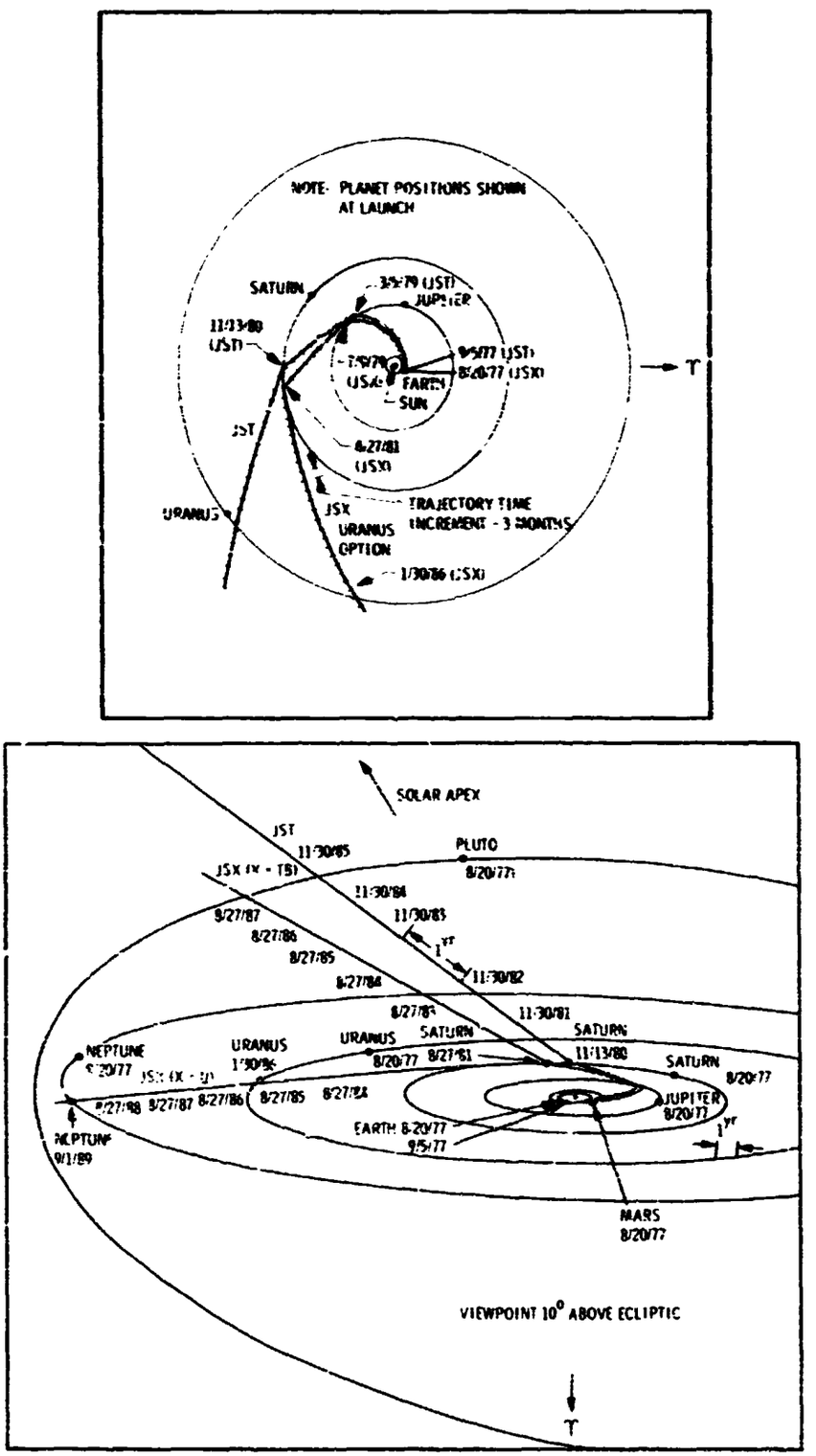

Figure 2. Heliocentric views of the Voyager trajectories.

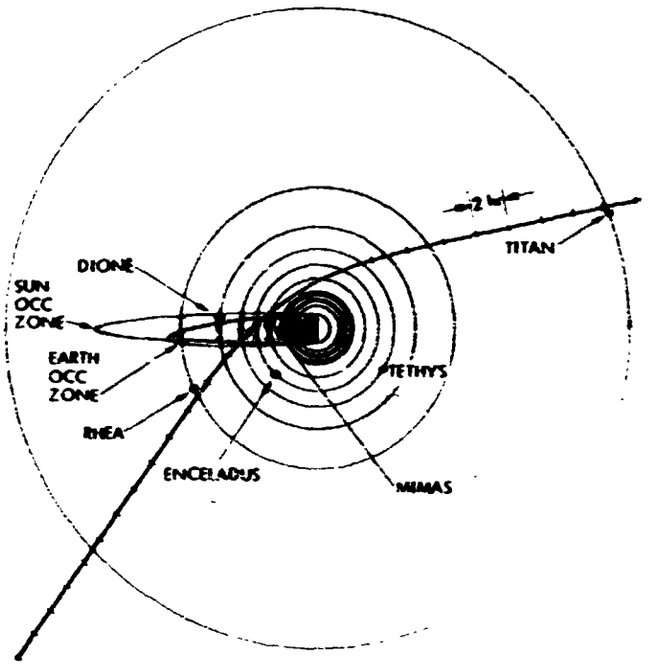

Figure 3. A view normal to the Saturnian equatorial plane of the JST encounter on November 12, 1980. The satellite positions are shown at satellite closest approach.

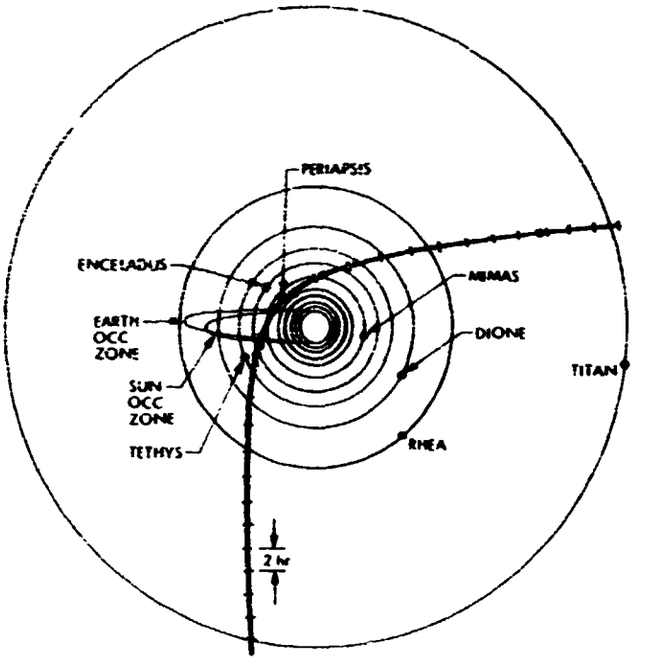

Figure 4. A view normal to the Saturnian equatorial plane of the JSX(X=U) encounter on August 27, 1981. The satellite positions are shown at satellite closest approach.

Since the study of atmospheric dynamics requires observations over an extended period of time, one of the key factors is the observing time available at a specified spatial resolution. Figure 5 illustrates the observing time as a function of resolution at Saturn for the narrow angle (NA) camera and the 1/4° field-of-view (FOV) of IRIS and PPS. Since even a very good resolution of 1" from the ground corresponds to ~7000 km at Saturn, the Imaging System will have significantly better resolution than ground-based telescopes throughout the 80 days (~2000 hr) prior to encounter, and there will be 30 hours during which IRIS and PPS will have resolution better than ~7000 km.

Latitude coverage is also important to a study of the atmosphere on a global scale. In fact, in a previous paper Tokunaga reported evidence that the temperature inversion is hotter in the South polar region than at the equator. As shown in Figure 6, the spacecraft latitude of the two Voyager flybys ranges from approximately -40° to +30°, providing useful coverage of higher latitudes in both hemispheres.

Studies of atmospheric structure require detailed observations of the pressure-temperature profile. The expected capability of the Voyager investigations is shown in Figure 7 which has been adapted from the Voyager Atmospheres Working Group Report. The figure indicates both the pressure range over which a given technique is expected to be useful and the expected scale height resolution of the measurement. The RSS measurement employs the dual-frequency radio occultation, while the IRIS measurement uses the pressure-broadened H_2 band at 250 to 500 cm^{-1} and the CH_4 band at 1306 cm^{-1} as temperature sounders. The UVS measurement in the upper atmosphere is a solar occultation measurement which should provide an altitude profile for H_2, CH_4, C_2H_6, and C_2H_2 absorption. Stellar occultations and terminator scans with PPS will also contribute to the determination of the pressure-temperature profile.

The same techniques will be applied in the study of Titan's atmosphere. Both R. A. Hanel and G. L. Tyler will report in subsequent papers on recent analyses of the expected capability at Titan.

SATELLITE STUDIES

A characterization of the surfaces of the satellites will be accomplished with a combination of high-resolution imaging, infrared spectral studies, and polarimetric

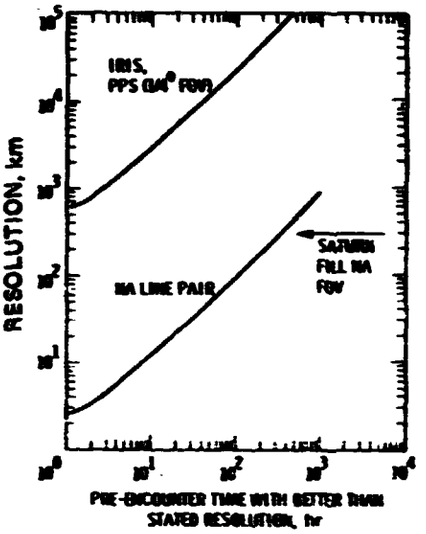

Figure 5. The length of time during which spatial resolution of Saturn's atmosphere exceeds a given value.

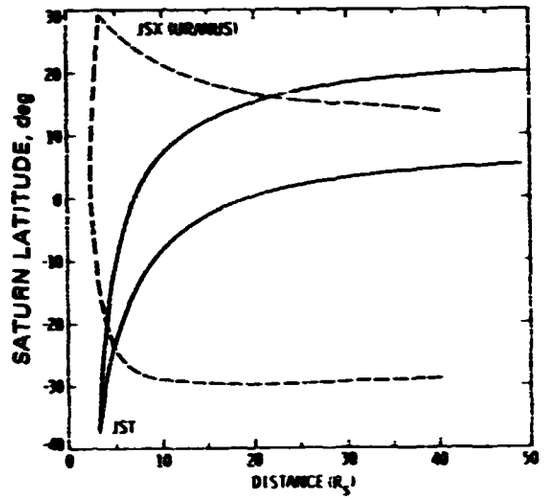

Figure 6. The subspacecraft latitude for the Voyager trajectories as a function of radial distance. For reference, note that $1R_S$ = 60000 km.

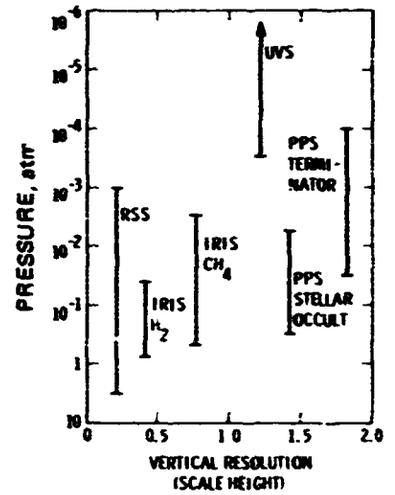

Figure 7. The vertical resolution and pressure range over which various techniques will yield information on the temperature-pressure profile in Saturn's atmosphere. This figure is adapted from the Voyager Atmospheres Working Group Report.

studies over a wide range of phase angles. The closest approach distances to the various satellites are indicated in Table 4 for all three possible trajectories.

Imaging resolution of the satellites SI through SVI will be significantly better than the 5 km/line pair resolution which is characteristic of the well-known mosaics of the half-lit disk of Mercury obtained by Mariner 10.

The densities of the satellites is also an important characteristic which will be studied by combining mass determinations from precise radio-navigation techniques with size determinations from the Imaging System. Figure 8, which is adapted from Fehleman *et al.* (1977), illustrates the expected capability. The uncertainty in the mass estimates is indicated by the labels on the diagonal solid lines, while the uncertainty in the volume estimates are indicated by the dashed lines. For this estimate, it has been assumed that the best estimate of the volume is uncertain to 0.4%, corresponding to a 1 pixel uncertainty in the diameter of a satellite image which fills the narrow-angle camera field-of-view. Thus, the mass of Titan (S6) will be determined to $\leq 0.02\%$, but

Table 4. Satellite Encounters

	Satellite	Closest Approach* (10^3 km)		
		JST	JSX(X=U)	JSX(X=TB)
SI	Mimas	89	315	116
SII	Enceladus	200	86	102
SIII	Tethys	416	92	150
SIV	Dione	163	503	91
SV	Rhea	74	648	199
SVI	Titan	7	667	15
SVII	Hyperion	884	480	869
SVIII	Iapetus	2400	918	1000
SIX	Phoebe	13500		7500

*Narrow angle camera resolution is 2 km/line pair at 100000 km.

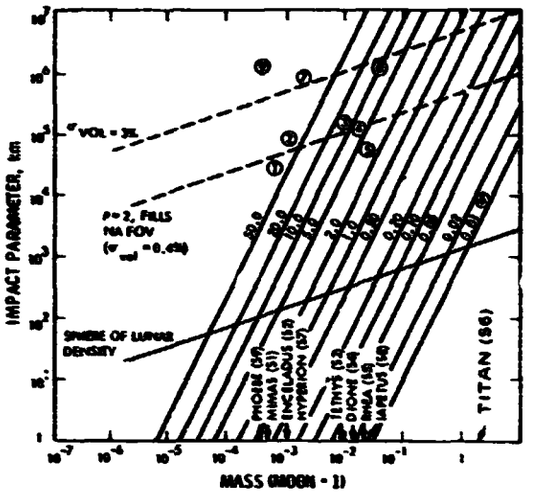

Figure 8. The percent error in mass and volume as a function of flyby distance and satellite mass. The diagonal solid lines are labeled with the mass uncertainties for a flyby velocity of 20km/sec, while the dashed lines indicate the volume uncertainty corresponding to 1 pixel in the narrow angle camera. Adapted from Eshleman et al., (1977).

the density will be uncertain to ~0.4%. For all other satellites, the density uncertainty will be dominated by the mass uncertainty which ranges from ~3% to ~15% for Rhea (S5), Dione (S4), Iapetus (S3), and Tethys (S3), and is >50% for all the others.

The interaction of the satellites with the magnetosphere is also an important objective which will be best studied during the close Titan flyby (7000 km) illustrated in Figure 9. The close flyby not only improves the detectability of any magnetic field at Titan, but also maximizes the probability that the spacecraft will intercept any magnetospheric wake, whether due to the corotation of the magnetosphere or due to a radial outstreaming (planetary wind).

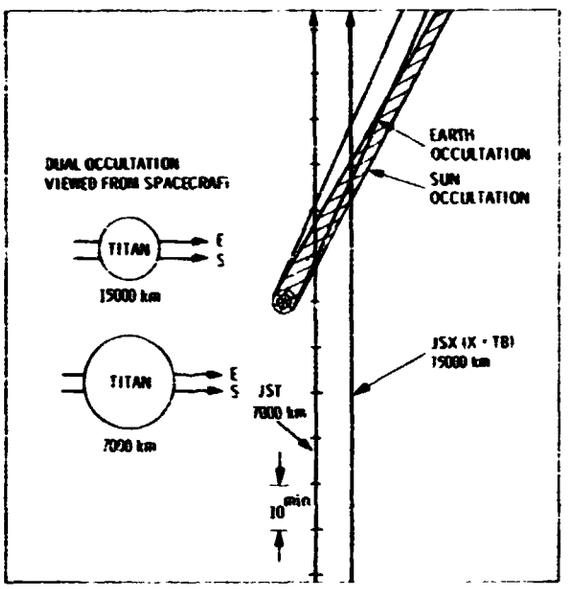

Figure 9. A view normal to Titan's orbital plane of the Voyager encounter. The JST encounter will be at 7000 km, while the JSX (X=TB) is nominally at 15000 km.

MAGNETOSPHERIC STUDIES

In addition to studying the interaction at Titan, Voyager will perform detailed measurements of the Saturnian magnetosphere, the evidence for which has been discussed by J. W. Warwick in a preceding paper. The spatial coverage of a possible magnetosphere is illustrated in Figure 10 which has been adapted from Scarf and Gurnett (1977). As indicated in the figure, the local times of the exit legs of JST and JSX(X=U) are quite different. Although not indicated, the latitudes of the exit legs are also quite different, with JST exiting at approximately +20° and JSX(X=U) at -30° (see Figure 6). Thus, JST and JSX(X=U) provide important complementary coverage of the magnetosphere.

The Voyager investigations provide broad coverage of the particle and wave phenomena expected at Saturn. Figures 11 and 12 from the Voyager Magnetospheres Working Group Report summarize the coverage. Note that the PRA frequency range includes the 300 kHz to 1 MHz interval in which Saturn signals have been detected by Brown (1975) and the PWS range includes the electron and ion plasmic and cyclotron frequencies expected at Saturn (Scarf and Gurnett, 1977).

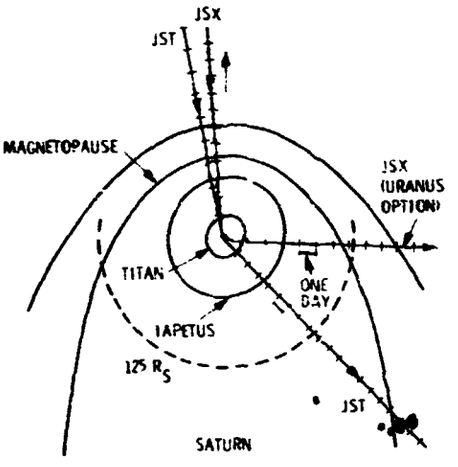

Figure 10. A view normal to Saturn's equatorial plane of the Voyager trajectories through a possible magnetosphere. Adapted from Scarf and Gurnett (1977).

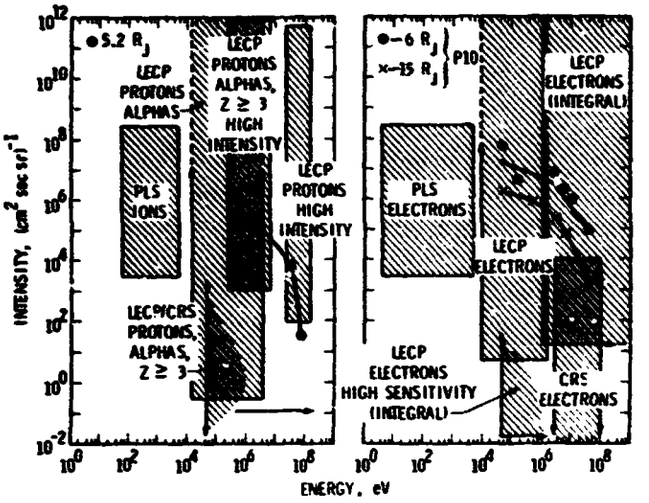

Figure 11. The intensity and energy coverage of electrons and ions by the Voyager instruments. The data points indicate the intensities observed by Pioneer 10 at Jupiter. This figure is from the Voyager Magnetospheres Working Group Report.

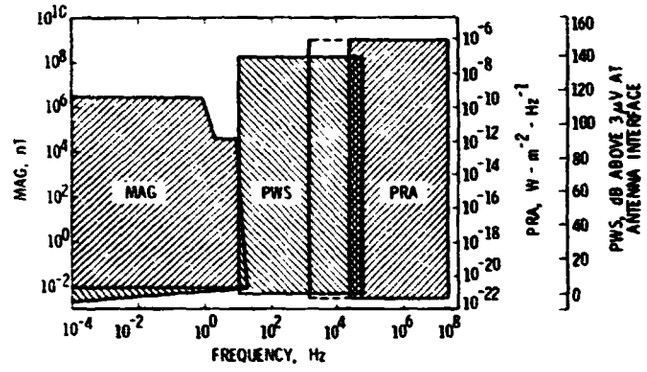

Figure 12. The frequency and intensity coverage of waves by the Voyager instruments. Adapted from the Voyager Magnetospheres Working Group Report.

RING STUDIES

The study of Saturn's Rings is also a primary Voyager objective which will be studied by several of the investigations. The Radio Science Team will use the attenuation and scattering of the dual-frequency radio to study particle size distribution and total amount of material in the ring as a function of radial distance from the planet. The JST trajectory was chosen so that the flyby geometry optimizes the high radial resolution which is possible with Doppler techniques as will be described by G. L. Tyler in a subsequent paper. Figure 13 illustrates the flybys as seen from Earth. Note that a radio occultation of the Rings occurs only on the outbound leg of JST.

Although the JSX(X=U) trajectory does not provide a ring occultation, it does provide a good viewing geometry for the scan platform instruments. IRIS will be used to study the eclipse cooling of the ring particles and to look for long wavelength cutoffs in the emitted radiation, while the PPS will view scattered light from the Rings at various phase angles and will observe stellar occultations by the Rings. Of course, the Imaging System will directly view the Rings to search for large objects ($\gtrsim$1 km) and to search for structure which may be related to Ring dynamics.

The estimated volume density sensitivity of the various observations is illustrated in Figure 14 which has been adapted from the Voyager Saturn's Rings Working Group Report. Assuming the upper limit to the E-Ring optical depth discussed by B. A. Smith in a preceding paper, the E-Ring will be $\sim$3 orders of magnitude below the PPS sensitivity if it is composed of mm-sized particles, but may just be detectable in the less likely event that the particles are micron-sized.

CONCLUSION

This is necessarily a rather brief overview of the Voyager capabilities for the study of the Saturnian system. Detailed planning of the observational strategies will begin a year from now, so that experience with the JST encounter at Jupiter can be folded into the plans for the Saturn encounter. In addition, results from the Pioneer 11 encounter with Saturn in September 1979 may significantly affect the Voyager observational strategy. Thus, the detailed scientific objectives of the Voyager Mission will continue to evolve within the general capability described in this paper.

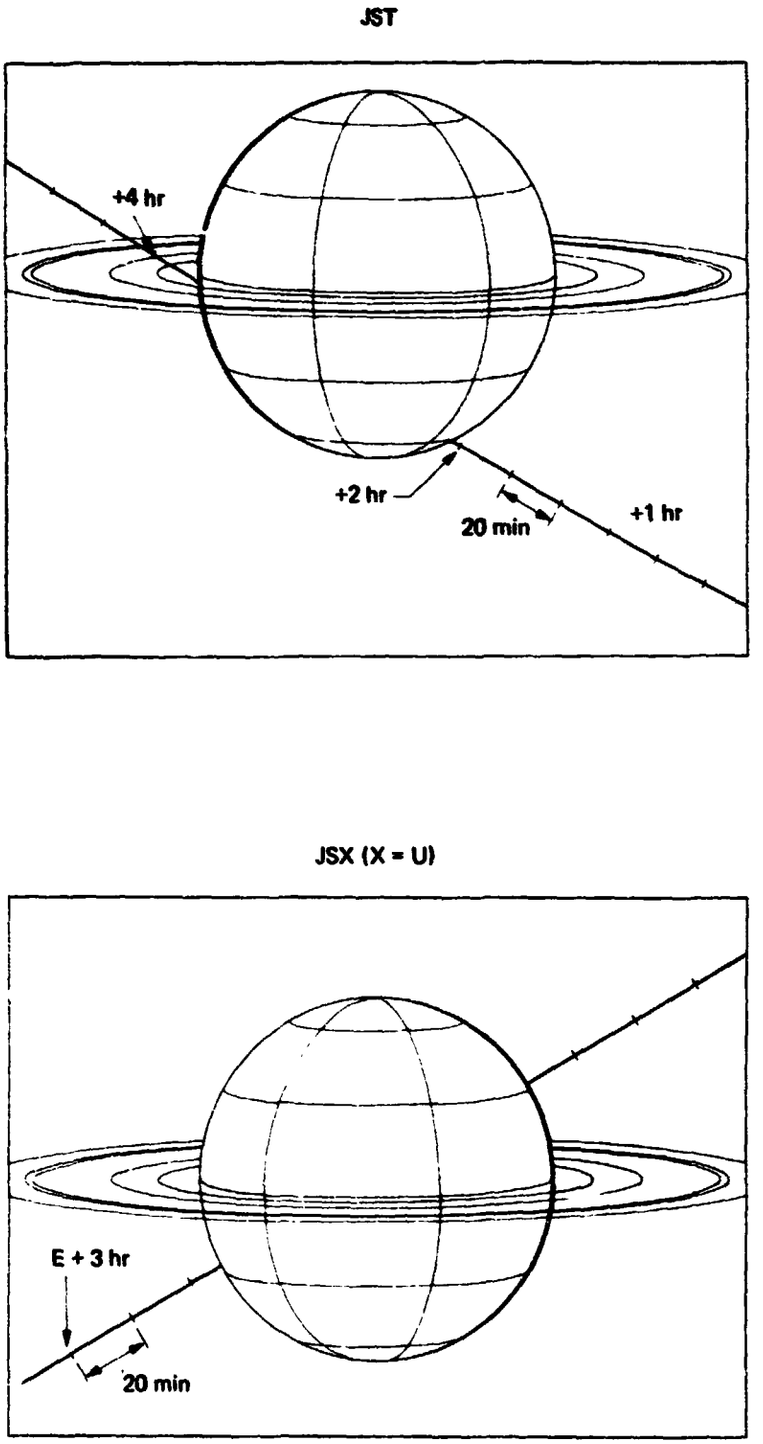

Figure 13. Earthviews of the Voyager encounter at Saturn

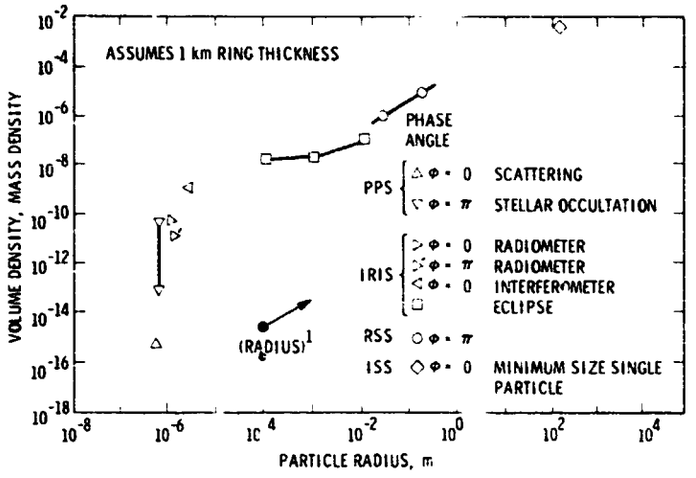

Figure 14. The estimated minimum detectable volume densities as a function of particle radius for various measurements of Saturn's Rings. The phase angles of the different observations are indicated. Note that the minimum detectable volume density scales linearly with the particle radius and inversely with ring thickness.

ACKNOWLEDGEMENTS

The Voyager Project is being carried out for the National Aeronautics and Space Administration by the Jet Propulsion Laboratory of the California Institute of Technology under contract NAS 7-100.

REFERENCES

Brown, L. W. (1975). Saturn radio emission near 1 MHz. *Astrophys. J. 198*, L89–L92.

Eshleman, V. R., Tyler, G. L., Anderson, J. D., Fieldbo, G., Levy, G. S., Wood, G. E., and Croft, T. A. (1977). Radio science investigations with Voyager. *Space Sci. Rev. 21*, 207–232.

Kohlhase, C. E., and Penzo, P. A. (1977). Voyager mission description. *Space Sci. Rev. 21*, 77–102.

Scarf, F. L., and Gurnett, D. A. (1977). A plasma wave investigation for the Voyager Mission. *Space Sci. Rev. 21*, 289–308.

Stone, E. C., ed. (1977). The Voyager Project. *Space Sci. Rev. 21*, 75–376.

Page intentionally left blank

VOYAGER IMAGING SCIENCE INVESTIGATIONS

Bradford A. Smith

Department of Planetary Sciences and Lunar and Planetary Laboratory
University of Arizona
Tucson, Arizona 85721

ABSTRACT

The Voyager Imaging Science Experiment objectives at Saturn include exploratory reconnaissance of Saturn, its satellites and its rings. The imaging cameras are described, along with an abbreviated discussion of specific objectives.

At the time of the NASA/JPL Saturn's Ring Workshop in 1973, I presented a description of the Mariner Jupiter/Saturn imaging experiment. Significant changes have taken place since that time: the Imaging Science Subsystem has evolved into one much better suited to meet the scientific objectives of the investigation, and the project has changed its name. Recently, the Voyager Imaging Science Team published a moderately detailed description of both the instrument and the scientific investigation (Smith *et al.*, 1977).

Figure 1 is a schematic representation of the medium resolution and high resolution cameras being flown on the two Voyager spacecraft. For reasons of historical significance only, these cameras are referred to as the "wide angle" and "narrow angle" cameras, respectively. The focal length of the wide angle camera is 200 mm, and the narrow angle camera is 1500 mm. Each camera employs a selenium-sulfur, slow-scan vidicon which provides an 800 × 800 array of 14-μm pixels, each digitized to 8 bits (256 levels of gray). The fields of view are 3°.2 and 0°.4. Additional camera characteristics are shown in Table 1.

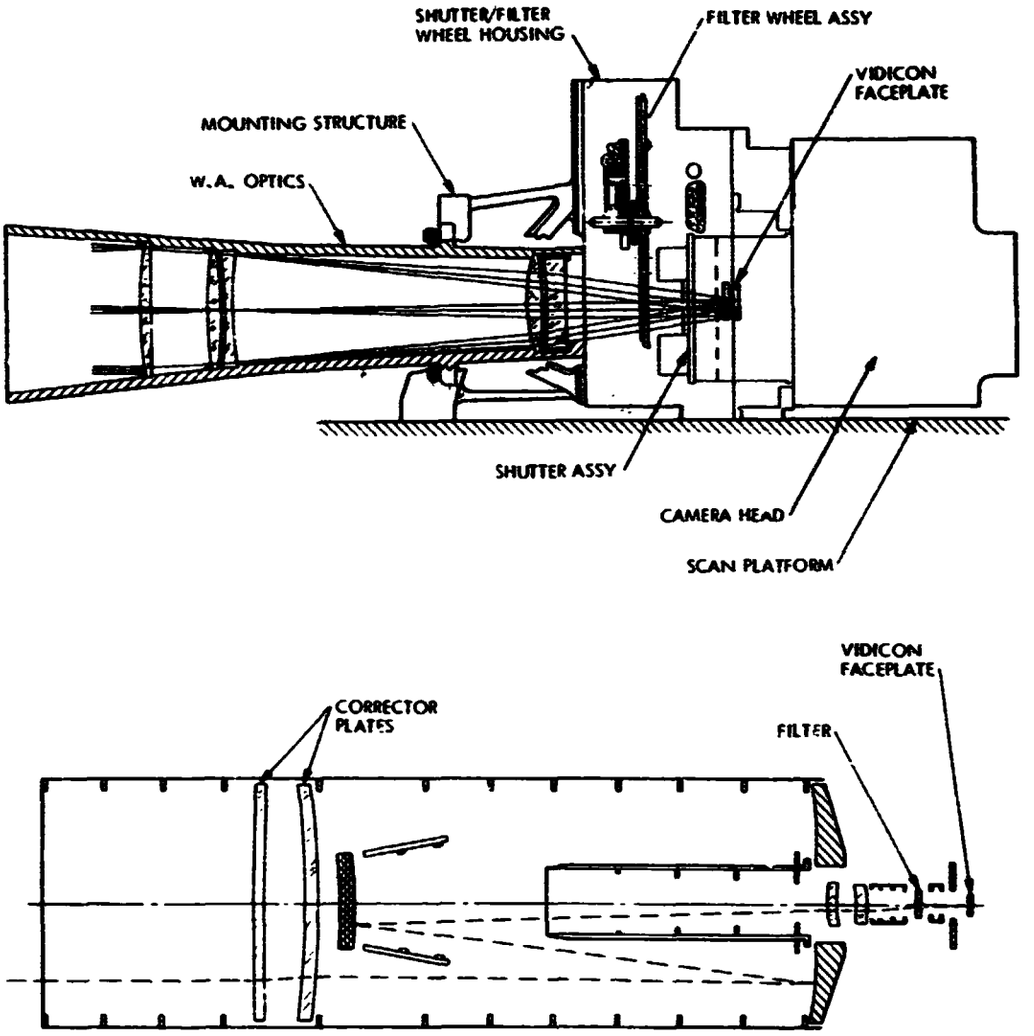

Figure 1. Imaging Experiment - Schematic Representation of the "Wide angle" and "narrow angle" Cameras for Voyager

Table 1. Imaging Science Subsystem Characteristics

Characteristic	Narrow angle camera	Wide angle camera
Focal length	1499.125 mm[a]	201.568 mm[a]
Focal number	F/8.5[a]	F/3.5[a]
Field-of-view	7.5 7.5 mrad	55.6 55.6 mrad
T/Number[b]	T/11.83[a]	T/4.17[a]
Nominal Shutter operation	0.05 to 15.36 sec	0.005 to 15.36 sec
Active Vidicon Raster	11.14 11.14 mm	11.14 11.14 mm
Scan lines per frame	800	800
Picture elements per line	800	800
Pixels per frame	640 000	640 000
Bits per pixel	8	8
Bits per frame	5 120 000	5 120 000
Nominal frame times	48 to 480 sec	48 to 480 sec
Video baseband	7.2 kHz	7.2 kHz
Video sampling frequency	14.4 kHz	14.4 kHz
Angle subtended by scan line	9.25 rad	69.4 rad
Nyquist Frequency	32 line pairs/mm	32 line pairs/mm
Resolution 10% Modulation at	36 line pairs/mm	36 line pairs/mm

[a]Actual data from prototype camera systems.

[b]T/Number – An effective F/number which includes obscuration and transmission losses.

Each camera has eight filters which cover a spectral range from 425 to 600 nm in the wide angle camera, and from 345 to 590 nm in the narrow angle camera. In addition, the wide angle camera has three narrow-band filters centered on the methane absorption bands at 541 and 619 nm, and on the sodium D_2 line at 589 nm.

Observational sequences for Saturn have not yet been developed, and there remains unanswered some crucial questions relating both to telemetry performance and to on-board, data-storage management throughout the Saturn encounter. Thus, it is not presently possible to discuss observational objectives and the sequences necessary to achieve them with the same degree of detail that I could now give for Jupiter. However, it is clear that telemetry rates will be lower at Saturn than at Jupiter and that inter-experiment sequencing conflicts will be much more serious. In other words, lower telemetry rates mean less information, no matter how clever we become in developing our observational sequences.

Arrival times at Saturn are 13 November 1980 for Voyager 1 and 27 August 1981 for Voyager 2. In the baseline plan we will begin imaging in the "observatory" phase 80 days before each encounter; that is, late August 1980 and early June 1981, respectively. At that time we will be a little less than 100 million km from Saturn and the resolution of our narrow angle cameras will be approximately 2000 km per line pair. This is about twice as good as the very best photographs taken from the Earth. Throughout the observatory phase resolution tends to increase linearly with time, reaching 2 to 3 km/lp on the disk of Saturn at the time of encounter. The best resolution on the rings may be a little higher still, but will eventually be limited by image smear caused by the motion of the spacecraft.

Scientific investigations of the satellites of Saturn will include distant imaging of the entire satellite system and near-encounter high resolution imaging of several satellites. At least some near-encounter imaging will be obtained over sub-hemispheric areas on all of the inner satellites: 3 km or better on Mimas, Enceladus, Tethys, Rhea, Dione, and Titan with 1 km or better on Mimas, Rhea, and Titan. Hyperion and Iapetus will be seen with resolutions of 10 to 20 km. The total attainable coverage of the surfaces of these satellites will be determined by actual data rates, sequencing conflicts and, to some extent, by image smear.

The following are among the scientific objectives to be pursued by the satellite subgroup within the Imaging Science Team:

Size and Shape: The sizes and shapes of most of the satellites will be determined with uncertainties between 0.1 and 1.0 percent.

Global High-Resolution Mapping: Between 20 and 40% of the illuminated hemispheres will be photographed in several colors. In some cases, the two spacecraft trajectories will provide balanced polar and equatorial coverage. These high-resolution observations will be used to examine the fine-scale details of major physiographic provinces and the nature of the transition regions.

Polar Volatiles: The polar regions will be explored for deposits and structures related to the past histories of these surfaces, including studies of the morphologies and interrelations of possible ice-related features. With equatorial-noon and polar temperatures ranging from ~100 K to ~30 K, stable ices should include water, certain sulfides, ammonia, and ammonium hydrates (Lebofsky, 1975). The polar regions, being at all times colder than other areas, may have acted as sinks for volatile materials originating elsewhere. These regions are, therefore, of special interest.

Titan: There is a lack of consensus in our understanding of Titan, and carefully planned spacecraft measurements are required if we hope to resolve these issues. The diameter and figure are the first priority. The next step is to establish whether this observation refers to the surface, or to a haze in a dense, molecular atmosphere, or to a uniform cloud layer. This might be accomplished by imaging observations in several colors. The suggestions that Titan may possess clouds, aerosols or even dust layers requires that it possesses weather systems. Titan is a slowly rotating planetary body with an orbital period of about 16 days, and thus, the circulation of the satellite atmosphere could represent an intermediate case between the baroclinic circulation typical of the mid latitudes of the earth and Mars and the symmetric Venus weather patterns.

In addition to the study of each satellite as an individual planetary body, we will, of course, pursue an intercomparison among all observed satellites in the Saturn system, and with those in the Jupiter system as well.

The Voyager mission provides a unique opportunity for the study of atmospheric systems very different from our own. At both Jupiter and Saturn, Voyager will achieve higher resolution and a longer observing time base than that obtained by Pioneer; both resolution and time are improved by a factor of about 50.

Throughout the observatory phase the disk of Saturn will be photographed in at least two colors (orange and ultraviolet) at five equally spaced longitudes during each rotation. Approximately three weeks before planetary encounter, the disk of Saturn will exceed the field of view of the narrow angle camera and mosaicking will be necessary. The extent to which global coverage with 2 × 2 and 3 × 3 mosaics can be maintained will depend upon data rates and tape recorder use. Eventually we will have to terminate this full disk coverage and concentrate on features of special interest identified and selected during the observatory phase.

During the observatory phase, observations in both space and time will provide information on the synoptic development, growth, and dissipation of atmospheric systems, and will provide the first opportunity to observe the zonal velocity field at the cloud tops. Unlike Jupiter, Saturn as seen from the Earth presents a dearth of nonaxisymmetric features necessary to measure zonal wind components. In fact, only 9 such features have ever been observed, leaving unknown the zonal velocities associated with most of the planet's axisymmetric structure.

The near encounter observational sequences of Saturn will be nearly identical to those carried out at Jupiter, in that a major objective of the Voyager mission involves a detailed comparison of the meteorologies of these two planetary atmospheres As an example, the Pioneer 11 observations of Gehrels *et al.* (1974) show that the axisymmetric structure terminates on Jupiter approximately 45° from the equator. The Voyager spacecraft trajectories, however, require the Jovian encounters to take place nearly in the equatorial plane, so that it will not be possible to make highest resolution observations of the Jovian polar regions. We do not yet know whether this transition also occurs in the Saturn atmosphere and, if so, at what latitudes. Fortunately, the Voyager trajectories make it possible to observe both the north and south poles of Saturn (see Figure 2) to complete the comparison of the Jovian and Saturnian meteorologies.

There are several types of observations of Saturn's Rings to be made with the wide and narrow angle cameras, which should yield information on the photometric properties of the particles and predicted radial drift displacements of particles within the rings. General profiles of the rings in reflection obtained during the observatory phase at nearly uniform phase angle may be used to interpret those obtained during encounter, when phase angle will vary greatly across the profile.

Strip sequences of images with high resolution taken across the rings will give information about minor divisions. If the strip is timed and placed so as to see the

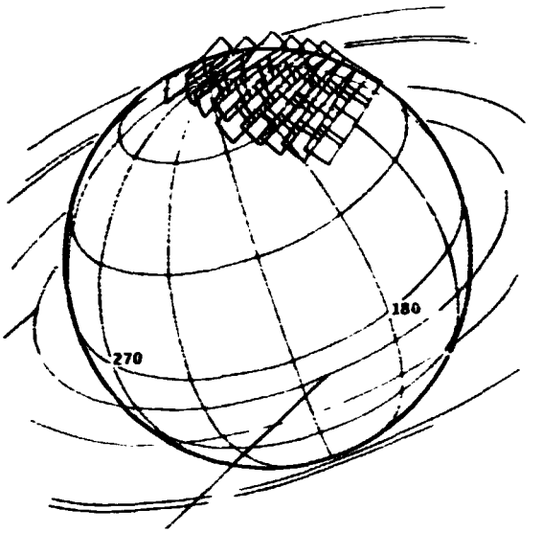

Figure 2. Typical Saturn Pole Coverage

turned-up illuminated outer edge of an inclination resonance as predicted by dynamical theory (Cook, 1978), a useful check on that theory will be obtained. If minor divisions are seen, we can establish lower limits on drift displacements across the corresponding resonances. The width of a division gives us the distance of drift during the age of the rings. Invisibility of a division gives us an upper limit on the distance of the drift or implies that the collision frequencies between particles are too high to allow the resonance to develop.

The existence of Ring D should be settled once and for all, and excellent profiles of Ring C and Cassini's Division will be obtained.

REFERENCES

Cook, A. F. (1978). Gravitational resonance in Saturn's rings II. To be published.

Gehrels, T., Coffeen, D., Tomasko, M., Doose, L., Swindell, W., Castillo, N., Kendall, J., and Baker, L. (1974). Imaging photo polarimeter experiment on Pioneer 10. *Science 183*, 318–320.

Lebofsky, L. A. (1975). Stability of frosts in the solar system. *Icarus 25*, 205–217.

Smith, B. A., Briggs, G. A., Danielson, G. E., Cook, A. F., Davies, M. E., Hunt, G. E., Masursky, H., Soderblom, L. A., Owen, T., Sagan, C., and Suomi, V. E. (1977). Voyager imaging experiment. *Space Science Rev. 21*, 103–127.

DISCUSSION

D. MORRISON: You talked about weather and clouds on Titan in a way that made me think you expected to see cloud patterns. Doesn't the large optical depth of haze suggest it would be more like looking down on Los Angeles on a smoggy day, where you see nothing?

B. SMITH: Yes. Although, if there are clouds above the haze, we'll see them.

J. POLLACK: I don't think we have good numbers for the optical depth of dust or haze on Titan right now. From that point of view I'd be a little hesitant to say we won't see exciting atmospheric features on Titan.

J. CUZZI: From what George Siscoe was saying about the sputtering going on at the outer edges of the rings, it would be especially interesting to look at the outer edge of the A ring.

G. ORTON: Do you have any filters that are located in the methane red bands?

B. SMITH: Yes. The 619 nm methane absorption band, and the band at 541 nm. The 541 nm filter was put on for Uranus. There is no hope of seeing that band on Saturn.

D. MORRISON: Is there any problem with scattered light for features like the D Ring or the inside of the Cassini division? Are you confident that your system has low enough scattered light levels, and that you will be close enough, to see into these regions?

B. SMITH: Absolutely confident.

WHAT THE VOYAGER INFRARED INVESTIGATORS HOPE TO LEARN ABOUT THE SATURN SYSTEM

R. A. Hanel

Laboratory for Extraterrestrial Physics, NASA Goddard Space Flight Center
Greenbelt, Maryland 20771

ABSTRACT

The Voyager infrared investigation uses a Michelson interferometer (IRIS) covering the spectral range from 200 to 3000 cm^{-1} (3.3 to 50 μm) and a bore sighted radiometer covering the range from 5000 to 25000 cm^{-1} (0.4 to 2 μm). The spectral resolution of the interferometer is 4.3 cm^{-1} and the field of view is 0.25°. Scientific results anticipated from the investigation of the Saturnian system are discussed; these are contrasted to those which were expected from the advanced interferometer (MIRIS), which was not qualified in time for flight.

INTRODUCTION

This paper summarizes what the Voyager Infrared Investigator Team expects to learn about the Saturnian system. The discussion addresses Saturn, its rings, Titan and the other smaller satellites. The format of this summary is similar to that of the team paper published in Space Science Review (Hanel, *et al.*, 1977), hereafter called paper one. However, in contrast to paper one the present discussion concentrates on Saturn, and takes account of the fact that the IRIS, rather than the MIRIS instrument, is on board Voyager.

An in-flight IRIS calibration is now available for the 200-2000 cm^{-1} range which shows that the instrumental performance is somewhat below expectation. The near infrared part of the spectrum (above 2000 cm^{-1}) will be calibrated shortly by

viewing the spacecraft mounted solar diffusing target. Figure 1 (similar to Figure 9 of paper one) shows the actually measured noise-equivalent-radiance (NER) of the Voyager 1 interferometer. The response has not changed since the initial cool down after launch is close to that during the final thermal vacuum test. The NER of the Voyager 2 interferometer after launch was similar to that of the Voyager 1 instrument, but has apparently not yet stabilized.

Also shown in Figure 1 are the NER values of the flight qualified MIRIS instrument as measured in a thermal vacuum chamber. Unfortunately, the instrument was qualified too late for the Voyager mission. Figure 2 illustrates the degree of improvement in the NER which can be obtained by averaging of spectra over indicated time intervals. Several radiometric data points obtained from the ground by Morrison *et al.* (1972) and Gillet *et al.* (1973) for Titan are shown for comparison. The Voyager scientific objectives defined in paper one are definitely affected by the substitution of IRIS for MIRIS. Objectives based on the analysis of the spectral range between 1000 cm^{-1} and about 3000 cm^{-1} will suffer in precision; objectives based on data from the 3000-7000 cm^{-1} range can not be accomplished at all. On the other hand the lower NER of IRIS compared to MIRIS between 200 and 900 cm^{-1} will benefit some objectives based on data in this spectral range; the lower spectral resolution of the IRIS instrument will affect other objectives, however. The discussion below treats the individual scientific objectives at Saturn following the overall format of paper one.

ATMOSPHERIC GAS COMPOSITION, ELEMENTAL ABUNDANCES AND ISOTOPIC RATIOS

Hydrogen to Helium Ratio

The hydrogen to helium ratio for Saturn will be derived primarily from the far infrared spectrum (200-800 cm^{-1}). Since the derivation will be made by using a large number of spectra the difference in performance between instruments becomes insignificant. The limit in the precision of the derived hydrogen to helium ratio is expected to be due to uncertainties in the knowledge of gas absorption coefficients and aerosol properties, rather than to random instrumental errors in the spectra. Thus, the objective of determining the H_2/He ratios as discussed in paper one seems obtainable.

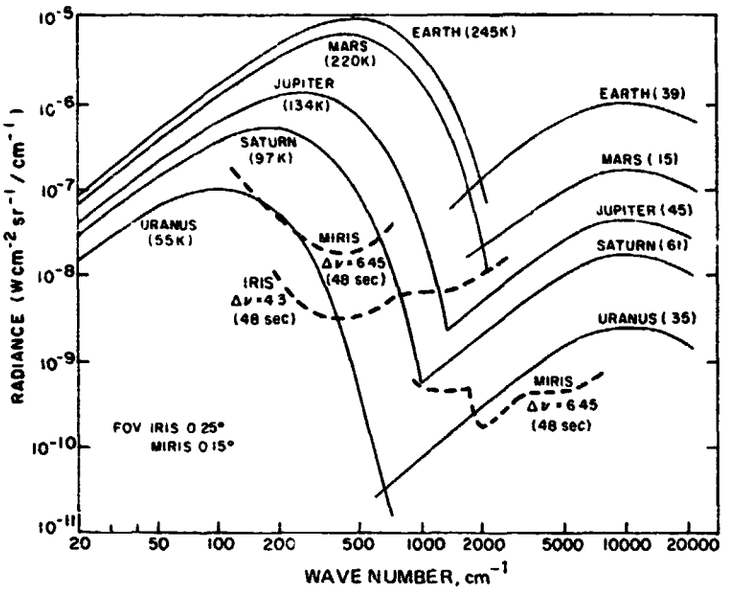

Figure 1 shows emitted and reflected radiance levels schematically for indicated brightness temperatures and albedos. Measured noise-equivalent-radiance values (NER) are shown for Voyager 1 (middle dashed line) and the far infrared (upper dashed line) and near infrared (lower dashed line) channels of MIRIS.

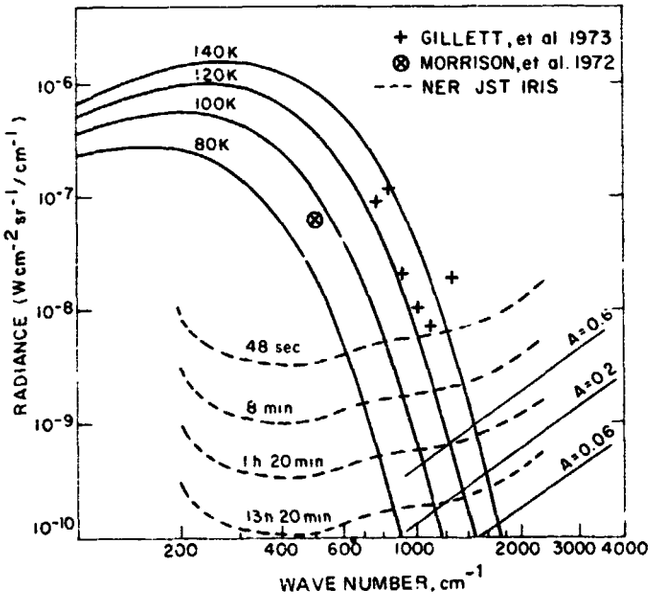

Figure 2 shows radiance versus wave number similar to Fig. 1, but on an expanded scale. The NER of IRIS is shown by dashed curves for individual spectra (48 sec) an average of 10 (8 min), 100 (1 h 20 min) and a total of 1000 spectra (13 h 20 min). Also illustrated are a few ground based measurements of Titan.

Methane

Information on the methane mixing ratios on Saturn and Titan will be based primarily on the 1306 cm^{-1} methane band in conjunction with temperatures derived from pressure induced H_2 lines. Instead of using individual MIRIS spectra an average over several hours of IRIS spectra will be required to obtain adequate precision. Since one hemisphere of Saturn fills the 0.25° field of view of IRIS about 10 days before encounter, and Titan fills the field of view about one day before closest approach to Titan, the original objective seems to be obtainable. However, an independent measurement of the mixing ratio in the upper stratosphere, based on the 3019 cm^{-1} CH_4 band, will probably not be possible.

Ammonia

Only the 200 to 275 cm^{-1} part of the rotation spectrum and the region near 900 cm^{-1} will be available. The 100 to 200 cm^{-1} range may have been useful to see uncondensed NH_3 in the lower atmosphere of Titan. However, the higher sensitivity of IRIS between 200 and 300 cm^{-1} might compensate for its more restricted spectral range.

Trace Constituents

The lack of sensitivity in spectral ranges of potential atmospheric windows (2000, 3700 and 6200 cm^{-1}) will hamper the search for unknown minor constituents severely. The availability of the 700 to 900 cm^{-1} range, on the other hand, may make a search for hydrocarbons (C_2H_2, C_2H_6) in the atmospheres of Saturn and Titan more productive.

Elemental Abundances

Without the prospect of good measurements in spectral ranges of potential atmospheric windows it seems probable that only the H_2/He and possibly the C/N ratios will be measurable with precision.

Isotopic Ratios

An observation of the D/H and C^{12}/C^{13} ratios may be possible by averaging all available Saturn spectra (20 days). The 2200 cm^{-1} CH_3D band and the 1306 cm^{-1} CH_4 band may then also provide adequate data for analysis. For Titan the same task seems marginal.

Clouds and Hazes

Lack of good near IR coverage will have a strong impact on specifying the particle composition and size, and the distribution of clouds and aerosols. Averages of carefully sorted groups of spectra (rather than individual measurements) may be usable. However, this will only allow parametrization of large areas, such as belts and zones rather than of local phenomena.

Temperature Profiles

Atmospheric temperatures are derived from the pressure induced lines caused by collisions between hydrogen molecules or between hydrogen and helium or methane molecules. On Titan collisions between methane molecules may also be important. Many of these pressure induced lines fall within the 200 cm^{-1} to 1000 cm^{-1} range where IRIS is sensitive. In the upper atmospheric layers (up to the 5 mbar level for Saturn and up to much lower pressures for Titan) the 1306 cm^{-1} methane band can be used. Depending on the actual atmospheric temperatures, spectra averaged over times ranging from 10 minutes to an hour will be required to obtain temperature profiles with adequate precision. In the 100 to 1000 mbar range individual spectra will be sufficient to yield a precision of 1 to 2 K with a vertical resolution of approximately one scale height. Thus, the task of deriving atmospheric temperatures on Saturn and Titan seems to be possible.

Dynamics and Heat Balance

Information on atmospheric motions is derived from the temperature field. For Saturn, good temperature data from the hydrogen lines will allow determination of the north-south temperature gradient; this will then be used to derive the east-west wind field.

Energy balance calculations require knowledge of both the total reflected and emitted energy. The radiometer provides a measure of the first and the interferometer of the second component. Derived compositional and temperature data will be used to extrapolate over part of the thermal spectrum. In thia case MIRIS would have been preferable but an adequate estimate of the local and total heat balance of Saturn can be expected from IRIS.

Satellites

The absence of the near infrared spectrum will make the identification of surface minerals and ices much more difficult; however, some far infrared features such as the 230 cm^{-1} water and the 280 cm^{-1} ammonia lattice modes fall within the IRIS range, as do features in the spectrum of silicates.

The measurement of the surface temperature and thermal inertia of the surface material can be carried out even if the satellite does not fill the field of view. This condition will occur more often with IRIS (0.25°) then it would have with MIRIS (0.15°). In the absence of strong spectral features a precise surface temperature can be established by fitting a Planck function to the measured spectrum.

Saturn's Rings

All properties of the rings derived from the thermal part of the spectrum and its variation with emission and phase angles and time can be accomplished by IRIS, while tasks based on the near infrared reflectivity will be severely limited. Particle sizes or thermal inertia can be estimated from the cooling curves depending on the mean size of particles.

SUMMARY

The scientific objectives formulated in anticipation of MIRIS being on board Voyager have to be modified because of the different parameters of the IRIS instrument. Tasks which depend on data in the 3000–7000 cm^{-1} range cannot be accomplished with IRIS. This will curtail but not eliminate the search for minor atmospheric constituents, the characterization of aerosols, and the surface composition of satellites and rings. Investigations based on data between 1000 and 3000 cm^{-1}, will suffer in precision or in spatial resolution due to longer averaging times required to compensate for the higher NER of IRIS compared to MIRIS. Finally, tasks based on the interpretation of the 200–1000 cm^{-1} range, such as temperature and hydrogen to helium measurements, will even gain to some degree by the lower NER of IRIS compared to MIRIS in this spectral region.

REFERENCES

Gillett F. C., Forrest W. J., and Merrill, K. M. (1973). 8-13 micron observations of Titan. *Astrophys. J. 184*, L93–L95.

Hanel R., Conrath B., Gautier D., Gierash P., Kumar S., Kunde V., Lowman P., Maguire W., Pearl J., Pirraglia J., Ponnamperuma C., and Samuelson R. (1977). The Voyager Infrared Spectroscopy and Radiometry Investigation. *Space Sci. Rev. 21*, 129–157.

Morrison D., Cruikshank D. P., and Murphy R. E. (1972). Temperatures of Titan and Galilean Satellites at 20 microns. *Astrophys. J. 173*, L143–L146.

DISCUSSION

J. CALDWELL: What spectral range will you use to look for the cloud features on Titan? If the clouds are methane ice, I'm skeptical that there will be features that you can identify. Certainly, the solids will have absorption features, at least at 8 μm and to shorter wavelengths, but there the gas which overlies the clouds will probably be completely opaque.

J. POLLACK: Water ice has a strong lattice band at about 45 μm, so he has some hope.

D. MORRISON: Could you say a few words about the capability of the instrument as a thermal radiometer for measuring the eclipse cooling and heating rates of the rings or the satellites? How low a temperature can you measure, and will your sequences allow you to observe dark side temperatures on the satellites or eclipse measurements of the rings?

R. HANEL: For a black body of 55 K, the radiometric signal to noise ratio is about 50 to 1.

D. MORRISON: Do you anticipate making measurements of ring eclipses or of the dark sides of the satellites?

R. HANEL: Yes.

VOYAGER RADIO OCCULTATION INVESTIGATIONS AT SATURN

G. L. Tyler and V. R. Eshleman

Radioscience Laboratory, Stanford University
Stanford, California 94305

ABSTRACT

Voyager will use dual-frequency 3.5 and 13 cm wavelength radio occultation techniques to study the atmospheres and ionospheres of Saturn and Titan, and the rings of Saturn. At Titan radio occultation is predicted to probe the atmosphere to the surface. The existence of a surface could be confirmed by detection of an obliquely scattered echo. At Saturn the two Voyager encounters will provide occultation measurements of temperate and equatorial regions of the atmosphere and ionosphere, and of the rings. The atmosphere will also be probed in polar regions during the deepest portions of the occultation. Both frequency and intensity data will be collected and jointly analyzed to study temperature-pressure profiles, and to derive information on atmospheric shape, turbulence, and "weather". For the rings, Voyager will provide measurements of the complex (amplitude and phase) radio extinction and angular scattering functions of the ring particles as a function of wavelength, polarization, and radial distance from Saturn. These observations will be used to infer the first several moments of the ring particle size distribution, the total amount of material in the rings, the radial distribution of material, and limits to possible particle shapes and constituents.

The Voyager radio occultation investigations discussed here are based on the use of the 3.5 and the 13 cm wavelength spacecraft transmitters and ground receiving systems which are also used for telecommunications. These studies are directed towards the atmospheres and ionospheres of Saturn and Titan, and the rings of Saturn. A number of other investigations are also planned, but will not be discussed here (Eshleman *et al.*, 1977).

Salient features of these investigations are the use of: a) harmonically related frequencies at the two wavelengths, b) considerably higher power levels than previous experiments, c) a new, radiation-hardened, highly stable spacecraft frequency standard, and d) improved phase, group-delay, and amplitude stabilities in spacecraft and ground radio systems. The resulting experimental precisions are given in Table 1.

When a spacecraft moves behind a planet as viewed from Earth, the radio path traverses the planet's atmosphere and ionosphere, and for Saturn, will also probe its system of rings. All of these regions affect the characteristics of the received radio signals, making possible the study of the vertical structure of these atmospheric regions, clouds, small and large scale variations associated with turbulence and weather, and fundamental characteristics of the ring particles and their disposition around Saturn. The atmosphere and ionosphere of Titan will also be studied by such occultation measurements. It is also expected that a reflection from the surface of Titan near the limb will be obtained during the occultation measurements. If this occurs, it will provide positive confirmation that the measurements reach the surface.

Table 1. Voyager Occultation Experiments at Saturn

Wavelength (cm)	S/N (1 s)	$\Delta P/P$(1000 s)	$\Delta f/f$(1 s)
3.5	6.3×10^4	<10%	2×10^{-12}
13	2.5×10^3	< 1%	2×10^{-12}

ATMOSPHERES

Saturn

Flyby trajectory characteristics of the two Voyager spacecraft at Saturn provide a good combination of conditions for radio occultation studies of its atmospheres and ionospheres. Figure 1 illustrates the paths of the radio image of the spacecraft as seen from Earth for the nominal JST and JSX trajectories. Note that both equatorial and polar regions will be probed, and that there will be both a near-central occultation and a more grazing occultation in which the spacecraft sets or rises, as seen from the Earth at large angles from the local vertical at the occulting body. Figure 2 provides a side

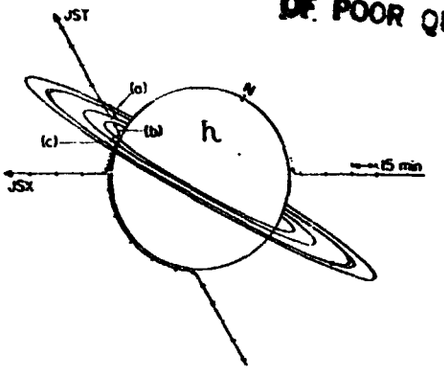

Figure 1. View from Earth of Voyager occultations at Saturn — *The spacecraft radio images follow the indicated paths for the JST and JSX trajectories at Saturn. Note that there is a near central and more grazing occultations. For JST at Saturn, region (a) provides a clear occultation of the rings and (b) a clear atmospheric occultation, while (c) is a combined ring and atmospheric occultation.*

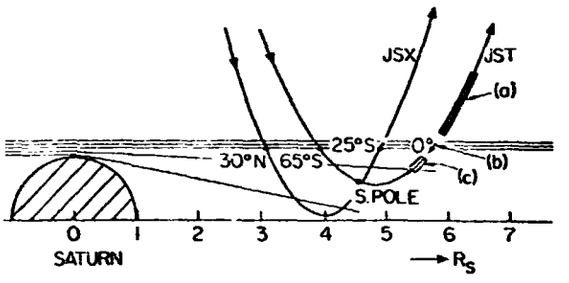

Figure 2. Side view of Voyager occultations at Saturn — *The trajectories are plotted in a rotating plane that instantaneously contains the earth, the spacecraft, and the center of the planet. The latitudes of occultation immersions and emersions are shown, and regions (a), (b), and (c) of Figure 1 are also illustrated here.*

view of the occultation geometry in a rotating plane that instantaneously contains the Earth, the spacecraft, and the center of Saturn. The figure is illustrated to scale. Occultation distances from the planetary limb to the spacecraft range about 3 to 6 R_S (Saturn radii).

For a central passage of a spacecraft behind Saturn, the trajectory would dip to zero in the vertical scale of Figure 2. At occultation entry and exit, the spacecraft would appear from the Earth to set and rise approximately normal to the limb of the planet, and the atmosphere would be sampled with height along a near-vertical path. Such a central passage is the optimum condition for occultation measurements of the vertical structure of the atmosphere. The JSX (Uranus) trajectory at Saturn is near optimum in this regard, while the JST trajectory gives occultation conditions in which the virtual image of the spacecraft enters the atmosphere along a path well away from the vertical. After modest penetration into the atmosphere, the image of the JST spacecraft, as viewed from Earth, will move approximately horizontally through the atmosphere, over south polar regions of Saturn, with spacecraft rise at emersion being over the equator in the western ansa. While such a non-central occultation will provide reliable vertical profiles over a smaller range of heights than is the case for central occultations, it is expected to be very useful in sampling conditions over a wide range of latitudes, in studying complex atmospheric structure due to turbulence and weather, and in helping to determine possible distortion of gravitational equipotentials from oblate spheroids, as discussed below.

Figure 2 shows illustrative radio ray paths in the regions behind Saturn. Measurements of the received frequency of the radio signals from the spacecraft provide precise information on the angle of refraction in the atmosphere. Knowledge of this angle as function of time, together with the spacecraft trajectory, makes it possible to estimate the refractivity of the atmosphere as a function of height. (Refractivity $\nu = n-1$, where n is the refractive index.) The profile of refractivity in turn can be used to determine the relative temperature and pressure as a function of height, and such relative profiles can be made absolute from knowledge of the atmospheric constituents (Fjeldbo and Eshleman, 1965; Kliore *et al.*, 1965; Eshleman, 1965).

The process of converting the observed signal frequencies into a height profile of refractivity, or a more general two or three dimensional refractivity model of the atmosphere, is not straightforward and in general cannot yield a unique result. The problem of determining refraction angles from any given atmospheric model is, by comparison, both straightforward and unique.

If one imposes the assumption that the atmosphere is spherically symmetric, there is a mathematical transform pair that allows computations in either direction, and in this case the profile computed from the refraction angles is the correct and only answer (Fjeldbo *et al.*, 1971). We are not aware of any other potentially applicable model where such a direct mathematical inversion has been identified. A different approach involves iteration downward in an atmosphere modeled by successive thin layers within each of which the refractivity is constant. While such a method has been used for the spherical case (Fjeldbo and Eshleman, 1968), it is potentially applicable with further development to any geometrical complexity that can be modeled in this way. The radio science team is preparing for both types of inversion approaches for the Voyager occultation experiments. The departure from spherical symmetry due to the oblateness of the major planets will be treated both by using a sequence of offset spherically-symmetric models to match the curvature of the equi-refractivity profiles at the occultation points (Kliore and Woiceshyn, 1976), and by the iterative process applied to the oblate spheroidal geometry. It is expected that this latter method may be made more complete with attempts to treat possible zone-belt differences and particular spot features in the atmospheres.

Important additional information about atmospheric structure can be obtained from the intensity of the dual-frequency signals received during occultation. Figure 2 illustrates the effects of differential refraction on intensity by showing that evenly spaced parallel rays to Earth connect with increasingly spread rays at the spacecraft for progressively lower ray passages through the atmosphere. Thus signal intensity decreases as the rays penetrate deeper into the atmosphere. Measured signal intensity can be inverted as discussed above for the frequency measurements, and should yield the same refractivity profiles if the changes in intensity are due solely to such atmospheric defocussing (Fjeldbo *et al.*, 1971). However, there are two other factors to consider, as discussed below.

Certain errors in profiles derived from Doppler frequency measurements undergo an inherent magnification deep in the atmosphere, but this does not occur in the intensity inversion process (Hubbard *et al.*, 1975; Eshleman, 1975). Thus cross-checks can be made to determine the onset of such magnified errors, with the possible result that the characteristics of such an error source could be measured. For example, profiles determined from Doppler measurements during the non-central occultations will be very sensitive to the assumed orientation of the local vertical (Hubbard *et al.*, 1975). At atmospheric levels where the signal intensity is reduced by a factor M (which could

reach values of thousands), an error in the local vertical of δ radians would produce a temperature error on the order of 200 Mδ% when the spacecraft sets or rises at an angle of 45° from the vertical (Eshleman, 1975). But if the temperature were known more accurately than this from the intensity measurements, or from other Voyager experiments, then the apparent error could provide information on the orientation of local equipotentials to an accuracy which could be important in the study of gravitational anomalies due to internal structure and atmospheric currents. The accuracy of the local vertical of the global gravity field of Jupiter as determined with Pioneer spacecraft is about one minute of arc (Anderson, 1976).

The second factor relative to the use of signal intensity measurements is that atmospheric absorption would add logarithmically to defocussing loss, but these two effects would be separable whenever the refractivity profile can be determined from the Doppler measurements (Fjeldbo *et al.* 1971). Microwave absorption in the atmosphere is expected due to cloud condensates, their vapors, or principal atmospheric constituents at low altitudes and hence high densities. The loss profile measured at the two radio frequencies would provide information on the location, density, and other characteristics of the clouds or other absorbing material.

Before absolute pressure and temperature profiles can be derived from the refractivity data, one must know either the composition or the temperature at some altitude level. For the Voyager missions, the IR and UV sensors are expected to yield complementary data on these parameters. Additional information may be obtained from the signal intensity measurements. For instance, if the altitude level of ammonia clouds could be identified in a microwave loss profile, one would know the approximate temperature at this altitude based on considerations involving vapor saturation. This temperature information would, in turn, allow us to use the scale height of the refractivity profile near the cloud level to estimate the mean molecular mass of the atmosphere. The mean molecular mass could in turn be utilized together with other data to establish limits on the abundance ratios between the principal atmospheric constituents.

Titan

The atmospheric occultation experiment is of special interest for Titan, the only satellite known to have an appreciable atmosphere. The trajectory for the JST mission includes a near-central passage behind Titan, under conditions which are

favorable for vertical profile measurements. The same general considerations discussed above also apply at Titan, except that oblateness is not expected to be important. While there is considerable uncertainty about atmospheric conditions at Titan (Hunten, 1974), it is expected that the radio occultation experiment can provide important atmospheric results over a wide range of altitudes, probably including conditions from the surface to heights where the atmospheric pressure is on the order of 1 mbar. At greater heights, ionospheric measurements would provide additional information as discussed below.

We have computed the radio propagation effects of the four model atmospheres of Titan (Paul Weisman, JPL; private communication) with the results that are summarized in Table 2 and Figure 3. In Table 2, the important parameters to compare are those for surface pressure, pressure for critical refraction, the near-limb signal

Table 2. Summary of Model Titan Atmospheres and Their Radio Effects

Model / Name	I Danielson	II Hunten	III Divine	IV Sagan
Principal Constituent	CH_4	N_2	N_2	Ne
Amount (km-A)	1.6	25	60	20
Second Constituent)	-	CH_4	CH_4	CH_4
Amount (km-A)	-	0.08	0.19	0.08
Scale Height (km)	31	18	28	66
Temperature (K)	76.0	76	122	204
Surface Pressure (bar)	0.015	0.40	0.96	0.23
Pressure for critical refraction (bar)	7.3	6.2	15.9	275
Near-limb signal (dB)	-13	-16	-14	-10
Bending angle at surface (radian)	5.36^{-4}	1.31^{-2}	1.54^{-2}	3.26×10^{-4}
Critical distance for a near limb maneuver (meters)	5.04^{9}	2.06^{8}	1.75^{8}	$8.27 \times 10^{+9}$

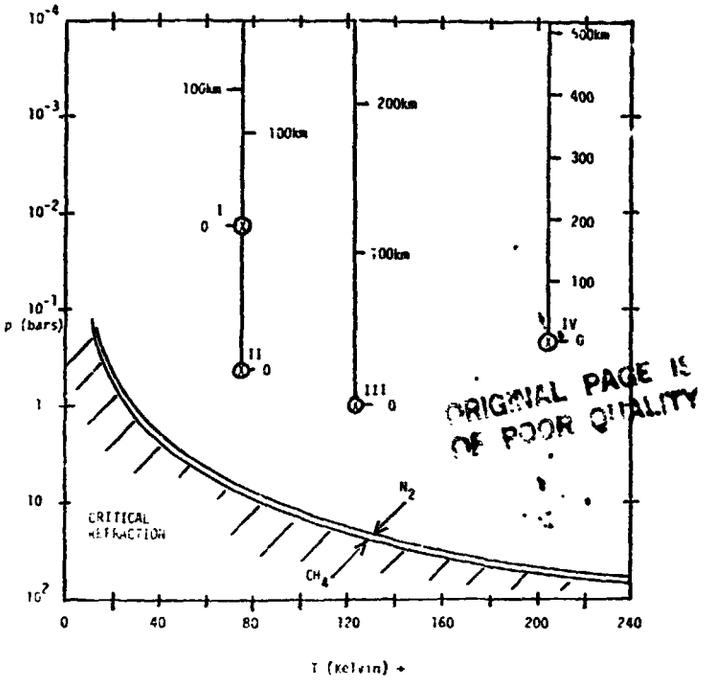

Figure 3. p-T Occultation space at Titan — *Figure illustrates the relationship of four model atmospheres (I-IV, see Table II) to the expected critical refraction level at Titan. Since critical refraction depends on the specific refractivity of the actual constituents, two illustrative cases, for pure atmospheres of N_2 and CH_4, are given.*

loss, bending angle at the surface and the critical occultation distance. Surface pressure and pressure for critical refraction compare the expected surface pressure with the pressure at the height at which the radius of curvature of a horizontal ray equals the radius of the ray. In all cases the critical height occurs at a level in the atmosphere that is more than one order of magnitude pressure greater depth than the expected surface pressure. The difference in these two pressures is the theoretical margin for occultation measurements to reach the surface.

In practical cases, signal strength must be considered as well. The entry under near-limb signal loss indicates the maximum signal loss due to atmospheric defocussing that will be encountered during occultation while observing signals from the closest limb of Titan. The difference between this loss and the initial signal-to-noise ratios (see Table 1) is available for study of absorption and scattering of the ray. Note that this difference typically is between two and three orders of magnitude in signal strength. To date, no potentially large sources of absorption have been identified.

The remaining two quantities indicate the margins for a successful no-limbing tracking, or a near-limb tracking maneuver occultation. The bending angle at the surface is always less than the Voyager 13 cm -3 dB half-beam width of 2.1×10^{-2} radians, although it can be larger than the -3 dB half-beam width of 5.9×10^{-3} radians at 3.5 cm wavelength. The critical distance is the maximum flyby distance at which a near-limb tracking maneuver can successfully track a surface ray. The Voyager occultation distance is planned to be about 3×10^{7} m, or about one order of magnitude less than the smallest value obtained for this quantity. At present the Voyager Radio Science Team plans to track the closest limb throughout the occultation.

Figure 3 illustrates the relationship of these models to the critical refraction levels of pure N_2 and CH_4. This figure allows easy estimation of proposed atmospheres to the critical occultation level.

Ionospheric Profiles

The vertical profiles of free electron concentration in an ionosphere can be found from the profile of refractivity, which in turn is determined in the same general way as described previously for the refractivity of the neutral atmosphere. However, there is an important difference in that the refractivity is also proportional to the square of the radio wavelength for ionospheres, while it is essentially independent of wavelength for neutral atmospheres. Thus the dual frequency measurements will be self-calibrating in the sense that ionospheric profiles derived from Doppler frequency differences will be independent of trajectory uncertainties and spacecraft oscillator instabilities (Fjeldbo *et al.* 1965). Ionospheric profiles will be obtained in conjunction with the atmospheric occultations at both Saturn and Titan.

RINGS OF SATURN

The Voyager encounters with Saturn provide an opportunity to study the ring system with radio occultation techniques. The JST trajectory includes a Saturn ring occultation following atmospheric occultation emersion. The JSX trajectory provides an optional retargeting for Titan encounter and ring occultation should the JST spacecraft fail prior to Saturn encounter.

The goals of these observations are to measure the complex (amplitude and phase) radio extinction and angular scattering function of the rings as a function of wavelength, polarization, and radial distance from Saturn. These observations would then be used to infer the first several moments of the ring particle size distribution, the total amount of material in the rings, the radial distribution of that material, and limits to possible particle shapes and constituents (Marouf, 1975).

As in atmospheric occultations, the 13 and 3.5 cm-λ radio waves will be transmitted from the spacecraft through the rings and received at Earth. The motion of the spacecraft will carry the geometric line of sight from the planetary occultation point within the western ansa (region (b) in Figures 1 and 2) outward through the entire ring system (region (a) in the figures). The complete phase, intensity, and polarization of the received signals at both wavelengths will be recorded at Earth. Note also from the figures that the complete ring plane will be crossed along a second path by the rays refracted through the atmosphere just prior to the atmospheric emersion of the spacecraft image (region (c) in the figures). This combined atmospheric and ring occultation will also be recorded.

It is expected that the received signal will consist of two principal components; a coherent signal that represents propagation directly through the rings, and an incoherent component which reaches the earth by scattering from particles that do not lie along the geometric straight-line path to Earth (Eshleman, 1973). Even though the rings consist of discrete particles, they interact with the radio wave in such a way as to produce average effects (per unit volume) on wave intensity and phase, much as does an atmosphere or ionosphere of discrete molecules or electrons. For the coherent signal, the rings can be characterized by their effective wave propagation constants. The coherent and incoherent components will be recognized and separated in the data on the basis of their spectral, time correlation, and polarization characteristics.

The first-order effects expected are shown in Figure 4. At each wavelength, the coherent component will be shifted in phase and attenuated due to the effective propagation constants of the ring material. If the concentration of ring particles varies with radial distance from Saturn, the progressive change in phase would correspond to small changes in the angle of refraction, so that it appears as a frequency shift in a manner that is analogous to an atmospheric occultation. Unlike atmospheric occultation, however, the reduction in the coherent signal intensity in ring occultation is expected to be due primarily to scattering of energy out of the direct path.

The phase of the coherent wave depends primarily on the total number of small particles per unit area projected normal to the spacecraft-to-Earth line-of-sight (i.e., the areal density). The precision of the phase data is limited by the oscillators employed. For frequency stabilities associated with the onboard oscillator, the threshold of detection would correspond to small ice particles whose areal density varies by about 20 g/cm^2 in a period of about 1000 s. Assuming a spacecraft velocity of 10 km/s in the plane of the sky, this gives a sensitivity to gradients in material of 2×10^{-3} $g/cm^2/km$, if the particles are small as compared with the radio wavelength.

The intensity of the coherent wave also carries important information about the ring particles. It appears that measurements of coherent signal extinction will be limited to an accuracy of about 10% at 3.5 cm-λ, and perhaps 1% at 13 cm, by systematic and slowly varying errors in spacecraft antenna pointing. For a simple model involving only optically thin regions and particles that are large relative to the wavelength, these errors would correspond to the same fractional error in the total projected area of the particles viewed against the plane of the sky. We estimate from current models for the B ring that this attenuation will be between 40 and 60 dB. As a result, the coherent wave may be below the limit of detection during portions of the ring occultation.

The incoherent signal illustrated in Figure 4 arises from scattering by ring particles with circumference greater than a wavelength. It can be analyzed in terms of the average angular scattering properties of the rings mapped into the frequency domain by the Doppler effect. This mapping can be understood in terms of the relative velocities between the spacecraft, ring particles, and the receiving station on Earth. Signals transmitted from the spacecraft illuminate ring particles at a frequency shifted by the instantaneous relative spacecraft-particle velocities. The component of the

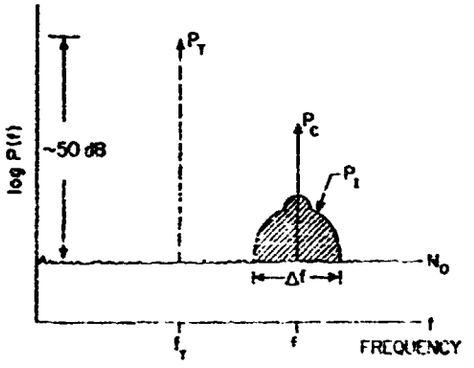

Figure 4. Signal characteristics during Saturn ring occultation — *Transmitted signal (P_T,f_T) is converted into coherent part (P_c,f_c) and incoherent part (P_I, Δf). System noise level N_0 is about 50 db below the received power in the absence of rings. Shape of incoherent spectrum schematically represents expected signature of a bimodal particle size distribution. Most scattering effects are wavelength dependent so that additional information is available by comparison of 13 and 3.5 cm results. Variation of incoherent spectrum with polarization is not illustrated.*

scattered wave that is re-radiated in the direction of the earth undergoes a second shift in frequency determined by the velocity of the particle relative to that of the Earth. The JST trajectory at Saturn was chosen in part so as to align the loci of constant Doppler shifts with the circumferential ring coordinate over a limited region of the ring plane. An example of one such set of Doppler loci is shown in Figure 5. As illustrated, each slice of the incoherent spectrum is closely associated with a portion of the rings at a constant radius from Saturn's center of mass. We estimate that the radial resolution achieved at 3.5 cm wavelength will be about 100 km, approximately 2% of the radial dimension of the Cassini division between the A and B rings. At 13 cm the resolution will be somewhat poorer due to the larger ring area illuminated at the longer wavelength, and the deviation of the Doppler loci from the ideal condition over the larger area.

A critical factor in the ring occultation experiment is the size of the particles relative to the size of the spacecraft antenna (3.66 m diameter). If the predominant particle size is greater than the spacecraft antenna size, then the forward scattering lobe will be narrower than the spacecraft antenna beamwidth. In this case, most of the scattered energy can be observed with a simple geometry in which the spacecraft antenna is always directed toward the geometric position of the Earth. However, particles smaller than the spacecraft antenna will produce forward diffraction lobes that are wider than the antenna beamwidth and no fixed condition of illumination will permit measurements of the entire scattering lobe. Current Earth-based radar observations indicate that many particles larger than about 2 cm in diameter are present in the rings, but give little hard information to constrain the upper size limits (Pollack *et al.* 1973). We cannot now predict which of the alternatives above best represents the conditions we will encounter or even if such conditions will be the same for all parts of the ring system.

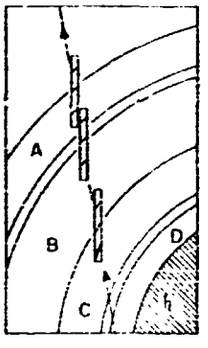

Figure 5. Radial resolution for incoherent signals in Saturn ring occultation measurements — *Figure represents ring plane with Saturn at lower right. Spacecraft is located below the plane of the rings out of the figure at the top of the page, earth above the ring plane out of the figure at the bottom of the page. Directed line from lower right to upper left is the path of the geometric ray between spacecraft and the earth. Boxes outline the ring plane area illuminated at three instants by the 3.5 cm antenna pattern. The one-half power contour is approximately an ellipse with axes given by the rectangle. Curved lines approximately tangent to the circumferential coordinates of the rings are loci of constant Doppler shift separated by 1 kHz. Measurement resolution is on the order of 20 Hz. Similar figure obtains at 13 cm wavelength except antenna beam intersection is larger and contours deviate from circumferential condition.*

The radio science team is planning to conduct the JST ring occultation experiment with the antenna directed toward the Earth. This strategy will yield the maximum signal-to-noise ratio for the coherent component. It will also yield the mean particle size and information on the particle size distribution, particularly if most of the particles are a few meters in diameter or larger. The effects of particles in the centimeter-to-meter size range will be recognizable in the data, although detailed information will not be available on the distribution of sizes in that range. We hope to obtain information on the intermediate-scale particles by incorporating an oblique scatter experiment in the JSX flyby, during which the spacecraft antenna will be directed toward the rings through a range of oblique scattering angles, but the feasibility of this has not yet been completely determined.

Polarization of the scattered waves is an independent observable which is germane to the study of the incoherent signal, and in principle, to the coherent wave as well. The polarization of the coherent wave will be modified by factors that depend primarily on particle shape if multiple scatter can be neglected, and by a combination of particle shape and multiple scattering in regions where the latter is important. Strong depolarization is observed in backscatter radar observations, and is one of the puzzling aspects of the ring system in these Earth-based experiments (Goldstein et al., 1977). For the coherent wave, we know of no particular reason to expect strong polarization effects, but this could occur if non-spherical particles have ordered orientations.

Polarization measurements will be made with coherent receiving systems for right and left hand circular polarization at each wavelength. The data can be processed to determine the complete properties of the waves -- intensity, axial ratio and orientation of the polarized part, and the intensity of the unpolarized part -- as a function of time and frequency. For the coherent signal, data processing based on polarization will improve the a posteriori signal-to-noise ratio.

The discussion above is expressed in terms of a simplified, single-scattering model. However, the fundamental experimental considerations of geometry and strategy do not depend on that model, but only on the assumption that the particles follow individual Keplerian orbits with few collisions. We expect to encounter a wide range of conditions as the radio beam moves outward through the ring system, and there may be no single scattering model or analysis technique which is appropriate over the full range. We are engaged in a continuing study of this experiment with emphasis on the sensitivity of data inversion to the experimental parameters, and on more complex models which include multiple scatter and polarization.

REFERENCES

Anderson, J. (1976). The gravity field of Jupiter. In *Jupiter* (T. Gehrels, ed.), pp. 113–121. University of Arizona Press, Tucson.

Eshleman, V. (1975). Jupiter's atmosphere: Problems and potential of radio occultation. *Science 189*, 876–878.

Eshleman, V. (1973). The radio occultation method for the study of planetary atmospheres. *Planet. Space Sci. 21*, 1521–1531.

Eshleman, V. (1965). Radar astronomy of solar system plasmas. In *Solar System Radio Astronomy*, (J. Aarons, ed.), pp. 267–293. Plenum Press, NY.

Eshleman, V., Tyler, G., Anderson, J., Fjeldbo, G., Levy, G., Wood, G., and Croft, T. (1977). Radio science investigations with Voyager. *Space Sci. Rev. 21*, 207–232.

Fjeldbo, G., and Eshleman V. (1968). The atmosphere of Mars analyzed by integral inversion of the Mariner IV occultation data. *J. Planet. and Space Sci 16*, 1035–1059.

Fjeldbo, G., and Eshleman, V. (1965). The bistatic radar-occultation method for the study of planetary atmospheres. *J. Geophys. Res. 70*, 3217–3226.

Fjeldbo, G., Kliore, A., and Eshleman, V. (1971). The neutral atmosphere of Venus as studied with the Mariner V radio occultation experiments. *Astron. J. 76*, 123–140.

Goldstein, R., Green, R., Perrengill, G., and Campbell, D. (1977). The rings of Saturn: Two frequency radar observations. *Icarus 30*, 104–110.

Hubbard, W., Hunten, D., and Kliore, A. (1975). Effect of the Jovian oblateness on Pioneer 10/11 Radio occultations. *Geophys. Res. Lett. 2*, 265–266.

Hunten, D. (ed.). (1974). *The Atmosphere of Titan. NASA SP-340*, NASA, Washington D.C. 185 pp.

Kliore, A., Cain, D., Levy, G., Eshleman, V., Drake, F., and Fjeldbo, G. (1965). The Mariner 4 occultation experiment. *Astronaut. Aeronaut 3*, 72–80.

Kliore, A., and Woiceshyn, P. (1976). Structure of the atmosphere of Jupiter from Pioneer 10 and 11 radio occultation measurements. In *Jupiter* (T. Gehrels, ed.), pp 216–237. University of Arizona Press, Tucson.

Marouf, E. (1975). The rings of Saturn: Analysis of a bistatic-radar experiment. Ph.D. dissertation. *Technical Report 3240-1 SU SEL 75-006*, Stanford Electronics Laboratories, Stanford University, Stanford, CA.

Pollack, J., Summers, A., and Baldwin, B. (1973). Estimates of the size of the particles in the rings of Saturn and their cosmogonic implications. *Icarus 20*, 263–278.

THE MAIN SCIENCE QUESTIONS AFTER VOYAGER

Panel I
E. Stone, Chairman, D. Hunten,
L. Tyler, J. Warwick

E. STONE: I would like to encourage the panel members to address not so much the implementation aspects of what they think ought to be done next, but to address what are the science issues, and of course that will lead them into some implementation questions which can be addressed. But I think one ought not be primarily focused on implementation issues for this panel. The first topic is Titan.

D. HUNTEN: It seems to me even before Voyager gets there we should have settled the issue of the surface temperature of Titan by the consensus of several radio measurements. My personal prejudice right now, of course, is that the temperature will turn out to be fairly large, around 200 K, with a pressure of at least 20 atmospheres. I could be wrong, but I'll proceed on the assumption that I'm not wrong about that particular aspect.

The surface temperature and pressure will then be a datum that Von Eshleman and Len Tyler could use for planning their occultation measurements of Titan: for example, whether or not to slew the antenna to optimize the radio occultation. So we'll have a good radio occultation measurement. The level of critical refraction for an adiabatic atmosphere seems to be quite deep, according to Tyler's presentation this morning, deeper than 20 atmospheres, maybe even 30 or 40.

There's a very good chance that they will be able to probe all the way to the true surface, although they could easily run into a layer of ammonia and if it's any warmer than 200 K, a layer of ammonia vapor is quite likely. So, again, it may be an apparent "surface," not a real one. Of course, if you get that glint, that bistatic glint, then you'll have it made.

Even if they don't get that deep, we'll have a very good idea about the true nature of the atmosphere, especially the mean mass. So we'll know whether the ideas

about nitrogen make any sense or not, because that will be found from the atmosphere above the cloud tops where we already know the temperature pretty well.

We'll also have a measurement of the ionosphere, presumably, which will probably be as mysterious as the ionosphere of Jupiter which we don't really understand.

We'll also have the data from the ultraviolet spectrometer which will have explored the torus of Titan and its upper atmosphere in the airglow mode, and looked for helium and presumably not found it. But we can't be absolutely sure until we look. And then it will have the solar occultation measurement, which will tell us quite a bit about the upper part of the atmosphere and tell us how high methane extends, in particular, which is quite a tricky thing because it's destroyed photochemically fairly rapidly.

And so with any luck, we'll have a very good idea of the basic physical properties of Titan: Its actual radius, its actual density, and the composition and general nature of the atmosphere.

So, the next question is what we'll want to know after that. Clearly, as far as atmospheric composition goes, we'd like to be a lot more certain than we ever can by remote sensing.

The Mars Viking landers detected several very important gases which simply aren't amenable to remote sensing: argon, nitrogen, and some isotopic ratios. That experience is a very good guide to what we'll want to do on Titan. We'll want a refined analysis of both major, medium and minor constituents of the atmosphere. Something for which Titan is already renowned, of course, is organic chemistry. We're going to have to pay a good deal of attention to that. Hopefully, we'll be smarter by then than we were when we designed Viking, and we'll know what to do about organic chemistry. Clearly, that's going to require a certain amount of laboratory work.

My personal predilection would be to try to learn something about the upper atmosphere of Titan also. I think this is one of the important insights that's come out of this meeting, something that perhaps should have been obvious but didn't occur to me, that methane is liable to be present at very high altitudes and subject to low energy proton bombardment, along with the nitrogen, if it's there, and produce a great deal of interesting chemistry right at the top of the atmosphere. So I think that emphasizes once more that aeronomy is more than a minor subject of interest to a few specialists. It actually does bear on quite important questions sometimes.

E. STONE: So your comments are really focused on two areas: One is the detailed composition of the atmosphere as a whole, which means a probe, and the other is the upper atmosphere composition, where one is possibly seeing some chemistry going on. So you're focusing on the chemistry of Titan's atmosphere as a key to the future objectives of both lower altitude and upper altitude chemistry.

D. HUNTEN: Yes. There is also a lot we'd like to know about the surface, but I'm mentally giving up on that for the moment and saying let's study it indirectly through what we can measure in the atmosphere.

J. CALDWELL: With any luck at all if the VLA observations work at one, two, and six centimeters, we should have some indication whether or not the thing that determines the opacity is in fact ammonia. So that uncertainty, along with the radio brightness temperature discrepancy, will hopefully be removed in the near future.

I would judge that the radio occultation is a very important experiment, and I would like to offer the maybe heretical viewpoint that it is more important than almost anything else Voyager can do on Titan. In particular, because of the possibility that the atmosphere is opaque at visual wavelengths, I am convinced that high resolution imaging of Titan is scientifically risky. Voyager should do the radio occultation right, and plan other experiments around.

E. STONE: Can we talk about what you think are the key questions after Voyager? Do you have anything to add to what Don had discussed, which was basically this question of composition?

J. POLLACK: I think another thing that a probe will do very nicely for us is on cloud structure, both in the sense perhaps of telling us something about the distribution of the aerosols, as well as the presence and location of major condensation clouds in the atmosphere.

I also think that we should look to try to get as much information on the dynamics of Titan's atmosphere as we can. And one subject that, for reasons I don't quite understand, I always seem to be bringing up is that the Doppler-shift velocity measurements are a very relevant way of seeing what the velocity shear is in planetary atmospheres, including Titan's atmosphere.

I think dynamics is certainly a very important area as a general objective.

D. MORRISON: Jim, as I recall a paper that you and Conway Leovy wrote, you predicted extremely sluggish dynamics on Titan. Are there really measurements that will reveal those kinds of motions? How important is that particular set of observations?

J. POLLACK: I would say it's extremely important because one of the general overall objectives in the planetary program is to use planetary atmospheres as sort of natural laboratories for meteorological studies to see how differences in their makeup (for example, rotation rate) affect the way in which their dynamics behave. Titan's rotation period of 16 days makes it an especially interesting case. Most planets are roughly one-day planets. And then we have Venus, which is a 100-day planet in terms of its rotation period. And Titan is very nicely intermediate. So I think it's quite important in that sense.

E. STONE: Is there anyone else who sees a principal science objective with respect to Titan that has not been addressed here?

S. CHANG: How about surface analysis? That is, an assessment of the volatile content versus the non-volatile content, for instance. And if there are a lot of volatiles there, what's the distribution between ices, organic matter, and so on?

You may get some information from the atmospheric analyses, both particle-wise, as well as molecular composition, but it may be difficult to extrapolate from those to the material actually on the surface.

E. STONE: Could I ask: Is a surface composition analysis an important part of the story of understanding atmospheric composition, or can one do atmospheric composition studies without a detailed understanding of the surface composition?

D. HUNTEN: One of the main reasons to be interested in atmospheric composition is the clues that it gives you about the surface and interior. It's not the only reason, but it's certainly a principal one. It's quite possible on Titan that the surface is kind of incompatible with the atmosphere. It may be a layer of oily tar or something like that. I think I'd go along with Sherwood and say the surface is an important objective, quite apart from whether we regard it as a feasible one. Can the bistatic radar tell a liquid from tar from a sheet of ice on the surface of Titan?

L. TYLER: I don't know about tar. We would not be able to tell ice from a soil of comparable roughness. Liquid depends on what kind of waves are propagating in it. If you have winds on Titan, yes, I think we'd know that.

D. MORRISON: I presume Voyager will answer the question as to whether Titan has an intrinsic magnetic field. I don't know how much it will tell about the moments of the gravity field, but I should think that understanding the degree to which the interior is differentiated, as derived from dynamical studies, would be an extremely important observation.

J. BLAMONT: If Titan is liquid inside, maybe the surface moves on top of this liquid. Why not? And, therefore, we are in a new situation. So, I wanted to ask if a computation has been done? Let's suppose that we have water. What's going to happen to the surface? Is it going to move with it? And, how? Maybe it would be interesting to try to do some small seismology experiment. I'm sorry to be kind of crazy, but if we are serious about Titan being liquid, then it may move.

D. HUNTEN: Jacques is suggesting that maybe the whole idea of a spherically stratified planet is too simplistic. It certainly is for the Earth. The Earth does exactly what you said, although on a very slow time scale. Maybe Titan has continental drift too.

S. CHANG: If the surface is a solid and one needs to belch gases from the interior into the atmosphere, does it make sense to have an experiment where you can measure the rate at which that kind of activity takes place or if it exists at all?

E. STONE: I think I would like to turn to Saturn's atmosphere and ask Jim Pollack to lead off with a 5-minute analysis of what should be done after Voyager.

J. POLLACK: Galileo gives us a very good starting point in terms of the general objectives for the Saturn atmosphere. Basically, a heavy stress is put on getting compositional information, particularly because of its relationship to some fundamental cosmogonic questions.

In addition, one would like to get information about cloud structure, and in addition, to study the dynamics of the atmosphere.

In the talk that I gave earlier, one thing that I mentioned is that Saturn could have a very interesting difference at the current time in terms of the factors responsible for its excess luminosity, mainly that it may be cold enough in the metallic region for helium to start segregating from hydrogen and for that to act as a source of excess energy. And the way to get at this is to have a very accurate measurement of the helium to hydrogen ratio and compare that accurate number to the accurate number you'd get from Galileo.

In terms of questions related to the origin and evolution of the Saturn system, it's important to get an assessment of what the amount of excess heavy elements are, particularly volatiles, and also silicates. This means finding out how much methane, ammonia, and water vapor is in the observable atmosphere, and in an indirect way, seeing if there is an excess of silicates in the envelope of Saturn.

In terms of dynamics, fair amounts can be learned from Voyager. It would be interesting having additional synoptic-type information from an orbiter and, in

addition, whatever information we can get about winds in the case of the Saturn atmosphere.

In the case of outer planets like Saturn, there is a thought that there may be a sequence of condensation clouds, beginning with the ammonia condensation clouds, then ammonium hydrosulfide clouds, and then finally, water vapor clouds.

The final point has to do with Saturn's magnetic field. The current thinking is that planets like Jupiter and Saturn have a dynamo mechanism for the magnetic field that's related to regions of high conductivity, namely, the metallic hydrogen region. Now, the interesting difference between Jupiter and Saturn is that the metallic region of Saturn has a much smaller volume than in the case of Jupiter. That means, for example, that you should have much more of a dipolar nature to a field that is produced by a more central region than in the case of Jupiter, so that learning about Saturn's magnetic field properties and comparing that to Jupiter's magnetic field properties could be an interesting exercise for the clues that it gives us about the origin of the magnetic field.

E. STONE: The point about the magnetic field is that you'd like to understand the magnetic field to some fairly high order, which you cannot do with a flyby.

L. TRAFTON: I think it might be interesting to try to study the dynamics in the neighborhood of the boundary of the shadow of the ring on the surface of the planet. There is some indication that the atmosphere may be more hazy when the percentage of the disk shaded by the rings is large, and this might be due to dynamical effects driven by the gradient between light and dark or hot and cold regions occurring at the edge of the ring shadow.

G. ORTON: I think radiometer studies are very important. So far, with the exception of possibly Uranus, Saturn represents one of the most oblique planets that has a studiable temperature. And we're seeing rather tremendous changes in thermal structure which seem to be tied closely with the amount of insolation taking place. There is a variety of things which should be dealt with in the synoptic sense.

J. POLLACK: What are the changes that you're referring to? Are they spatial or temporal?

G. ORTON: Both. If you're sitting at the pole, then you're seeing changes throughout the year. If you're sitting at the Equator, then you're going to go through the ring shadow.

D. MORRISON: Since Saturn appears to have much stronger driving forces for atmospheric motion because of its obliquity and because of the ring shadows, is it not a little strange that it seems to have many fewer atmospheric storms that are visible from Earth than Jupiter?

G. ORTON: One possible reason for the difference is the complex atmospheric structure. On Saturn, the haze may be greater, so we don't see the dynamical effects as well as in Jupiter.

B. SMITH: Also, Saturn is twice as far away. However, I believe Saturn is actually less active. There is a point I would like to make with regard to the ring shadow. When seen by Voyager, it will be a fairly narrow projection on the equatorial region, whereas in the late 80's, the shadow will cover a very, very large part of the southern hemisphere.

D. MORRISON: It may be important to look again with a spacecraft when the ring is open. As now planned, SOP[2] will arrive at Saturn in 1991, while the tilt is still large. But if the mission slips to the mid 1990's, we'll be back looking at Saturn in the same situation as Voyager.

J. WARWICK: The discovery and initial exploration of the non-thermal radio emission properties of Saturn will be accomplished on Voyager. We have really no secure idea as to what will appear. If we see nothing, all right. But what we see may well be only exploited on further spacecraft. It certainly won't be studied usefully from the ground or near the Earth.

E. STONE: So there is always the point that we don't know some of the questions we need to ask and we won't know them.

Let's summarize the questions that we have identified for Saturn:

(1) The probe will allow us a direct compositional comparison with Jupiter.

(2) It also allows us to do a more detailed, specific study of clouds and temperature structure, and possibly dynamics.

(3) Synoptic observations have been identified for dynamical studies, including effects of the ring shadow.

(4) Finally, the higher order details of the magnetic and gravity field may tell us about the difference between the internal structure of Saturn and that of Jupiter.

I would like now to move on to the other satellites, and ask Dale to lead off.

D. CRUIKSHANK: There is a serious lack of hard information about any of the satellites and even about the existence of some of them. In this sense, trying to decide

what should be done from a post-Voyager probe is a little like sitting in the Court of Queen Isabella the day after Columbus set sail and trying to figure out how to explore the Mississippi River and the Rocky Mountains. You don't even know if they're there.

So the kinds of things that I could put on the list are all the fairly obvious ones that have surely appeared on countless planning documents in preparation for a spacecraft already en route.

One important thing, though, is that Voyager and the Galileo experience, in imaging the Galilean satellites, will tell us a lot about the effects of large and medium-scale topography on such Earth-observable parameters as the solar and orbital phase functions. This will help us to interpret the data we now have on the satellites of Saturn.

From an orbiting spacecraft, the satellites should all be mapped at the highest possible spatial resolution. This permits people to do studies of the morphology of any features of any topography that might be seen. One can use crater counts to understand something about the flux of large impacting particles in the early history of the solar system in that neighborhood of the solar system. This will be the first opportunity to study close up the morphology of satellites that are almost surely ice or other frozen volatiles.

There have been papers by Torrence Johnson and others on what kind of morphology might be expected on such very low-density frozen satellites, and it is different from the kind of thing that we see on the Moon and Mercury and presumably the Galilean satellites. So there's a whole new area there.

It's important to study the distribution of the frozen volatiles on the surfaces of the satellites of Saturn and particularly to search for things other than water ice. Ammonia ice, in particular, is a very important one because ammonia ice on the surface almost certainly reflects ammonia ice in the interior, or some ammonia mixture in the interior. And because ammonia has a profound effect on the melting temperature of a water-ammonia ice mixture, it will have a great influence on the question of the thermal history of the interior.

So the detection of some other materials in the frozen ice on these satellites is very important. And, of course, once you find it, you'd like to look at its distribution around the surface. Now, how to do that is still an open question, because the presence of water ice tends to mask the presence of anything else. If further laboratory studies show that remote sensing either further in the infrared or the ultraviolet can resolve

other things from water ice, then that will provide the criteria on which any instrument to do this would be designed.

Interior structure and thermal history can also be investigated using the gravitational moments of the satellites, and by repeated close passages of the spacecraft to at least one or two of the satellites, one could presumably determine some of these crucial things.

One should search for atmospheres and ionospheres of at least the largest of the satellites of Saturn, and this can be done nicely by well-proven occultation experiments.

We know that frozen water vapor even at a very low temperature has a finite vapor pressure, and so there must be some molecules in an atmosphere surrounding an icy satellite even at 100 K. Whether or not we can detect it is another question, but the occultation technique is a very powerful one.

D. HUNTEN: The atmosphere of Mercury was detected by ultraviolet spectroscopy, not by occultation techniques. Generally UV is much more sensitive.

D. CRUIKSHANK: I don't care how you find an atmosphere. But there is a molecular atmosphere surrounding an icy satellite at 100 K. Let's go find it. And let's also find out if it's been dissociated by solar ultraviolet to form oxygen and all the things that people are talking about surrounding the Galilean satellites which haven't yet been found.

The question of the interaction of the surface materials, the ices or whatever, on the satellites with the magnetospheric particles is of interest too. Have the ices been modified to some degree that we can't determine from the ground? That's something that needs to be looked at, both in the laboratory well in advance of any spacecraft experiments, and also done on the spacecraft itself.

We should also be trying to understand the interaction of the surfaces of the satellites with any extended ring particles in Ring E. Is the diffusion time of particles radial to Saturn in this extended range so fast that, for example, every time a satellite makes an orbit it sweeps up a new batch, or is the diffusion time so slow that each satellite has carved out for itself a wake which it continually maintains? Those are the kinds of scientific questions that I think need to be answered.

D. MORRISON: I would make a special point of Iapetus because some asymmetries in photometric properties are seen on almost every satellite as a general phenomenon. Iapetus is such an extreme example that I would think that no matter what Voyager tells us, we're going to want to follow up in a detailed way to understand

the photometric asymmetry of Iapetus, and what it is telling about Phoebe or ring particles or magnetosphere or whatever. It's almost surely telling us something about more than just Iapetus itself.

R. MURPHY: I think it would be important to try and extend our knowledge of what the inventory of satellites around Saturn actually is.

B. SMITH: Well, Voyager will do a lot of that, particularly if you're talking about the inner satellites. For faint outer satellites, it is best done from the ground with large telescopes.

D. MORRISON: We should remember that we have yet to really see any satellite anyway, except Phobos and Deimos. I bet you that as soon as we've looked at the Galilean satellites, let alone when Voyager gives its first glimpse of the Saturn satellites, we'll think of a whole myriad of new problems.

E. STONE: Let's move on to the next topic which is the rings. Jeff, could you lead off.

J. CUZZI: I think a study of the rings is important from two standpoints: first is their own origin, and the second is that they provide an extremely important boundary condition on the protoplanetary nebula.

There are different ways of getting at these two topics:

(1) Through the size and size distribution of the particles themselves. The radius limits and slope of the power law distribution, and their variations with radial distance are important for questions of ring formation and evolution. In particular, the size of the largest particles is a critical number.

(2) Through the composition of the particles. Are there any silicates and if so, in what amounts? Do the amounts vary with radial distance? What causes the reddening of the rings, relative to the satellites?

Size distribution information is especially important near the ring boundaries and in the Cassini division because that's where the dynamics influence the rings the most strongly.

As far as the global structure of the rings themselves, there are three important things:

(1) The local microstructure of, for instance, the nonaxisymmetric brightness variations in the A Ring, and telling us something about gravitational perturbations which could be very important for learning how planets themselves form.

(2) By observing the edges of the various ring boundaries, you learn the dynamical strengths of the resonances. That is, how effectively are the resonances keeping the particles in, and hence how much mass has been lost over the age of the solar system. Do the thickness and volume density vary near the resonances? This could indicate that the resonances may be sources of particle dispersions, and may affect estimates of the age of the rings.

(3) The mass of the rings. I suspect that to get very good J_2 and J_4 on the planet, we might need a better estimate of the mass than Voyager can provide, so I think repeated orbits would be very important.

L. TRAFTON: What about inhomogeneity with depth perpendicular to the rings?

J. CUZZI: That has to do with the stratification of sizes, which is an interesting thing to look at. The way you get at that is probably with the repeated radar observations. The best way to do the size distribution studies would be by doing lots of bistatic radar mapping.

L. TRAFTON: Is there any particular reason to expect the top side of the ring to look just like the bottom side?

J. CUZZI: Yes, it would be symmetric about the midplane. But it wouldn't be at all surprising to find little particles going much farther up than big particles.

D. CRUIKSHANK: We should look for atmospheres of the rings for the same reason that we should look for atmospheres of the satellites.

J. CALDWELL: Is this out of the range of possibilities for Voyager?

R. HANEL: No, we plan to do that, looking just at a time when we pass through the ring plane. Of course, with IRIS we'll be limited primarily to water vapor, methane, and ammonia.

L. HUNTEN: UVS will be looking for atomic hydrogen.

D. MORRISON: I would venture the prophecy that the rings will seem increasingly important as we learn about other ring systems. The differences are so striking between Uranus rings and the Saturn rings. We don't know if Neptune has a ring system. If there are other ring systems and we find them differing in significant and poorly understood ways from the Saturn system, I expect it will increase our motivation to understand the Saturn system better.

D. CRUIKSHANK: I think we need to find out if the rings are accreting or if they're a steady state; or if they're slowly evaporating, if particles are flowing from

the rings onto the atmosphere of the planet, or if there is any change in the rings at all that could be observed by, say, an orbiter rather than a flyby.

B. SMITH: Quite apart from the scientific interest of particle sizes in the so-called E Ring, if they are the wrong size (mm range) it constitutes a potential hazard for any Saturn orbiter making multiple passes through that ring plane. I don't know how to get the answer before SOP[2]. During the 79/80 ring plane passage we should get very reliable measurements of the optical thickness from the outer edge of the visible rings all the way out to Titan. However, to translate that into particle size is another problem.

E. STONE: In September 1979, of course, Pioneer 11 will be penetrating the ring plane. It's a single, one sample test of particle size.

D. MORRISON: Because of the inclination of the rings, studies from an orbiter which has a long lifetime may be especially valuable. The opportunity to look from above, from below, edge-on, over a period of years as the tilt changes may allow us to answer some questions that seem difficult right now, and that are not going to be well answered by any single snapshot view.

I believe there are people who still question the antiquity of the rings, and I would expect that one motivating factor behind some of these dynamical and size distribution studies might be to understand if the rings have been there since the formation of the solar system.

L. TYLER: I think the radar experiment on Voyager will determine mean particle size and the width of the distribution function. If we can get some scattering away from the straightforward direction, that is, some phase-angle coverage, then I think we can begin to say something about the size distribution referenced to some model, but I think it would still be open to question.

E. STONE: Let's move along to the last, final topic which is the magnetosphere. George, would you lead off?

G. SISCOE: I'd like to start by addressing the questions that have to do with the two things about Saturn's magnetosphere that make it interesting in comparison with all the other magnetospheres, namely, the presence of Titan and the rings.

It seems to me that what the Voyagers will do for us is to identify the grossest features related to the presence of Titan and the rings. These will tell us what general class of physics to apply, but they will leave undefined most of the important details.

The Pioneer and Voyagers will almost certainly determine for us the magnetic field at Saturn, and we will learn from that information whether Titan is inside or

outside the magnetosphere. No matter which it is, the interaction with Titan is going to be important and even interesting.

If Titan lies outside the magnetosphere part of the time, then, of course, there will be a solar wind interaction. Even in this case, however, Titan will pass through the tail of the magnetosphere, and the entire magnetospheric tail population will then be important as a boundary condition to Titan physics.

If Titan lies inside the magnetosphere all the time, there are still two possibilities: it might be that the solar wind convection sweeps away Titan generated particles faster than they diffuse inward, so that the picture I described before does not apply. Then the main magnetospheric particle populations affecting Titan might be solar wind particles that have entered into the tail. The other possibility is the one that I described, with a fully involved magnetosphere and a fully engaged Titan torus. The important physical parameters in this case relate to the particle transport problem, which means the diffusion coefficient, if our present thinking on the problem is correct.

Then going on to the rings, I do not know how well the Voyagers will define for us the inner edges of the particle population, on which information is needed, so that we can get a good idea of the absorption boundaries. That measurement should be done in detail from a more protracted series of observations from an orbiter. It is a very important measurement that couples the diffusion coefficient and the absorption process.

The question of the E Ring might be solved in this way, as was noted by Brad Smith, since the particles might disappear faster than they should if they are only interacting with the A Ring. Also, I think that the subject that [illegible] brought up about the flux tube interaction with Titan [illegible] from the point of view of comparative studies [illegible] and radio emissions could be well investigated from an orbiter.

One would also like to look very carefully at the effects of satellites other than Titan to determine the individual particle environments of the satellites. As has been demonstrated in the case of Jupiter's satellites, one can obtain the diffusion coefficient at the location of the orbits from differential measurements across the orbit.

Going on to more general things, it is important from the point of view of magnetosphere studies to obtain a detailed morphology of the magnetosphere particle populations and their time variations which cannot be obtained from one or two passes through a magnetosphere. One would like to have a long-lived data gathering system

to look at variations which are probably going on at time scales of months, the intrinsic time scale of the transport processes.

E. STONE: The Pioneer 11 trajectory will take the spacecraft inside the L shell which is connected to the outer edge of the A Ring; in fact, it will continue on in, into the C Ring region. So Pioneer 11 will, for energetic particles at least, see the interface between the energetic particle population and the ring material.

What Pioneer 11 will not do is measure the plasma environment at the same time. So, in that sense, there is an essential missing ingredient in understanding the interaction of the rings. Voyager will not, in fact, get close enough to the A Ring to do the job.

L. COLIN: Why do you say the plasma will not be measured?

E. STONE: The Pioneer 11 does not have a magnetospheric plasma instrument on it. There is some chance there may be some plasma information from John Wolfe's solar wind instrument, but it will be necessarily limited at best.

G. SISCOE: Since we will have the Galileo observations of Jupiter, the new data which would be acquired at Saturn by an orbiter take on more importance because the intercomparison of these two planets, which are so much alike in other ways, essentially extends their joint value beyond the sum of the two separately. It would give very important data upon which to base a science of comparative magnetospheres.

D. MORRISON: Why not compare the magnetospheres of Jupiter and Earth?

G. SISCOE: Because of the gap to run the theories from one to the other. It's much easier, for example, to go from Earth to Mercury, where the theories actually appear to allow you to do that. But you can't do that from Earth to Jupiter. There's also good reason to think you could do it from Jupiter to Saturn, and so you could have that class of magnetospheres defined and checked.

SATURN ORBITER DUAL PROBE MISSION

Richard P. Rudd

Jet Propulsion Laboratory, California Institute of Technology
Pasadena, California 91103

ABSTRACT

With the completion of the flybys of Saturn by the Pioneer 11 and Voyager spacecraft in 1979 and 1981 the reconnaissance phase of the Saturn system investigation will be completed. The logical follow on mission is one that provides the capability for detailed long duration observations of the planet and its satellites. This requires a Saturn orbiting spacecraft with remote sensing capability and with maneuvering capability to tour the satellites of Saturn. The described Saturn Orbiter Dual Probe mission and spacecraft combines three systems into a multi-purpose Saturn exploration package that can satisfy the exploration objectives. The spacecraft, as currently envisioned, consists of

(1) Saturn Orbiter
(2) Saturn Probe
(3) Titan Probe or Lander

This single spacecraft provides the capability to conduct *in situ* measurements of the Saturn and Titan atmospheres, and, possibly the Titan surface, as well as a variety of remote sensing measurements. The remote sensing capabilities will be used to study the surfaces, interiors and environments of Saturn's satellites, the rings of Saturn, Saturn's magnetosphere, and synoptic properties of Saturn's atmosphere.

Based on the 1975 report of the Space Science Board (1975), the recommended post-Voyager Saturn exploration objectives are:

(1) Intensive investigation of the atmosphere of Saturn including in situ measurements of the chemical composition made with an atmospheric probe.

(2) The determination of regional surface chemistry and properties of the surface features of satellites and properties of ring particles.

(3) Intensive investigation of the satellite Titan.

These objectives require, in addition to a Saturn orbiting spacecraft, a Saturn atmospheric probe and a Titan atmospheric probe or lander.

This paper discusses an example Saturn Orbiter Dual Probe (SOP^2) mission that satisfies these exploration objectives. The example spacecraft is a multi-purpose Saturn exploration package consisting of three separate spacecraft systems. These systems are:

(1) Saturn Orbiter

(2) Saturn Probe

(3) Titan Lander*

The Saturn Orbiter is the bus vehicle for the Saturn Probe and Titan Lander providing all propulsive maneuver capability necessary to deliver each of these vehicles. The Saturn Probe is deployed from the Saturn approach trajectory and the Titan Lander is deployed from Saturn orbit. Based on Jupiter Orbiter Probe (JOP) spacecraft studies by JPL and Titan Lander studies by the Martin Marietta Corporation, the necessary mass for each subspacecraft system is:

(1) Saturn Orbiter (less propellant tanks and propellant)	~590 kg
(2) Saturn Probe (no propulsive capability)	~200 kg
(3) Titan Lander (no propulsive capability)	~225 kg

The launch time period under consideration is 1986 utilizing a single space shuttle launch with the Interim Upper Stage (IUS) booster. This launch year should allow adequate time to incorporate knowledge gained by the Voyager flybys into the SOP^2 spacecraft design. This is of particular importance to the design of the Titan Lander where the current range of Titan atmosphere models is large. Based on a 1986 launch, the Saturn delivery mass capability for standard ballistic trajectories is inadequate to conduct the desired mission. A single shuttle launch is capable of delivering less than 900 kg to Saturn in this mode. Considering the orbiter propellant and tankage necessary to achieve Saturn orbit and perform all other necessary propulsive maneuvers, a delivery mass of approximately 2000 kg or greater is required. The exact mass requirement varies as a function of Saturn approach speed, V_∞. It

*This paper refers to the Titan vehicle as a lander, however, a less complicated atmospheric probe is also under consideration

would be possible with multiple shuttle launches (probably 3) with on-orbit stacking of IUS to provide the required delivery mass capability with a standard ballistic trajectory mode. Other Earth-Saturn transfer modes investigated to achieve an adequate Saturn delivery mass capability include gravity assist techniques and low thrust, ion drive. The gravity assist mode (VEGA or ΔVEGA) utilizes swingbys of Venus and/or Earth to add energy to the spacecraft orbit. Inherent to the VEGA or ΔVEGA mode is a long flight time of 7.5 to 8 years in addition to the necessity of executing an *additional* propulsive maneuver near Earth of approximately 2 km/s. Discussions of these gravity assist techniques are contained in Roberts (1975) and Martin Marietta Corporation (1976). The low thrust, ion drive mode also has long flight times, 7 to 8 years, if the current baseline Encke '87 system parameters are used. System performance improvements could however reduce flight time. In comparison to these delivery modes a combined ion drive/gravity assist mode utilizing an Earth swingby was found to provide the greatest Saturn delivery mass capability. Using this technique, mass delivery capabilities in excess of 2800 kg with flight times of 6 to 8 years are possible. Table 1 summarizes these different Earth-Saturn transfer modes. The

Table 1. 1986 Earth-Saturn Transfer Modes

Option	Saturn Delivery Mass,* kg	Saturn Flight Time, yr	Saturn Approach Speed, V_∞	Mission
Direct Ballistic	<900	5.7	5.4 km/s	Flyby and probe or lander mission possible
Ballistic Gravity Assist	2400 - 2600	7 - 8	5.9 km/s	Baseline Mission possible
Ion Drive	2100 - 2200	7 - 8	6.0 - 5.0 km/s	Baseline Mission possible
Ion Drive/ Gravity Assist	2800+	6 - 8	7.5 - 5.5 km/s	Baseline Mission possible

*Saturn Approach Mass, Not Mass in Orbit

baseline SOP[2] mission incorporates the low thrust, ion drive mode into its design. Major events of the baseline SOP[2] mission are described in Table 2 and illustrated in Figure 1. Spacecraft launch occurs in 1986 using a single space shuttle/IUS combination. The spacecraft consists of the Saturn Orbiter/Saturn Probe/Titan Lander combination and an ion drive propulsion module. The ion drive module provides low thrust capability for the initial 2 1/2 to 3 1/2 years after launch. at which time it is jettisoned and the spacecraft continues on a ballistic trajectory to Saturn.

Approximately 65 days before Saturn encounter the Saturn Probe is separated from the Saturn Orbiter on a pre-established trajectory to enter the Saturn atmosphere. The separation conditions had previously been established by propulsive maneuvers executed by the Saturn Orbiter. Following probe separation, approximately 60 days before encounter, the orbiter executes another propulsive maneuver to deflect its trajectory away from Saturn impact. This deflection is accomplished to establish a periapsis altitude of four Saturn radii (4 R_S) and to optimize the encounter time to maximize the Saturn Probe to Saturn Orbiter relay link data return capability. Figure 2 is an illustration of the probe entry and the orbiter passing overhead receiving the relay link.

Targeting options for the entry probe are best described by referring to the representative B-plane plot for Saturn Probe targeting contained in Figure 3. Saturn approach is from the north with a major portion of the planet being illuminated. The shaded band from the top to the bottom of the figure is the region of aim-points which result in an entry on the night side of the terminator. To the right of the band is a region of aim-points which miss Saturn entirely while to the left is a region of aim-points which result in entry on the daylight side of the terminator. The dot pattern shading in the lower right hand corner area of the plot is the region of trajectories which pass through the rings of Saturn. The curved edge of this region represents the innermost visible edge of the crepe ring. Three arcs (dashed lines) representing targeting for entry angles of -10, -20, and -30 degrees are shown parallel to the terminator. Another set of lines labelled from 15°N through 10°S are target points for entry at various latitudes on Saturn. The line labelled 0° is the equator. Any trajectory aimed between the equator and the edge of the crepe ring must necessarily pass through the ring plane and therefore through any ring particles as yet unobserved inside the crepe ring. Therefore, it is preferable, if possible, to land in the northern latitudes. For entry angles more shallow than -13 deg, it is not possible to land north of the equator. In order to avoid having a steeply inclined orbit and possible

Table 2. Baseline Mission Scenario

Time Relative to Probe Entry	Events	Comments
E - 750 days	Pre-Saturn Navigation Maneuver	$\Delta V \approx 5$ m/s
E - 70 days	Pre-Probe Separation Nav. Maneuver	$\Delta V \approx 5$ m/s
E - 65 days	Saturn probe separation from bus	Mechanical separation
E - 60 days	Bus deflection maneuver	$\Delta V = 77$ to 100 m/s (probe does not have maneuver capability)
E - 4 to 10 days	Pre-insertion Nav. Maneuver	$\Delta V = 10$ m/s
E + 0	Saturn Probe entry	Entry angle of 7.5 deg
E + 1/2 hr	Orbiter overhead from probe	Orbiter and probe have same radius vector
E + 2 1/2 hr	Insertion into Saturn orbit of periapsis 4 R_S and period 159.4 days	$\Delta V = 990$ to 1963 m/s
E + 79.7 days	Periapsis raise from 4 to 19 R_S	$\Delta V = 590$ m/s
E + 85 to 100 days	Pre-Titan Nav. Maneuver	$\Delta V + 20$ m/s
E + 159.4 days	Titan encounter pump-down and/or plane change	Saturn orbit period reduced to 31.9 days
E + 165 to 180 days	Pre-Titan Nav. Maneuver	$\Delta V = 20$ m/s
E + 191 days	Titan lander approach and entry	40 kg of landed science; 225 kg Titan approach mass
E + 0.5 to 1 year	Satellite/ring tour	$\Delta V = 50$ m/s

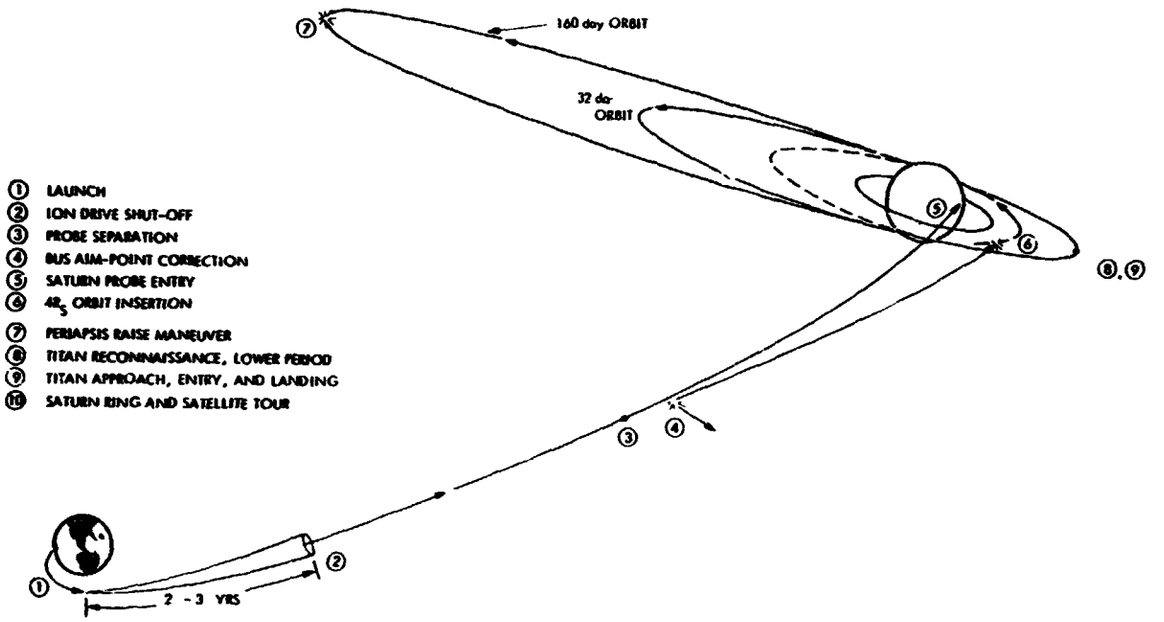

Figure 1. Baseline Mission Scenario

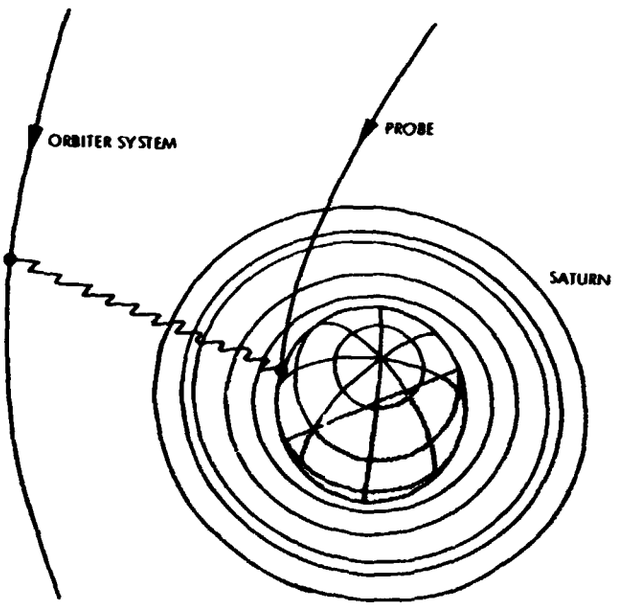

Figure 2. View from North Ecliptic Pole of Probe Entry

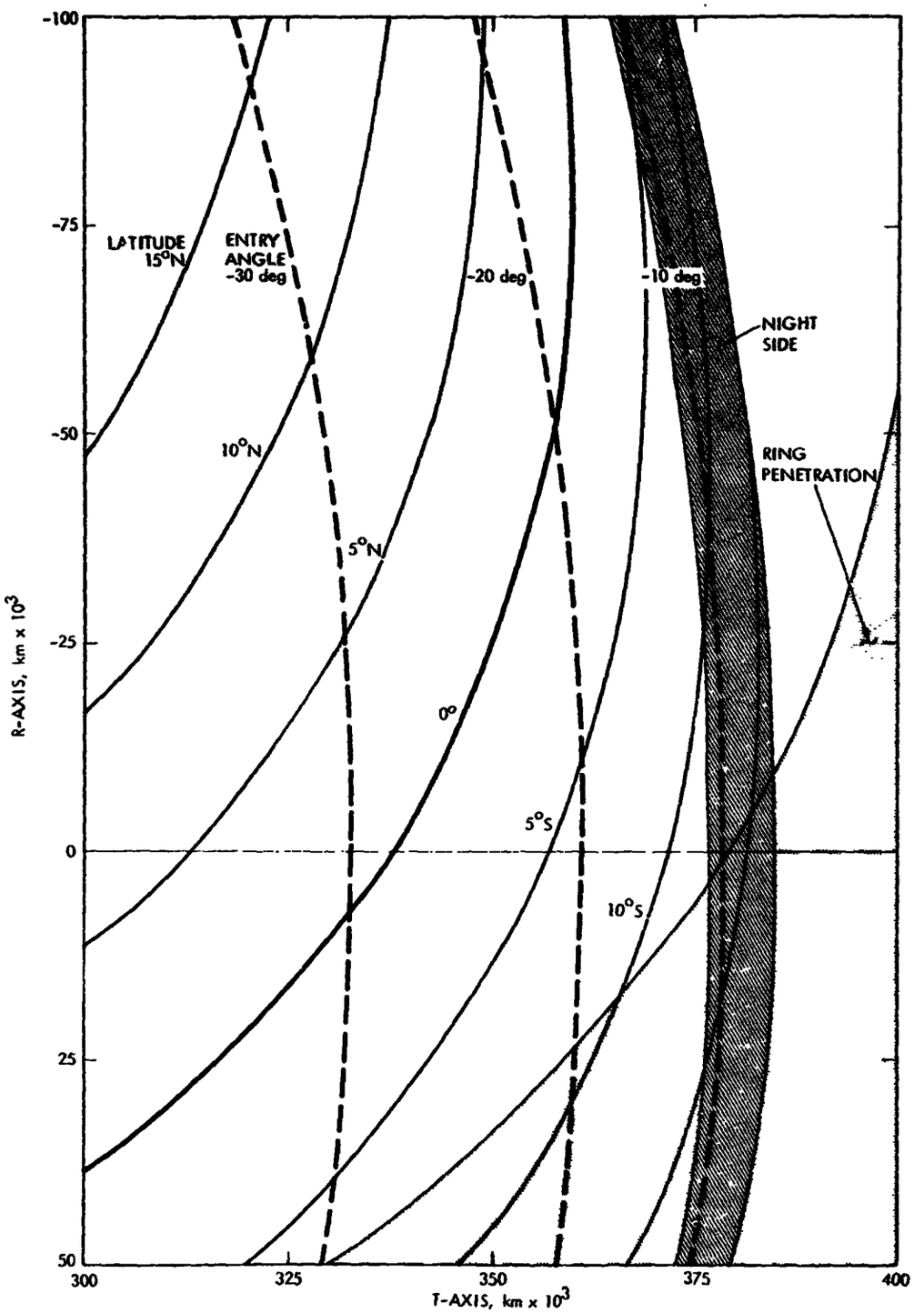

Figure 3. Saturn B-plane Mapping, Saturn Probe Entry Design

requirements for large plane changes, it is preferable to land as close as possible to an R value of 0, that is, near the lower part of the plot. A good aim-point for this approach trajectory would thus be for an entry angle of about -30 degrees, and an entry just north of the equator.

The Saturn entry environment is less severe than the Jupiter environment with the entry velocity being 27 km/s instead of the 48 km/s at Jupiter. Entry can occur at relative flight path angles of -6 to -40 degrees. The maximum axial load in this range of flight path angles is approximately 360 Earth Gs and a maximum dynamic pressure of approximately 600 kN/m^2 as compared to JOP's nominal of 385 Earth Gs and 800 kN/m^2. The convective heating rate is approximately 40% of a JOP entry. Using a JOP staging scheme the Saturn entry to a pressure altitude of 10 bars can be up to two hours duration which places stringent relay requirements on the orbiter as it flys overhead. Figure 4 illustrates representative relay link margins as a function of periapsis altitude and indicates the rationale for selecting a periapsis altitude of 4 R_S. A zero link margin is defined as that signal to noise ratio, 10 dB, required to support 100 bps (a preliminary JOP specification).

Approximately 2 1/2 hours after Saturn Probe entry the orbiter propulsion system is used to slow the spacecraft, inserting the Saturn Orbiter/Titan Lander systems into a Saturn orbit with periapsis radius of 4 R_S and an orbit period of approximately 160 days. This is illustrated in Figure 5 as well as other pre-Titan landing major events. Near the first apoapsis, ($\approx$184 R_S), approximately 80 days after orbit insertion, an orbiter propulsive maneuver is executed to increase the periapsis radius to $\approx$19 R_S in preparation for the first Titan encounter to occur approximately 80 days later. During this Titan encounter, the influence of Titan's gravitational field is used to "pump down" the orbit period to 31.9 days (twice the Titan period) and possibly change the plane of the orbit. During one of the subsequent Titan encounters the Titan Lander is separated from the orbiter on a pre-established entry trajectory for Titan entry and landing. The orbiter then executes a propulsive deflection maneuver similar to that performed in support of the Saturn Probe deployment. During Titan entry and landing, data are relayed to the Saturn Orbiter for playback to Earth. If the Titan Lander is intended to survive only a few hours after landing, the orbiter could be released after receiving the lander data to begin its satellite/ring tour. If the lander is intended to survive for months after landing, the orbiter will continue its Titan encounters to receive additional data from the lander. This assumes there will not be any direct playback between the Titan Lander and Earth ground stations.

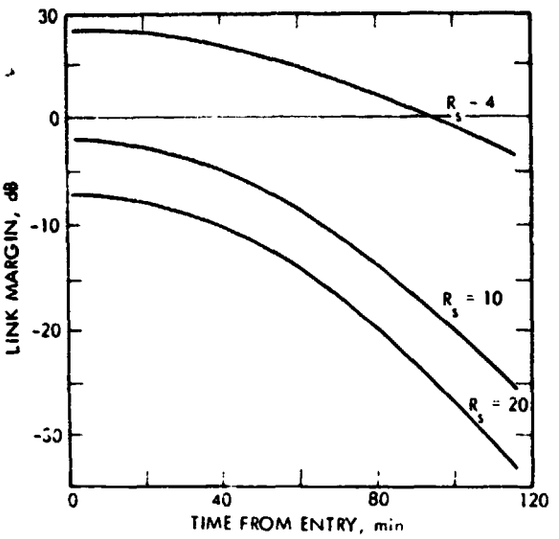

Figure 4. Link Margin vs Time from Entry (Periapsis Variation)

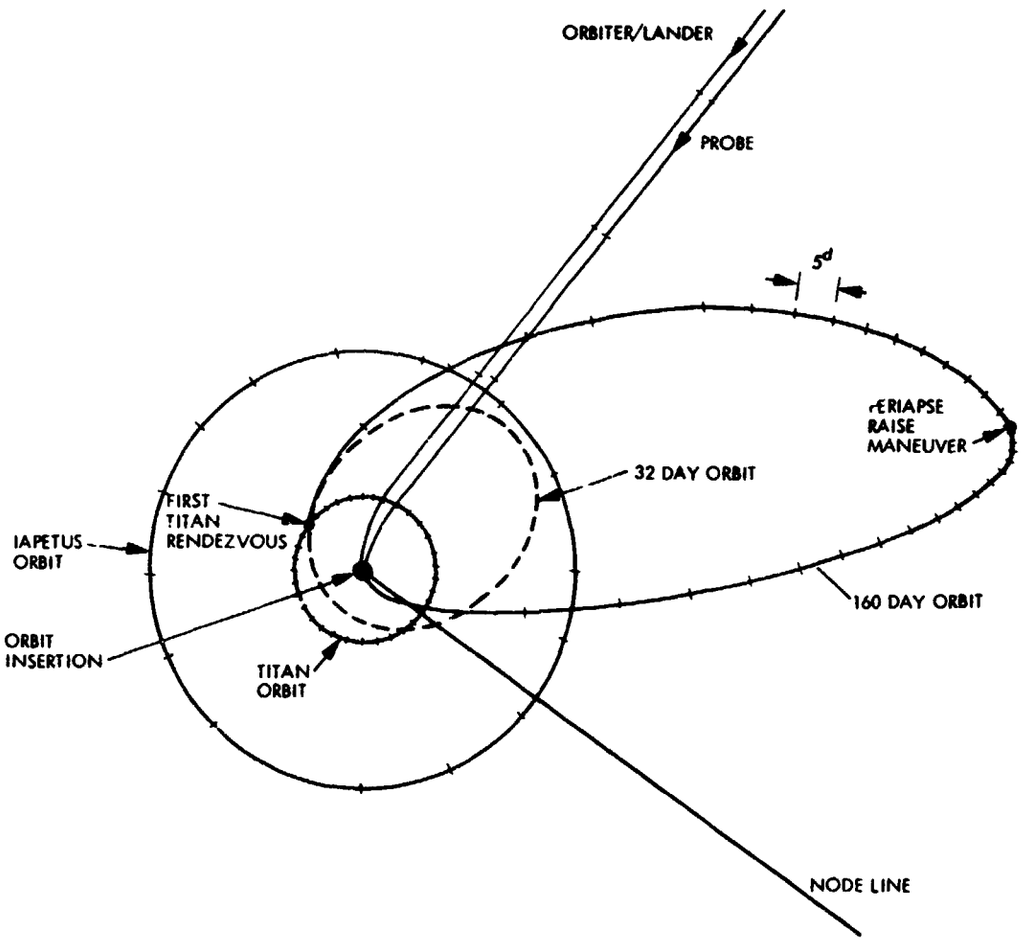

Figure 5. Pre Titan Landing Orbit Sequence

Another option for the Titan Lander would be to provide it with a propulsive and RF command reception capability. After separation from the orbiter the lander would, using its propulsion system, insert itself into a Titan orbit. After several revolutions, during which Titan is observed from orbit, the lander enters Titan's atmosphere and lands on its surface sending back data to the Saturn Orbiter via relay link. In this option the Saturn Orbiter would probably be in a nearly circular orbit at Titan distance ($\approx$20 R_S) but inclined with respect to Titan's orbit. This option would significantly increase the Saturn delivery mass delivery requirements and could mean even longer flight times or require a combination of low thrust and gravity assist modes.

Titan entry speeds for delivery from Saturn orbit range from 2.4 to 7 km/s. For the orbit previously described (periapsis radius of 19 R_S and an orbit period of 31.9 days) the entry velocity is approximately 2.8 km/s. For comparison purposes, the entry speed for delivery from Titan orbit varies between 1.7 and 2.4 km/s.

Titan appears to be the least difficult of any of the major Solar System bodies on which to mechanize a landing. It is expected that a Titan soft landing can be achieved with a lander vehicle of considerably less complexity than, say, the Viking or Surveyor vehicles. The current state of knowledge of Titan's atmosphere will probably not permit the design of a single cost effective lander for all atmosphere models. Surface pressure, just one of many parameters characterizing the Titan atmosphere, differs by a factor of 500 among the four models being considered, Figure 6. The Titan occultation data from the Voyager flybys in 1981 will be most important in hopefully reducing the range of atmosphere models that must be considered for SOP[2]. Titan landers can probably be configured without complex attitude or altitude control systems, the most complex device required being a parachute and/or simple touchdown cushion. For the super-thick Titan atmosphere model not even a parachute is required.

Descent trajectory profiles for the four atmosphere models are shown in Figure 7 for lander delivery from the previously described Saturn orbit. The ballistic coefficient of 100 kg/m^2 represents a 225 kg lander with a 2.25 m^2 aeroshell. For these trajectories the maximum axial load is significantly less than 10 Earth Gs, which is a representative upper limit that would not impact lander design. In fact, for an entry speed of 2.9 km/s flight path angles up to -90 deg still do not result in axial loads of 10 Earth Gs for any of the atmospheres. The shallowest entry angle is approximately -25 deg where skipout occurs. The maximum axial load experienced in

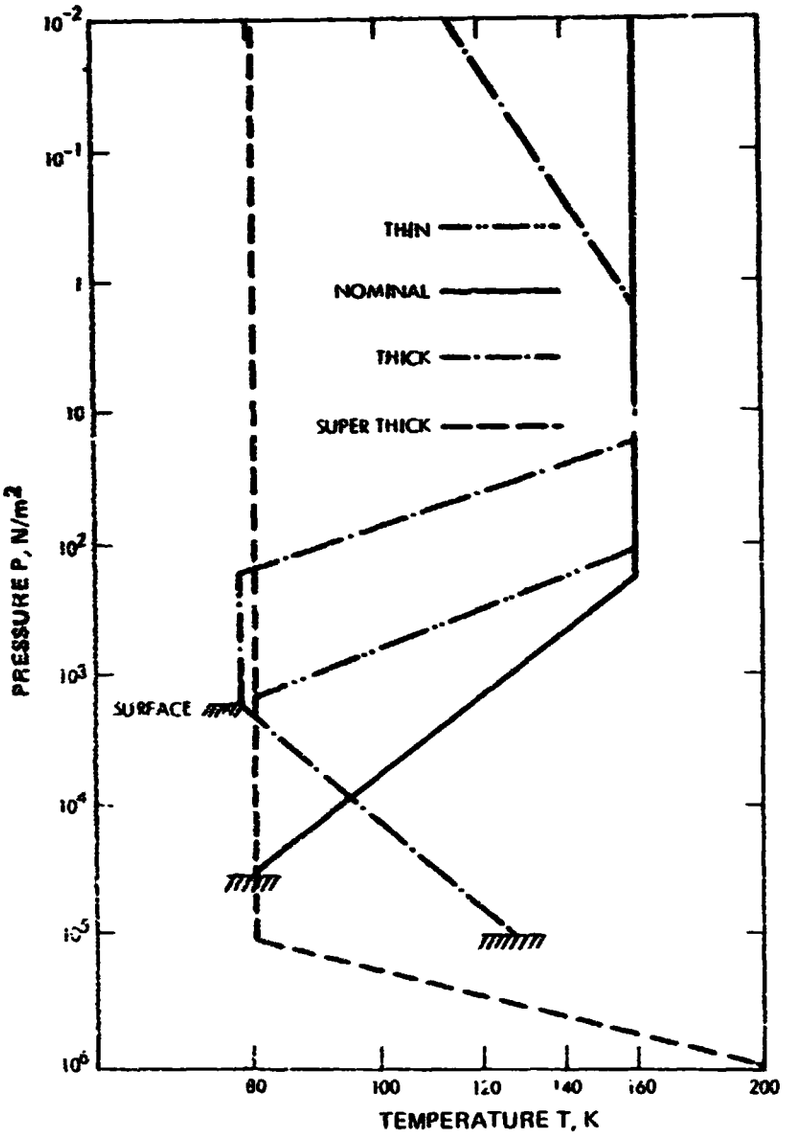

Figure 6. Pressure Temperature Profiles of Engineering Models of Titan's Atmosphere

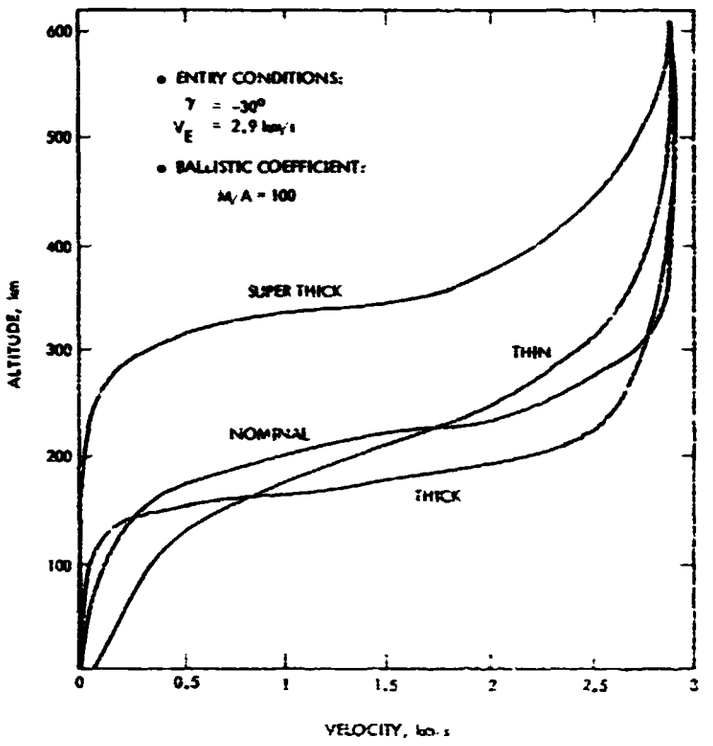

Figure 7 Descent Profiles

the nominal atmosphere as a function of entry speed, flight path angle and ballistic coefficient is illustrated in Figure 8. For reference the Viking value is shown on the chart. The peak heating rate and integrated heating input has a minor effect on lander mass. Considering worst case values requires a heat shield of approximately 5% of the lander mass.

Terminal descent to a landing with a maximum touchdown velocity of 10 mps is possible in all atmospheres with only a parachute. In the super thick atmosphere the parachute primarily provides attitude control during descent. In all cases the parachute can be deployed at a 2 km altitude. The thin atmosphere provides the worst environment for terminal descent requiring the largest parachute to achieve an acceptable (<10 mps) touchdown velocity. It turns out that the parachute size needed for the thin atmosphere is almost the same size as the Viking parachute. The variation in touchdown velocity with parachute size or ballistic coefficient is illustrated in Figure 9. It is readily apparent that parachute size becomes important only if the thin atmosphere is considered.

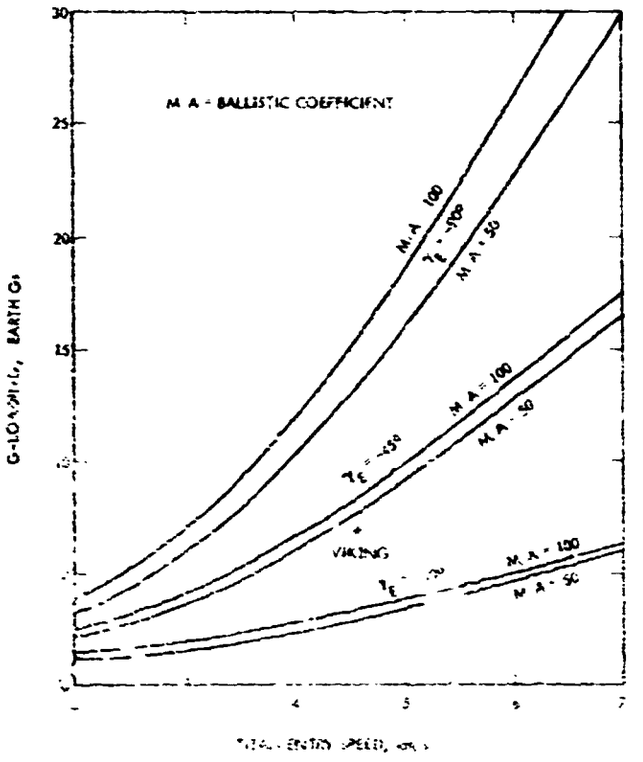

Figure 8. G-loading for Titan Entry, Nominal Atmosphere

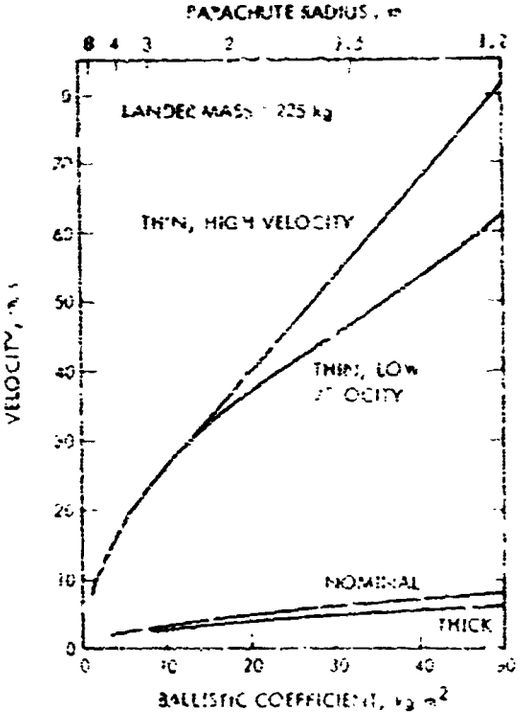

Figure 9. Touchdown Velocity

Flight times from entry to touchdown vary from 30 min to in excess of 4 1/2 hours depending on the atmosphere, aeroshell ballistic coefficient, parachute size and altitude of parachute deployment. If the model atmosphere range can be narrowed down it is possible to control the time spent in descent by proper sizing and staging strategies.

Data transmission from the Lander would be relayed through the orbiter vehicle as it passes by Titan. If the lander were designed to survive only a few hours after landing this relay would take place during the initial overflight of the orbiter during entry and landing. If the lander were designed to survive for an extended period of time the orbiter would pass by Titan periodically to receive the relay from the lander. Figure 10 illustrates the variation in orbiter range and elevation as viewed by a lander on the surface of Titan at the anti-Saturn point, a Saturn Orbiter in a 32 day period, and 20 R_S periapsis radius orbit that is coplanar with the orbit of Titan. Line of sight from lander to orbiter is maintained for several days around closest approach for relay data transmission purposes.

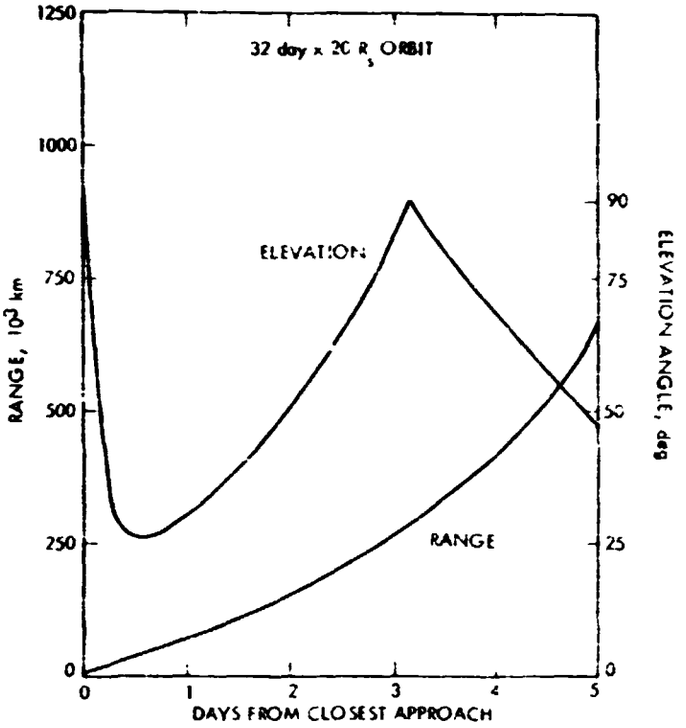

Figure 10. Saturn Orbiter - Titan Range, Elevation, 32 Day x 20 R_s Orbit

In order to conduct a satellite tour it is necessary to make orbit changes using gravity assist pumping and cranking techniques. Of all the Saturn satellites Titan is the only one that can be used effectively for these purposes. Large period changes of 100 days are possible with a single encounter as are inclination and apsidal rotation changes of 10s of degrees per encounter. With this capability a tour is possible; however, encounters with other satellites of Saturn will have to be found on trajectories which are targeted back to Titan. Reference 2 (Roberts, 1975) contains a detailed discussion of Titan pumping and cranking capability and also some examples of possible satellite tours.

The information contained in this paper was derived primarily from the results of the 1977 Saturn Mission Options Study (Wallace, 1977). This reference contains additional details, parametrics and considerations for interested readers.

REFERENCES

Report on Space Science (1975). National Academy of Sciences—National Research Council, Washington, D.C., 228 pp.

Roberts, P. H. (1975). The Saturn Orbiter Study, Final Report. *JPL Internal Document 760-126*, pp. 3−1 to 4−7.

Martin Marietta Corporation (1976). A Titan Exploration Study-Science, Technology, and Mission Planning Options, Final Report. *MCR-76-186*, pp. A−39 to A−50.

Wallace, R. A. (1977). 1977 Saturn Mission Options Study *JPL Internal Document 710-6*, pp. 1−1 to 2−1.

DISCUSSION

D. MORRISON: Have you gone through any exercises to see how many satellite encounters you might get in a year or 18 months in orbit?

R. RUDD: In a year's time, right now I would be guessing, but I would say it's like 3 or 4, not including Titan.

D. MORRISON: One every second orbit or something of that sort?

J. CALDWELL: In what ways do you get hurt if you design a probe for a very thin atmosphere and it turns out to be thicker than you expected when you designed it?

D. HERMAN: You have to use the orbiter as a relay, so if the descent rate is very, very slow, it's conceivable that you lose communication before you can get to the lower atmosphere.

D. MORRISON: At what pressure level does the probe become subsonic and start taking data? That's extremely important for us because one of the things we want to know from this group is whether a Titan probe is worthwhile. If there is a possibility of a very thin atmosphere, we don't know if we can get any probe data at all.

R. RUDD: I don't have an answer to that.

D. HUNTEN: We need to know, given an atmosphere, let's say take two extremes, one that's practically pure hydrogen and one that's practically pure nitrogen, when do you reach Mach 1 slowing down, is it at 1 mbar, 10 mbars, or a hundred millibars? For Jupiter, it's 100 mbars, and that's disappointing. It's presumably much less for Titan, but the question is, how much less.

R. RUDD: I will try to get the answer from JPL. (Answer: In the range of atmospheres that were studied, the probe reaches Mach 1 at 2-5 mbar.

J. CALDWELL: Is it possible to arrange the orbit such that you intersect Titan at different points in Titan's orbit, so that you don't always have to see the same side of Titan.

R. RUDD: Yes. That will happen with apsidal rotations.

D. MORRISON: You'd have to rotate the line of apsides, which is a step-wise process, in order to look at different sides. You can't, given just one intersection with Titan, arbitrarily choose to intersect at some completely different point in its orbit the next round.

OUTER PLANET PROBE MISSIONS, DESIGNS AND SCIENCE

Lawrence Colin

NASA-Ames Research Center
Moffett Field, California 94035

ABSTRACT

This paper reviews the similarities and differences of atmosphere entry probe missions, designs and science appropriate to certain solar system objects. In particular, the evolution of techniques and concepts from the Pioneer Venus Multiprobe Mission to the Galileo Jupiter Probe leading to Saturn and Titan probe concepts is traced. Candidate payloads for Saturn and Titan probes are suggested such that maximum inheritances from the earlier programs may be realized. It is clear, however, that significant Supporting Research and Technology efforts are required to develop mission-peculiar technology for probe exploration of the Saturnian system.

INTRODUCTION

Outer planet atmospheric probe missions have been accorded serious study since the early 1970's. A "common" probe design for application both to Jupiter and Saturn/Uranus has been emphasized. To a great extent these studies were stimulated by the Ames Planetary Atmospheres Entry Test (PAET) mission and have benefited from the development efforts of the Pioneer Venus Multiprobe mission. (There is a certain amount of spillover from the Viking Entry Probe and Lander program, but this has been minimal due to the relatively benign Mars entry environment.)

To a lesser extent, atmospheric probes and landers on Titan have also been studied. Surface penetrators which have been studied mainly for application to Mars, have also received preliminary study for Titan and the Galilean satellites. All of the

contemplated missions--Pioneer Venus (PV) Multiprobe, Jupiter Orbiter Probe (JOP) (recently designated "Galileo"), Saturn Orbiter with Probes to Saturn and Titan (SOP^2)--are severely constrained, particularly with regard to probe weight (thus scientific payload weight) and cost. "Combined" missions, e.g., an all-purpose atmospheric probe-lander-penetrator concept or even a combination of two of the three alternatives, may not be realizable. This is not to say that combinations or very ambitious missions would not actually be cost-effective and it is strongly recommended that such approaches be studied seriously and the required compromises elucidated at an early stage. It is clear that even the simplest mission to Saturn/Titan severely pushes the Shuttle/IUS capabilities; therefore new propulsion systems, orbital assembly techniques, or PV type missions, i.e., separate Orbiter and Probe launches, will need to be developed to evolve a cost-effective, scientifically valuable program. In fact, Solar Electric Propulsion is currently being considered for this purpose.

The purpose of this paper is to summarize existing programs and studies as they pertain to an SOP^2 mission. The results of this Saturn Workshop, particularly the feasibility of candidate payloads, will thus have a basis in reality appropriate to NASA's current technological base and anticipated resources for exploration of the Saturnian system beyond Pioneer and Voyager.

GALILEO

The Galileo mission was approved by Congress as a FY 78 new-start in the Summer of 1977. Shortly thereafter tentative scientific payloads were announced by NASA Headquarters. (The Galileo program is managed by JPL and they are also developing the Orbiter which will carry the Probe to Jupiter. ARC is managing the Probe portion of the mission including development and integration of the Probe experiments. Only the Probe-related features are discussed in this paper.) Two competitive Probe system design studies were completed by McDonnell Douglas and Hughes Aircraft/General Electric in December 1977; an RFP for the Probe development and execution phase was issued in January 1978; hardware proposals were received in March 1978 leading to selection of the Hughes/GE team in June 1978. The Probe design, Probe experiments and Probe mission strategy are currently in a state of conceptual design. Thus, we are only able to describe a "baseline" or "strawman" picture at this point.

Probe Mission Strategy

Key elements of the Galileo Probe mission are listed in Table 1, which also contains a comparison with the PV Multiprobe program. After about 1000 days in transit (from a January 1982 launch to September 1984 arrival), the Orbiter will release the Probe some 100 days prior to encounter with Jupiter. The Probe will enter the Jovian atmosphere (the entry is defined to begin at 450 km above a pressure level of 1 bar; all altitudes below are referenced to this level) near the evening terminator with a relative velocity of 48 km/s (>100,000 mph) at a shallow relative entry angle of -9.35 at a latitude of 5.5° S (South Equatorial Zone). Inertial values are 60 km/s and -7.5° respectively. After the Probe experiences enormous aerodynamic braking forces and heating during which the heatshield will ablate about half its weight, the Probe will deploy a parachute near Mach 1 to slow the Probe rapidly. The forward and aft heatshields (i.e., deceleration module) will then be ejected exposing the descent module (currently containing six experiments: see below) to the environment. Scientific measurements will be made in the pressure range 0.1-10 bars (~50 km to -100 km) during the next 30 min. The Probe may free-fall below 10 bars continuing to make scientific measurements for another 15 minutes to about 20-30 bars (-160 km) where the Probe mission will terminate. (Termination will occur due either to thermal failure or insufficient Orbiter-to-Probe communications margins.) The main parachute size (~2 m) and its jettison time will be selected to ensure this pressure range-time goal (based on a "nominal" atmosphere defined by the Galileo Project Science Group). Certain limited experimental data will also be collected prior to entry and during entry into the sensible atmosphere above 0.1 bar. These data will be stored on the Probe to be transmitted together with the lower atmosphere data back to the overflying Orbiter (~4 R_J range) for transmission to Earth.

Probe Design

Key elements of the Galileo Probe design are listed in Table 2, which also contains a comparison with the PV Probe's features. The Galileo Probe consists of a quasi-spherical descent module of 80-90 cm base diameter containing the scientific instruments, encased in a deceleration module consisting of a conical forward and spherical aft heatshield. The forward shield will be about 120 cm base diameter and

Table 1. Comparison of Mission Factors

	Pioneer Venus Large Probe		Pioneer Venus Small Probe	Galileo Probe
Launch Date		August 1978		January 1982
Launch Vehicle - Type		Atlas/Centaur		Shuttle/IUS
- Capability, kg		910		1500*
Trajectory Type		I		II
Transit Time, Days		125		1049*
Encounter Date		December 1978		September 1984*
Entry Speed, km/s		11.6		48.3**
Entry Angle, deg	-25 to -45		-20 to -75	-9.35
Maximum Deceleration, G_E	315		190 to 550	320
Descent Regime - bars		0.07 to 100		0.1-10 (20-30)
- K		232 to 750		110-350 (400-450)
Descent Time, min	55		57	30 (45)
Descent Velocity, m/s	55 - 10		70 - 10	400 - 50

*1800 KG, 1275 days and November 1984 for a Mars gravity-assist strategy (recently determined to be required to meet total mass constraints)

**relative to atmosphere; inertial velocity is 60 km/s

Table 2. Comparison of Probe Designs

	Pioneer Venus Large Probe	Pioneer Venus Small Probe	Galileo Probe
Mass - Total, kg	314	90	250
Science, kg	29.3 (34 max)	3.5 (4 max)	21 (25 max)
Science Volume, cc	31625 (40000 max)	3110	24400 (27000 max)
Science Power, W	92.8 (106 max)	9.8 (10 max)	48
Science (and s/c) Data, b/ps	256/128	64/16	150
Store, bits	3072	3072	32000
Heatshield - Type, Fore	Carbon Phenolic	Carbon Phenolic	Carbon Phenolic
Aft	low dens. elastomeric	low dens. elastomeric	phenolic nylon
- Mass, kg	33	9	100
Pressurized, psia	8 - 30	4 - 30	No
Staged	Yes	No	Yes
Base Dia, cm	142	76	120
Half-Cone Angle, deg	45	45	45
Radiation Protection Requirements	No	No	Yes
Communications Link	Direct	Direct	Relay thru Orbiter

will be a spherically tipped cone some 45° half-angle. The height of the Probe is about 90 cm. The total Probe weight is 250 kg (maximum) accommodating some 21 kg (25 kg max) of scientific instruments. The heatshield itself weighs about 100 kg (total) and is ablated significantly by the severe heating peculiar to Jupiter entry. The descent module is vented in a controlled fashion to the ambient environment.

Scientific Instruments and Objectives

There are six experiments selected tentatively for the Galileo Probe. These are listed in Table 3 and compared with those being flown on PV. Key instrument

Table 3. Probe Experiments

	Pioneer Venus Large Probe	Pioneer Venus Small Probe	Galileo Probe
Temperature, Pressure, Acceleration (Single Experiment)	X	X	X
Neutral Mass Spectrometer	X		X
Gas Chromatograph	X		
Helium Abundance Detector			X
Solar Flux Radiometer	X		
Infrared Radiometer	X		X
Net Flux Radiometer		X	
Nephelometer	X	X	X
Cloud Particle Size Spectrometer	X		
Lightning Detector			X
	7	3	6

characteristics are listed in Table 4. The major features and scientific objectives are discussed below. Final confirmation of the experiments is expected in October 1978.

Temperature, Pressure, Acceleration (PI: Alvin Seiff/Ames Research Center) - Together these measurements comprise the Atmospheric Structure Experiment. The experiment consists of a temperature sensor and pressure transducers exposed to the ambient flow during the descent regime (below 0.1 bars), a 3-axis accelerometer located at the descent module center-of-gravity operating during both entry and descent, and associated electronics. The primary objective is to reconstruct atmospheric state profiles (pressure, temperature, density) from the point where the sensible atmosphere is detectable ($\sim 10^{-6}$ g_E) to end of mission. Secondary objectives include determination of atmospheric mean molecular weight, horizontal wind velocity and wind shear (requires Doppler tracking), neutral flow velocity and turbulence intensity and scale.

Neutral Mass Spectrometer (PI: Hasso Niemann/Goddard Space Flight Center) - The instrument consists of a quadrupole mass spectrometer operating over the mass range 1-52 AMU plus two higher mass numbers (probably 84 and 131 AMU (Kr and Xe)). The primary objectives are to determine vertical variations of the

Table 4. Key Galileo Probe Science Instrument Characteristics

Instrument	Mass KG	VOL cm^3	Avg Pwr w	Descent Data Rate BPS
Atmosphere Structure (T, p, g)	3.0	3600	6	20.5*
Neutral Mass Spectrometer	9.5	9400	18	28
Helium Abundance Detector	1.2	2400	1	2
Net Flux Radiometer	3.0	3500	6	16
Nephelometer	2.5	3000	5	8
Lightning, Radio Emissions	1.8	2000	2	5*

*Does not include pre-entry/entry requirements.

chemical composition of the Jovian atmosphere within the above mass range with a threshold of about 10^{-8} or 10 ppb mixing ratio. An enrichment cell system is used to increase the ratio of minor to major constituents for analysis of trace constituents and the determination of some isotope ratios in a few samples. Noble gas concentration and isotope ratios are also to be obtained through the use of scrubbers. Samples are ingested into the system through direct glass-capillary pressure-reducing leaks connected to an inlet system located near the Probe stagnation point.

Helium Abundance Detector (PI: Ulf von Zahn/Univ. of Bonn) - This is another composition device dedicated to precise (0.1%) determination of the He/H_2 ratio in the Jovian atmosphere. A Jupiter atmosphere sample is ingested into a cell contained within the Probe. A miniature optical interferometer is used to compare the refractive index of this sample to that of a reference gas mixture contained within the Probe. Measurements are made in the range 3-8 bars only.

Net Flux Radiometer (PI: Robert Boese/Ames Research Center) - This experiment consists of a multichannel radiometer (0.3-30, 0.3-2000, 20-30, 30-40, 40-60 micrometers plus possibly two other channels) measuring ambient radiation in 50° cones alternately centered ±50° from the Probe horizontal. The primary objectives are to measure the net flux of solar energy (assuming a dayside entry) and planetary emission, determine location of cloud layers, measure mixing ratios of selected constituents and to study the opacity of clouds and aerosols.

Nephelometer (PI: Boris Ragent/Ames Research Center) - This experiment consists of a single-wavelength, multiple-angle (5) scattering nephelometer. The primary objectives are to determine the vertical extent, structure and microphysical characteristics (particle size distribution, number density, physical structure) of the Jovian clouds.

Lightning and Radio Emission Detector (PI: Louis Lanzerotti/Bell Labs) - This experiment consists of both electromagnetic and optical sensors. The former operate in the frequency domain (3, 15, 100 kHz narrow band) and the time domain (1 Hz-100 kHz; 16 s resolution). A ferrite core coil is used as an antenna. The optical sensor is a photodiode connected to a lead-glass fisheye lens. The primary objectives are to determine if lightning exists on Jupiter and measure basic physical characteristics; determine scale size of cloud turbulence; study electrification; look for evidence of precipitation, sources of heat and acoustic shock waves; measure RF noise levels. As a secondary objective, the electromagnetic sensor will be operated

pre-entry, below 3 R_J altitude, to measure the component of Jupiter's magnetic field perpendicular to the Probe spin axis.

This brief summary of experiments on the Galileo Probe is provided as background to aid in selection of candidate payloads for Saturn and Titan atmospheric Probes. There are other potential experiments of course, some of which have already been proposed. A listing of both Category 1 experiments and non-Category 1 experiments proposed for Galileo is given in Table 5 and some are discussed briefly below.

Gas Chromatograph

This potentially very valuable composition experiment (particularly for the study of heavy organic molecules at sensitivities of about 1 ppb) was not chosen for Galileo primarily because of resource constraints (mass and dollars).

Table 5. Galileo Proposed Probe Experiments Not Selected

Catetory I	Mass, kg
Gas Chromatograph*	4-6
Energetic Particle Detector	1-2
Ion Mass Spectrometer*	3-4
Neutral Mass Spectrometer (Aeronomy)*	4-5
Electron Temperature Probe*	2-3
Non-Category I	
Alpha-Scatter Composition Detector	
Microwave Radar Precipitation Detector	
Cloud Imager	
Magnetometer*	
Retarding Potential Analyzer*	
Ortho/Para H_2 Ratio	

*PV derivatives

Energetic Particle Detector, Ion Mass Spectrometer, Neutral Mass Spectrometer, Electron Temperature Probe

These very valuable radiation and aeronomy instruments would operate in the pre-entry regime (ionosphere and magnetosphere). One or more of these may yet be added to the Galileo payload prior to payload confirmation.

Pioneer Venus Comparisons

Tables 1, 2, 3 and 4 contain some useful data comparing PV and Galileo with regard to mission factors, Probe designs and experiments. The inheritances provided to Galileo by PV have been important and we are certain those provided to the Saturn and Titan Probes by Galileo will also be.

Major mission factor similarities and differences are highlighted in Table 1. Although the Shuttle/IUS launch capability (1500 kg, or 1800 kg with a Mars gravity assist) is significantly greater than that of the Atlas/Centaur (910 kg), the additional mass plus a good deal more, is consumed by Galileo *Orbiter* requirements compared to the PV bus (Fly-by) because of the orbit insertion/operations requirements. The order-of-magnitude longer transit times (1049 or 1275 vs 125 days) for Galileo translate into more stringent reliability requirements for the experiments and Probe subsystems. However, the most significant difference between the two Probe missions results from the tremendous entry speeds of the Jupiter Probe (48.3 km/s) in a H_2-He environment versus the Venus Probes (11.6 km/s) in a CO_2 environment. Note that the difference lies not in the structural requirements for survival (g-loading is similar) but in the entry heating or thermal protection requirements. This will be further discussed subsequently. Note also that although the *entry* requirements are more severe at Jupiter, operation in the *descent* regime is more benign. Galileo Probe operation will terminate at about 30 bars and 450 K after 45 mins, whereas the PV Probes will operate for about 60 minutes reaching 100 bars and 750 K.

Referring to Table 2, the Galileo Probe mass (250 kg) is between the PV Large Probe (314 kg) and Small Probe (90 kg), the increase in heatsheld being offset by no pressure vessel penalty. The same is true for the pertinent science parameters (mass, volume, power, data rate). The much more severe entry requirements for Galileo are reflected in the much higher required heatshield weights (100 kg or 40% of Probe mass

compared to 33 and 9 kg for the PV LP and SP respectively). The design of the heatshield is the single most important concern of the Galileo program. On the other hand, the more benign descent environment on Jupiter permits the use of a vented probe, with attendant savings, hopefully, in instrument design and possibly simpler thermal control considerations. Added difficulties at Jupiter, not thought to be of the same magnitude as entry heat protection, are the requirement for survival through the radiation belts of Jupiter, and design of the probe-to-orbiter RF link sufficient to perform satisfactorily in the poorly understood absorbing atmosphere and cloud environment.

Referring to Table 3, one sees the experiment inheritance provided to Galileo by PV. The Gas Chromatograph and Cloud Particle Size Spectrometer were the only PV experiments not carried over to Galileo; however, two new Jupiter-oriented experiments were added to Galileo. The multiple-scattering-angle nephelometer on Galileo, compared to the backscattering only nephelometer on PV, will provide much of the types of data potentially available from the Particle Size Spectrometer; as mentioned earlier there is no true counterpart on Galileo of the PV Gas Chromatograph.

SATURN/TITAN PROBES

Only very preliminary studies of Probe missions to Saturn and its satellite, Titan, have been performed. There are, of course, many options and all must be given adequate study to determine an optimum strategy for exploration of the Saturnian System. The options range from a simple flyby bus that would carry a simple atmospheric probe to Saturn and/or Titan to a sophisticated orbiter that targets a sophisticated atmospheric probe to Saturn and a combination atmospheric probe-lander to Titan. From a *Probe* standpoint, this range of options allows a broad spectrum of possibilities. For the purposes of this paper, we have adopted a middle ground within the range of options and focus on a SOP^2-type mission which is derived from and thus benefits directly from the Galileo experience. However, scientific payload options are suggested for a more sophisticated mission as well.

A Candidate "Baseline" SOP^2 Mission Strategy

The "baseline" SOP^2 mission encompasses atmospheric Probe exploration of both Saturn and Titan and a Saturn Orbiter with multiple satellite encounters, with launch in 1986. The mission can be accomplished by the addition of a Titan Probe to the Galileo Orbiter, which, we believe, can be added without extensive alteration to the Orbiter, and by the use of the Galileo Probe with a lighter weight heatshield and associated structure as the Saturn Probe. Therefore costs should be held to a minimum through extensive inheritance of Galileo Orbiter and Probe and perhaps the scientific instrumentation aboard at least the Saturn Probe. One possible SOP^2 mission sequence is listed in Table 6.

Probe Design Requirements

For the SOP^2 mission described above, typical entry conditions for the Probes are listed in Table 7, compared with the Galileo Probe. Note that whereas the Galileo Probe must be targeted to a shallow entry angle to minimize peak heating while still avoiding skip-out, the greater ephemeris uncertainties associated with Saturn and Titan require much steeper entry angles. Despite this, requirements for structural survival and entry heat protection are much simpler for Saturn than Jupiter and are trivial for Titan. Table 8 lists the potential Probe, Science and Heatshield masses and compares these with the PV and Galileo Probes. The differences in Saturn and Titan Probe masses are illustrative only. Other mixes are indeed feasible.

Candidate Payloads

Saturn Probe

At this point it seems plausible to consider the PV and Galileo Probe instruments as reasonable candidates for the Saturn Probe (see Tables 3, 4 and 5). Note that the 20 kg capability for the latter compares well with the Galileo payload of 21-25 kg (Table 8).

Table 6. Nominal SOP[2] Mission Sequence at Encounter

- Target spacecraft for Saturn atmosphere entry point
- Separate Saturn Probe
- Retarget for near-equatorial Saturn orbit with $R_p = 3R_s$ (outside rings)
- Transmit Saturn Probe entry and descent data to orbiter for transmission to earth
- Perform Saturn-orbit injection to apoapsis for Titan-commensurate period (~144 days)
- Raise periapsis radius R_p for Titan encounter
- Separate Titan Probe (ΔV on probe for entry)*
- Transmit Titan-Probe entry and descent data to orbiter
- Pump down to 32 day orbit
- Perform orbital maneuvers as required for remainder of mission

*May follow pump-down to 32-day orbit

Table 7. SOP[2] and Galileo Probe Entry Conditions

	Saturn	Titan	Jupiter
Entry Velocity (Rel) - km/s	29	6	48
Entry Angle (Rel) - deg	-30	-60	-9.35
Maximum Decel - g_E	365	11	300
Peak Heating Rate - KW/cm^2	5	0.1	40

Table 8. Comparison of Probe Designs

	Saturn Probe	Titan Probe	Pioneer Venus Large Probe	Pioneer Venus Small Probe	Galileo Probe
Total Mass, kg	143	110	314	90	250
Science Mass, kg	20	20	29.3	3.5	25
%	14.0	18.0	9.3	3.9	10.0
Heatshield Mass, kg	37	9	33	9.5	100
%	26	8.2	10.5	10	40

Titan Probe

The Ames Research Center has embarked on a six-month Phase A study of a Titan "Probe" applicable to a potential SOP[2] mission. The options to be studied are listed in Table 9. The minimum Probe (~175 kg) would be an atmospheric probe only (note that this minimum weight is now thought to be more realistic than the 110 kg shown in Table 8 considered by Martin-Marietta earlier). A somewhat more complex probe (~215 kg) would permit several hours operation at the surface after completing the atmospheric phase. Finally, a fully combined atmospheric and surface-oriented probe (400 kg) might survive for several months. The candidate payloads are suggestive only, but are hopefully representative and compatible with the total payload weights. The actual candidate payload list for the study will be selected as a result of the Workshop.

The most recent, in-depth study of a Titan Probe mission was performed by Martin-Marietta (A Titan Exploration Study - Science Technology and Mission Planning Option, Vols. I and II, Final Report, NASA CR 137847, Contract NAS 2-8885, June 1976). The following candidate payloads are abstracted from that study and are based on significant personal interactions of Martin-Marietta personnel with the scientific community. Table 10 lists candidate Titan atmospheric probe instruments. The blocked list is basic and fits reasonably well the capability given in Table 8. Table 11 lists a candidate Titan lander payload and Table 12 a Titan penetrator payload.

Table 9. Titan Probe Matrix

Element	Scope		
	Approach and Atmosphere	Approach, Atmosphere and Short Surface Operation	Approach, Atmosphere and Long Surface Operation
Mass, kg	≤175	≤ 215	≤ 400
Operation	Can "die" at impact	Impact plus several hours	Impact plus several months
Payload			
Atmosphere	P, T, Accelerometer Neut. Mass Spec. Gas Chromatograph Cloud Sensor Net-Flux Radiometer	P, T, Accelerometer Neut. Mass Spec. Gas Chromatograph Cloud Sensor Net-Flux Radiometer	P, T, Accelerometer Neut. Mass Spec. Gas Chromatograph Cloud Sensor Net-Flux Radiometer
Surface		Impact Accelerometer α P, X, Neutron, γ Spectrometer	Impact Accelerometer α P, X, Neutron, γ Spectrometer
Environment			Meteorology Pictures Active Sampler DTA GCMS

Recommendations

Given the current state of knowledge of the Saturnian system, and the extra knowledge expected from the Pioneer and Voyager fly-bys, and given our current spacecraft, Probe and scientific instrument technological capabilities a few general observations suggest themselves. The major scientific questions associated with the Saturn atmosphere and Titan atmosphere closely parallel those associated with Jupiter and Venus. Thus the Galileo Probe payload should match nicely the payload required of a Saturn Probe and a Titan Atmospheric Probe. The major deficiency is a Gas Chromatograph. It is recommended that SRT studies be supported to develop and maintain our GC competence.

Table 10. Titan Atmospheric Probe Science Payload

Instrument	Characteristics
Atmospheric MS	1-50 AMU, 3 measurements/scale height
Organic MS	50-250 AMU, 1 measurement/scale height
GC	1-3 analyses, up to 3-carbon
UV Photometer	Solar Pointing, 220, 260, > 280 nm bands
Accelerometer	Entry
T, P Transducers	3 measurement/scale height
Impact Transducer	Surface location, penetrability
Expanded Organic Analysis	
IR Radiometer	IR balance
Visible Light Monitor	Solar pointing
Nephelometer	Galileo
Cloud Particle Size Analyser	Pioneer Venus
Ion MS	Ionosphere Measurement
RPA or Plasma Probes	Charged particles in ionosphere
X-ray Fluorescence Spectrometer	P, S, Cl, Ar Detection

With regard to Titan *surface* measurements, unique problems exist. Firstly, knowledge of surface characteristics is so poor that it is probably unwise to plan, in a first mission, for a penetrator payload or even a very sophisticated lander payload. The best compromise appears to be a Titan Probe that is primarily atmospheric-oriented yet incorporates a minimum of surface observations intended to facilitate design of the next exploratory effort (i.e., the mid-range probe shown in Table 9). Again the Galileo-derived scientific instruments should apply well to the atmospheric portion of the payload. SRT studies are required to develop the surface-oriented payload.

Examination of the Titan Probes will doubtless turn up a few significant features which do not derive from PV or Galileo. In the case of the long duration Probe, in particular, truly severe thermal control problems will arise because of the temperature (and winds ?) uncertainty. Also electrical power requirements will differ greatly.

Table 11. Titan Lander Science Payload

Instrument	Characteristics
Combined GCMS/Life Detection	Viking GCMS + Kok experiment
Meteorology	T, P, wind
Sunlight Monitor	Visible, UV?
Imagery	One panorama
Surface Sampler	Scoop/Chisel (viscid surface?)
Wet Chem. Amino Acid Analysis	ABLDI
Expanded Organic Analysis	
Seismometer	Passive, Active?
Neutron Activation, Scatter	Elements, Isotopes
Passive Gamma-ray Spectrometer	K, U, cosmic ray, nuclides
XRFS, X-ray Diffraction	Heavy elements, crystal structure
Heat Flow	Temperature, gradient, thermal conduction
Microwave Radiometer	Subsurface temperature profile
Sonar Sounder	Layer detection
Drill Sampler	1-10 m
Particle Size Analyzer	Regolith characteristics
Age Dating	Ices, organics?
Upper Atmosphere Life Detect.	Sampler
Listening Devices	Audio, EM, lightning, thunder

A major requirement at an early date is for an in-depth tradeoff analysis of SOP^2 mission options given a Shuttle/IUS propulsion system and advanced propulsion systems, e.g. Solar Electric. At this point it is impossible to intelligently "size" the mission, i.e., allocate mass between Orbiter, Saturn Probe and Titan Probe spacecraft and science instruments.

Table 12. Titan Penetrator Science Payload

Instrument	Characteristics	Mass (Kg)	Power (Watts)
Accelerometer	Physical Properties of Surface Material	0.3	1.0
Temperature Array	Soil temperature, thermal conductivity	2.0	0.1
MS	10-300 AMU	6.5	27.5
Expanded Organic Analysis*		8.8 kg	28.6 W
Passive Seismometry	Viking		
Active Seismometry	Explosive Charges		
Neutron Activation	Elements, Isotopes		
Passive Gamma-ray Spectrometer	K, U, Activated Nuclides		
XRFS	Elements		
X-ray Diffractometer	Crystal Structures		
Heat Flow	Temperature Profile		
Magnetometer	Sensitivity?		

*The following instruments are optional

GALILEO ORBITER SPACECRAFT AND INSTRUMENTATION

David Morrison

Office of Space Science
NASA Headquarters
Washington, DC 20546

ABSTRACT

The Galileo Jupiter orbiter and its science investigations are briefly described as a baseline design for a Saturn orbiter.

INTRODUCTION

An essential element of the proposed SOP^2 mission is a long-lived Saturn orbiter. The orbiter spacecraft will release the atmosphere probes to both Saturn and Titan and will serve as the relay point for transmitting the probe data to Earth; it will then remain in orbit for two or more years investigating the planet, its rings and satellites, and its magnetosphere.

As presently envisioned, the SOP^2 orbiter is modeled closely on the Galileo Jupiter orbiter, just as the SOP^2 probes are expected to be derivatives of the Galileo probe (Colin, 1978). In this paper, I briefly describe the Galileo orbiter and its scientific investigations as examples of the type of spacecraft and associated science that could be launched to Saturn in the mid-1980's. It is important to note, however, that these Galileo designs are not fixed at the time of this writing (spring 1978), and that in any case signficant modifications, particularly in scientific experiments, could be accommodated for SOP^2.

THE GALILEO SPACECRAFT

The Galileo orbiter is a new departure in planetary spacecraft. In the past, these spacecraft have been either three-axis stabilized (the Mariner/Voyager class) or spin stabilized (the Pioneer class). The Mariner vehicles are optimized for remote sensing, since they are highly stable platforms from which pointed experiments, such as those involving cameras and spectrometers, can be carried out. They are also capable of highly controlled maneuvers when necessary. The simple spinning spacecraft, in contrast, provide a superior base for particles and fields experiments, which need to scan many directions rapidly to characterize the space environment of the spacecraft. The Galileo orbiter is designed to incorporate both spinning and stable mounts for scientific experiments.

The bulk of the Galileo orbiter is designed to spin around an Earth-oriented axis at several rpm. Included in this spinning section are the large telemetry antenna, the selenide radioisotope power generators, the retropropulsion system, and most of the spacecraft structure and electronics. Attached to this spinning spacecraft is a despun platform for remote sensing instruments, with a connecting bearing across which power and telemetry signals can be transmitted During cruise or when the propulsion engines are being used, this despun section can be spun-up to rotate with the rest of the spacecraft.

The Galileo communication system makes use of an S-band (about 12 cm wavelength) uplink, or command system, and both S-band and X-band (about 3 cm wavelength) downlink capabilities. The bulk of the science data will be transmitted at X-band using an Earth-directed 4.8-meter antenna with a beam-width of less than a degree. The maximum data rate from Jupiter is 115.2 kilobits per second. With even modest improvements in transmitting and receiving capabilities over the next few years, at least a comparable data rate should be achieved by SOP^2 from Saturn.

The Galileo retropropulsion system used to insert the spacecraft in orbit and to modify the orbit subsequently is being provided by the Federal Republic of Germany. This engine has a thrust of 400 Newtons, and a substantial fraction of the orbiter mass consists of fuel for orbit insertion and navigation needed for close flybys of the Galilean satellites. If SOP^2 uses an ion drive engine, the burden on the chemical retropulsion system is somewhat decreased.

Science experiments are mounted on both the spinning and despun sections of the Galileo orbiter. The magnetometer and plasma wave experiments are on a long

spinning boom, while other particles and fields experiments are mounted closer to the spin axis. On the despun section, a scan platform provides the base for the imaging camera and the other remote sensing telescopes that are bore-sighted with it. The expected absolute pointing accuracy is 0.2 degree, with short-term jitter of less than 0.1 degree.

Galileo Scientific Investigations

A science payload for Galileo was tentatively selected in August 1977, with determination of the final selection scheduled for October of 1978. The description given here refers to the tentative selection and may not represent the final Galileo payload.

Seventeen investigations were selected for Galileo, sixteen involving instruments, and one dealing with the scientific capabilities of the radio-telemetry system. Six of these are probe investigations, as described in the companion paper by Colin (1978). The other ten are on the orbiter. These experiments are listed in Table 1 and briefly described below, beginning with those on the scan platform.

Table 1. Tentatively Selected Science Investigations for the Galileo Jupiter Orbiter

PI	Investigation
M. Belton, Kitt Peak	Imaging (CCD, 1500-mm focal length)
R. Carlson, JPL	Near Infrared Mapping Spectrometer
C. Hord, U. Colorado	Ultraviolet Spectrometer
A. Lacis, Goddard Institute	Photopolarimeter/Radiometer
M. Kivelson, UCLA	Magnetometer
D. Gurnett, U. Iowa	Plasma Wave Spectrometer
L. Frank, U. Iowa	Plasma
D. Williams, NOAA	Energetic Particles
R. Grard, ESTEC	Electron Emitter
E. Gruen, MPI Kernphysik	Dust

The Imaging Investigation is actually a series of related investigations being carried out by an Imaging Science Team consisting of thirteen individually selected scientists. The camera is provided by NASA. The optics, a 1500-mm focal length catadioptric telescope and 8-position filter wheel, are Voyager hardware. However, Galileo will be the first planetary spacecraft to use the new CCD (charge coupled device) detectors, with their high quantum efficiency, linearity, large dynamic range, and extended infrared responsivity. The Galileo camera will use an 800 × 800 pixel frame, with a resolution of 20 microradians per line pair.

Also on the scan platform is the NIMS, or Near-Infrared Mapping Spectrometer. This instrument is designed primarily to identify and map mineralogical units on the Galilean satellites, but it will also be used for cloud studies and temperature sounding of the Jovian atmosphere. Its spectral sensitivity covers most of the infrared reflectance region where diagnostic spectral features of ices and silicate minerals appear. The spectral resolving power is about 100 and the angular resolution is 0.5 milliradians. Galileo is the first spacecraft to carry a NIMS-type instrument.

A Fastie-Ebert ultraviolet spectrometer (UVS) is bore-sighted with the imaging and NIMS telescopes. This UVS is designed primarily to study the composition and structure of the upper atmosphere of Jupiter and the tenuous atmospheres of the satellites. The wavelength range is from 110 to 430 nm, with spectral resolution of about 1 nm. Similar spectrometers have been flown before on Pioneer Venus and Voyager.

The final scan-platform instrument is a photopolarimeter/radiometer, designed primarily for study of cloud and haze properties on Jupiter. A 10-cm telescope and 16-position filter wheel allow measurements in a number of spectral bands in the visible and near-IR. A similar instrument is on Pioneer Venus, while other photopolarimeters have flown to the outer planets on Pioneers 10 and 11 and Voyager.

The next four instruments in Table 1 obtain coordinated data aimed at understanding the physical dynamics of the Jovian magnetosphere and the plasma processes that affect it. All have major inheritance from Voyager, Pioneer Venus, and other planetary and Earth-orbiting spacecraft. First of these is the Magnetometer, mounted on a boom on the spinning part of the spacecraft. Dual triaxial fluxgate magnetometers are used, sensitive to magnetic fields over the dynamic range from near 1 milligamma to as high as 16 kilogamma.

Also mounted on the magnetometer boom are the antennas for the Plasma Wave Spectrometer, which directly measures the varying electric and magnetic fields in the Jovian plasma. Frequency range is from 6 Hz to 300 kHz.

The Plasma investigation will measure both positive ions and electrons in the plasma over an energy range from 1 eV to 50 keV. Energy spectra will be determined as a function of direction over essentially the entire celestial sphere. Miniature mass spectrometers will also identify several major ionic species, including several components of the extended atmosphere of Io.

An Energetic Particles experiment, also mounted on the spinning section of the Galileo orbiter, consists of a series of particle telescopes to determine the energy and angular distribution of protons, electrons, and ions trapped in the Jovian magnetosphere. The energy ranges up to 11 MeV for electrons and 55 MeV per nucleon for ions. This experiment can also measure the composition of the trapped ions from He through Fe.

The final two experiments are also mounted on the spinning part of the orbiter. The Electron Emitter is designed to clamp the spacecraft potential to that of the surrounding plasma. The Dust investigation has the goal of determining the physical and dynamical properties of small dust particles or micrometeorites in the Jovian environment. Mass, velocity, and charge can be determined over the mass range from 10^{-10} to 10^{-6} gram. This is a much higher sensitivity than has been achieved in past experiments to measure dust in the outer solar system.

Possible Modifications for Saturn

If the Galileo spacecraft proves satisfactory for the Jupiter mission, it will probably need only slight modifications for Saturn. The interfaces will need substantial alteration to accommodate the ion drive propulsion system and the second probe, but the basic spacecraft need not change significantly. Less radiation shielding will be required, but the spacecraft power sources and telemetry rate may need enhancement if the performance at Saturn is to equal that expected of Galileo at Jupiter.

More substantial changes may be needed in the scientific payload. On Galileo, there is a heavy emphasis on particles and fields measurements; we do not yet know if Saturn has a substantial magnetosphere, and it is possible that after the Pioneer 11 and Voyager flyoys we will not conclude that a similar emphasis in this area is needed for a Saturn orbiter.

In the remote sensing area, however, our present limited knowledge suggests two additions to the payload. Interest in atmospheric dynamics on Saturn and perhaps also on Titan argues for the addition of a second, wide-angle CCD camera to obtain synoptic global-scale images. Such coverage will be very limited on Galileo, but in the case of Jupiter many goals in atmospheric dynamics can perhaps be carried out by the Space Telescope. For Saturn, in contrast, imaging from an orbiter seems to be required. The second new instrument suggested by discussions at this workshop is a submillimeter radiometer for studies of the rings. A great deal of information on particle sizes and bulk composition may reside in radiation emitted at wavelengths from 100 μm to 1 mm, and no existing spacecraft instrument operates in this area.

At present, of course, all of these suggestions concerning the detailed spacecraft design and science payload of a SOP^2 mission are highly speculative. Only after the Pioneer 11 and Voyager flybys will we have the information needed to assess these issues properly. The purpose of the present exercise is to show that even the unmodified Galileo orbiter and science instruments are reasonably well suited to a Saturn mission.

REFERENCES

Colin, L. (1978). Outer Planet Probe Missions, Designs, and Science. In this volume.

A METHOD OF EXPLORATION OF THE ATMOSPHERE OF TITAN

Jacques Blamont

CNES and Service d'Aeronomie du CNRS
Centre National
D'Etudes Spatiales
129 Rue de L'Universite - 75007 Paris

ABSTRACT

A new type of hot-air balloon, with the air heated by natural sources, is described here. The vehicle was developed at the Service d'Aéronomie du CNRS, in Paris, France. Buoyancy is accomplished by either solar heating or utilizing the IR thermal flux of the planet to heat the gas in the balloon. Altitude control is provided by a valve which is opened and closed by a barometer. The balloon is made of an organic material which has to absorb radiant energy and to emit as little as possible.

THE SELF-BUOYANT MONTGOLFIERE

Principle

A new type of vehicle was developed at the Service d'Aeronomie du CNRS, in Paris, France, during 1977 by J.-P. Pommereau and A. Hauchecorne (1977).

It is a hot-air balloon, where the air is heated by natural sources. We call *solar montgolfiere* a hot-air balloon whose buoyancy is provided by solar heating and *infrared montgolfiere* a hot-air balloon whose buoyancy is provided by the IR thermal flux of the planet (Earth or other).

A montgolfiere is a balloon made of an organic material defined by its weight g (gm^{-2}), its emissivity ϵ and its transmissivity α, both thermooptical coefficients defined over all wavelengths. The balloon is open at the bottom and at the top by two very large apertures. The aperture at the top can be closed by a valve.

The potential of the system can be discussed with the help of the thermal buoyancy per unit volume P defined as

$$P = \left| \frac{T_b - T_a}{T_b} \right| \rho_a$$

where T_b is the temperature of the balloon, T_a and ρ_a respectively the temperature and the density of the ambient atmosphere.

A model of the system relating the parameters defining the balloon (radius r, g, α and ϵ) to the buoyancy and therefore to the total weight of the balloon (weight of the balloon and payload), including the spectral dependence of α and ϵ, the actual shape of the balloon, convection inside and outside the balloon has been computed for different types of atmospheres (Pommereau and Hauchecorne, 1977).

The Solar Montgolfiere

Because of the large value of the solar flux, the system is fairly simple. In this case, the balloon is made of a single material which has to absorb the solar light and to emit as little as possible (α large, ϵ small). When the top valve is closed, the solar energy heats the inner gas and the balloon ascends; a barometer opens the valve at a predetermined altitude and the balloon descends to another predetermined altitude where the barometer closes the valve. A series of vertical explorations is thus obtained during the day.

The Infrared Montgolfiere

Because of the geometry, the balloon is made of two hemispheres of different infrared emissivity. Ideally, the emissivity has to be zero for the upper hemisphere and one for the lower hemisphere. Over a region when the upward IR flux is defined by a brightness temperature T_R, the temperature of the gas inside the balloon T_B would become equal to T_R in the absence of convection losses.

Detailed computations show that the thermal buoyancy is not large in the majority of circumstances and therefore acrobatics permitted to the solar montgolfiere may not be permitted to the IR montgolfiere: a mere survival of the balloon during the

night can be hoped for. A typical value of the buoyancy on the Earth is 100 g m^{-3} during the day and 10 g m^{-3} during the night for a flux coming from the sun of 1940 W m^{-2} at the top of the atmosphere and a flux generated by the Earth at night varying with the nature of the clouds from 110 W m^{-2} to 300 W m^{-2}.

It is obvious that when the buoyancy is small the payload is also small and therefore the IR montgolfiere has to be very large. A limit is set to its dimensions by the mechanical properties of a thin structure.

State of the Art

The first launches of solar montgolfieres were performed with complete success in Pretoria (Union of South Africa) on Feb. 17th and Feb. 25th, 1977 by a crew of the Service d'Aeronomie. The volume was 300 m^3, the weight 50 g m^{-2}, and the payload 2 kg. As predicted, the two balloons performed a series of 4 vertical excursions between 15 and 19 km of altitude. The measured temperatures inside and outside the balloon were fitted to the theoretical model; their values showed that the IR montogolfiere should work (Pommereau *et al.*, 1977a). The program was then adopted by CNES which developed, according to the specifications of the Service d'Aeronomie, and launched from Aire-sur-l'Adour (France) an IR montgolfiere on December 19th, 1977, with complete success. The volume was 5800 m^3, the weight 25 g m^{-2}, and the payload 10 kg. The balloon had no top valve since the test was only intended to prove the survivability during the night. It drifted during 66 hours over Southern Europe performing as predicted, culminating at noon at 24 km and bottoming at the end of the night around 19 km, and was destroyed by a preset timer without which it would still be flying today (Pommereau *et at.*, 1977b; Bezaudun, 1977).

CNES and the Service d'Aéronomie have initiated a program of applications of the system to the study of the stratosphere, starting with two launches from Pretoria in April 1978.

During the same time, CNES is studying the possible use of the concept for the exploration of the Venus atmosphere, a joint venture with the Soviet Union, with an approved launch in 1983.

THE MONTGOLFIERE IN THE ATMOSPHERE OF TITAN

A preliminary study (Hauchecorne and Pommereau, 1978) has been completed of the feasibility of both solar and IR montgolfieres in the atmosphere of Titan for the three atmospheric models described in the NASA document "The environment of Titan" (1975) (NASA, 1976).

The Titan IR Montgolfiere

The emissivity ϵ of the upper hemisphere of the balloon is assumed to be 0.05 towards the outside and 0.90 towards the inside; the lower hemisphere is assumed to be transparent.

With the "thin" and "nominal" models, the temperature of the atmosphere is higher than the temperature on the ground: the buoyancy is therefore zero and the montgolfiere cannot work.

With the thick model, using the albedo measurements of Younkin (A = 0.20 and T_B = 85 K) the upward infrared flux can be assumed to be 3.0 W m^{-2} at the tropopause. Below the tropopause, we suppose that the difference between the upward IR flux and the black body emission at the atmospheric temperature increases linearly from zero on the ground to 1.1 W m^{-2} at the tropopause. Figure 1 shows that the buoyancy of the balloon in this model is inferior to 3 g m^{-3}; therefore the IR montogolfiere is impossible in practice.

The Titan Solar Montgolfiere

The balloon is completely covered by a thin metallic film in order tc reduce the IR emissivity and by a thin varnish for total absorption of visible solar light.

$$\epsilon_{IR} = 0.05 \qquad \alpha_{sol} = 0.60$$

The visible solar flux above the atmosphere is 15 W m^{-2} and is supposed not to be absorbed by the atmosphere. No cloud can exist in the "thin" and "nominal" models, but there is a strong possibility of clouds below the tropopause in the "thick"

model; the buoyancy of the solar montgolfiere is plotted on Figure 1. With the "thin" model, a buoyancy of only 8 g m^{-3} is obtained on the ground, which makes the system very hard to fly. However with the two other models, the solar montgolfiere flies easily: a montgolfiere with a buoyancy of 20 g m^{-3} could explore the region from 0 to 35 km in the "nominal" model and from 0 to 75 km in the "thick" model.

Figure 2 shows the payload available with a montgolfiere made with a material weighing 20 g m^{-2} and a buoyancy of 20 g m^{-3}. A typical example would be a relatively small balloon of 4000 m^3 whose weight would be 25 kg and the payload 50 kg. This balloon is in the class of the successful IR montgolfiere of December 1977.

The temperature of the fabric would be low. With the skin temperature above the ambient temperature by 100°C, we are faced with a temperature of the material of -100°C. A large number of products (fiber glass, kevlar, polypropylene film) retain their mechanical properties in this range, even down to -200°C.

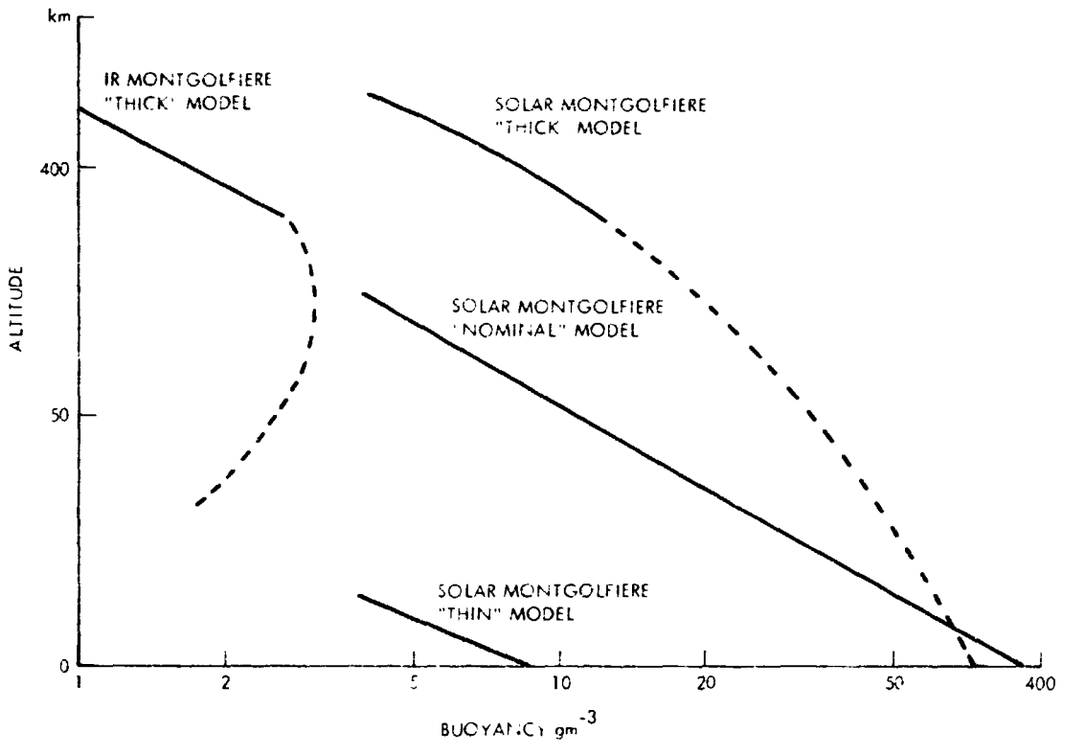

Figure 1 Buoyancy of a Montgolfiere in the Atmosphere of Titan

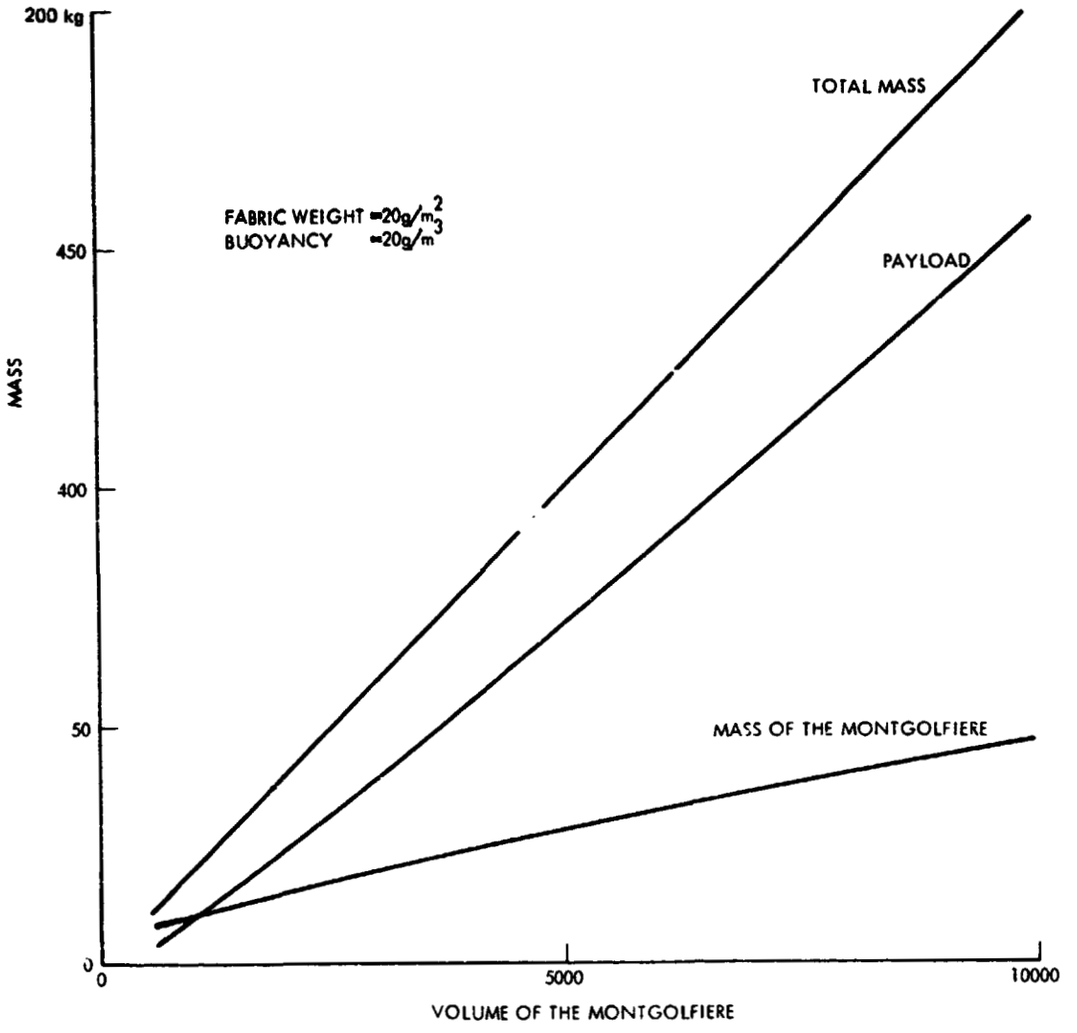

Figure 2. Payload of the Montgolfiere as a Function of the Volume

A Possible Mission

The scientific objective is a vertical exploration of the Titan atmosphere. A solar montgolfiere is injected near the subsolar point, drifts in the winds, exploring an extended range of altitudes. The value of the range cannot be determined today as it depends on the model chosen. The advantage of the use of the montgolfiere can be best understood by considering it as *a parachute which can ascend* in specified conditions.

A 4,000 m^3 montgolfiere could fly up to a pressure of around 50 millibars and down to an altitude determined by the solar flux available after absorption through the clouds. Should the "ultrathick" model of Hunten be proven to describe the situation, the system would fly from 180 km down to at least the tropopause level at 100 km of altitude where the pressure is 1 bar, and explore even the region below the clouds if their optical thickness is not too great.

When the balloon approaches the terminator, it slowly descends to the ground and allows an exploration of the lower layers. The vertical structure of the wind velocity field can be deduced from the measurement of the position of the montgolfiere. Therefore, if a real time analysis can be obtained, it could become feasible to maintain the system a long time in the sunlit hemisphere by commanding the valve from the Earth in order to either maintain the system at an altitude where the wind velocity is minimum, or vary the altitude in a vertical gradient around an altitude of zero wind velocity.

With a nominal payload of 50 kg, a scientific package of 15 kg could be accommodated, the remnant of the weight being allocated to a RTG, a transmitter, an omnidirectional antenna, a command receiver and a mechanical structure.

In these 15 kg, a measurement of the vertical structure of temperature and pressure, a chemical analysis of the atmosphere (organic molecule mass spectrometer and gas chromatograph similar to Pioneer Venus's of a weight of 3 kg) a nephelometer, an IR radiometer, a measurement of the nature of the cloud particles (α backscattering, X ray fluorescence spectrometer and other) perhaps a camera for obtaining pictures of the clouds or of the landscape could be placed. Data on general circulation, wind velocity and field including vertical gradients and vertical motions are deduced from the motion of the balloon. The main interest of the mission is that transport phenomena and their interaction with the physicochemical properties of the atmosphere are investigated.

In this configuration, the total payload is 75 kg (50 kg for the gondola and 25 kg for the montgolfiere). A comparison with the Galileo probe where the total weight is 250 kg for a heat shield of 100 kg and a science payload of 25 kg, shows that a Titan probe of less than 250 kg which would need a heat shield of less than 20 kg, could accommodate a payload of 100 kg, and therefore the 4,000 m^3 montgolfiere and its gondola. The proposed Titan probe therefore would be in the class of the Galileo probe and of the Saturn probe.

The data would be transmitted to the orbiter which would also have to locate the gondola. The necessity of maintaining a communication link suggests a circular orbit in the equatorial plane of Titan, since it is likely that the general circulation and therefore the motions of the balloon would have a large zonal component. The altitude would have to be chosen as a trade off between different requirements but 20,000 km could be a reasonable figure.

More than one balloon could be released; the exact number would depend on the payload capacity at injection.

The mission can be defined with more accuracy after the Pioneer and Voyager encounters with Titan.

REFERENCES

Bezaudun J. (1977). Vol d'une montgolfiere IR. *Internal CNES Memo.* CT/PRT/BA/EE/ 0Go.

Hauchecorne, A., and Pommereau, J. P (1978). Faisabilite d'une montgolfière dans l atmosphere de Titan. *Internal S/ Memo.*

The environment of Titan, 1975 (1976). NASA-SP8122. 45 pp.

Pommereau, J. P., and Hauchecorne, A. (1977). La montgolfiere infra-rouge, etude theorique. *Internal report. SA 275 G.*

Pommereau, J.-P Hauchecorne, A., Viret, F., Baribeau. M., de Luca, A. François, D., Leclère, M., Nizou, Y., and Poiet, G. (1977a). Essais au dol et en vol d'une montgolfière volaire. *Internal report. SA 273 G.*

Pommereau, J.-P., François. D., Hauchecorne, A., Nizou. Y., Schneider, J.-P., Viret, F., Baribeau, M., Bezaudun, J., and Rougeron, M (1977b). *Sondages verticaux atmosphériques. Internal report SA 304 G*

DISCUSSION

J. POLLACK: In your evaluations of the buoyancy, what assumptions did you make about the absorption of sunlight by the Axel dust above the balloon?

J. BLAMONT: I supposed that the balloon was above the clouds. There was no allowance for absorption by a haze at higher altitudes.

BASELINE SCIENCE PAYLOAD FOR SOP[2]

Panel 2
G. Orton, Chairman, J. Blamont, L. Colin, G. Siscoe, D. Morrison, J. Pollack

G. ORTON: We would like to discuss baseline science and baseline payloads for SOP[2].

J. POLLACK: One important element for a probe payload is a capability to determine atmospheric composition. A second thing is information about cloud and aerosol properties, such as size and location. Third, we would like to have information on the winds themselves. That's an important piece of meteorology. Doppler tracking capability could give us information on how the vertical winds vary as a function of altitude.

I would also like to get some information on the surface of Titan. We have to think seriously about what types of instruments might be feasible. The real problem is we've got to expand our horizons a bit beyond things like alpha scattering experiments, which are directed towards silicates, since on Titan the things we'll want to go after are primarily the ices and organics.

I also think that if one goes far enough to speak about a lander that stays around and operates for a while on the surface, there's quite a bit one could get from imaging information. One could get information on properties and particles in the atmosphere and monitor how they change.

G. ORTON: For Titan do you see any need for additional or modified instrumentation from the Galileo Jupiter probe or a Saturn probe in order to more fully exploit the possibility and the extent of organic compounds?

J. POLLACK: Well, I certainly think that one would have to consider a gas chromatograph very seriously. When you have a wide enough range of possibilities as to compositions that you're going after, you would like to cut in several dimensions so

that you can best pin down what you're looking at. A mass spectrometer gives a nice cut in one dimension. A gas chromatograph gives you a cut in a complementary direction.

D. MORRISON: What kind of gas chromatograph capability would be required to provide a substantial orthogonal data set to what you would get with a mass spectrometer?

J. POLLACK: I think the gas chromatograph that was proposed for Galileo gives you a first order answer to that question. There was an electron capturing device that was proposed as a primary detector; for certain C and N compounds it had enormous sensitivity. With certain selected compounds of particular organic interest, it has very high sensitivity.

S. CHANG: There's a particular advantage in Titan, too, because you don't have the enormous excess of hydrogen and helium to deal with. If you are interested in looking for trace organics, you already have the three order of magnitude advantage over the case in Jupiter. Furthermore, the non-condensable gases that comprise the major portion of the atmosphere are nitrogen and methane, and if you are interested in three more orders of magnitude of concentration, these can be swept through. The concentration mechanism can be used to further enhance your detection capability. I think it's a very sensitive and high-resolution method.

J. CUZZI: What about imaging on the way down?

J. POLLACK: I think there are radiation experiments that give you more valuable data than imaging would on the way down, but once you get to the surface, then it's a different ballgame. On the way down, I really don't see that imaging does too much.

D. HUNTEN: I would like to mention that we should consider where we'll be in instrument development after Pioneer Venus, because a number of the proposals that have been made – Doppler tracking, gas chromatography, and so on – are being implemented on Pioneer Venus. We'll have a much better handle on how well these things actually work in the real world by about a year from now.

J. BLAMONT: As far as the dynamics are concerned, I don't believe that with one single probe you can learn something. Just imagine that you would have Mariner 4 as the only description of Mars. What do you learn? Nothing.

But I think it's easier to send entry probes to Titan than to Jupiter. Therefore, I think that at least you have to find a way of having more than one vertical

probe. This is essentially why I made the presentation of the hot air balloon, because you want to have more than one vertical profile of the wind.

If you obtain only one single measurement of circulation, you'll have nothing. Even if you have one good Doppler measurement, you won't go very far from there.

G. ORTON: As far as your idea about the hot air balloon, it's going to be necessary to wait in order to know whether the atmosphere will or will not support a balloon.

J. BLAMONT: It's possible to have a hot air balloon which would fly at 10 millibars. We are just starting to study this and we hope to be able to provide you with a list of possibilities.

J. CUZZI: At Ames, we talked a little bit about sub-surface measurements, like sticking a penetrator in the ground. I would be interested in hearing what people have to say about that.

J. POLLACK: One of the really fundamental things that you'd like to know is the heat flow. And I'm not quite sure how easy it would be to implement it on the lander, but that certainly would be one of the important things to do.

D. HUNTEN: I would like to suggest that anybody who is advocating a heat flow measurement should take one or two plausible models for the heat flow of Titan and combine them with the heat conductivity of, let's say, solid water ice or solid tar or liquid tar, and see if it's within orders of magnitude of it being feasible. I would be very surprised if any such measurement is possible.

S. CHANG: There may be some interesting things resulting from sub-surface chemical analysis, too; composition may vary significantly with depth below the surface.

D. HUNTEN: I'd like to raise a plea again for pre-entry science, which hasn't really been discussed in this particular panel. Measurements of the ionosphere and upper atmosphere have been quite seriously considered for Galileo, but had to be abandoned because of the high cost and added mission complexity. But Titan is a relatively easy and a very interesting place in which to make some measurements of positive ion chemistry and, preferably, even upper atmospheric composition. The highest priority instrument is an ion mass spectrometer. The optimum complement is what Pioneer Venus carries, which is a neutral mass spectrometer, ion mass spectrometer, ion trap, and Langmuir probe.

Sherwood Chang has made the proposal that a good deal of the organic aeronomy that goes on in Titan may be going on in the upper atmosphere, mediated by auroral particle bombardment. This adds to the excitement of these kinds of measurements.

G. ORTON: The distinguishing characteristics between pre-entry and probe science are, I assume, that pre-entry is pre-Mach 1.

D. HUNTEN: Well, even more than that. It's done at heights where the mean-free path is long enough or the vacuum is good enough so you don't need vacuum pumps; the region of the ionosphere, or a little bit above.

L. COLIN: You want a candidate Saturn probe payload. Let me suggest a list of high-priority instruments and low-priority instruments, with the high-priority instruments in order of priority:

(1) In the area of composition: a neutral mass spectrometer and a gas chromatograph.

(2) For atmospheric structure: temperature, pressure, and accelerometer measurements.

(3) For cloud structure: the multiple scattering nephelometer that we have on Galileo.

(4) For dynamic experiments: Doppler ratio tracking or possibly balloon techniques.

(5) For thermal balance, the net flux radiometer, which hopefully will tell us why the winds are being driven the way they are.

(6) Finally, a plea again for pre-entry science; I listed two instruments: An ion mass spectrometer and a retarding potential analyzer.

That adds up to a total of seven hardware instruments, which I think is in the right ballpark.

That leaves for lower priority experiments, a helium abundance detector, a cloud particle size spectrometer, and a lightning radio emission detector. Among aeronomy instruments, in a lower priority are the electron temperature probe and neutral mass spectrometer. And finally, the magnetospheric-type experiments of low priority, such as an energetic particle detector and a magnetometer.

D. MORRISON: For the Saturn probe, should magnetospheric experiments be given such low priority? In the extensive debates over where to target Pioneer 11

at Saturn, some very cogent sounding arguments were made that one really wanted to measure the energetic particle and magnetic field profiles in the regions of interaction with the ring particles and inside them in the gap where the D Ring may or may not extend all the way to the surface of the planet. Only with a Saturn probe that has an extensive magnetospheric complement of instruments can we study that aspect of magnetospheric physics. Is that a reasonable argument?

J. POLLACK: I think the thing that would worry me on an argument like that is the question of priorities; in other words, you are getting a one-shot sample so that, in the case of magnetic field, you get a hint of the asymmetries, but you really wouldn't be able to actually define that asymmetry. So from that point of view, I wouldn't put it in as high a priority class.

E. STONE: If you just trade, say, the magnetospheric experiments on a probe versus magnetospheric experiments on an orbiter, my own impression is that a comprehensive magnetospheric orbiter package will, in the end, yield much more science about the magnetosphere than would the package on the probe.

D. MORRISON: Suppose you were considering just an energetic particle detector as part of the pre-entry science on the probe. Would you put it as low priority as Larry did?

E. STONE: A simple energetic particle experiment on the probe could give us some information about the magnetic field direction, as well as something about whether or not there are particle sources inside of the visible rings. Whether one would rank that as high as the first seven you listed, I don't know. I think it may well be high up in the second category.

D. HERMAN: Let me ask a question about the need for a GC into Saturn. I heard a debate at a Physical Sciences Committee meeting between John Lewis and Carl Sagan, where John calculated the abundance of organics that would exist in Jupiter, if they do exist, and that dictated the kind of sensitivity you need in a GC. Using whatever model you wish, if there are organics in the atmosphere of Saturn, what would you anticipate is a relevant abundance?

J. POLLACK: I think it depends how you define the word "organics". If you are speaking about amino acids or something like that, I would be surprised if there were measurable quantities. If, on the other hand, you are speaking about a variety of other interesting compounds that are more plausible on other grounds, I think it's an entirely different situation.

Let me just give you a couple of examples of surprises that we have encountered in the case of Jupiter, which is why I think there is a wider range of possibilities in the real case than one might predict on very simple grounds: We know that there are measurable quantities of both carbon monoxide and phosphine in the atmosphere of Jupiter.

D. HUNTEN: Measurable by a GC?

J. POLLACK: Yes. In fact, that was explicitly part of our GC proposal for Galileo. Just to explain that a little bit more, the reason that we think that these compounds are actually there in the case of Jupiter is that they get manufactured by thermodynamics at very high temperatures in deep layers, and then get mixed up quickly, so it would be nice to see some of those vertical gradients to understand how the compounds get up there.

G. ORTON: Do we need a dedicated helium-hydrogen instrument? Should one measure helium for its contribution to cosmogony? The answer, I think is very definitely yes.

D. HUNTEN: I think it's another mildly interesting thing to do in about the same class as, let's say, pre-entry science.

G. ORTON: On the record we have clear differences of opinion.

D. MORRISON: I am confused by the vehemence of your assertion, Don, that the helium abundance is only mildly interesting. If I understood Jim correctly, he is saying that there appears to be a discrepancy between theory and observation in the internal heat source of Saturn. By determining the helium ratio, we might find the clue to that discrepancy. It would seem to me that if that argument is valid, then measuring the helium is in the same class as measuring the internal heat source of Saturn for understanding what went on at the time the planet was formed.

D. HUNTEN: I don't disagree, except I'm not sure that once we've measured the helium we will have the ultimate solution to that particular puzzle. There's a near infinity of solutions even once you know the helium.

J. POLLACK: Perhaps you could enlarge on that, Don? Tell me the near infinity.

G. ORTON: That would take a long time.

D. HUNTEN: In anything as complicated as a planet, a unique explanation of anything that complicated practically never happens, Jim. In the context of today's theories, yes, it may discriminate but that doesn't mean we find the true answer.

J. POLLACK: Let me just explain my remark and then you could just very quickly just take a look, on a quantitative basis that is, to what energy sources you have available. And the only thing that's going to produce something of the right order of magnitude is some type of gravitational energy release, and so the real focus of trying to understand the excess heat source is to understand the mechanism of gravitational energy release. A desirable accuracy would be one percent of the ratio of helium to hydrogen.

D. CRUIKSHANK: With all humility and great trepidation, I would like to ask a question about deuterium. No one has mentioned deuterium and I realize it's been found spectroscopically on Saturn recently. But I wonder if it's something that should be given attention in a probe measurement. It seems like a number we'd like to know on Titan, at least, and it may relate to whether or not the Titan atmosphere is the original atmosphere or a secondary atmosphere.

D. HUNTEN: I think you raise a good point. Isotopic ratio measurements tend to be taken for granted as a primary objective, but should be brought out explicitly.

S. CHANG: Is it possible that because there are differences between the densities of Saturn and Jupiter, that Saturn is not only somewhat chemically fractionated, but also isotopically fractionated from the point of view of the stable elements, light elements as well as the rare gases. Would that be a particularly interesting measurement; that is, by comparison with Jupiter, would there be an anomalous elemental fractionation pattern or isotopic pattern?

J. POLLACK: Recent suspicion has been that it's much more an elemental than it is isotopic. Elemental, in the sense that it's hydrogen-helium versus rocky and icy material.

D. MORRISON: I have talked about the orbiter payload already, but I have a couple of general comments. Saturn missions are difficult because Saturn is a long way away, and several things work against us:

(1) We have less knowledge than on nearer planets from ground-based studies on which to base mission plans.

(2) The missions are of longer duration and that means if we have to build upon the knowledge from one mission to go on to the next, the interval between them is longer. It is difficult to talk meaningfully about a Saturn mission before we've had any spacecraft to Saturn, and I conclude that

we should not now foreclose any options. The uncertainty is particularly severe in things having to do with the magnetosphere, but there are other areas as well.

In reference to the payload on an orbiter, there are three major questions in my mind about science priorities:

(1) The role of magnetospheric physics and measurements. They were omitted by the Space Science Board, but perhaps one just cannot make a judgment on that until after Pioneer 11 has gone there.

(2) Synoptic Saturn studies. The Space Science Board did not recommend synoptic studies of Jupiter, where we know there is a lot of atmospheric motion that's reflected in the visible appearance, but is has recommended, although at a fairly low priority, synoptic studies of Saturn for a Saturn orbiter. I suspect that until we have Voyager pictures, we won't have a feel for whether those kinds of studies are likely to be very useful or not.

(3) Although, given enough time, the SOP[2] orbit can almost be selected at will, I suspect there will be some kind of conflict between ring observations and satellite observations. Most of the ring studies will require cranking up to moderately high inclinations, and that makes it much harder, although not impossible, to encounter other satellites. If we really want to do a detailed comparison of 4 or 5 or 6 Saturn satellites, we might find that in conflict with the kind of extensive ring measurements that we would also want to do.

J. POLLACK: Given the flexibility to change the inclination, wouldn't you choose to have an equatorial inclination most of the time, but then at some point change to an inclination that would let you do the rings and then go back again?

D. MORRISON: The Saturn system has a kind of atmospheric dynamics in it that is absent from Jupiter because of the changing tilt of the rings and of the pole. This argues for a relatively long orbiter mission that's phased to the inclination of the rings and pole. For a good ring study, we would like to get above the rings, below the rings, to see them under different illumination angles; observe their thermal emission, for instance, under different heating regimes.

The season and the ring shadow may also influence our study of the motions of Saturn's atmosphere. Both rings and weather argue for a mission lasting several

years. The next question is the arrival time. The maximum ring exposure corresponds to a flat maximum several years long. If we got on the tail end of that maximum, say at about 20°, in the next three years they'd go down through zero tilt. That might be a very attractive range of times to make orbiter observations.

W. WELLS: Or arrive at zero and go up?

D. MORRISON: Yes. But you wouldn't want to arrive just plus or minus one to two years of zero. For one thing, you'd duplicate Voyager too much. That's around 1995. And you wouldn't want to arrive right when they were maximum full open either, because it's such a flat maximum. These times are 1988 or 2002.

E. STONE: I would be very surprised if, in fact, the magnetosphere is not an important part of the Saturn system. It will surely be an important part of understanding what's going on with Titan, some aspects of the rings, and possibly the other satellites with their curious surface characteristics.

Voyager will not have the appropriate geometry of flyby, except for Titan, to do much in the way of assessing the environment around the satellites, and it does not have the capability for the mass analysis of plasma.

In fact, one is almost sure after Voyager to have the same situation we had after Pioneer at Jupiter, that the magnetosphere is an important part of understanding the Saturnian system. The combination of experiments which are on Galileo are the typical complement which is basic in the sense that they make a coupled set in terms of their interactions.

G. SISCOE: I would like to agree with what Ed said. It seemed to me that what the Space Science Board did was to react to the absence of hard data on the magnetic field of Saturn as contrasted to Jupiter, where we knew there was a strong magnetic field before the Pioneers went. I think that the way to proceed is to assume that if the magnetosphere were as big as it could be, then it would be a very important scientific objective, both from the point of view of the magnetospheric science and also from the point of view of what it does to the Saturnian system.

J. POLLACK: I would like to turn to a type of instrument that is not on Galileo but might profitably be part of an SOP^2 orbiter: a multi-channel infrared radiometer for the 20 μm - 1 mm wavelength region. It would be directed towards getting information on the composition of the ring particles at different positions within the rings. Such an experiment would also be nice to have for both Titan and for Saturn to do atmospheric sounding.

M. KLEIN: I would like to suggest that you consider longer wavelengths than 1 mm. There are several reasons:

(1) There is a one-meter probe relay antenna hanging on the spacecraft already. You could make use of that after the probe has gone as a very efficient microwave antenna to probe the atmosphere. You can do synoptic mapping of Saturn's atmosphere itself, looking for large scale circulations, changes in the ammonia relative humidity, if it has belts and zone-type structure like Jupiter.

(2) You can look at the very cold temperatures of the satellites, particularly the night-side temperatures of the satellites. This is easy to measure with a microwave system, whereas I don't know about the infrared.

(3) Probably less significant, you might be able to do some magnetospheric studies by measuring synchrotron emission if you have a long enough wavelength - (around 30 cm).

J. CUZZI: I want to reemphasize that I think this millimeter region is extremely important for studying the rings. In this region the ring particle behavior goes from that of absorbing and emitting to that of scattering. It's a transition region, where the action is and where we're going to learn the most. It's going to tell you about particle size, composition, impurities, and structure. We want to learn the maximum particle size, and how absorbing they are, whether they have silicates, and this is where to look. The range is probably down to a couple of hundred μm.

D. MORRISON: I think that's an interesting point, and I would ask the question more broadly. The things Saturn has that Jupiter doesn't are Titan and a ring system. We've talked a lot about Titan; for the ring system it's fair to ask the question: How do you modify the payload to take advantage and attack the problems associated with that unique element. Infrared and millimeter radiometry is one way, and perhaps there are some other ideas.

J. CUZZI: We haven't really talked about doing any bistatic radar.

G. ORTON: It's been mentioned. Any of it's advocates care to stand up and be counted at this point?

J. CUZZI: I'll stand up. That's the second important handle on the rings, and I should elaborate on that a little bit more.

Presumably, there'll be another two-wavelength radio-science experiment. I think that would be extremely nice, 3 and 12 cm or something like that. It would be extremely valuable. I would support a two frequency (S and X band) telemetry. It could be used for extensive bistatic radar mapping of the rings. And it would be nice to have the orbit cranked to 10° inclination. I would also support the desire to have the rings inclined by about 20° when we get there.

It would also be nice to be able to take the orbit and slew it around once so you can look at different parts of the rings from different angles, elevation angles, and investigate the size distribution.

L. TYLER: By bistatic, I think you mean phase angle coverage at centimeter wavelengths.

J. CUZZI: Yes, the spacecraft bouncing radar off the rings and being received at the Earth, both from above and below, and at all different scattering angles.

J. POLLACK: To contrast this a little bit, what Voyager will be doing, primarily, is something with scattering angles of half a degree or so, and the things that Jeff Cuzzi was mentioning could go up to maybe 30° scattering angles. And if backscatter is possible, it can give shape information.

G. COLOMBO: (1) I would consider very important a study of a mission whereby the spacecraft is periodically and sequentially transferred, with minimum energy expenditure, from a Saturn orbiter to a Titan orbiter, and vice versa. This will allow detailed study of both long and short term variations in the Titan and Saturn atmospheres and a complete exploration of the inner Saturn satellite system and planet. Of particular interest is the region between Rhea and Titan for the reason outlined in the next paragraph. I emphasize here that the mass of Titan is large enough to give quite a large flexibility in the maneuvering capability with relatively small consumption of the propellant of the auxiliary propulsion systems. Typical trajectories of the restricted three body problem may be used as reference. The efficiency of the satellite Rhea in a similar role may also deserve some consideration. The other satellites may be too small and the relative velocity may be too large for gravity assisted maneuvering. (2) I consider very crucial a deep survey of the intersatellite region between Rhea and Titan and just outside Titan. The similarity of the dynamical environment inside the belt between Mars and Jupiter and the dynamical environment between Rhea and Titan lead us to think that a belt of sparse and relatively small objects may be present similar to the asteroidal belt. We should also look for Trojan type objects in the triangular Lagrangian position. Besides it seems probable that Hyperion is one of the members of a family of smaller objects just outside the Titan orbit.

(3) Concerning the inner Saturn system, we expect the existence of a swarm of small limited number of bodies between Mimas and the ring A of Saturn. In particular we think that the inner boundary of ring B could be caused by a resonance effect due to bodies orbiting Saturn just outside the Roche limit. In fact, from photometric observations of the light curve of Iapetus, eclipsed by the rings, it seems now clear that the outer boundary of ring A is 2000 km inside the circular orbit of a hypothetical satellite, or swarm of small bodies in a 3 to 2 orbital resonance with Mimas. This possible satellite(s) could excite a strong resonance (2 to 1) at the inner boundary of ring B causing the conspicuous drop in density at this boundary distance from the planet.

(4) The near Saturn environment may be quite different from the Jupiter environment both in regard to energetic particles and intersatellite solid (meteor or meteorite) components. This characteristic should allow a better exploration of the inner system than that which will be done with Galileo on the Jupiter inner system. The density of the solid component of the intersatellite space and rings may require a re-examination of any mission profile when more information will be available from the Voyager mission and in 1979 from the Pioneer flyby. A very intense observation program both from ground and from the space telescope will be crucial in the mission planning. We wanted to emphasize the difficulty we are encountering at present in optimizing the mission because of lack of information.

CONCLUSIONS AND RECOMMENDATIONS: EXPLORATION OF THE SATURN SYSTEM

Summarized by

Donald M. Hunten

Department of Planetary Science and Lunar and Planetary Laboratory
The University of Arizona
Tucson, Arizona 05724

Areas of Investigation

In its *Report on Space Science 1975*, the Space Science Board adopted as policy the report of its Committee on Planetary and Lunar Exploration (COMPLEX). The section on "Saturn objectives" (pp. 47-49) begins by pointing out that the flybys of Pioneer 11 and Voyagers 1 and 2 will complete the reconnaissance phase of Saturn investigation. COMPLEX then "anticipates that [follow-on] missions will have the following principal goals, in order of importance:

(1) Intensive investigation of the atmosphere of Saturn ...

(2) Determination of regional surface chemistry and properties of the surface features of satellites and properties of ring particles ...

(3) Intensive investigation of Titan ...

(4) Atmospheric dynamics and structure ...

... The comparative planetology of the satellites will also be of great interest

... The rings of Saturn are potential treasure-houses of information ...

"For these reasons, we consider it essential that NASA be in an adequate posture to initiate exploration of the Saturnian system in the middle 1980's following the reconnaissance of this system."

The present Workshop and report constitute an early step towards reaching this posture.

COMPLEX's omission of the magnetosphere was presumably intentional. Indeed, its outer parts can be expected to be similar to the corresponding regions around Jupiter. But the inner magnetosphere may be a different story. Even since

1975 we have increasingly realized the profound effects that charged-particle bombardment can have on Jupiter's inner satellites, particularly Io. Io emits vast quantities of sodium, sulfur, and presumably other materials into the surrounding space, most probably because of sputtering by energetic particles. Its ionosphere also is thought to be generated by particles rather than solar photons. Similarly, the gases emitted may be a major, even dominant, source for the magnetosphere. Though Titan lies farther from its primary than does Io, important effects in both directions are expected, and the influence on ring particles could be even more important. Thus, it seems to us essential to be able to explore the inner magnetosphere, both as a phenomenon in itself and as an aspect of the Saturnian environment. While we agree that all four of the COMPLEX goals are important, we add another:

(5) Exploration of the inner magnetosphere and its relationship to the rings and satellites.

It is desirable that a mission to Saturn contribute significantly to the study of all five goals.

Scientific Questions and Their Investigation

In this section we state what, in our view, are the most important questions concerning the various bodies and media in the Saturn system, and attempt to predict what the state of knowledge will be late in 1981, when Pioneer 11 and Voyagers 1 and 2 will have performed their flybys. Account is also taken of the likely progress in ground-based measurements, and the competition, even beyond 1981, from Earth-orbiting telescopes.

Study of the present state of the Saturn system is of great interest. Certain results have added interest because they bear on questions of history and origin, and they are highlighted. Since we did not discuss priorities between the various areas, they are arranged in decreasing order of mass.

Saturn The basic state of the atmosphere is described by its composition, temperature profile, and cloudiness. With this information, further questions, such as energy balance, mass transport, and condensation can be investigated; knowledge of the radiation fields is very helpful. We expect to find abundances of volatile elements similar to solar (or Jovian) values, but any deviations will be of particular interest.

Segregation of helium in the interior has been suggested, and most current analyses give an enrichment of the heavier elements. Information on the bulk composition and internal state also comes from the mean density, the gravitational moments, the heat flow, and the magnetic field. Many of these data bear on theories of Saturn's origin. In particular, it might be possible to decide between the models of a core instability or a gas instability. Isotopic ratios, particularly within the noble gases, are of particular interest because they can be compared with data for Earth, Mars, and soon Venus and Jupiter.

The primary tool for most of the measurements suggested above is an entry probe with instruments directly measuring the atmosphere and the radiation field. Important support comes from an orbiter which can place the single profile from the probe in its global context. Conversely, the probe data give calibration and improved confidence in the less direct orbiter measurements.

Another area of interest is the ionosphere and the neutral upper atmosphere in which it lies. "Pre-entry" measurements have had to be omitted from Galileo, but the Saturn mission offers another chance to measure the composition and energy budget of this strange region. Saturn's ionosphere should resemble that of Jupiter, which is not understood except in the framework of *ad-hoc* assumptions.

The general circulation of Saturn's atmosphere has features absent from Jupiter: the 27° equatorial inclination and the enormous shadowing of solar input by the rings. Studies of this circulation will be of particular interest. Evaluation of the global zonal velocity field on Saturn requires observations (over several rotations) of discrete, nonaxisymmetric cloud features distributed at various latitudes over the disk. Although only 9 such features have been observed to date, the very best ground-based photographs obtained at a rate of a few per year show additional features at the limit of ground-based detectability. Thus we have some confidence that improved resolution will yield the data necessary to evaluate the zonal wind system at the top of the clouds on Saturn. Although the present document stresses the capability of an imaging system aboard an orbiter, important contributions may also be possible by the Space Telescope. Infrared sounding from the orbiter can give information on the driving forces.

Because of its substantial obliquity and the unique rings of high optical depth, Saturn is expected to demonstrate many seasonal changes. For the planet, the alternating illumination of the poles and the varying size and position of the ring shadow provide drives for the atmosphere that are not present in Jupiter. For the rings

themselves, the absorption of sunlight and hence the temperature vary dramatically, and the changing geometry offers possibilities for determining the properties of the rings and of their individual particles that could not be obtained in any one "snapshot" view. Voyager and Pioneer will visit Saturn while the ring tilt is near zero. In order to complement these studies and to obtain the greatest scientific return from this orbiter mission we recommend:

(1) The orbiter be at Saturn during a period when the rings are fairly wide open, preferably more than 20°.

(2) The duration of the mission should be sufficient to track the effects of changing tilt, for instance by observing from a tilt near 20° down to a tilt of less than 5°. (The variation from 20° to 0° requires about three years). The time period from about 1992 to 1995 fits these criteria of timing and duration.

Of scientific importance is the nature of temporal variations of features and fluxes (uv-visual and thermal) in Saturn's atmosphere. Longterm variations of a seasonal nature as well as short-term variations of spots, etc. shed light on the meteorology. Also, spatial dependence of temporal phenomena is relevant to structure as well as meteorology. Examples are the bright equatorial belt motions and the polar zone, both of which differ in appearance from temperate latitudes. Of special interest is the study of dynamical phenomena near the boundaries of the Ring shadow - the heat input gradient at these boundaries may drive dynamical processes, create hazes, etc. affecting the atmosphere globally on a seasonal time scale.

Titan Much of the discussion of Saturn also applies to its largest satellite. But the nature of this "planet" is different in many ways: it likely has a liquid interior and probably a solid surface. The atmosphere is substantial and must be made of a heavier gas, with nitrogen the most popular at present, but including enough methane to be very obvious spectroscopically. This methane may form a dense cloud deck, and there is in addition a dark, high-altitude haze. Cloud measurements are even more important than for Saturn.

The location of Titan's surface is still highly debatable, but there is good prospect that the debate will be settled in a year or two. As discussed in Chapters 8 and 9, we now have two radio measurements of the surface temperature, one implying a "low" pressure (~1 bar) and the other a "high" pressure (~20 bars). Further

measurements now in progress with the Very Large Array support support the low value. Radio-occultation measurements from the flybys of 1979-81 should also indicate the location of the surface, simply by its interception of the radio beam. Or, if the apparent surface is really an absorbing layer in the atmosphere, the experiment will give a characteristically different answer.

In any case, even the lowest pressure consistent with present data is ample to support a highly productive probe mission. The same things should be measured as for Saturn (as well as Venus and Jupiter), but with far greater emphasis on organic chemistry. Pre-entry measurements are of great interest here as well, for Titan's atmospheric composition is unique, except perhaps for that of the primitive Earth.

Meteorologically, Titan is again a special case, though the deep version of the atmosphere has much in common with that of Venus. Titan rotates much faster than Venus and shares the seasonal geometry of Saturn. Imaging of Titan could, however, prove very disappointing, as we have no evidence whether its atmosphere contains photographable detail that would permit its motions to be traced. Fortunately, the requirements for imaging of Saturn, the rings, and the other satellites should assure that Titan is well covered.

It is expected that photolysis of Titan's methane provides a copious source of H_2 and H to a torus that occupies much or all of its orbit. Lyman-α emission from the H atoms has probably been detected. The corresponding Io torus has been seen in several emission lines, but it does not extend all the way around the orbit because the atoms are ionized by impact of magnetospheric electrons. Titan's torus may not be so limited, and it should be much more accessible to direct study. H_2, which should be an important component, is difficult or impossible to sense remotely.

Other Satellites The Saturn system is a miniature solar system; in a sense it even has an asteroid belt (the rings) and could have a closer analog near Titan's orbit. A complete inventory is needed, particularly of the inner region; Earth-based searches, rather than Voyager, will contribute to this. Systematics of the mean densities as a function of distance are of particular interest, quite apart from the intrinsic importance of the density as a constraint on the interior composition. Densities should be obtained to a few percent; the

requirements for masses and especially radii are correspondingly stringent. Large satellites may have liquid interiors, and their gravitational moments are of interest. The outer satellites may perhaps have been captured; their sizes, shapes, and general morphology, particularly for Phoebe, should be revealing. The interactions of the satellites with the rings, particularly ring E, need to be explored.

Surface morphology (craters and their distribution; other topography) should be studied on representative large and small satellites (diameters greater than 1000 and less than 500 km). Voyager is expected to do an excellent job on parts of the surfaces of most of the inner satellites. Surface compositions (apart from the known water ice) should be measured. Iapetus is of special interest, with its remarkable hemispherical asymmetry in albedo and ice cover; we do not know whether this is a survival from its origin or a feature due to its present environment.

Icy satellites are expected to have at least a tenuous atmosphere, and their nature and interactions with the magnetosphere are of interest.

Such physical studies can hardly be carried out for all the satellites, and we recommend as a minimum set (in addition to Titan); Iapetus, one icy inner satellite, and preferably one outer satellite.

Rings Saturn's rings are still among the least-understood objects in the solar system. We do not know their origin or whether they are evolving rapidly; and we are baffled by the almost total lack of resemblance between the ring systems of Saturn and Uranus. The particles may have condensed in their present form or originated by breakup of a large body or bodies. Earth-based studies may have missed completely the largest particles in which most of the mass may reside. Whatever we can learn about these matters will bear directly on our ideas of planet formation.

Questions about the rings divide naturally into two categories: the collective properties and the properties of the individual particles. Collective properties include the total mass and its radial distribution, and the physics behind the divisions and edges. Knowledge of these matters might lead to elucidation of the nature of the rings of Uranus. An azimuthal variation is now well established. The size distribution of the particles and its variation with distance from Saturn are of prime importance, as is the composition and

nature (distribution of minerals and ices in a typical particle). The rings should have at least a tenuous atmosphere, which should mediate their interaction with both the magnetic field and the magnetospheric charged particles. There may also be an interaction with Saturn's atmosphere.

Pioneer 11 and the Voyagers should do a respectable job on many of these objectives. Indeed, they may get considerably closer to the rings than an orbiter will, and should therefore be in a better position to disentangle the gravitational effect of the rings from that of Saturn. It may be in the properties of the individual particles, or the statistics of these properties, that the Saturn Orbiter could make its best contribution. Experiments such as bistatic radar and submillimeter radiometry have been suggested here, and additional ideas would be welcome.

Saturn's Magnetosphere The existence of Saturn's magnetosphere is not yet demonstrated, but is expected both on general principles and judging from the limited data now available. On the assumption that there is a substantial magnetosphere, there are three major points of interest: 1) Magnetospheric effects on Saturn, its rings, satellites, and in particular on Titan and its torus. 2) the effects on the magnetosphere of the rings and the Titan torus, which are unique to Saturn, and 3) the general magnetospheric data which will contribute to the subject of comparative astrophysical magnetospheres.

1) The magnetospheric particle precipitation into Saturn's atmosphere, as in the cases of Earth and Jupiter, probably will have interesting observable effects on the atmosphere, e.g., auroras and hot spots. Ablation of the rings by magnetospheric particle sputtering and the associated redistribution of ring material now appears likely to be an important process. Similarly sputtering of the surfaces of the satellites might account for photometric satellite characteristics. The effects of magnetospheric particles on Titan aeronomy and the Titan torus is likely to be of major importance as both a loss mechanism for the torus and as an energy supply for aeronomical processes and high altitude organic chemistry, in particular chemistry of nitrogen, since N_2 is not efficiently dissociated by photons.
2) The massive ionized particle source represented by the Titan torus and the spatially extended absorption boundary represented by the rings constitute important and unique variations of magnetospheric

parameters compared with any other planet. The variations they provide are sufficiently radical to lead to a magnetosphere of great intrinsic interest, and also to provide hard and clear data with which to test magnetospheric theories that deal with particle transport. Also important in this regard is the distinct possibility that the Titan source might lead to a non-linearly evolved magnetospheric configuration analogous to what occurs at Earth during geomagnetic storms. Since the source in this case would be well specified, the situation is ideally suited to the study of the non-linear response.

3) The comparison of Jovian and Saturnian magnetospheric characteristics provides a unique opportunity to provide for increased understanding of the general subject of astrophysical magnetospheres. The approximate similarity of the Jovian and Saturnian solar wind and planetary parameters (exclusive of those mentioned above under Item 2) makes it possible to determine how magnetospheric features and processes vary with changes in these parameters and so to test the theories that address such variations. This is important in connection with the general problem of developing a theory of astrophysical magnetospheres encompassing the range from small planetary magnetospheres such as at Mercury and Earth, giant planetary magnetospheres, and stellar magnetospheres.

The two Voyager spacecraft will provide magnetospheric coverage at 3 local times. Both spacecraft will enter the magnetosphere at $\leq 10^{\circ}$ to the Saturn-sun line, with exits at ~90° for JSX(X = U) and ~135° for JST. Thus, for a nominal magnetosphere, JST will traverse the dawn flank of a possible magnetotail at distances of $\geq 200\ R_S$. Along with Pioneer 11, these missions will give an excellent reconnaissance of the magnetosphere, along with some information on the possible sources and sinks of ions. The potential of a Saturn orbiter to explore many more regions and obtain the time dimension, can be assessed definitively after the Pioneer and Voyager encounters, but we expect the value of the orbital studies to be great.

Orbiter and Probe Experiments

In considering potential experiments for a Saturn mission, we shall take Galileo as a convenient point of departure, since it includes an orbiter and a probe for intensive study of the Jupiter system. A few additional candidates are carried by Voyager. Finally, we draw attention to a few areas where development or improvement of instruments should be encouraged. The science complements of Voyager and Galileo have been summarized in earlier chapters, but are reproduced for reference in Tables 1 and 2.

Table 1. Voyager Experiments

Imaging Science	Magnetic Fields
Radio Science	Plasma
Infrared Interferometer Spectrometer	Low Energy Charged Particles
Ultraviolet Spectroscopy	Cosmic Ray
Photopolarimetry	Plasma Wave
Planetary Radio Astronomy	

Table 2. Galileo Experiments (tentative)

Probe	
Atmospheric Structure	Nephelometer
Mass Spectrometer	Net Flux Radiometry (visible and infrared)
Helium Abundance Interferometer	Lightning
Orbiter	
Imaging	Electron Emitter
Radio Science	Magnetometer
Near Infrared Mapping Spectrometer	Plasma
Ultraviolet Spectrometer	Plasma Wave Spectrometer
Photopolarimeter Radiometer	Energetic Particles
Dust	

An ideal mission would carry a combination of Galileo and Voyager experiments, as well as a small number of new ones. Although some priority judgements will eventually be needed, we do not attempt to make them here. We do, however, call attention to some of the issues as they can be seen today.

Orbiter Experiments An imaging system is essential for study of planet, rings, and satellites. The CCD detector now being designed for Galileo is nearly ideal, but the limitations of a single focal length are being keenly felt. Every effort should be made to find a solution to this problem; options might be a compromise focal length, a variable focal length, or two cameras.

For infrared studies, the same issue will be faced as for Galileo: the requirements for spectral mapping of satellite surfaces and for sounding of atmospheres are not easily (if at all) reconcilable in a single instrument. And a powerful instrument of the latter type (IRIS) will have been carried past Saturn and Titan by the Voyagers. A possible compromise is to carry a far-infrared filter instrument to supplement the near-infrared mapper. But, in view of the importance of atmospheres in the Saturn system, the implications must be carefully examined.

Polarimetry is another experiment that has great value for study of atmospheres (particularly those with clouds) and surfaces. But again it will have had two opportunities on Voyager, as will ultraviolet spectroscopy. UV measurements will also be taken from Earth orbit, and their value on an orbiter will have to be re-assessed. One unique measurement is made during eclipse (or "solar occultation"), with the advantages of high sensitivity and the ability to detect unexpected gases. On Mariner 10, this method set the strongest limit on Mercury's atmosphere, and the dayglow mode actually detected H and He. Some of the most interesting tenuous gas will actually be directly available to the orbiter, and its direct measurement may be the preferred option. A mass spectrometer with this objective was proposed for Galileo, but could not be flown because of weight limitations. Dust particles are also of interest, even though they have far less effect on the magnetosphere, and an experiment such as the one on Galileo would be suitable.

Instruments for magnetospheric science have evolved to a standard package, the last 5 in Table 1 or 4 in Table 2. They should be equally suitable for Saturn, as long as they are carried by a spacecraft with a spinning section.

Radio-science measurements of atmospheres and ionospheres can be made with the telemetry carriers. A variety of proposals have been made for other experiments, such as bistatic radar and passive radiometry. The applicability of the Voyager Planetary Radio Astronomy experiment to Saturn should be assessed after their Saturn encounter.

Ring studies deserve special attention. Most of the investigations suggested for satellite surfaces, in particular imaging, are applicable here. But there is a special class of far-infrared and radio experiments that shows great promise. The behavior of the rings changes from absorbing/emitting at middle-infrared wavelengths to scattering at centimeter wavelengths. Thus the wavelength range between these limits contains information crucial to our understanding of the range of particle sizes and the bulk particle composition. We therefore suggest that effort be initiated to produce sub-millimeter range radiometers or spectrometers for use on a Saturn orbiter. The desired range of interest is at least from several hundred microns to several millimeters. Compositional studies of the rings and satellites will be aided by added spectral capability from 20 m wavelength longward. Atmospheric studies will be greatly aided by extending the wavelength. In addition, bistatic radar studies at S and X band, with polarization capability, will be of significant value in studying the particle size distribution.

Orbit Design Close encounters with Titan permit large changes in the eccentricity and inclination of the orbit. The opportunity therefore exists, at least in principle, to tailor the orbit successively for various investigations. The need to pass near Titan at every revolution ensures that there will be plenty of coverage of this important object. It will be desirable to have some orbits that go outside, and some inside, that of Titan. For ring studies, an inclination of at least 5-10° is suitable, and the ring inclination (as seen from Earth) should be similar. Such an inclination, with a fairly close approach, would also permit investigation of the ring mass and Saturn's gravitational moments.

While it would be desirable to make close approaches to all the satellites, most objectives would be satisfied by detailed study of Titan, Iapetus, and one inner satellite such as Rhea. It would be desirable to add one small, outer satellite to this list. In addition to remote sensing, measurements may include mass, shape, mean density, magnetic field, atmosphere, and interaction with the magnetosphere.

Iapetus, with its notable asymmetry, should be encountered at more than one orbital phase to give the best possible coverage of the whole surface.

The variety of orbits suggested above will be excellent for coverage of the inner magnetosphere. The outer parts, and the tail, are expected to be less distinctive in comparison with Jupiter, and an extended tail orbit is of low priority. In any case, we anticipate 7 passes through other outer regions from Pioneer 11, Voyagers 1 and 2, and the incoming leg of the orbiter-probe mission.

Probe Experiments Probes for Saturn and Titan have so much in common that it is convenient to discuss them together initially. Problems peculiar to Titan are addressed in the next section. The basic instrument for measuring composition is still the mass spectrometer, particularly valuable because it can measure the unexpected as well as the expected. The Galileo instrument is furnished with enrichment cells for noble gases and for absorbable compounds, later driven off by heat. Further development along such lines is desirable, and may even lead to a full-blown GCMS (gas-chromatograph--mass spectrometer) such as operated successfully on Viking. Progress along such lines is desirable for Saturn and particularly so for Titan. An alternative is to have a separate GC, which gives some redundancy but lacks the power of the combined instrument. A special measurement of the helium abundance included for the Galileo Probe is desirable for Saturn only.

The primary package for atmospheric structure is the combination of accelerometer, pressure gauge, and thermometer. Clouds and hazes are important on both Titan and Saturn, and a Galileo-type nephelometer is suitable to measure them. Such a nephelometer, with several scattering angles, is a partial substitute for the Pioneer Venus cloud particle size spectrometer.

Doppler tracking of the probe is a method of studying atmospheric motions; it is an important part of the Pioneer Venus mission (and earlier Veneras) but is not in the current baseline for Galileo because of the cost impact. Collection and analysis of dust (particularly the dark material in the stratosphere) is of interest for both Saturn and Titan. It has never been implemented on previous missions because of doubts about its feasibility, but further work is desirable. A radar altimeter for the Titan probe would also be useful. Such an instrument was included in early studies for Pioneer Venus, but had to be deleted because of its weight and the difficulty of accommodating the antenna. A similar cost-benefit tradeoff will be necessary for Titan.

Unless we learn more than currently foreseen about the nature of Titan's surface, it will not make sense to carry instruments for detailed surface study. The probe should do a good job on the atmosphere but also try to diagnose the general nature of the surface. An indication of its hardness or softness would be important. Imaging is a possibility; other experiments that could be considered are a seismometry mode of the accelerometer, differential thermal analysis, and nuclear methods. It must be remembered that heavy elements may be rare or absent; carbon, nitrogen, and oxygen probably dominate. Ideas, research, and development are needed here.

If Titan's atmosphere is mostly N_2, it is unusually favorable for support of a balloon. Some attention might be paid to this technique, which could be particularly useful for study of atmospheric circulation, although it is probably premature for an initial probe mission.

Instruments for pre-entry science include neutral and ion mass spectrometers, an ion retarding potential analyzer, and a Langmuir probe. For Saturn, an energetic particle detector would be of interest.

Probe Mission Profiles For Saturn, a descent time of 30-45 minutes is suitable, similar to the Galileo Jupiter descent profile. It is highly desirable to reach the 300-350 K level, below the water cloud base. Further penetration should be treated as an "extended mission", desirable for reconnaissance but not an engineering requirement.

For Titan, a period of survival on the surface is desirable, even though primary emphasis should be on the atmosphere. Presumably, the total time will be limited by the duration of the relay link to the orbiter. If practical experiments are identified that require a much longer duration, a second relay period could be considered for the next approach of the orbiter to Titan. The probe-lander would have to be put into a low-power data-gathering mode. A precedent exists in Viking.

Planetary quarantine for Titan should receive considerable study. The Space Science Board has recommended assumption of a very small probability of growth for the Jovian planets, including Saturn. Quarantine requirements can, therefore, be satisfied by standard clean-room techniques. But Titan has quite a different composition from Jupiter and Saturn, and some of the relevant factors are not so unfavorable to the growth of terrestrial organisms. If we can be certain that the surface temperature is not far above 200 K, this factor alone should be enough to prevent any growth.

Engineering Questions

Ring Hazards Current knowledge of the hazard due to the ring particles is summarized in Smith in Chapter 7. Pioneer 11 and the Voyagers will tell us far more, and these data will be eagerly awaited.

Magnetosphere Hazards We have essentially no empirical information about high-energy particle fluxes around Saturn. Even with Jupiter as a model, theoretical expectations are extremely uncertain; they are summarized by Siscoe, Chapter 7. Again, we must await receipt of data from Pioneer 11 and the Voyagers.

☆U.S. GOVERNMENT PRINTING OFFICE: 1979-635-004/36

1050-119